Desert Research Institute

Ilias Kavouras, David DuBois, George Nikolich, and Vicken Etyemezian
755 East Flamingo Road, Las Vegas, Nevada 89119
Phone: (702) 862-5362; E-mail: ilias.kavouras@dri.edu

Albuquerque/Bernalillo County Community-Scale Air Toxics Monitoring and Risk Assessment Project

Final Technical Report prepared for the Albuquerque Environmental Health Department

February 2010

Foreword

This report is compiled and submitted in fulfillment of USEPA Assistance Agreement - XA96637091. The AEHD and DRI thank the USEPA for their continued support of air quality monitoring and risk assessment in Albuquerque/Bernalillo County.

Disclaimers

This report was prepared by Desert Research Institute (DRI) as an account of work sponsored by the City of Albuquerque Environmental Health Department (AEHD). Neither the City of Albuquerque, members of the AEHD, DRI nor any person acting on their behalf: (1) makes any warranty, express or implied, with respect to the use of any information, apparatus, method, or process disclosed in this report, or (2) assumes any liabilities with respect to the use, inability to use, or damages resulting from the use or inability to use, any information, apparatus, method, or process disclosed in this report.

Although the information in this document has been funded wholly or in part by the United States Environmental Protection Agency and the Environmental Health Department of the City of Albuquerque to the Desert Research Institute, it may not necessarily reflect the views of the US EPA and AEHD and no official endorsement should be inferred.

DRAFT

Acknowledgements

We greatly appreciate the support from Mr. V. Louis Jaramillo, MPH - Originator and Grant Proposal Author (AEHD), Mr. Fabian Macias - Air Quality Assurance and Project Manager (AEHD), Mr. Ken Lienemann - Air Monitoring Supervisor and Principal Analyst (AEHD), Mr. Dan Gates - Air Quality Assurance Officer (AEHD), Ms. Christella Armijo - Grants and Financial Management (AEHD), Mr. Dwayne Salisbury - Lead Air Monitoring Specialist and Instrumentation Setup and Programming (AEHD), Mr. David Garcia - Air Monitoring Specialist (AEHD), Ms. Angela Reyes - Air Monitoring Specialist (AEHD), Ms. Denise Huff - Air Monitoring Specialist (AEHD), Mr. Michael Doherty - Instrumentation Setup and Programming (AEHD).

We would like to thank Mr. Francis Thomas - Field Assistant (DRI), Mr. Robert Powell - Field Assistant (DRI), Ms. Lycia Ronchetti - Business Manager (DRI), Ms. Alexandra Nikolich - Administrative Assistant (DRI) and Ms. Jacqueline Mason - Administrative Assistant (DRI).

We greatly appreciate the support from George Boyden, who allowed us to put instrumentation on the Sandia Tramway. We acknowledge the assistance from the Albuquerque FAA Flight Standards Office staff John Dewitt and John Wenzel and the help from Sandy Gregory of the City of Albuquerque's Parks and Recreation in reserving the parking lot at the Albuquerque International Balloon Fiesta Park at no cost to us.

DRAFT

Executive Summary

Air toxics include heavy metals, polycyclic aromatic hydrocarbons (PAHs), and volatile organic compounds (VOCs), many of which could, at elevated concentrations, have adverse health consequences. The potential risks associated with exposures to multiple air toxics may be greatest for residents of urban communities, where air toxics may be accumulated from regional, city, and local sources. A study was carried out in Albuquerque, New Mexico, by the Albuquerque Environmental Health Department (AEHD) to determine the levels, spatial variations, temporal trends, local sources, and regional sources of air toxics. The Desert Research Institute (DRI) was contracted by AEHD to analyze the measurements of air toxics in order to obtain a better understanding of the conditions that affect the levels of air toxics in the region. This report summarizes the results of the study, which relied on a measurement campaign that was carried out from September 1, 2007, to March 31, 2009.

Collection of daily samples on a 1-in-6 day schedule of air toxics was carried out by AEHD using canisters and high-volume (filter and polyurethane foam (PUF)) samplers at air quality monitoring sites in Del Norte, North Valley, and South Valley. Selection of sites was based on population, land use, and prevailing wind patterns, which are north-northeasterly during the winter and southerly/southeasterly during the summer. The New Mexico Scientific Division Laboratory (NMSLD) analyzed canisters for VOCs using gas chromatography-mass spectrometry (GC-MS). The Eastern Research Group Inc (ERG) analyzed the particulate filters for heavy metals using the induced coupled plasma-mass spectrometry (ICP-MS) method, and the particulate filter/PUF absorbent for PAHs with GC-MS techniques. A portion of the particulate filter analyzed for PAHs was also analyzed by DRI for elemental carbon (EC) and organic carbon (OC) using the thermal/optical reflectance (TOR) method. During the two intensive monitoring periods (IMPs) in February 2008 and June 2008, DRI obtained hourly VOC measurements using a continuous gas chromatography system. Vertical profiles of meteorological conditions were obtained using a Vaisala tethered balloon equipped with radiosondes. Supplemental data were also obtained to assist in the analysis effort. Those datasets included meteorological and air quality data from the AEHD monitoring network and air mass backward trajectories using the National Oceanic and Atmospheric Administration (NOAA) HYbrid Single Particle Lagrangian Integrated Trajectory (HYSPLIT) model at several different elevations, locations, and durations. In addition, $PM_{2.5}$ speciation data for Albuquerque collected under the framework of the U.S. Environmental Protection Agency's (USEPA) $PM_{2.5}$ Chemical Speciation Network (CSN) for the period of January 2007 – February 2009 were retrieved and analyzed by positive matrix factorization (version 2) (PMF2) to identify and quantify the sources of $PM_{2.5}$ and correlate them to air toxics.

The total PAHs concentrations at all sites ranged from 40.04 to 181.11 ng/m^3 at Del Norte, from 34.90 to 323.85 ng/m^3 at North Valley, and from 18.04 to 228.64 ng/m^3 at South Valley, with naphthalene being the dominant PAH in all samples (more than 70 percent of total PAHs). For heavy metals, the total concentration varied from 6.13 to 39.76 ng/m^3 at Del Norte, from 6.01 to 52.83 ng/m^3 at North Valley, and from 5.73 to

122.03 ng/m^3 at South Valley. The highest levels were measured for manganese (more than 60 percent of total metal concentrations), while trace amounts of mercury and beryllium were detected. VOCs were composed of a mixture of aromatic and chlorinated hydrocarbons with total concentration from 0.1 to 18.7 ppbv at Del Norte, from 0.1 to 8.7 ppbv at North Valley, and from 0.1 to 15.4 ppbv at South Valley. The levels of aromatic hydrocarbons were higher than those measured for chlorinated, with toluene being the predominant compound. Chloromethane and dichloromethane were the most significant chlorinated hydrocarbons. The concentrations of particulate OC ranged from 2.7 to 24.9 μg/m^3 at Del Norte, from 0.3 to 23.8 μg/m^3 at North Valley, and, from 2.7 to 31.5 μg/m^3 at South Valley. Particulate EC concentrations ranged from 0.4 to 7.9 μg/m^3 at Del Norte, from 0 to 9.8 μg/m^3 at North Valley, and from 0.6 to 7.3 μg/m^3 at South Valley. OC represented more than 80 percent of total carbon in Albuquerque.

The hourly concentrations of VOCs followed a bimodal distribution for aromatic VOCs. The first peak was correlated with the morning commute hours. Later in the day, concentrations of all gaseous pollutants decreased because of the combined effects of changes in the atmospheric chemistry and an increase in the height of the boundary layer. Emissions from the evening commute and biomass burning as well as the descent of the boundary layer triggered a second mode in late evening. The levels of chlorinated compounds increased during the daytime, reached their peak concentrations in early afternoon, and then declined and remained low during the nighttime.

The comparison of levels of air toxics measured in Albuquerque with those measured in other urban areas under the frame of National Air Toxics Trends Sites (NATTS) and Urban Air Toxics Program (UATP) showed that: (*i*) the concentrations of VOCs and PAHs in Albuquerque were comparable to those measured nationwide; (*ii*) lower heavy metals levels were measured in Albuquerque than in other urban areas. Note that PAHs and heavy metals were only measured during winter in Albuquerque, which is when the highest PAHs levels tend to occur due to higher emissions, shallow boundary layers, and reduced destruction by photochemistry.

Strong seasonal variation (warm vs. cold period) was observed for aromatic hydrocarbons and 1,3-butadiene with the highest levels being measured during the cold period. On average traffic flow may not vary significantly in Albuquerque; however, the observed trend may be associated with increased emissions from school buses during the cold period (as compared to summer), especially at the Del Norte location, where the monitoring site is adjacent to a school. A similar trend was also observed for OC and EC, providing additional evidence of the importance of traffic emissions.

The day-of-week trends of air toxics concentrations in Albuquerque showed that the lowest concentrations for VOC, OC, and EC were measured on Sunday, followed by a drastic increase on Monday. Different patterns were observed for the rest of the week with levels being high during weekdays and followed by a moderate decrease on Saturday. This “Monday peak” has been observed in other areas, especially for fine particulate matter ($PM_{2.5}$) and its precursors, but it is not attributable to a specific cause.

Note that weekday/weekend trends could not be evaluated for PAHs and heavy metals because of the limited number of samples.

The Pearson correlation coefficient, absolute and relative concentration differences, and the coefficient of divergence were used to assess temporal and spatial characteristics of air toxics in Albuquerque. For PAHs, better associations among the three sites were observed for heavier PAHs, which are present mostly in the particulate phase, as compared to volatile PAHs. Taking into account that reaction losses were not significant, the differences among PAHs at the three sites were probably related to emissions from local sources of volatile PAHs as compared to the rather uniform emissions of combustion-related heavier PAHs. A relatively uniform spatial and temporal variation was observed for particulate heavy metals, OC, and EC. For VOCs, poor to moderate associations were observed among the three sites and were probably caused by strong variations in emissions from sources. Note that VOCs react quickly with atmospheric oxidants (e.g. OH radicals). These processes usually result in a strong spatial and temporal pattern.

The sources of PAHs and VOCs were reconciled using concentration diagnostic ratios. Note that only qualitative information can be obtained using this approach. For PAHs, a mixture of emissions from traffic, oil residues, and wood burning was identified. The comparison of the relative distributions of PAHs measured in Albuquerque to those emitted from three types of woodstoves showed a good correlation with emissions from non-catalytic woodstoves. The values for toluene/benzene, xylene/benzene, and xylene/toluene ratios in Albuquerque were within the range of values measured in other urban areas in the U.S. and on highways, indicating that traffic was the major source of aromatic VOCs. The good correlations between PAHs, VOCs, and some heavy metals (namely, arsenic, cadmium, chromium, and lead) indicated a common origin.

In addition to source reconciliation using concentration diagnostic ratios, a source apportionment effort to identify and quantify the sources of $PM_{2.5}$ in Albuquerque (Del Norte site) and relate them to air toxics levels was undertaken. $PM_{2.5}$ chemical speciation data measured under the framework of the $PM_{2.5}$ CSN network at Del Norte location were used. Five source categories were identified for Albuquerque:

(1) Secondary particulate nitrate aerosol (NO_3^-) formed from the oxidation of NO_x,
(2) Secondary particulate sulfate aerosol (SO_4^{2-}) formed from the oxidation of SO_2,
(3) Primary $PM_{2.5}$ emissions from vehicle exhaust,
(4) Road and mineral dust, and
(5) A mixture of primary $PM_{2.5}$ biomass burning emissions and secondary organic aerosol (SOA) formed from the oxidation of VOCs.

Particulate NO_3^-, SO_4^{2-}, and biomass burning/SOA accounted for about 80 percent of $PM_{2.5}$ mass on an annual basis, with biomass burning/SOA and NO_3^- being more important in winter and SO_4^{2-} being the dominant aerosol type in summer. Primary traffic emissions of particulate matter and road dust represented about 25 percent in summer but less than 15 percent in winter. However, contributions from sources with infrequent, sporadic, or seasonal characteristics may also be important for days in which a lower percentage of $PM_{2.5}$ mass was explained by the five source categories. Particulate NO_3^- is

usually formed through the oxidation of locally emitted nitrogen oxides from traffic (NO and NO_2) to nitric acid (HNO_3) that can be neutralized by free ammonia (NH_3) and condense to form ammonium nitrate particles (NH_4NO_3). The analysis of correlations and linear relationships between $PM_{2.5}$ source contributions and air toxics concentrations for the December 2008 to February 2009 period indicated that the vast majority of aromatic VOC was strongly associated with the NO_3^- source category, providing additional evidence of the significant role of traffic emissions of air toxics and $PM_{2.5}$ in Albuquerque. A large fraction of PAHs was also associated with the NO_3^- source category, indicating that PAHs are mostly emitted in the form of hot gases that eventually condense to form particles as the temperature decreases. This is also in agreement with the detection of minor quantities of PAHs associated with the primary traffic emissions sources. Biomass burning was also a major source of air toxics. Finally, a small fraction of PAHs and heavy metals was associated with road dust, indicating that dust particles that are mechanically released into the air by traffic may be contaminated by oil residues and vehicle exhausts.

The back-trajectory calculations for air masses arriving in Albuquerque at five different elevations (10, 100, 500, 1000, and 2000 m) showed similar paths by air masses near the ground compared to those at higher elevations. Three different routes were identified from northwest New Mexico, including the Four Corners area, central/south New Mexico along the I-25 corridor, and central Arizona including the Phoenix urban area. Air masses backward trajectories intersected air toxic point sources emitting more than 500 ton/year in the Four Corners region and central Arizona, and intersected a number of smaller sources (emissions of less than 50 tons/year) in southern New Mexico, southwest Colorado, and Phoenix. This pattern was in effect for air trajectories arriving at Albuquerque during the first IMP (February 2008). During the second IMP (June 2008), air masses at all elevations were moving extremely slowly through central Arizona and New Mexico and lingering over Albuquerque for a long period of time.

As part of an air quality study for the City of Albuquerque to support a community scale air toxics risk assessment, meteorological measurements were collected to help understand the wind patterns and transport of pollutants within the air basin. The study was organized into two parts, with a winter and summer Intensive Monitoring Period (IMP). Instruments included a tethered balloon system, an instrumented aerial tramway, a laser celiometer, and a network of surface-based sites. The surface measurements varied over a range of elevations from 1,500 m at the Rio Grande River to over 3,100 m on the Sandia mountain range. This study also compares the pseudo profiles with the tethered balloon and nearby twice daily radiosonde measurements at the airport.

A wind field modeling study was undertaken as part of the Air Toxics Risk Assessment for the city of Albuquerque. The purpose of the modeling study was to determine wind flows in the area to help understand data collected during the study and to shed light on the distribution of pollutants in the valley. This was accomplished by applying the CALMET diagnostic meteorological model to wind measurements from surface monitors in the area for the winter and summer IMPs. Simulated wind fields for each of the IMPs are also documented in this report. During the night, local circulations developed with

westerly, northwesterly, and northerly drainages from the western plateau toward the river valley. Wind speeds were low. During the day, mainly southwesterly/southerly flows developed from the cooler valley floor air toward the warmer air over the slope. Wind speeds and the mixing depth were higher during the day compared to the nighttime. Model results were derived using sparse measurements, and in some cases cannot fully represent atmospheric flows and thermal stability in this complex terrain.

The USEPA's coupled HAPEM/TRIM.Risk model was used to estimate annualized non-cancer and cancer risks associated with exposures to air toxics in Albuquerque/Bernalillo County using EPAs Reference Concentration (RfC) and Unit Risk Estimate (URE). Risks were estimated for air toxics with sample completeness for more than 50 percent of the year, namely, benzene, toluene, xylene, and methylene chloride. The annual hazard quotient (AHQ) values for all toxics were typical for urban communities dominated by traffic emissions and similar to those estimated for other urban areas in the U.S. and did not indicate significant health risks. The annualized cancer risks for benzene and methylene chloride were lower than 1-in-a-million. These estimates were in the same range with those obtained in NATTS sites.

Table of Contents

List of Figures

List of Tables

List of Acronyms

AAMS	Ambient Air Monitoring Section Supervisor
ABCAQCB	Albuquerque/Bernalillo County Air Quality Control Board
ACR	Annual Cancer Risk
AEHD	Albuquerque Environmental Health Department
AHQ	Annual Health Quotient
AQ	Air Quality
AQD	Air Quality Division
AQS	Air Quality System
ATP	Air Toxics Program
CAAA	Clean Air Act Amendments
CABQ	City of Albuquerque
CALMET	California Meteorological Model
CD	Central Database
CDROM	Compact Disk
CHAD	Consolidated Human Activity Database
CO	Carbon monoxide
COD	Coefficient of Divergence
CSN	Chemical Speciation Network
DAVE	Data Analysis and Visualization Engine
DELCD	Dry Electrolytic Conductivity Detector
DQA	Data Quality Assessment
DQI	Data Quality Indicators
DQO	Data Quality Objectives
DRI	Desert Research Institute
EC	Elemental Carbon
EDAS	Eta Data Assimilation System
EIB	New Mexico Environmental Improvement Board
ERG	Eastern Research Group, Inc,
FAA	Federal Aviation Authority
FID	Flame Ionization Detector
GC	Gas Chromatography
GC-MS	Gas Chromatography-Mass Spectrometry
GPS	Global Positioning System
HAP	Hazardous Air Pollutants
HAPEM5	Hazardous Air Pollutant Exposure Model
HYSPLIT	HYbrid Single-Particle Lagrangian Integrated Trajectory
IARC	International Agency for Research on Cancer
ICP-MS	Induced Coupled Plasma-Mass Spectrometry
IMP	Intensive Monitoring Period
IMPROVE	Interagency Monitoring of Protected Visual Environments
ISCLT	Industrial Source Complex-Long Term
IUATS	Integrated Urban Air Toxics Strategy

MBL	Measurement blanks
MDL	Method Detection Limit
MW	Molecular Weight
NATA	National Air Toxics Assessment
NATTS	National Air Toxics Trends Sites
NIST	National Institute for Standards and Traceability
NMED	New Mexico Environment Department, Air Quality Bureau
NMSLD	New Mexico Scientific Laboratory Division
NOAA	National Oceanic and Atmospheric Administration
NOx	Nitrogen oxides
NSHE	Nevada System of Higher Education
O3	Ozone
OC	Organic Carbon
PAHs	Polycyclic Aromatic Hydrocarbons
PC	Personal Computer
PCMP	Pilot City Monitoring Program
PI	Principal Investigator
PID	Photoinozation Detector
PM_{10}	Particles with aerodynamic diameter less than 10 μm
$PM_{2.5}$	Particles with aerodynamic diameter less than 2.5 μm
PMF	Positive Matrix Factorization
PUF	Polyurethane Foam
RfC	Reference Concentration
QA	Quality Assurance
QAO	Quality Assurance Officer
QAPP	Quality Assurance Project Plan
QAR	Quality Assurance Report
QC	Quality Control
SOA	Secondary Organic Aerosol
SOP	Standard Operation Procedure
TBD	To be determined
TBS	Tethered Balloon System
TO	Technical Order
TOR	Thermal Optical Reflectance
TOT	Thermal optical Transmittance
TRIM	Total Risk Integrated Methodology
TSA	Technical Systems Audit
UATMP	Urban Air Toxics Monitoring Program
URE	Unit Risk Estimate
USEPA	United States Environmental Protection Agency
UV	Ultraviolet
VOC	Volatile Organic Compounds
WOE	Weight of Evidence

1 Background

The 1990 Clean Air Act Amendments (CAAA) included the identification and classification of 188 chemical compounds as Hazardous Air Pollutants (HAPs) (air toxics, hereafter) that require specific attention, long-term monitoring, health-risk assessment, and eventually regulation because of their association with long-term severe health effects. As part of this study, the AEHD contracted NMSLD and ERG Inc. to analyze samples for PAHs, heavy metals, VOCs, and carbonyls, and contracted DRI to coordinate and conduct the IMPs – including hourly monitoring of VOC, tethered balloon-based measurements, complete a source apportionment, relate source contributions to measured air toxics, utilize dispersion models, and apply health risk assessment models for air toxics exposure. The analysis of the data was designed to meet the following objectives:

- measure ambient concentration levels of air toxics within specific community settings and geographic and demographic regions in the city of Albuquerque,
- assess spatial variations in air toxics concentrations,
- identify and evaluate the impact of local air toxics sources,
- quantify the relative contributions from local sources and long-range transport to air toxics,
- determine the impact of meteorological conditions on diurnal, daily, and seasonal time scales, and
- assess adverse health impacts from exposure using risk assessment models

This study utilized: (*i*) air toxics sampling at the three fixed sites with a collection frequency of 1-in-6 days, and (*ii*) two intensive monitoring periods (IMPs) with continuous monitoring of ground-level air toxics and vertical profiling of VOCs, commonly associated pollutants, and meteorological parameters. The monitors were installed at sites that are part of the Air Quality Monitoring Network. In addition to field measurements, $PM_{2.5}$ aerosol composition data were retrieved via the $PM_{2.5}$ Chemical Speciation Network (CSN) run by the U.S. Environmental Protection Agency (USEPA), at Del Norte, and analyzed by positive matrix factorization to apportion the sources of $PM_{2.5}$.

The remainder of Chapter 1 of this report provides a brief background on air toxics in Bernalillo County. In Chapter 2, we provide information on the data validation. Results of the air toxics characterization and patterns are presented in Chapter 3. The outcomes of the advanced analyses, including source apportionment, meteorological modeling, backward trajectories, and risk assessment, are presented in Chapter 4. Chapter 5 summarizes the conclusions from this work. Details on the transport modeling and the experimental configurations during the two IMPs are included in Appendices A and B, respectively. A Central Database (CD) was also prepared.

1.1 City of Albuquerque and Air Toxics

A map of the Albuquerque area, showing major interstate highways, land use, and the 10 existing local air quality (AQ) monitoring sites, is presented in Figure 1-1. The estimated

2006 population for Albuquerque was 504,949 (Bernalillo County: 635,139 residents). The city of Albuquerque extends over an area of 180 square miles and has a population density of 2,483 residents/sq/mile (U.S. Census Bureau 2009). The city is located by the Rio Grande River and the intersection of I-40 and I-25 highways. It is divided into ten distinct communities, namely, Northwest Mesa, Southwest Mesa, South Valley, Central Albuquerque, North Valley, Near Heights, Mid-Heights, East Gateway, Foothills, and North Albuquerque. Urban growth and recent improvements in the transportation network have contributed to Albuquerque's development of industry and as a regional service area.

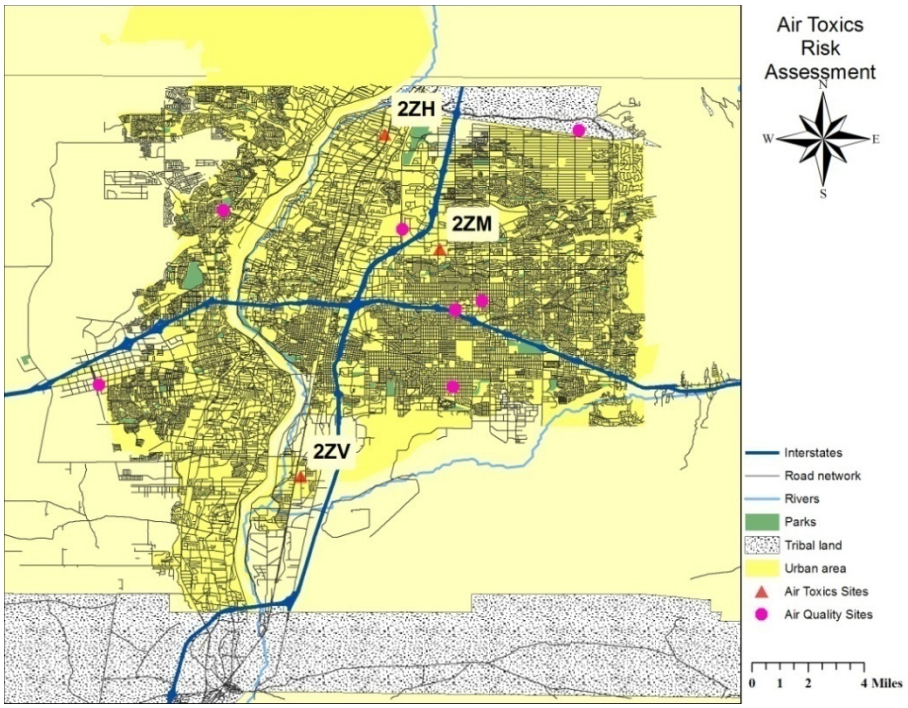

Figure 1-1 Map of Albuquerque/Bernalillo County showing the boundaries of the urban area, tribal lands and parks; major highways and road network and; the locations of air quality (magenta circles) and air toxics (red triangles) sites.

Figure 1-2 shows the land use in Albuquerque, with residential communities covering most of the area. Commercial, industrial, and manufacturing activities are located along Interstates 25 and 40, while the airport is on the south. The major industries include manufacturing (electronic equipment, semiconductors, missile guidance systems, surgical appliances, transportation equipment and parts), printing and publishing, and food processing. The U.S. Air Force, the Department of Energy, and the University of New Mexico are major regional employers with processes requiring permits from the AQD.

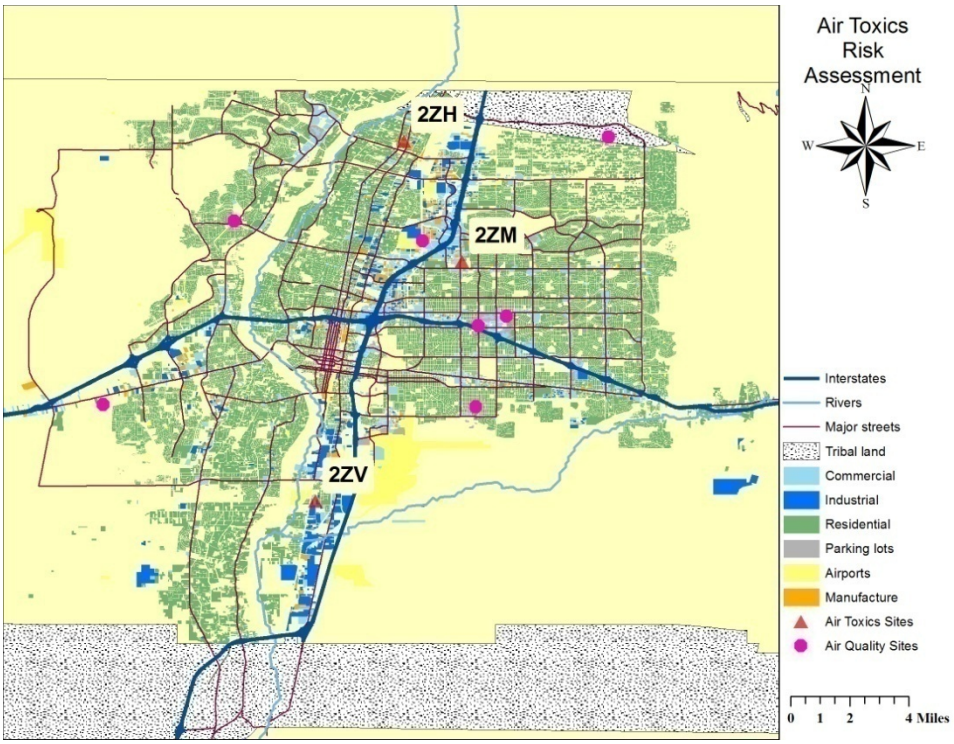

Figure 1-2 Map of Albuquerque/Bernalillo County showing land use, road network, and the locations of air quality (magenta circles) and air toxics (red triangles) sites.

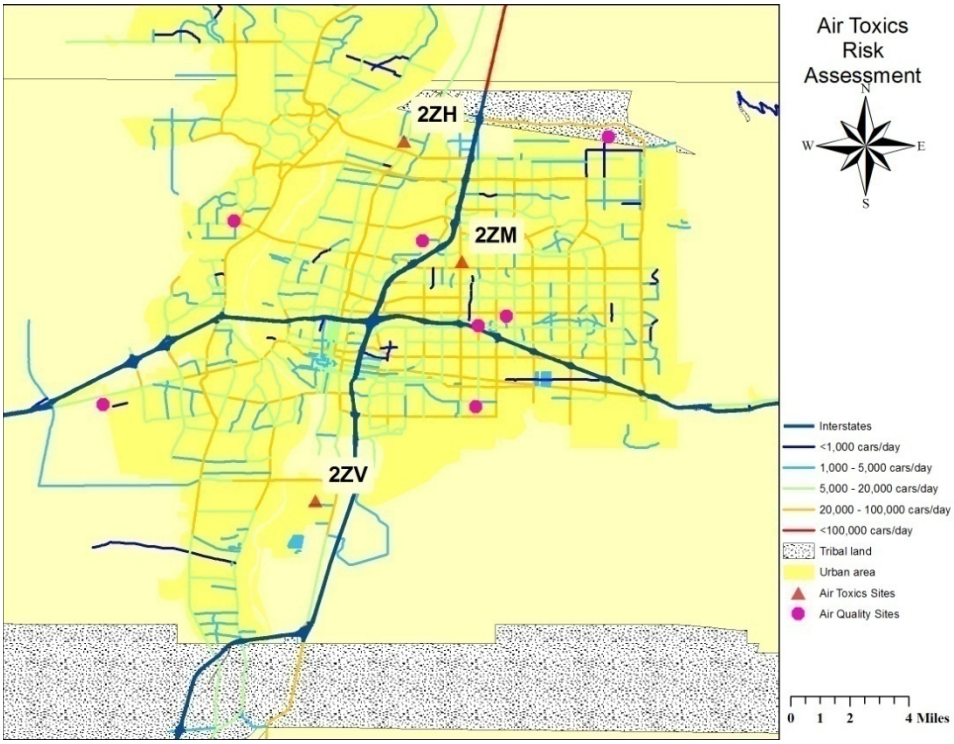

Figure 1-3 Map of Albuquerque/Bernalillo County showing traffic volume in 2007 and the locations of air quality (magenta circles) and air toxics (red triangles) sites. (Traffic volume data were obtained from the New Mexico Department of Transportation.)

The annual average daily traffic for the interstates and major roads in the city of Albuquerque is shown in Figure 1-3. Analysis of traffic data obtained by the New Mexico Department of Transportation at the Wyoming Blvd / North of Montgomery intersection did not show a consistent monthly variation for traffic volume. The highest traffic volumes were measured in April and October, while the lowest was measured in January. On a daily basis, the traffic flow remained relatively constant on weekdays and decreased by 20 to 30 percent on weekends.

The locations and annual emissions of the major point sources of air toxics in Albuquerque are presented in Figure 1-4. The data is from the USEPA's National Emission Inventory (NEI) estimates for the year 2005. The data have not been verified against AQD data. The data represent estimated annual emissions in tons/year.

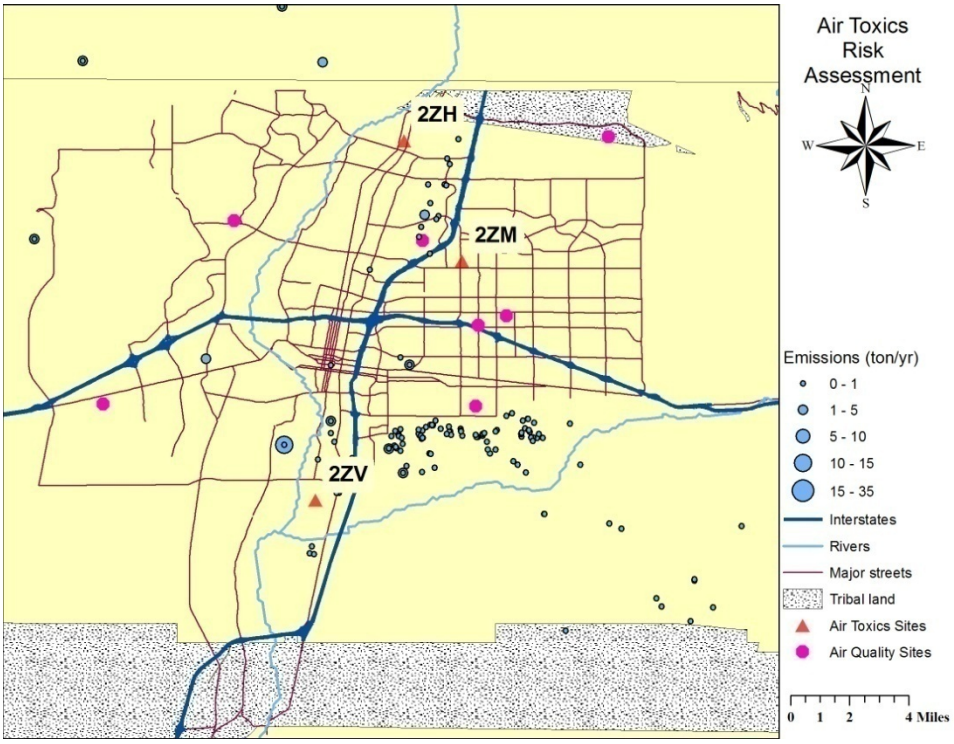

Figure 1-4 Point sources of air toxics emissions and the air location of the quality and air toxics monitoring sites. Emissions are in tons/year. (Emissions data were obtained from the USEPA NEI 2005.)

The implementation of CAAA led to the development of the Integrated Urban Air Toxics Strategy (IUATS) and the Air Toxics Program (ATP), which included the detailed investigation of a subset of 33 HAPs such as aromatic hydrocarbons (e.g. benzene and its derivatives), halocarbons, heavy metals (e.g. As, Hg, Ni), polycyclic aromatic hydrocarbons (PAHs), and diesel particles in order to minimize cumulative public health risks in urban areas.

Table 1-1 Urban air toxics data from Rio Rancho, Bernalillo, and Albuquerque during the PCMP study (The New Mexico Environment Department 2004)

Compound	Mean Conc ($\mu g/m^3$)	URE ($m^3/\mu g$)	RfC (mg/m^3)	Toxicity
Benzene	1.6	7.80E-06	0.03	0.05
Chloroform	1.5		0.098	0.01
Dichlorobenzene	0.6	1.10E-05	0.8	0.00
Ethyl-benzene	0.9		1	0.00
Dichloromethane	3.5	4.7E-07	1	0.00
Toluene	4.1		0.4	0.01
Xylenes	2.1		0.1	0.02
Formaldehyde	2.9	5.5E-09	0.0098	0.30
Acetaldehyde	2.5	2.20E-06	0.009	0.28

The National Air Toxics Assessment (NATA) program, a major component of ATP, has been developed to monitor ambient concentrations, evaluate the impact of sources nationwide, and assess the health risks. Other nationwide programs such as the Urban Air Toxics Monitoring Program (UATMP) launched in 2001 and the Pilot City Monitoring Program (PCMP) in 2001-2002 include year-long measurements of HAPs in up to 30 urban areas. Some data from that study appear in Table 1-1.

1.2 The Air Toxics Risk Assessment Study

The study was divided in three major tasks: (*i*) field measurements; (*ii*) data analysis and modeling; and (*iii*) risk assessment modeling.

The field measurement component included measurements of polycyclic aromatic hydrocarbons and heavy metals in Del Norte (Site Code: 2ZM; AIRs number: 35-001-0023), North Valley (Site Code: 2ZH; AIRs number 350011013)) and South Valley (Site Code: 2ZV; AIRs number: 350010029) on a 1-in-6 day frequency. The schedule and frequency of sampling is presented in Table 1-2. Samples were collected by AEHD staff and analyzed by NMSLD and ERG Inc. In addition, two intensive monitoring periods (IMP) during which hourly measurements of VOCs at Del Norte and frequent profiles of meteorology and air quality at Fiesta Balloon Park were measured, were carried out in February and June 2008. Other supplementary measurements include temperature and relative humidity on fixed locations and on the route of the Sandia Tramway. Details of the monitoring, the instrumentation used for the monitoring of volatile organic compounds, O_3, and meteorological parameters ,as well as supplemental measurements taken during the study are described in the intermediate progress report (Kavouras, DuBois, et al., 2008).

Table 1-2 Sampling period and frequencies of HAPs

Compounds	Period	Location and frequency
PAHs	December 2008 - March 2009	3 sites; 1-in 6 days
Heavy metals	December 2008 - March 2009	3 sites; 1-in 6 days
VOCs (24-hr canister samples)	September 2007-August 2008 and December-March 2008	3 sites; 1-in 6 days
VOCs (1-hr GC-measurements)	February and June 2008	1 site; Every hour

The data analysis and modeling component included the investigation of patterns and trends of air toxics concentration and identification of local and regional sources. This was accomplished by a combination of statistical analysis, transport modeling, and source apportionment modeling. Transport regional modeling was carried out by the computation of the air mass backward trajectories from September 2007 to March 2009 using the NOAA's HYSPLIT (Version 4.9) and CALMET. The sources of particulate matter were apportioned by using 2-D positive matrix factorization (PMF) on $PM_{2.5}$ aerosol speciation data obtained from the USEPA's CSN.

The risk assessment modeling included the identification of risks associated with exposures to air toxics in Albuquerque. Analysis was done using the USEPA HAPEM5.0 to determine the personal exposures to air toxics and the TRIM.Risk to evaluate the hazardous and cancer risks. For this analysis, annual average concentrations were required and thus analysis was done for VOCs detected in all three monitoring sites in more than 50 percent of the valid samples.

2 Data Validation

2.1 Data Completeness

Table 2-1 shows the data completeness for each 24-hr measurement. PAHs and heavy metals were recorded for more than 60 percent of sampling days (with the exception of dibenz[a,h]anthracene). Note that for these compounds, samples were only collected during the December 2008 to March 2009 period. For aromatic hydrocarbons and chlorofluorocarbons more than 50 percent of samples were obtained, while a limited dataset was obtained for the other VOCs. Note that for VOCs, samples were collected from September 2007 to September 2008 and from December 2008 to March 2009.

Table 2-1 Data completeness for each parameter

Compound	Del Norte				North Valley				South Valley			
	Samples expected	Samples Available	Valid Samples	Percent Valid	Samples expected	Samples Available	Valid Samples	Percent Valid	Samples expected	Samples Available	Valid Samples	Percent Valid
PAHs												
Naphthalene	15	15	15	100%	15	15	15	100%	15	14	14	93%
Acenaphthylene	15	15	14	93%	15	15	15	100%	15	14	12	80%
Acenaphthene	15	15	15	100%	15	15	15	100%	15	14	14	93%
Fluorene	15	15	15	100%	15	15	15	100%	15	14	14	93%
Phenanthrene	15	15	15	100%	15	15	15	100%	15	14	14	93%
Anthracene	15	15	15	100%	15	15	15	100%	15	14	14	93%
Retene	15	15	15	100%	15	15	14	93%	15	14	14	93%
9-Fluorenone	15	15	15	100%	15	15	15	100%	15	14	14	93%
Fluoranthene	15	15	15	100%	15	15	15	100%	15	14	14	93%
Pyrene	15	15	15	100%	15	15	15	100%	15	14	14	93%
Benzo[a]anthracene	15	15	9	60%	15	15	10	67%	15	14	11	73%
Chrysene	15	15	15	100%	15	15	15	100%	15	14	14	93%
Cyclopenta[cd]pyrene	15	15	15	100%	15	15	15	100%	15	14	14	93%
Benzo[b]fluoranthene	15	15	15	100%	15	15	15	100%	15	14	14	93%
Benzo[k]fluoranthene	15	15	15	100%	15	15	15	100%	15	14	14	93%
Benzo[e]pyrene	15	15	15	100%	15	15	15	100%	15	14	14	93%
Benzo[a]pyrene	15	15	15	100%	15	15	14	93%	15	14	14	93%
Perylene	15	15	9	60%	15	15	10	67%	15	14	11	73%
Benzo[g,h,i]perylene	15	15	15	100%	15	15	15	100%	15	14	14	93%
Indeno[1,2,3-cd]pyrene	15	15	15	100%	15	15	15	100%	15	14	14	93%
Dibenz[a,h]anthracene	15	15	3	20%	15	15	7	47%	15	14	4	27%

Compound	Del Norte				North Valley				South Valley			
	Samples expected	Samples Available	Valid Samples	Percent Valid	Samples expected	Samples Available	Valid Samples	Percent Valid	Samples expected	Samples Available	Valid Samples	Percent Valid
Coronene	15	15	15	100%	15	15	15	100%	15	14	14	93%
Heavy metals												
Antimony	19	17	17	89%	19	19	19	100%	19	19	19	100%
Arsenic	19	17	17	89%	19	19	19	100%	19	19	19	100%
Beryllium	19	17	17	89%	19	19	19	100%	19	19	19	100%
Cadmium	19	17	17	89%	19	19	19	100%	19	19	18	95%
Chromium	19	17	17	89%	19	19	19	100%	19	19	19	100%
Cobalt	19	17	17	89%	19	19	19	100%	19	19	19	100%
Lead	19	17	17	89%	19	19	19	100%	19	19	19	100%
Manganese	19	17	17	89%	19	19	19	100%	19	19	19	100%
Mercury	19	17	13	68%	19	19	15	79%	19	19	16	84%
Nickel	19	17	17	89%	19	19	19	100%	19	19	19	100%
Selenium	19	17	17	89%	19	19	19	100%	19	19	19	100%
VOCs												
Acrylonitrile	80	1	1	1%	79	2	1	1%	79	1	1	1%
Benzene	80	70	63	79%	79	67	66	84%	79	60	54	68%
Bromomethane	80	0	0	0%	79	1	0	0%	79	0	0	0%
1,3-Butadiene	80	55	51	64%	79	49	48	61%	79	35	35	44%
Carbon tetrachloride	80	39	38	48%	79	49	48	61%	79	25	25	32%
Chlorobenzene	80	0	0	0%	79	1	0	0%	79	0	0	0%
Chloroethane	80	0	0	0%	79	1	0	0%	79	0	0	0%
Chloroform	80	0	0	0%	79	1	0	0%	79	2	2	3%
Chloromethane	80	46	42	53%	79	40	39	49%	79	37	36	46%
1,2-Dibromoethane	80	0	0	0%	79	1	0	0%	79	0	0	0%
1,2-Dichlorobenzene	80	0	0	0%	79	1	0	0%	79	1	1	1%
1,3-Dichlorobenzene	80	0	0	0%	79	1	0	0%	79	0	0	0%
1,4-Dichlorobenzene	80	1	1	1%	79	1	0	0%	79	3	3	4%
1,1-Dichloroethane	80	0	0	0%	79	1	0	0%	79	0	0	0%
1,2-Dichloroethane	80	0	0	0%	79	1	0	0%	79	0	0	0%
1,1-Dichloroethene	80	0	0	0%	79	1	0	0%	79	0	0	0%
cis-1,2-Dichloroethene	80	0	0	0%	79	1	0	0%	79	0	0	0%
1,2-Dichloropropane	80	0	0	0%	79	3	2	3%	79	1	1	1%
cis-1,3-Dichloropropene	80	0	0	0%	79	1	0	0%	79	0	0	0%
Trans-1,3-Dichloropropene	80	0	0	0%	79	1	0	0%	79	0	0	0%
Ethylbenzene	80	55	53	66%	79	56	55	70%	79	47	46	58%

Compound	Del Norte				North Valley				South Valley			
	Samples expected	Samples Available	Valid Samples	Percent Valid	Samples expected	Samples Available	Valid Samples	Percent Valid	Samples expected	Samples Available	Valid Samples	Percent Valid
Trichlorofluoromethane	80	70	64	80%	79	65	64	81%	79	56	55	70%
Dichlorodifluoromethane	80	72	66	83%	79	67	66	84%	79	58	56	71%
Trichlorotrifluoroethane	80	46	44	55%	79	59	58	73%	79	38	38	48%
Dichlorotetrafluoroethane	80	0	0	0%	79	1	0	0%	79	1	1	1%
Hexachloro-1,3-butadiene	80	1	1	1%	79	2	1	1%	79	0	0	0%
Methylene_Chloride	80	72	57	71%	79	69	59	75%	79	66	63	80%
Styrene	80	1	0	0%	79	1	0	0%	79	2	2	3%
1,1,2,2-Tetrachloroethane	80	0	0	0%	79	1	0	0%	79	0	0	0%
Tetrachloroethene	80	6	6	8%	79	3	2	3%	79	4	4	5%
Toluene	80	71	65	81%	79	63	62	78%	79	57	55	70%
1,2,4-Trichlorobenzene	80	1	1	1%	79	1	0	0%	79	1	1	1%
1,1,1-Trichloroethane	80	0	0	0%	79	1	0	0%	79	0	0	0%
1,1,2-Trichloroethane	80	0	0	0%	79	1	0	0%	79	0	0	0%
Trichloroethene	80	1	1	1%	79	1	0	0%	79	1	1	1%
1,2,4-Trimethylbenzene	80	48	47	59%	79	48	47	59%	79	39	39	49%
1,3,5-Trimethylbenzene	80	9	9	11%	79	8	7	9%	79	18	18	23%
Vinyl chloride	80	0	0	0%	79	1	0	0%	79	0	0	0%
m/p-Xylenes	80	68	61	76%	79	62	59	75%	79	55	54	68%
o-Xylene	80	58	55	69%	79	58	55	70%	79	49	47	59%
Organic and Elemental Carbon												
OC	67	67	67	100%	67	61	61	91%	67	62	62	93%
EC	67	67	67	100%	67	61	61	91%	67	62	62	93%
Total Carbon	67	67	67	100%	67	61	61	91%	67	62	62	93%

Table 2-2 shows the days for which there were more than fifteen (15) valid hourly measurements for VOCs at the Del Norte site. Sometimes fewer than fifteen valid measurements were collected because of repeated calibration and blank tests, especially during the first IMP.

Table 2-2 Data completeness for online VOCs at the Del Norte site [(x) indicates the days for which there were more than 15 valid hourly measurements]

Date	IMP1	Date	IMP2
2/12/2008		6/17/2008	x
2/13/2008	x	6/18/2008	x
2/14/2008	x	6/19/2008	x
2/15/2008	x	6/20/2008	x
2/16/2008	x	6/21/2008	x
2/17/2008		6/22/2008	x
2/18/2008	x	6/23/2008	x
2/19/2008	x	6/24/2008	x
2/20/2008		6/25/2008	x
		6/26/2008	x
		6/27/2008	x
		6/28/2008	x
		6/29/2008	x
		6/30/2008	

The percentage of valid measurements for which the measured concentrations were higher than the method detection limit for each compound is presented in Table 2-3. Air toxics with less than 50 percent valid and measureable samples were excluded from the analysis, because the measured concentrations were associated with a high degree of uncertainty.

Table 2-3 Percentage of valid samples with measured concentrations above the method detection limit (Italic letters indicate air toxics with less than 50% valid samples that were excluded from the data analysis)

Compound	Del Norte	North Valley	South Valley
PAHs			
Naphthalene	100%	100%	100%
Acenaphthylene	100%	100%	100%
Acenaphthene	100%	100%	100%
Fluorene	100%	100%	100%
Phenanthrene	100%	100%	100%
Anthracene	100%	93%	100%
Retene	100%	100%	100%
9-Fluorenone	100%	100%	100%
Fluoranthene	100%	100%	100%
Pyrene	100%	100%	100%
Benzo[a]anthracene	67%	60%	64%
Chrysene	100%	100%	100%
Cyclopenta[cd]pyrene	73%	87%	79%
Benzo[b]fluoranthene	100%	93%	100%

Compound	Del Norte	North Valley	South Valley
Benzo[k]fluoranthene	67%	73%	64%
Benzo[e]pyrene	93%	67%	79%
Benzo[a]pyrene	73%	79%	71%
Perylene	56%	90%	55%
Benzo[g,h,i]perylene	100%	100%	100%
Indeno[1,2,3-cd]pyrene	100%	87%	100%
Dibenz[a,h]anthracene	*0%*	*86%*	*25%*
Coronene	80%	60%	79%
Heavy metals			
Antimony	100%	100%	100%
Arsenic	100%	100%	100%
Beryllium	71%	79%	100%
Cadmium	100%	100%	100%
Chromium	100%	100%	100%
Cobalt	100%	100%	100%
Lead	100%	100%	100%
Manganese	100%	100%	100%
Mercury	*46%*	*73%*	*63%*
Nickel	100%	100%	100%
Selenium	100%	100%	100%
VOCs			
Acrylonitrile	*0%*	*0%*	*0%*
Benzene	86%	89%	72%
Bromomethane			
1,3-Butadiene	*43%*	*23%*	*71%*
Carbon tetrachloride	*-3%*	*0%*	*0%*
Chlorobenzene			
Chloroethane			
Chloroform			*100%*
Chloromethane	100%	100%	100%
1,2-Dibromoethane			
1,2-Dichlorobenzene			*100%*
1,3-Dichlorobenzene			
1,4-Dichlorobenzene	*100%*		*100%*
1,1-Dichloroethane			
1,2-Dichloroethane			
1,1-Dichloroethene			
cis-1,2-Dichloroethene			
1,2-Dichloropropane		*100%*	*100%*
cis-1,3-Dichloropropene			
Trans-1,3-Dichloropropene			

Compound	Del Norte	North Valley	South Valley
Ethylbenzene	*32%*	*38%*	*52%*
Trichlorofluoromethane	78%	94%	69%
Dichlorodifluoromethane	95%	97%	91%
Trichlorotrifluoroethane	*0%*	*2%*	*8%*
Dichlorotetrafluoroethane			*0%*
Hexachloro-1,3-butadiene	*100%*	*100%*	
Methylene Chloride	56%	51%	51%
Styrene			*50%*
1,1,2,2-Tetrachloroethane			
Tetrachloroethene	*17%*	*0%*	*25%*
Toluene	97%	97%	98%
1,2,4-Trichlorobenzene	*100%*		*0%*
1,1,1-Trichloroethane			
1,1,2-Trichloroethane			
Trichloroethene	*0%*		*0%*
1,2,4-Trimethylbenzene	*30%*	*38%*	*64%*
1,3,5-Trimethylbenzene	*100%*	*100%*	*100%*
Vinyl chloride			
m/p-Xylenes	59%	63%	59%
o-Xylene	98%	96%	96%
Organic and Elemental Carbon			
OC	100%	100%	100%
EC	100%	98%	100%
Total Carbon	100%	100%	100%

3 Data Characterization

This section contains the analysis of daily concentrations and trends of PAHs, heavy metals, VOCs, OC, and EC measured at the three sampling sites, as well as hourly VOCs levels measured at Del Norte site. The concentrations of air toxics were also compared to those measured at 50 sites of the NATTS/UATP programs and 2002 NATA estimates. In addition, the results of the source characterization of fine particulate matter and PAHs using PMF modeling and concentration diagnostic ratios, respectively, are presented and compared to obtain qualitative and quantitative information on the sources of air toxics in Albuquerque.

3.1 Concentration Levels

3.1.1 PAHs

A series of twenty parent PAHs (from naphthalene to coronene), retene (1-methyl-7-isopropyl-phenanthrane), and 9-fluorenone were identified at the three monitoring sites. The concentration ranges (of individual PAHs for the three monitoring sites for the January-March 2009 period are given in Figure 3-1 -through Figure 3-20. The boxes represent the 25%, 50% (median), and 75% percentiles, and whiskers show the 5% and 95% percentiles and "x" show the minimum and maximum concentrations. The open squares show the mean value. Prioritized chronic dose-response values (RfC (for non-cancer) and URE (for 1-in-million cancer)) for naphthalene, benzo(a)anthracene, benzo(b)fluoranthene, benzo(k)fluoranthene, and benzo(a)pyrene were also included in the plots . For these compounds, ambient measured concentrations were significantly lower than the RfC and URE (1-in-million) values.

The collected total (gas + particulate) PAHs identified in the analyzed samples had total concentrations from 40.04 to 181.11 ng/m^3 at Del Norte, from 34.90 to 323.85 ng/m^3 at North Valley, and from 18.04 to 228.64 ng/m^3 at South Valley. Naphthalene was the dominant PAH, representing more than 70 percent of total PAHs concentrations. The lowest concentrations were measured for coronene.

Figure 3-22 through Figure 3-35 show the daily concentrations of PAHs at Del Norte, North Valley, and South Valley. With the exception of naphthalene, the highest concentrations were measured in January, followed by a decrease in February and March.

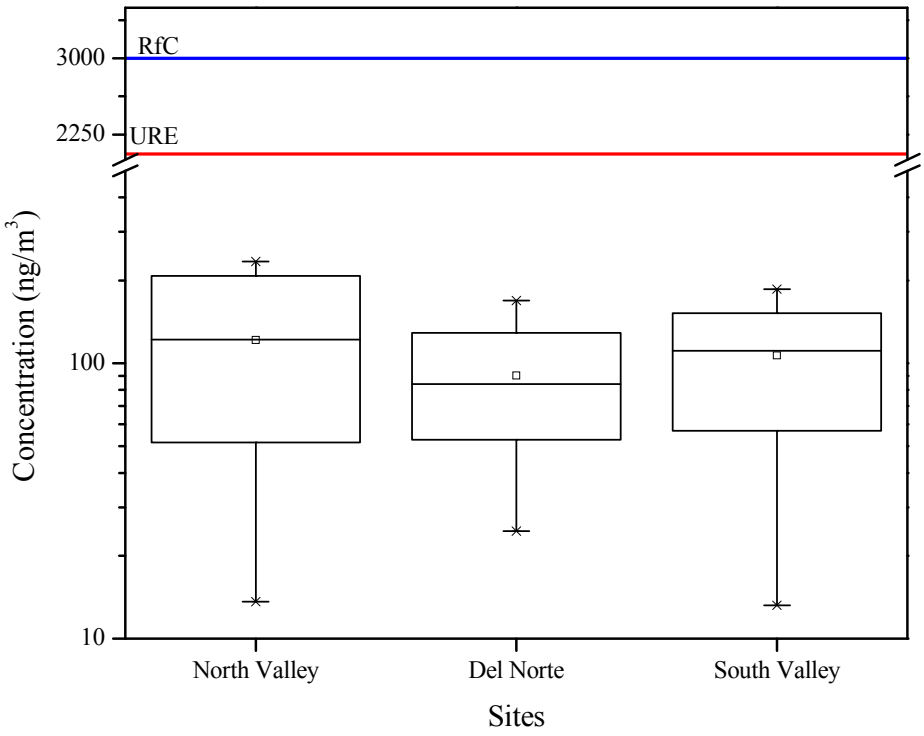

Figure 3-1 Concentrations of naphthalene at the three locations and the RfC (non-cancer chronic inhalation; blue line) and URE (cancer chronic inhalation; red line)

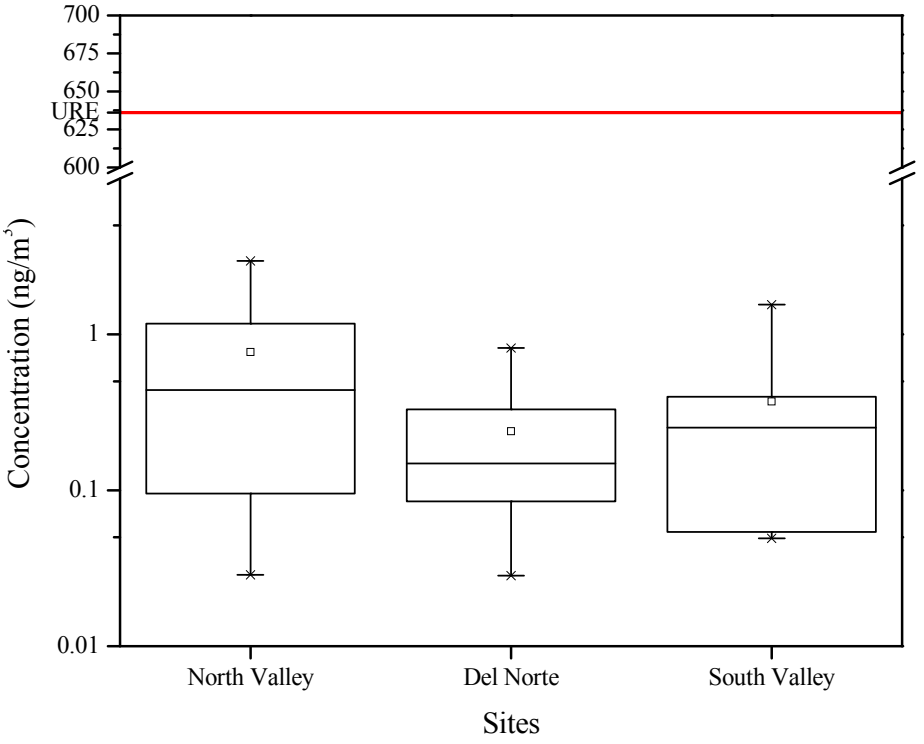

Figure 3-2 Concentrations of benzo(a)anthracene at the three locations and the URE (cancer chronic inhalation; red line)

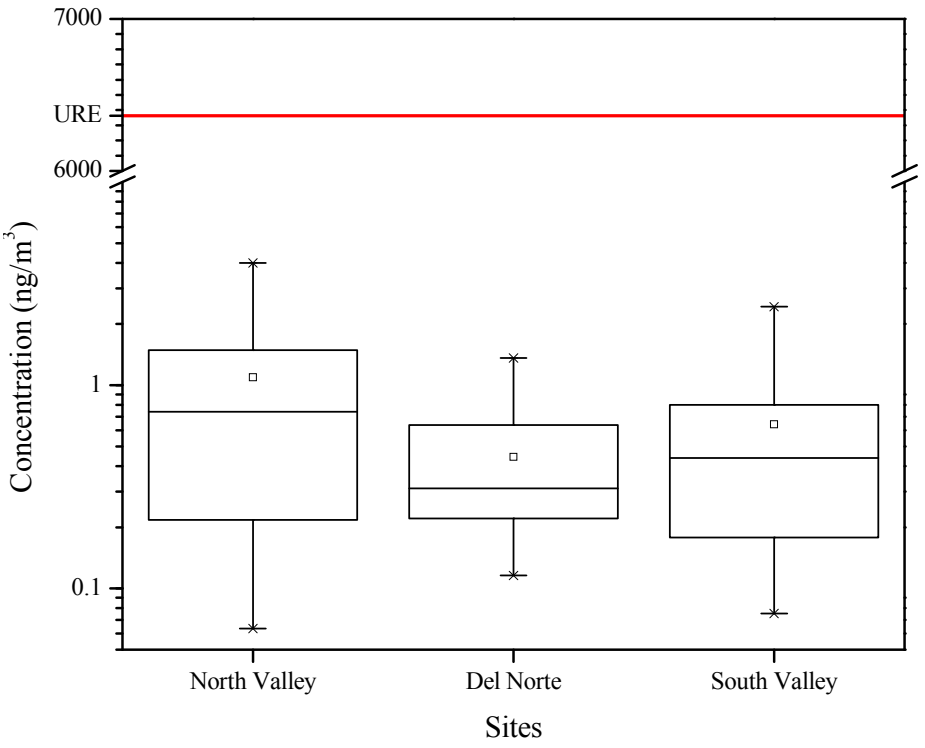

Figure 3-3 Concentrations of chrysene at the three locations and the URE (cancer chronic inhalation; red line)

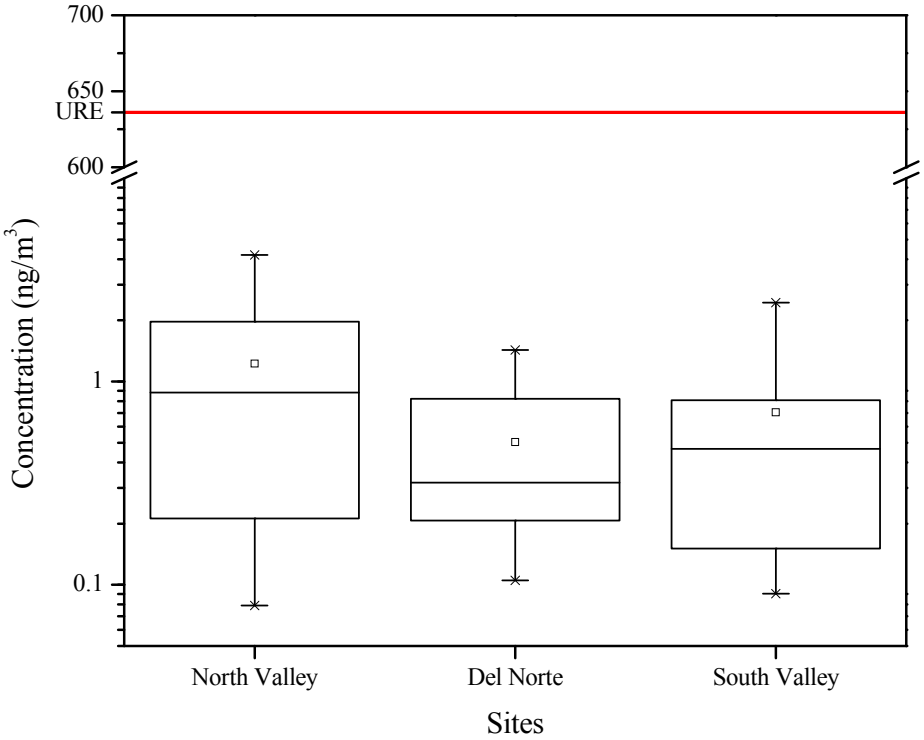

Figure 3-4 Concentrations of benzo(b)fluoranthene at the three locations and the URE (cancer chronic inhalation; red line)

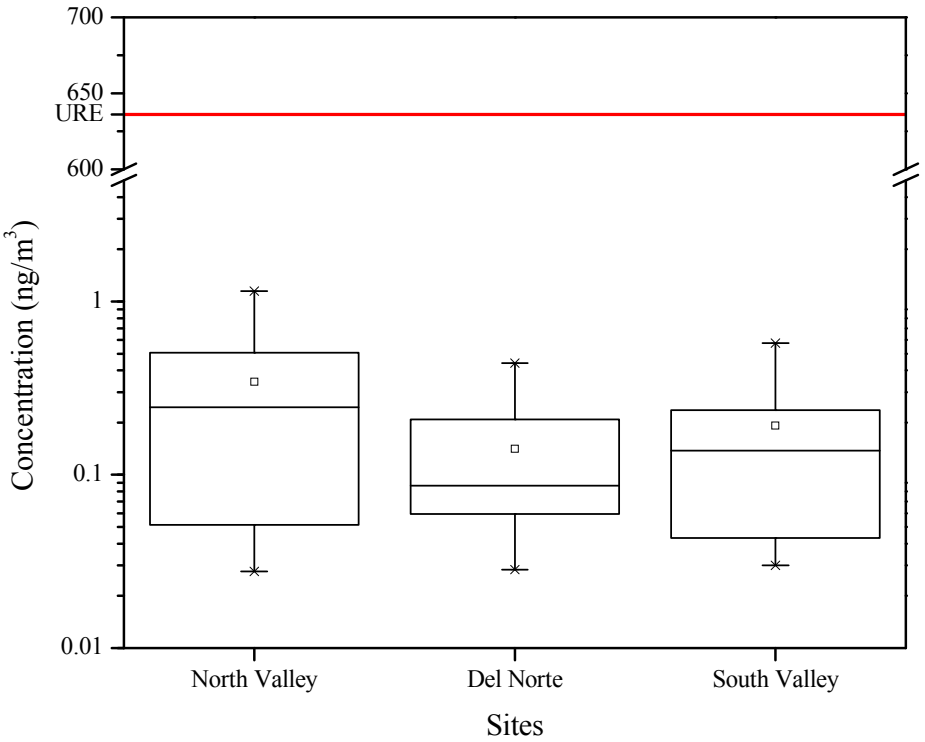

Figure 3-5 Concentrations of benzo(k)fluoranthene at the three locations and the URE (cancer chronic inhalation; red line)

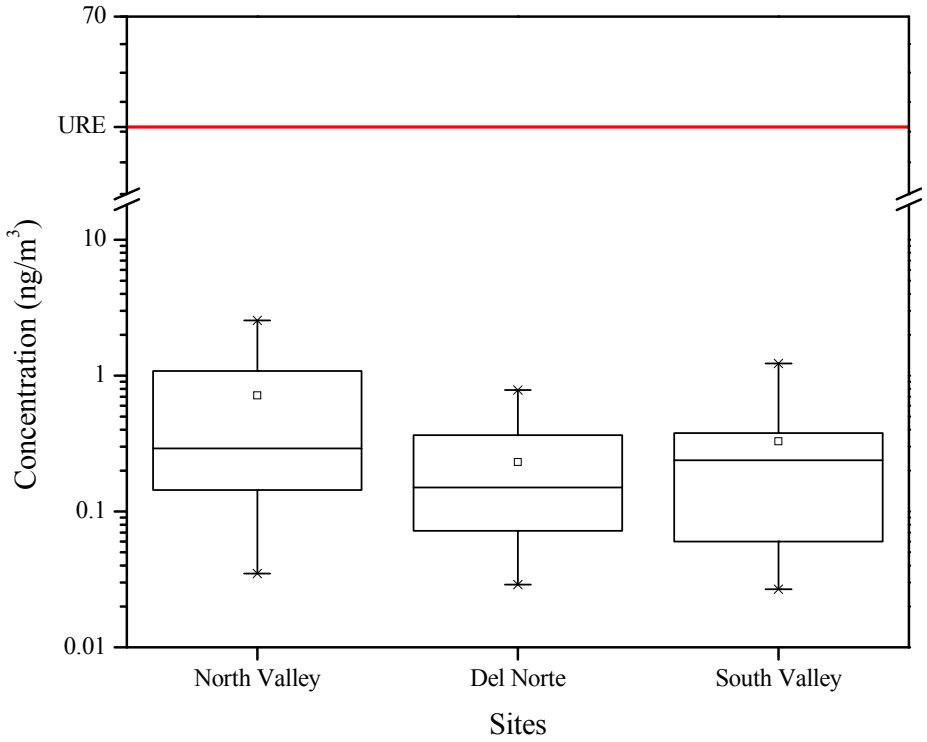

Figure 3-6 Concentrations of benzo(a)pyrene at the three locations and the URE (cancer chronic inhalation; red line)

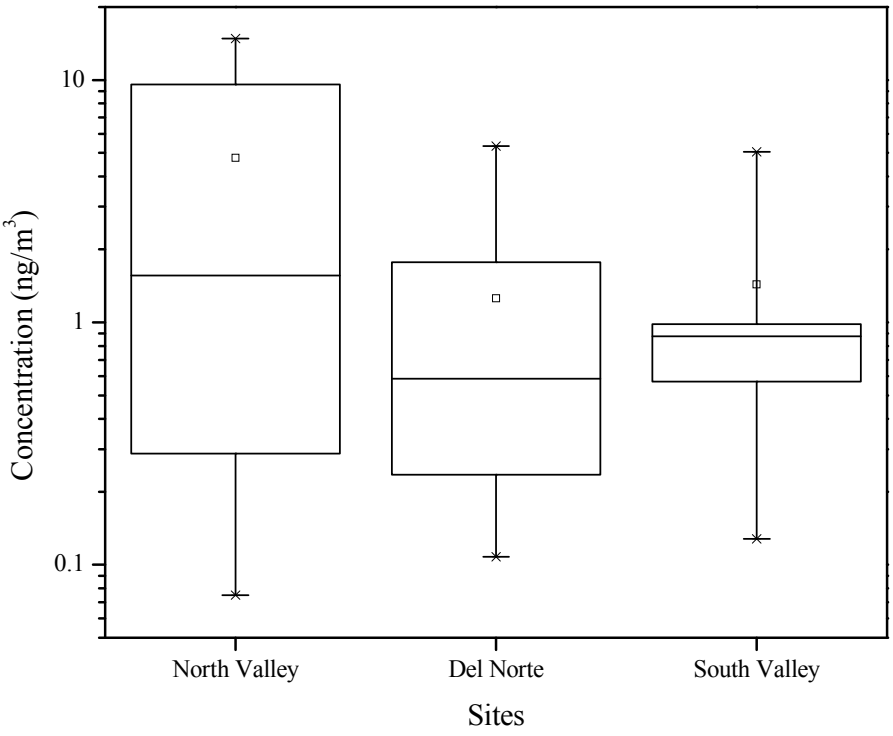

Figure 3-7 Concentrations of acenaphthylene at the three locations

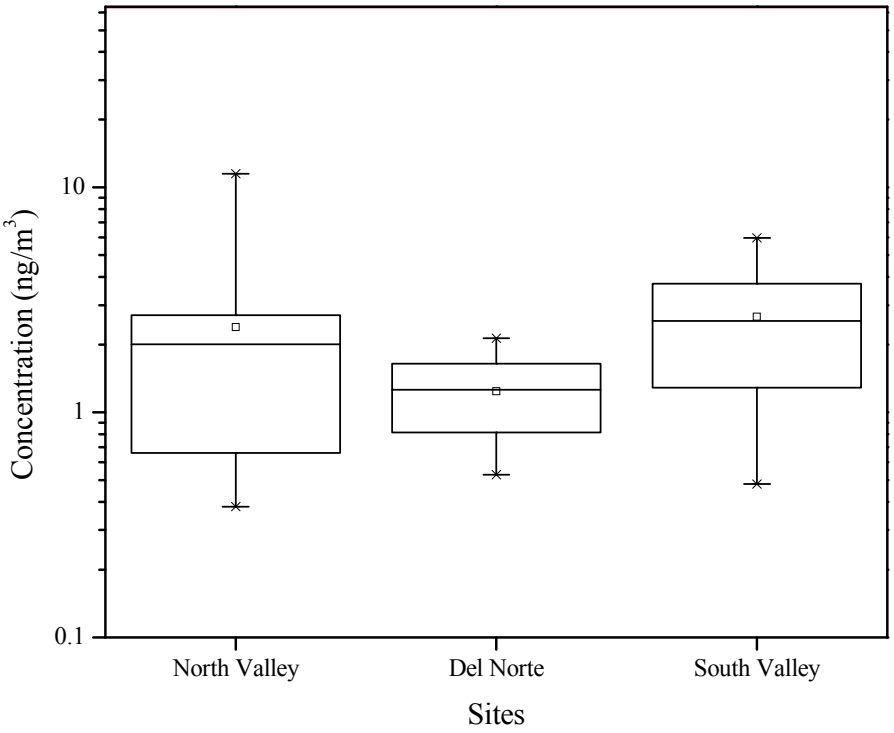

Figure 3-8 Concentrations of acenaphthene at the three locations

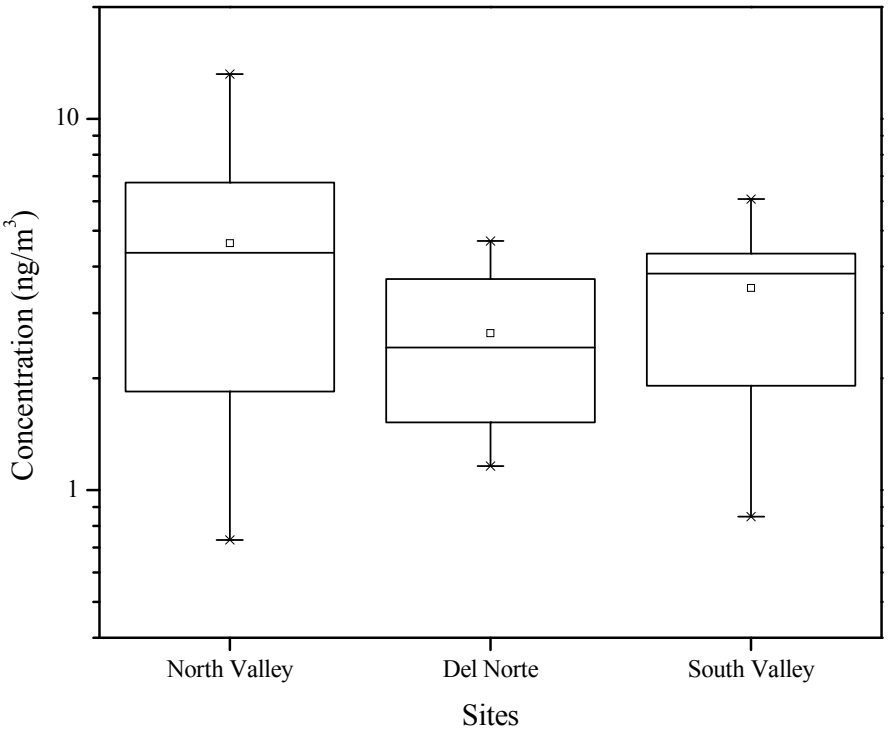

Figure 3-9 Concentrations of fluorene at the three locations

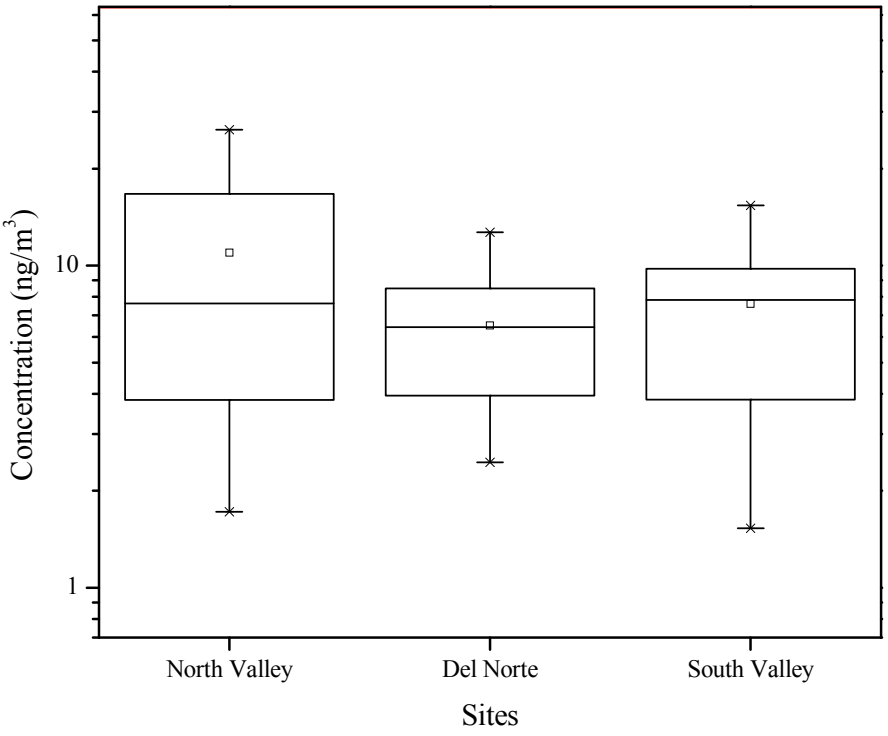

Figure 3-10 Concentrations of phenanthrene at the three locations

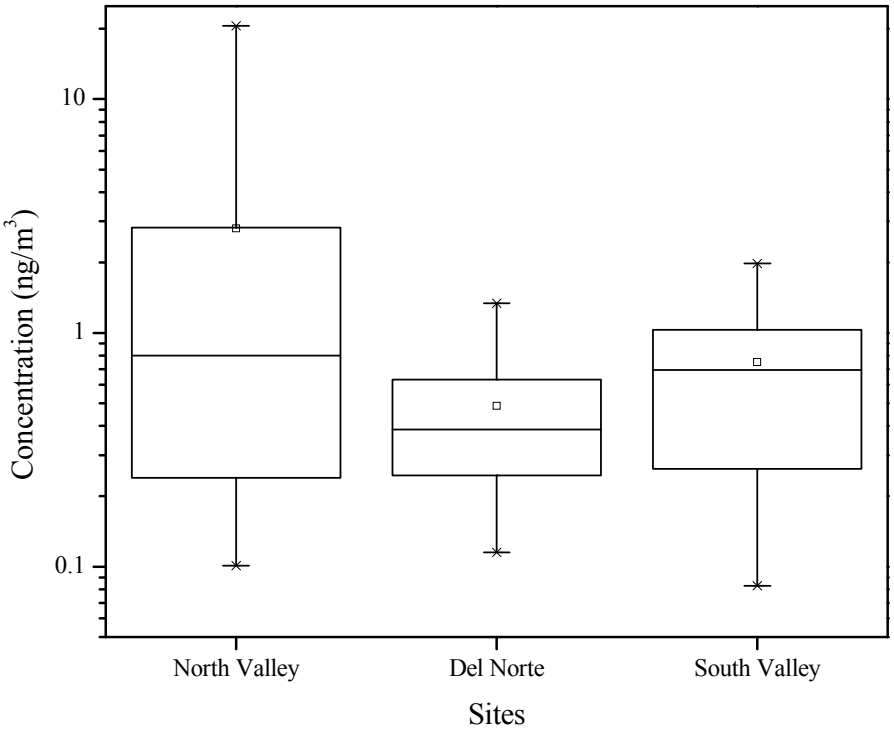

Figure 3-11 Concentrations of anthracene at the three locations

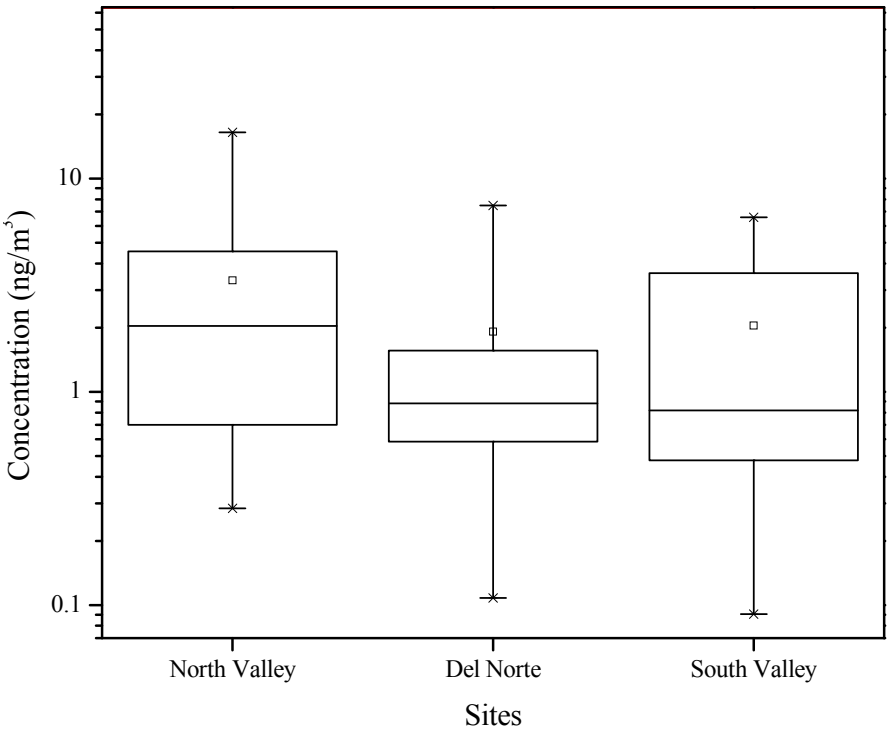

Figure 3-12 Concentrations of retene at the three locations

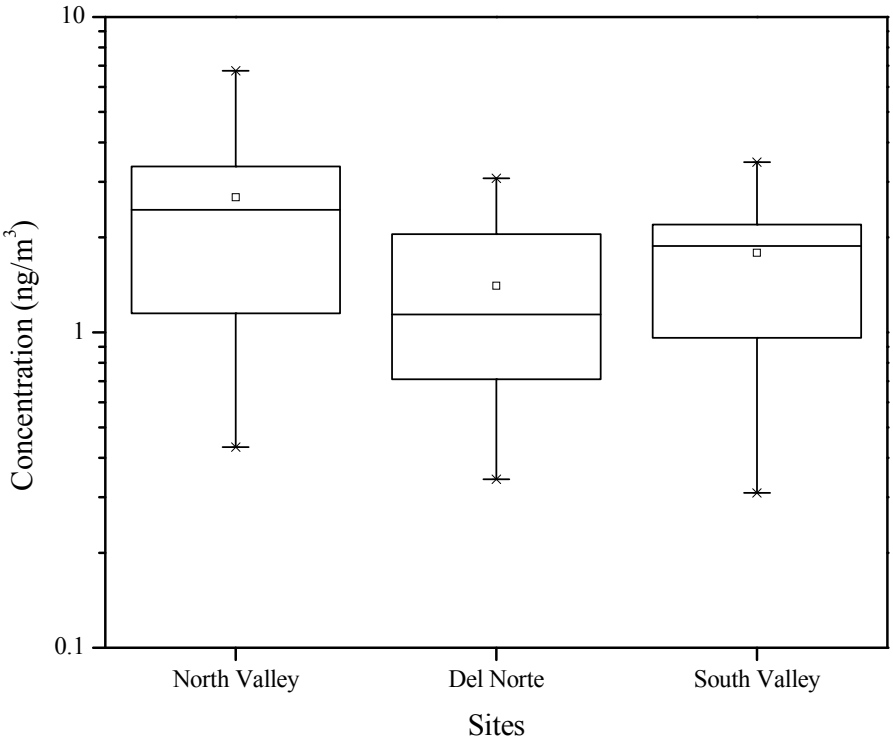

Figure 3-13 Concentrations of 9-fluorenone at the three locations

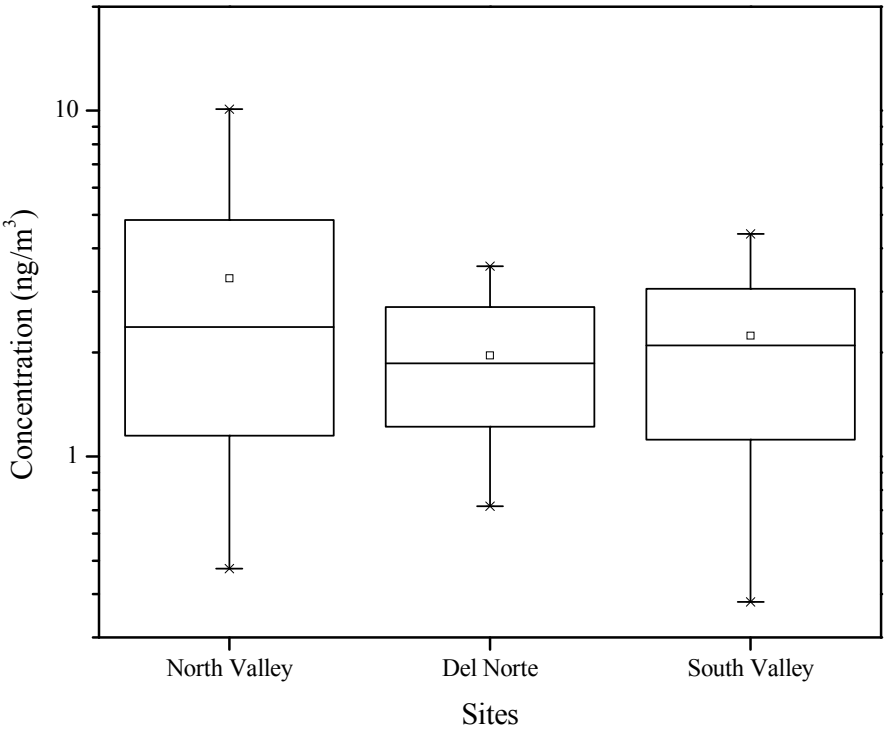

Figure 3-14 Concentrations of fluoranthene at the three locations

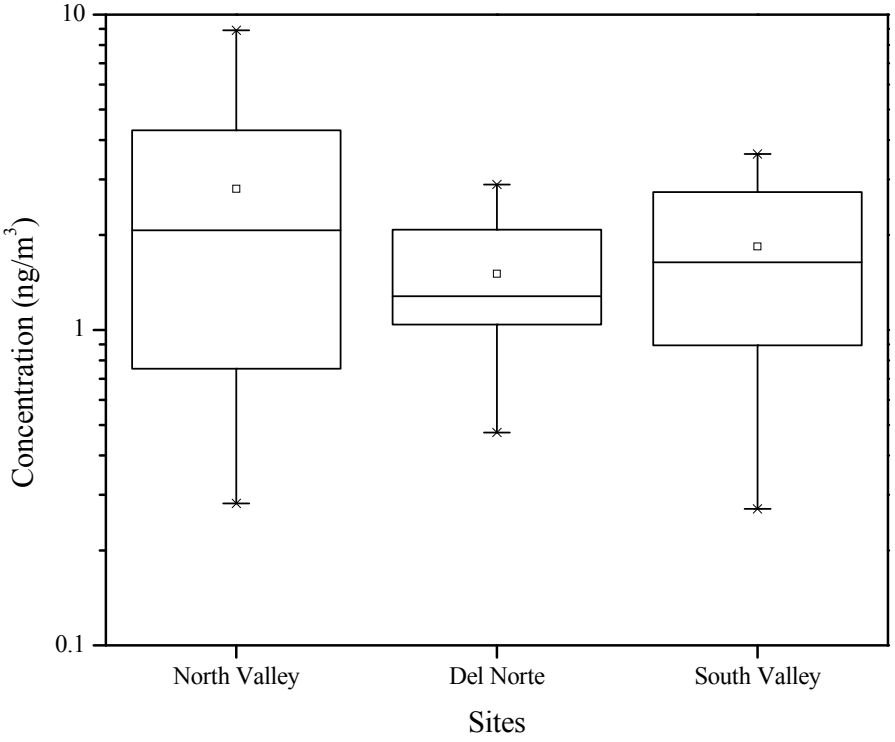

Figure 3-15 Concentrations of pyrene at the three locations

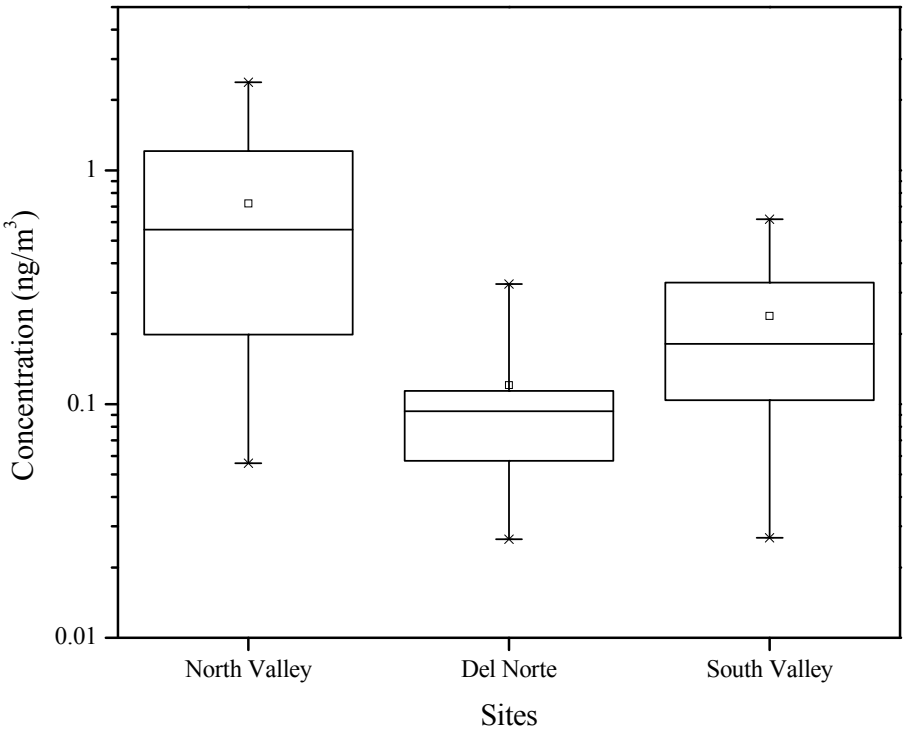

Figure 3-16 Concentrations of cyclopenta[cd]pyrene at the three locations

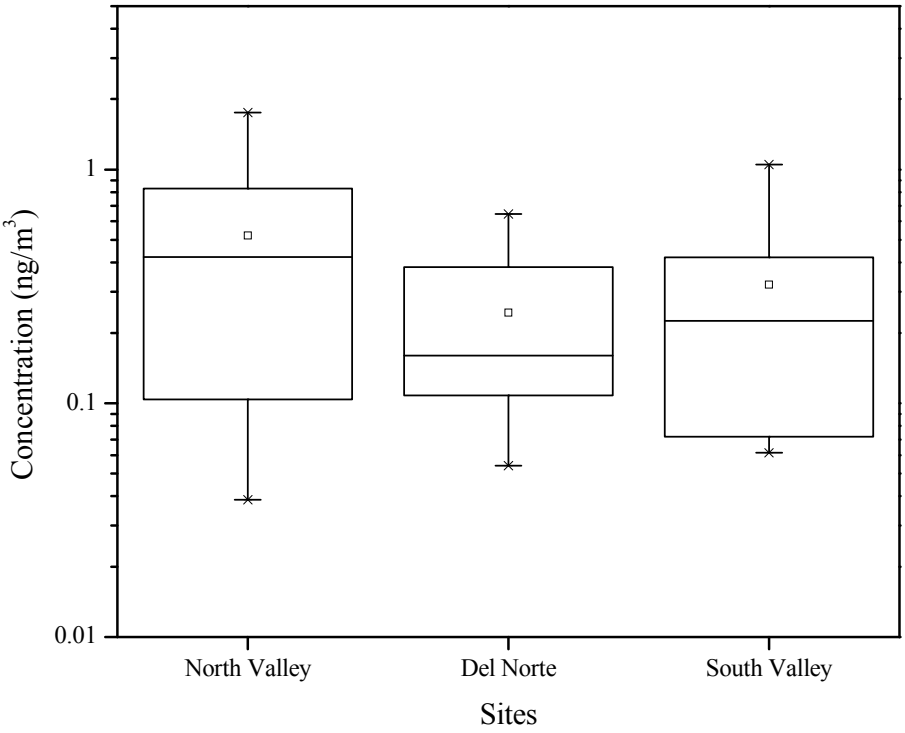

Figure 3-17 Concentrations of benzo(e)pyrene at the three locations

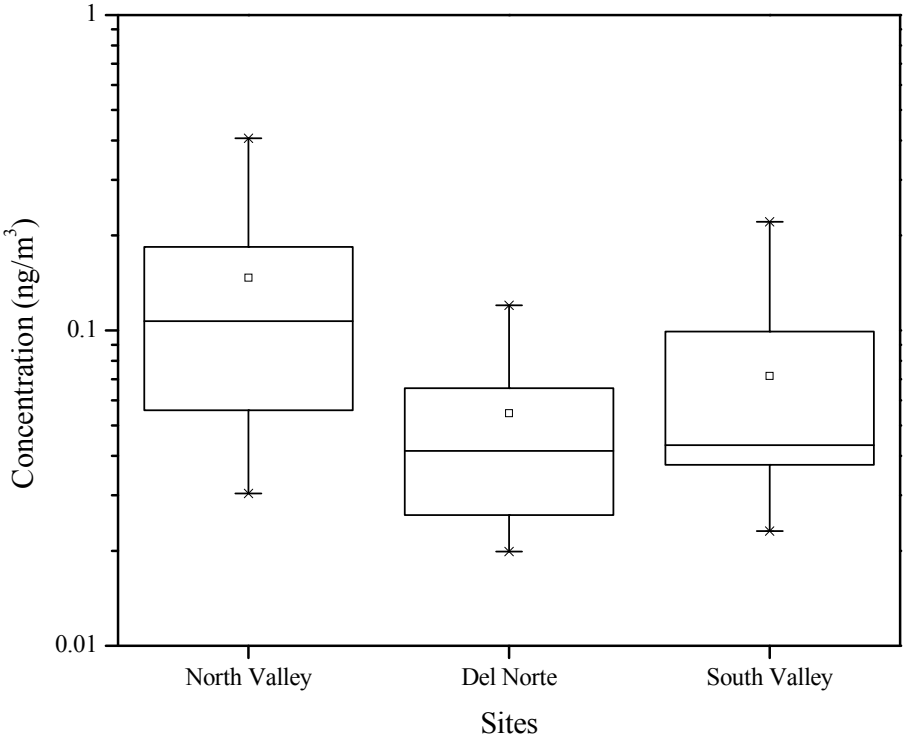

Figure 3-18 Concentrations of benzo(ghi)perylene at the three locations

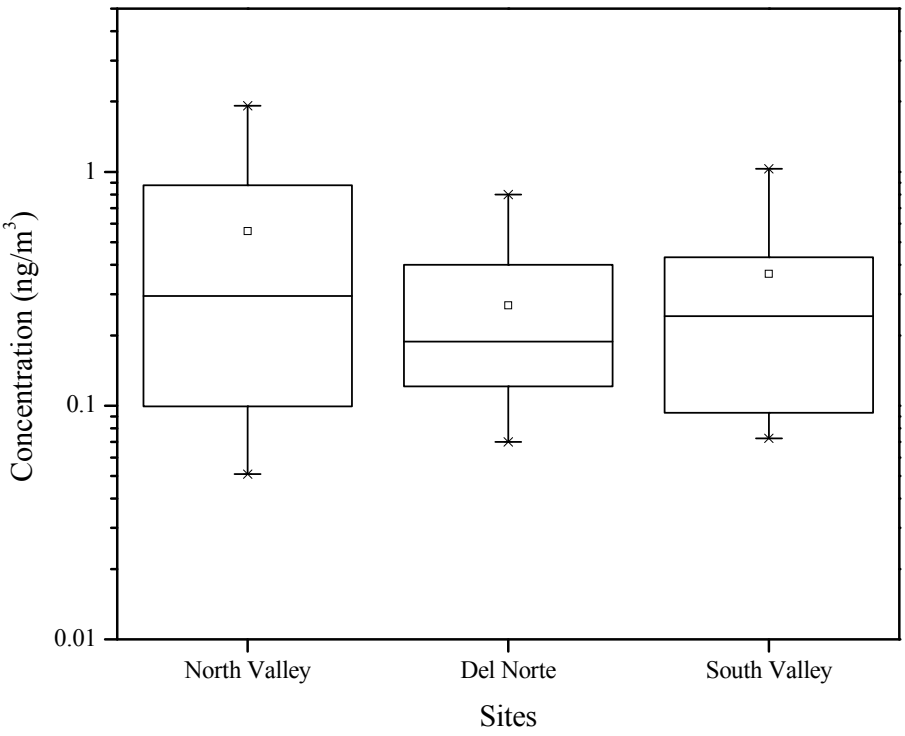

Figure 3-19 Concentrations of indeno[1,2,3-cd]perylene at the three locations

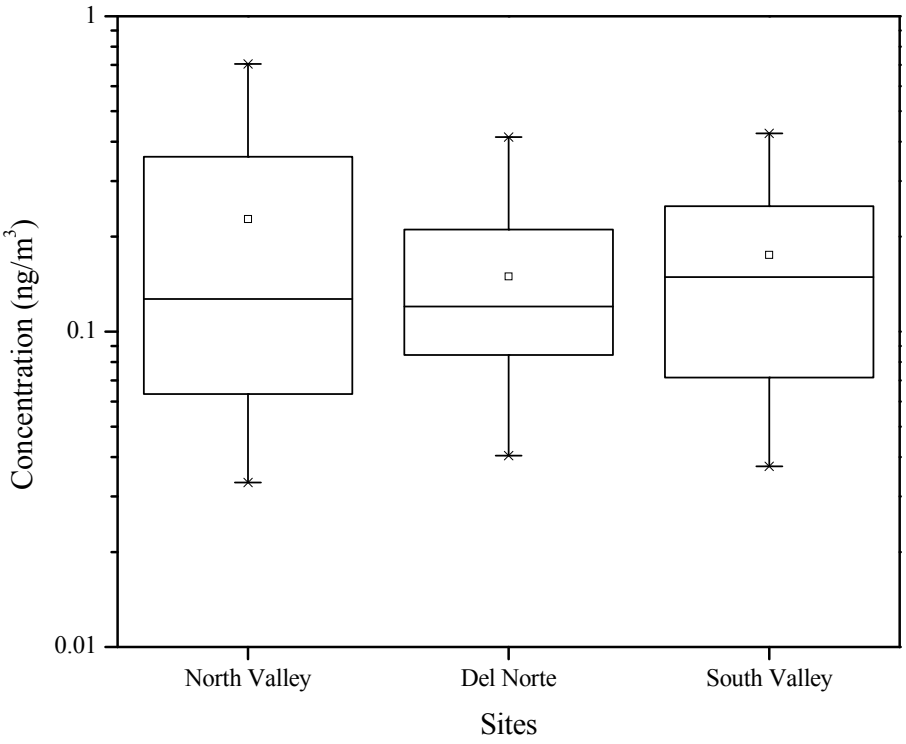

Figure 3-20 Concentrations of coronene at the three locations

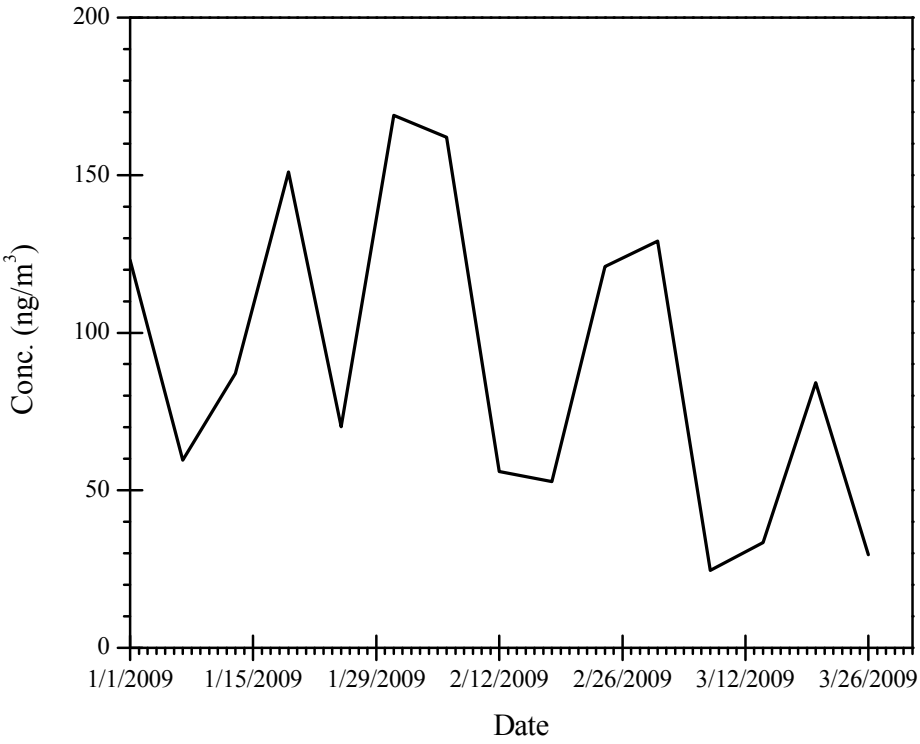

Figure 3-21 Variation of naphthalene at Del Norte

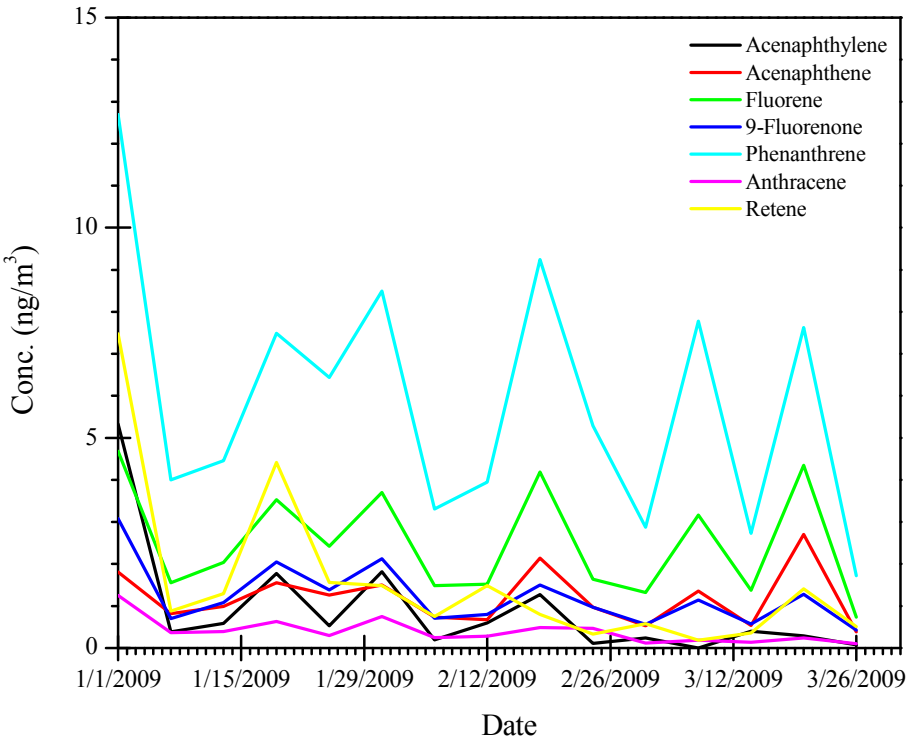

Figure 3-22 Variation of 3-aromatic-ring PAHs at Del Norte

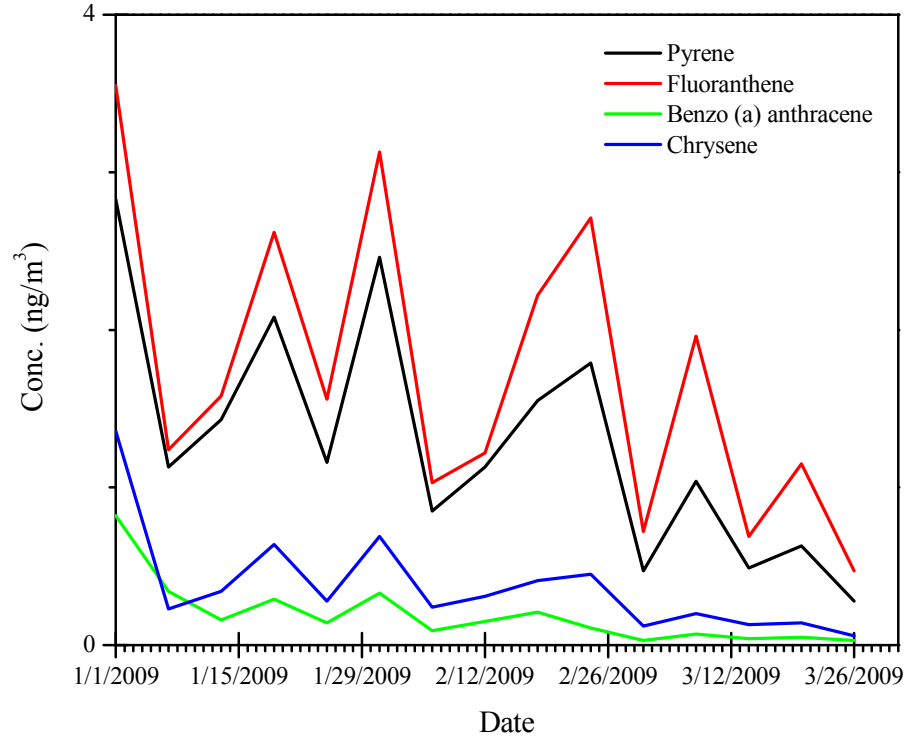

Figure 3-23 Variation of 4-aromatic-ring PAHs at Del Norte

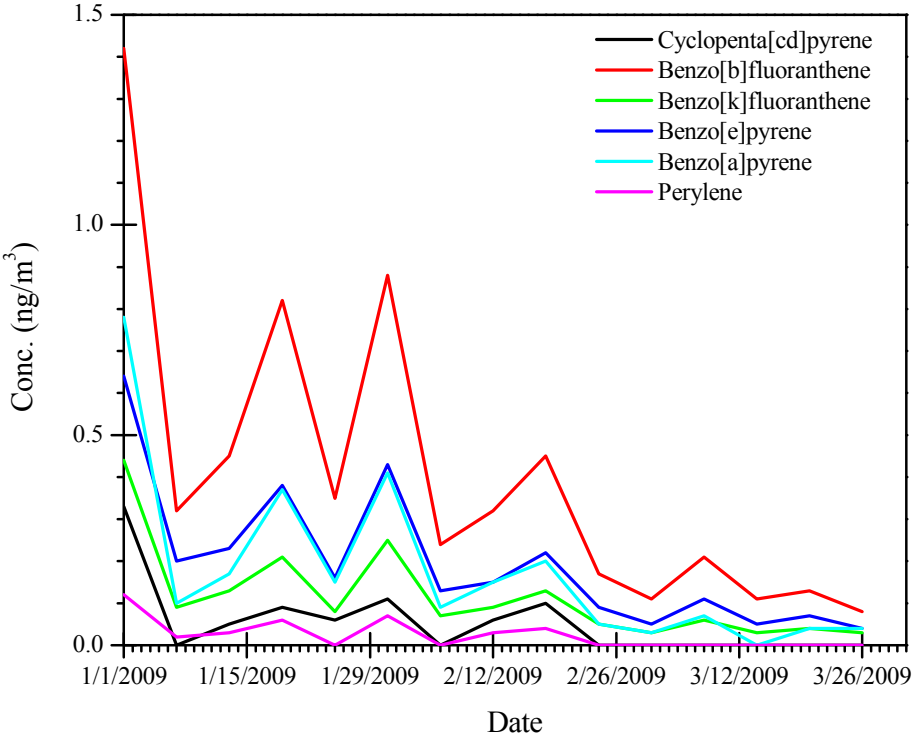

Figure 3-24 Variation of 5-aromatic-ring PAHs at Del Norte

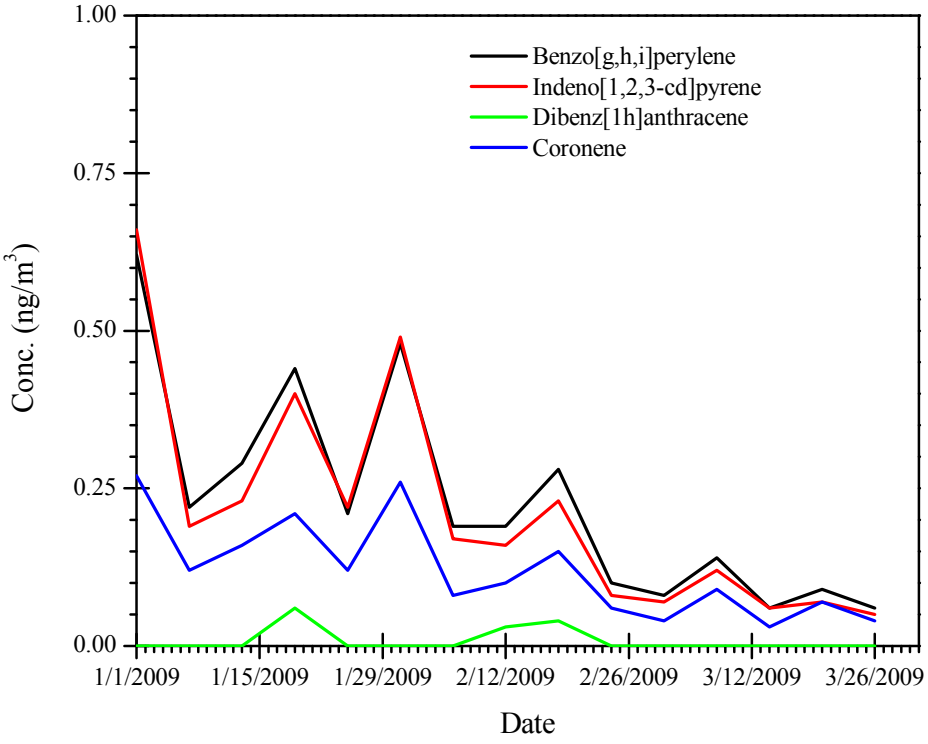

Figure 3-25 Variation of 6-aromatic-ring PAHs at Del Norte

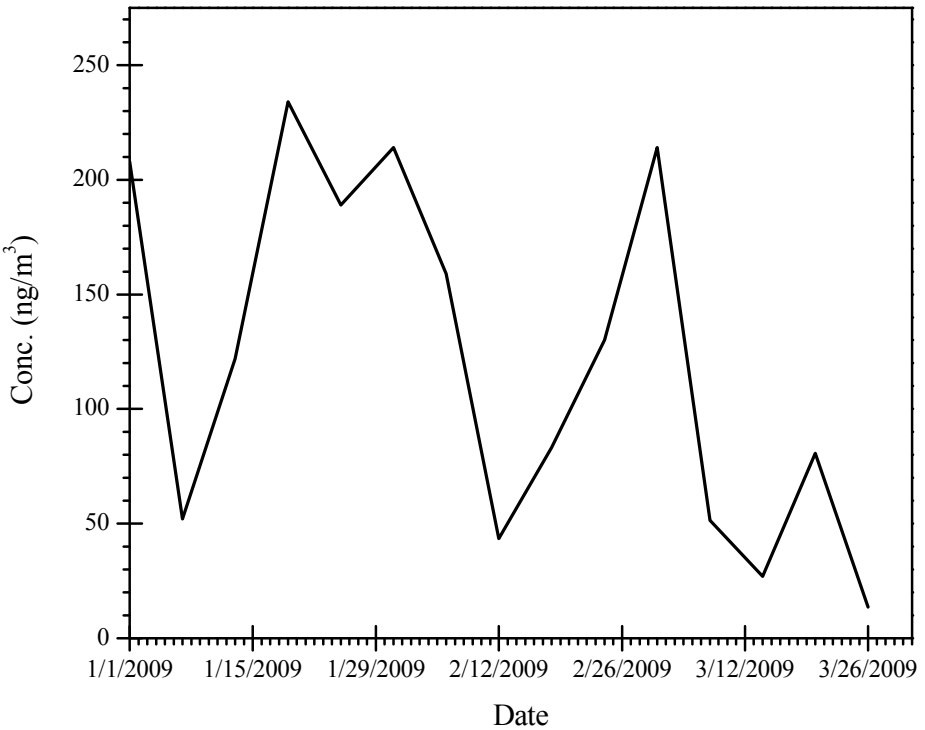

Figure 3-26 Variation of naphthalene at North Valley

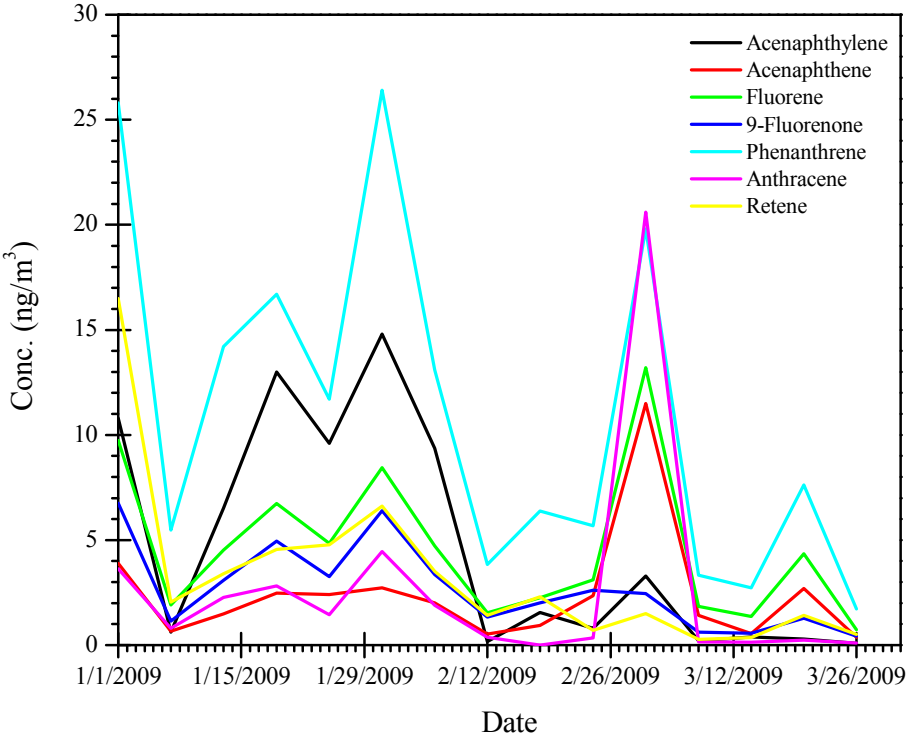

Figure 3-27 Variation of 3-aromatic-ring PAHs at North Valley

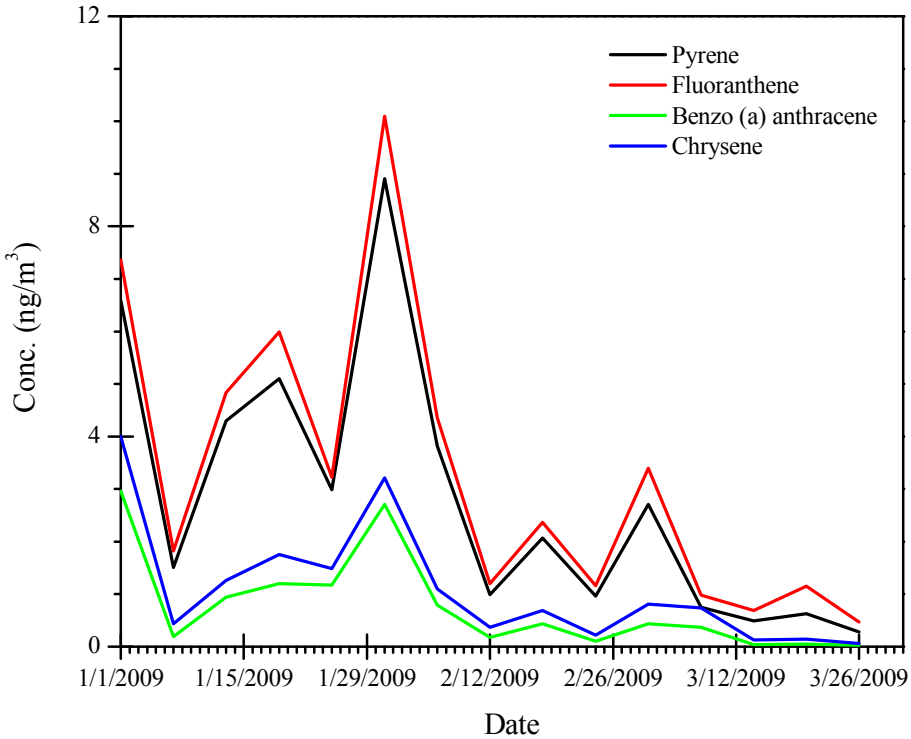

Figure 3-28 Variation of 4-aromatic-ring PAHs at North Valley

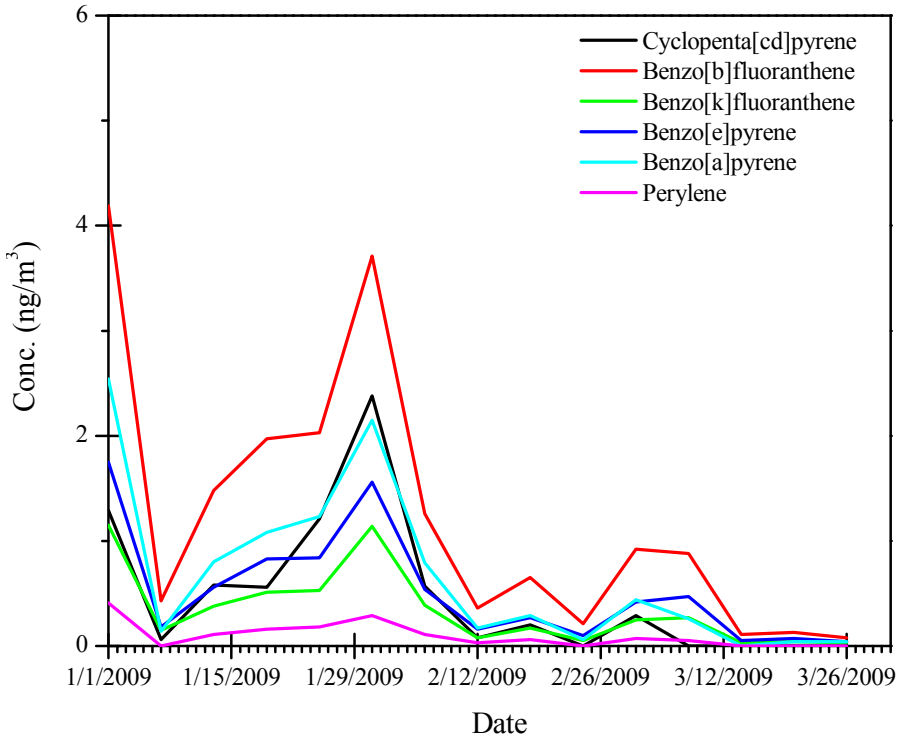

Figure 3-29 Variation of 5-aromatic-ring PAHs at North Valley

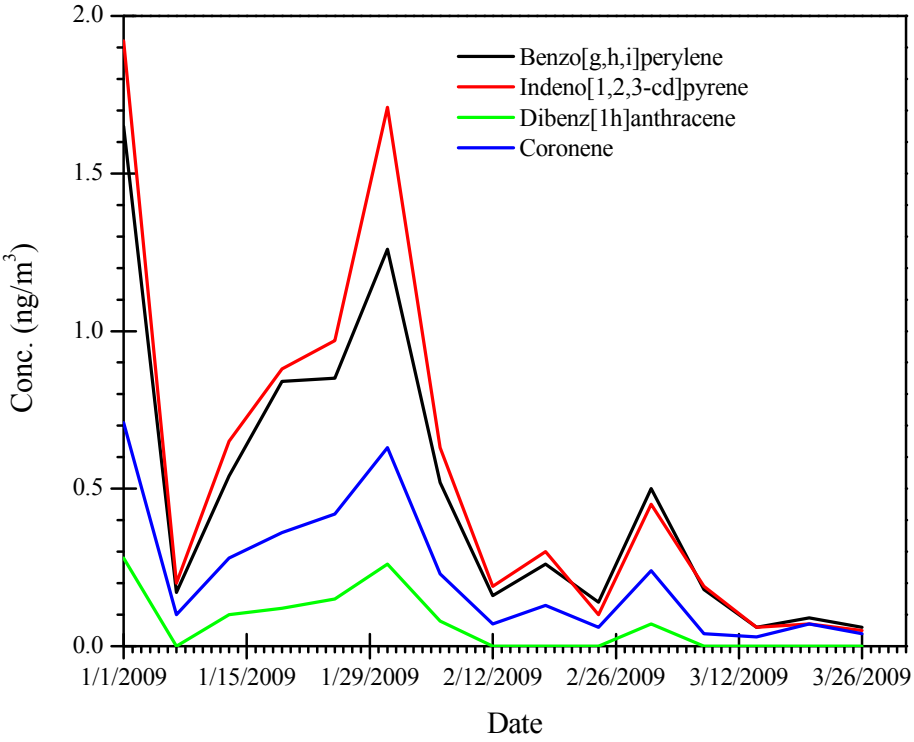

Figure 3-30 Variation of 6-aromatic-ring PAHs at North Valley

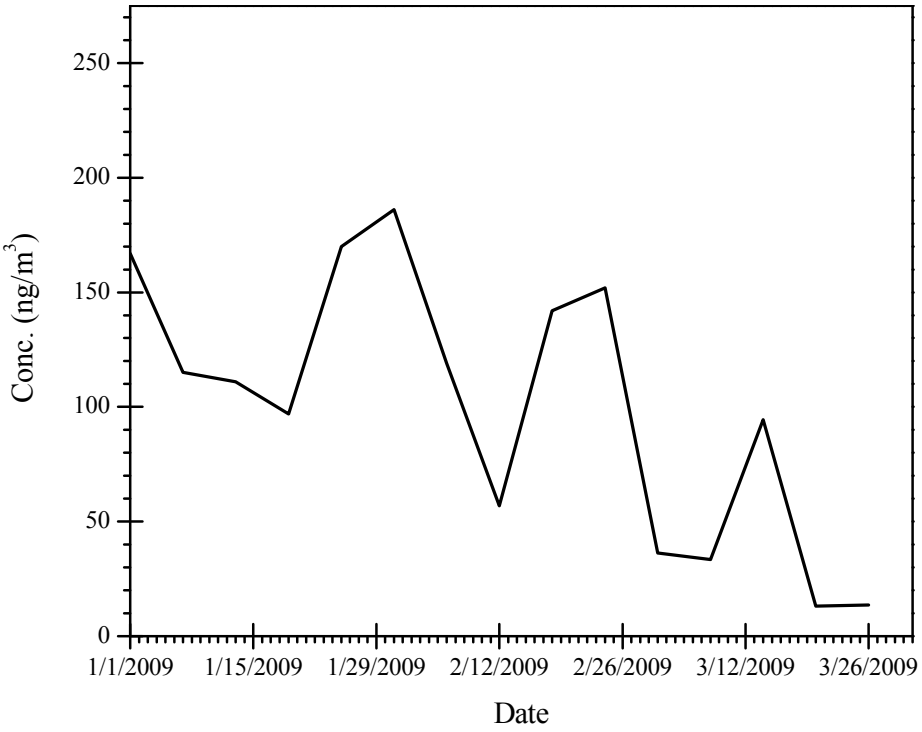

Figure 3-31 Variation of naphthalene at South Valley

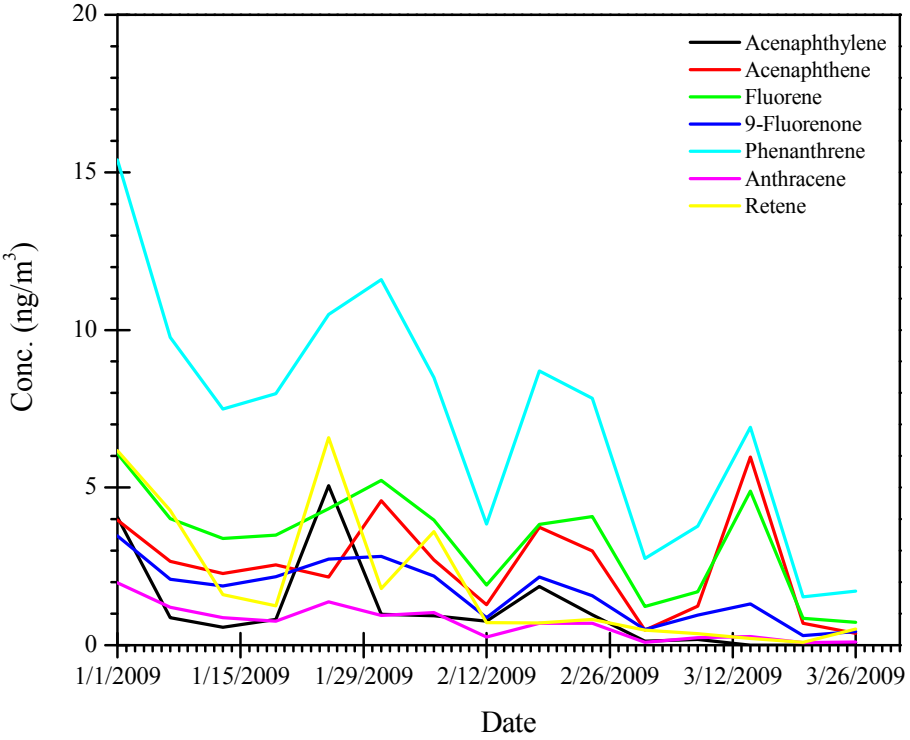

Figure 3-32 Variation of 3-aromatic-ring PAHs at South Valley

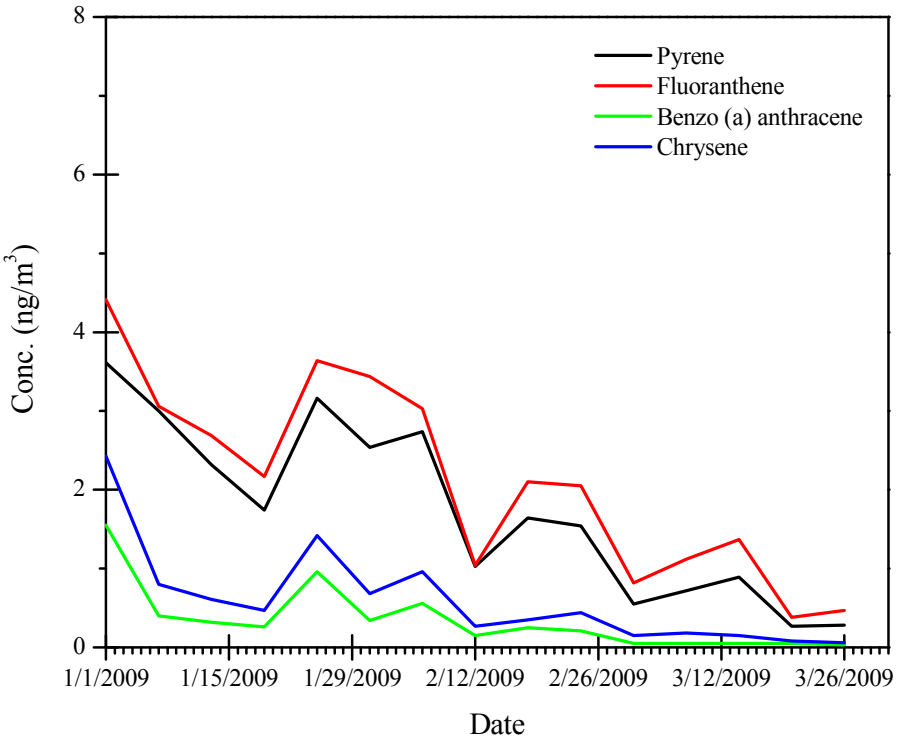

Figure 3-33 Variation of 4-aromatic-ring PAHs at South Valley

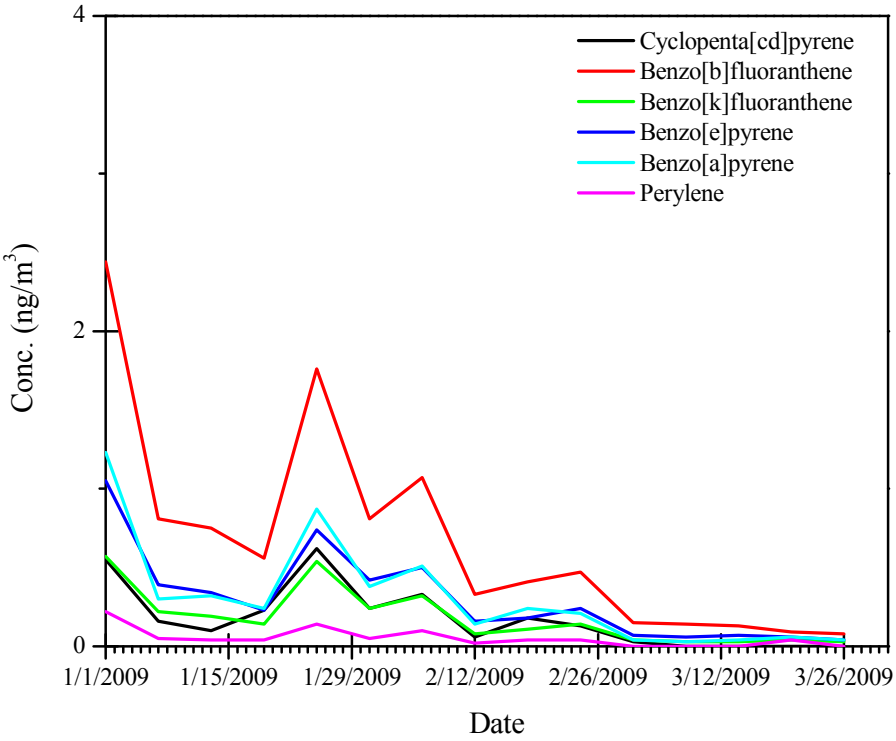

Figure 3-34 Variation of 5-aromatic-ring PAHs at South Valley

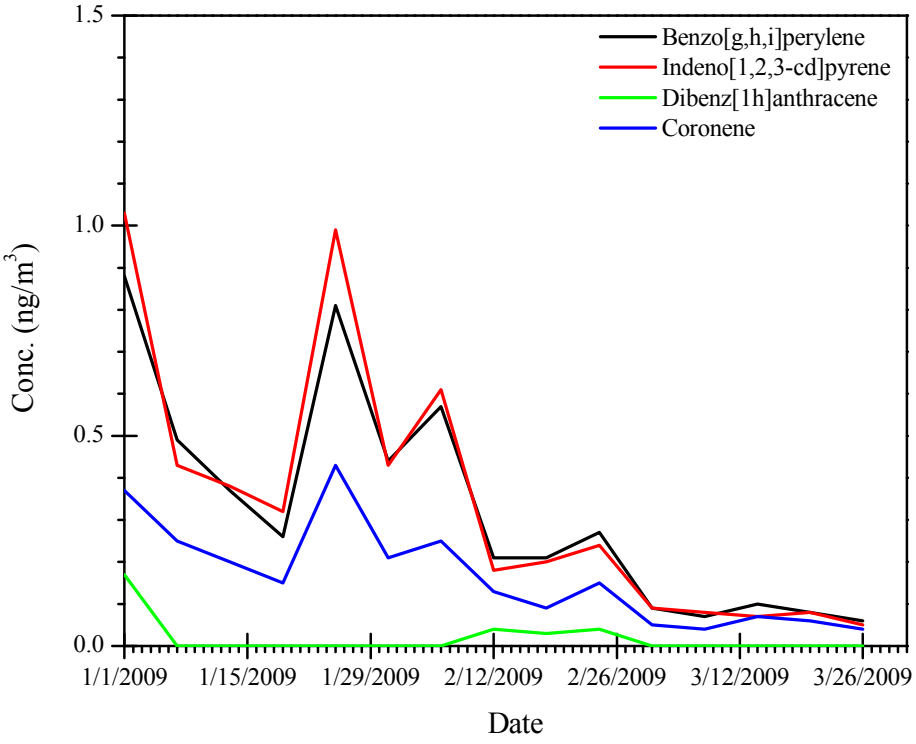

Figure 3-35 Variation of 6-aromatic-ring PAHs at South Valley

3.1.2 Heavy Metals

The concentration ranges of individual heavy metals for the three monitoring sites for the December 2008 to March 2009 period are given in Figure 3-36 through Figure 3-45. The boxes represent the 25%, 50% (median), and 75% percentiles, and whiskers show the 5% and 95% percentiles and "x" show the minimum and maximum concentrations. The open squares show the mean value. Prioritized chronic dose-response values (RfC (for non-cancer) and URE (for 1-in-million cancer)) for Arsenic (As), beryllium (Be), cadmium (Cd), chromium (Cr), cobalt (Co), lead (Pb), manganese (Mn), mercury (Hg), nickel (Ni) and selenium (Se) compounds were also included in the plots.

The heavy metals measured in the collected samples had total concentrations from 6.13 to 39.76 ng/m^3 at Del Norte, from 6.01 to 52.83 ng/m^3 at North Valley, and from 5.73 to 122.03 ng/m^3 at South Valley. Manganese was the dominant metal, representing more than 60 percent of total metal concentrations. The lowest concentrations were measured for beryllium.

Figure 3-46 through Figure 3-48 show the daily concentrations of heavy metals at Del Norte, North Valley, and South Valley, respectively. The highest concentrations were measured in late January, February, and March.

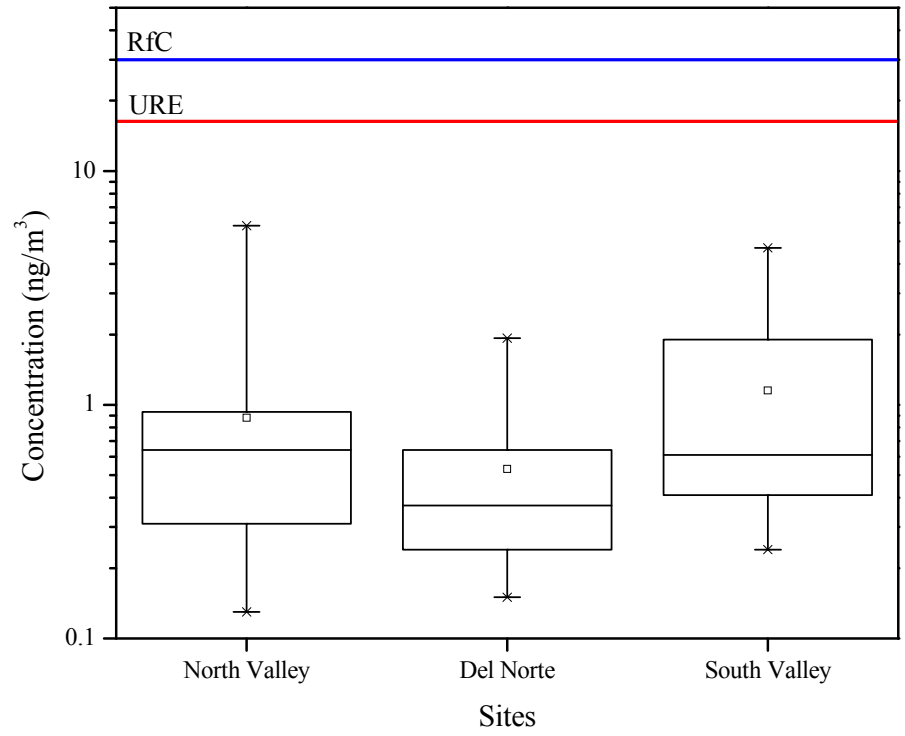

Figure 3-36 Concentrations of As compounds at the three locations and the RfC (non-cancer chronic inhalation; blue line) and URE (cancer chronic inhalation; red line)

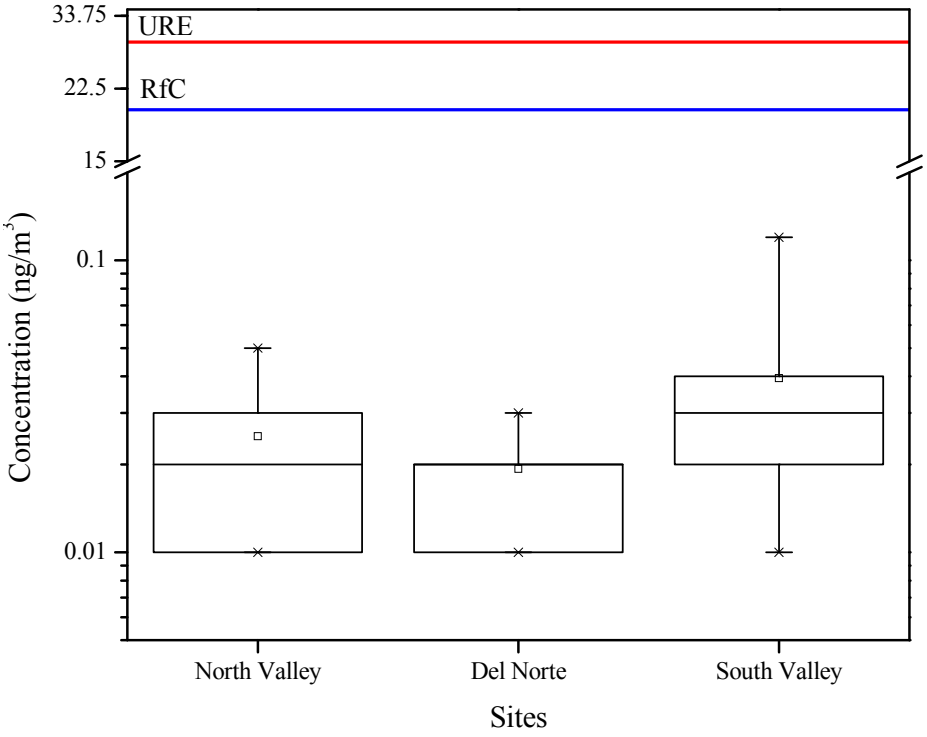

Figure 3-37 Concentrations of Be compounds at the three locations and the RfC (non-cancer chronic inhalation; blue line) and URE (cancer chronic inhalation; red line)

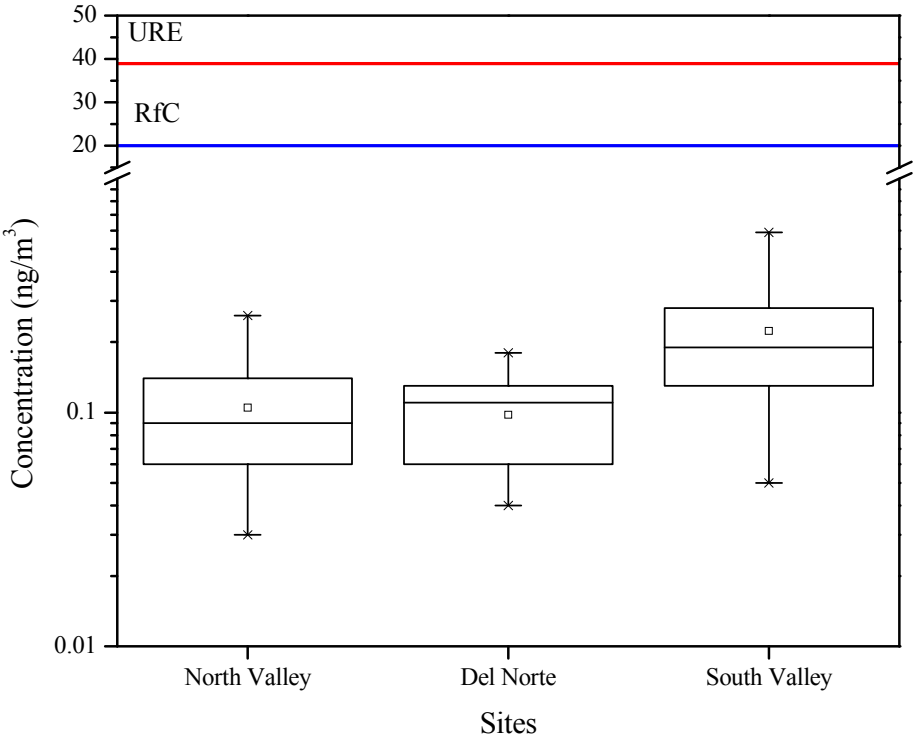

Figure 3-38 Concentrations of Cd compounds at the three locations and the RfC (non-cancer chronic inhalation; blue line) and URE (cancer chronic inhalation; red line)

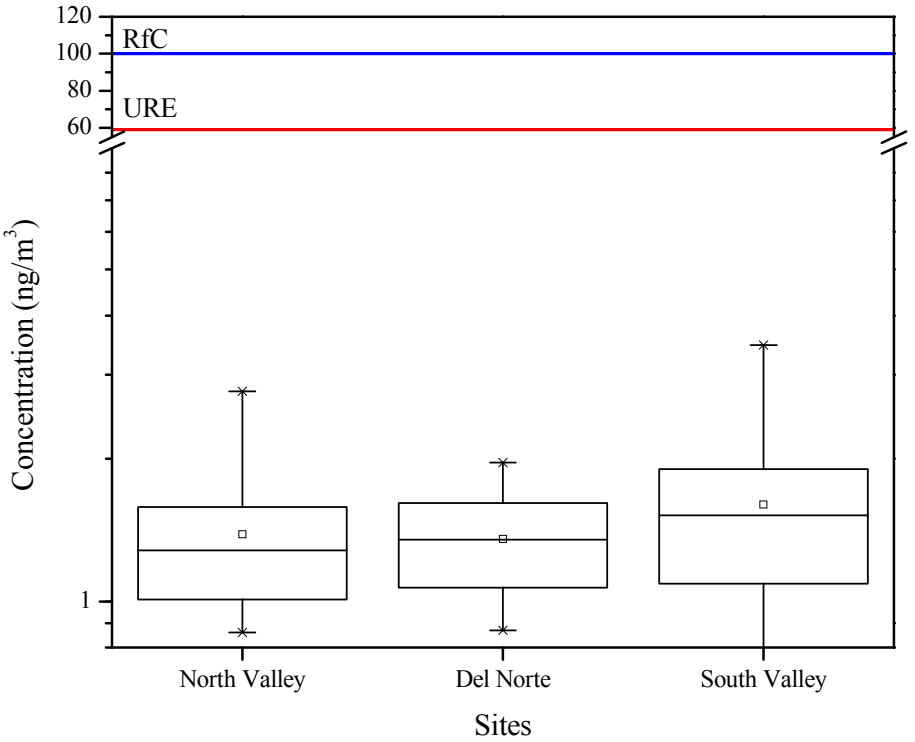

Figure 3-39 Concentrations of Cr compounds at the three locations and the RfC (non-cancer chronic inhalation; blue line) and URE (cancer chronic inhalation; red line)

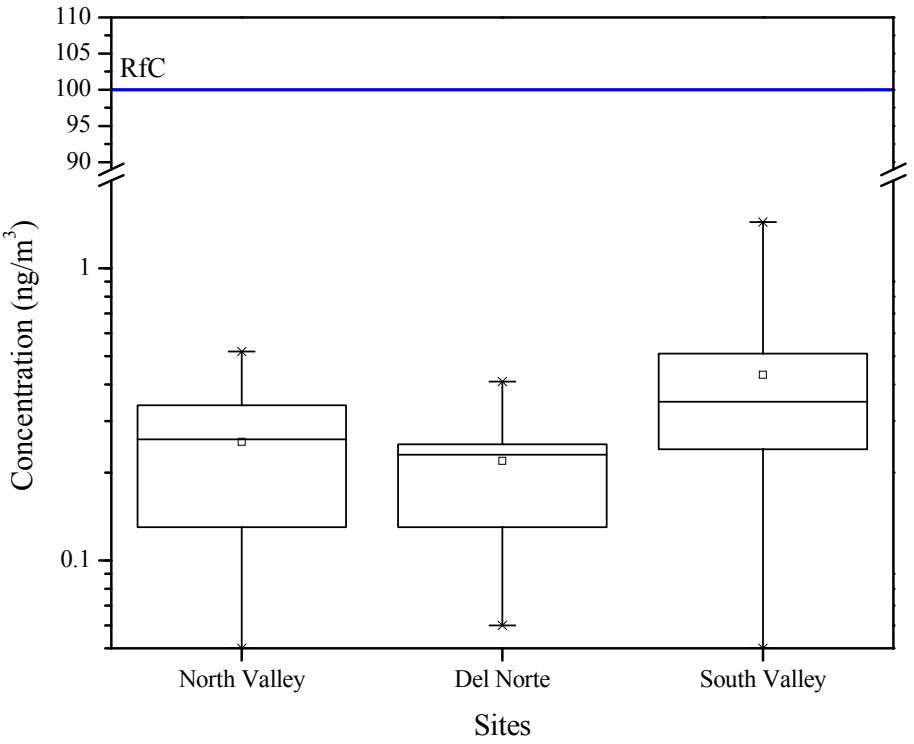

Figure 3-40 Concentrations of Co compounds at the three locations and the RfC (non-cancer chronic inhalation; blue line)

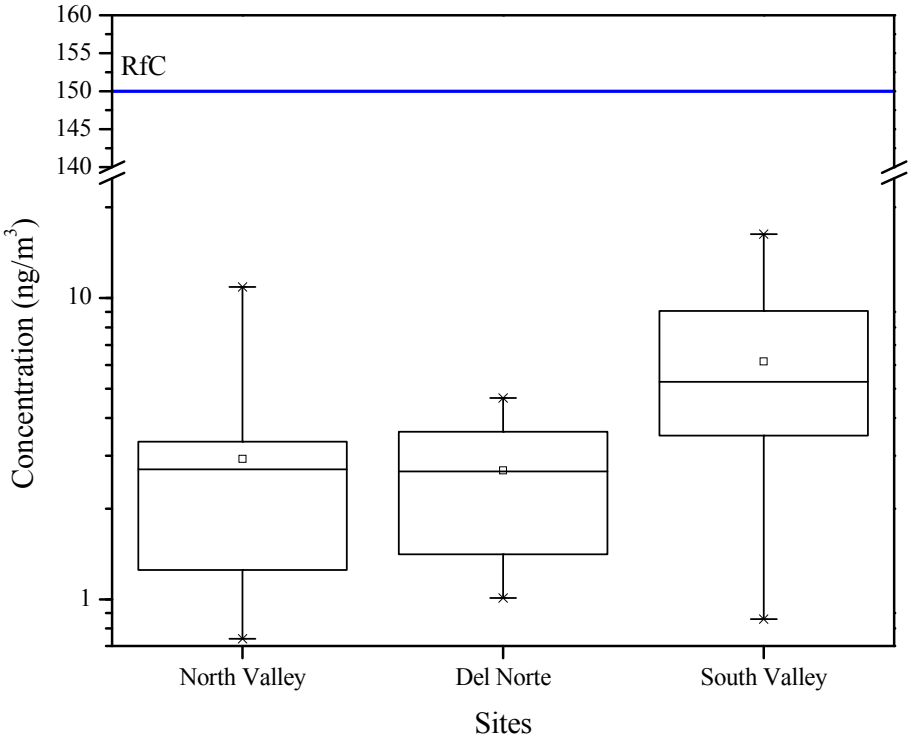

Figure 3-41 Concentrations of Pb compounds at the three locations and the RfC (non-cancer chronic inhalation; blue line)

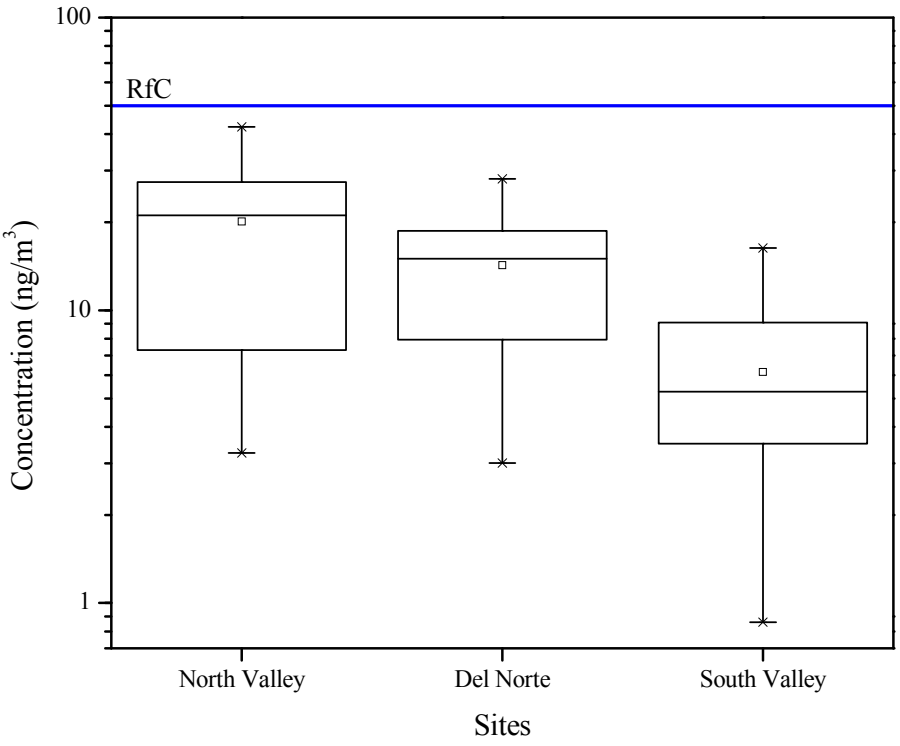

Figure 3-42 Concentrations of Mn compounds at the three locations and the RfC (non-cancer chronic inhalation; blue line)

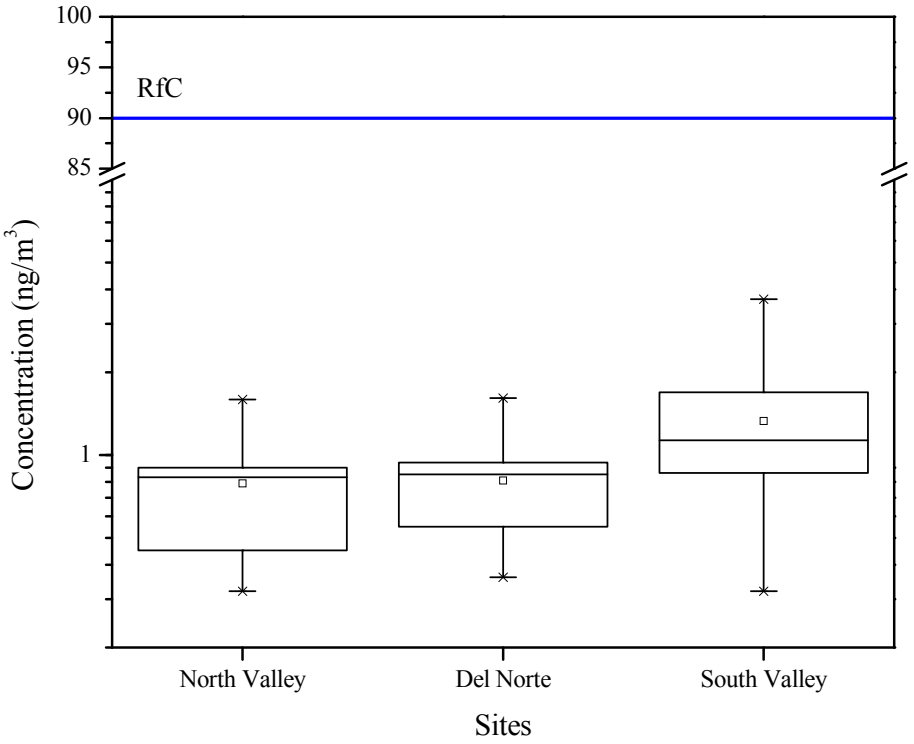

Figure 3-43 Concentrations of Ni compounds at the three locations and the RfC (non-cancer chronic inhalation; blue line)

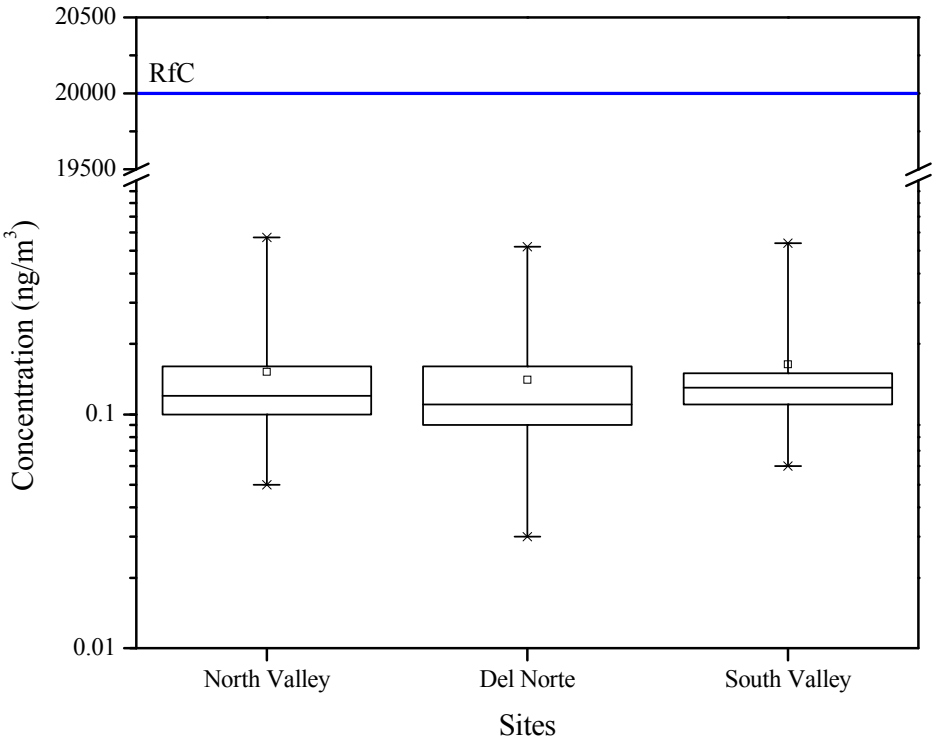

Figure 3-44 Concentrations of Se compounds at the three locations and the RfC (non-cancer chronic inhalation; blue line)

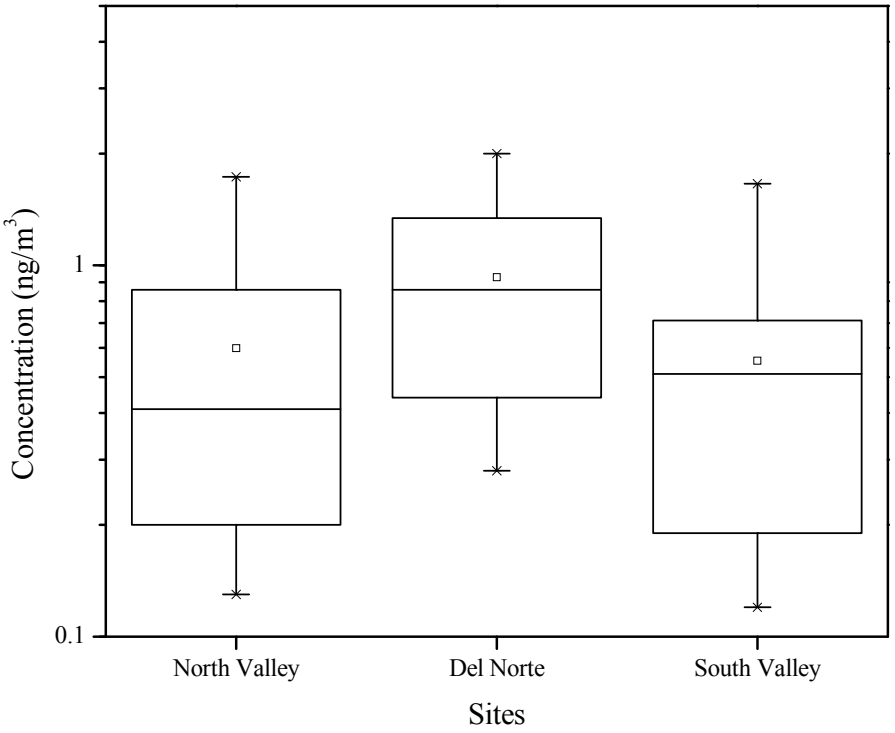

Figure 3-45 Concentrations of Sb compounds at the three locations

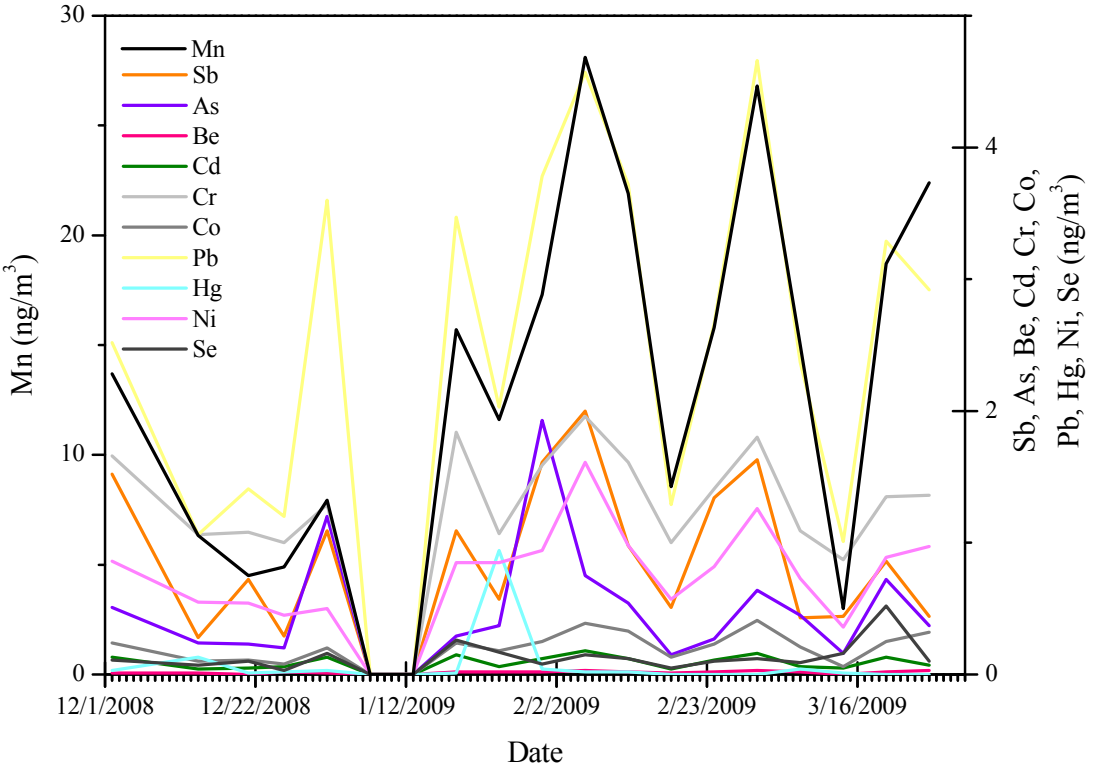

Figure 3-46 Variation of heavy metals concentrations at Del Norte

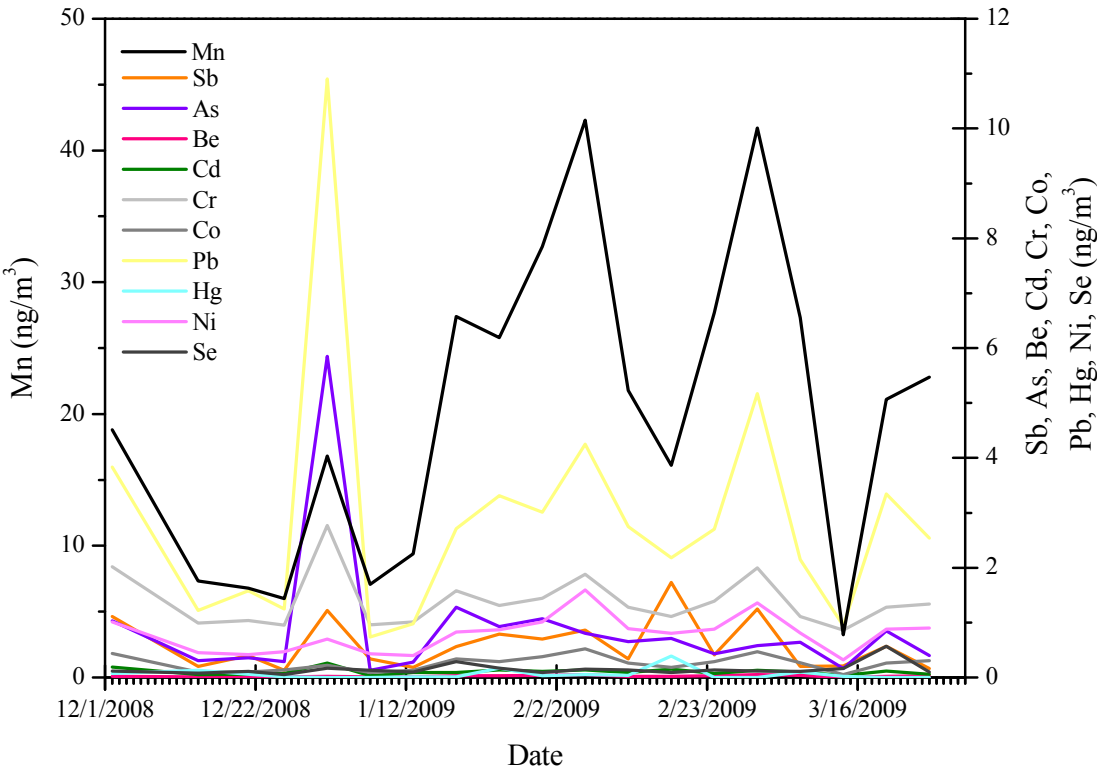

Figure 3-47 Variation of heavy metals concentrations at North Valley

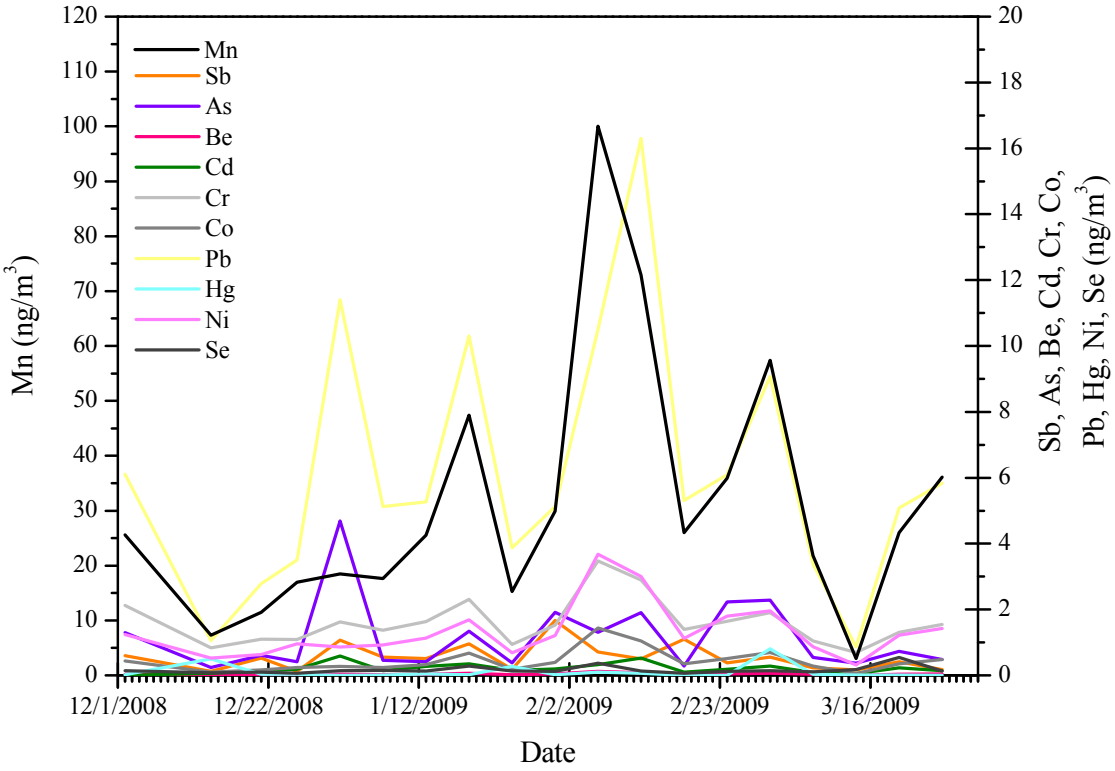

Figure 3-48 Variation of heavy metals concentrations at South Valley

3.1.3 VOCs

3.1.3.1 24-hr Measurements at Three Locations

The 24-hr concentration ranges of individual VOCs measured using canister samples for the three monitoring sites for the December 2008 to March 2009 period are given in Figure 3-49 through Figure 3-55. The boxes represent the 25%, 50% (median), and 75% percentiles, and whiskers show the 5% and 95% percentiles and "x" show the minimum and maximum concentrations. The open squares show the mean value. Prioritized chronic dose-response values (RfC (for non-cancer) and URE (for 1-in-million cancer)) for benzene; toluene; *m*-, *o*- and *p*-xylenes, chloromethane, and dichloromethane were also included in the plots.

The total concentrations of the VOCs measured in the collected samples ranged from 0.1 to 18.7 ppbv at Del Norte, from 0.1 to 8.7 ppbv at North Valley, and from 0.1 to 15.4 ppbv at South Valley. Figure 3-56 through Figure 3-61 show the variations of unsaturated and chlorinated hydrocarbons at the three monitoring sites. Toluene was the major component of unsaturated hydrocarbons, while chloromethane and methylene chloride dominated the fraction of chlorinated hydrocarbons.

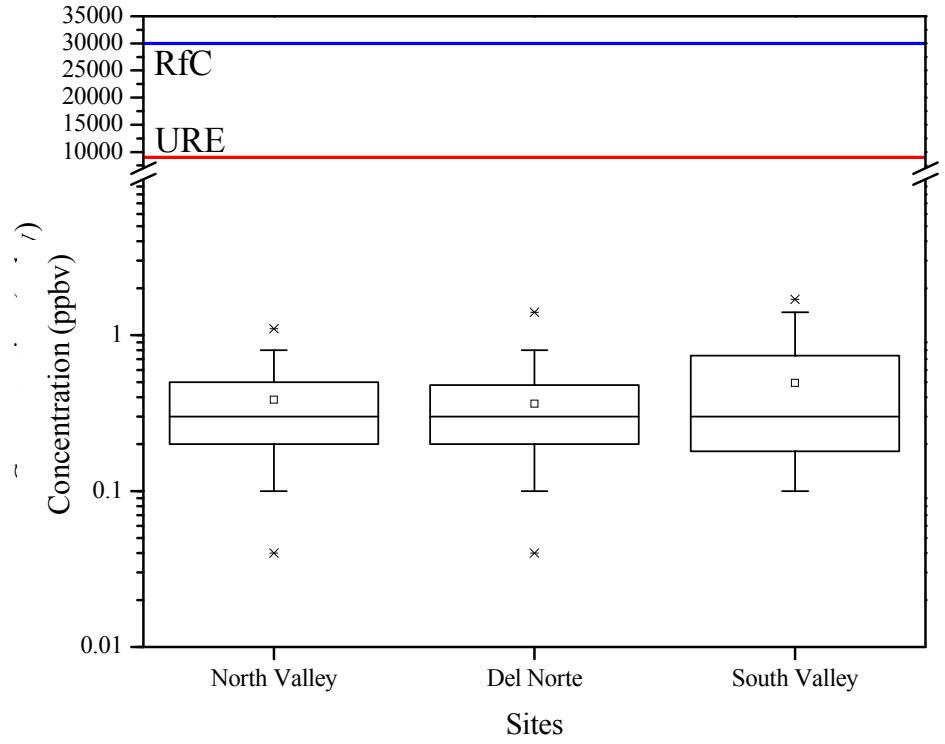

Figure 3-49 Daily concentrations of benzene at the three locations and the RfC (non-cancer chronic inhalation; blue line) and URE (cancer chronic inhalation; red line)

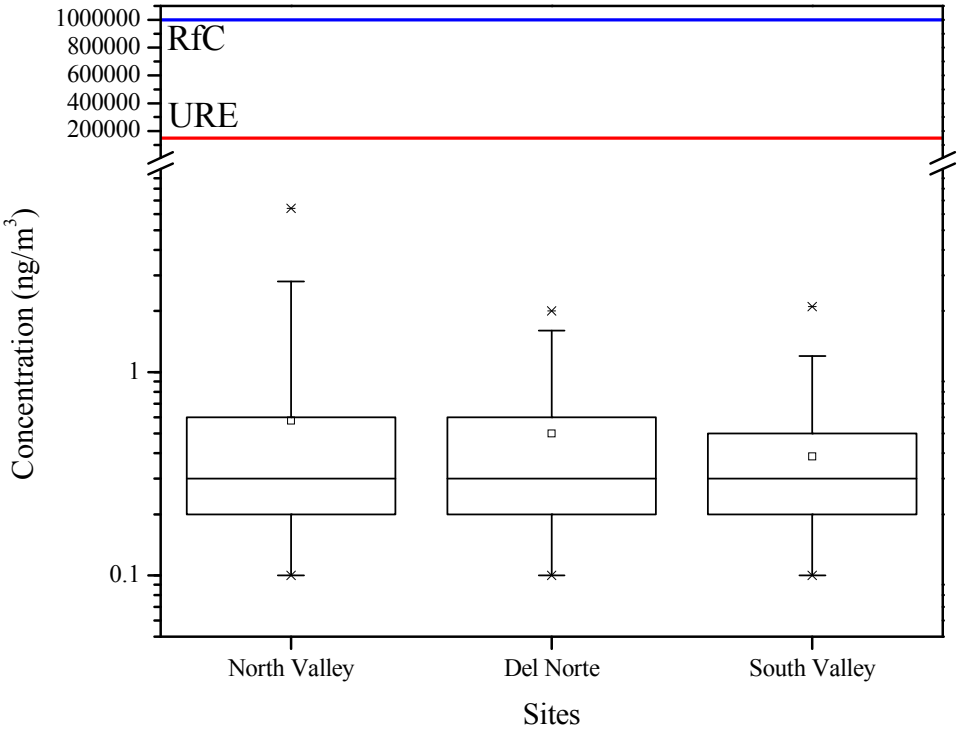

Figure 3-50 Daily concentrations of methylene chloride at the three locations and the RfC (non-cancer chronic inhalation; blue line) and URE (cancer chronic inhalation; red line)

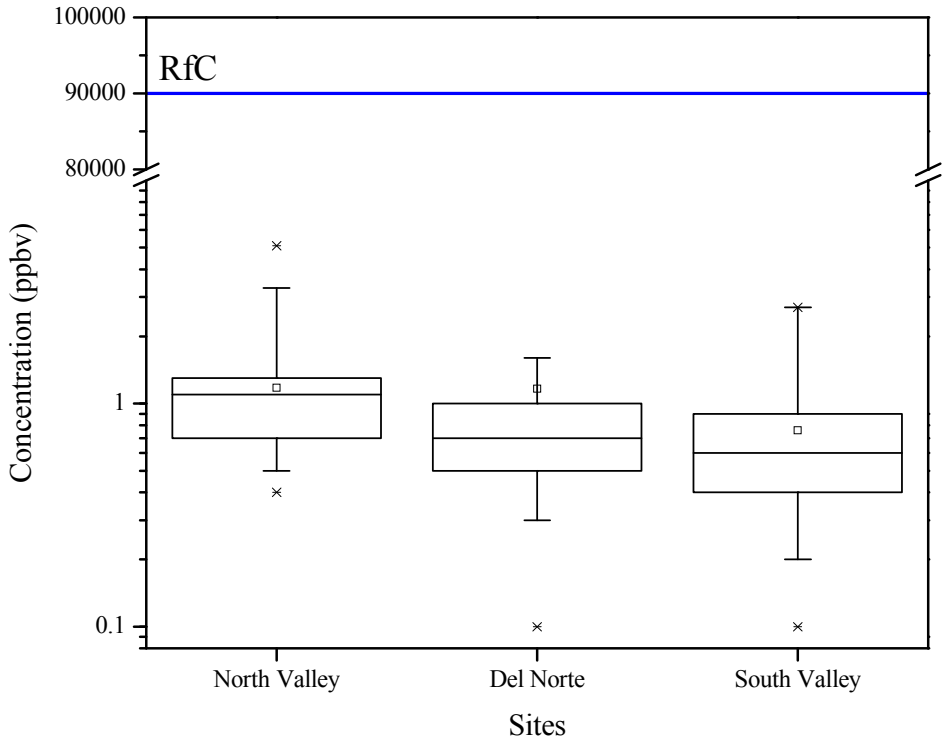

Figure 3-51 Daily concentrations of chloromethane at the three locations and the RfC (non-cancer chronic inhalation; blue line)

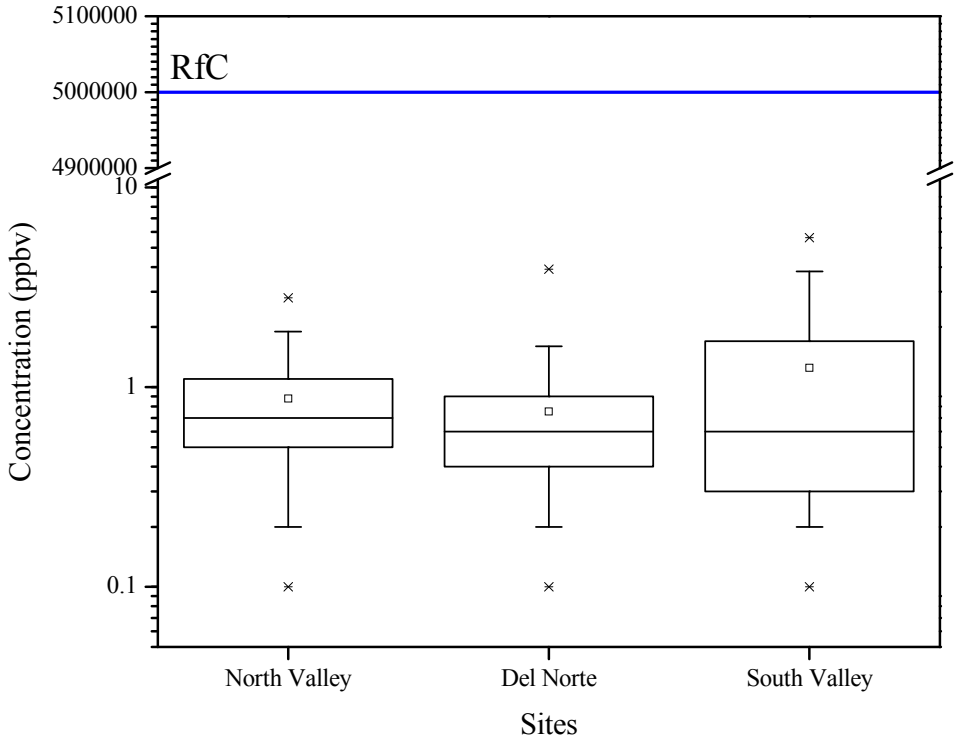

Figure 3-52 Daily concentrations of toluene at the three locations and the RfC (non-cancer chronic inhalation; blue line)

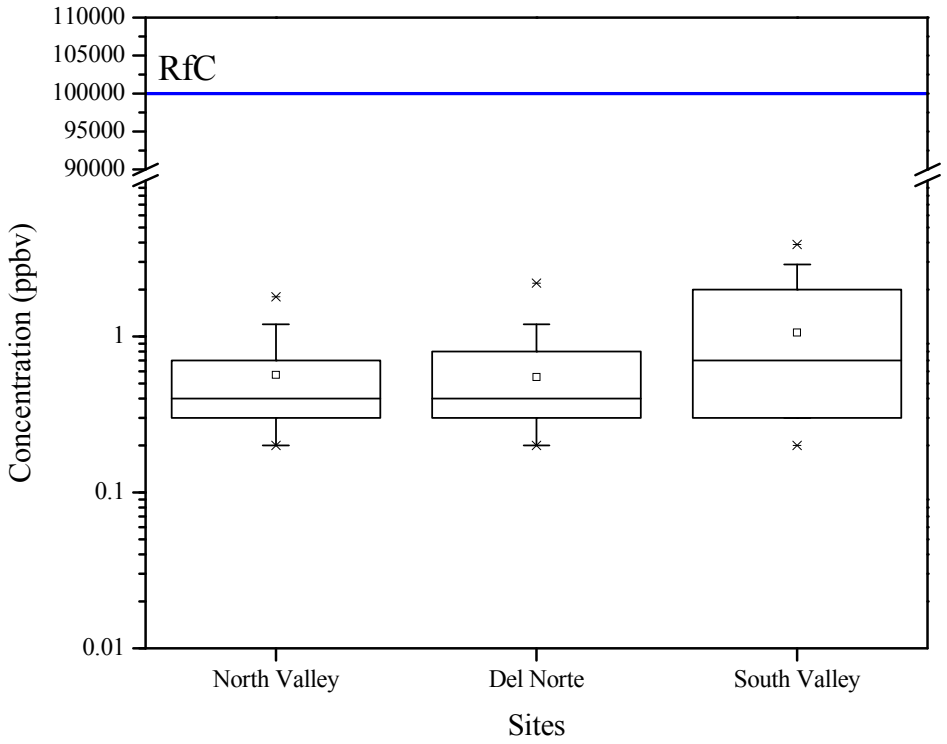

Figure 3-53 Daily concentrations of total xylenes at the three locations and the RfC (non-cancer chronic inhalation; blue line)

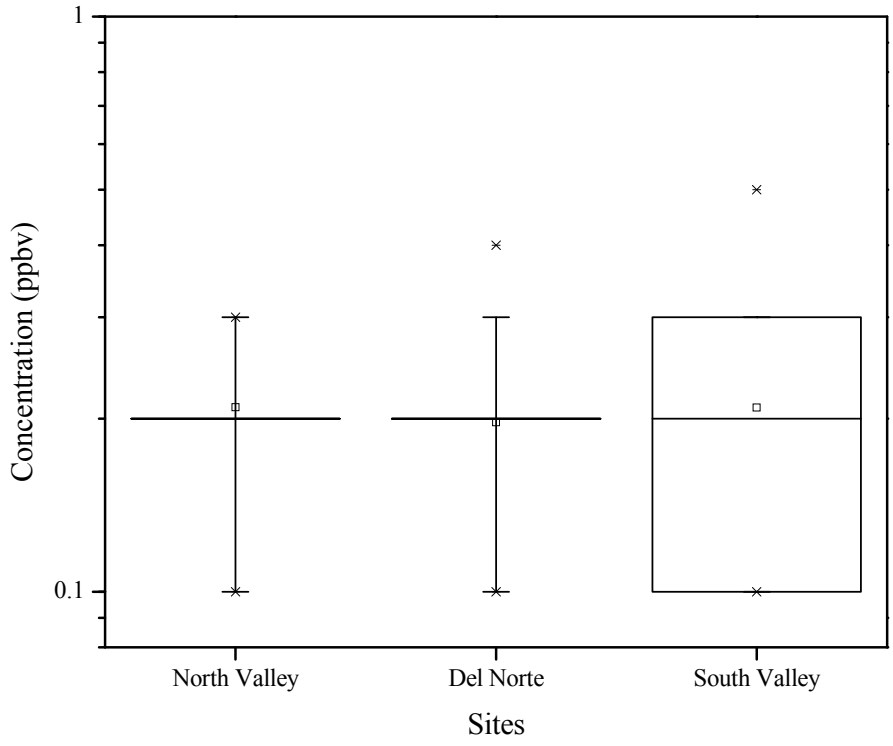

Figure 3-54 Daily concentrations of trichlorofluoromethane at the three locations and the RfC (non-cancer chronic inhalation; blue line)

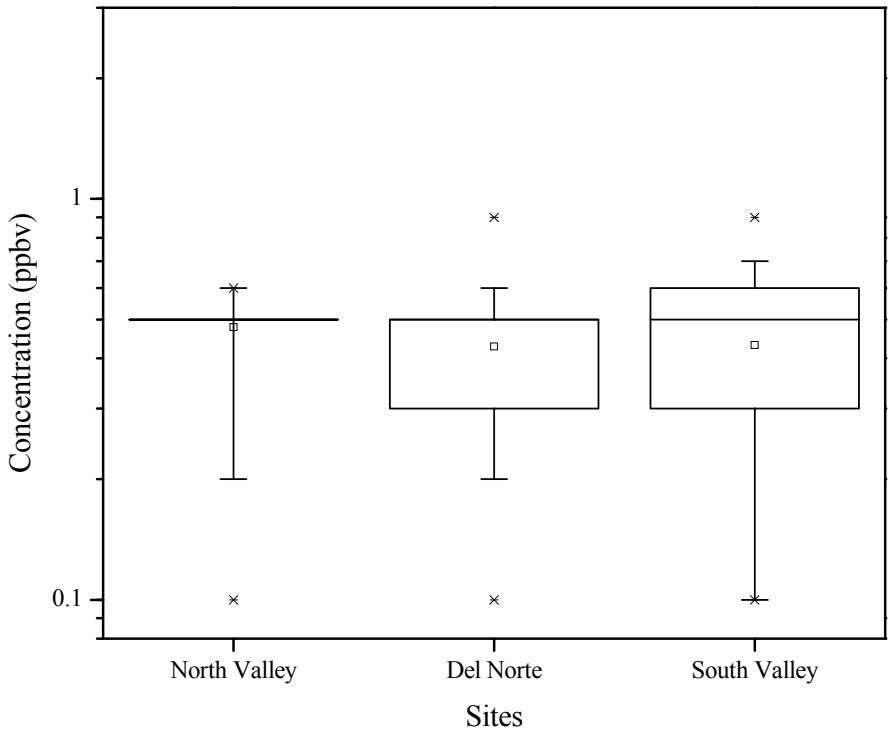

Figure 3-55 Daily concentrations of dichlorodifluoromethane at the three locations and the RfC (non-cancer chronic inhalation; blue line)

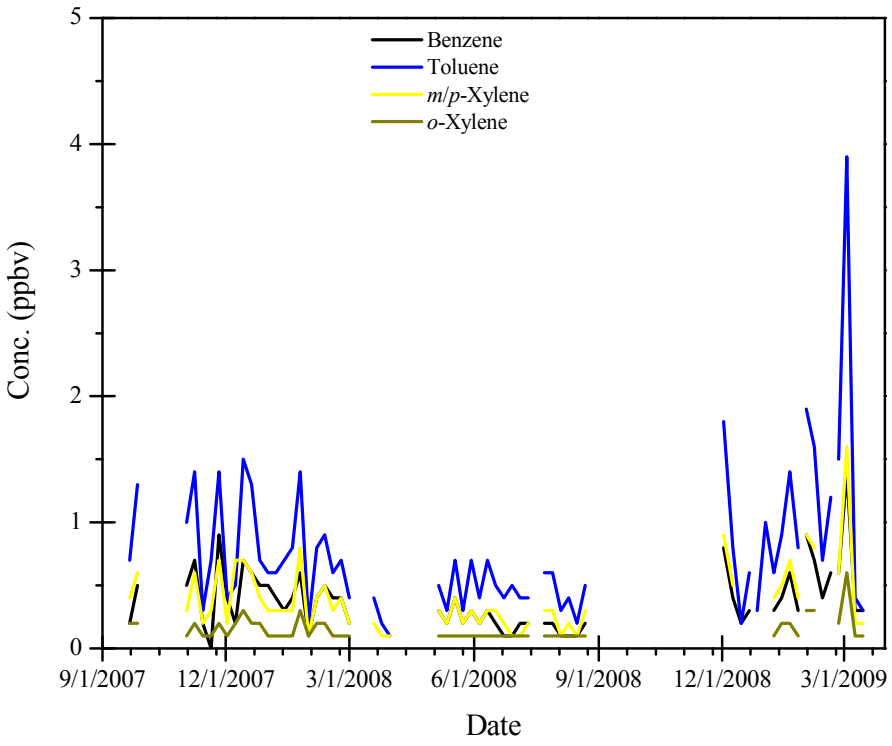

Figure 3-56 Variation of unsaturated hydrocarbons at Del Norte

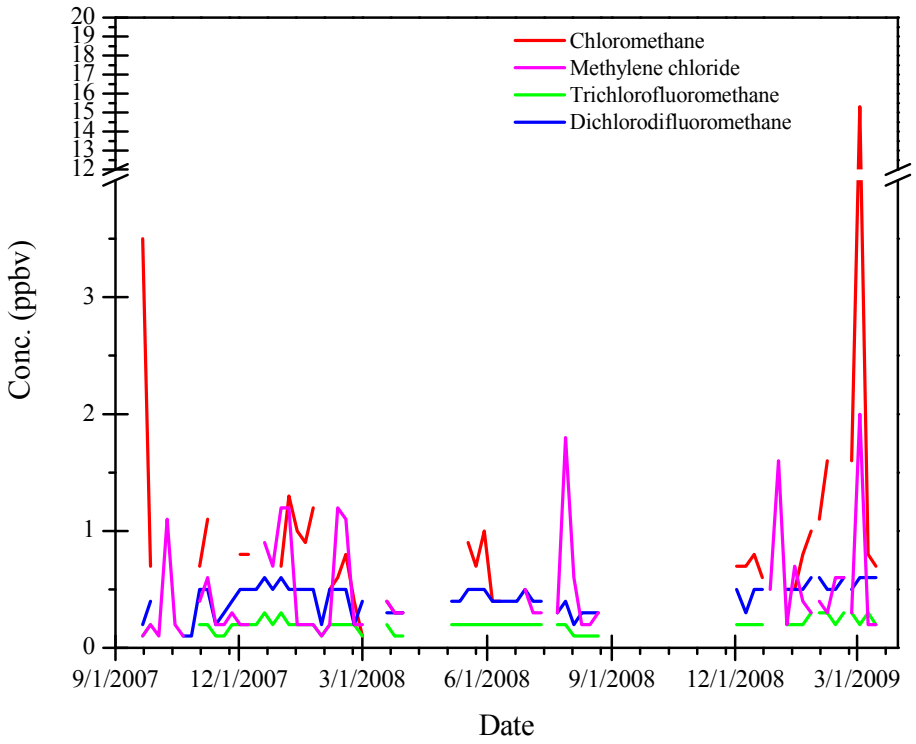

Figure 3-57 Variation of chlorinated hydrocarbons at Del Norte

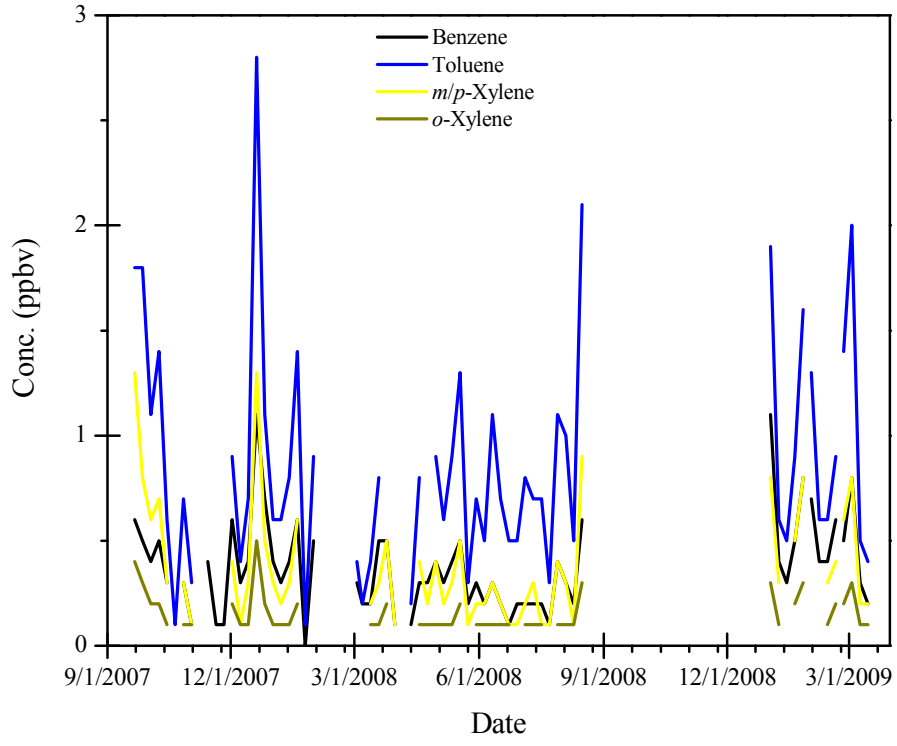

Figure 3-58 Variation of unsaturated hydrocarbons at North Valley

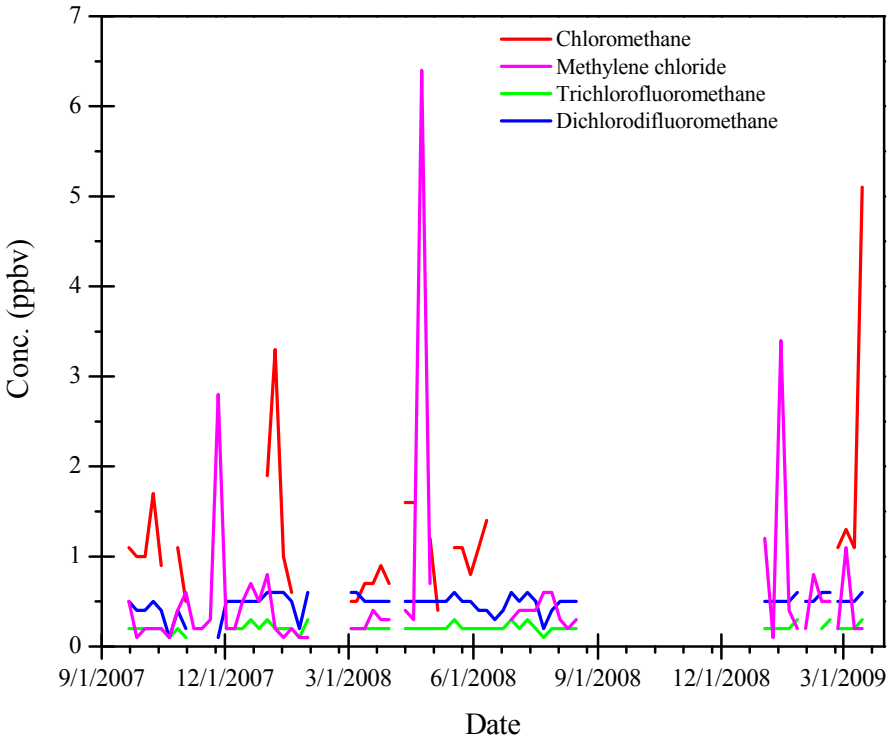

Figure 3-59 Variation of chlorinated hydrocarbons at North Valley

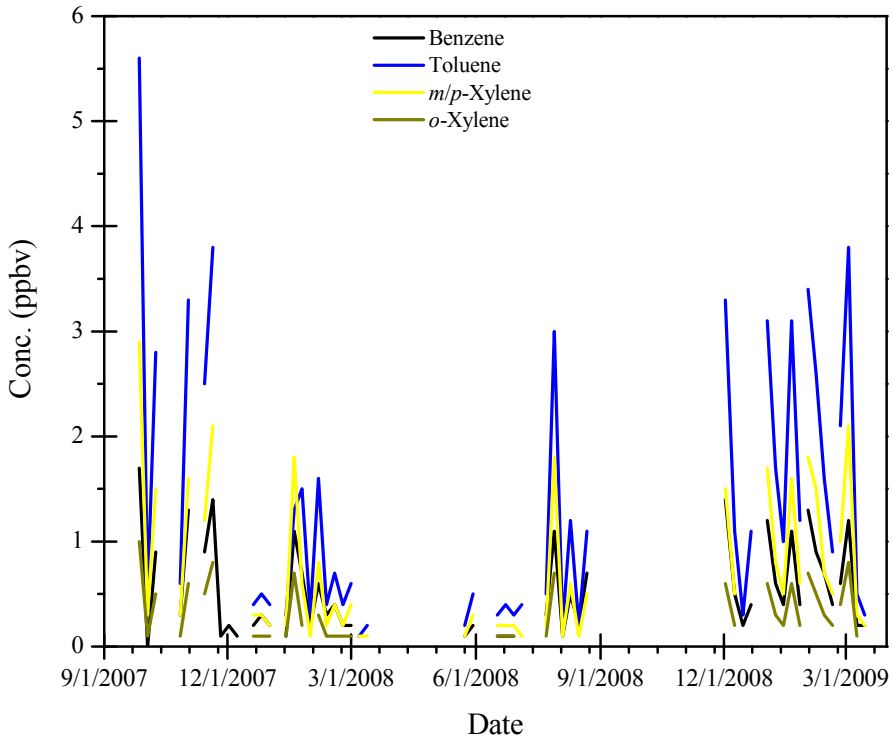

Figure 3-60 Variation of unsaturated hydrocarbons at South Valley

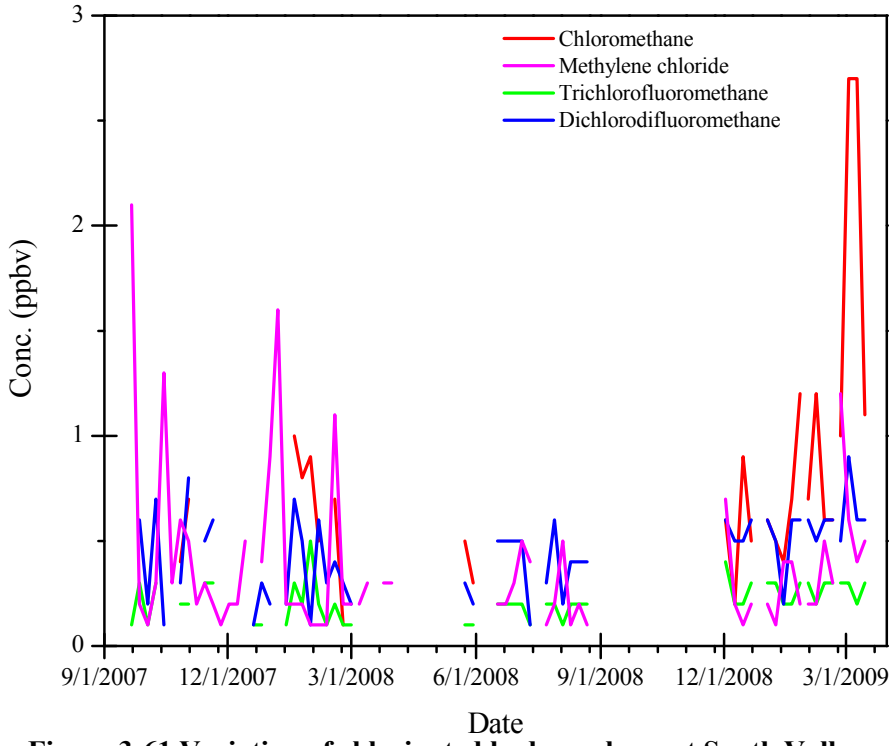

Figure 3-61 Variation of chlorinated hydrocarbons at South Valley

3.1.4 Hourly Measurements at Del Norte

Table 3-1 presents the 1-hour minimum, maximum, mean (and standard deviation) concentrations of hydrocarbons measured at the Del Norte site in Albuquerque during the two Intensive Monitoring Periods (IMPs). The following compounds were identified and quantified: benzene, bromomethane,1,3-Butadiene, carbon tetrachloride, chlorobenzene, chloroform, chloromethane, 1,2-dichlorobenzene, 1,3-dichlorobenzene, 1,4-dichlorobenzene, 1,1-dichloroethane, 1,2-dichloroethane, 1,1-dichloroethene, cis-1,2-dichloroethene, cis-1,3-dichloropropene, trans-1,3-dichloropropene, ethylbenzene, trichlorofluoromethane, hexachloro-1,3-butadiene, methylene chloride, styrene, 1,1,2,2-tetrachloroethane, Tetrachloroethene, Toluene, 1,2,4-trichlorobenzene, 1,1,1-trichloroethane, 1,1,2-trichloroethane, trichloroethene, 1,2,4-trimethylbenzene, 1,3,5-trimethylbenzene, cinyl chloride, m/p-xylenes, o-xylene, 1-ethyl-4-methylbenzene, 3-chloro-1-propene. The concentrations of aromatic hydrocarbons (benzene and its alkylated derivatives) were higher than those measured for halogenated hydrocarbons. The highest 1-hour concentrations were measured for benzene (40.7 ppbv during IMP1 and 4.4 ppbv during IMP2) and toluene (24.4 ppbv during IMP1 and 7.1 ppbv during IMP2). Higher average concentrations were measured for benzene, toluene, and *m/p*-xylenes as compared to the other detected organic compounds.

Figure 3-62 through Figure 3-64 show the 24-h mean concentrations of measured VOCs for the two IMPs. Analysis of patterns showed that most of the organic compounds followed a clear temporal cycle with the highest levels being measured during the winter IMP. The day-to-day variation of aromatic VOCs may be related to temporal patterns of emissions from local sources as well as to local meteorology. For example, traffic

emissions, which are more important on weekdays, and stagnant conditions, which are created by high-pressure systems, result in the accumulation of pollutant levels, whereas passage of weather fronts can trigger faster dilution and lower concentrations. The sources and trends are presented in a later section.

For two monitoring days in IMP1 and three monitoring days in IMP2, canister samples of VOCs were also collected and analyzed by NMSLD using a GC-MS instrument. Figure 3-65 and Figure 3-66 show the comparison of concentrations measured with the two instruments at Del Norte during IMP1 and IMP2, respectively. For all VOCs, the correlation coefficients were higher than 0.75 (Chloromethane: 1.00; Methylene chloride: 0.75; Benzene: 0.92; Toluene: 0.96; M/p-Xylene: 0.85; and o-Xylene:0.85), indicating a good agreement. However, concentrations measured using the online GC were higher than those measured with the canister sampling and analysis in the laboratory (with the exception of methylene chloride).

Table 3-1 The minimum, maximum, mean (and standard deviation) concentrations of hourly VOCs (in µg/m^3) at Del Norte during the two IMPs

	February 12-20, 2008	June 17-30, 2008
Benzene	0 - 40.7; 3.7 (5.4)	0 - 4.4; 1.3 (0.7)
Bromomethane	0.5 - 1.9; 0.6 (0.4)	0 - 1.4; 0.4 (0.2)
1,3-Butadiene	0.2 - 1.3; 0.4 (0.3)	0 - 0.8; 0.2 (0.2)
Carbon tetrachloride	0 - 2.3; 0.5 (0.4)	0 - 1.2; 0.3 (0.2)
Chlorobenzene	0.5 - 3.9; 0.8 (0.6)	0 - 1.8; 0.5 (0.3)
Chloroform	0 - 6.7; 0.4 (0.7)	0 - 0.9; 0.2 (0.2)
Chloromethane	0 - 12.1; 1.3 (1.4)	0 - 2.8; 0.8 (0.5)
1,2-Dichlorobenzene	0 – 4.1; 0.3 (0.4)	0 – 0.7; 0.2 (0.1)
1,3-Dichlorobenzene	0 – 3.5; 0.3 (0.3)	0 – 0.6; 0.2 (0.1)
1,4-Dichlorobenzene	0 – 6.6; 0.5 (0.6)	0 – 1.1; 0.3 (0.2)
1,1-Dichloroethane	0 - 4.6; 0.1 (0.4)	0 - 0.3; 0.1 (0.1)
1,2-Dichloroethane	0 - 1.8; 0.3 (0.3)	0 - 0.7; 0.2 (0.1)
1,1-Dichloroethene	0 – 1.0; 0.1 (0.1)	0 - 0.3; 0.1 (0.1)
cis-1,2-Dichloroethene	0 - 0.1; 0.1 (0)	0 – 0.1; 0.1 (0)
cis-1,3-Dichloropropene	0 – 3.0; 0.7 (0.5)	0 - 1.6; 0.4 (0.3)
Trans-1,3-Dichloropropene	0.1 - 5.2; 0.6 (0.7)	0 - 1.4; 0.4 (0.3)
Ethylbenzene	0.1 - 5.9; 0.6 (0.9)	0 - 0.8; 0.1 (0.1)
Trichlorofluoromethane	0 - 6.4; 1.4 (1.3)	0 - 3.3; 0.9 (0.6)
Hexachloro-1,3-butadiene	0 - 5.6; 0.4 (0.6)	0 - 0.8; 0.2 (0.1)
Methylene Chloride	0 - 4.8; 1.2 (0.9)	0 - 2.7; 0.7 (0.5)
Styrene	0 – 6.0; 0.6 (0.8)	0 – 1.0; 0.2 (0.2)
1,1,2,2-Tetrachloroethane	0.1 - 5.1; 0.8 (0.7)	0 - 1.7; 0.5 (0.3)
Tetrachloroethene	0.4 - 3.4; 0.6 (0.5)	0 - 1.4; 0.4 (0.3)
Toluene	1.8 - 24.4; 3.2 (2.8)	0 - 7.1; 1.9 (1.3)
1,2,4-Trichlorobenzene	0.1 – 2.0; 0.3 (0.3)	0 - 0.7; 0.2 (0.1)
1,1,1-Trichloroethane	0 - 10.4; 0.7 (1.4)	0 - 1.5; 0.4 (0.3)
1,1,2-Trichloroethane	0.1 - 3.1; 0.3 (0.4)	0 - 0.7; 0.2 (0.1)
Trichloroethene	0 - 3.1; 0.5 (0.5)	0 - 1.2; 0.3 (0.2)
1,2,4-Trimethylbenzene	1.3 - 56.6; 2.1 (4.5)	0 - 3.1; 0.5 (0.4)
1,3,5-Trimethylbenzene	0 - 32.4; 1.3 (2.5)	0 - 3.9; 0.3 (0.4)
Vinyl chloride	0.1 - 1.6; 0.4 (0.4)	0 – 1.0; 0.3 (0.2)
m/p-Xylenes	2.2 - 20.6; 3.1 (2.9)	0 - 5.4; 1.3 (1.0)
o-Xylene	0 - 5.3; 0.6 (0.8)	0 - 0.9; 0.1 (0.1)
1-Ethyl-4-methylbenzene	0 - 13.4; 1.3 (1.6)	0 – 3.0; 0.8 (0.5)
3-Chloro-1-propene	0 - 9.3; 0.3 (1.1)	0 - 0.7; 0.2 (0.1)

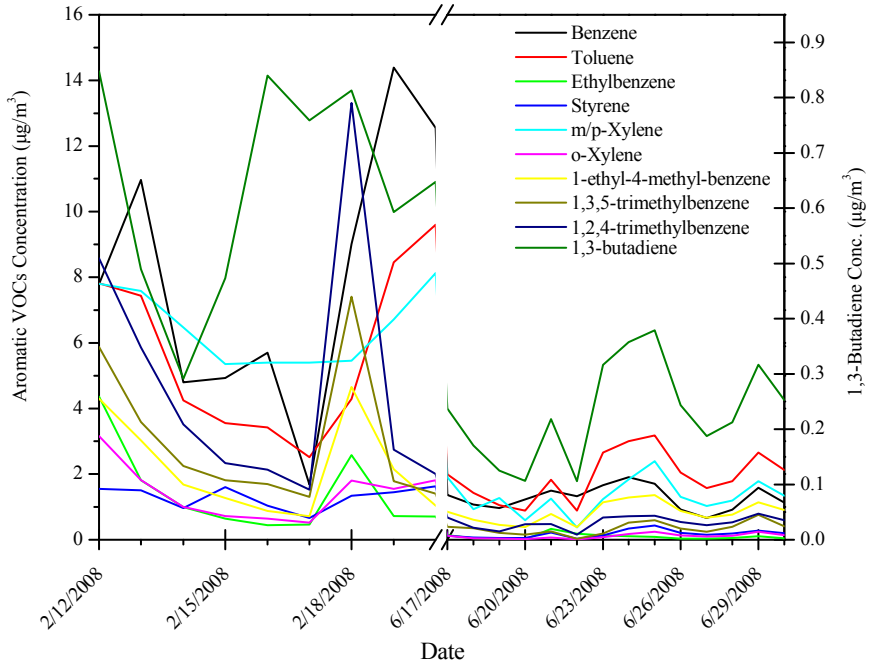

Figure 3-62 Variation of aromatic hydrocarbons and 1,3-butadiene during the two IMPs

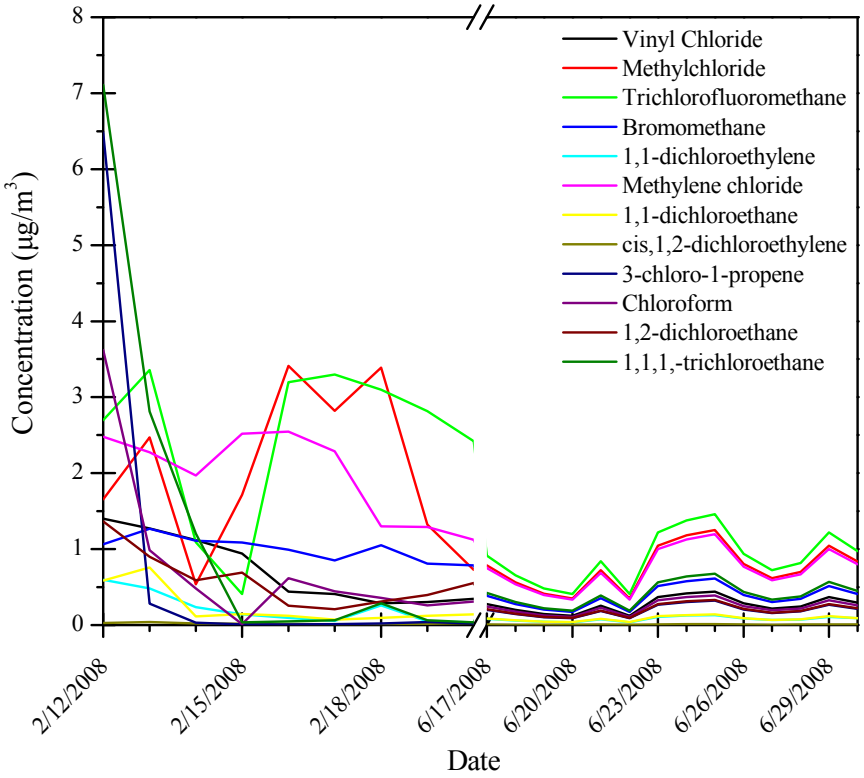

Figure 3-63 Variation of chlorinated hydrocarbons during the two IMPs

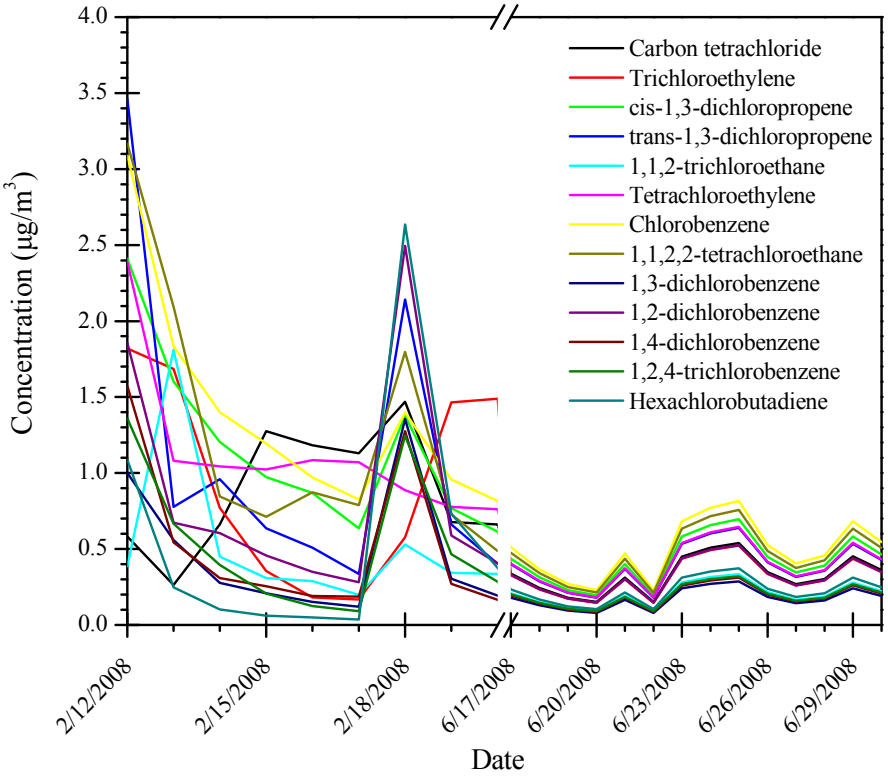

Figure 3-64 Variation of chlorinated hydrocarbons during the two IMPs

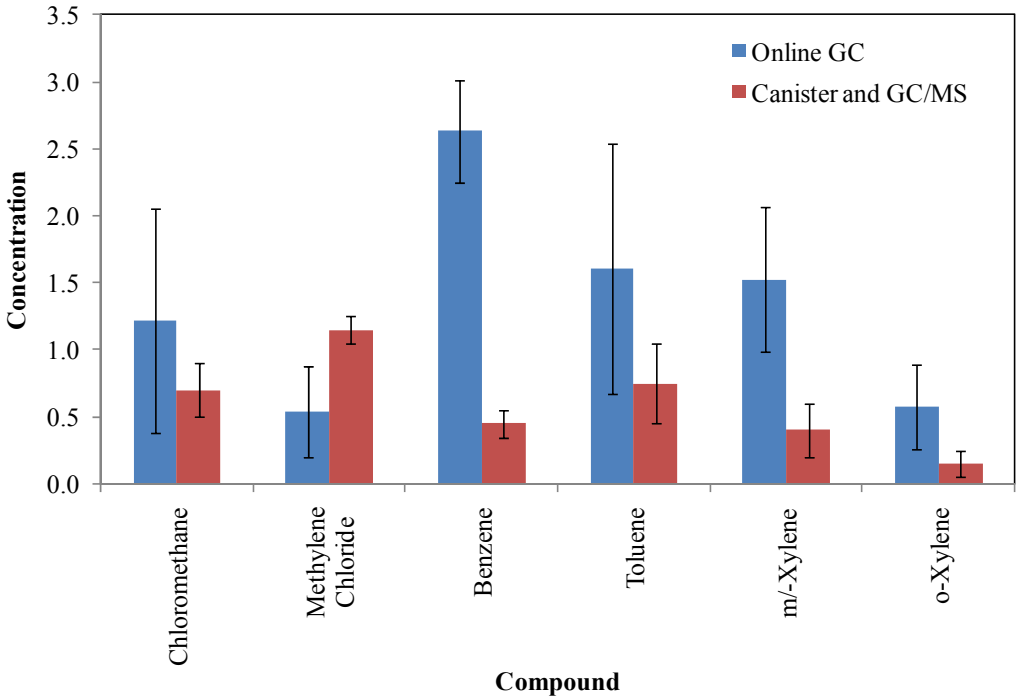

Figure 3-65 Comparison of VOCs measured with online GC and canister (analysis by GC-MS) at Del Norte on February 12 and 18, 2008

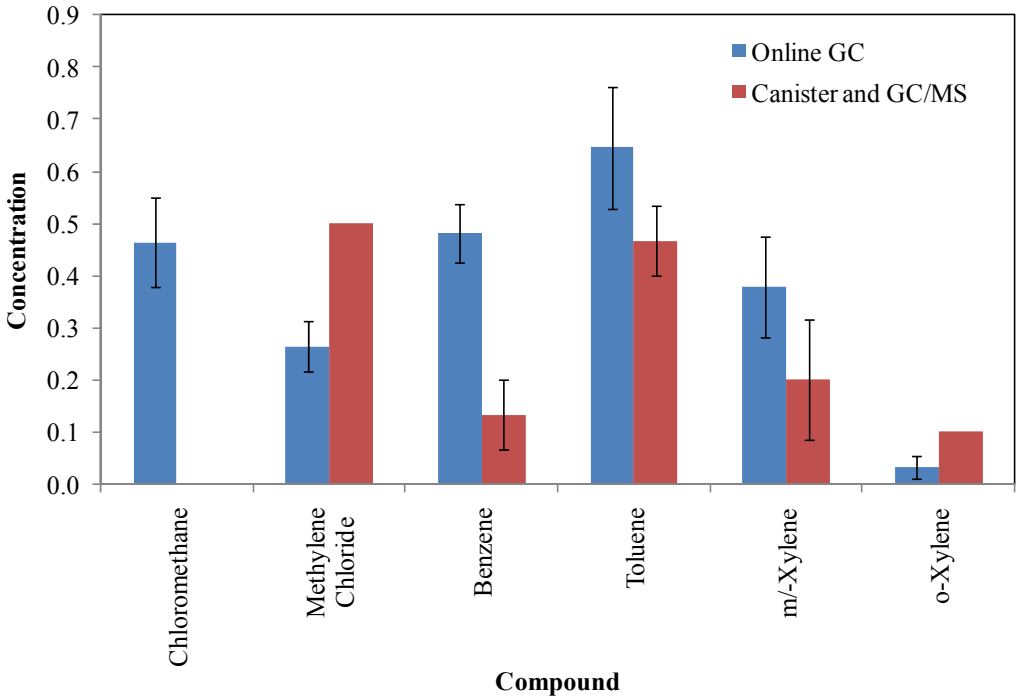

Figure 3-66 Comparison of VOCs measured with online GC and canister (analysis by GC-MS) at Del Norte on June 7, June 23, and June 29, 2008

3.1.5 Organic Carbon and Elemental Carbon

Table 3-2 shows the mean, standard deviation (σ), minimum, and maximum concentrations of organic carbon, elemental carbon, and total carbon (TC) of aerosol samples collected at the three sites from September 2007 to March 2009. Organic carbon concentrations varied from 2.7 to 24.9 μg/m^3 at Del Norte, from 0.3 to 23.8 μg/m^3 at North Valley, and from 2.7 to 31.5 μg/m^3 at South Valley. Elemental carbon levels ranged from 0.4 to 7.9 μg/m^3 at Del Norte, from 0 to 9.8 μg/m^3 at North Valley, and from 0.6 to 7.3 μg/m^3 at South Valley. Note that a 1-cm punch of quartz fiber filter used for the collection of PAHs was used to measure OC and EC during the entire monitoring period; data on PAHs were not available for the same period due to laboratory recovery problems. The later does not invalidate the OC and EC measurements.

Organic carbon accounted for 83 percent, 80 percent, and 79 percent of total carbon at South Valley, North Valley, and Del Norte, respectively. Figure 3-67 through Figure 3-69 show the daily concentrations of OC, EC, and TC at Del Norte, North Valley, and South Valley, respectively. Similar temporal trends were drawn for OC, EC, and TC at all sites, indicating a common origin for OC and EC. Higher levels were generally observed in the winter as compared to the spring and fall (no measurements were obtained in the summer).

Table 3-2 The minimum, maximum, mean (and standard deviation) concentrations of organic carbon and elemental carbon (in µg/m^3) at Del Norte, North Valley, and South Valley

	Del Norte		North Valley	South Valley
	Primary	Collocated		
Organic carbon	2.7 - 24.9; 8.6 (3.7)	0.3 - 26.7; 10.2 (7.0)	0.2 - 23.8; 10.3 (5.2)	2.7 - 31.5; 11.7 (6.9)
Elemental carbon	0.4 - 7.9; 2.3 (1.4)	0 - 10.2; 3.3 (2.8)	0 - 9.8; 2.5 (1.8)	0.6 - 7.3; 2.3 (1.4)
Total carbon	3.3 - 32.9; 10.9 (5.0)	0.3 - 37; 13.4 (9.7)	0.2 - 33.7; 12.8 (6.7)	3.6 - 34.8; 14.0 (7.8)

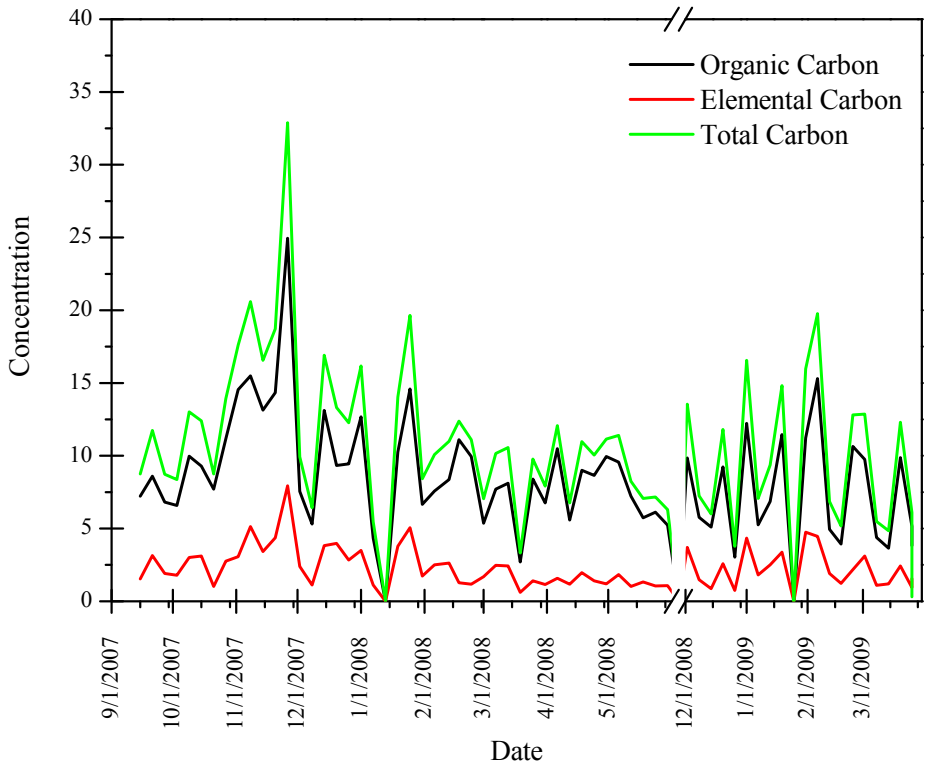

Figure 3-67 Variation of organic, elemental, and total carbon at Del Norte

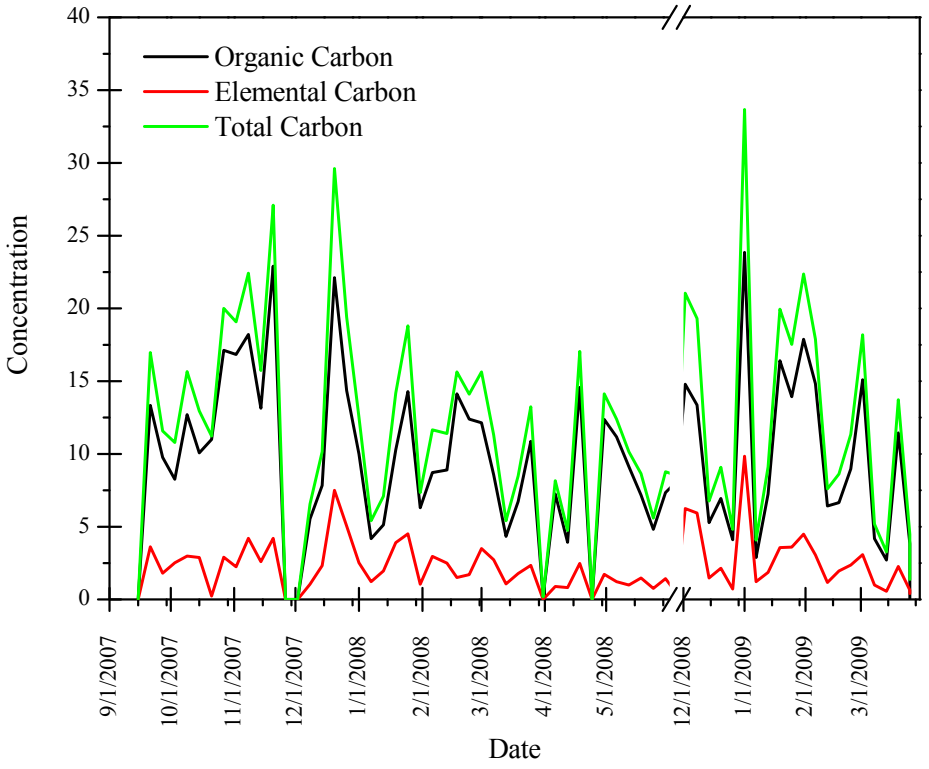

Figure 3-68 Variation of organic, elemental, and total carbon at North Valley

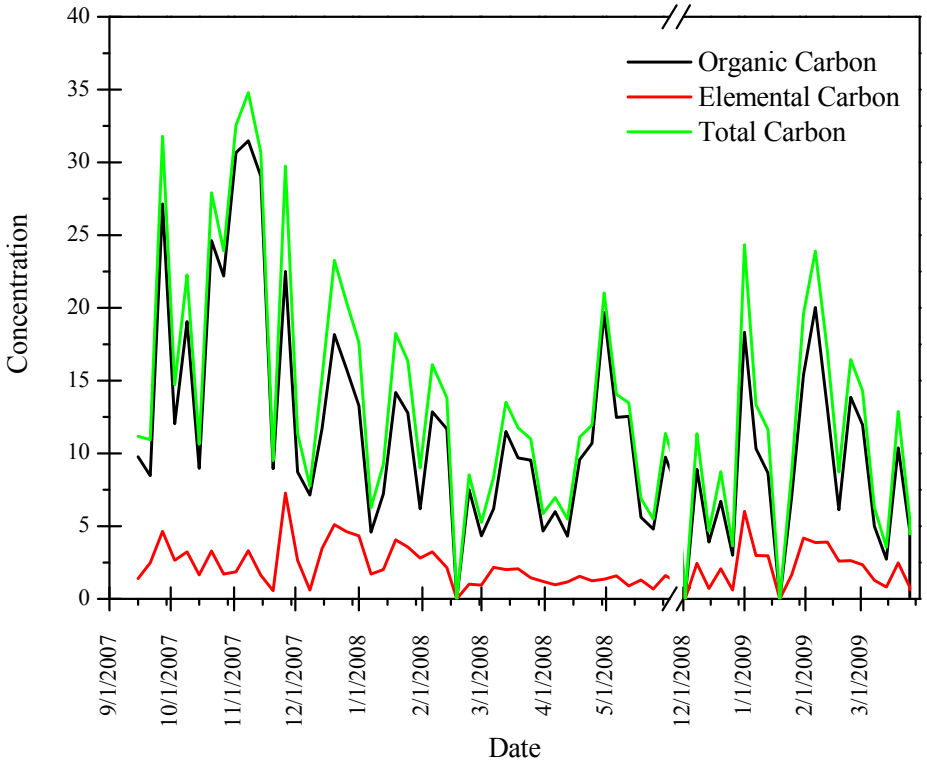

Figure 3-69 Variation of organic, elemental, and total carbon at South Valley

3.1.6 Comparison with NATTS/UTAP Ambient Measurements

The concentrations of air toxics were also compared to levels of air toxics at 50 sites around the U.S. (Arizona, California, Colorado, Washington DC, Florida, Illinois, Indiana, Kentucky, Massachusetts, Michigan, Mississippi, Missouri, New Jersey, New York, Oklahoma, Puerto Rico, Rhode Island, South Carolina, South Dakota, Tennessee, Texas, Utah, Vermont, Washington, and Wisconsin) as shown in Figure 3-70 through Figure 3-72. Note that for PAHs and heavy metals, only wintertime concentrations were measured in this study as compared to annual averages in the NATTS/UATP network. The comparisons also include the USEPA's RfC and URE values. Note that there are RfC and URE threshold values for a limited number of air toxics.

For PAHs, the concentrations measured at the three locations were within the range of those measured elsewhere in the U.S. and significantly lower than threshold values for chronic non-cancer and cancer health effects. Elevated concentrations of perylene, anthracene, acenaphthylene, and benzo(k)fluoranthene at the North Valley site are probably associated with increased emissions from wood burning in the winter (perylene is a tracer of wood burning and is not emitted from fossil fuel combustion). Detailed discussion of sources of PAHs is presented in Section 4.1.

Similarly, for heavy metals, ambient concentrations measured in this study were comparable (or lower) to those measured at NAATTS/UATP sites and lower than the

threshold values for chronic non-cancer and cancer health effects. Note that heavy metals were only measured during the winter.

The levels of 24-hr VOCs in Albuquerque were comparable to those measured nationally and at least five orders of magnitude lower than the USEPA's RfC and URE threshold values for non-cancer and 1-in-million cancer outcomes.

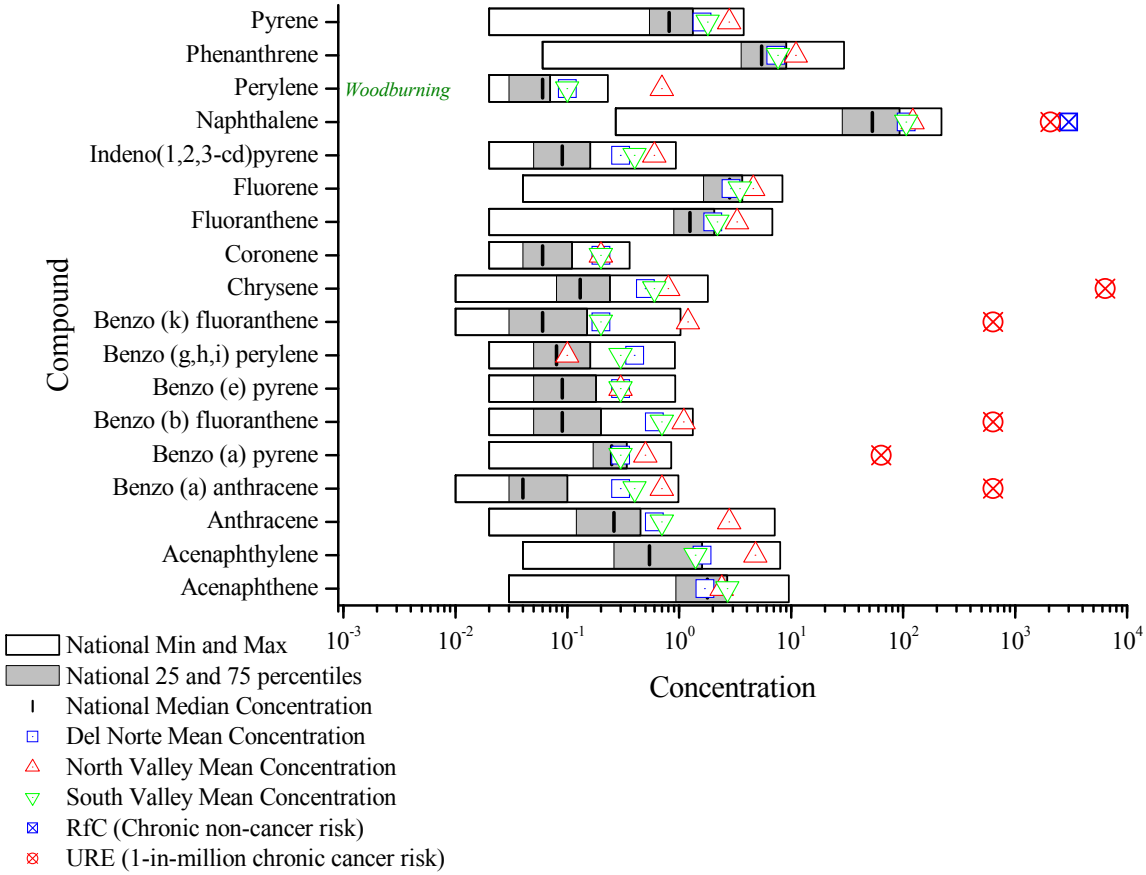

Figure 3-70 Comparison of mean concentrations of PAHs (in ng/m^3) measured at the three sites with those measured at NAATS/UATP sites and the RfC (non-cancer chronic inhalation; blue square) and URE (cancer chronic inhalation; red circle)

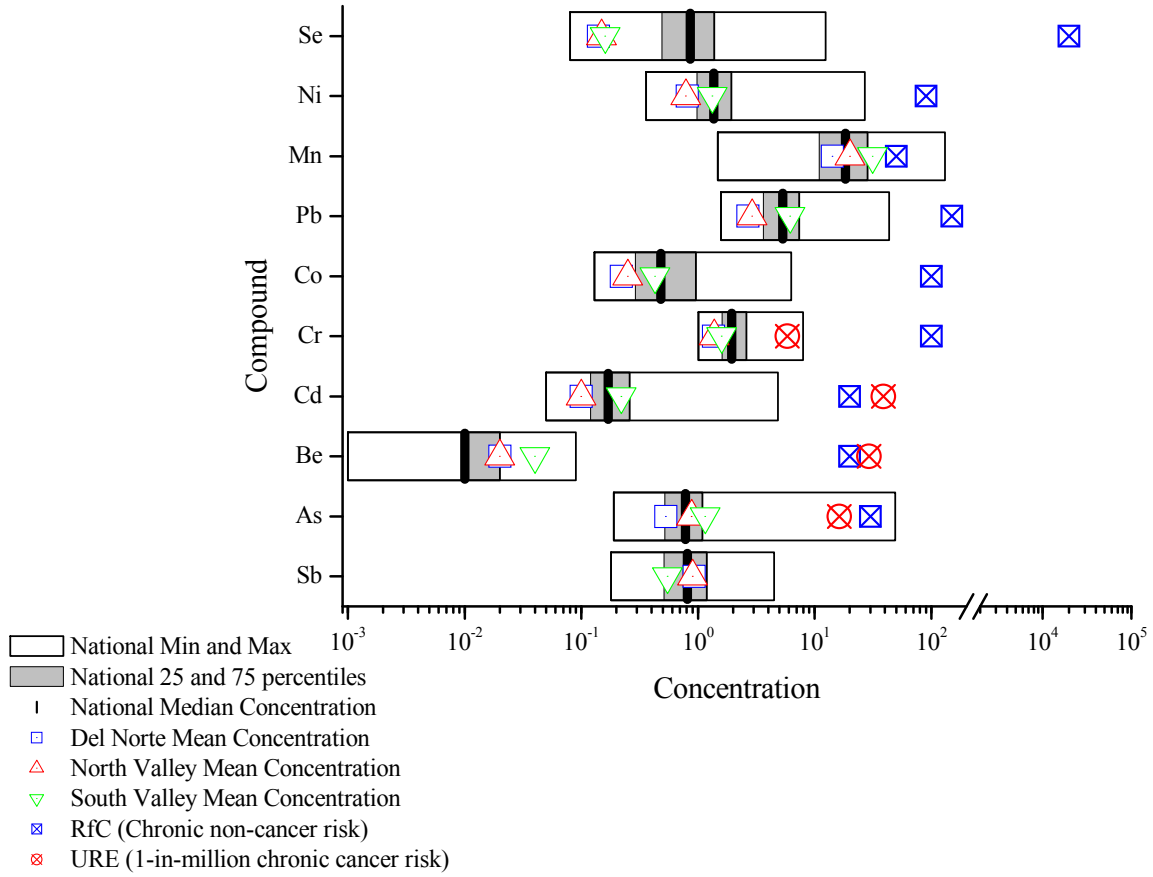

Figure 3-71 Comparison of mean concentrations of heavy metals (in ng/m^3) measured at the three sites with those measured at NAATS/UATP sites and the RfC (non-cancer chronic inhalation; blue square) and URE (cancer chronic inhalation; red circle)

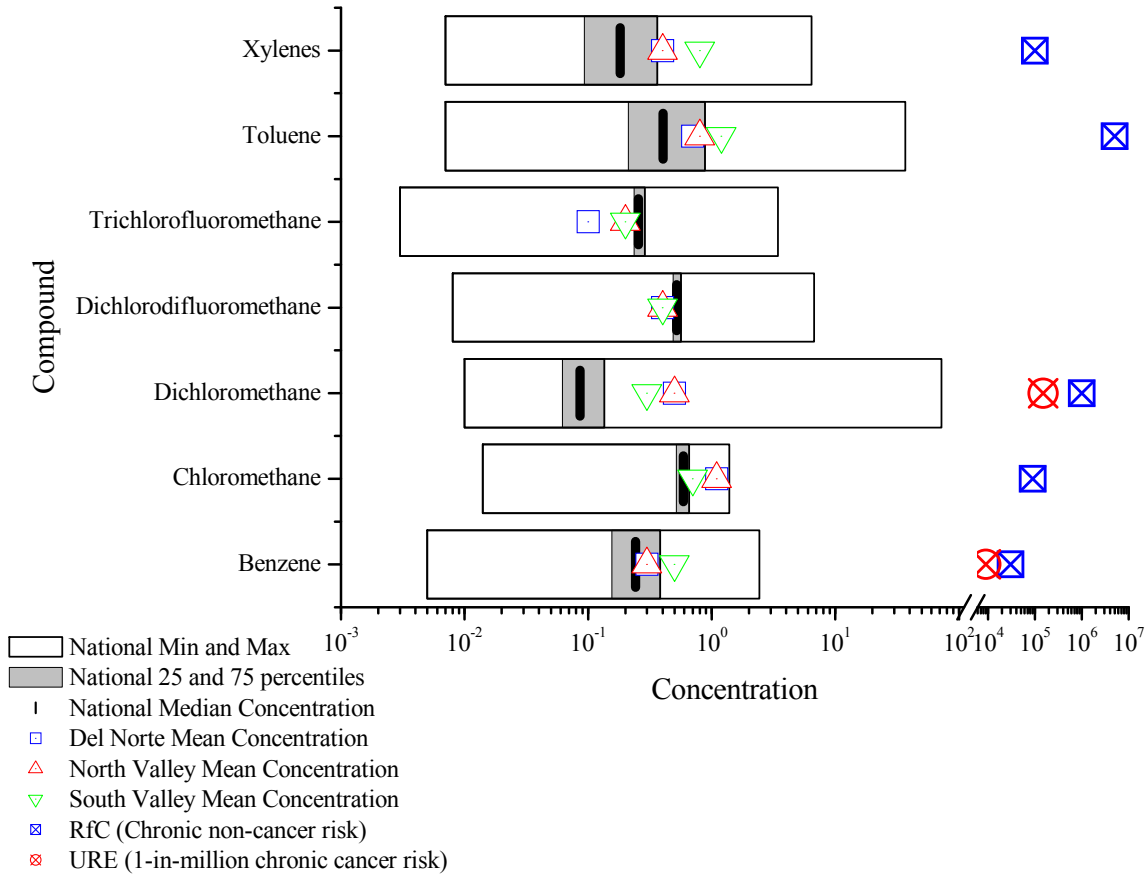

Figure 3-72 Comparison of mean concentrations of VOCs measured at the three sites with those measured at NAATS/UATP sites and the RfC (non-cancer chronic inhalation; blue square) and URE (cancer chronic inhalation; red circle)

3.2 Temporal Variability

This section evaluates the seasonal (for VOCs, EC, and OC), day-of-the-week (for VOCs, EC, and OC) and hourly (for VOCs) trends. PAHs and heavy metals were only measured during the winter.

3.2.1 Seasonal Variation

Given the number of samples collected per month, two periods were defined: a warm period from April 15 to October 15 and a cold period from October 15 to April 15. The mean (and standard deviation) concentration of VOCs, EC, and OC during the warm and cold periods are reported in Table 3-3 through Table 3-6 for the three sites. In addition, the outputs of the *t*-test (*F*-ratio and significance level) used to test the null hypotheses

$$H_{o,i}: \mu_{warmperiod} = \mu_{\text{coldperiod}}$$

are also presented. The null hypothesis, tested at the $\alpha = 0.05$ significance level, was that the VOC concentrations were not different for each period. Results showing statistically significant *F*-values (with *p*-value < 0.05) indicated that the between-groups variation

was higher than that estimated within groups and therefore the null hypothesis was rejected.

Aromatic hydrocarbons emitted from traffic (benzene and its alkylated derivatives) also showed a strong seasonal profile for the Del Norte site, but not for the other two sites. While traffic characteristics were not measured in this study, this variability may be caused by the increased traffic emissions from school buses at the adjacent high school, in San Mateo and Montgomery Blvds., and/or the shallow boundary layer in morning.

Table 3-3 Mean (and standard deviation) concentrations of individual VOCs measured at Del Norte during the warm and cold periods, the *F*-ratio, and significance of the mean difference between the two periods

	Warm Period			Cold Period			t-test	
	n	Mean	σ	n	Mean	Σ	F	*p*-value
Benzene	21	0.2	0.1	42	0.4	0.3	9.766	0.003
Chloromethane	8	1.0	1.0	34	1.2	2.5	0.092	0.764
Trichlorofluoromethane	21	0.2	0.0	43	0.2	0.1	0.289	0.593
Dichlorodifluoromethane	22	0.4	0.1	44	0.5	0.2	0.980	0.326
Methylene Chloride	15	0.4	0.5	42	0.5	0.5	0.360	0.551
Toluene	21	0.5	0.2	44	0.9	0.7	7.886	0.007
m/p-Xylenes	21	0.3	0.1	40	0.5	0.3	9.216	0.004
o-Xylene	21	0.1	0.0	34	0.2	0.1	13.859	0.000

Table 3-4 Mean (and standard deviation) concentrations of individual VOCs measured at North Valley during the warm and cold periods, the *F*-ratio, and significance of the mean difference between the two periods

	Warm Period			Cold Period			t-test	
	n	Mean	σ	n	Mean	σ	F	Sign.
Benzene	26	0.3	0.1	40	0.4	0.3	6.477	0.013
Chloromethane	13	1.1	0.3	26	1.2	1.0	2.398	0.130
Trichlorofluoromethane	26	0.2	0.0	38	0.2	0.1	1.604	0.210
Dichlorodifluoromethane	26	0.5	0.1	40	0.5	0.1	0.109	0.743
Methylene Chloride	17	0.7	1.5	42	0.5	0.7	1.381	0.245
Toluene	25	0.9	0.5	37	0.9	0.6	0.632	0.430
m/p-Xylenes	26	0.4	0.3	33	0.4	0.3	0.126	0.724
o-Xylene	23	0.1	0.1	32	0.2	0.1	0.342	0.561

Table 3-5 Mean (and standard deviation) concentrations of individual VOCs measured at South Valley during the warm and cold periods, the *F*-ratio, and significance of the mean difference between the two periods

	Warm Period			Cold Period			t-test	
	n	Mean	σ	n	Mean	σ	F	Sign.
Benzene	16	0.4	0.5	38	0.6	0.4	0.005	0.946
Chloromethane	7	0.5	0.2	29	0.8	0.6	1.975	0.169
Trichlorofluoromethane	19	0.2	0.1	36	0.2	0.1	2.515	0.119
Dichlorodifluoromethane	19	0.4	0.2	37	0.5	0.2	0.289	0.593
Methylene Chloride	19	0.4	0.5	44	0.4	0.3	0.778	0.381
Toluene	17	1.0	1.5	38	1.3	1.2	0.004	0.949
m/p-Xylenes	17	0.6	0.8	37	0.7	0.6	0.001	0.978
o-Xylene	13	0.3	0.3	34	0.3	0.2	0.092	0.763

With respect to seasonal variation of OC and EC, distinct differences were observed among the three sites. For Del Norte, EC and OC concentrations measured during the cold period were higher than those measured during the warm period. This may be indicative of seasonal variations of emission from sources nearby the monitoring site (e.g. school buses and traffic in Del Norte). This trend was also observed at North Valley. However, no significant differences were observed in South Valley.

Table 3-6 Mean (and standard deviation) concentrations of organic carbon and elemental carbon measured during the warm and cold periods, the *F*-ratio, and significance of the mean difference between the two periods

	Warm Period			Cold Period			T-test	
	n	Mean	σ	n	Mean	σ	F	Sign.
Del Norte								
Total OC	19	7.4	1.9	48	9.0	4.2	7.178	0.009
Total EC	19	1.6	0.8	48	2.5	1.5	6.499	0.013
Total C	19	9.0	2.5	48	11.6	5.5	7.238	0.009
North Valley								
Total OC	13	9.9	2.8	48	10.4	5.7	7.561	0.008
Total EC	13	1.9	1.0	48	2.6	1.9	2.833	0.098
Total C	13	11.8	3.5	48	13.0	7.3	6.745	0.012
South Valley								
Total OC	15	11.9	5.9	47	11.7	7.3	1.011	0.319
Total EC	15	1.8	1.0	47	2.5	1.5	2.284	0.136
Total C	15	13.7	6.7	47	14.2	8.2	1.691	0.198

3.2.2 Weekday/Weekend Variation

The weekday/weekend variation of VOCs, OC, and EC at the Del Norte, North Valley, and South Valley sites are depicted in Figure 3-73 through Figure 3-78. In addition, one-way analysis of variance was used to test the null hypotheses

$$H_{o,i}: \mu_{weekday} = \mu_{weekend}$$

which assumes that there was no difference in the concentration of a given *i* parameter by the day of the week.

The lowest concentrations for VOCs, especially for aromatic VOCs at Del Norte, were measured on Sundays, probably due to reduced emissions from traffic on Sundays as compared to weekdays. An increase was observed beginning on Mondays, followed by a moderate decrease on Tuesdays and Wednesdays. Ambient levels increased on Thursdays and Fridays. In most cases, the Saturday mean concentration was comparable to that measured on Sundays. The difference between the highest concentrations and those measured on Sundays were generally greater than 70 percent. The highest difference was measured for methylene chloride (237 percent). Similar weekly profiles were also observed at the North Valley and South Valley sites. The concentrations for weekdays were comparable to those measured on Saturdays. The difference between the highest weekday and Sunday concentrations were between 20 and 70 percent (481 percent for methylene chloride) at North Valley and higher than 150 percent (only 29 percent for chloromethane) at South Valley.

For EC and OC, a strong weekday/weekend variation was also observed, with the lowest concentrations being measured during the weekend and the highest concentrations being measured on Tuesdays at Del Norte and North Valley and Thursdays at South Valley. A decrease of EC and OC concentrations was also observed on Wednesdays at Del Norte and North Valley. On average, the concentrations of EC and OC measured during the weekdays were up to 500 percent more than those measured during weekdays.

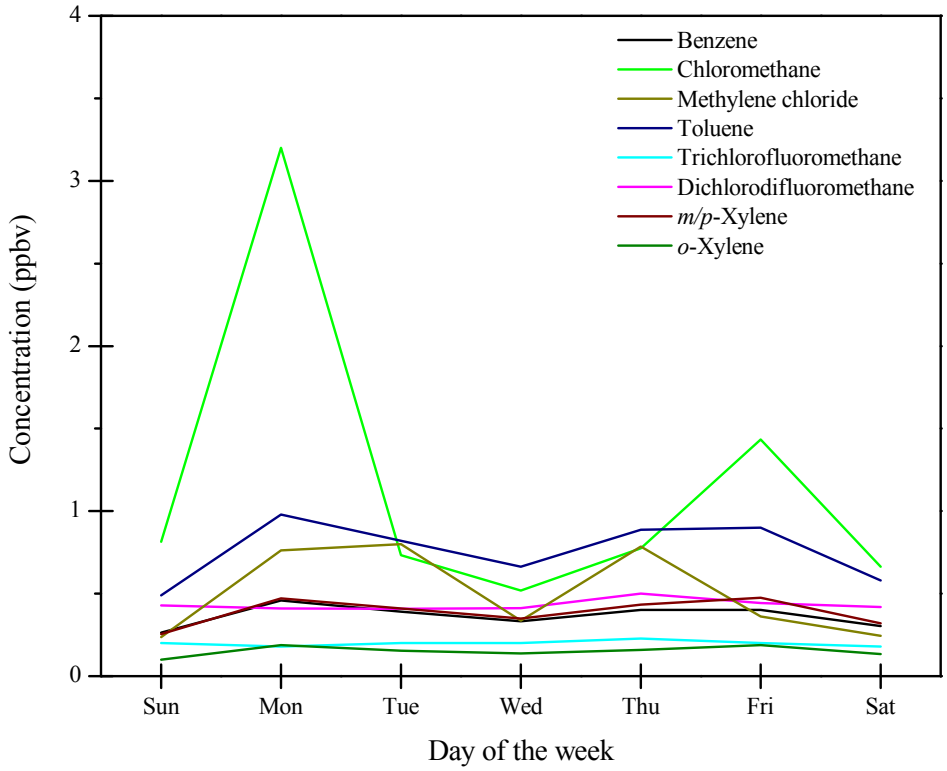

Figure 3-73 Day-of-the-week variation of VOCs at Del Norte

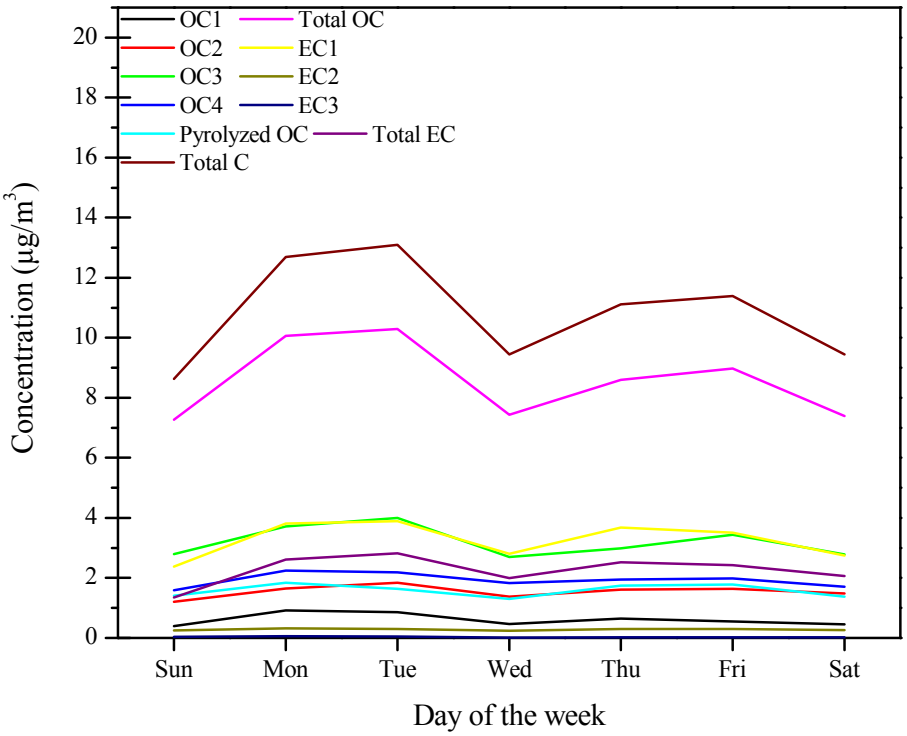

Figure 3-74 Day-of-the-week variation of VOCs at North Valley

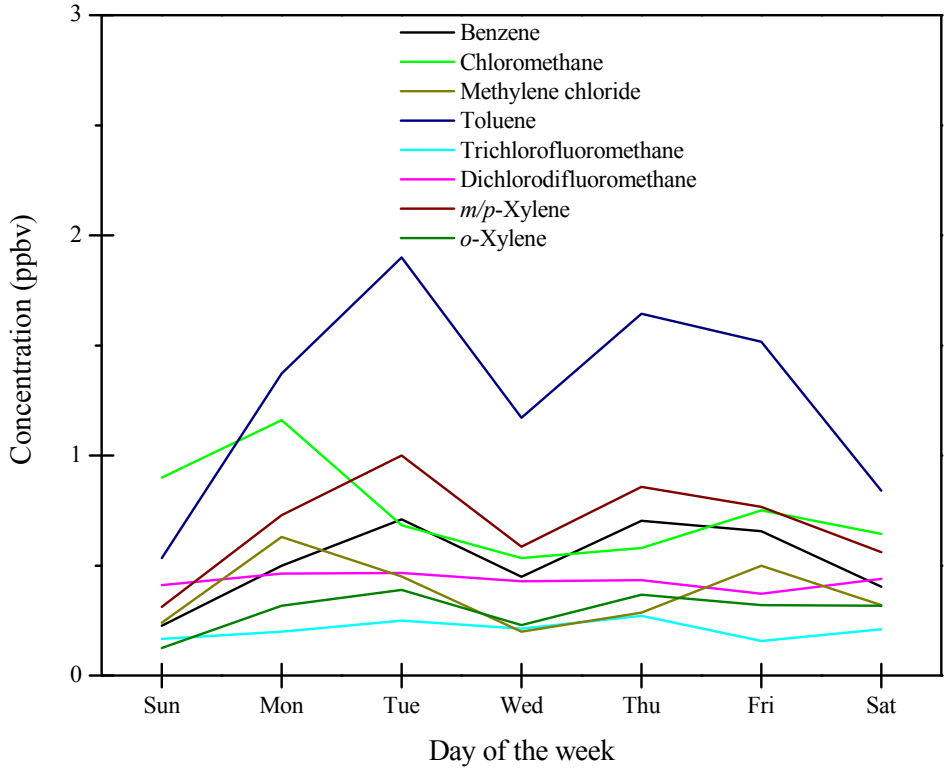

Figure 3-75 Day-of-the-week variation of VOCs at South Valley

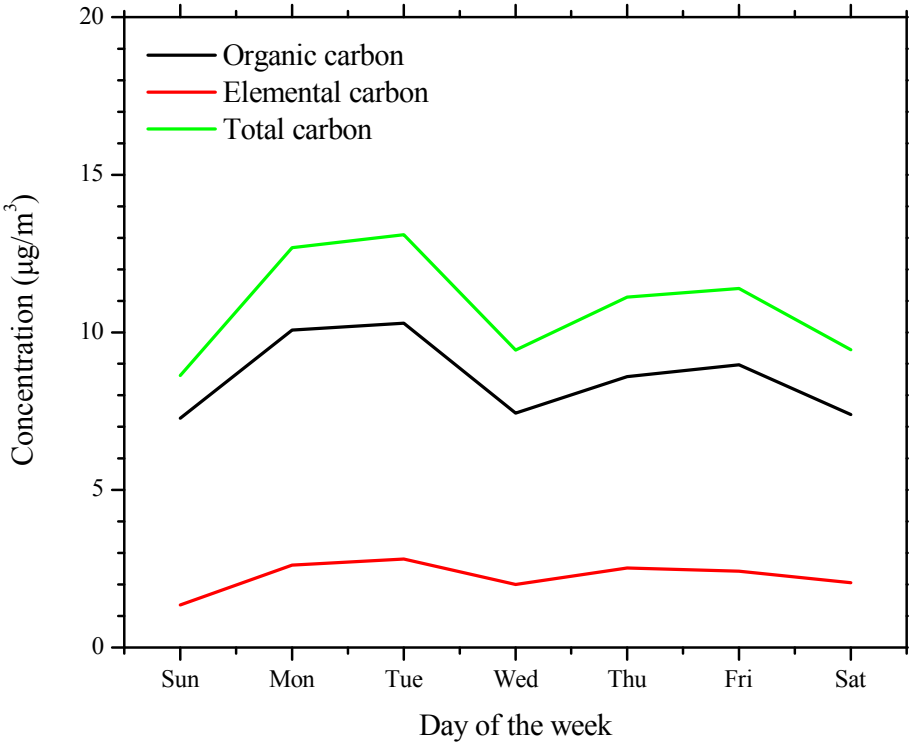

Figure 3-76 Day-of-the-week variation of organic carbon and elemental carbon at Del Norte

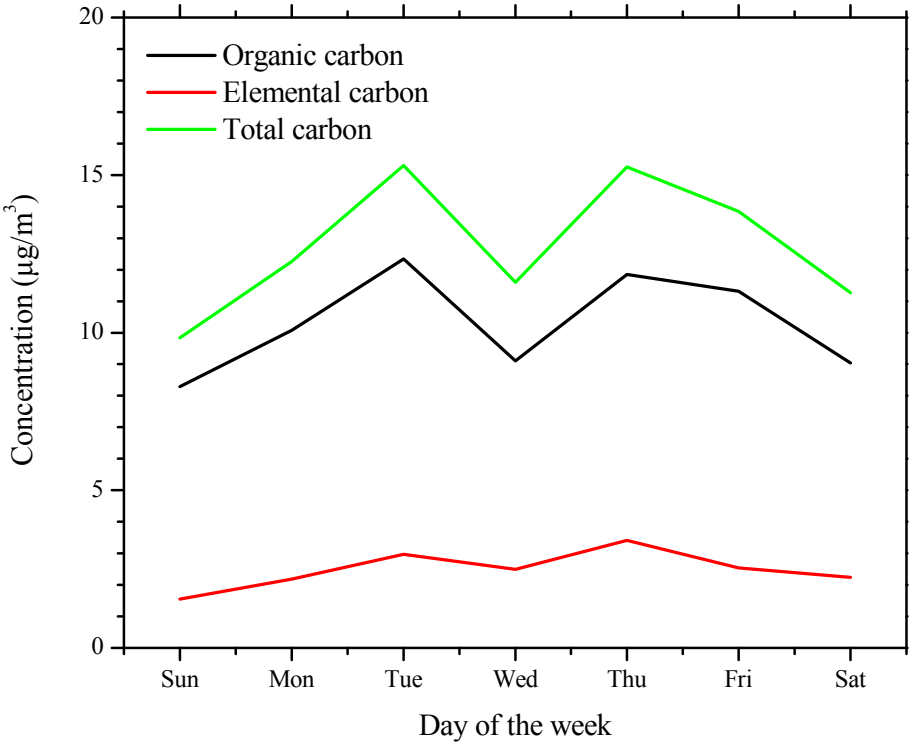

Figure 3-77 Day-of-the-week variation of organic carbon and elemental carbon at North Valley

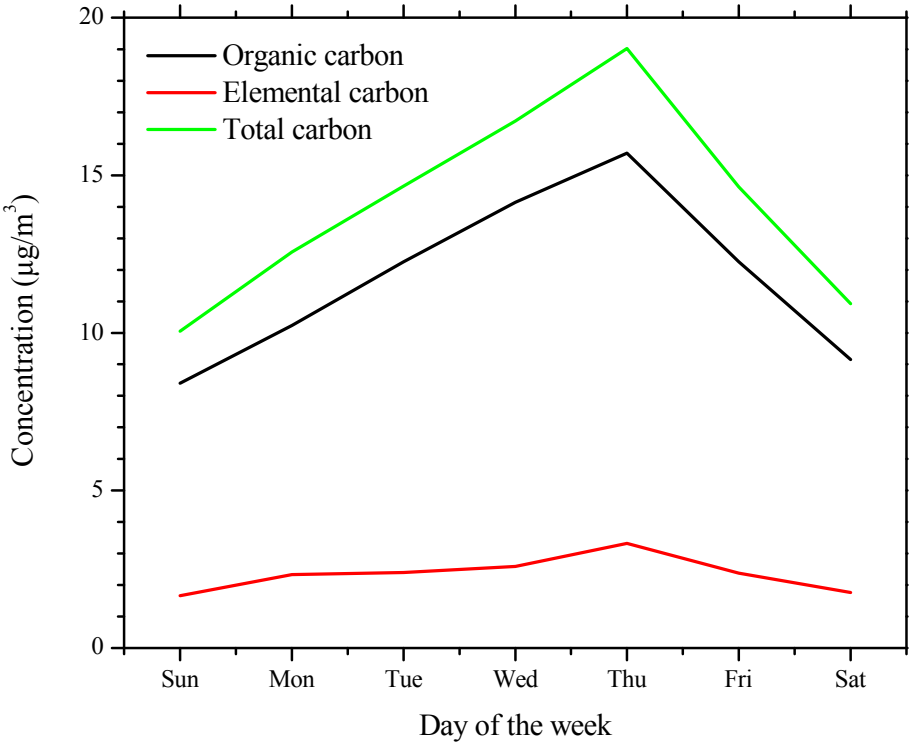

Figure 3-78 Day-of-the-week variation of organic carbon and elemental carbon at South Valley

3.2.3 Hourly Variation

Figure 3-79, Figure 3-80, and Figure 3-81 show the variation of aromatic (and 1,3-butadiene) hydrocarbons and chlorinated hydrocarbons at the Del Norte site for both IMPs. The diurnal profiles of aromatic hydrocarbons followed a typical two-mode pattern with local maxima in the early morning (peak at 9:00-10:00) and the evening (20:00-21:00). More specifically, the concentrations increased rapidly in the early morning, reaching their maximum levels at about 9:00 because of traffic emissions during the morning rush hours (6:00-9:00). Then, levels followed a downward trend until the early afternoon. The lowest concentration was measured at 18:00.

The first mode was clearly associated with commuter traffic. The second mode was less pronounced. Finally, a single-mode pattern with a maximum at 15:00 was observed for heavier aromatic hydrocarbons (1,2,4-trimethyl-benzene, 1,3,5-trimethylbenzene and 1-ethyl-4-methylbenzene). For chlorinated hydrocarbons, the highest concentrations were measured in the afternoon (14:00 – 17:00); however, a less clear diurnal profile was observed for most of them.

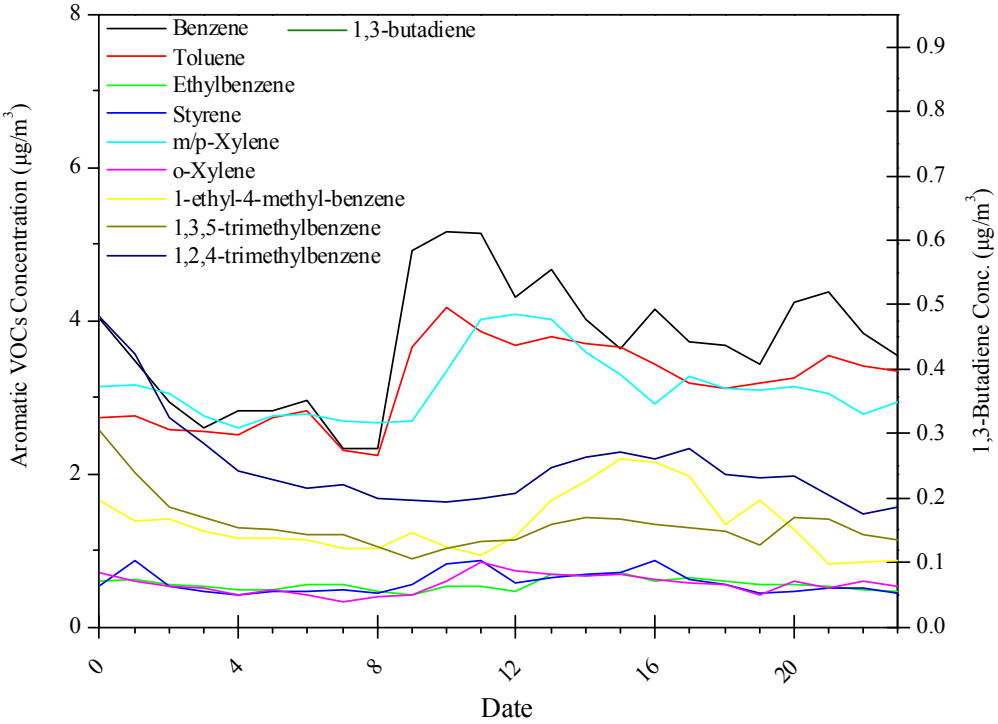

Figure 3-79 Hourly variation of hydrocarbons at Del Norte

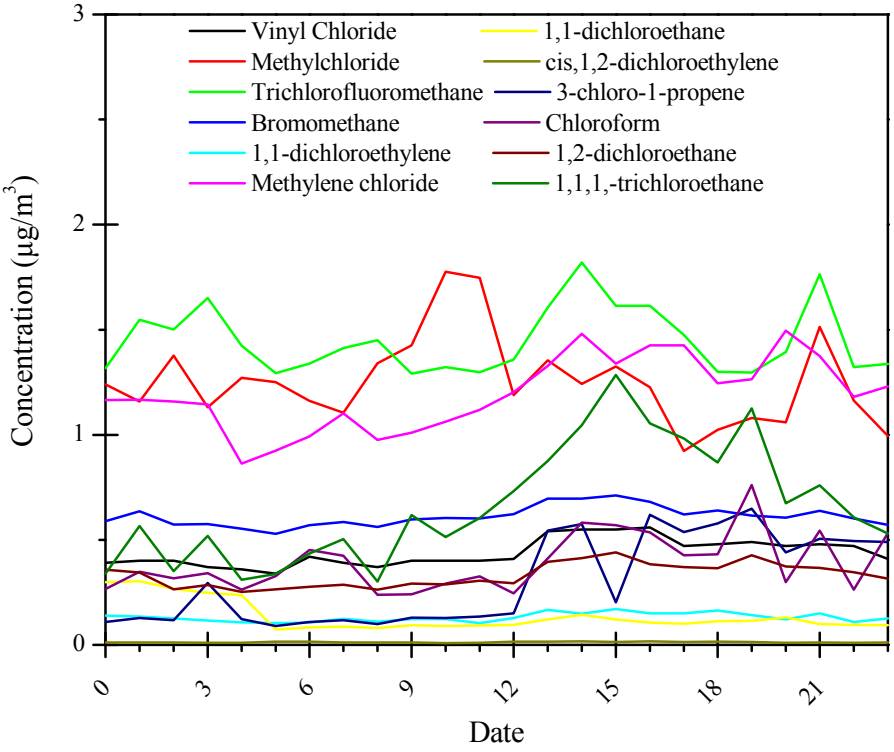

Figure 3-80 Hourly variation of chlorinated hydrocarbons at Del Norte

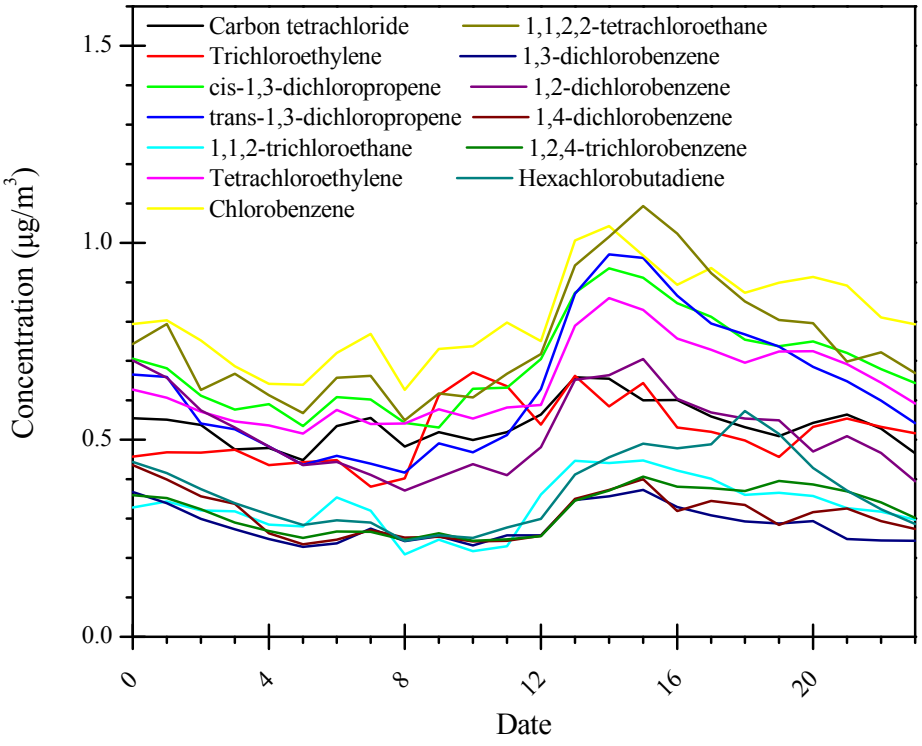

Figure 3-81 Hourly variation of chlorinated hydrocarbons at Del Norte

3.3 Spatial and Temporal Correlations

The purpose of this section is to determine the spatial and temporal characteristics of air toxics using a set of data analysis tools. These include:

- The Pearson correlation coefficient (r) to determine whether there is a uniform temporal profile (concentrations decrease or increase simultaneously). Pearson's correlation reflects the degree of linear relationship between two variables. High (>0.70) correlation coefficient values indicate a positive linear relationship between variables, while negative values suggest a strong inverse correlation.
- The absolute (ΔC) and the relative difference ($\%\Delta C/Ref$) of 24-hr paired concentration differences between two sites. The relative difference was computed as the percentage of the absolute concentration difference to the reference site concentration. For the needs of this study, we used Del Norte as a reference site for air toxics because of its central location with respect to the other sites in Albuquerque. Positive values indicate that air toxics concentrations at the site were higher than those measured at Del Norte. Median absolute and relative differences provided an indication of systematic differences between the sites, whereas site-to-site variation was quantified using the standard deviation.
- The coefficient of divergence (COD) was used to assess the spatial uniformity of measurements with respect to the concentration levels. The COD was estimated as follows:

$$COD = \sqrt{\frac{1}{p} \cdot \sum_{i=1}^{p} \left(\frac{C_{ij} - C_{ik}}{C_{ij} + C_{ik}} \right)^2}$$

where p is the total number of paired measurements and C_{ij} and C_{ik} are the measured concentrations at the reference and comparison sites on the i-th day, respectively. The COD was computed using 24-hr concentrations at Del Norte for the reference values. COD values vary from 0 to 1, with COD values close to unity being indicative of strong spatial variation.

3.3.1 PAHs

Figure 3-82 shows the correlation coefficient for individual PAHs for the three monitoring sites. PAHs can be categorized in two groups based on the variation of correlation coefficient for each pair of measurement sites. The first group is composed of low molecular weight (MW) PAHs, from naphthalene to pyrene, in which a large variation of R values (from 0.15 to 0.98) was observed. On the other hand, for heavier PAHs (from cyclopenta[cd]pyrene to coronene), similar R values were computed for each pair of measurement sites, indicating a uniform temporal variation. These variations may be explained by differences in emission and atmospheric lifetimes. For example, low MW PAHs mostly originate from sources with strong spatial variation, such as oil residues and fugitive emissions, whereas heavier PAHs are produced primarily from combustion-related processes (e.g. vehicular engines) that tend to be homogeneously distributed in an urban area. In addition, PAH lifetimes may vary from a few hours to years for photolysis and reactions with atmospheric oxidants (the lifetime of the benzo[a]anthracene that is absorbed on coal fly ash and wood smoke are >1000 hours and 25 min, respectively (Kamens, et al. 1988)). They depend on a large numbers of factors,

including atmospheric conditions, the phase (gas/particle), and the physical and chemical composition of particulate matter.

In a previous study, the ratios of benzo[a]pyrene to benzo[e]pyrene (BaP/BeP) and perylene to benzo[e]pyrene (Per/BeP) were applied to determine reaction-related losses of PAHs (Arey, et al. 1987). For the three monitoring sites in Albuquerque, the BaP/BeP ratio varied from 0.81 to 1.09, which is close to the values estimated by Arey et al. (1987) for nighttime PAHs (0.76), indicating that degradation of PAHs was not significant. Similarly, the Per/BeP ratio (from 0.16 to 0.21) was comparable to that computed at night. The relative importance of different sources at each monitoring site may account for the observed differences of the correlation coefficients.

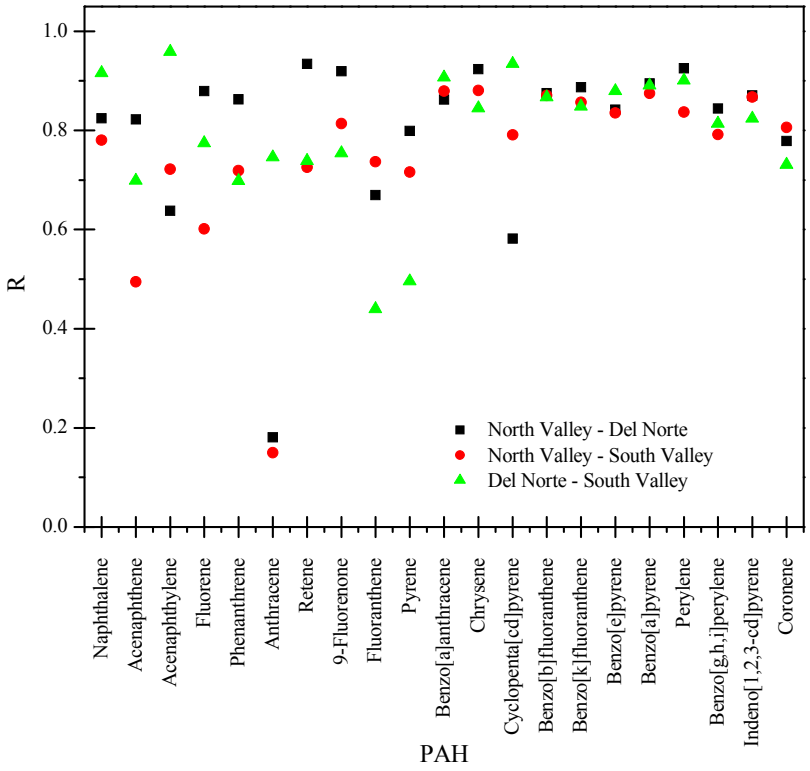

Figure 3-82 Pearson correlation coefficients of paired measurements for individual 24-hr PAHs

Table 3-7 shows the distribution (median and standard deviation) of the 24-hour absolute (ΔC) and relative differences (%ΔC/Ref) among measurements at South Valley, North Valley, and Del Norte. In general, median ΔC and %ΔC/Ref values were high, indicating a strong spatial variation in the valley on a day-to-day basis. This was more pronounced for the North Valley site, where levels of individual PAHs were from 40 to 420 percent higher than those measured at Del Norte. The spatial pattern of PAH concentrations was also demonstrated by the high COD values. The analysis of the site-to-site variation of O_3 concentrations, expressed by the standard deviation of %ΔC/Ref values, suggested strong local common characteristics for each site, probably due to differences in source contributions.

Table 3-7 Absolute (ΔC) and relative (%ΔC/Fixed) differences (median and σ) of daily concentrations of PAHs, and mean COD for all PAHs (Del Norte site was used as the reference site).

	North Valley					South Valley				
	Median ΔC	σ (ΔC)	Median % $\Delta C/C_{ref}$	σ (%ΔC)	COD	Median ΔC	σ (ΔC)	Median %$\Delta C/C_{ref}$	σ (%ΔC)	COD
Naphthalene	28.6	45.8	47.5	58.3	0.975	23.9	20.5	27.4	35.8	0.974
Acenaphthylene	2.0	4.1	159.1	533.4	0.287	0.0	0.6	7.4	122.9	0.432
Acenaphthene	0.5	2.9	44.9	134.0	0.559	1.6	1.1	124.3	99.3	0.352
Fluorene	1.1	2.6	42.8	63.1	0.517	1.4	1.0	41.4	59.9	0.500
Phenanthrene	3.5	5.0	57.9	70.2	0.753	1.5	2.7	23.9	64.1	0.715
Anthracene	1.1	5.9	152.0	1198.7	0.460	0.2	0.4	58.4	110.1	0.428
Retene	1.0	2.5	105.0	176.7	0.428	0.0	1.4	15.8	158.4	0.408
9-Fluorenone	1.1	1.2	75.8	67.2	0.317	0.4	0.6	33.0	80.2	0.276
Fluoranthene	1.2	1.7	50.0	76.2	0.383	0.4	1.1	24.2	77.2	0.339
Pyrene	1.1	1.5	65.1	80.7	0.512	0.3	0.9	27.6	83.7	0.665
Benzo[a]anthracene	0.3	0.6	166.4	223.1	0.346	0.0	0.2	17.6	157.5	0.304
Chrysene	0.4	0.8	94.4	126.1	0.341	0.1	0.4	50.0	113.4	0.482
Cyclopenta[cd]pyrene	0.5	0.4	418.2	626.6	0.585	0.1	0.1	83.3	100.0	0.759
Benzo[b]fluoranthene	Aq0.4	Qaa	103.8	Qaa	Q	0.0	0.4	27.3	108.3	0.472
Benzo[k]fluoranthene	0.1	0.2	90.6	179.3	0.674	0.0	0.1	7.7	114.1	0.774
Benzo[e]pyrene	0.2	0.3	85.5	155.0	0.554	0.0	0.2	20.0	87.8	0.656
Benzo[a]pyrene	0.2	0.5	120.0	217.6	0.512	0.0	0.2	5.0	147.2	0.690
Perylene	0.1	0.1	133.3	88.4	0.857	0.0	0.0	16.7	71.4	0.904
Benzo[g,h,i]perylene	0.1	0.3	57.7	98.0	0.572	0.0	0.1	10.5	68.8	0.626
Indeno[1,2,3-cd]pyrene	0.1	0.4	91.6	108.6	0.549	0.0	0.2	14.3	82.6	0.627
Coronene	0.0	0.1	9.2	87.3	0.757	0.0	0.1	25.0	69.6	0.763

3.3.2 Heavy Metals

Figure 3-83 shows the correlation coefficient for the heavy metals for the three monitoring sites. The *R* values ranged from 0.45 to 0.99, indicating a relatively uniform temporal variation of heavy metals concentrations among the three sites. Table 3-8 shows the distribution (median and standard deviation) of the 24-hour absolute (ΔC) and relative differences (%ΔC/Ref) among measurements at South Valley, North Valley, and Del Norte. In general, there were no significant differences between the North Valley and Del Norte sites. With the exception of Cr and Se, the levels of metals at South Valley were elevated to those measured at Del Norte. These may be associated with emissions from local activities. Note that these levels are lower than the RfC (for non-cancer) and URE (for cancer) threshold values (see Figure 3-71). An analysis of sources of heavy metals is presented later.

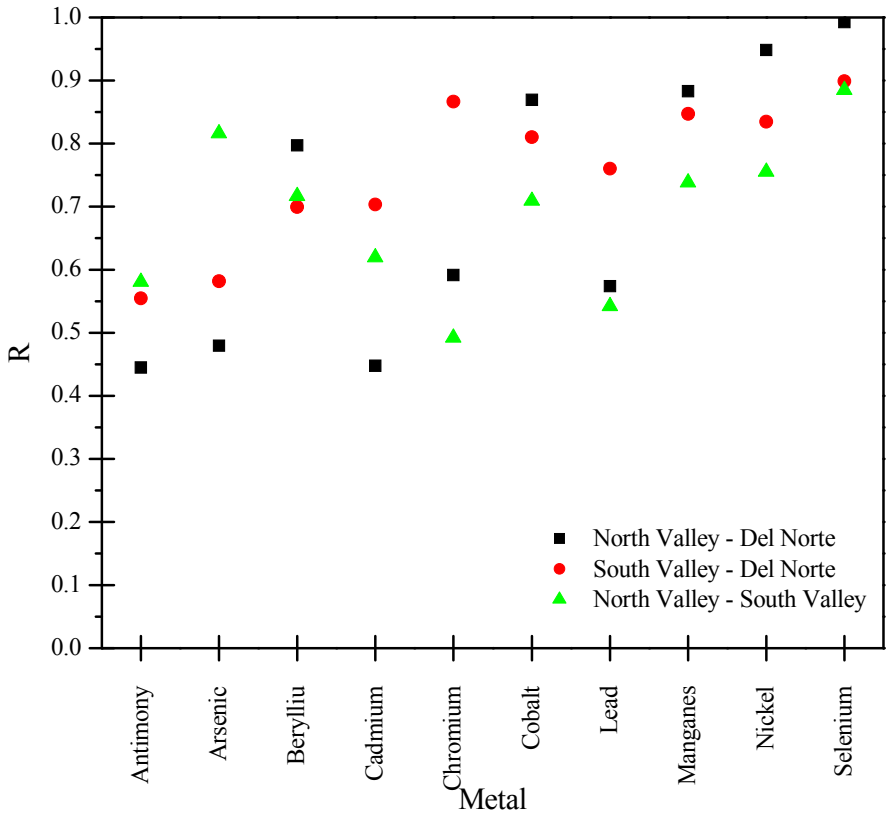

Figure 3-83 Pearson correlation coefficients of paired measurements for individual 24-hr heavy metals

Table 3-8 Absolute (ΔC) and relative (%ΔC/Fixed) differences (median and σ) of daily concentrations of heavy metals, and mean COD for all heavy metals (Del Norte site was used as the reference site).

	North Valley					South Valley				
	Median ΔC	σ (ΔC)	Median $\%\Delta C/C_{ref}$	σ (%ΔC)	COD	Median ΔC	σ (ΔC)	Median $\%\Delta C/C_{ref}$	σ (%ΔC)	COD
Antimony	-0.3	0.5	-48.6	73.4	0.349	-0.3	0.5	-57.1	45.9	0.380
Arsenic	0.1	1.2	42.2	138.2	0.329	0.2	0.9	105.0	185.4	0.411
Beryllium	0.0	0.0	0.0	0.0	0.346	0.0	0.0	100.0	104.1	0.447
Cadmium	0.0	0.1	-7.7	80.0	0.231	0.1	0.1	91.7	97.7	0.387
Chromium	0.0	0.4	-1.5	30.1	0.104	0.1	0.5	9.0	29.1	0.126
Cobalt	0.1	0.1	26.1	31.3	0.153	0.2	0.3	56.0	85.0	0.323
Lead	0.0	1.9	1.5	55.2	0.170	2.9	3.2	99.7	99.0	0.386
Manganese	7.5	6.0	50.5	39.0	0.226	12.1	18.9	114.2	84.6	0.372
Nickel	0.0	0.1	2.4	17.1	0.078	0.4	0.6	47.4	59.4	0.260
Selenium	0.0	0.0	10.0	23.4	0.110	0.0	0.1	16.7	41.3	0.162

3.3.3 VOCs

Figure 3-84 shows the correlation coefficient for individual VOCs for the three monitoring sites. Correlation coefficients vary from -1 to 0.6, indicating unrelated or poor temporal association between the sites. Table 3-7 shows the distribution (median and standard deviation) of the 24-hour absolute (ΔC) and relative differences (%ΔC/Ref) among measurements at the South Valley, North Valley, and Del Norte sites. The high median and standard deviation %ΔC/Ref values indicated a strong spatial variation in the valley on a day-to-day basis. A rather moderate spatial variation was suggested by the low COD values. Overall, it appeared that VOCs were strongly dependent on a daily basis on local sources near the site such as the traffic emissions, domestic heating emissions, AC units, and dry cleaners.

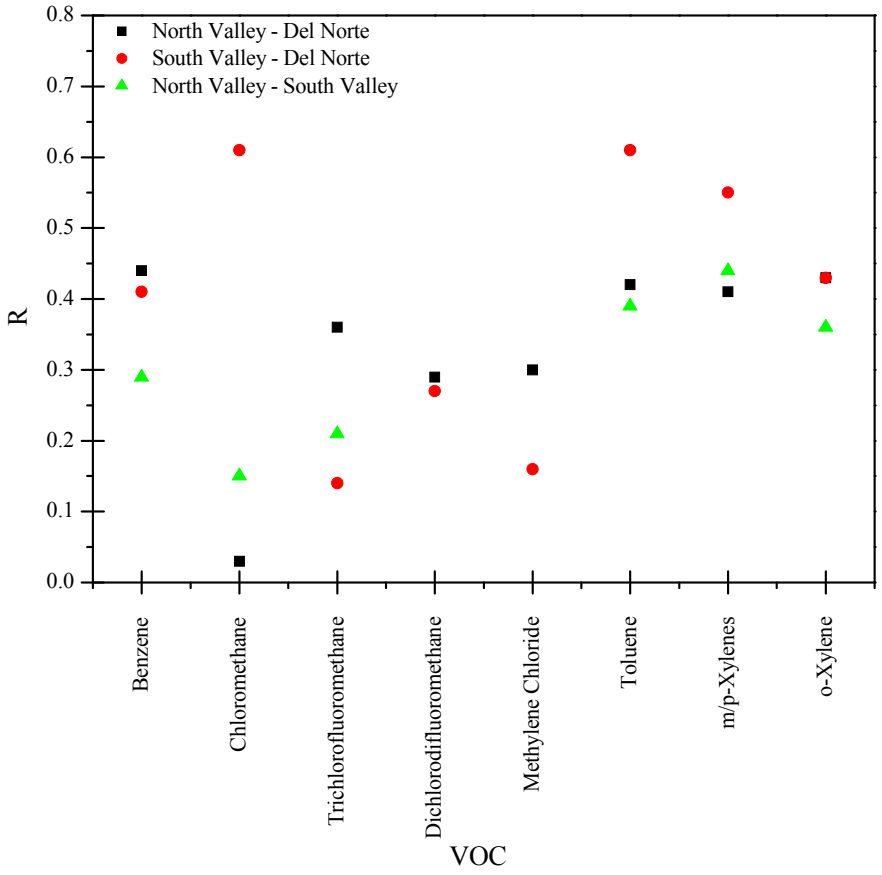

Figure 3-84 Pearson correlation coefficients of paired measurements for individual 24-hr VOCs

Table 3-9 Absolute (ΔC) and relative (%ΔC/Fixed) differences (median and σ) of daily concentrations of VOCs, and mean COD for individual VOCs (Del Norte site was used as the reference site).

	North Valley					South Valley				
	Median ΔC	σ (ΔC)	Median %ΔC/C_{ref}	σ (%ΔC)	COD	Median ΔC	σ (ΔC)	Median %ΔC/C_{ref}	σ (%ΔC)	COD
Benzene	0.1	0.3	33	141	0.354	0.1	0.4			0.366
Chloromethane	0.3	3.2	57	148	0.367	-0.1	2.6	-23	105	0.318
Trichlorofluoromethane	0.1	0.1	50	72	0.177	0.1	0.1	50	106	0.248
Dichlorodifluoromethane	0.1	0.2	25	106	0.235	0.1	0.2	20	115	0.273
Methylene chloride	-0.1	0.8	-25	201	0.336	-0.1	0.7	-40	351	0.377
Toluene	0.1	0.7	33	169	0.320	0.1	1.1	40	156	0.338
m/p-Xylenes	-0.1	0.3	-22	171	0.326	0.2	0.6	67	186	0.345
o-Xylene	0.1	0.2	100	92	0.222	0.2	0.3	100	235	0.367

3.3.4 Elemental Carbon and Organic Carbon

Figure 3-85 shows the correlation coefficient for OC, EC, and total carbon for the three monitoring sites. Table 3-10 shows the distribution (median and standard deviation) of the 24-hour absolute (ΔC) and relative differences (%ΔC/Ref) among measurements at the South Valley, North Valley, and Del Norte sites. The correlation coefficients for OC and EC fractions were higher than 0.5, indicating very good temporal associations among the three sites. Despite strong daily variation (as indicated by the high %ΔC/Ref standard deviation values), the comparison of concentrations showed that for the OC that account for the large of total t fraction of total carbon, there were no significant quantitative differences among the three sites. This was further supported by the low-to-moderate values of the COD.

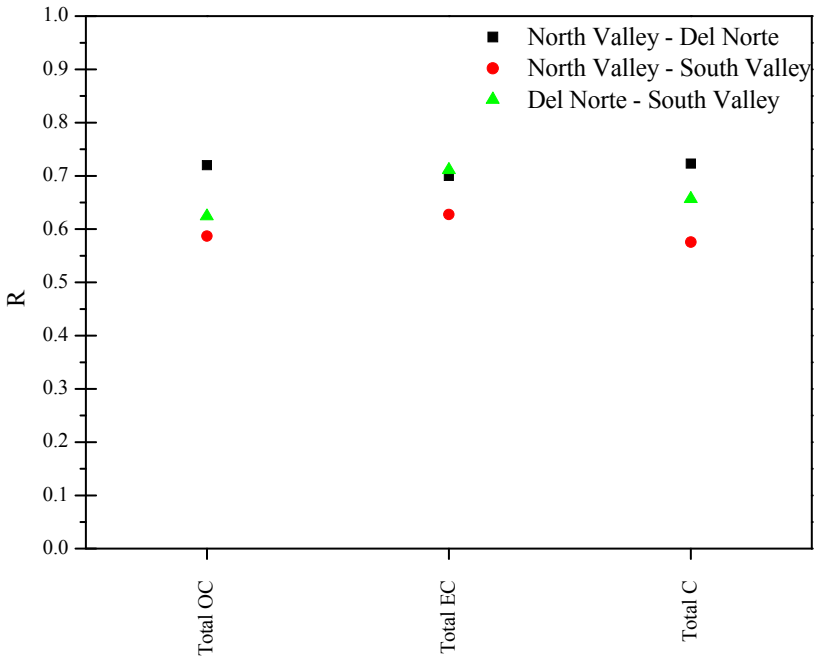

Figure 3-86 Pearson correlation coefficients of paired measurements for 24-hr TC, EC, OC

Table 3-10 Absolute (ΔC) and relative (%ΔC/Fixed) differences (median and σ) of daily concentrations of organic, elemental and total carbonm and mean COD for OC, EC, and total carbon (Del Norte site was used as the reference site).

	Median ΔC	σ (ΔC)	Median $\%\Delta C/C_{ref}$	σ (%ΔC)	COD
			North Valley		
Total OC	1.5	3.7	17.2	46.3	0.207
Total EC	-0.1	1.3	-3.9	63.0	0.237
Total Carbon	1.5	4.7	12.3	47.3	0.204
			South Valley		
Total OC	2.0	5.5	26.2	69.3	0.218
Total EC	-0.1	1.1	-8.5	58.7	0.209
Total Carbon	1.9	6.0	20.7	64.1	0.204

4 Advanced Analyses

4.1 Source Characterization

PAHs are ubiquitous pollutants of the atmosphere and originate primarily from combustion of contemporary and fossil organic material. Emissions from gasoline and diesel-powered vehicle exhaust, fugitive sources, unburnt oil residues, environmental tobacco smoke (ETS), wood burning, and industrial sources are the major sources of PAHs (Rogge, Hildemann, and Mazurek M, et al. 1993) (Rogge, Hildemann, et al. 1993) (Rogge, Hildemann, et al. 1994) (Benner, et al. 1995). PAH concentration diagnostic ratios (characteristic of anthropogenic emissions) are used to reconcile their presence in the atmosphere with potential emission sources (Grimmer, Jacob and Nauhack 1983) (Sicre, et al. 1987) (Pyyssalo, et al. 1987).

The PAHs concentration diagnostic ratios included:

(i) Fluoranthene to (Fluoranthene and Pyrene) [Fl/(Fl+Py)];
(ii) Benzo[a]anthracene to (Benzo[a]anthracene and Chrysene/Triphenylene (BaA/(BaA+CT)];
(iii) Benzo[e]pyrene to (Benzo[e]pyrene and Benzo[a]pyrene) [BeP/(BaP+BeP)] and;
(iv) Indeno[1,2,3-cd]pyrene to (Indeno[1,2,3-cd]pyrene and Benzo[ghi]perylene) [IP/(IP+BgP)].

Typical values for emissions sources, including the values measured in this study and in other urban, suburban, and rural locations are presented in Table 4-1. Note that values obtained from references were computed for particulate PAHs, while total PAHs (particulate and gas phase) were measured in this study. For PAHs from naphthalene to anthracene, more than 90 percent were in the gas phase (Finlayson-Pitts and Pitts, Chemistry of the Upper and Lower Atmosphere 1999). More than 50 percent of PAHs from fluorene to chrysene were usually in the gas phase, whereas more than 90 percent of heavier PAHs (from benzo[e]pyrene to coronene) were associated with particulate matter.

The mean [Fl/(Fl+Py)] ratio was similar for the three sites (from 0.56 ± 0.01 to 0.57 ± 0.01) and comparable to those computed from emissions from diesel and gasoline vehicles. In addition, [BaA/(BaA+CT)] mean values ranged from 0.32 ± 0.06 to 0.36 ± 0.02 and were similar to those calculated for diesel engines. For these two diagnostic ratios, the values were comparable to those measured in other urban and suburban locations, underscoring the contribution of traffic-related activities. The mean [BeP/(BeP+BaP)] obtained in our study values (from 0.49 ± 0.02 to 0.56 ± 0.02) compared with the corresponding values for used motor oil residues and wood combustion. The mean [IP/(IP+BgP)] values (from 0.479 ± 0.01 to 0.51 ± 0.01) were higher than those measured for cars and diesel emissions, but comparable to those observed in suburban locations and in Temuco, Chile (Kavouras, Koutrakis, et al. 2001) (Tsapakis, et al. 2002). The later urban area was characterized by significant contribution of wood burning emission to $PM_{2.5}$ and PAHs concentrations. The analysis of

concentration diagnostic ratios in Albuquerque indicated a mixed origin for with contributions from traffic and wood burning.

Table 4-1 PAHs concentration diagnostic ratios measured in Albuquerque compared to source ratios and other areas.

	Fl/(Fl+Py)	BaA/(BaA+CT)	BeP/(BeP+BaP)	IP/(IP+BgP)
This study				
Del Norte	0.57 ± 0.01	0.32 ± 0.03	0.56 ± 0.02	0.47 ± 0.01
North Valley	0.56 ± 0.01	0.36 ± 0.02	0.49 ± 0.02	0.51 ± 0.01
South Valley	0.56 ± 0.01	0.34 ± 0.02	0.53 ± 0.02	0.50 ± 0.01
Sources				
Diesel engines	0.60 - 0.70	0.38 - 0.64	0.29 - 0.40	0.35 – 0.37
Gasoline engines	0.40	0.43	0.60 - 0.80	0.18
Wood combustion	0.74	0.56	0.48	
Crude oil	0.18 ± 0.06	0.16 ± 0.12	0.87 ± 0.10	
Used motor oil	0.36 ± 0.08	0.50	0.64 ± 0.10	0.25 ± 0.05
ETS	0.46 ± 0.03	0.17 ± 0.03	0.34 ± 0.13	0.65 ± 0.13
Ambient aerosol				
Urban	0.54 ± 0.06	0.34 ± 0.02	0.70 ± 0.02	0.30 ± 0.02
Suburban	0.54 ± 0.17	0.31 ± 0.09	0.73 ± 0.15	0.59 ± 0.27
Rural	0.75 ± 0.11	0.20 ± 0.09	0.79 ± 0.09	0.61 ± 0.04
Santiago de Chile	0.41 ± 0.10	0.16 ± 0.08	0.46 ± 0.27	0.32 ± 0.22
Temuco	0.57 ± 0.08	0.41 ± 0.01	0.41 ± 0.08	0.47 ± 0.02

Figure 4-1 and Figure 4-2 show the relative distribution of emissions factors for three different types of woodstoves and concentrations of PAHs at the three sites, respectively. Emission factors were retrieved from USEPA AP-42 Chapter 1.10 Residential Wood Stoves (US EPA 1996). Catalytic and non-catalytic woodstoves decrease emissions using a ceramic catalyst coated with a noble metal and by mixing the smoke plume with fresh, preheated makeup air that enhances further combustion, respectively. The total emission factor for PAHs presented in Figure 4-1 were 0.443 lb/ton for conventional woodstoves, 0.269 lb/ton for non-catalytic woodstoves and 0.222 lb/ton for catalytic woodstoves. A comparison among the three woodstove types showed that there were significant qualitative differences for acenaphthylene (about 50 percent of conventional woodstove emissions and 30 percent for catalytic woodstove emissions), benzo(a)anthracene (5 and 10 percent for conventional and catalytic woodstoves emissions, respectively, and negligible amounts for non-catalytic woodstoves), and phenanthrene (about 35 percent for non-catalytic woodstoves and less than 25 percent for the other two types). The relative distribution of PAHs measured at the three sites (without naphthalene) showed that phenanthrene (more than 30 percent) was the dominant PAH followed by fluorene (more than 10 percent). The relative distribution profiles for all three sites were comparable among each other and similar to that observed for non-catalytic woodstoves.

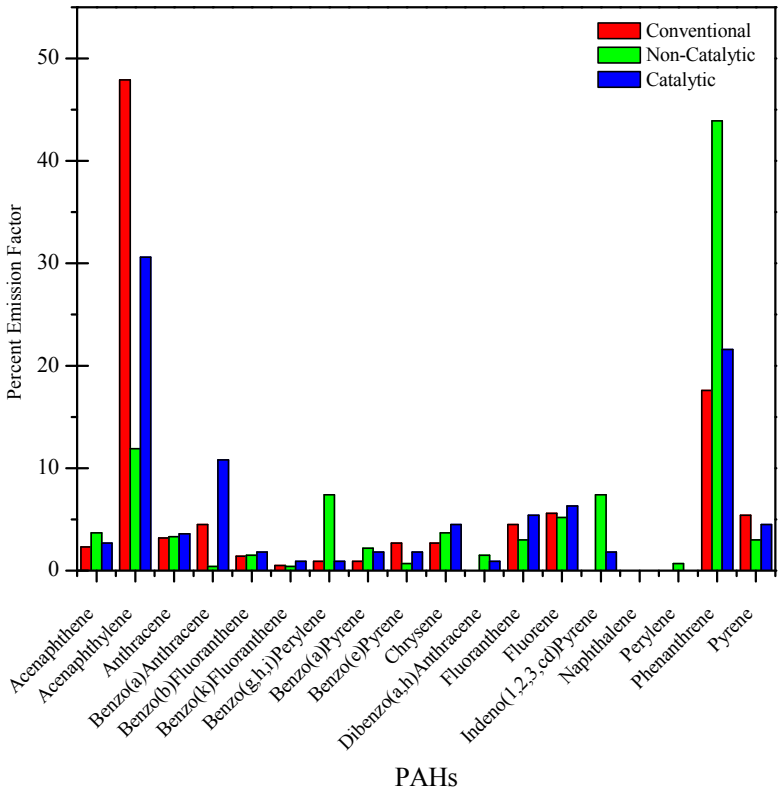

Figure 4-1 Relative distribution of PAHs emitted from different types of woodstoves

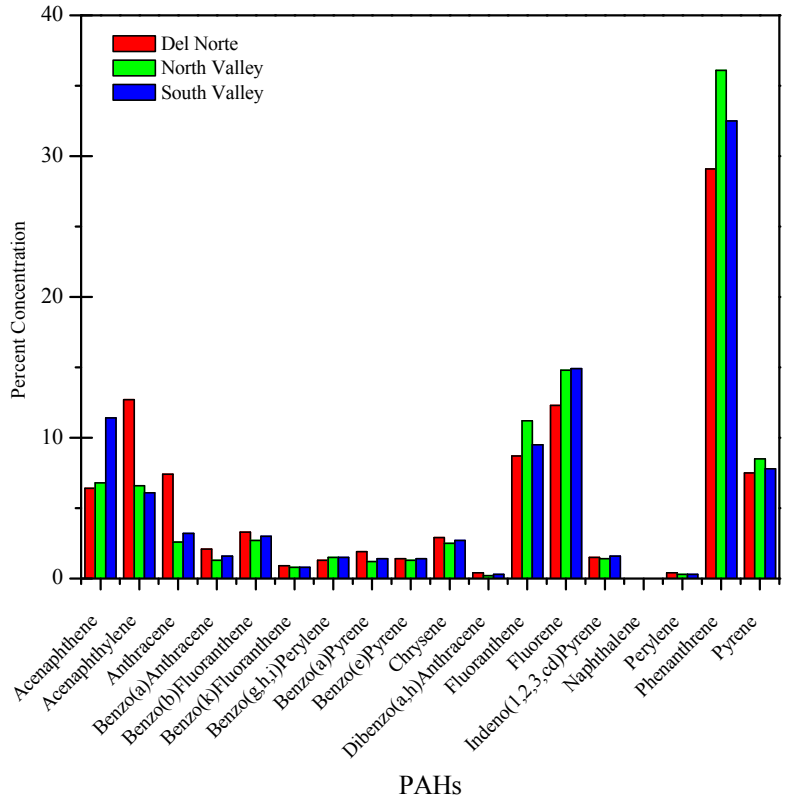

Figure 4-2 Relative distribution of PAHs at the three monitoring sites in Albuquerque

Table 4-2 shows a comparison of toluene/benzene, (*m/p*)-xylene/benzene and (*m/p*)-xylene/toluene ratios in Albuquerque and other major urban areas in the U.S., including data from highway tunnels. The range of values for the concentration ratios is the outcome from the differences in vehicle fleet composition and age, fuel composition, use of ethanol, and emission regulations for different urban areas and monitoring periods. For example, because of regulations controlling benzene emissions, the ratio of toluene/benzene increased by almost a factor of two in Los Angeles (from 1.9 to 3.5). In our study, the toluene/benzene ratios were 2.02 ± 0.13 at Del Norte, 1.88 ± 0.10 at North Valley, and 2.49 ± 0.14 at South Valley. These values are comparable to those estimated for most of the other urban areas and the highway tunnels. The (*m/p*)-xylene/benzene and (m/p)-xylene/toluene ratios varied from 0.88 ± 0.05 to 1.34 ± 0.06 and from 0.46 ± 0.01 to 0.53 ± 0.02, respectively, and fall within the range of those computed for the other urban areas, providing evidence of the substantial contribution of automobile emissions on aromatic VOCs levels in all locations.

Table 4-2 Concentrations ratios for benzene, toluene, and (m/p)-xylenes in Albuquerque compared to other urban areas and in highway tunnels in the U.S.

	Toluene/ Benzene	**(*m/p*)-Xylene/ Benzene**	**(*m/p*)-Xylene/ Toluene**
Del Norte	2.02 ± 0.13	1.12 ± 0.07	0.53 ± 0.02
North Valley	1.88 ± 0.10	0.88 ± 0.05	0.46 ± 0.01
South Valley	2.49 ± 0.14	1.34 ± 0.06	0.53 ± 0.02
Urban areas			
15 urban locations in the U.S.	1.7	0.7	0.4
Los Angeles, CA	1.9-3.5	0.8-1.2	0.2-1.6
Chicago, IL	0.8	0.3	0.4
Oakland, CA	2.0	0.9	0.5
Phoenix, AZ	2.7	1.4	0.5
Denver, CO	2.5	1.3	0.5
Houston, TX	1.8	0.9	0.5
Philadelphia, PA	2.3	1.3	0.6
Pittsburgh, PA	1.7	0.3	0.3
San Jose, CA	1.8	1.3	0.7
Boston, CA	2.3	1.2	0.5
St. Louis, MO	0.7	1.1	1.6
40 urban location in U.S.	2.1		
Highway Tunnels			
Caldecott	1.2-1.4	0.8-1.1	0.52-0.60
Fort McHenry	1.2-1.6	1.2-2.5	0.7-2.1
Tuscarora	1.3-1.4	0.8-1.0	0.6-0.7
Van Nuys	1.7	1.1	0.64
Cassiar	1.6	0.7	0.47

For heavy metals, there is insufficient information on the sources and emissions. In an effort to reconcile the sources of heavy metals, their correlations with VOCs and PAHs were examined. The correlations between the different groups of air toxics measured in this study for the three sites are presented in Table 4-3 to Table 4-5.

In general, a range of correlations were observed among PAHs, VOCs, and heavy metals. As anticipated, the *R* values were higher than 0.6 for PAHs and aromatic hydrocarbons. In addition, some heavy metals were also strongly correlated with heavier PAHs and aromatic hydrocarbons (arsenic, cadmium, chromium, and lead) with associations being higher at the North Valley and South Valley sites as compared to those at Del Norte. These correlations provide additional evidence of their common origin from traffic and other combustion-related activities.

Table 4-3 The minimum and maximum correlation coefficients between individual compounds for each compound group at Del Norte

	Metals	PAHs	VOCs
Metals			
PAHs	-0.35 – 0.94		
VOCs	-0.66 – 0.88	-0.66 – 1.00	

Table 4-4 The minimum and maximum correlation coefficients between individual compounds for each compound group at North Valley

	Metals	PAHs	VOCs
Metals			
PAHs	-0.50 – 1.00		
VOCs	-1.00 – 0.80	-1.00 – 1.00	

Table 4-5 The minimum and maximum correlation coefficients between individual compounds for each compound group at South Valley

	Metals	PAHs	VOCs
Metals			
PAHs	-0.74 – 0.94		
VOCs	-0.37 – 0.69	-0.61 – 0.99	

Overall, this analysis indicated that the dominant source of PAHs and VOCs (aromatic hydrocarbons) in Albuquerque is traffic with important contributions from wood burning and oil residues. Vehicular emissions also appeared to be responsible for some of the heavy metals. No significant differences were observed among the three sites. To further evaluate the contribution of aerosol sources on air toxics, the outcomes of fine PM source apportionment were analyzed in conjunction with air toxics concentrations for the December 2008 to February 2009 period.

4.1.1 $PM_{2.5}$ Source Apportionment

4.1.1.1 Chemical composition

The daily $PM_{2.5}$ chemical composition data for Albuquerque were obtained through the USEPA Community Speciation Network Air Quality System program (www.epa.gov/aqs). Aerosol samples collected on a 1-in-6 days frequency from January 2007 to February 2009 were retrieved. Major ions (NH_4^+, Na^+, K^+, NO_3^-, and SO_4^{2-}), four fraction of organic carbon, elemental carbon, and 48 elements (from Na to Pb) were measured.

The mean $PM_{2.5}$ and concentrations of chemical species (in $\mu g/m^3$) for the entire study period (January 2007 to February 2009), the two IMPs (February and June 2008), and the winter of 2008/2009 (December 2008 to February 2009)) during which samples for PAHs and heavy metals were analyzed are given in Table 4-6. In addition, the concentration ratios of soil elements, SO_4^{2-}-to-S and the NH_4^+-to-SO_4^{2-} molar ratio, and the percentage of NO_3^- neutralized by NH_4^+ during the January 2008 to February 2009 period and the December 2008 to February 2009 periods are presented in Table 4-7.

Table 4-6 Chemical analysis of $PM_{2.5}$ for Albuquerque, New Mexico. Concentrations are in µg/m^3

	January 2007 – February 2009 (n=129)				February 11-20, 2008 (n=2)				June 17-30, 2009 (n=3)				December 2008 – February 2009 (n=13)			
	% n	*mean*	σ^a	*max*	*% n*	*mean*	σ^a	*max*	*% n*	*mean*	σ^a	*max*	*% n*	*mean*	σ^a	*max*
$PM_{2.5}$ mass	96	6.1	3.1	19.2	100	3.6	0.3	3.8	100	8.5	2.5	11.4	100	7.1	4.8	19.2
Ammonium,NH_4^+	94	0.384	0.249	1.530	100	0.194	0.015	0.204	100	0.405	0.174	0.581	100	0.358	0.22	0.756
Sodium, Na^+	94	0.244	0.497	4.250	100	2.147	2.974	4.250	100	0.100	0.014	0.116	92	0.036	0.02	0.073
Potassium, K^+	42	0.080	0.122	0.786	50	0.023		0.023	100	0.072	0.041	0.119	38	0.134	0.109	0.325
Nitrate, NO_3^-	94	0.581	0.640	4.130	100	0.743	0.435	1.050	100	0.260	0.084	0.357	100	0.892	0.616	2.040
Sulfate, SO_4^{2-}	95	0.815	0.490	3.700	100	0.386	0.052	0.423	100	1.257	0.446	1.760	100	0.420	0.171	0.685
OC1	95	0.639	0.342	2.030	100	0.570	0.059	0.612	100	0.408	0.121	0.533	100	0.991	0.435	2.030
OC2	95	1.077	0.385	2.250	100	0.960	0.269	1.150	100	1.230	0.118	1.360	100	1.254	0.302	1.910
OC3	95	0.812	0.304	2.070	100	0.673	0.190	0.807	100	1.103	0.09	1.160	100	0.833	0.243	1.330
OC4	95	0.77	0.435	3.050	100	0.640	0.360	0.894	100	0.954	0.117	1.070	100	0.788	0.497	1.910
Pyrolyzed OC-TT	24	0.309	0.596	2.460	50	0.374		0.374	100	0.187	0.026	0.212	38	0.790	0.953	2.350
Total OC	95	3.377	1.282	8.710	100	3.030	0.099	3.100	100	3.883	0.376	4.310	100	4.173	1.585	7.370
Total EC	93	0.539	0.377	2.170	100	0.503	0.059	0.545	100	0.212	0.112	0.315	100	0.772	0.375	1.380
Sodium, Na	52	0.026	0.034	0.251	*n.d.*				100	0.023	0.014	0.039	46	0.023	0.021	0.062
Magnesium, Mg	47	0.016	0.021	0.103	*n.d.*				66	0.017	0.023	0.033	23	0.013	0.013	0.028
Aluminum, Al	86	0.052	0.061	0.437	100	0.013	0.011	0.021	100	0.084	0.059	0.150	69	0.027	0.032	0.106
Silicon, Si	96	0.150	0.146	0.985	100	0.069	0.014	0.079	100	0.228	0.122	0.339	100	0.085	0.063	0.272
Phosphorous, P	3	0.002	0.002	0.004	*n.d.*				*n.d.*				7	0.001		0.001
Sulfur, S	96	0.278	0.181	1.410	100	0.116	0.020	0.130	100	0.387	0.164	0.573	100	0.129	0.064	0.246
Chlorine, Cl	79	0.008	0.009	0.062	100	0.002	0.001	0.002	66	0.007	0.002	0.008	76	0.006	0.006	0.020
Potassium, K	96	0.060	0.092	0.820	100	0.035	0.002	0.037	100	0.096	0.038	0.140	100	0.072	0.087	0.341
Calcium, Ca	95	0.075	0.063	0.387	100	0.046	0.017	0.058	100	0.103	0.069	0.169	100	0.05	0.039	0.160
Scandium, Sc	3	0.001	0.001	0.002	50	0.001		0.001	*n.d.*				*n.d.*			
Titanium, Ti	66	0.005	0.005	0.028	100	0.002	0.003	0.004	33	0.009		0.009	38	0.003	0.001	0.004
Vanadium, V	50	0.002	0.002	0.011	50	0.001		0.001	*n.d.*				15	0.002	0.002	0.003
Chromium, Cr	29	0.001	0.002	0.011	*n.d.*				*n.d.*				46	0.001	0.001	0.002
Manganese, Mn	74	0.002	0.001	0.005	100	0.001	0.001	0.002	*n.d.*				69	0.001	0.001	0.003
Iron, Fe	96	0.070	0.049	0.312	100	0.065	0.02	0.079	100	0.06	0.027	0.077	100	0.064	0.037	0.160

	January 2007 – February 2009 (n=129)				February 11-20, 2008 (n=2)				June 17-30, 2009 (n=3)				December 2008 – February 2009 (n=13)			
	% n	*mean*	σ^a	*max*	*% n*	*mean*	σ^a	*max*	*% n*	*mean*	σ^a	*max*	*% n*	*mean*	σ^a	*max*
Cobalt, Co	44	0.001	0.001	0.002	50	0.001		0.001	*n.d.*				53	0.001	0.001	0.001
Nickel, Ni	55	0.001	0.001	0.005	50	0.001		0.001	*n.d.*				30	0.001	0.001	0.001
Copper, Cu	92	0.005	0.005	0.038	100	0.006	0.002	0.007	100	0.002	0.001	0.002	100	0.004	0.004	0.011
Zinc, Zn	85	0.005	0.004	0.026	100	0.004	0.005	0.007	66	0.002	0.002	0.003	84	0.005	0.003	0.009
Gallium, Ga	23	0.001	0.001	0.001	*n.d.*				33	0.001		0.001	7	0.001		0.001
Arsenic, As	53	0.001	0.001	0.002	100	0.001	0.001	0.001	66	0.001	0.001	0.001	46	0.001	0.001	0.002
Selenium, Se	32	0.001	0.001	0.002	50	0.001		0.001	33	0.001		0.001	15	0.001	0.001	0.001
Bromine, Br	91	0.002	0.001	0.006	100	0.002	0.001	0.003	100	0.003	0.001	0.003	92	0.002	0.001	0.006
Rubidium, Rh	45	0.001	0.001	0.001	50	0.001		0.001	33	0.001		0.001	7	0.001		0.001
Strontium, Sr	37	0.002	0.002	0.014	50	0.001		0.001	100	0.001	0.001	0.002	46	0.003	0.002	0.006
Yttrium, Y	13	0.001	0.001	0.002	*n.d.*				*n.d.*				30	0.001	0.001	0.001
Zirconium, Zr	19	0.001	0.001	0.003	50	0.001		0.001	33	0.001		0.001	7	0.001		0.001
Niobium, Nb	11	0.001	0.001	0.003	50	0.001		0.001	*n.d.*				7	0.001		0.001
Molybdenum, Mo	5	0.001	0.001	0.002	50	0.001		0.001	*n.d.*				7	0.001		0.001
Silver, Ag	17	0.004	0.003	0.012	50	0.004		0.004	*n.d.*				30	0.007	0.004	0.012
Cadmium, Cd	14	0.003	0.004	0.015	50	0.002		0.002	*n.d.*				15	0.008	0.010	0.015
Indium, In	21	0.005	0.005	0.019	50	0.003		0.003	33	0.001		0.001	30	0.009	0.002	0.011
Tin, Sn	18	0.006	0.005	0.016	*n.d.*				33	0.008		0.008	30	0.011	0.007	0.016
Antimony, Sb	19	0.009	0.008	0.025	50	0.005		0.005	33	0.010		0.01	30	0.013	0.012	0.025
Cesium, Cs	16	0.002	0.002	0.005	50	0.001		0.001	33	0.001		0.001	15	0.004	0.001	0.005
Barium, Ba	17	0.005	0.007	0.033	50	0.002		0.002	33	0.006		0.006	7	0.001		0.001
Lanthanum, La	11	0.002	0.002	0.007	*n.d.*				*n.d.*				7	0.003		0.003
Cerium, Ce	5	0.003	0.006	0.017	*n.d.*				*n.d.*				*n.d.*			
Samarium, Sa	14	0.001	0.001	0.005	50	0.001		0.001	*n.d.*				*n.d.*			
Europium, Eu	6	0.003	0.002	0.006	*n.d.*				33	0.006		0.006	*n.d.*			
Terbium, Tb	6	0.001	0.001	0.003	*n.d.*				*n.d.*				*n.d.*			
Hafnium, Hf	9	0.002	0.002	0.005	*n.d.*				33	0.002		0.002	23	0.002	0.002	0.005
Tantalum, Ta	8	0.003	0.002	0.007	*n.d.*				*n.d.*				30	0.004	0.002	0.007

	January 2007 – February 2009 (n=129)				February 11-20, 2008 (n=2)				June 17-30, 2009 (n=3)				December 2008 – February 2009 (n=13)			
	% n	*mean*	σ^a	*max*	*% n*	*mean*	σ^a	*max*	*% n*	*mean*	σ^a	*max*	*% n*	*mean*	σ^a	*max*
Tungsten, W	13	0.002	0.001	0.006	*n.d.*				*n.d.*				30	0.003	0.002	0.006
Iridium, Ir	11	0.001	0.001	0.002	*n.d.*				33	0.001		0.001	7	0.002		0.002
Gold, Au	11	0.001	0.001	0.003	*n.d.*				*n.d.*				15	0.002	0.002	0.003
Mercury, Hg	20	0.002	0.001	0.006	50	0.001		0.001	66	0.002	0.001	0.003	15	0.001	0.001	0.001
Lead, Pb	43	0.001	0.001	0.008	100	0.001	0.001	0.001	66	0.002	0.001	0.003	38	0.004	0.002	0.008

[a] The σ was not calculated for compounds for which less than 2 measurements were obtained and σ was equal to 0 for compounds in which measured concentrations did not vary.
n.d.: Not detected

The mean ratios for Al/Si, Al/Ca, and K/Fe were 0.30 ± 0.01, 0.61 ± 0.03, and 0.98 ± 0.15, respectively. These ratios were somewhat lower but comparable to those estimated for samples collected at the Interagency Monitoring of Protected Visibility Environments (IMPROVE) sites in the western United States (Al/Si: 0.31 to 0.43, K/Fe: 0.67 to 0.78, Al/Ca: 1.4 to 1.7) when soil dust was the major component of particulate matter (I. G. Kavouras, V. Etyemezian, and D. W. DuBois, et al., 2009). The EC/OC ratio values (0.15 ± 0.01) were lower than those determined for traffic-dominated urban aerosol, indicating the possible contribution of smoke aerosol that generally contains more OC than EC. Sulfur (S) was in the form of SO_4^{2-} with a SO_4^{2-}-to-sulfur ratio of 3.00 ± 0.03. The mean NH_4^+/SO_4^{2-} and $NH_4^+/(NO_3^-+2SO_4^{2-})$ molar ratios for the two periods were 2.77 ± 0.15 and 0.77 ± 0.01 respectively, suggesting that SO_4^{2-} aerosols were mostly in the form of $(NH_4)_2SO_4$ in the winter and $(NH_4)HSO_4$ in the summer, while NO_3^- appeared to be partially neutralized by the NH_3 (Malm, et al. 2004).

Table 4-7 Mean concentration (± standard error) and molar ratios at Albuquerque for the January 2007 to February 2009 period

Parameter	Jan.08-Feb.09
Al/Si	0.30 ± 0.01
Al/Ca	0.61 ± 0.03
K/Fe	0.98 ± 0.14
EC/OC	0.15 ± 0.01
SO_4^{2-}/S	3.00 ± 0.03
NH_4^+/ SO_4^{2-} molar ratio	2.77 ± 0.15
NH_4^+/ $(NO_3^-+2SO_4^{2-})$ molar ratio	0.77 ± 0.01

4.1.1.2 Positive Matrix Factorization

The sources of $PM_{2.5}$ in Albuquerque, New Mexico, were identified and quantified using Positive Matrix Factorization (PMF) receptor modeling. PMF is a statistical-based approach that determines the profiles of aerosol sources and source strengths for each sample period in order to reduce the difference between measured and PMF-estimated particle mass concentration ((Paatero and Tapper, Positive Matrix Facotrization: a non-negative factor model with optimal utilization of error estimates of data values 1994) (Paatero 1997). Concentrations of *m* aerosol species for *n* sampling days are described by the product of two matrices, G (*nxp*), which is the source contribution matrix with *p* sources, and F (*pxm*), which is the source profile matrix, and a residual component *E* (*nxm*) as described below:

$$\mathbf{X=GF+E} \qquad \mathbf{(1)}$$

$$\boldsymbol{Q} = \sum_{\boldsymbol{i=1}}^{\boldsymbol{n}} \sum_{\boldsymbol{j=1}}^{\boldsymbol{m}} \left(\frac{\boldsymbol{e_{ij}}}{\boldsymbol{h_{ij} S_{ij}}} \right)^{\mathbf{2}} \qquad (2)$$

$$e_{ij} = x_{ij} - \sum_{k=1}^{p} g_{ik} f_{kj} \qquad (3)$$

where s_{ij} is the uncertainty in the measured concentration x_{ij}, and h_{ij} is a filter function to handle outliers in the dataset, as follows

$$\boldsymbol{h_{ij}} = \begin{cases} \mathbf{1} & \boldsymbol{if} \left|\boldsymbol{e_{ij}/s_{ij}}\right| \leq \boldsymbol{a} \\ \left|\boldsymbol{e_{ij}/s_{ij}}\right|/\boldsymbol{a} & \boldsymbol{otherwise} \end{cases} \quad (4)$$

where α is the outlier threshold distance. The PMF2 algorithm applies a least-squares approach to solve the factor analysis by considering that sources profiles and contributions are not negative during the optimization analysis. The F_{peak} parameter introduces rotation of resolved factors to clarify the meaning of these factors; however, the factor solutions are mathematically equivalent.

The number of factors (sources) is defined by the user, based on a trial-and-error approach and a combination of statistical tests, outputs of the model, and comparison with existing source profiles. These tests include the *Q* value, the largest element in the *rotmat* matrix, and the highest individual column mean (*IM*) and standard deviation (*IS*) from the scaled residual matrix.

$$\boldsymbol{IM} = \max_{\boldsymbol{j=1,2,\ldots m}} \left(\frac{\mathbf{1}}{\boldsymbol{n}} \sum_{\boldsymbol{i=1}}^{\boldsymbol{n}} \boldsymbol{r_{ij}} \right) \quad (5)$$

$$IS = \max_{j=1,2,..m} \left(\sqrt{\frac{1}{n-1} \sum_{i=1}^{n} \left(r_{ij} - \overline{r_j}\right)^2} \right) \quad (6)$$

The same tools are also used to determine the most appropriate rotation (defined by the F_{peak} value) of the factors. The optimum solution should be within the range of factors (or F_{peak} values) in which *Q* remains relatively constant, *IM* and *IS* drop significantly, and the highest element in *rotmat* increases. The final acceptable solution was identified by trial and error in order to obtain reasonable results.

In this effort, chemical species associated with more than 75 percent missing measurements were excluded from the analysis. Missing concentration data were replaced by the geometric mean of the measured concentrations while missing uncertainties were substituted with four times the geometric mean of measured uncertainties. In the PMF2 model, the robust method with a α=4.0 was applied. The error model "-12" (that uses observed values) was selected.

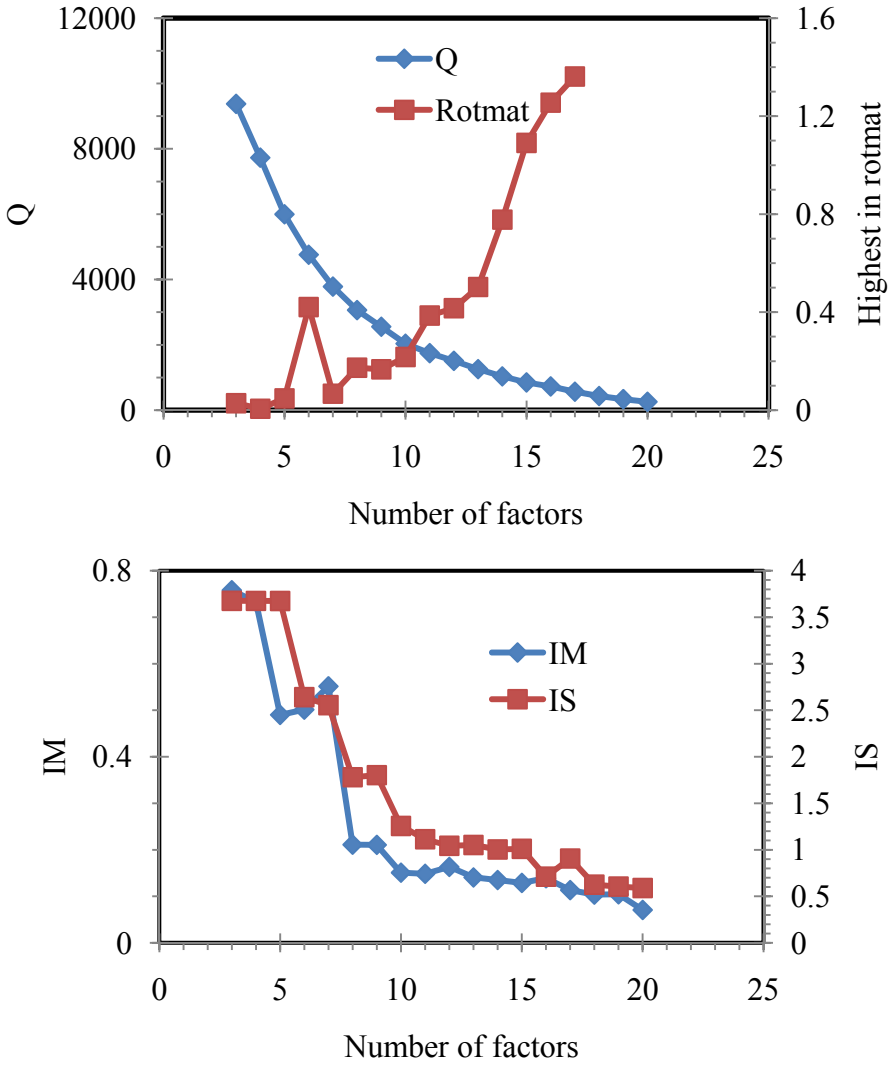

Figure 4-3 Variation of (a) *Q*, the highest element in rotmat, and (b) *IM* and *IS* for different numbers of factors

Figure 4-3 shows the trends of *Q*, the highest element in *rotmat*, *IM*, and *IS* for models with 3 to 20 factors. For more than 6 factors, the *Q* value did not change significantly, indicating that most of the variation was explained by five to six factors. A sudden increase of the highest element in *rotmat* when the number of factors increased from five to six indicated that six or more factors had excessive rotational freedom. The sharp decrease of *IM* and *IS* for five or more factors further supported that the optimum solution should lie between four and six factors. The four-factor model was rejected because two factors, namely biomass burning and traffic emissions, were merged into a single factor.

The profiles on the five-factor model were identified prior to rotations; however, to further clarify the loadings, a set of models with F_{peak} values from -5.0 to 5.0 was executed. Models with F_{peak} values lower than -1.5 or higher than 1.5 did not converge

into a solution. Similarly, Figure 4-4a-b shows the trends of *Q*, highest element in *rotmat*, *IM*, and *IS* for models with F_{peak} from -1.5 to 1.5. A sudden increase of the highest element in *rotmat* for F_{peak}=0 was observed when the lowest *Q* value was computed. In addition, a sharp increase of *IS* for F_{peak}=-1.0 supported that the solution with F_{peak}=-0.5 was the most appropriate rotation.

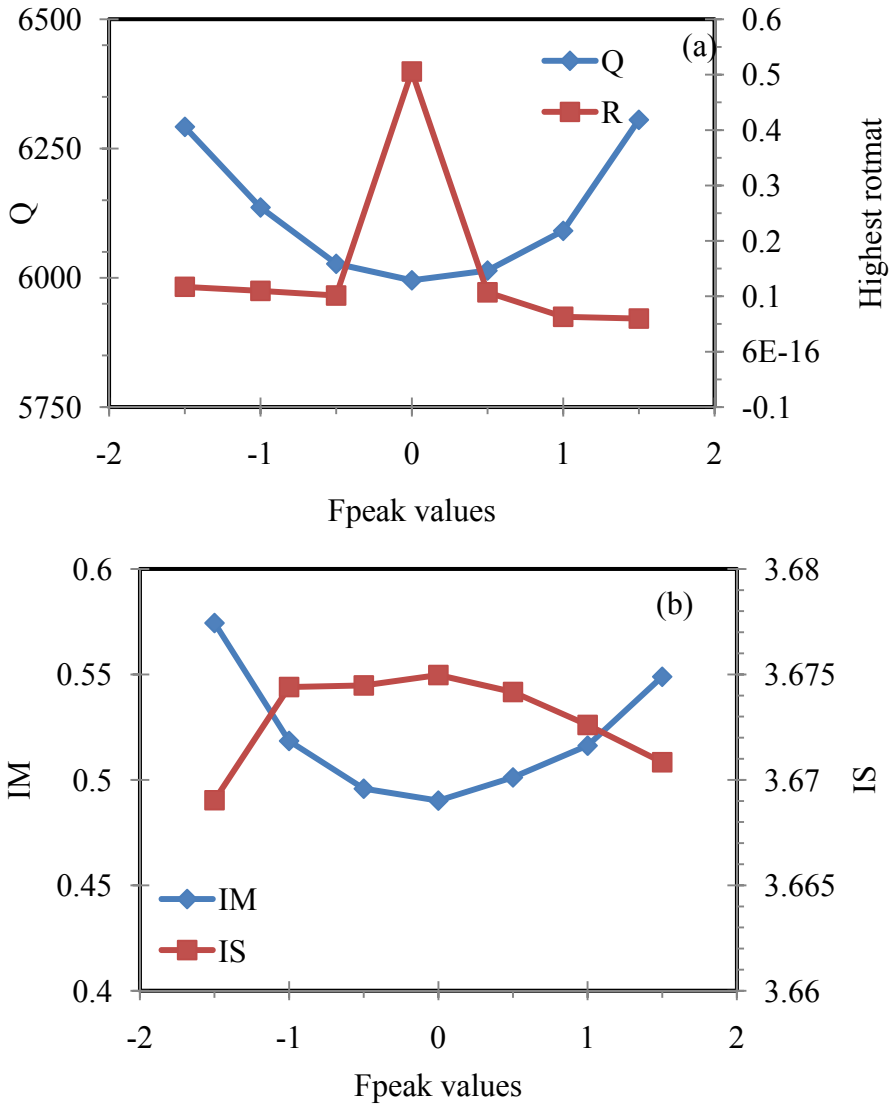

Figure 4-4 Variation of (a) *Q*, the highest element in *rotmat*, and (b) *IM* and *IS* for different rotations

The source contributions can be estimated by regressing daily $PM_{2.5}$ mass concentrations on factor contributions (*G* matrix) as follows

$$\boldsymbol{PM_{2.5}} = \boldsymbol{a} + \sum_{\boldsymbol{j=1}}^{\boldsymbol{p}} \boldsymbol{b_j} \cdot \boldsymbol{g_{jk}} \qquad (7)$$

where $PM_{2.5}$ is the particle-associated mass concentration (in μg/m^3) for the sample k, g_{ik} is the rotated factor score of source j in sample k, b_j is the regression coefficient of the g_{ik}-to-mass concentration, and a is the unexplained component. The agreement between the calculated and estimated mass concentrations was examined by the percent root mean square error, which is defined as follows:

$$\%\boldsymbol{RMSE} = \frac{\left|\boldsymbol{PM_{2.5}^{measured}} - \boldsymbol{PM_{2.5}^{calculated}}\right|}{\boldsymbol{PM_{2.5}^{measured}}} \cdot \mathbf{100} \qquad (8)$$

4.1.2 Source Apportionment

The comparison between measured and estimated $PM_{2.5}$ mass concentrations, using the five-factor PMF model, is shown in Figure 4-5. The calculated and measured mass and elemental concentrations are in an acceptable agreement with a slope of 0.70251 and an intercept of 1.3 μg/m^3 (R = 0.83) (blue line in Figure 4-5). The estimated mass concentrations were lower ($PM_{2.5}$: measured 6.0 ± 0.2 μg/m^3 vs. estimated 5.6 ± 0.2 μg/m^3). The %RSME was 17%.

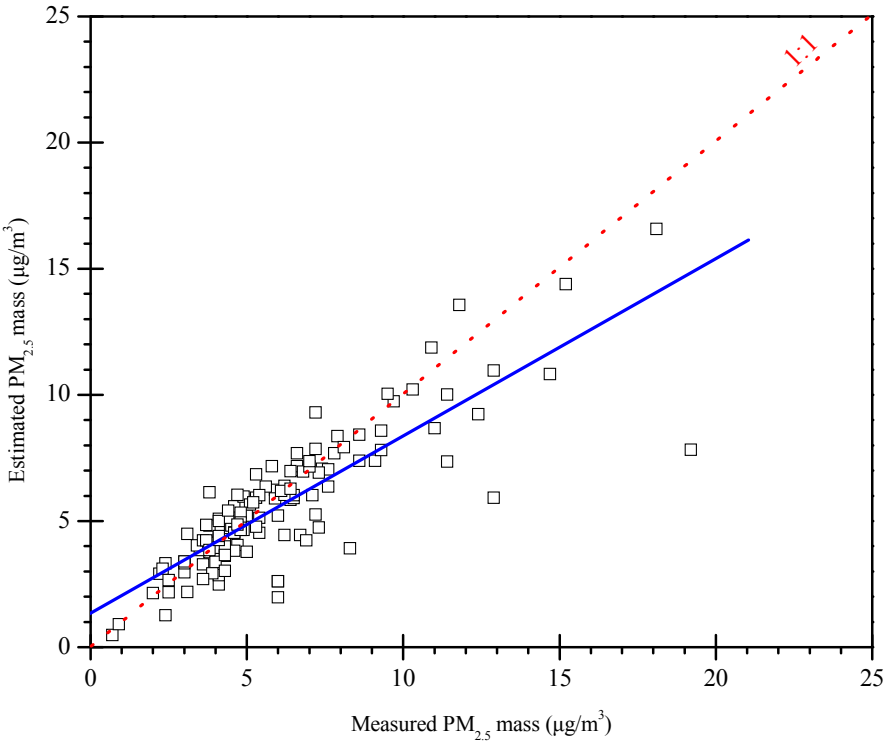

Figure 4-5 Measured vs. PMF-calculated 24-hr $PM_{2.5}$ mass concentration using $PM_{2.5}$ chemical speciation data from CSN network for the January 2007 – February 2009 period

The profiles of the five retained factors are shown in Figure 4-6. Mean source contributions to $PM_{2.5}$ mass for the January 2007 – February 2009, the two IMPs (February and June 2008) and the Air Toxics period (December 2008 – February 2009) periods are depicted in Figure 4-7, while Figure 4-8 shows the contribution of each source to individual daily samples.

Primary particulate matter for traffic

The strong correlations of the first factor with OC and EC indicated the contribution of primary particulate emissions from automobiles. Furthermore, factor loadings of S, SO_4^{2-}, Pb, Al, Ni, and V were also associated with motor vehicle emissions. Automobile emissions were responsible for 5.9 percent during the January 2007 to February 2009 period, 3.9 percent in February 2008, 11.9 percent in June 2008, and 7.9 percent during the December 2008 to February 2009 period, of $PM_{2.5}$ mass, respectively. The contributions of traffic-related emissions did not change significantly over the January 2007 to February 2009 period with the exception of two episodes on July 5, 2007, and July 5, 2008, which can be attributed to increased emissions from traffic or particulate matter from fireworks during the previous night.

Road dust

Road dust was identified as a source of $PM_{2.5}$ in Albuquerque. Most of the measured concentrations of crustal elements Al, Si, Ca, Fe, and Ti were associated with this source. In addition, fractions of organic carbon, elemental carbon, and other elements, such as Br, As, Cu, Zn, and K, were also associated with this factor because of the resuspension of urban soil containing these elements. Water-soluble ions (Na^+, K^+, and SO_4^{2-}) may be attributed to road-sanding material (Etyemezian, et al. 2002). The contribution of road dust to $PM_{2.5}$ mass represented 10.7 percent for the January 2007 to February 2009 period. During the two IMPs, road dust accounted for 4.9 percent in February 2008 and 15.3 percent in June 2008. This is due to dry conditions in the spring and summer that favor the resuspension of dust by vehicles. Mineral particles in the summer may be associated with elevated emissions from unpaved roads.

Biomass burning and secondary organic aerosol

The third factor, biomass burning, includes a mixture of secondary aerosols including some from traffic emissions. Biomass burning includes wildfires, prescribed burning, and agricultural fires, as well as wood burning. CO, CO_2, NO_x, light hydrocarbons, CH_3Cl, CH_3Br, polycyclic aromatic hydrocarbons (PAHs), formaldehyde, formic and acetic acids, methanol, R-hydroperoxides, NH_3, HCN, acetonitrile, nitric acid, peroxyacetylnitrates (PAN), SO_2 and particulate matter have been reportedly directly emitted during the flaming, smoldering, and pyrolysis stages (Finlayson-Pitts and Pitts, Chemistry of the upper and lower Atmosphere, 1999). In addition to primary emissions, SOA are formed through the condensation of hot vapors and the gas-to-particle conversion of gas-phase precursors to low volatility compounds. The highest contributions of these sources were identified during the January to February 2009 period. This source contributed 31.9 percent during the January 2007 to February 2009 period and 43.5 percent of $PM_{2.5}$ mass during the December 2008 to February 2009 period. During the two IMPs, this source accounted for 54.8 percent and 119.1 percent. Assuming that domestic wood burning is the dominant source in winter and wildfires/prescribed burning are observed in summer, it is confirmed that emissions from wood burning for domestic heating make a significant contribution to particulate matter concentration in the Albuquerque area.

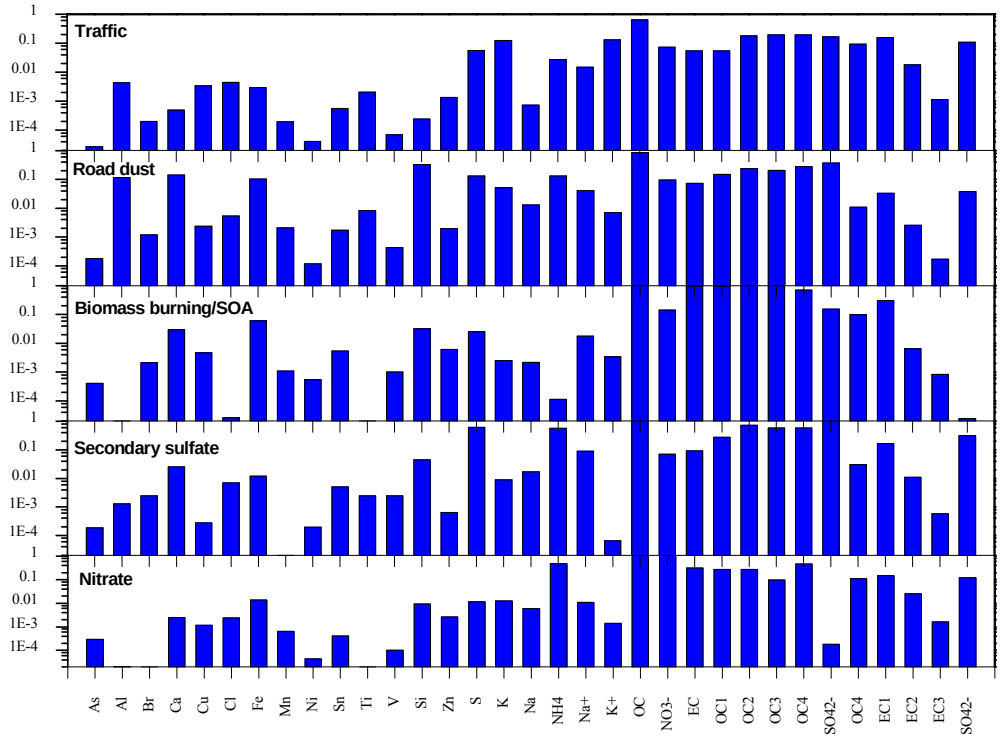

Figure 4-6 Source profiles for $PM_{2.5}$ sources in Albuquerque, New Mexico

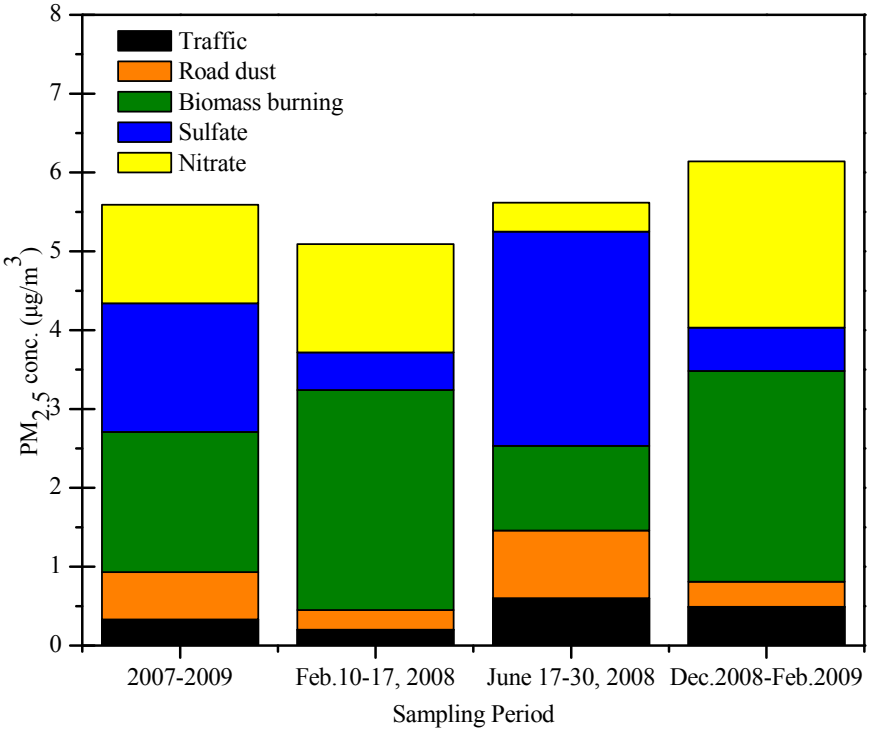

Figure 4-7 Modeled mean contributions of sources to $PM_{2.5}$ mass based on chemical speciation data collected at Del Norte

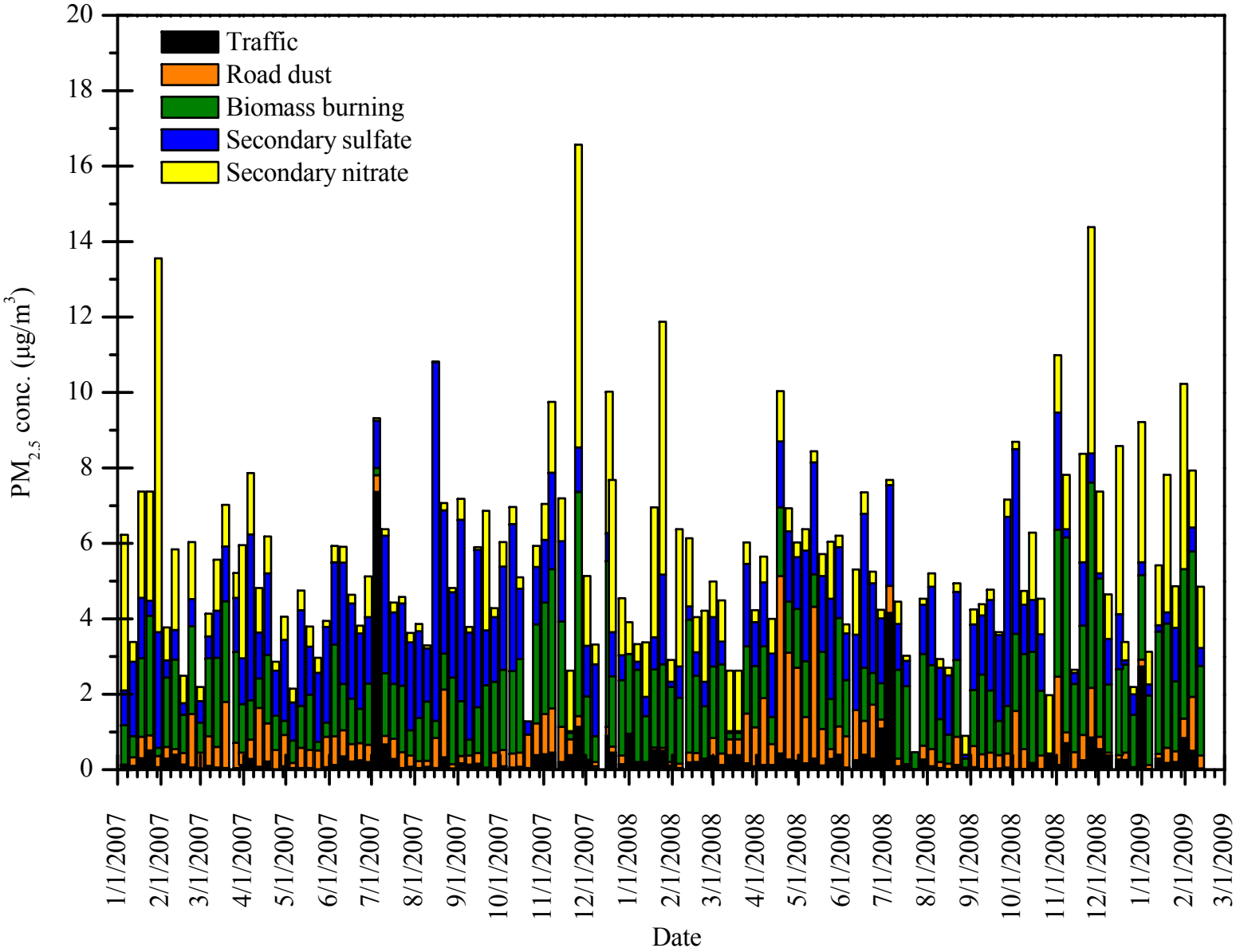

Figure 4-8 Modeled daily variations of source contributions to $PM_{2.5}$ mass based on chemical speciation data collected at Del Norte

Secondary sulfate

A separate factor for secondary SO_4^{2-} aerosol was resolved. This source showed strong associations with elemental S, NH_4^+, EC, and OC (Figure 4-6). Furthermore, a small fraction of Al, Ni, and V, was associated with this factor. The contribution of this source to $PM_{2.5}$ was ~29.2 percent for the January 2007 to February 2009 period and 8.9 percent for the December 2008 to February 2009 period. The contribution of secondary sulfate was 9.5 percent in February 2008 and 48.4 percent in June 2008, indicating an important seasonal variation.

Secondary nitrate

Finally, the fifth factor was attributed to particulate NO_3^- with high loadings of NH_4^+ and SO_4^{2-} and minor loadings of the volatile fractions of organic carbon (OC1) and elemental carbon. NO_3^- appeared to be a major component of fine particulate matter in the winter whereas only minimal amounts were observed in the spring, fall, and summer. For the entire measurement period, NO_3^- accounted for 22.3 percent of $PM_{2.5}$. The contribution of particulate NO_3^- to $PM_{2.5}$ mass during February 2008 and December 2008 to February 2009 were 26.9 percent and 34.4 percent, but only 6.6 percent in June 2008.

4.1.3 Contribution of $PM_{2.5}$ Sources to Air Toxics Concentrations

The associations between air toxics concentrations and $PM_{2.5}$ source contributions during the December 2008 to February 2009 period were examined using correlation and regression analysis. The Pearson correlation coefficients are presented in Table 4-8. Table 4-9 shows the contributions of $PM_{2.5}$ sources to air toxics concentrations, estimated and measured concentrations, and the %RSME based on the regression of air toxics concentrations against the $PM_{2.5}$ source contributions (all non-negative contributions are included).

PAHs are present in both emissions and ambient air in the gas and particulate phases. A fraction of them are directly emitted from tailpipes in the particulate phase, which is in agreement with the good correlations with $PM_{2.5}$ mass and direct traffic emissions in this study. In addition, a large fraction of PAHs (especially volatile PAHs such as naphthalene and phenanthrene) are released into the air in the gas phase and partition between gas and particulate phase as the temperature decreases. This is a possible explanation for the very good correlations between PAHs and the nitrate source, a source that is closely associated with traffic emissions of NO and NO_2. It is further corroborated by the good correlations of aromatic hydrocarbons (benzene, toluene, xylenes, and ethylbenzene) with $PM_{2.5}$, traffic contribution, and nitrate contribution.

The significant role of traffic was also identified by the moderate correlations of aromatic hydrocarbons with road dust. Road dust was also strongly correlated with heavy metals. The strong associations between benzene alkylated derivatives and the biomass burning/SOA source indicated they played an important role of SOA formation in the region, as they react with OH radicals from 10 to 50 times faster than benzene. The moderate to high *R* values for heavy metals may be related to woodburning emissions of heavy metals. Finally, sulfate source, a regional source, was only correlated to mercury

and trichlorotrifluoromethane, contaminants with more regional and global characteristics.

The largest quantities of PAHs were associated with the nitrate source, followed by biomass burning and direct particulate emissions from traffic sources. This indicated that nitrate in Albuquerque is largely associated with local traffic emissions as compared to other regional sources and that gas-to-particle conversion of hot PAHs vapors is the dominant pathway for the accumulation of PAHs in the particulate phase. A fraction of PAHs were also associated with road dust, suggesting that road dust was contaminated by vehicle exhausts and oil residues.

Road dust was also responsible for less than 20 percent of heavy metals concentrations.

Biomass burning appeared to be a major contributor to air toxics especially volatile (form naphthalene to pyrene) PAHs. Aromatic hydrocarbons were associated with both traffic and biomass burning emissions. In general, good agreements between estimated and measured concentrations were observed. The %RSME varied from 0 to 55 percent with the highest values being computed for chlorinated hydrocarbons.

Table 4-8 Correlations (higher than 0.50) between individual air toxics, measured $PM_{2.5}$, and its modeled source contributions at Del Norte (bold: R > 0.75)

Compound	PM2.5	Traffic	Road dust	Biomass burning / SOA	Sulfate	Nitrate
Antimony			0.80	**0.91**		0.52
Arsenic		0.57				0.78
Beryllium			0.62			
Cadmium	0.63		0.71	0.72		0.55
Chromium	0.55		0.72	**0.82**		
Cobalt			**0.80**	0.63		
Lead	0.54		0.70	0.60		0.63
Manganese			**0.84**	0.61		
Nickel			**0.95**	0.62		
Selenium	0.74					
Naphthalene	0.74		0.60	**0.83**		0.73
Acenaphthylene	0.59	**0.90**				**0.81**
Acenaphthene	0.76	0.67				0.78
Fluorene	0.73	0.72		0.51		**0.82**
9-Fluorenone	0.70	0.76				**0.84**
Phenanthrene	0.63	**0.83**				0.76
Anthracene	0.56	0.76				**0.85**
Retene	0.71	0.79				**0.92**
Pyrene	0.67	0.69		0.61		0.79
Fluoranthene	0.70	0.71		0.56		0.75
Cyclopenta[cd]pyrene		**0.88**				0.75
Benzo[a]anthracene		**0.82**				0.77
Chrysene	0.63	**0.88**				**0.82**
Benzo[b]fluoranthene	0.65	0.77		0.51		**0.87**
Benzo[k]fluoranthene	0.61	**0.84**				**0.82**
Benzo[e]pyrene	0.63	0.76		0.52		**0.85**
Benzo[a]pyrene	0.62	**0.81**				**0.86**
Perylene	0.52	0.80				**0.82**
Benzo[ghi]perylene	0.63	0.66		0.62		**0.88**
Indeno[123,cd]pyrene	0.58	0.68		0.57		**0.86**
Coronene	0.53	0.51		0.71		**0.82**
Benzene	0.60	**0.85**	0.57	**0.92**		**0.82**
Chloromethane		0.53	**0.93**			
Trichlorotrifluoroethane					0.54	
Methylene Chloride		**0.85**				
Toluene	0.60		0.60	**0.92**		0.73
m/p-Xylenes	0.58	0.78	0.54	**0.89**		0.75
o-Xylene		**0.87**	0.58	**0.98**		0.54

Table 4-9 Contributions of $PM_{2.5}$ sources to concentrations of air toxics during the December 2008 – February 2009 period based on chemical speciation data collected at Del Norte

Compound	Traffic	Road dust	Biomass burning / SOA	Sulfate	Nitrate	*Estimated*	Measured	% RSME
Antimony	0.08 ± 0.02	0.19 ± 0.03	0.93 ± 0.11	-		0.99 ± 0.16	1.10 ± 0.18	-1
Arsenic	0.08 ± 0.10	0.08 ± 0.12	-	-	0.43 ± 0.2	0.59 ± 0.42	0.67 ± 0.19	-22
Cadmium	0.01 ± 0.01	0.02 ± 0.01	0.03 ± 0.05	-	0.02 ± 0.02	0.07 ± 0.09	0.11 ± 0.01	-7
Chromium	-	0.12 ± 0.08	0.44 ± 0.31	-	0.08 ± 0.11	0.64 ± 0.50	1.46 ± 0.12	-2
Cobalt	-	0.06 ± 0.02	-	-	0.03 ± 0.03	0.09 ± 0.05	0.22 ± 0.03	-12
Lead	-	0.62 ± 0.17	-	-	0.80 ± 0.25	2.68 ± 0.41	2.92 ± 0.39	-4
Manganese	-	5.27 ± 1.34	-	-	1.55 ± 1.96	6.82 ± 3.30	13.96 ± 2.61	-18
Nickel	-	0.21 ± 0.05	0.28 ± 0.18	0.10 ± 0.06		0.59 ± 0.29	0.84 ± 0.12	-4
Selenium	-	0.01 ± 0.02	-	0.03 ± 0.03	0.04 ± 0.03	0.08 ± 0.08	0.14 ± 0.03	-5
Naphthalene	3.05 ± 7.20	13.94 ± 13.37	53.51 ± 70.22	3.66 ± 15.06	31.74 ± 21.25	105.9 ± 127.1	109.73 ± 16.7	-3
Acenaphthylene	0.70 ± 0.08	0.20 ± 0.10	-	-	1.07 ± 0.19	1.97 ± 0.37	1.81 ± 0.66	-24
Acenaphthene	0.10 ± 0.07	0.04 ± 0.13	0.37 ± 0.67	0.19 ± 0.14	0.34 ± 0.20	1.04 ± 1.21	1.30 ± 0.15	-6
Fluorene	0.34 ± 0.15	0.25 ± 0.28	0.73 ± 1.46	0.31 ± 0.31	0.97 ± 0.44	2.60 ± 2.64	2.99 ± 0.45	-3
9-Fluorenone	0.26 ± 0.09	0.13 ± 0.18	0.54 ± 0.92	0.24 ± 0.20	0.73 ± 0.28	1.90 ± 1.67	1.76 ± 0.33	-4
Phenanthrene	1.13 ± 0.42	0.59 ± 0.78	0.71 ± 4.09	0.89 ± 0.88	2.32 ± 1.24	5.64 ± 7.41	7.22 ± 1.19	-7
Anthracene	0.11 ± 0.04	0.08 ± 0.05	-	-	0.34 ± 0.09	0.53 ± 0.18	0.66 ± 0.15	-8
Retene	0.63 ± 0.13	-	-	-	2.43 ± 0.30	2.36 ± 0.43	3.06 ± 0.96	-6
Pyrene	0.23 ± 0.09	0.18 ± 0.14	0.63 ± 0.72	-	0.41 ± 0.27	1.45 ± 1.22	1.85 ± 0.29	-3
Fluoranthene	0.30 ± 0.13	0.29 ± 0.25	0.55 ± 1.32	0.09 ± 0.28	0.54 ± 0.40	1.77 ± 2.38	2.25 ± 0.35	-3
Benzo[a]anthracene	0.09 ± 0.03	-	-	-	0.16 ± 0.08	0.31 ± 0.11	0.37 ± 0.10	-21
Chrysene	0.15 ± 0.01	0.07 ± 0.02	-	-	0.25 ± 0.03	0.50 ± 0.06	0.60 ± 0.15	-1
Benzo[b]fluoranthene	0.13 ± 0.04	0.08 ± 0.07	0.18 ± 0.34	-	0.34 ± 0.13	0.73 ± 0.58	0.74 ± 0.17	-4
Benzo[k]fluoranthene	0.05 ± 0.01	0.03 ± 0.01	-	-	0.09 ± 0.02	0.17 ± 0.04	0.21 ± 0.05	-7
Benzo[e]pyrene	0.05 ± 0.02	0.05 ± 0.02	-	-	0.16 ± 0.04	0.29 ± 0.08	0.35 ± 0.07	-5
Benzo[a]pyrene	0.08 ± 0.03	0.05 ± 0.05	0.04 ± 0.27	0.01 ± 0.06	0.20 ± 0.08	0.37 ± 0.49	0.35 ± 0.10	-3

Compound	Traffic	Road dust	Biomass burning / SOA	Sulfate	Nitrate	*Estimated*	Measured	% RSME
Benzo[ghi]perylene	0.04 ± 0.02	0.03 ± 0.03	0.15 ± 0.17	-	0.15 ± 0.06	0.37 ± 0.28	0.40 ± 0.07	-7
Indeno[123,cd]pyrene	0.05 ± 0.03	0.05 ± 0.04	0.06 ± 0.23	-	0.19 ± 0.09	0.35 ± 0.39	0.40 ± 0.08	-10
Coronene	0.02 ± 0.02	0.01 ± 0.04	0.12 ± 0.22	0.01 ± 0.05	0.07 ± 0.07	0.22 ± 0.40	0.20 ± 0.04	-11
Benzene	0.12 ± 0.08	0.02 ± 0.03	0.29 ± 0.16	0.01 ± 0.03	0.10 ± 0.05	0.54 ± 0.35	0.48 ± 0.07	-2
Chloromethane	0.28 ± 0.11	0.28 ± 0.04	-	-	-	1.29 ± 0.15	0.81 ± 0.11	-55
Methylene Chloride	0.22 ± 0.05	-	-	-	-	0.49 ± 0.05	0.50 ± 0.12	-32
Toluene	0.01 ± 0.04	0.01 ± 0.06	1.23 ± 0.25	0.13 ± 0.07	0.21 ± 0.1	1.59 ± 0.52	1.03 ± 0.15	0
m/p-Xylenes	0.05 ± 0.13	0.01 ± 0.05	0.49 ± 0.26	0.06 ± 0.06	0.09 ± 0.08	0.69 ± 0.58	0.60 ± 0.08	-4
o-Xylene	0.03 ± 0.01	0.01 ± 0.01	0.19 ± 0.02	-	-	0.19 ± 0.04	0.21 ± 0.03	0

4.2 Air Transport and Circulation

The meteorological conditions and air circulation were also investigated to measure stability across the city during the two IMPs using a tethered balloon system, an instrumented aerial tramway, a laser ceilometer, and a network of surface-based sites. In addition, USEPA's CALMET, NOAA's HYSPLIT, and models were utilized to obtain information on local and regional circulation. A detailed analysis of meteorological measurements and inputs/outputs of CALMET are presented in Appendix A. A summary of air mass backward trajectories is presented below.

Backward trajectories with a resolution of one hour and going back ten days were generated for Albuquerque for the September 1, 2007 to March 31, 2009 period at 1-hour intervals using the NOAA HYSPLIT trajectory model (Draxler and Hess, 1995) and Eta Data Assimilation System (EDAS) meteorological fields as inputs. Starting heights were 10 m, 100 m, 500 m, 1000 m, and 2000 m above ground level. The residence time, defined as the fraction of the total time of back trajectories that the airmass was over a given area of 0.25 degree latitude by 0.25 degree longitude, was computed.

The paths of air masses arriving in Albuquerque at five different elevations for each hour during the entire monitoring period were used to compute the cell residence times of air masses as an indicator of the possible contribution of upwind sources to air toxics concentrations. Figure 4-9 through Figure 4-13 show the spatial variation of residence times at different elevations, including interstate highways and the locations of major air toxics point sources, while the residence time for February 2008 and June 2008 for trajectories at 500 m are compared in Figure 4-14 and Figure 4-15, respectively. These maps show that at all elevations the air masses originated from:

(a) The south/central New Mexico and El Paso area, and followed the I-25 corridor north to Albuquerque, where there are a number of air toxics sources that each emit less than 100 tons/year.
(b) The northwest New Mexico and the Four Corners area, where there are a number of large point sources emitting more than 500 tons/year of air toxics and a large number of air toxic sources with annual emissions between 50-100 tons/year;
(c) Central Arizona, including the Phoenix metropolitan area (along the I-40), intersecting an air toxic source with annual emission of more than 500 tons/year and several point sources in Phoenix.

No significant differences were observed for the normalized residence time during the IMP1 (February 2008). During the second IMP (June 2008), air masses appeared to move slowly and remain for longer periods of time over the Albuquerque area. Some influence from Phoenix urban areas was also observed, while air masses spent little or no time over the Four Corners region and southeast New Mexico. These distinctive patterns for the two IMPs suggested that air masses in the summer may be influenced more by emissions from urban areas while contributions from regional sources may be more important in wintertime.

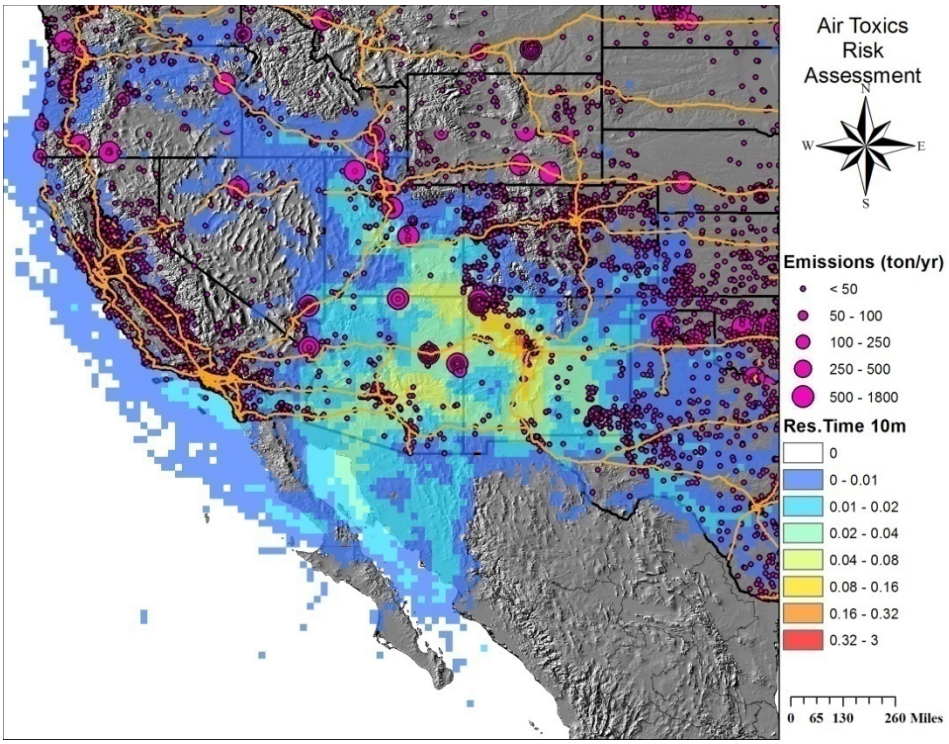

Figure 4-9 Normalized residence time of air mass arriving in Albuquerque at 10 m during the entire monitoring period, the locations of air toxics point sources, and interstate highways

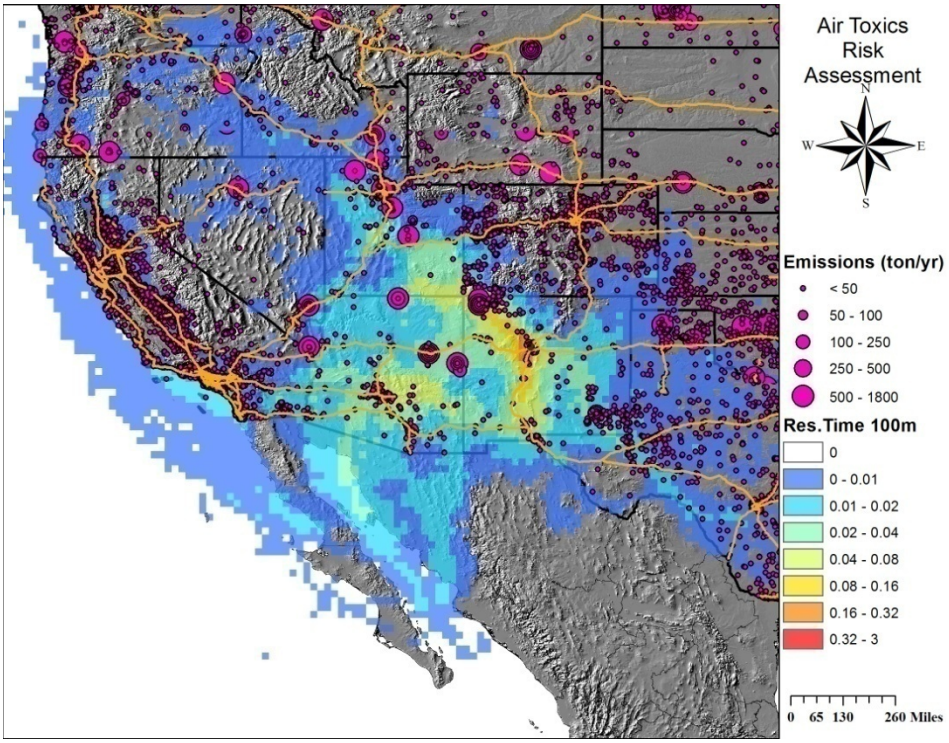

Figure 4-10 Normalized residence time of air mass arriving in Albuquerque at 100 m during the entire monitoring period, the locations of air toxics point sources, and interstate highways

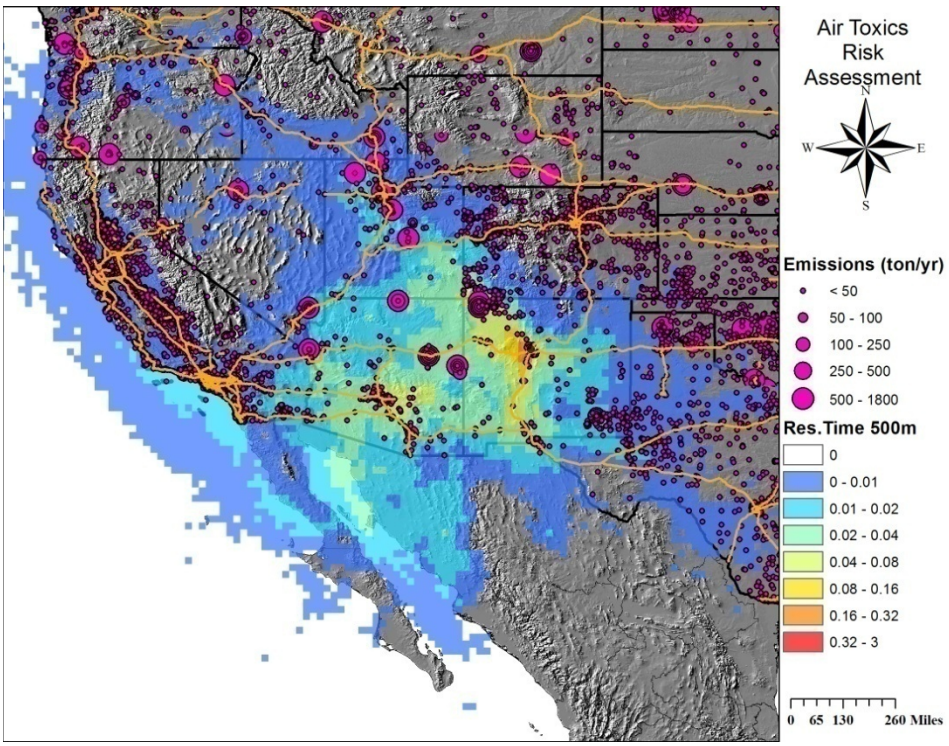

Figure 4-11 Normalized residence time of air mass arriving in Albuquerque at 500 m during the entire monitoring period, the locations of air toxics point sources, and interstate highways

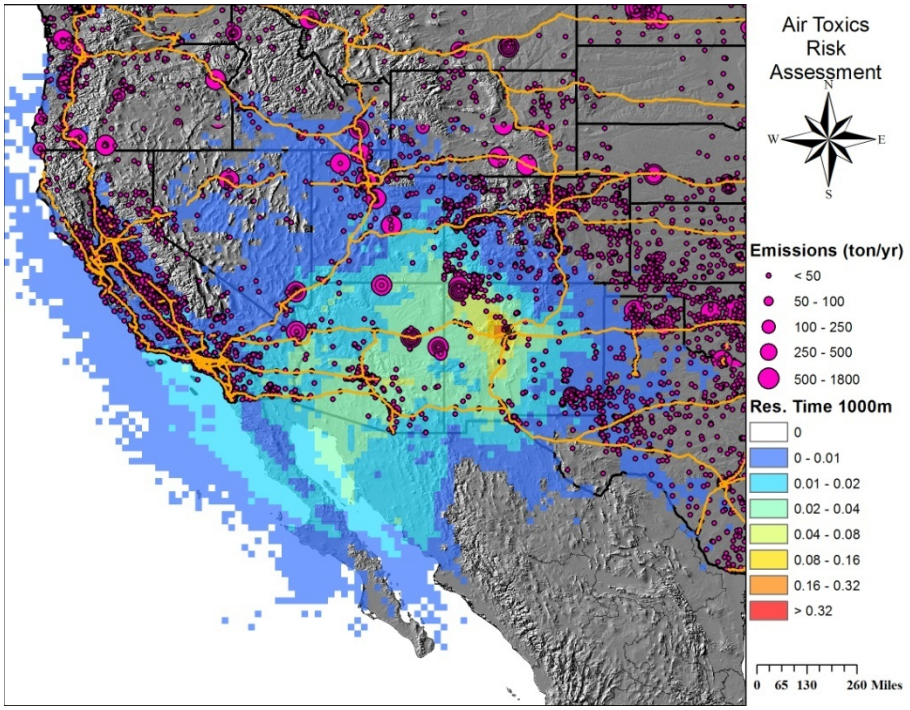

Figure 4-12 Normalized residence time of air mass arriving in Albuquerque at 1000 m during the entire monitoring period, the locations of air toxics point sources, and interstate highways

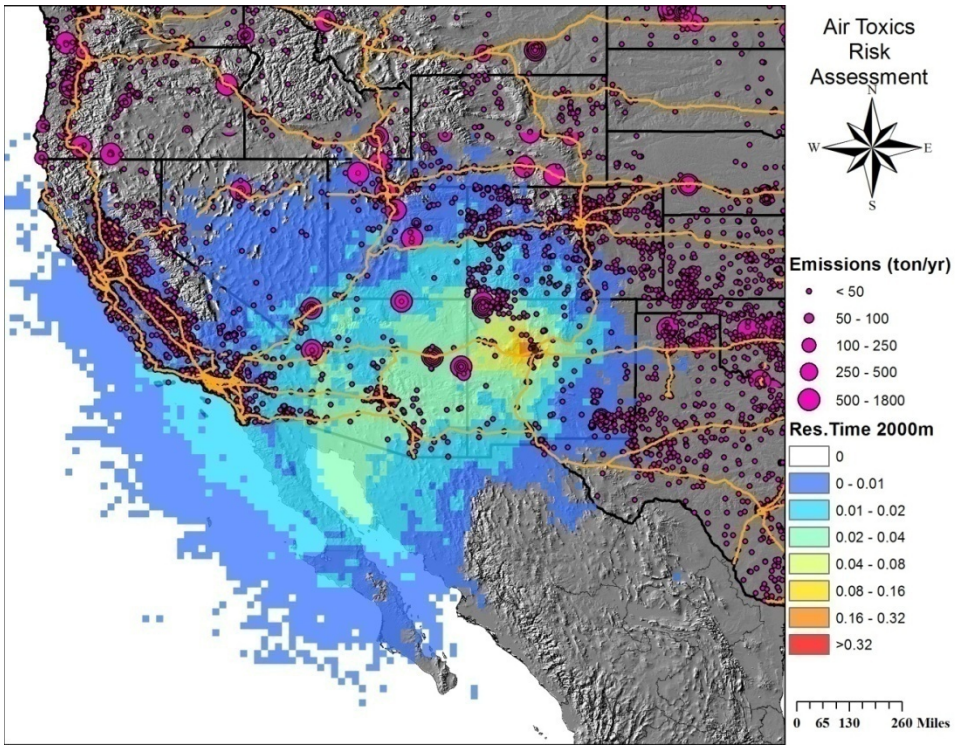

Figure 4-13 Normalized residence time of air mass arriving in Albuquerque at 2000 m during the entire monitoring period, the locations of air toxics point sources, and interstate highways

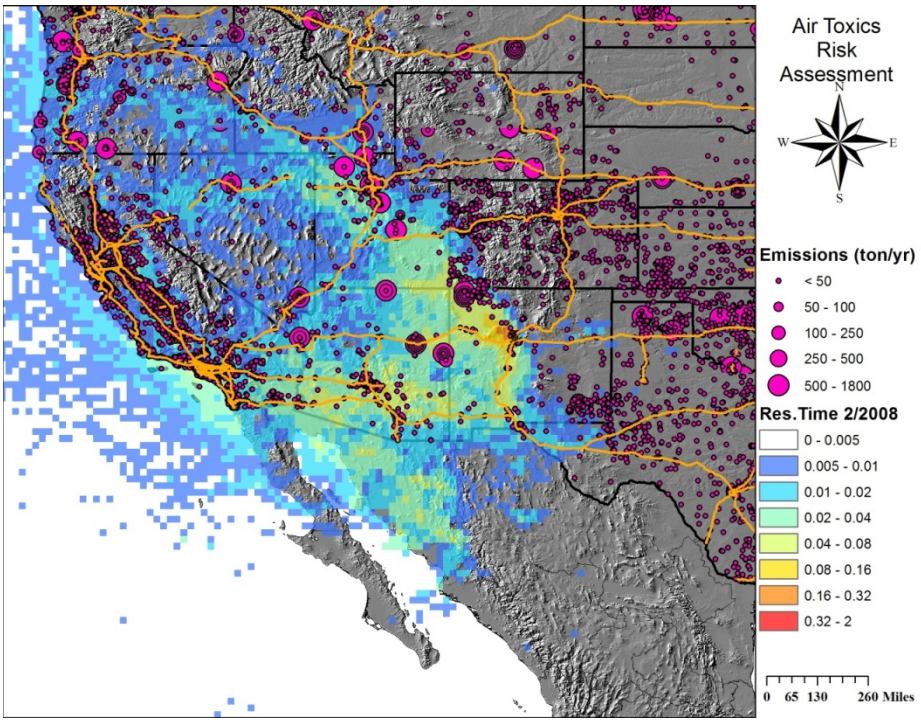

Figure 4-14 Normalized residence time of air mass arriving in Albuquerque at 500 m during the first IMP (February 2008), the locations of air toxics point sources, and interstate highways

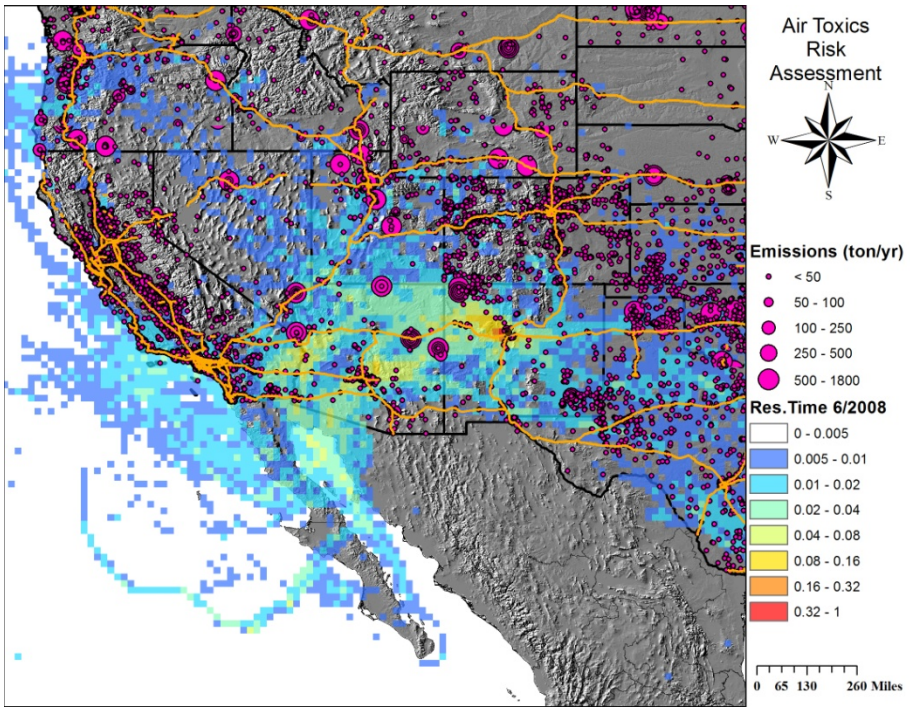

Figure 4-15 Normalized residence time of air mass arriving in Albuquerque at 500m during the second IMP (June 2008), the locations of air toxics point sources, and interstate highways

4.3 Risk Assessment

The risk assessment was conducted for specific air toxics for which more than 50 percent of valid measurements were obtained during a year. These included: benzene (SAROAD Code: 45201), methylene chloride (SAROAD Code: 43802), Toluene (SAROAD Code: 45202) and xylenes (SAROAD Code: 45102).

Table 4-10 Health effects of air toxics and weight of evidence for cancer by the International Agency for Research on Cancer (IARC) and USEPA

	Non-Cancer	Cancer evidence	
		IARC[a]	USEPA[b]
Benzene		1	CH
Toluene			
Xylenes			
Methylene chloride		2B	B2

[a] *IARC WOE = weight-of-evidence for carcinogenicity in humans (1 - carcinogenic; 2A – probably carcinogenic; 2B - possibly carcinogenic; 3 - not classifiable; 4 - probably not carcinogenic).*

[b] *USEPA WOE = weight-of-evidence for carcinogenicity under the 1986 USEPA cancer guidelines, as superseded for specific compounds by the 1999 interim guidelines (1986 guidelines: A - human carcinogen; B1 - probable carcinogen, limited human evidence; B2 - probable carcinogen, sufficient evidence in animals; C - possible human carcinogen; D - not classifiable E - evidence of non-carcinogenicity. 1999 guidelines: CH - carcinogenic to humans; LH - likely to be carcinogenic; SE - suggestive evidence for carcinogenicity; InI - inadequate information to determine carcinogenicity; NH - not likely to be carcinogenic*

The USEPA's TRIM.Risk model was used to calculate human health cancer risks and chronic hazards by combining exposure estimates with toxicity value and using non-probabilistic exposure-response values. The exposure modeling is done using HAPEM5. Toxicity values used for TRIM.Risk calculations include inhalation unit risk estimates (UREs) for assessment of cancer risk and chronic reference concentrations (RfCs). The principles, methodology and applications for each model are given elsewhere (ICF Consulting 2005) (USEPA 2005). The flow diagram of coupled HAPEM and TRIM.Risk model is presented in Figure 4-16. The output of the model is then processed in a tabular format by the Data Analysis and Visualization Engine (DAVE).

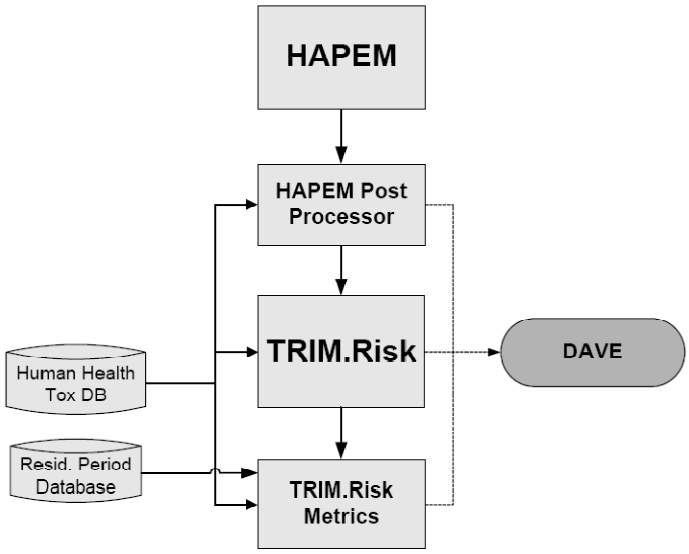

Figure 4-16 Flow diagram of HAPEM/TRI.Risk model (obtained from (US Environmental Protection Agency 2005))

4.3.1 Exposure Characterization

The USEPA HAPEM5 model was used to estimate personal exposure based on measured ambient concentrations. The model uses the U.S. Census Bureau as the primary source of most population demographic data, which is organized in predefined tracts divided into a set of cohorts based on gender and age (see Table 4-11)

Table 4-11 Population code for each combination of gender and age

	Gender	
Age range	Male	Female
0 – 4	1	6
5 – 11	2	7
12 – 17	3	8
18 – 64	4	9
65 and older	5	10

The HAPEM5 requires annual-averaged air quality data in the Industrial Source Complex-Long Term (ISCLT) format. Because measurements were obtained in three locations, each U.S. Census tract was assigned to the nearest monitoring site. Figure 4-17 shows the U.S. Census tracts, the associated monitoring sites, the two interstate highways, and the locations of the air toxics point sources. The operating parameters for the HAPEM model are presented in Table 4-12. The details to setup and run HAPEM are described elsewhere (ICF Consulting, 2005) .With the exception of air quality files that were generated based on measured concentrations, the rest of the files were part of the HAPEM5 package.

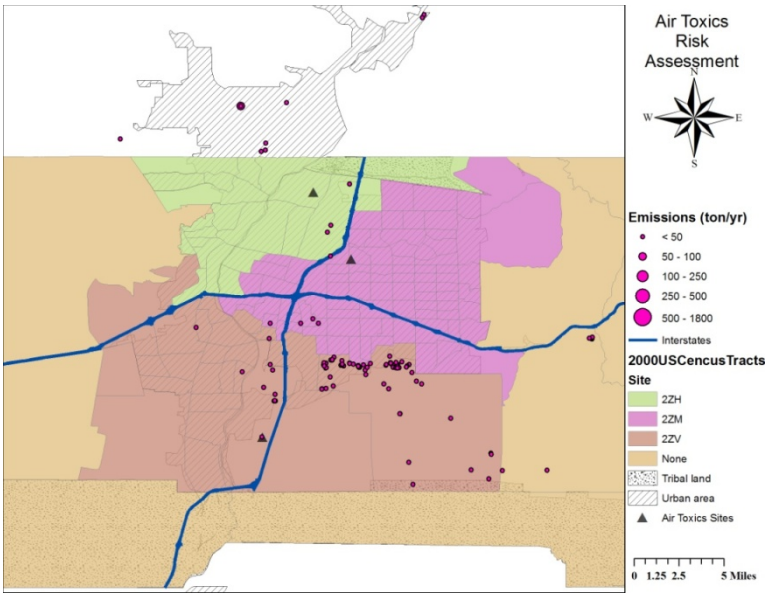

Figure 4-17 Map of Albuquerque showing the representative monitoring site for each 2000 U.S. Census tract, the locations of point sources and monitoring sites of air toxics, and the boundaries of urban and tribal areas.

Table 4-12 HAPEM5 operating parameters

Description	Input File
Activity File	durhw.fix.txt
Cluster File	durhw_cluster.txt
Population File	CENSUS2000.txt
Commuting File	comm2000.txt
State FIPS file	STATEFIP.DAT
Cluster Transition File	clustertransa.txt
Factors File	gas_factors.txt
AutoPduct File	autogarage.txt
Air Quality File	Files generated based on concentrations levels

The estimated exposures to the target air toxics for different age groups of male and female population in Albuquerque are presented in Table 4-13. Exposure estimates were comparable for different age groups for both males and females.

Table 4-13 Modeled exposures (in µg/m^3) of males to target air toxics in Albuquerque based on measurements obtained during the September 2007 – August 2008 and December 2008-March 2009 periods at the three monitoring locations

	Age				
Compound	0 – 4	5 – 11	12 – 17	18 – 64	65 and older
		Males			
Benzene	1.29 ± 0.02	1.30 ± 0.02	1.28 ± 0.02	1.28 ± 0.01	1.31 ± 0.02
Toluene	3.37 ± 0.06	3.38 ± 0.06	3.34 ± 0.06	3.31 ± 0.05	3.41 ± 0.06
Xylenes	2.76 ± 0.07	2.77 ± 0.07	2.74 ± 0.07	2.72 ± 0.05	2.79 ± 0.07
Methylene Chloride	1.77 ± 0.02	1.77 ± 0.02	1.75 ± 0.02	1.74 ± 0.01	1.79 ± 0.02
		Females			
Benzene	1.29 ± 0.02	1.29 ± 0.02	1.28 ± 0.02	1.28 ± 0.01	1.30 ± 0.02
Toluene	3.36 ± 0.06	3.36 ± 0.06	3.33 ± 0.06	3.32 ± 0.06	3.38 ± 0.06
Xylenes	2.76 ± 0.07	2.76 ± 0.07	2.73 ± 0.07	2.73 ± 0.06	2.77 ± 0.07
Methylene Chloride	1.77 ± 0.02	1.76 ± 0.02	1.75 ± 0.02	1.74 ± 0.02	1.77 ± 0.02

4.3.2 Risk Characterization

For inhalation risk assessments using non-probabilistic exposure-response (i.e., toxicity) values, TRIM.Risk combines toxicity values with human inhalation exposure estimates obtained from HAPEM and population-specific information to derive annual hazard quotient (AHQ) and annual cancer risk (ACR).

4.3.2.1 AHQ

The USEPA's prioritized Chronic Dose-Response Values for non-cancer were used to estimate the AHQ and ACR based on the exposure estimates. The values of chronic dose-response for non-cancer (RfC) and acute dose-response values are presented in Table 4-14.

The AHQ is defined as the ratio between the exposure concentration and the RfC.

$$\mathrm{AHQ} = {}^{\text{Exposure Concentration}}/_{\mathrm{RfC}} \qquad (9)$$

Thus, the risk for non-cancer health outcomes due to exposures to air toxics increases for high AHQ values. Exposures to toluene and methylene chloride were associated with very low AHQ values. The mean AHQ values for benzene and mixed xylenes were 0.0430 and 0.0275, respectively, however, these values are typical in urban communities dominated by traffic emissions and similar to those estimated for other urban areas in the U.S.

Table 4-14 Prioritized Non-Cancer Chronic Dose-Response Values and Acute Dose-Response Values for Screening Risk Assessments [a]

	Benzene	Methylene chloride	Toluene	Xylenes (mixed)
Prioritized Chronic Dose-Response Values				
RfC (mg/m^3)	0.03	1	5	0.1
Acute Dose-Response Values				
AEGL-1 (1-h) (mg/m^3)	170	690	750	560
AEGL-1 (8-h) (mg/m^3)	29		750	560
AEGL-2 (1-h) (mg/m^3)	2600	1900	4500	4000
AEGL-2 (8-h) (mg/m^3)	640	210	2400	1700
ERPG-1 (mg/m^3)	170	690	750	
ERPG-2 (mg/m^3)	2600	1900	1900	
MRL (mg/m^3)	0.029	2.1	3.8	8.7
REL (mg/m^3)	1.3	14	37	22
IDLH/10 (mg/m^3)	160	800	190	390

[a] *AEGL = Acute exposure guideline levels for mild effects (AEGL-1) and moderate effects (AEGL-2) for 1- and 8-hour exposures. ERPG = U.S. DOE Emergency Removal Program guidelines for mild or transient effects (ERPG-1) and irreversible or serious effects (ERPG-2) for 1-hour exposures. MRL = ATSDR minimum risk levels for no adverse effects for 1 to 14-day exposures. REL = California EPA reference exposure level for no adverse effects. Most, but not all, RELs are for 1-hour exposures. IDLH/10 = One-tenth of levels determined by NIOSH to be imminently dangerous to life and health, approximately comparable to mild effects levels for 1-hour exposures.*

Table 4-15 Annualized Hazard Quotient in Albuquerque

	Mean	Median	Minimum	Maximum	Std Deviation
Benzene	0.0430	0.0407	0.0341	0.0617	0.0058
Toluene	0.00839	0.00752	0.00636	0.01350	0.00177
Xylenes	0.0275	0.0242	0.0203	0.0485	0.0074
Methylene Chloride	0.00587	0.00595	0.00410	0.00770	0.00070

Figure 4-18 to Figure 4-20 present the cumulative frequencies of AHQ values for the air toxics. Because exposure concentrations are not spatially uniform, these plot show that about 70 to 80 percent of the population residing in Albuquerque may be exposed to concentrations of benzene, toluene, and xylenes with AHQ below the average for the entire population, while the remaining 20% – 30% may be exposed to concentrations that are above the local average but are below the level of health concerns. The similarities between these compounds are probably because of the large contribution of traffic to their levels. For methylene chloride, about 60 percent of the population will be exposed to levels with AHQ higher than the average.

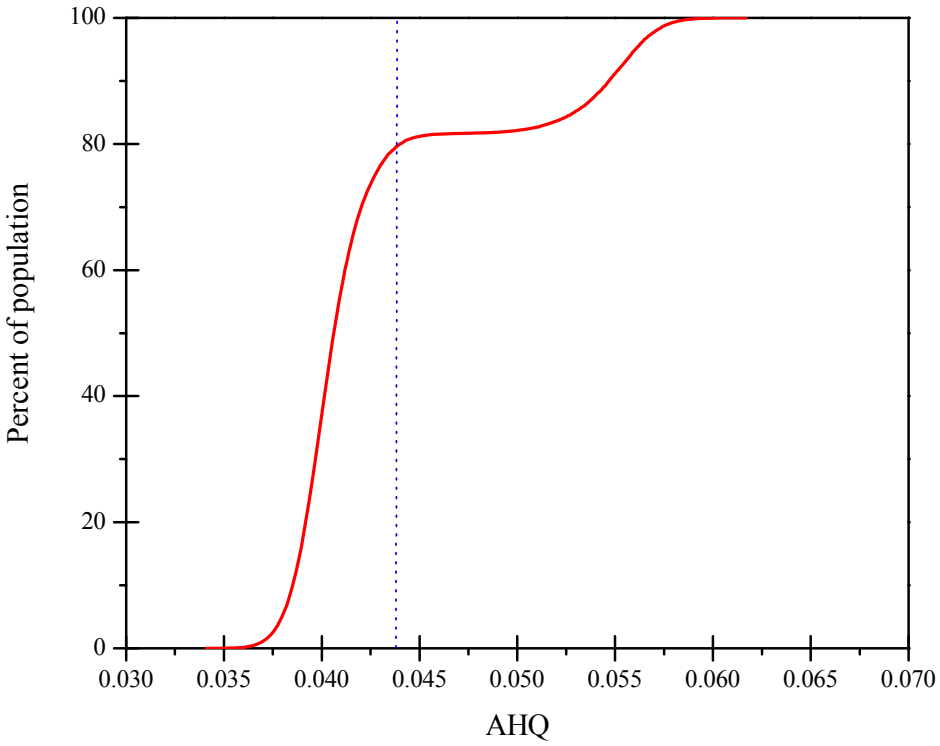

Figure 4-18 Cumulative frequencies of AHQ for population exposed to benzene

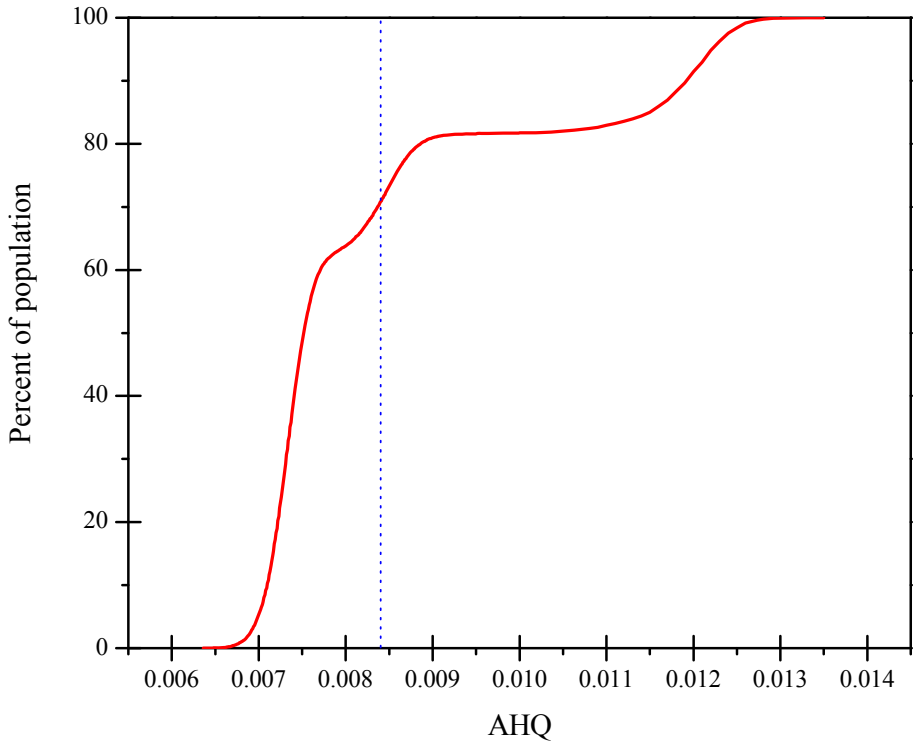

Figure 4-19 Cumulative frequencies of AHQ for population exposed to toluene

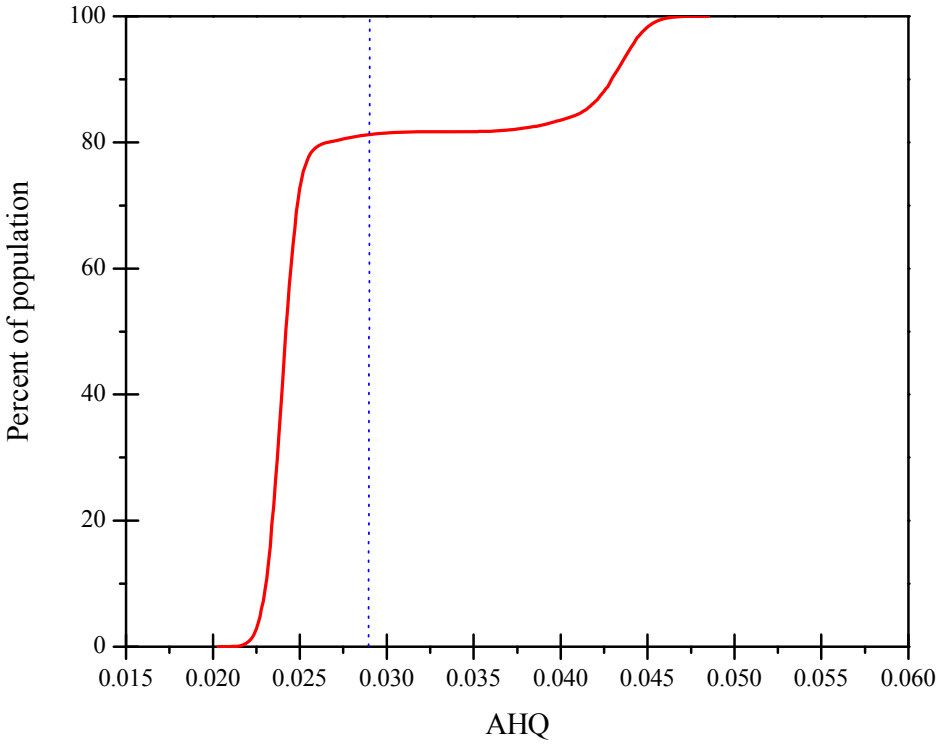

Figure 4-20 Cumulative frequencies of AHQ for population exposed to xylenes

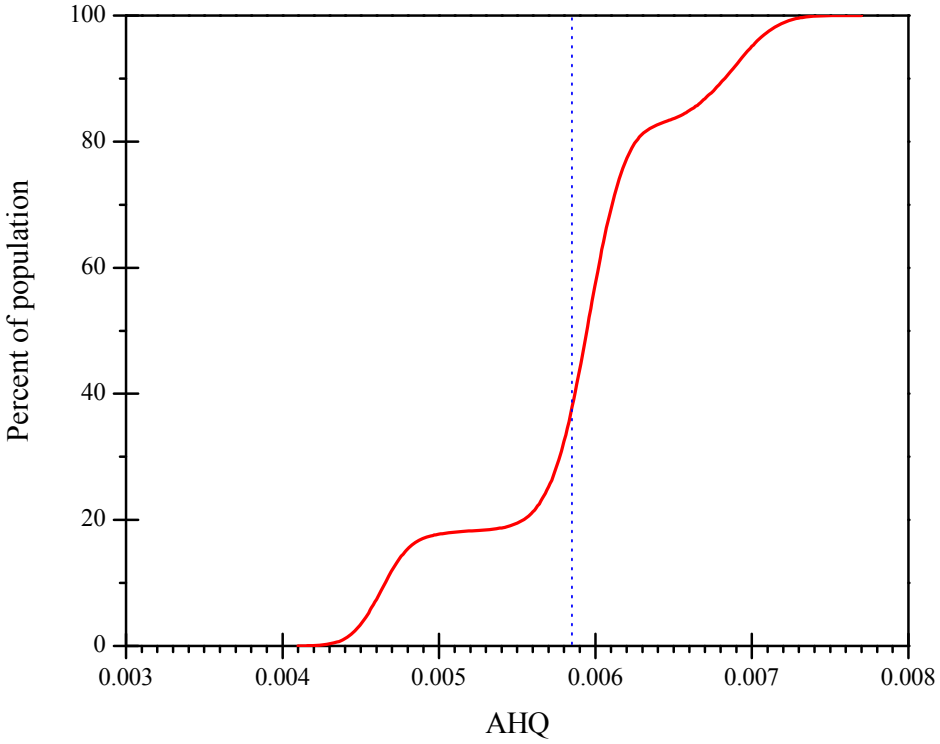

Figure 4-21 Cumulative frequencies of AHQ for population exposed to methylene chloride

4.3.2.2 ACR

The USEPA's prioritized Chronic Dose-Response Values of chronic dose-response for cancer (URE) are presented in Table 4-16. The ACR is defined as the product between the exposure concentration and the URE for a lifetime of 70 years.

$$\mathrm{ACR} = {}^{(\mathrm{ExposureConcentration} \cdot \mathrm{URE})}/_{70} \qquad (10)$$

Table 4-16 Prioritized Cancer Chronic Dose-Response Values and Acute Dose-Response Values for Screening Risk Assessments

Compound	URE ($m^3/\mu g$)	Cancer risk (in one million)			
		Mean	Median	Min	Max
Benzene	$7.80\ 10^{-6}$	0.143706	0.136	0.114	0.206
Methylene Chloride	$4.7\ 10^{-7}$	0.011821	0.012	0.00826	0.0155

The annualized cancer risks for the two air toxics are low, indicating that for a lifetime of 70 years the cumulative cancer risk for exposures to the four air toxics would be less than 1-in-a-million. These estimates were in the same range with those obtained in NATTS sites.

5 Conclusions

The concentrations levels, spatiotemporal trends, sources and health risks of air toxics (PAHs, heavy metals and VOCs) in the City of Albuquerque/Bernalillo County were examined under the framework of an EPA-funded study by AEHD, DRI, NMSLD and ERG Inc. Samples were collected in three locations from September 2007 to August 2008 (only VOCs) and from December 2008 to March 2009 (VOCs, PAHs and heavy metals). In addition, two intensive monitoring periods in which VOCs were continuously monitored and data on local air circulation using a tethered-balloon system were obtained, were carried out in February 2008 and June 2008. Concentrations of air toxics in the three monitoring locations were comparable to those measured in other urban areas nationwide and substantially lower than the prioritized chronic dose-response threshold values for non-cancer (RfC) and cancer (URE) outcomes. Analysis of spatial and temporal trends showed that (1) higher VOCs concentrations were measured during the cold period; (2) lowest VOCs concentrations were measured in weekends as compared to weekdays; (3) strong spatial pattern for VOC. For PAHs and heavy metals, a rather uniform spatial variation was observed.

Analysis of chemical speciation data using positive matrix factorization identified the contribution of five sources to $PM_{2.5}$ particle mass, namely, secondary NO_3^-, secondary SO_4^{2-}, primary emissions from traffic, road dust, and secondary organic aerosol-biomass burning. Biomass burning and particulate NO_3- accounted for most of $PM_{2.5}$ mass during the winter, while SO_4^{2-} was mostly present in the summer. Primary particulate emissions and road dust contributed about 25 percent of $PM_{2.5}$ mass.

The molecular markers approach was used to reconcile the sources of PAHs and VOCs. The mean values of the Fl/(Fl + Py), BaA/(BaA + CT), BeP/(BeP + BaP) and IP/(IP + BgP) diagnostic ratios were indicative of a mixed origin from combustion of fossil fuels and biomass burning. Analysis of air toxics concentrations using the source contributions for $PM_{2.5}$ mass indicated that traffic and biomass burning are the major source of VOCs and PAHs, while some quantities of PAHs and heavy metals were also associated with the resuspension of contaminated road dust.

The health risks associated with exposures to air toxics measured in this study were examined using the EPA-approved TRIM.Risk model coupled with HAPEM5 to estimate exposure concentrations. The analysis was completed for air toxics with more than 50 percent valid measurements over a year. The estimated total inhalation non-cancer and cancer risk for benzene, toluene, xylenes and methylene chloride were similar to those estimated for other urban areas in the U.S. and did not indicate significant health risks.

6 Literature

Benner, B A, et al. "Distinguishing the contributions of residential wood combustion and mobile source emissions using relative concentrations of dimethylphenanthrane isomers." *Environmental Science and Technology*, 1995: 2382-2389.

Department of Environmental Quality. "2005 Air Quality Monitoring Data Summary." Boise, Idaho, 2005.

Desert Research Institute. *Quality Assurance Project Plan: City of Albuquerque Air Toxics Risk Assessment Study.* Las Vegas: DRI, 2007.

Draxler, R R, and G D Hess. "An overiveiw of the HYSPLIT_4 modelling system for trajectoreis dispersion and deposition." *Aistralian Meteorological Magazine*, 1995: 295-308.

Etyemezian, V, et al. *Treasure Valley Road Dust Study: Final Report.* Final , Las Vegas, NV: Desert Research Institute, 2002.

Fehsenfeld et al. "Emissions of volatile organic compounds from vegetation and the implication for atmospheric hemistry." *Global Biogeochemical Cycles*, 1992: 389-430.

Finlayson-Pitts, B J, and J N Pitts. *Chemistry of the Upper and Lower Atmosphere.* Academic Press, 1999.

Finlayson-Pitts, B J, and Jr, J N Pitts. *Chemistry of the upper and lower Atmosphere.* London, UK: Academic Press, 1999.

Fujita, E M, D E Campbell, W Stockwell, P T Roberts, W Main, and L R Chinkin. *Weekend/weekday ozone observations in the South Coast Air Basin, Volume I-Executive Summary.* Final, Atlanta, GA: Desert Research Institute and Sonoma Technology, 2002.

Grimmer, G, J Jacob, and K M Nauhack. "Profile of the polycyclic aromatic hydrocarbons from crude oils_inventory by GC GC/MS. PAH in Environmental Materials Part 3." *Frezenius Z Analytical Chemistry*, 1983: 29-36.

Harrison et al., , D. "Ambient isoprene and monoterpene concentration in a Greek fir (Abies Borissi-regis) forest. Reconciliation with emissions measurements and effects on measured OH concentrations." *Atmospheric Environment*, 2001: 4699-4711.

Jacob, D J, E W Gottlieb, and M J Prather. "Chemistry of a polluted cloudy boundary layer." *JOurnal of Geophysical Research*, 1989: 12975-13002.

Kamens, R, Z Guo, J Fulcher, and D Bell. "Influence of humidity, sunlight, and temperature on the daytime decay of polyaromatic hydrocarbons on atmospheric soot particles." *Environmental Science and Technology*, 1988: 103-108.

Kavouras, I G, D W DuBois, V Etyemezian, and G Nikolich. *Air City Risk Assessment in Albuquerque, New Mexico.* Progress, Las Vegas, Nevada: Desert Research Institute, 2008, 46.

Kavouras, I G, D W DuBois, V Etyemezian, and G Nikolich. *Ozone and its precursor in the Treasure valley, Idaho.* Final, Las Vegas, Nevada: Desert Research Institute, 2008.

Kavouras, I G, V Etyemezian, D DuBois, J Xu, and M Pitchford. "Source reconciliation of dust sources in western United States." *Journal of Geophysical Research-Atmospheres*, 2009: D02308.

Koracin, D, et al. "Dispersion modelling for Treasure Valley, Idaho." *Journal of Air and Wastes Management Association* (Desert Research Institute), 2000: 174-185.

Kuhns, et al, and et al. *Treasure Valley Secondary Aerosol Study.* Final, Las Vegas, Nevada: Desert Research Institute, 2000.

Kuhns, H, et al. "The Treasure Valley Secodanry Aerosol Study I: Measurement and Equilibrium Modeliing of Inorganic Secondary Aerosol and Precursotrs for SOuthwestern Idaho." *Atmospheric Environment*, 2003: 4511-4524.

Logan, J A, M J Prather, F C Wofsy, and M B McElroy. "Tropospheric Chemistry: A global Perspective." *Journal of Geophysical Research*, 1981: 7210-7254.

Lonati, G., M Guigliano, P Butelli, L Romele, and R Tardivo. "Major chemical components of PM2.5 in Milan (Italy)." (Atmospheric Environment) 39 (2005): 1925-1934.

Lovejoy, E R, D R Hanson, and L G Huey. "Kinetics and products of the gas-phase reactions of SO3 with water." *Journal of Physical Chemistry*, 1996: 19911-19916.

Marr, L C, D R Balck, and R A Harley. "Formation of a photochemical pollution in central California 1. Development of a revised mobile vehicle emissions inventory." *JOurnal of Geophysical Research*, 2002: S1-S9, doi:10.1029/2001JD000689.

Martin, R, H Westberg, E Allwine, L Ashman, C Farmer, and B lamb. "Measurement of isoprene and its oxidation products in a central Pensylvania decideous forest." *Journal of Atmospheric Chemistry*, 1991: 1-32.

model, HAPEM.

Motallebi, N, H Tran, B E Croes, and L C Larsen. "Day-of-week patterns of particulate matter and its chemical components at selected sites in California." *Journal of Air and Wastes Management Association*, 2003: 876-888.

Paatero, P. "Least-squares formulation of robust non-negative factor analysis." *Chemometrics and Intelligent Laboratory Systems*, 1997: 23-35.

Paatero, P, and U Tapper. "Positive Matrix Facotrization: a non-negative factor model with optimal utilization of error estimates of data values." *Environmetrics*, 1994: 111-126.

Potukichi, S, and A S Wexler. "Identifying solid-aqueous phase transitions in atmospheric aerosols. II. Acidic solution." *Atmospheric Environment*, 1995: 3357-3364.

Pyyssalo, H, et al. "Polyclic organic material in urban air. Fractionation, chemical analysis and genotoxicity of particulate and vapour phases in an industrial town in Finland." *Atmospheric Environment*, 1987: 1167-1180.

Rogge, W F, L Hildemann, A Mazurek M, G R Cass, and B R.T Simoneit. "Sources of fine organic aerosol. 2. Non-catalyst and catalyst-equipped automobiles and heavy-duty diesel trucks." *Environmental Science and Technology*, 1993: 636-651.

Rogge, W F, L Hildemann, M A Mazurek, G R Cass, and B.R.T Simoneit. "Sources of fine organic aerosol. 3. Road dust, tire debris, and organoimetallic brake lining dust: roads as sources and sinks." *Environmental Science and Technology*, 1993: 1892-1904.

Rogge, W F, L Hildemann, M A Mazurek, G R Cass, and BRT Simoneit. "Sources of fine organic aerosol. 6. Sigarette smoke in the urban area." *Environmental Science and Tehcnology*, 1994: 1375-1388.

Seinfeld, J H, and S N Pandis. *Atmospheric Chemistry and Physics: From Air Pollution to Climate Change.* New York: Wiley-Interscience, 1998.
Sicre, M A, J C Marty, A Saliot, X Aparicio, J Grimalt, and J Albaiges. "Aliphatic and aromatic hydrocarbons in diffrent sized aerosol ove the Mediterranean Sea: Occurence and Origin ." *Atmospheric Environment*, 1987: 2247-2259.
The New Mexico Environment Department. "Corrales Environmental health Evaluation Community Process Summary Report." 2004.
The New Mexico Environment Department. "Corrales Environmental Health Evaluation Community Process Summary Report." Final, 2004.
U.S. Census Bureau. *State and County QuickFacts.* 2009.
U.S. Environmental Protection Agency. *Air Toxics Risk Assessment Reference Library.* EPA-453-K-04-001A, Office of Air Quality Planning and Standards, 2004.
US EPA. *AP 42, Fifth Edition Compilation of Air Pollutant Emission Factors, Volume 1: Stationary Point and Area Sources.* 1996.
White, W H, and P T Roberts. "On the nature and originas of visibility-reducing aerosol in the Loas Angeles air basin." *Atmospheric Environment*, 1997: 803-812.

Appendices

A. Albuquerque/Bernalillo County Community Scale Air Toxics Monitoring and Risk Assessment Project - Modeling Summary

B. Albuquerque/Bernalillo County Community Scale Air Toxics Monitoring and Risk Assessment Project – Experimental Methods

APPENDIX A

Albuquerque/Bernalillo County Community Scale Air Toxics Monitoring and Risk Assessment Project - Modeling Summary

Table of Contents

INTRODUCTION

Background

As part of an air quality study for the City of Albuquerque to support a community scale air toxics risk assessment, a network of temperature sensors were used to measure stability across the city. The Albuquerque urban area is bounded to east by a mountain range and is situated in broad valley. The study was organized in two parts, with a winter and summer intensive operational period. Instruments included a tethered balloon system, an instrumented aerial tramway, a laser ceilometer and a network of surface based sites. The surface measurements varied over the range of elevations from 1500 m to over 3100 meters on the mountain range. This study also compares the pseudo profiles with the tethered balloon and nearby twice daily radiosonde measurements at the airport. The paper reports some observations from the study and discusses some of the issues in using pseudo profiles for estimating atmospheric stability. The methods and results of this study are described in this report.

Project Goals and Objectives

The main goal of this portion of the project was to collect meteorological data and to investigate the wind flow patterns and atmospheric conditions that will help give insights and details about the coupling among HAPs levels, sources and meteorology. The scope of the analysis was limited to primarily data collected during the IMPs. Specific project objectives were:

- Document atmospheric conditions necessary to understand the wind flow patterns during the two Intensive Monitoring Periods in 2008
- To simulate and analyze wind speeds and directions and provide a conceptual model of the atmospheric conditions relevant to pollutant transport and dispersion in the Albuquerque metropolitan area during the IMPs

Technical Approach

A combination of transport models and analysis of the existing meteorological monitoring data was applied in order to understand the transport of pollutants in the Albuquerque area. A wind rose analysis of the existing surface meteorological network was completed to help understand inter- and intra-valley differences in wind flow patterns. The analysis looked at up- and down valley as well as up- and down-slope winds from the mountains in the context of diurnal and seasonal cycles. The CALMET diagnostic meteorological model was used to generate local-scale wind fields within the greater Albuquerque area. CALMET was run with hourly data from the City of Albuquerque's meteorological monitoring network and National Weather Service airport data and twice daily airport radiosondes. Tethersonde data collected during the IMP was used to supplement the upper air measurements taken at the airport and as input to CALMET. The CALMET model output will be necessary for running a local dispersion model such as CALPUFF. To obtain a regional perspective (and identify regional

transport of HAPS), HYSPLIT was employed to calculate multi-day back-trajectories. The inputs for HYSPLIT are provided by either the 40-km or 12-km EDAS model data from NOAA's Atmospheric Research Laboratory. Since comprehensive toxics emission inventory is neither part of this proposed work nor available for the Albuquerque area from prior studies, a reasonably accurate cumulative source dispersion modeling analysis will not be possible.

Air quality models are commonly used for permitting planned sources, determining the pollutant contributions from existing sources, and estimating human exposure (Moschandreas et al., 2002). These source-oriented models simulate how emissions from point, line, and area sources disperse and transport in the atmosphere. They are most often applied to estimate ground-level concentrations of emitted pollutants that might increase human exposure beyond acceptable levels.

All models are simplifications of reality. Simplifying assumptions must be made because input data are usually sparse, emissions may be sporadic or poorly characterized, and the random nature of atmospheric movements can never be completely known. Exact correspondence between dispersion model estimated and measured concentrations are rare. However, when dispersion models are validly applied, the general characteristics of emitted plumes can be determined and ambient concentrations can be estimated within stated uncertainties. These estimates become more reliable with longer averaging periods as random variations over shorter periods cancel each other in the long-term averaging.

EPA's CALMET diagnostic atmospheric model is most appropriate for estimating wind fields for this application. CALMET interpolates between available meteorological measurements with user-given constraints about terrain and flow obstructions. It does not require expensive super-computers. More accurate "prognostic" models, such as Mesoscale Model 5 (MM5) and the Weather Research and Forecasting model (WRF), solve complex physical equations rather than interpolate between measurements. These models require substantial set up and computational resources that are beyond the scope of this project, although they might be considered in future projects. CALMET can estimate where and when low winds speeds occur. Winds from CALMET can be coupled with the CALPUFF dispersion model.

Merely running modeling software on a computer and obtaining results is insufficient for a valid air quality study. The results must be examined with respect to measurements to determine model performance. The results must also be consistent with conceptual models of air quality emissions, dispersion and transport.

Study area and sampling network

Figure 1 designates the area of interest, including locations of various terrain features and population center within the Albuquerque metropolitan area.

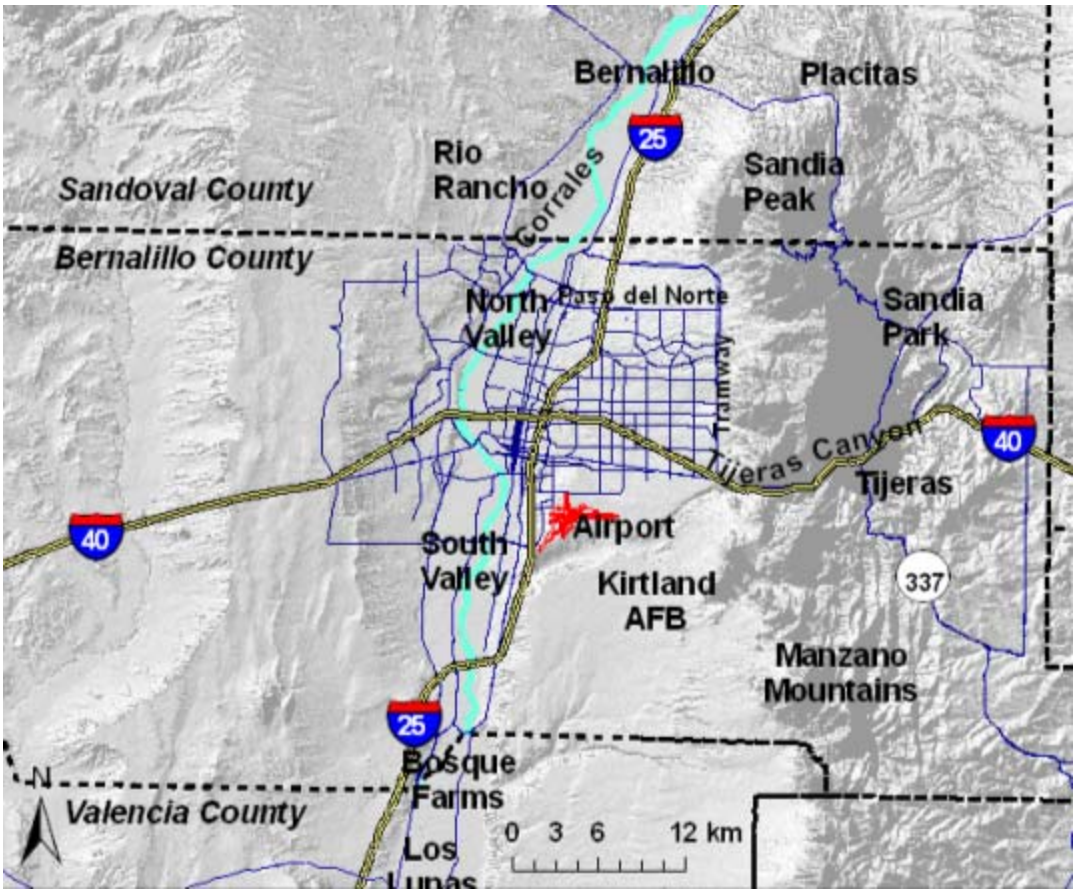

Figure 1. Study area showing major locals within the valley

The data discussed in this section included primary measurements or those included in the QAPP and those that were called "supplemental" or not included in the QAPP and were to help us understand the air transport patterns during the two IMPs.

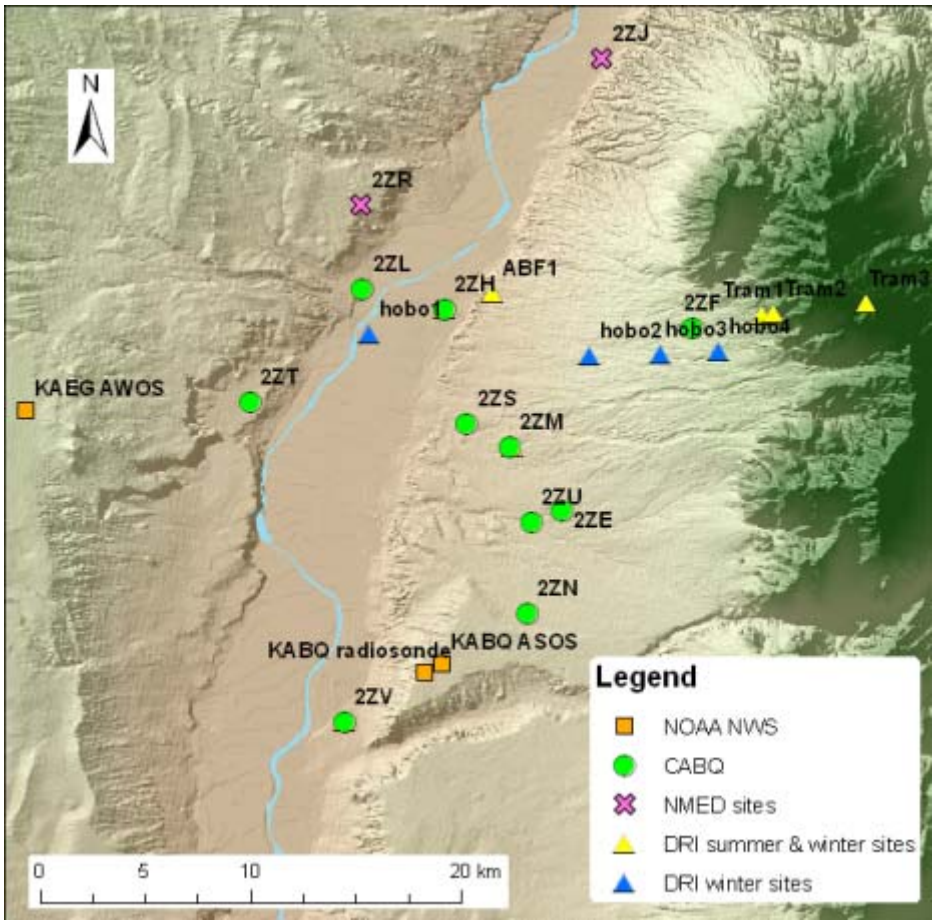

Figure 2. Study sites. Supplemental sites operated by DRI are shown as triangles. Other sites such as the Double Eagle KAEG and sites operated by the New Mexico Environment Department are also shown for reference.

SUMMARY OF THE WINTER STUDY

The winter study is important to the analysis of peak air quality events since that is the time of the year when temperature inversions are frequent and pollutants build up during multi-day stagnant periods.

Daily Project Activity and Meteorological Conditions

This section describes the general meteorological conditions during the winter intensive monitoring period from February 12 to 18, 2008. The meteorological summaries relied on twice daily 500 mb height/vorticity maps, surface station maps, GOES satellite imagery, National Climatic Data Center station summaries and observations made during the study. The twice daily radiosonde data in the form of skew-T plots are presented in Appendix D.

February 12, Tuesday

The synoptic weather pattern characterizing the start of the IMP is that of a transition between a trough and a building upper level ridge. At this point in the synoptic cycle

there are northwest winds aloft. This was a dry and cool day with mostly light winds and mostly sunny skies. Maximum temperatures reached in the upper 50s °F in the valley. The airport temperature reached 55°F as the maximum and 32°F as a low. Forecasted mixing heights for the middle Rio Grande Valley were expected to be 3,000 foot AGL with northwest winds 16 knots. This is in the fair ventilation category with a product of 48,000 knot-feet. Evening forecasts were for mostly clear skies and minimum temperatures in the range of 24 to 28°F in the valley, humidities in the 52 to 72 percent range and north winds 10 to 15 mph becoming terrain dominated 5 to 10 mph. Tram instrumentation and HOBO sensors were installed at the tram top and base by noon. The blue tram car held the instrumentation today. Several inches of snow cover was observed at the top of the tram and Sandia Ski area. Visibility was very good from the tram top at 11:45 am. Preparations were made at the balloon fiesta park for operating the tethered balloon tomorrow. Tram instrumentation was downloaded from the data loggers at 6 pm. A total of 12 up and down tram profiles were measured by the instrumentation today.

February 13, Wednesday (CABQ sample day)

The day started with clear skies and mild temperatures. It was warmer than yesterday with winds increasing. Forecasts for the area included highs in the upper 50s to lower 60s with west winds 10 to 20 mph in the afternoon. In the evening the area was partly cloudy with lows in the 30s and southwest winds 10 to 15 mph. In advance of a cold front approaching from the west, winter storm warnings went up in the evening for the mountainous areas to the north. Tethered balloon operations began at 9:20 am. As the sun came up, there was some haze visible toward the east. For several profiles we used the particle counter and VOC analyzer on the balloon. The tetherline broke at approximately 1:38 pm. Tethered balloon operations were terminated at that point. The airport temperature reached 62°F as the maximum and 28°F as a low. A total of 6 tethered balloon profiles were collected today. A total of 29 up and down tram profiles were measured by the instrumentation today. The first tram up profile was started at 7:59 am and the last profile started at 9:30 pm.

February 14, Thursday

On the large scale a closed low was over southern Nevada and surface low over the Four Corners. The 500 mb map at 12 UTC (5 am) showed moderate positive vorticity advection over the Four Corners. This system will bring in a winter storm over the area starting from the Four Corners and drifting east throughout the day. Strong cold front moved south across the state today. Forecast for today was mostly cloudy with some isolated rain showers in the afternoon. A wind advisory was issued for the south central mountains and high plains. The morning started off with clear skies with a few clouds over the Sandia Mountains. The morning sounding at the airport showed an inversion at around 200 m AGL with clouds at 600 mb. Dewpoint temperature at the surface was -7 ºC. By the afternoon the airport sounding showed a dry unstable surface layer with no signs of an inversion and clouds did not show up until nearly 500 mb. Surface dewpoint depression was 30ºC at 4 pm. By 5 pm high clouds covered the metro area but no precipitation. The high temperatures for the day were in the upper 50s in the valley with southwest winds from 10 to 20 mph and gusts to 30 mph. The airport temperature reached 64°F as the maximum and 42°F as a low. Gusty east winds through Tijeras

Canyon of 15 to 30 mph and gusts to 40 mph were the result of the cold front moving through the region during the night hours. Vertical profiling with the tram started today but no vertical profiling with the balloon. There were a total of 17 profiles with the tram starting at 8:04 am and ending at 5:30 pm. HOBO® dataloggers were placed along Paso del Norte in the evening that measures temperature and humidity from the Rio Grande River to Tramway Boulevard.

February 15, Friday

A closed low aloft centered over southern Arizona and associated surface trough drove the weather on Friday. Morning skies started off with clouds but higher than the Sandia Peak. The morning airport sounding showed an inversion cap at 187 m AGL at about 4 am local time. Based on this sounding cloud heights were at 581 mb or 2870 meters AGL. Dewpoint at the bottom of the sounding was at -5ºC indicating a slightly moister airmass compared to yesterday. Clouds remained over the region all day with some breaks near mid-day. Strong easterly winds blowing through the canyon influenced portions of the valley throughout the day. Forecasted peak winds were in the 20 to 35 mph range with gusts of 50 to 55 mph were possible. Gusty winds were observed in the afternoon with some blowing dust in the valley downwind of the canyon. The afternoon airport sounding showed clouds around 575 mb, at a height of 2950 meters AGL. The high temperatures at the airport reached 52ºF and 37°F as a low. There were a total of 28 profiles with the tram starting at 7:58 am and ending at 8:26 pm. No vertical profiling with balloon today. Today we discussed with the local FAA on ways to start balloon soundings and rebuild our tethered balloon system. The local FAA representative, Mr. John Dewitt, approved the use of an alternate balloon (< 6' diameter), going no more than 500' above ground height and staying below 500' from a cloud base. We agreed this would work for the remaining portion of the project and ordered more 5 and 6 foot diameter latex balloons. The HOBO® dataloggers continued to measure T and RH today.

February 16, Saturday

The closed upper low moved slowly east and by the morning it was over southern New Mexico. The morning started off wet with some snow showers. The morning's airport sounding indicated a new airmass was in the region with a surface dewpoint at the freezing point of 0ºC. Combined with a temperature of 0ºC (low temperature of the day) gave it a RH of 100 percent. Snow was falling throughout the valley in the morning but no accumulations. The airport ASOS accumulated a total of 0.09 inches of precipitation. The airmass was forecasted with a little cooler air but didn't cool below freezing. In fact the day's high temperature reached 55 ºF at the airport. By afternoon the closed upper low was over the Permian Basin in Texas. Precipitation moved off toward the east with some snow showers and freezing rain north of I-40 and east of I-25. In fact most of the precipitation fell in the eastern part of the state with snow accumulation ranging from 2.5 to 7 inches near Clines Corners. Only 2 inches of snow accumulation was measured at the Sandia Ski area by 2:27 pm. By evening the sky was partly sunny with some lingering clouds over the mountains. The airport temperature reached 55°F as the maximum and 32°F as a low. Testing of a new balloon system was done today in the afternoon at 2:19 pm. However winds were too high to continue so no vertical profiling

today. There were a total of 37 profiles with the tram starting at 8:10 am and ending at 10:55 pm. The HOBO dataloggers continued to measure T and RH today.

February 17, Sunday

Finally a break in the storm systems allowed us to start soundings with the new balloon today. We started the soundings at 4:41 am and concluding at around 7:30 am. On the synoptic scale an upper level ridge builds over the western US following the storm system from the previous few days. Winds were from the northwest at this point in the developing ridge. Overnight a cold front passed over the valley that brought in a new airmass. The morning airport sounding showed an inversion at 647 mb or at 1992 meters AGL. Surface dewpoint of the sounding was -6ºC. By daybreak a few clouds were observed over Sandia Peak but otherwise clear skies. The forecast for today called for partly cloudy skies, breezy and northwest winds 10 to 20 mph increasing to 15 to 25 mph in the afternoon with gusts up to 35 mph. At the airport the morning low was 36°F while the high was 52°F. Tethered balloon operations commenced again at the balloon fiesta park at 4:41 am. To comply with FAA regulations, we went no higher than 152 meters AGL (500'). The day started out with clear skies, with some terrain forced clouds over the Sandia Mountains. The first balloon sounding showed a low level inversion up to 80 meters AGL. By 7:20 am, the winds were too high to safely operate the balloon, so we terminated the day. A back door cold front passed through the area in the afternoon that brought in a dry airmass as the dewpoints drop. This was verified during the afternoon airport sounding measuring a surface dewpoint of -17.6ºC. The airport recorded a 40 mph peak wind gust during this event. There were a total of 27 profiles with the tram starting at 8:03 am and ending at 9:48 pm. The HOBO® dataloggers continued to measure T and RH today.

February 18, Monday (CABQ sample day and President's Day)

Monday started off with clear skies and cool temperatures. On the synoptic scale the strong upper level trough that affected the area the past few days has moved east and a upper level ridge continues to build with a weakening northwest flow aloft. With this type of pattern we typically see a warming trend and tranquil conditions. The new milder weather system brought in lighter winds and shift in wind direction. This calm weather should last for at least another day until the next storm system arrives on Wednesday afternoon. The morning low at the airport reached 25ºF on Monday. The morning airport sounding showed a shallow inversion 125 m and a more defined one around 1582 meters AGL. The surface dewpoint temperature on the sounding was –8.7ºC. The forecast for today called for sunny skies, light winds and near seasonal temperatures in the upper 50s. The afternoon airport sounding showed an unstable mixed layer through 700 mb. Above that (above 1454 m AGL) there was a very dry free tropospheric layer. Flew new balloon today, with profiles starting 3:33 am. The near ground temperature at the start of the first profile was slightly below freezing at -1.5°C. By 3:55 am there was a sharp drop in ambient temperature and a wind shift to the southwest. At 8:11 am the near surface temperature inversion had eroded. We did notice smoke from a wildfire north of Albuquerque after 1 pm. The smoke plume travelled east looking from the balloon fiesta location and was not visible after 2 pm. By 3 pm, there were numerous cirrus clouds covering the sky. The tethered balloon soundings ended at 4:13 pm due to increasing

winds aloft. The high at the airport reached 56ºF with high clouds moving in from the west. The morning low at the airport was 25°F. Unfortunately no tram profiles were obtained on this date due to a power problem on the instrument package. The HOBO® dataloggers continued to measure T and RH today.

February 19, 2008, Tuesday (pack up day)

Tuesday was another calm day with zonal flow aloft over central New Mexico. Since yesterday was the last official day of the intensive operational period, all sites were packed up today. Tuesday started out with clear skies and calm winds. A weak shortwave travelled over the area in the afternoon bringing in high clouds. Forecast for Tuesday called for partly cloudy skies, highs in the upper 50s, southwest winds 10 to 15 mph.

Tethered Balloon Profiles

The purpose of the tethered balloon measurements was to collect detailed profiles of meteorological variable in order to improve or understanding of transport of toxic air pollutants in the Rio Grande Valley. Measurements were focused on capturing the pre-dawn atmospheric stability and subsequent expansion of the mixed layer just after sunrise.

The Vaisala DigiCORA instrument package on the tethered balloon includes a fast response temperature and humidity sensor, a cup anemometer and a wind vane. The data acquisition is similar to one used on radiosondes and collects a measurement from each sensor once per second. Clearance from the FAA was given to fly the balloon between sunrise and sunset up to a height of 450 meters above the ground at the Balloon Fiesta Park. Prior to sunrise and after sunset the tethered balloon was permitted to fly only up to 150 meters (500 feet). Before launching the balloon each morning we contacted the airport flight tower to notify them that we were operating the balloon. Similarly, at the end of each day we notified them that we were quitting for the day. Typical ascent and descent rates were in the range of 0.5 to 0.75 meters per second. Deviations from these rates were made while bringing the system down to avoid thunderstorm wind gusts.

On February 13 the official sunrise was at 6:51 am mountain standard time but the sun rose above the Sandia Mountains approximately 10 minutes after that. Tethered balloon operations began on February 13 at 9:33 am. Figure 3 summarizes the eight profiles made on this day. Wind barbs are defined using standard meteorological definitions such as north as up and 5 knots per barb. Potential temperatures in Kelvin are displayed in the background to visually identify stable and unstable layers where potential temperature is defined as

$$\theta = T\left(\frac{p_0}{p}\right)^{R/C_p}$$

And p = pressure, p_0 = 1000mb, T = temperature, R = gas constant, and C_p = specific heat of air at constant pressure. Stable layers are defined when the potential temperature increases with height or

$$\frac{\partial \theta}{\partial z} > 0$$

and unstable layers are for conditions when the potential temperature profile decreases with height or

$$\frac{\partial \theta}{\partial z} < 0$$

Notice in Figure 3 that the first profile at 9:33 am indicated a stable layer at 200 meters above the ground. The atmosphere was unstable after that and showed considerable warming in the lower 50 meters before heating the layers aloft. The two shorter profiles at 10:57 and 11:05 were for testing the ozone and particle samplers up to 100 meters. Unfortunately the tether line snapped after the 12:17 pm profile and the balloon soundings didn't commence again until February 17. However the first two soundings provided useful information about the post-sunrise evolution of the boundary layer and some value for the depth of the nocturnal stable layer.

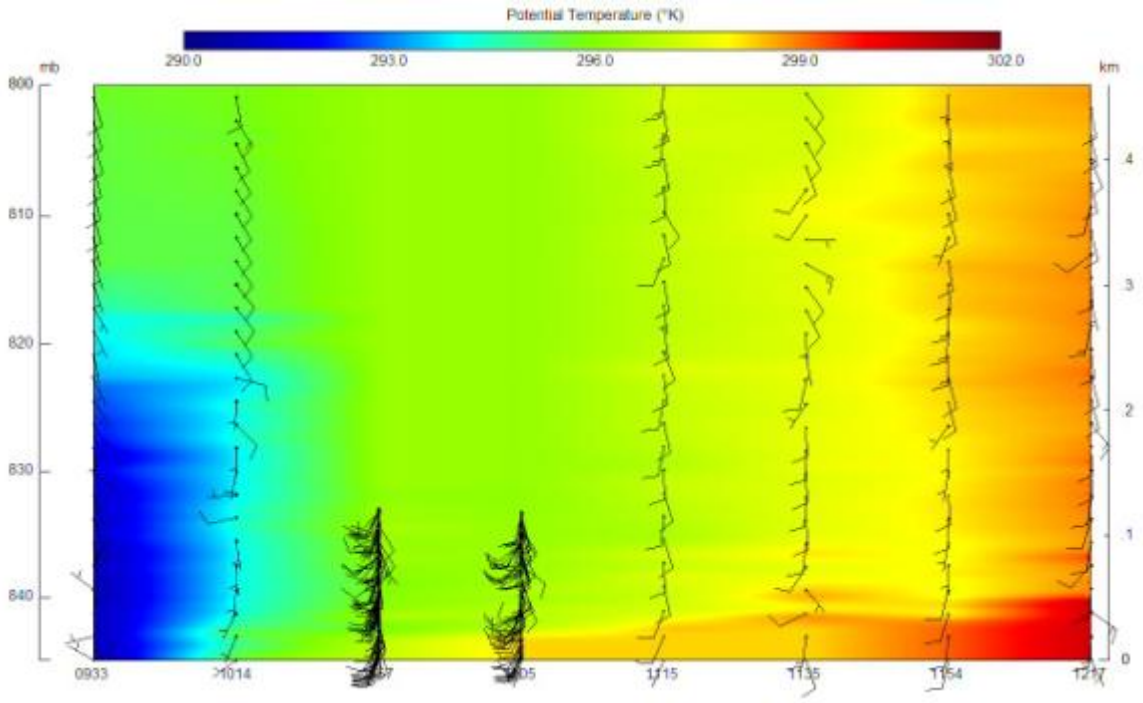

Figure 3. Potential temperature soundings from the tethered balloon during February 13, 2008.

Since the soundings on February 17 started earlier in the day before sunrise, profiles indicated the presence of a residual layer in the evening. This can be seen in stable layer in Figure 4 from 4:41 to 5:11 am. The stable layer was shallow and was approximately 50 meters above the ground. Since it was before sunrise, no profiles were taken above 150 meters. It was interesting to see a thin cool layer ($\Delta\theta \approx 2K$) near the surface that existed through 7:30 am. This 30 meter thick layer was probably a surface effect from the cool ground. On February 18, the stable layer was present at the same strength as the previous day but was a little higher, ranging from 50 to 100 meters above the ground up till sunrise. By 8 am, the stable layer has eroded and was no longer visible.

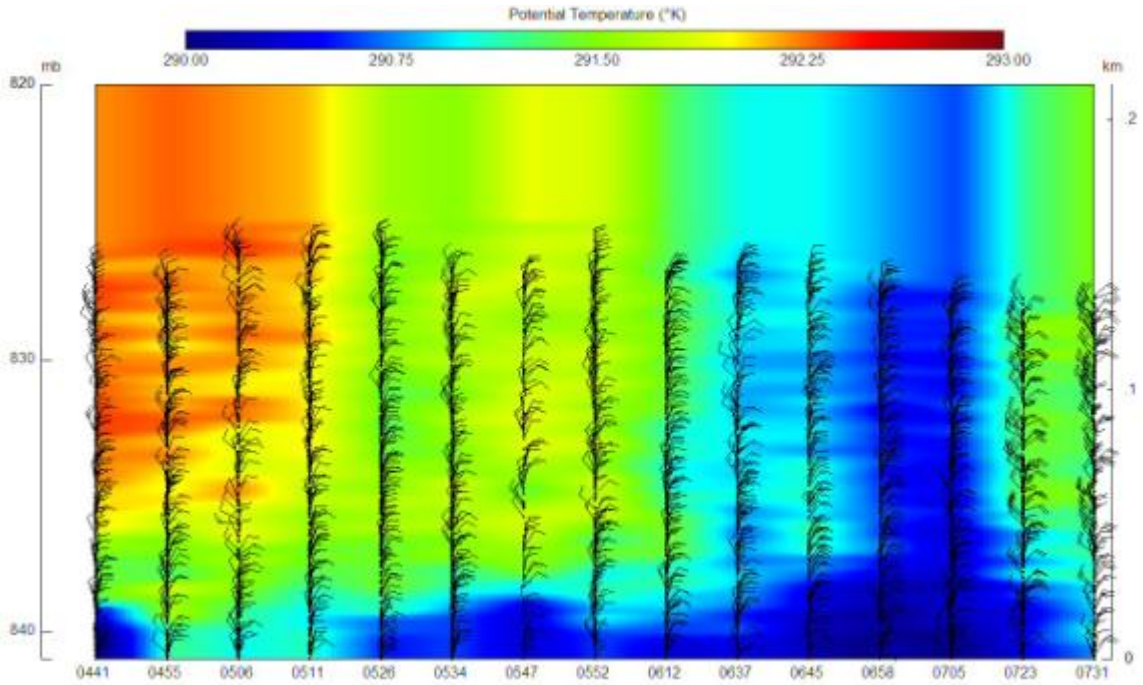

Figure 4. Potential temperature soundings from the tethered balloon during February 17.

The next plot shows the soundings on February 18. There were 23 soundings at the fiesta park on this day. A stable layer was present in the morning soundings and varied in height over time. By 7:50 am the stable layer had eroded and the ground started to warm up from the sun.

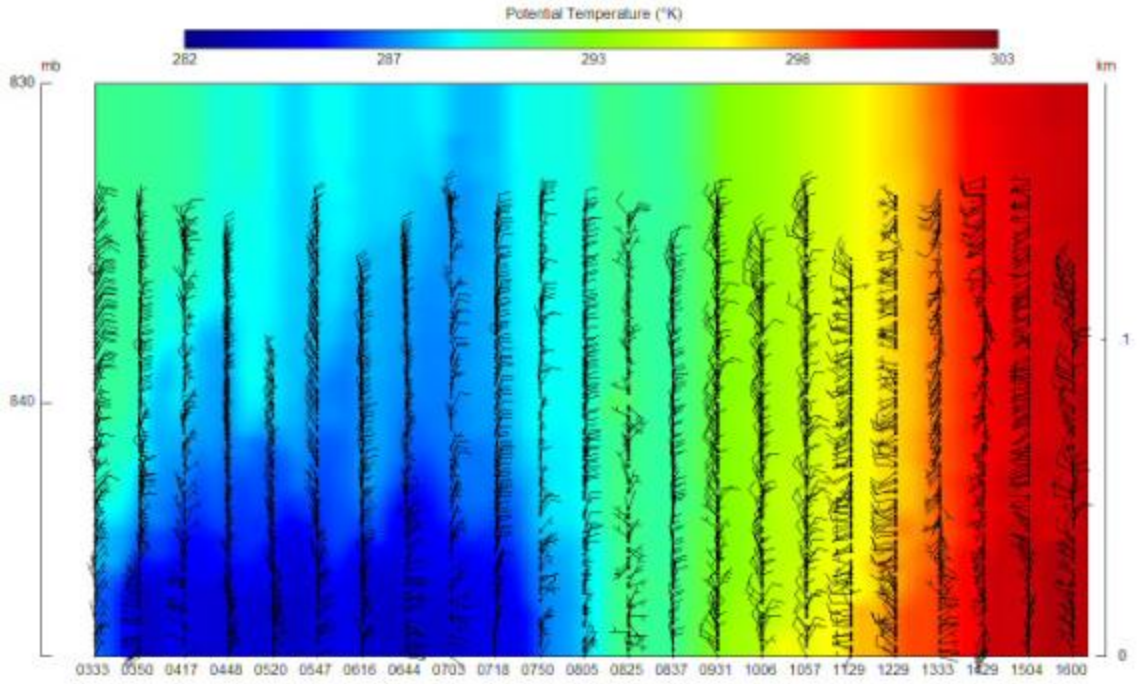

Figure 5. Potential temperature soundings from the tethered balloon during February 18

During this IMP an instrumented 20 foot meteorological tower was deployed at the balloon fiesta park to measure winds, temperature, relative humidity at 10-minute intervals at the base of the tethered balloon. Figure 6 shows the wind measurements taken during this time. The wind direction shows the daily transitions from northerly to southerly flows and corresponded well to the lower level tethered balloon measurements.

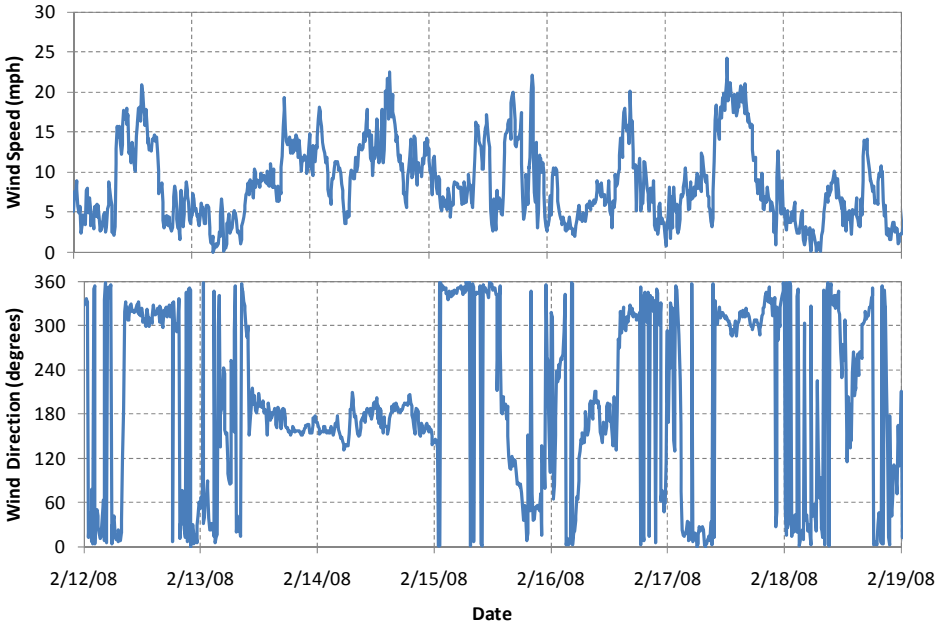

Figure 6. Wind measurements at the balloon fiesta park during the winter IMP

Detailed plots of the tethered balloon data are presented in Appendix B. Here we present plots of mixing ratio, relative humidity, temperature, potential temperature, equivalent potential temperature, v-component of wind speed, and scalar wind speed.

Sandia Tramway Profiles

In order to obtain a near continuous record of temperature profiles from maximum height of the tethered balloon up to 3 kilometers, we employed a temperature/relative humidity sensor on the Tramway. The Tramway regularly travels from the base up to the top seven days of the week from around 8 am to the evening. During the winter study the tram took on average 15 minutes from top to bottom and occasionally makes the trip in 12 minutes and as long as 32 minutes.

To convert the pressure measured on the tram to an altitude, we derived an expression based on first principles. The first assumption is that the atmosphere behaves as an ideal gas. The ideal gas law is

$$p = \rho R_d T$$

Where p is the pressure, ρ is the density of the air, R_d is the gas constant and T is the air temperature. The second assumption is that the atmosphere is in hydrostatic balance. This assumption is valid in our case since we are not dealing with thunderstorms or tornadoes. The hydrostatic equation is expressed as the following equation.

$$dp = -\rho g dz$$

Where p is pressure, g is the gravitational constant and z is the height. This equation implies that pressure decreases as a function of height. Now substituting the density from the ideal gas law into the hydrostatic equation results in

$$dz = -\frac{R_d T}{gp} dp$$

Now this can be integrated from a height, z_1 to a height z_2 and corresponding pressures p_1 and p_2.

$$\int_{z_1}^{z_2} dz = -\int_{p_1}^{p_2} \frac{R_d T}{gp} dp$$

Upon integration we solve for z_2 as a function of pressure and temperature.

$$z_2 = z_1 + \frac{R_d T}{g} \ln(\frac{p_1}{p_2})$$

This was implemented with p_1 as the pressure measured at the tram's lowest point, z_1 was the elevation of the tram's lowest point (1,999 meters MSL), T being the measured temperature, and with p_2 as the measured pressure at some elevation z_2. The lowest point was obtained when the tram was docked at the base.

Figures 6 to 11 show the tram profiles for February 12 to 17, 2008. Notice that the ground heated up the sounding as it passed close to the tram towers. The ground effects from the tram tower can be seen at about 2,200 and 2,700 MSL in the figures. Ground effects were more prominent in the raw one second temperature profile plots in Appendix C. Figures 6 to 11 were averaged into 100-meter vertical averages to smooth out the effects of ground heating but still retained the overall temperature trend. Averaging to 100-meter segments divided the profile data into 11 points. Surprisingly there were very few indications of a stable layers in the tram temperature profiles. The only strong indication of a stable layer can be seen in the 8:12 am profile on February 16, 2008 near the top of the tram. Unfortunately we did operate the tethered balloon during that day.

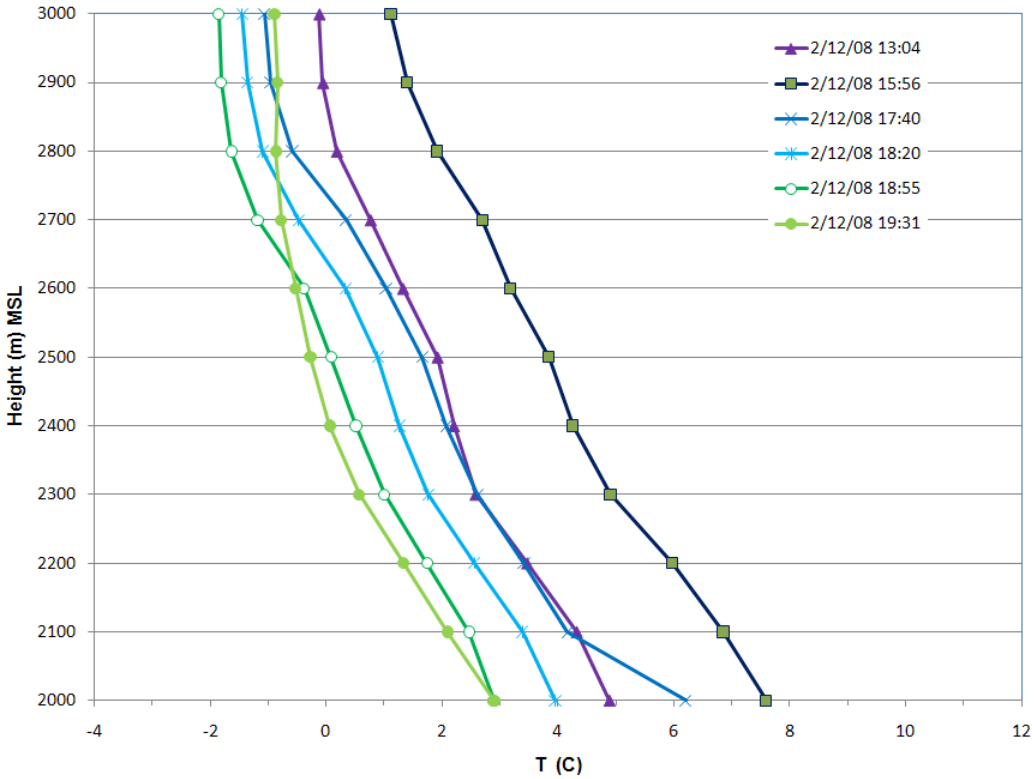

Figure 7. Tram temperature profiles on February 12, 2008

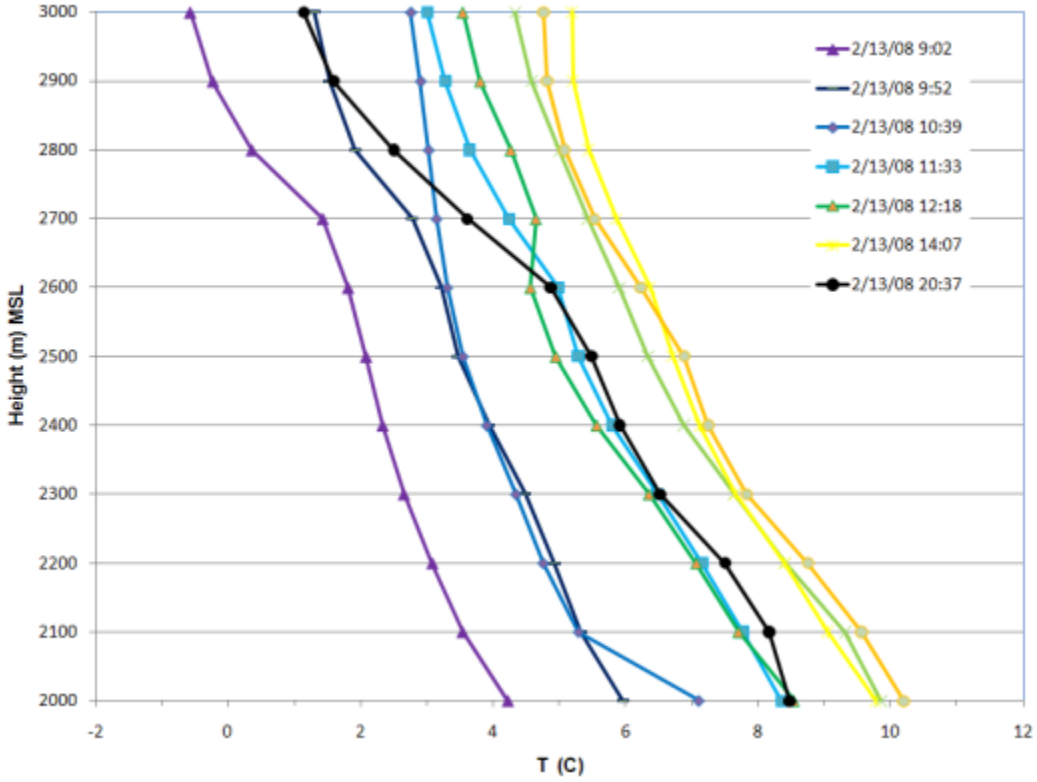

Figure 8. Tram temperature profiles on February 13, 2008

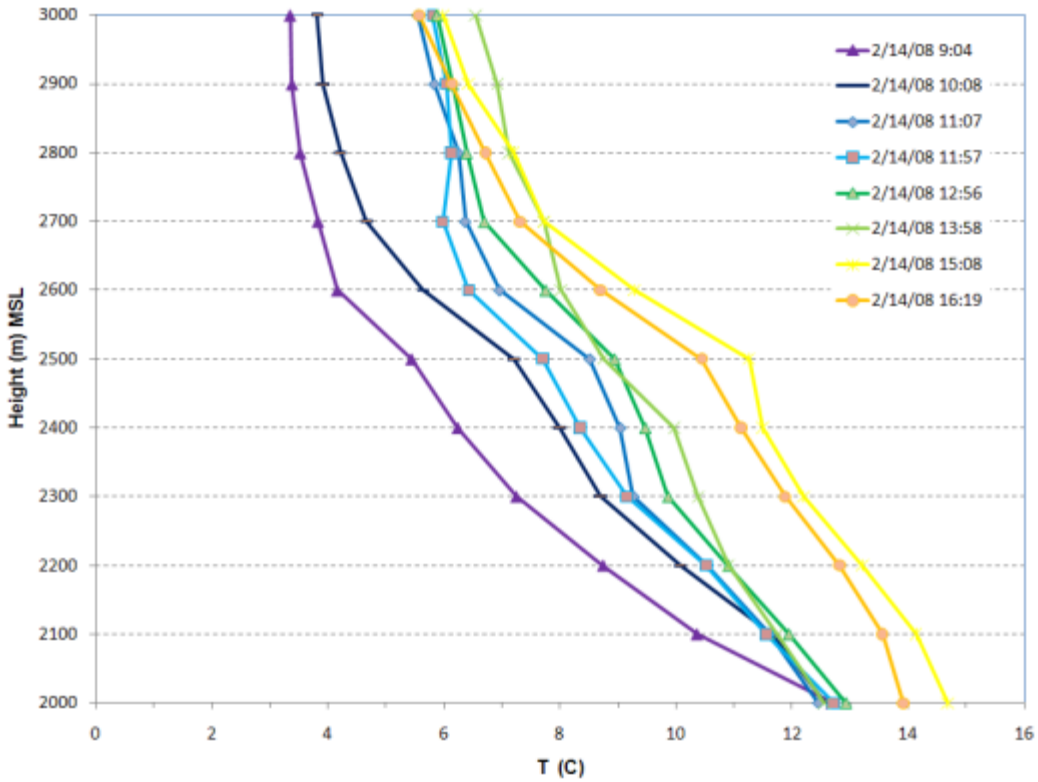

Figure 9. Tram temperature profiles on February 14, 2008

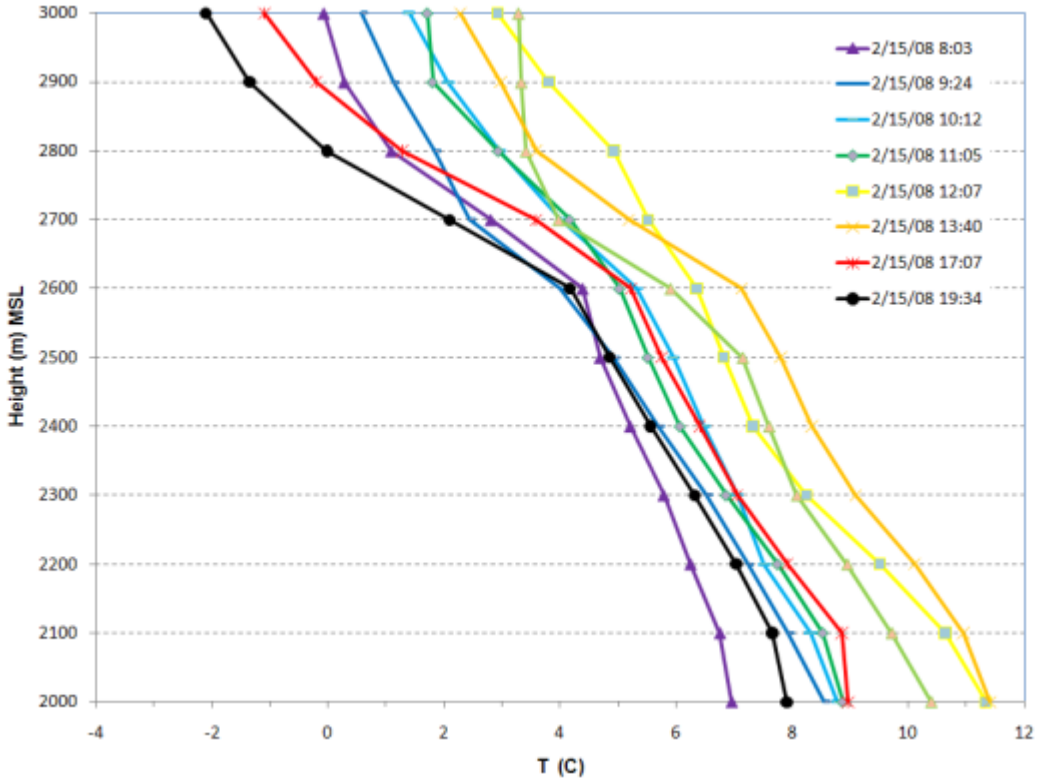

Figure 10. Tram temperature profiles on February 15, 2008

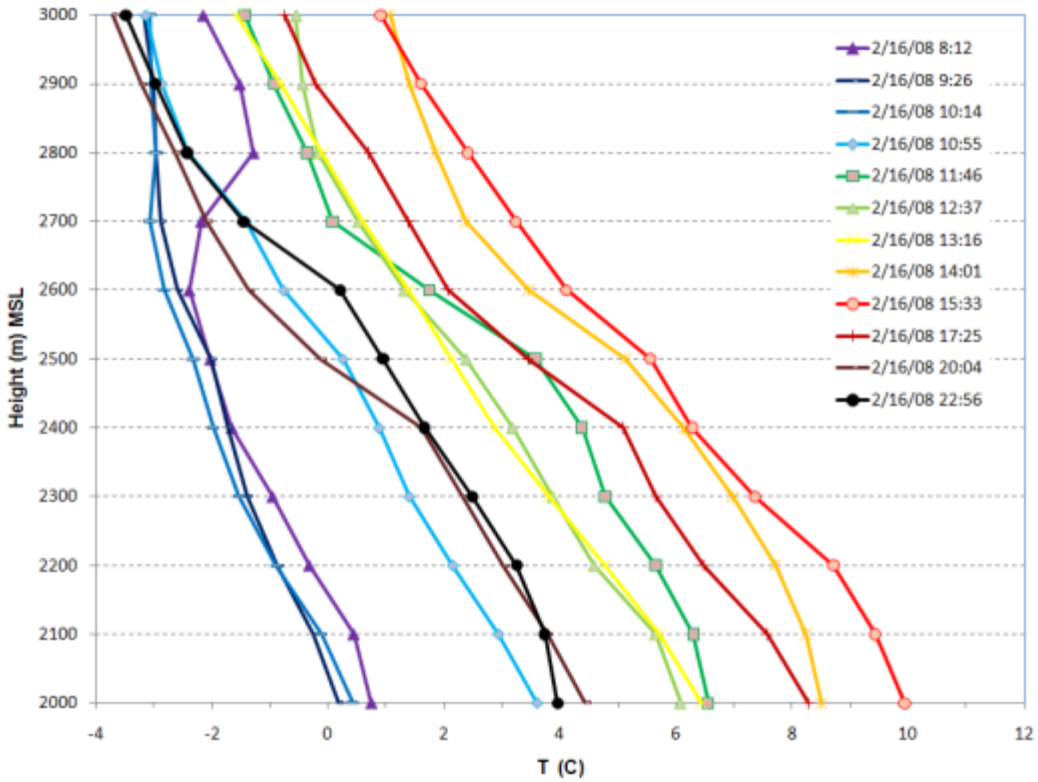

Figure 11. Tram temperature profiles on February 16, 2008

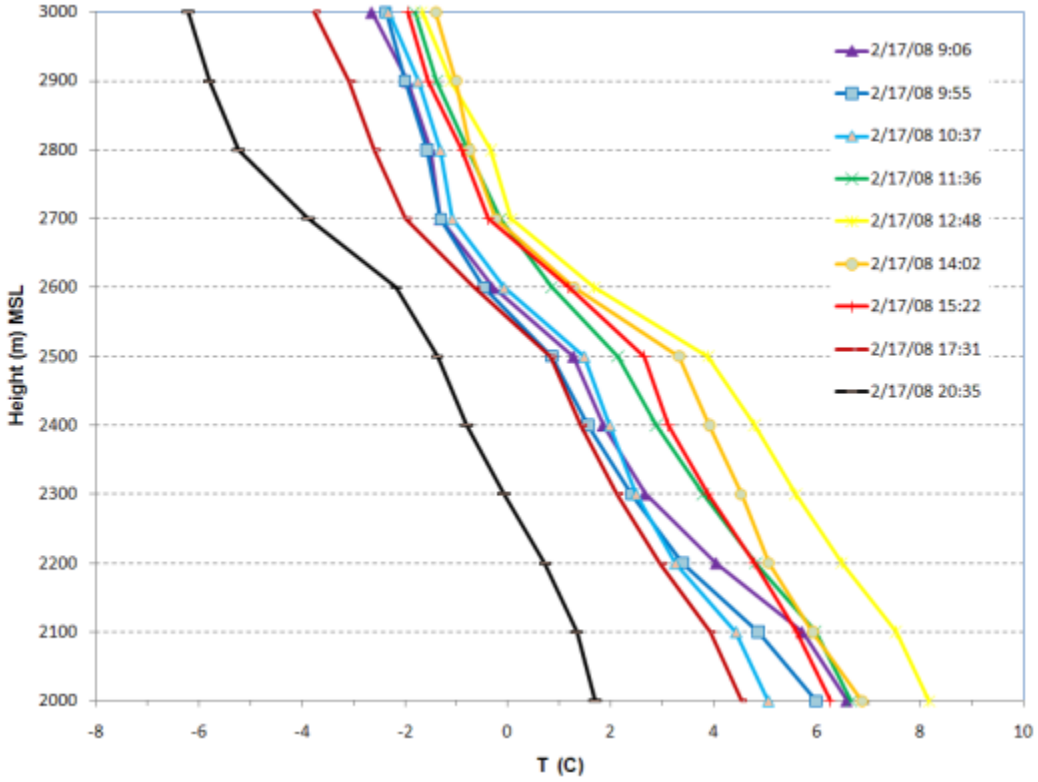

Figure 12. Tram temperature profiles on February 17, 2008

Pseudo-Temperature Profiles

We augmented our tethered balloon profile measurements with a method to gather pseudo-vertical temperature profiles using HOBO® temperature sensors at various elevations in the valley. The tethered balloon system provided profiles from 1,547 m (5,075 feet) to a maximum height of 2,012 m (6,600 feet) above mean sea level as dictated by the FAA. HOBO® temperature/relative humidity sensors were placed on an east to west transect from the Rio Grande River to the top of the Sandia Tramway as shown in Figure 12. These were installed during the late evening of February 14th. Data collection started on the 15th and the data loggers recorded temperatures every minute. The locations of the sensors were chosen at increments of approximately 100 meters in elevation from the Rio Grande River. The Rio Grande River sensor location was chosen on the east side of the river on the east bound side of Paso del Norte Boulevard. The sensor was placed in a shielded container and hung on the back of traffic sign. A handheld GPS recorded the location and approximate elevation. This was repeated for the remaining three other HOBO® sensors travelling east on Paso del Norte.

This method has been done successfully during other field programs (Fast et al. 2004; Whiteman et al., 2004; Whiteman et al., 2000) to measure profiles of temperature. This type of method yields a pseudo-profile since the measurements are not located at one location but spaced apart over several kilometers.

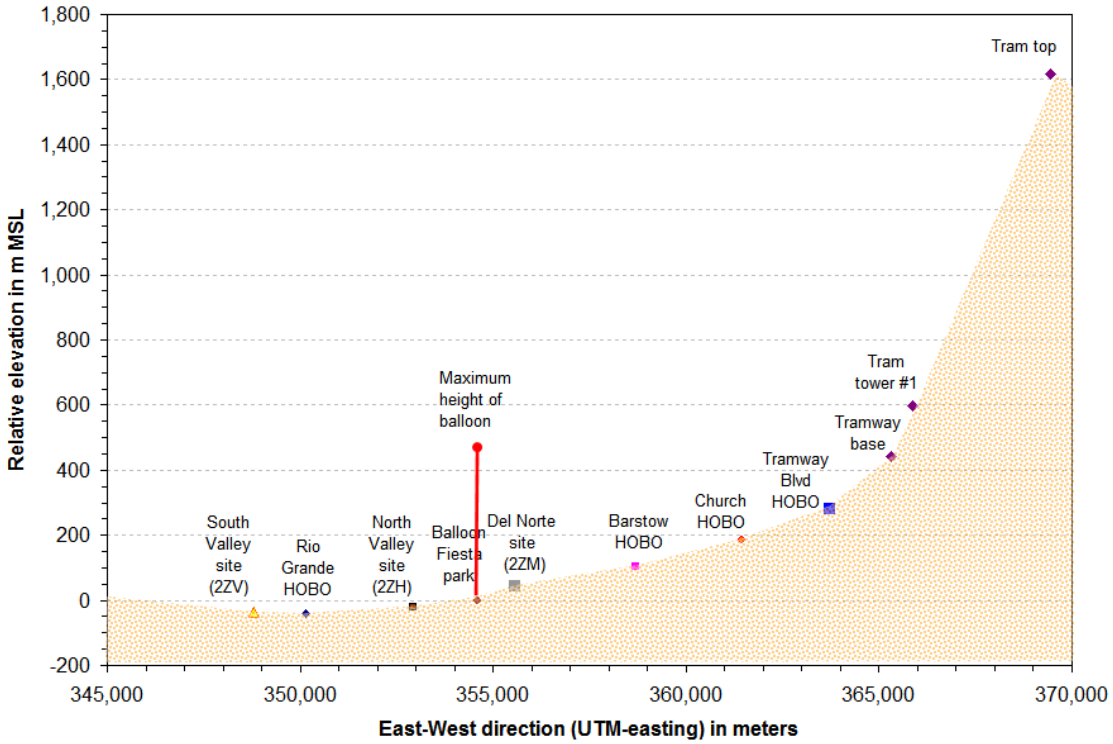

Figure 13. East to west elevation cross section during the winter IMP. Shaded area is approximate ground elevation.

Measuring temperature near the ground does have its limitations however. Close to the ground we are influenced by surface heating and the effect varies from one location to

another as the surface material changes. Despite this limitation, we were successful in obtaining vertical profiles over a cross section of the valley. Table 1 lists the location of each temperature measurement site in the winter IMP.

Table 1. Pseudo-profile temperature measurement locations.

Site Name	UTM-E (m)	UTM-N (m)	Elev (m)
Just east of Rio Grande on Paso del Norte approximately 1 meter from guard rail. HOBO attached to street sign	350146	3894556	1505
Southwest corner of the intersection of Barstow and Paso del Norte. HOBO attached to a telephone pole in a dirt lot	358710	3893407	1648
Near the southeast corner of the intersectionof Hamilton Steet and Paso del Norte. Near the Sandia Presbyterian Church (10704 Paseo del Norte NE). HOBO attached to a telephone pole about 5 meters off of sholder of road	361436	3893424	1732
The northwest intersection of Tramway Blvd and Paso del Norte. The HOBO was attached to a street sign	363698	3893506	1829
Located on a trail east of the Tramway building at about the same elevation as the tram gondola as it sits in the building	365395	3895179	2003
HOBO installed on the roof of the Tram museum at the top and attached to the radio transmitter pole on southwest corner of building	369473	3895673	3131

Figure 13 shows the time series of temperatures for all six HOBO® sites across the valley transect. With the exception of the tram top site (T2), the site located near the Rio Grande River (P1) recorded both the highest temperature on the afternoon of the 15th and also the lowest on the morning of the 18th. On February 18 the conditions were right for a cold pooling of air toward the lowest elevations of the valley.

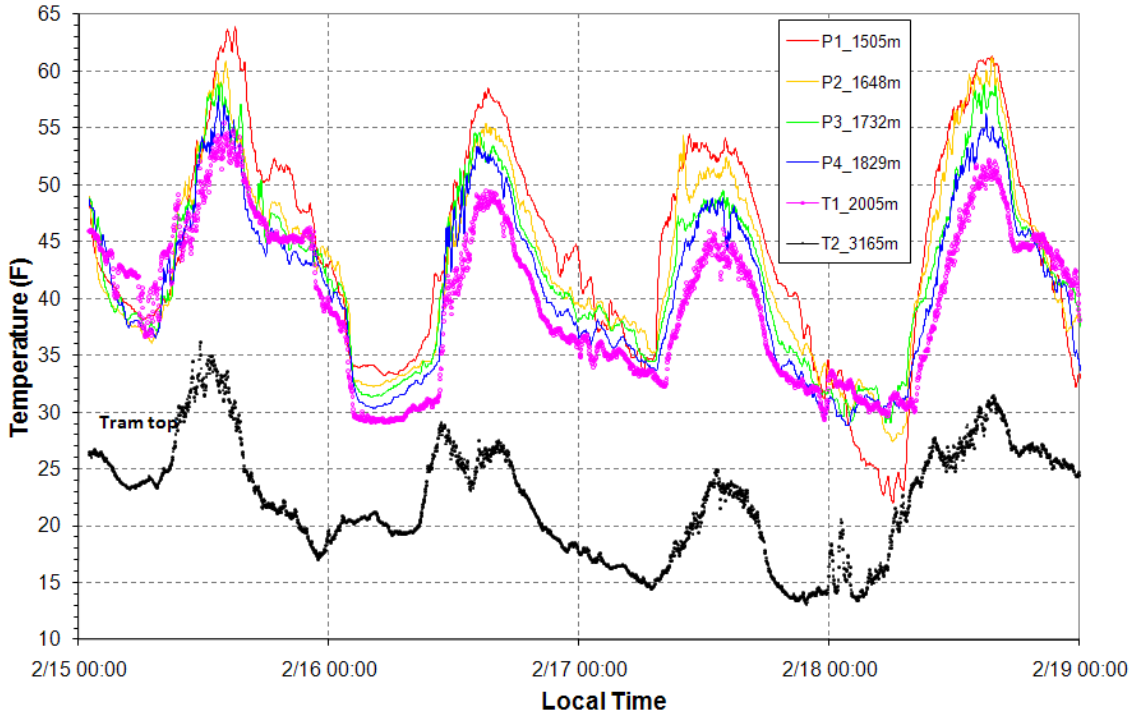

Figure 14. HOBO temperatures during the winter IMP.

Table 2 shows a summary of the minimum daily temperatures recorded at each site. Daily minimum values are highlighted and in bold. On two of the days, the lower

elevation sites recorded the lowest temperatures of the IMP. For the remaining days, the higher elevation sites recorded the lowest daily minimum temperatures.

Table 2. Pseudo temperature profile sites and minimum daily temperatures during the winter IMP. The columns are arranged in order of elevation going from lowest to highest from the left.

	HOBO P1- Rio Grande	F1- Fiesta	Airport ASOS	HOBO P2- Barstow	HOBO P3- church	HOBO P4- Tramway	Foothills COOP	HOBO Tram base	HOBO Tram top
Date	**1505m**	**1546m**	**1619m**	**1648m**	**1732m**	**1829m**	**1865m**	**2003m**	**3131m**
2/12/2008		33.8	32				30		
2/13/2008		24.8	28				30		
2/14/2008		45.9	42				42		
2/15/2008	38.2	36.7	37	**36.1**	36.9	36.5	33	36.7	17.0
2/16/2008	33.2	32.5	32	32.2	31.3	30.3	**27**	29.1	17.6
2/17/2008	31.2	35.6	36	32.2	31.5	29.5	30	**29.3**	13.1
2/18/2008	**22.0**	24.4	25	27.4	29.0	28.8	25	29.7	13.4
2/19/2008	30.1	**25.9**	31	28.6	31.8	28.4	27	37.5	24.1

Note: F1 was at 6 m, T2 at 4 m, others at 1.5 meters

Figures 14, 15, and 16 shows the pseudo-temperature profiles every third hour from February 15 to 19. Stable layers are seen on February 15 starting at midnight, and on February 18.

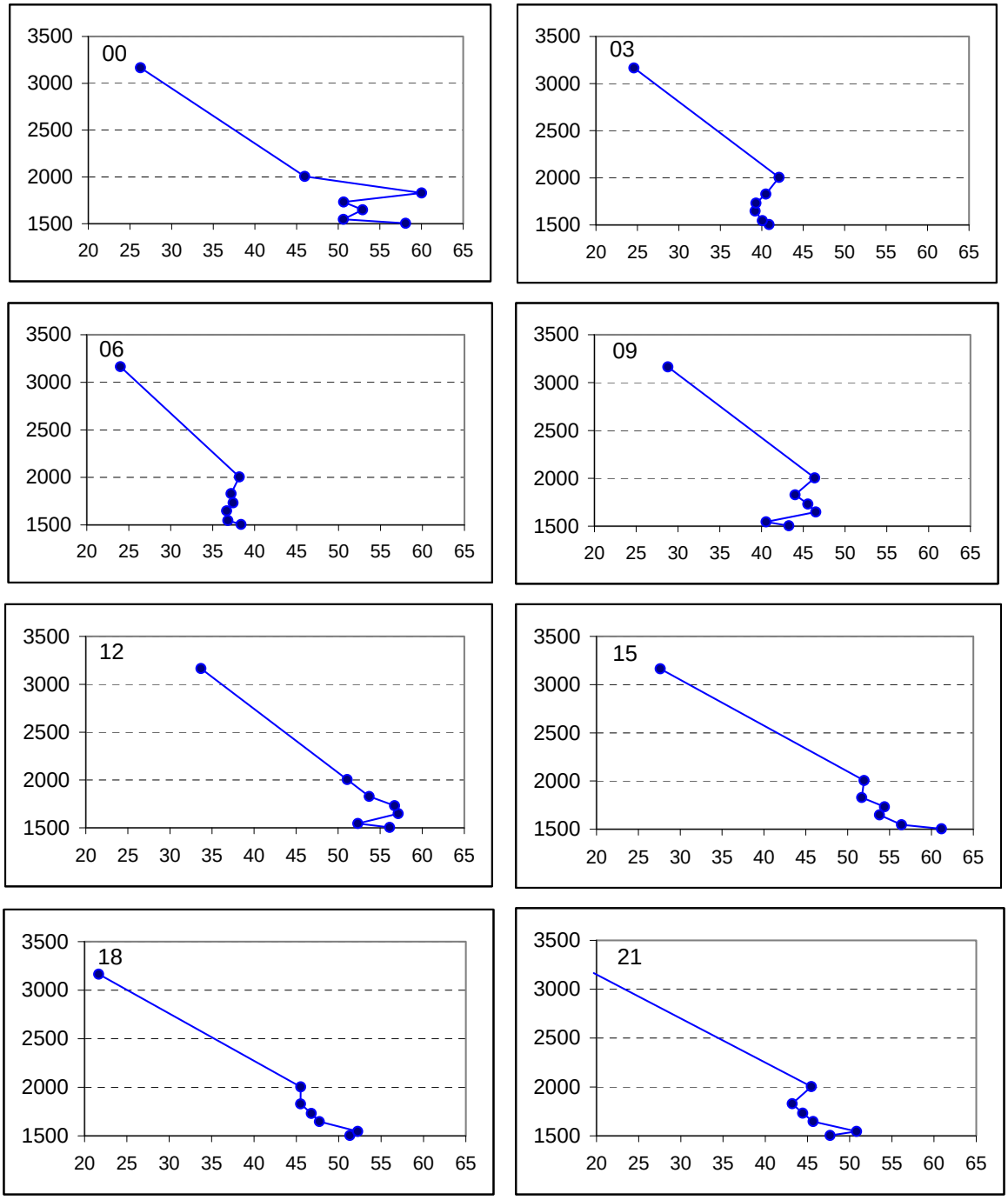

Figure 15. February 15, 2008 pseudo vertical temperature profiles every third hour. Vertical axis is height above mean sea level in meters and horizontal axis is ambient temperature in ºF. Time of day in local time is noted in the upper left hand corner of each plot.

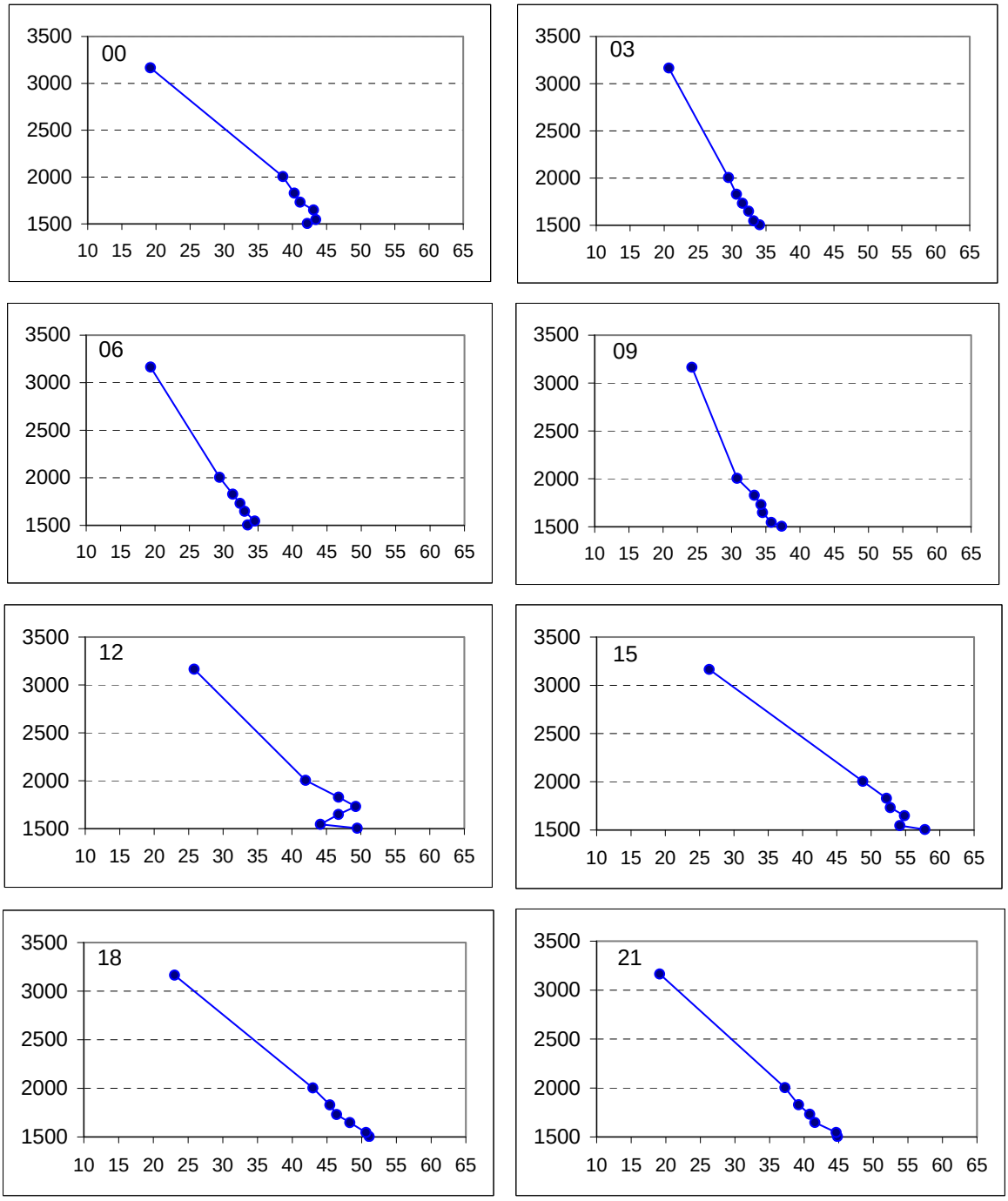

Figure 16. February 16, 2008 Pseudo vertical temperature profiles. Vertical axis is height above mean sea level in meters and horizontal axis is ambient temperature in ºF. Time of day in local time is noted in the upper left hand corner of each plot.

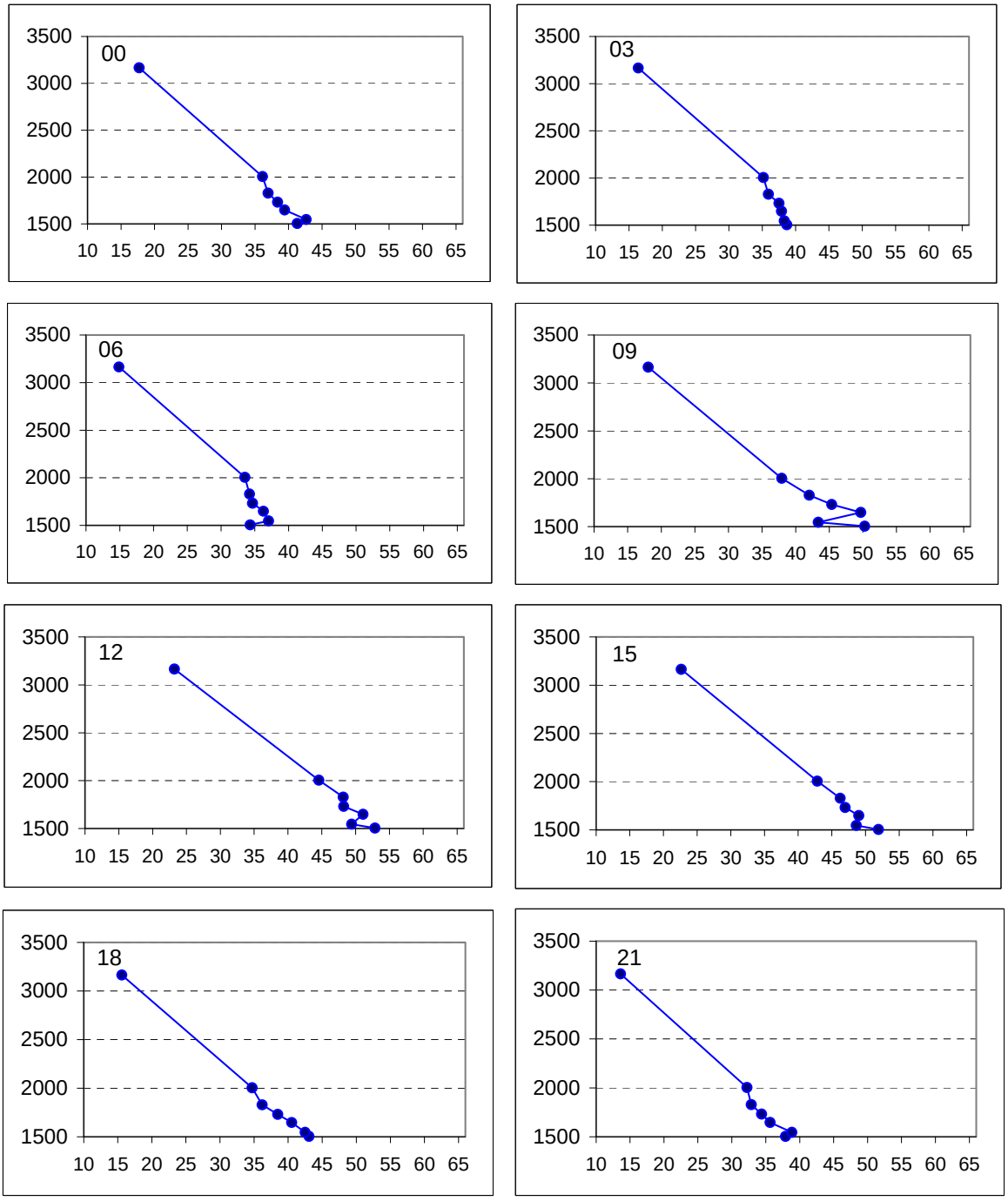

Figure 17. February 17, 2008 Pseudo vertical temperature profiles. Vertical axis is height above mean sea level in meters and horizontal axis is ambient temperature in ºF. Time of day in local time is noted in the upper left hand corner of each plot.

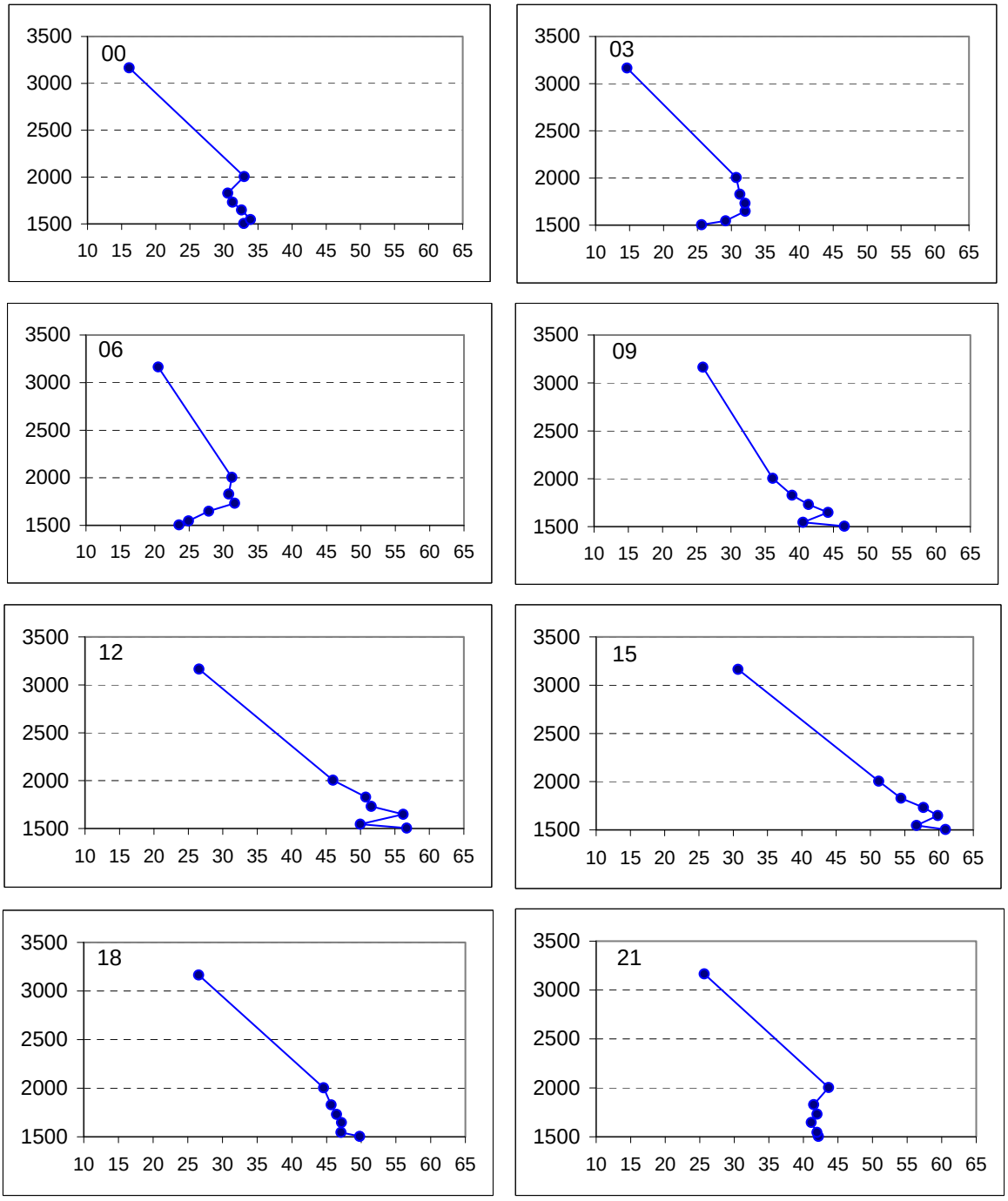

Figure 18. February 18, 2008 Pseudo vertical temperature profiles. Vertical axis is height above mean sea level in meters (MSL) and horizontal axis is ambient temperature in ºF. Time of day in local time is noted in the upper left hand corner of each plot.

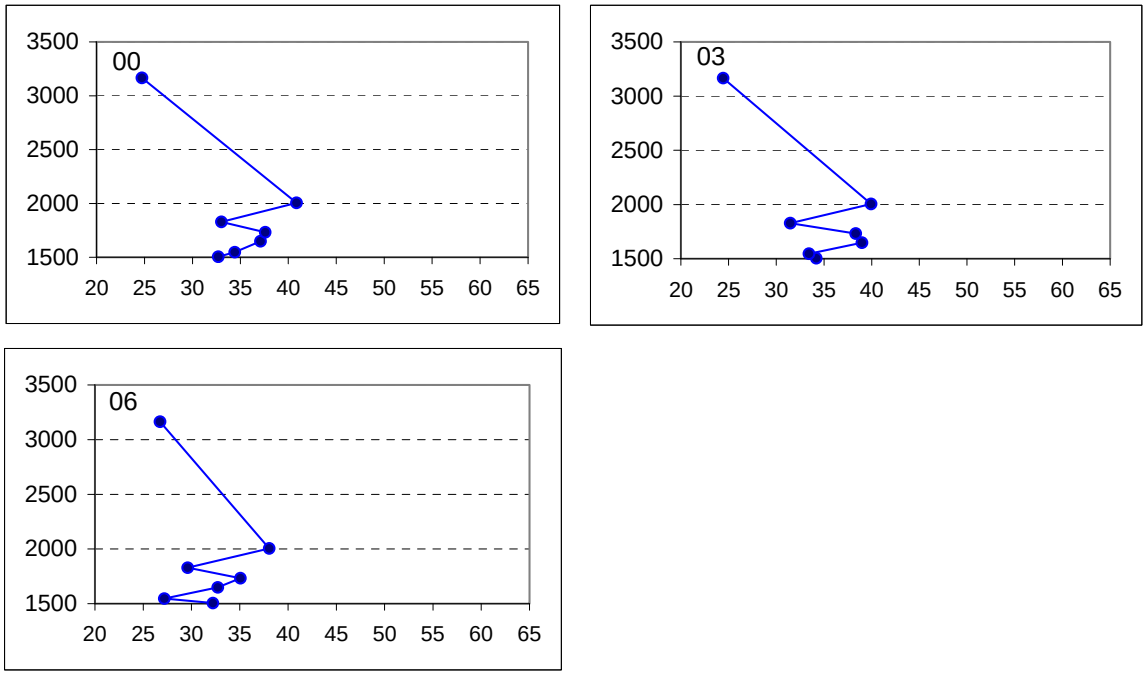

Figure 19. February 19, 2008 Pseudo vertical temperature profiles. Vertical axis is height above mean sea level in meters and horizontal axis is ambient temperature in ºF. Time of day in local time is noted in the upper left hand corner of each plot.

SUMMARY OF THE SUMMER STUDY

The summer intensive monitoring period extended from midnight June 17 to midnight on June 30, 2008.

Daily Project Activity and Meteorological Conditions

This section describes the general meteorological conditions during the summer intensive monitoring period. The meteorological summaries relied on twice daily 500 mb height/vorticity maps, surface station maps, National Climatic Data Center station summaries and observations made during the study.

June 17, Tuesday (CABQ sample day)

The area was under the influence of an upper level ridge and partly sunny skies. Early in the morning of the 17th there were east canyon winds and hourly winds were sustained at 23 mph (10 m/s) at from midnight to 1 am MDT as a result of a back door cold front. A pulse of moisture was seen mainly in the eastern part of the state but could be seen in town as the morning dewpoint temperatures were high in the mid 50s °F and dropped off after noon back to the upper 20s. Highs were in the mid 90s throughout the city. High temperature was 96 °F at the airport. Winds were light early in the day but turned breezy in the afternoon with 10 mph winds from the W and WNW. The eastern part of the state had an active day with severe thunderstorms. This was a 1 in 6 sample day for the City of Albuquerque air toxics study. During this period, the DRI Gas Chromatograph (GC)

was installed, tested and ran. A total of 47 up/down profiles were collected on the tram today. Tethered balloon vertical profiles were not collected today.

June 18, Wednesday
The area was still under the influence of an upper level ridge and partly sunny skies. This day started off similar to June 17 with early morning moisture pushing in from the east along with east canyon winds. At midnight winds at the airport were from the east at 27 mph and dropped to below 10 mph by 2 am. Dewpoint temperatures were again in the upper 50s F in the morning. The morning low was 68 °F at the airport. Later on in the day, Albuquerque was under clear skies and light winds. High temperature was 96 °F at the airport. In the afternoon, convection to the south of the region in Valencia and Socorro counties brought in gusty southerly winds. A total of 46 up/down profiles were collected on the tram today. Vertical profiles with the tethered balloon system were not collected today.

June 19, Thursday
The upper level ridge was still influencing the area but was flattening out, showing some weakening. The morning low was 67 °F at the airport while the high topped at 95 F. Convective activity mainly occurred to the east of the area, resulting in a mostly clear day. Some of those storms were severe and some tornado activity was seen over Harding County. A backdoor cold front from a short wave over Oklahoma pushed its way in the eastern part of the state in the evening. As a result of this front, dewpoint temperatures were seen increasing to the 55 degree mark by 10 pm along with high east canyon winds. Maximum wind gusts of 45 mph were observed at the airport at 10 pm. A total of 49 up/down profiles were collected on the tram today. Vertical profiles from the tethered balloon system were not collected today.

June 20, Friday
The morning started out with the results from the cold front pushing in a moist air mass. The morning low was again 67 °F at the airport. Dewpoint temperatures stayed within the 50 °F range all morning and into the early afternoon. Strong easterly winds continued through the morning and were over 15 mph from midnight until 8 am. Convective activity peaked in the valley in the mid-afternoon hours and brought brief gusty winds and some showers, although in trace amounts. High temperatures were moderated by the afternoon convective activity and peaked at 88 °F at the airport. Today preparations were made for balloon measurements to take place on June 21. A total of 66 up/down profiles were collected on the tram today.

June 21, Saturday
Moisture remained in the region, providing more fuel for convective activity in the Albuquerque area. East winds were steady throughout the morning peaking in intensity between 6 and 7 am, with gusts in the 33 to 37 mph range. Skies were clear in the morning except for low clouds covering the tops of the Sandia Mountains. In the afternoon, convective activity controlled the weather with cloud cover from 3 pm to around 9 pm. As seen in Figure 20 some haze could be seen but the visibility was overall good with no signs of wildfire smoke.

Severe weather continued in the eastern and southern part of the state throughout the day and into the night. The skies cleared up in the late evening hours in the Rio Grande Valley with southerly to south-southeasterly wind. Similar to the previous day, the high temperature was limited to cloud cover and reached 88°F at the airport. Normal highs for this day were 92°F and the normal low was 61°F. Vertical profiles were not collected today.

Figure 20. Photo at 3:48 pm from top of Sandia Peak looking west toward Albuquerque

June 22, Sunday

The summer intensive study began under an upper level high with clear skies and calm surface winds. The upper level high shifted west toward the Baja Peninsula with low wind aloft. The forecast for the day in the Rio Grande Valley included isolated showers and thunderstorms after noon, partly cloudy, with a high near 92 °F. An easterly wind between 5 to 10 mph becoming southwest was forecasted. Chance of precipitation was 20 percent. Less moisture streamed in to the region compared to earlier in the week, resulting in less convective activity today. However, convection was active in the western part of the state from the Jemez down to the Gila Mountains. Data collection was started on the tram in the morning. Initial testing was done at the balloon fiesta park in the afternoon in preparation for an early start on the 22nd. Some vertical profiles were collected with the tethered balloon starting at 5:13 pm and were completed by 7:45 pm due to high winds. Unfortunately the data collection hard drive crashed at that time before it was backed up for the night. No data was recovered although some screen shots were taken when the profiles were being recorded. Tram measurements were conducted successfully on this day.

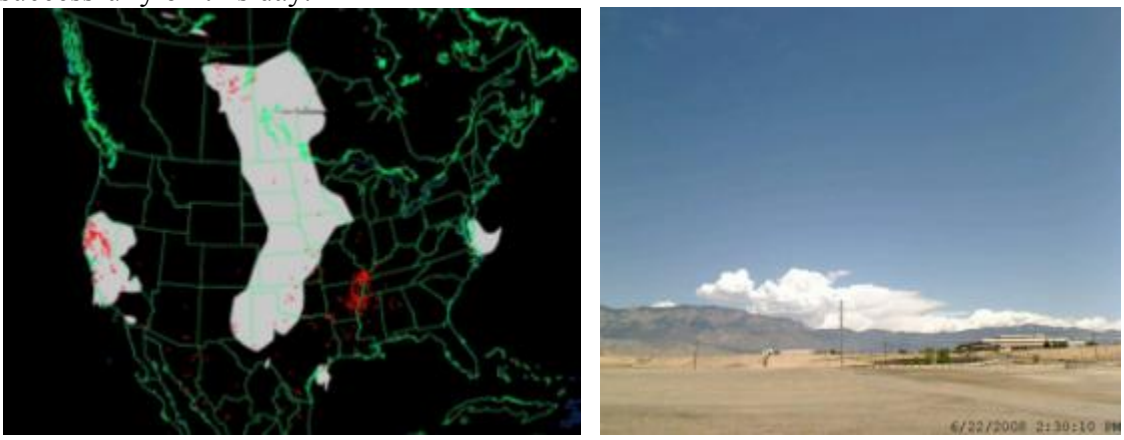

Figure 21. Smoke plumes the NOAA HMS on the 22nd at 02:37 UTC (8:37 pm MDT) and view of convection over the Sandia Mountains at 2:30 pm MDT

June 23, Monday (CABQ sample day)

Today the Albuquerque area is located on the eastern periphery of a large 500 mb ridge extending west to east from the Pacific Ocean to NW Chihuahua. The morning low

temperature was 66 °F at the airport. The day started off with cloud cover and isolated showers over the Sandia mountain range. We observed mammatus clouds overhead at around 6:40 am as seen in Figure 22. As omninous as it looked, it usually indicates a weakening storm cell where subsiding air that initially was lofted from an updraft, and then lost momentum. It briefly cleared up around 8 am but the convection started to pick up at 2 pm. A short wave to the west travelling to the east added to the dynamics and threat of thunderstorms. After spending the morning using a replacement laptop and installing the software, tethered balloon soundings started at 12:45 pm at the balloon fiesta location. While no precipitation fell, the small convection clouds produced brief gusts and downdrafts that caused us to end the day of sampling at the balloon fiesta park. At around 5:30 pm (23:30 UTC), a strong downdraft produced high winds from the west and lofted dust and debris through the city as Figure 22 shows. High temperatures were moderated by the afternoon convective activity and peaked at 92 °F at the airport. An east canyon wind characterized the evening wind transport. Tram measurements were conducted successfully on this day.

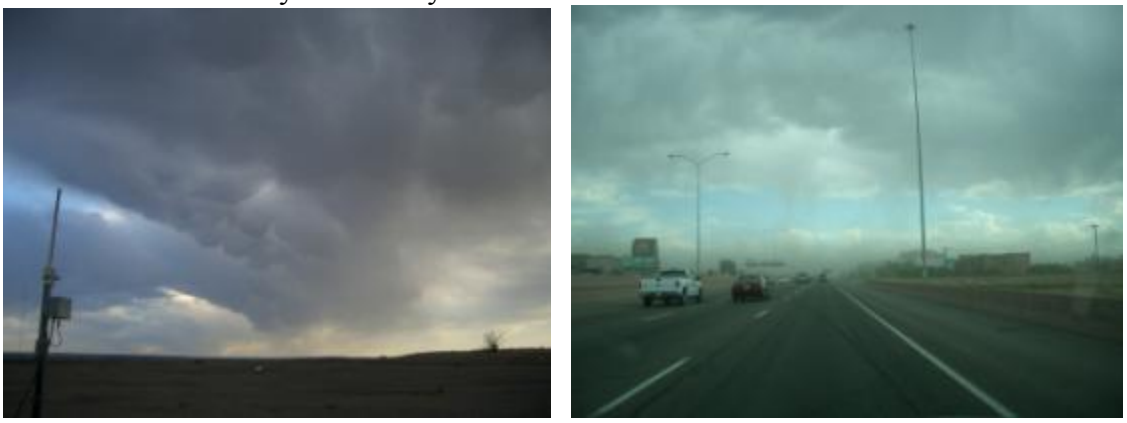

Figure 22. Mammatus cloud formation at 6:48 am (left) and blowing dust across I-25 near Osuna exit at 5:37 pm (right) on June 23

June 24, Tuesday

The day started off with clear skies with some clouds to the west. The main synoptic pattern was an elongated upper level high the stretched from Baja to southwestern New Mexico. Tethered balloon measurements were started at the balloon fiesta park at 5:58 am MDT. As the sun was rising, there was some indication of a thin whispy smoke plume over the Sandia Mountains.

Figure 23. Thin plumes over Sandia Mountains (left) right before sunrise at 6:02 am and Blowing dust at Balloon Fiesta Park at 3:27 pm (right)

Upon examination of early morning visible GOES imagery, a haze layer can be seen over the central mountain chain as the sun comes up. According to the NOAA Hazard Mapping System smoke product, an aged smoke plume that originated from the California fires travelled to the Four Corners and the west edge of the Jemez by the evening of June 23. It is likely that some of this plume was transported to central New Mexico overnight. Smoke from the southeast Arizona fires were also likely transported to the Rio Grande Valley overnight. There were fires in the Lincoln National Forest and in the Organ Mountains in southern New Mexico but the smoke plumes from these fires travelled in an easterly direction toward Texas. The Big Springs fire started on June 23 and was reported today as a wildfire in the Cibola National Forest. This fire was burning 25 miles southeast of Albuquerque on the east facing slope of the Manzano Mountain Range. To provide more dynamics to the convection, a shortwave trough propagated across the state during the middle of the day and peak heating period. Winds were light right after sunrise with the tethered balloon measuring no more than 3 m/s from ground to 400 meters AGL. A very shallow 0.05 °C/m inversion up to 40 meters AGL was observed at 7 am. By 2 pm MDT, clouds were covering much of central NM. Tethered balloon operations were terminated at 3:15 pm due to threat of high winds and a dust cloud to the west travelling toward the site. As anticipated, a strong downburst swept across the balloon fiesta park by 3:30 pm blowing much dust and debris at the site. High temperatures were again moderated by the afternoon convective activity and peaked at 91 °F at the airport. Similar to past days, an east canyon wind characterized the late evening wind transport. Tram measurements were conducted successfully on this day.

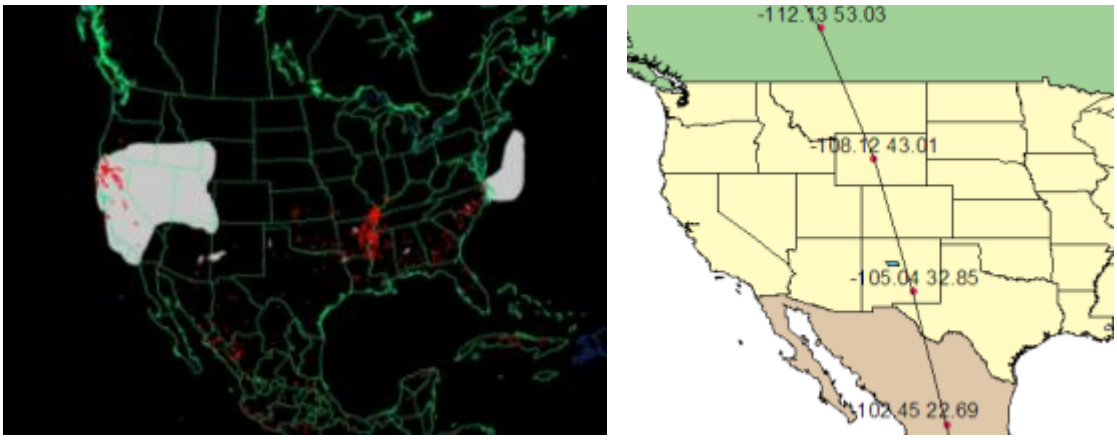

Figure 24. On left smoke plumes from NOAA HMS as of 03:20 UTC (June 24, 9:20 pm MDT) and path of CALIPSO from the morning

A unique opportunity to observe regional air quality using data collected by the satellite based CALIPSO lidar is presented here. The CALIPSO track on June 24, 2008 is shown below as the black line in the figure below. The points in the track correspond to reference markers on the CALIPSO quick look backscatter plot. The satellite passed over central NM around 20:20 UTC (2 pm local time). The satellite based lidar shows elevated aerosol east of the study area potentially remnants of the Big Spring fire plume in the eastern Manzano Mountains. The aerosol shows up as an orange color (number 3) in the feature type plot below. The plot below that is the 532 nm backscatter intensity and shows the aerosol layer as a faint yellow region.

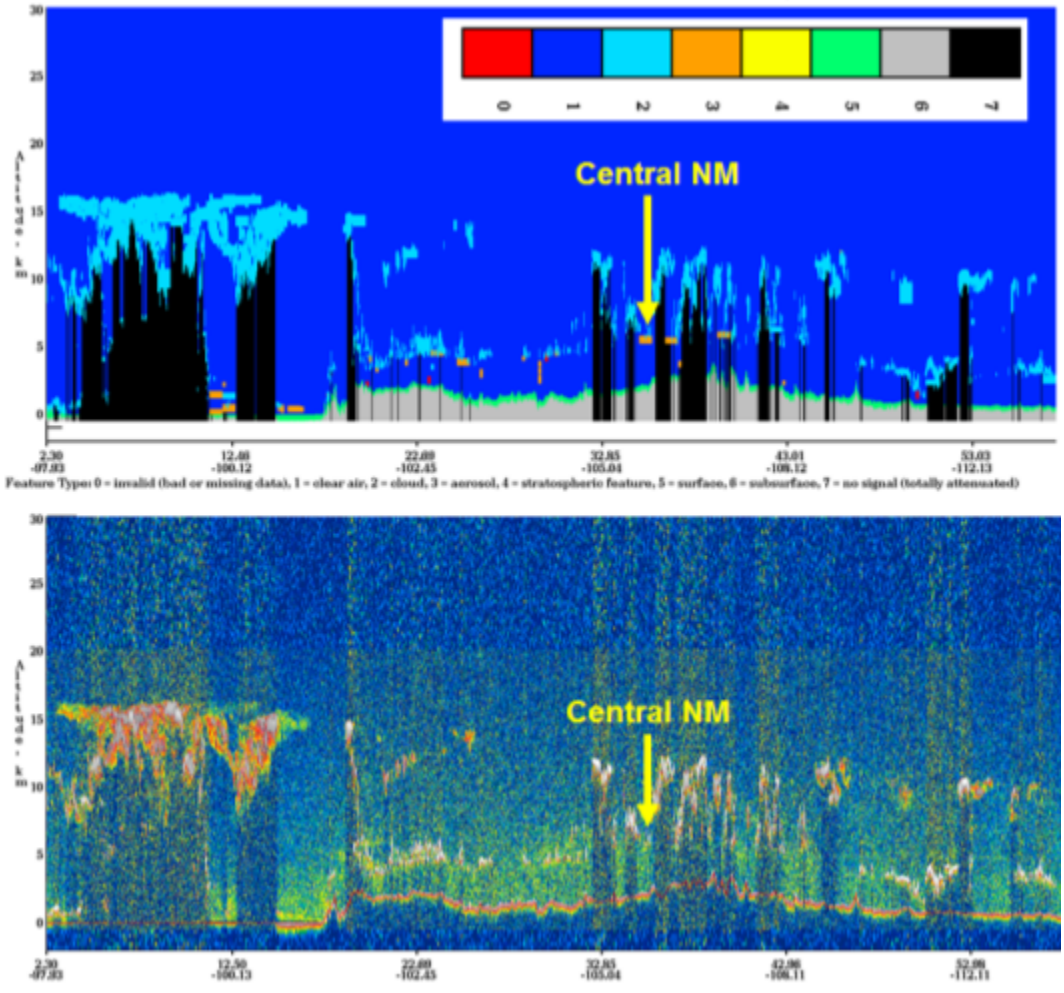

Figure 25. CALIPSO backscatter profiles on the morning of June 24, 2008

The high intensity backscatter returns in the above figure are from convective clouds. The labeled point (-105.04, 32.85) shows up in the backscatter plot with a convective cloud top over 12 kilometers above mean sea level. The GOES visible image from 20:30 UTC on is shown below with an approximate path of CALIPSO shown in yellow.

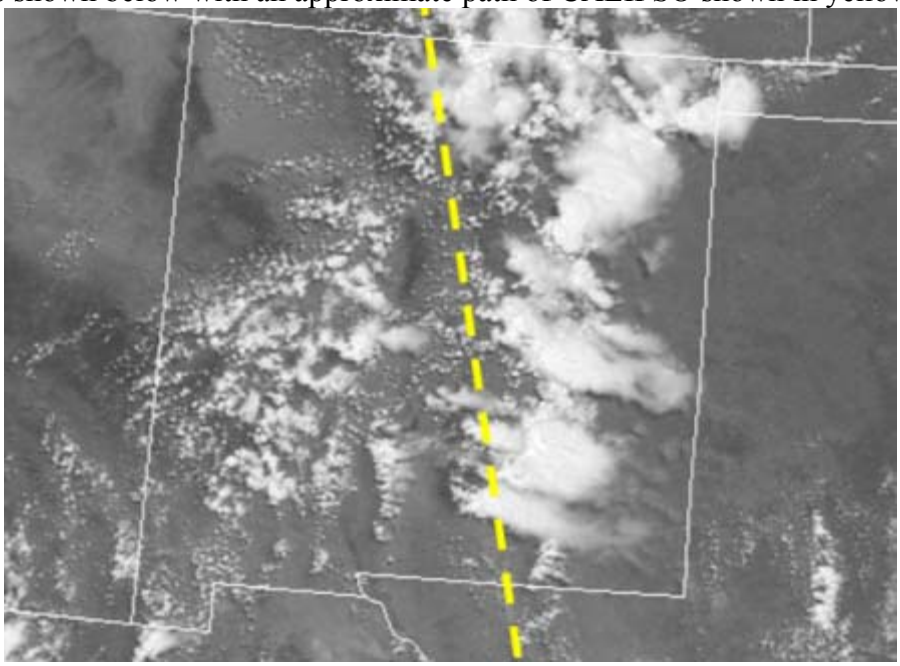

Figure 26. GOES visible image from 20:30 UTC with CALIPSO path in yellow

Earlier in the day, a dispersed smoke plume can be seen in GOES images from the Big Spring fire. As the morning progressed, the smoke plume drifted eastward out of the study area. Based on photographic documentation in the morning before sunrise, the smoke plume was primarily aloft and could be seen as a very thin haze looking east over the Sandias. Smoke outlines from the NOAA HMS product in the afternoon (21:32 UTC) show no major plumes over central NM.

Figure 27. Smoke and fire locations from the NOAA HMS at 21:32 UTC.

June 25, Wednesday

The weather forecast for the 25th included isolated showers and thunderstorms after noon with partly cloudy skies, and a high near 95 in Albuquerque. The winds were forecasted to be from the southwest between 5 and 10 mph and the chance of precipitation was 10 percent. The day started off with high clouds over the Rio Grande Valley and breezy. Winds at the airport were between 8 and 9 mph at sunrise. Tethered balloon operations were postponed today due to threat of thunderstorms. We used this day to prepare for the next few days of sampling and to buy a new hard drive for the tethersonde laptop, install the software and look at the data collected so far. Based on the NOAA Hazard Mapping System smoke plume product, haze was widespread over central New Mexico primarily from the fires in southeastern Arizona. Because of high clouds and scattered convection, it was difficult to verify this finding. The smoke plume from the Big Spring fire travelled easterly and away from the Rio Grande Valley as seen in Figure 21.

Figure 28. On the left, the Big Spring Wildfire smoke plume is shown as viewed from Highway 14 near Tajique at 5 pm looking west. Right figure shows wind vectors at the 700 mb (~10,000 ft) height at 21 UTC (3 pm local time). The approximate fire location is indicated by the red dot.

High temperatures were again moderated by the afternoon convective activity and peaked at 92 °F at the airport. Tram measurements were conducted successfully on this day.

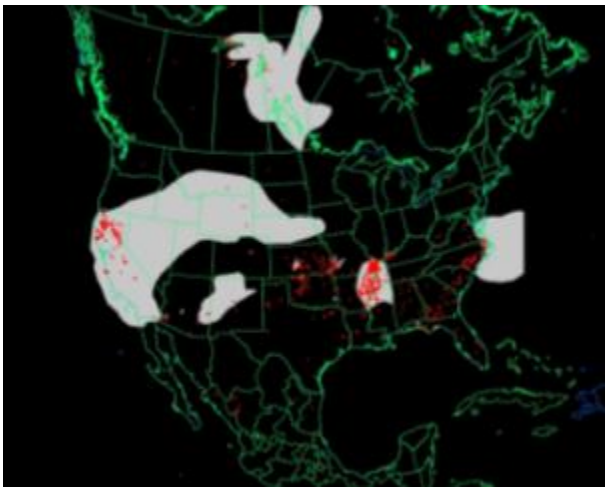

Figure 29. Smoke plumes from the NOAA HMS analysis on the evening of June 25, 2008 at 02:45 UTC (8:45 pm MDT)

June 26, Thursday

The primary synoptic scale change is the 500 mb high moves from southern New Mexico westward to the NM/Arizona border. The day started out with clear skies with winds below 5 m/s up to 400 meters AGL. The forecast is for another day of isolated showers and thunderstorms with partly cloudy skies and a high near 93 °F. A west wind of 5 to 10 mph becoming south was forecasted. The chance of precipitation was 10 percent. Based on the NOAA Hazard Mapping System smoke plume product, haze was widespread over northeast New Mexico primarily from the Big Spring fire. By the morning the Big Spring fire burned 1,900 acres of piñon-juniper forest and was 10 percent contained. Tethered balloon operations started at the balloon fiesta park at 10:59 am MDT. The ceilometer was collocated with the tethered balloon today to compare the aerosol back scattering profile with the measurements of meteorology. The afternoon forecast again predicted for scattered showers and gusty winds in the lower and mid Rio Grande Valley. Cumulus clouds quickly built up 2 pm to the west of the site and virga was observed in some small patches. By 2:25 pm, winds started to climb near 10 m/s at the 400 meter level. At that point the balloon starts to get uncontrollable, so we decided to terminate the day. The tethered balloon operations were concluded by 2:53 pm MDT. By 6 pm, the NWS issued a special weather statement that said that to expect wind gusts to 50 mph in the Albuquerque metropolitan area until 6:30 pm. Peak wind gusts of 39 mph were recorded at the airport between 5 and 6 pm from the southwest. High temperatures were again moderated by the afternoon convective activity and peaked at 91 °F at the airport.

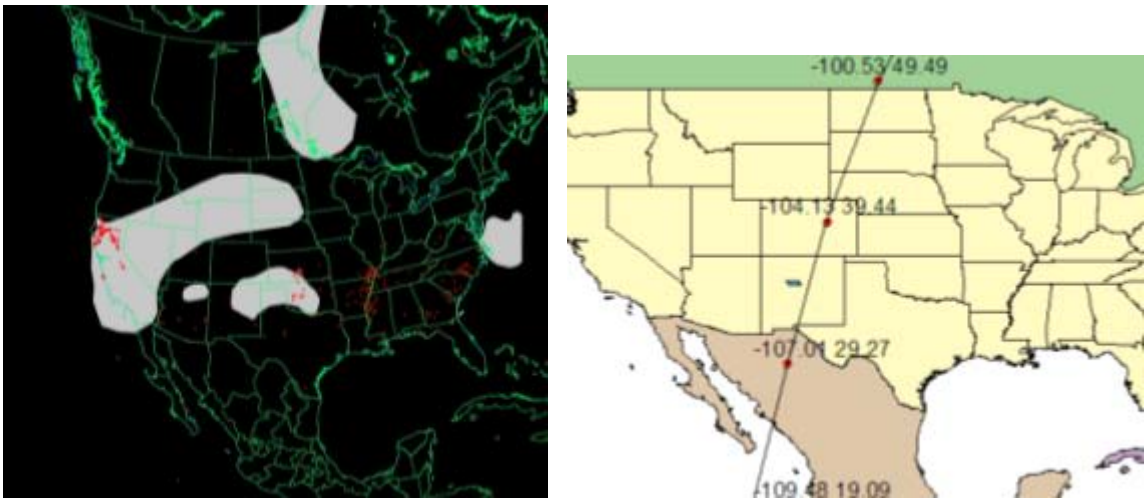

Figure 30. Smoke plumes from the NOAA HMS analysis on the evening of June 26, 2008 at 21:27 UTC (3:27 pm MDT) and CALIPSO path

On June 26 CALIPSO again passed over east central NM in the early morning at 09 UTC. The CALIPSO track is shown below as the black line. The points in the track correspond to reference markers on the CALIPSO quick look backscatter plot.

CALIPSO again shows elevated aerosol east of the study area potentially remnants of the Big Spring fire plume from the day before. The yellow arrow points to a point directly east of Bernalillo county. Aloft aerosol around 5 kilometers MSL show up as an orange color (number 3) in the feature type plot below. The plot directly below that is the 532 nm backscatter intensity and shows the aerosol layer as a faint yellow region mixed in with the cloud cover.

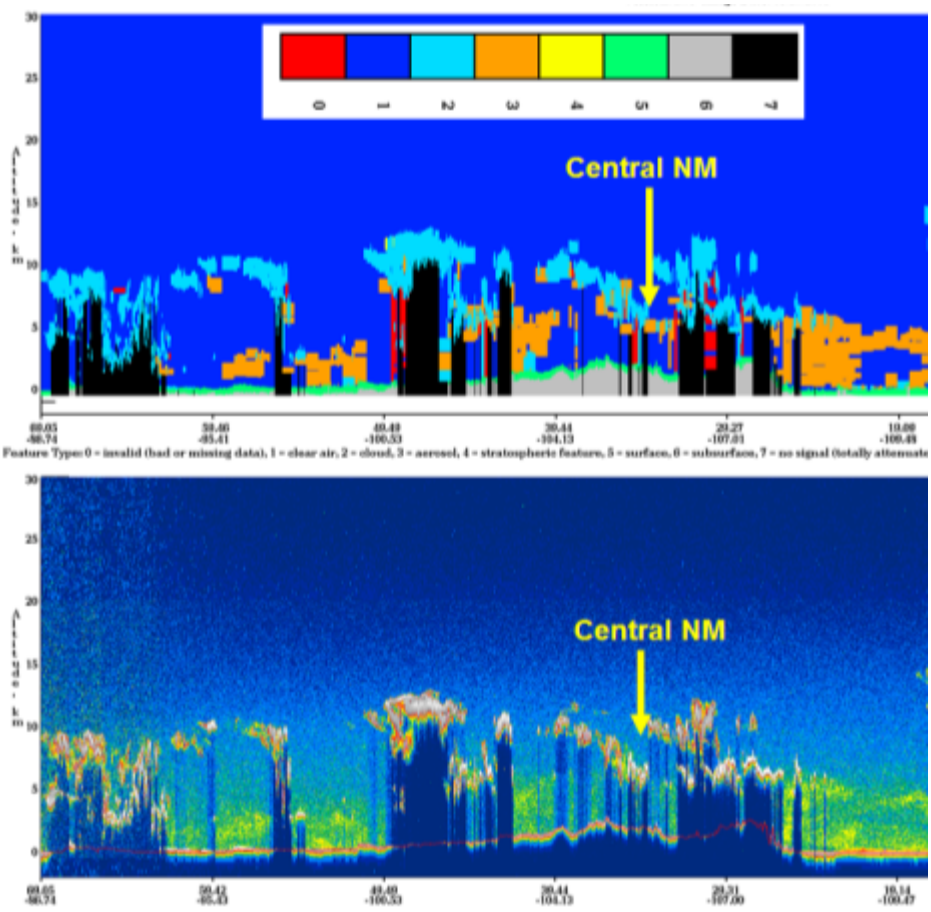

Figure 31. CALIPSO backscatter

At 09 UTC in the morning, there were clouds covering much of central NM as shown in this GOES infrared image from 08:38 UTC. Clouds show up as yellow to blue areas in the IR image below. The red areas are without clouds. The blue areas are colder than the yellow and usually indicate higher clouds. The black dashed line shows an approximate CALIPSO track across New Mexico.

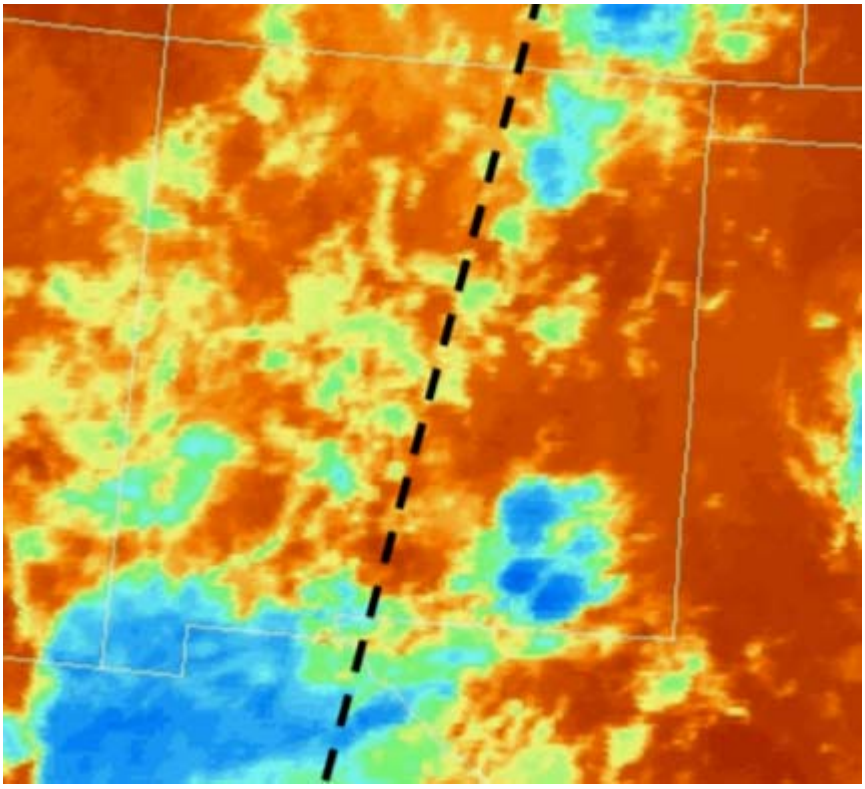

Smoke outlines from the NOAA HMS product in the afternoon (21:27 UTC) show a wide-spread plume over northeast quadrant of NM. Much of that appears to be from the Big Spring fire. The location of that fire shows up as a red dot in the map below.

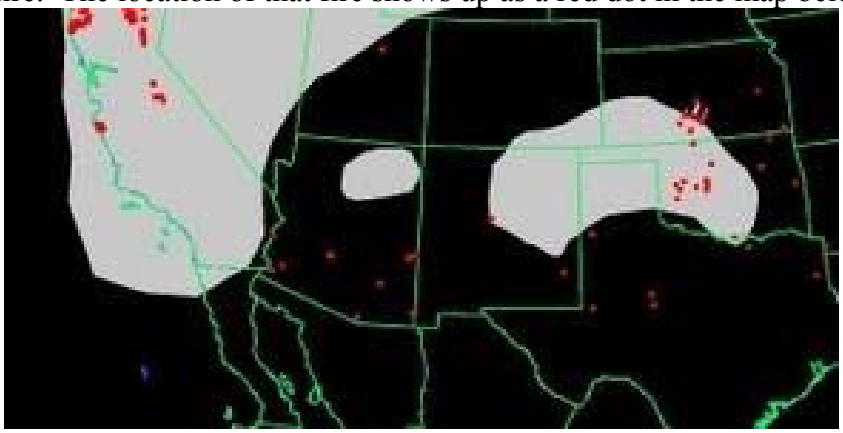

Figure 32. NOAA HMS for 21:27 UTC

June 27, Friday

The major synoptic weather pattern for this day is a cut-off upper level high over Northern Mexico. This pattern usually signifies a blocking pattern and the weather at the surface is dry with above normal temperatures. Today's forecast called for partly cloudy skies, isolated showers and thunderstorms, some with little or no rain in the afternoon. The expected high temperatures were in the lower to mid 90s. Winds were forecasted to

be from the northwest from 10 to 20 mph in ther afternoon. Tethered balloon operations were started at 3:50 am MDT at the balloon fiesta park. The day started out with high clouds mainly toward the east and south. Winds were light, below 3 m/s from the south through the lowest 400 meters based on the 6:53 am sounding. After 7 am, the skies started to cloud over. The 7:30 am sounding showed that winds were from the south in the lowest 250 meters and from the north to north-west above that. At 9 am, the balloon sounding measured the top of an inversion at around 275 meters AGL. The sounding revealed moist air from the south and drier air from the northwest. By 9:30 am the ceilometers measured a clear cloud base at 4,630 meters AGL. By 10 am the area was completely covered by clouds with a base of 4,690 meters. At that time, there were westerly winds aloft between 300 to 400 meters, and southerly winds near the surface. Tethered balloon sounding were terminated at 12:55 pm MDT due to threat of downdrafts from clouds. High temperatures were moderated by the afternoon cloud cover and peaked at 87 °F at the airport.

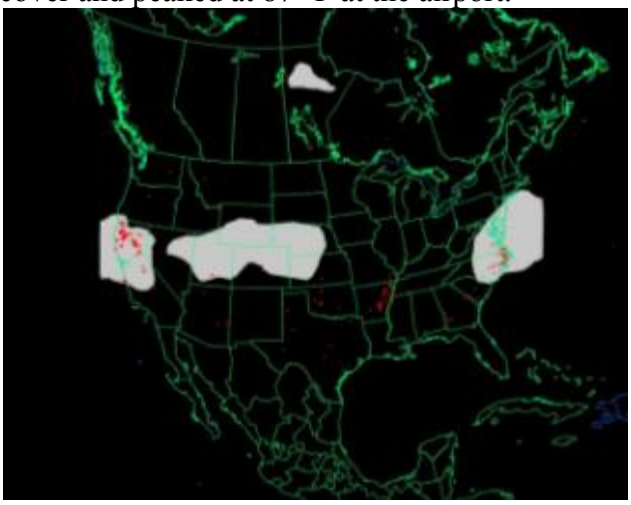

Figure 33. Smoke plumes from the NOAA HMS analysis on the afternoon of June 27, 2008 at 20:25 UTC (2:25 pm MDT)

June 28, Saturday

The area is under the influence of a weak upper level low system centered over southeastern New Mexico. At the surface a cold front pushed through northeastern NM in the morning and propagated across the state. The forecast for the 28th was calling for isolated showers and thunderstorms, mostly cloudy, with a high near 85. East wind between 10 and 15 mph. Chance of precipitation is 20 percent. Tethered balloon soundings began at 5:38 am MDT under partly cloudy skies. The ceilometer was again collocated with the balloon for comparison. Although the official sunrise was 5:55 am, the sun crested the Sandia peak at 6:26 am MDT. Dewpoint temperatures were in the low 40s in the morning and upper 40s in the afternoon and evening in the Rio Grande Valley. The skies overhead partly cleared by 8 am. Winds at the surface were from the NW and turning to the SE above 115 meters AGL. By 9 am, the area was clouded over. Balloon operations were terminated at 9:33 am MDT due to a threat of thunderstorms. The ceilometer was moved to the DelNorte, 2ZM, site by 10 am. By 3:27 pm, the National Weather Service issued a high wind advisory until 11 pm in the Rio Grande

Valley with strong east canyon winds. Although most of the day was cloudy, the high temperature of 92 °F was observed during a clear period at 2 pm at the airport. High east canyon winds were observed as forecasted starting at 5 pm and lasted all night.

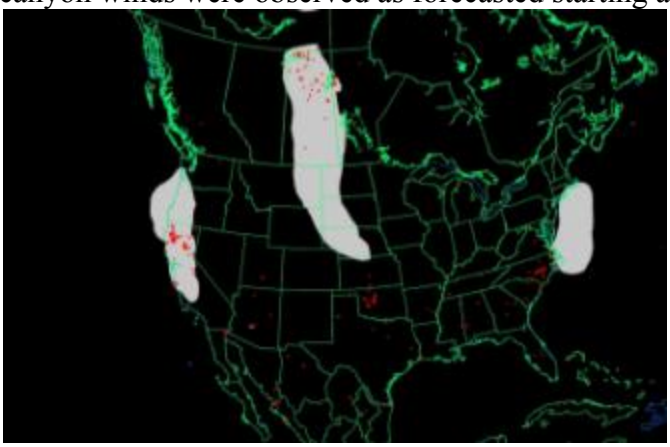

Figure 34. Smoke plumes from the NOAA HMS analysis on the evening of June 28, 2008 at 01:37 UTC (7:37 pm MDT)

June 29, Sunday (CABQ sample day)

The major synoptic weather feature during this day is the 500 mb upper level high over the central Rockies with a mesolow system remaining to the south in northern Mexico. The National Weather Service forecast for the 29th included isolated showers and thunderstorms with mostly cloudy skies and a high near 85 °F. East wind between 10 and 15 mph. Chance of precipitation is 20%. Both the NAM and RUC models predicted some light precipitation in the late morning. East canyon winds remained throughout the morning and diminished by the afternoon. Tethered balloon operations were started at 5:46 am MDT under scattered high clouds. Some Kelvin-Helmholtz instability clouds were observed over the Sandia Mountain range at 10:21 am. This type of cloud formation indicates a region of wind shear or rapidly changing wind speed as a function of height. Balloon operations were terminated at 10:51 am due to a threat of high winds and thunderstorms. As predicted, most of the day, the winds at the airport were from the east at 10 to 15 mph. Strong thunderstorms and outflow were observed in the afternoon after 5 pm over the Sangre de Cristo Mountains. The Albuqueque Sunport ASOS measured 0.5 inches of rain at 6 pm. High temperatures were moderated by the afternoon cloud cover and peaked at 84 °F at the airport.

Figure 35. Smoke plumes from a HMS analysis on the afternoon of June 29, 2008 at 22:55 UTC (4:55 pm MDT)

Tethered Balloon Data

Tethered balloon operations began on June 22 at 5:13 pm with profiles up to 150 meters AGL. However, the data was lost due to a hard drive crash soon after the last profile was collected. Data recovery was attempted but with no success. A couple of digital camera screen shots were taken during that day but were not digitzed.

The summary of data collected on June 23 is shown in the figure below. The day started off with variable southerly to southwest winds. Only profiles to 150 meters were collected on this day. Later on in the afternoon the winds shifted from a southerly and southeast direction to westerly.

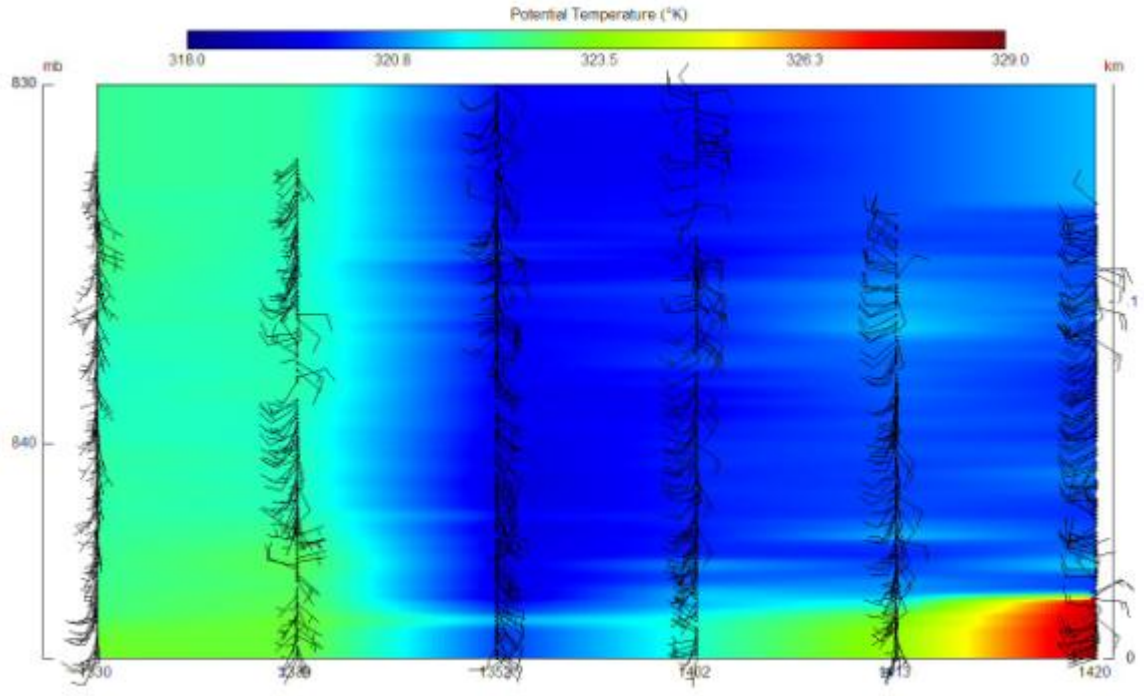

Figure 36. Tethered balloon wind and potential temperature profile summary for June 23, 2008.

June 24 started off with light and variable winds with a more northerly component. Winds later turned from a southerly direction by 10 am. A visible stable layer showed up in the early morning and was in the range of 200 to 300 meters deep. By 10 am this stable layer had disappeared owning to strong heating of the ground.

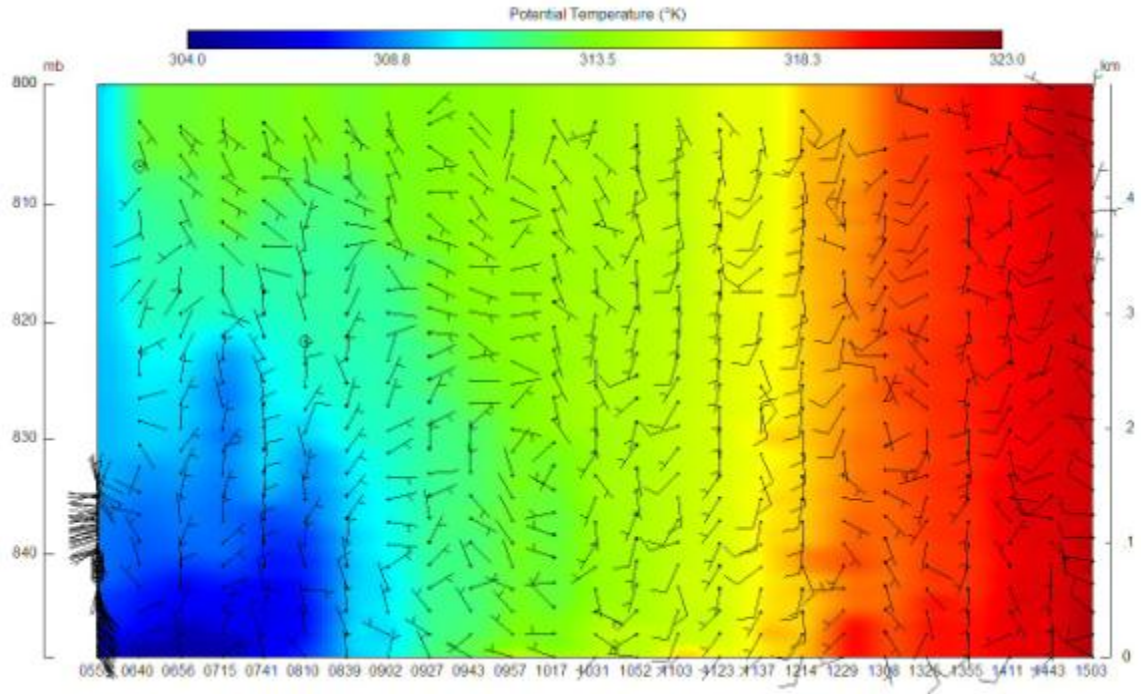

Figure 37. Tethered balloon wind and potential temperature profile summary for June 24, 2008.

No tethered balloon measurements were taken on June 25 because of the unpredictable winds that started off the day. We decided to cancel flights on this day rather than risk having problems with the balloon.

Very little temperature variation can be seen within the bottom 450 meters of the atmosphere on June 26. The early soundings showed a west to southwest flow but turned highly variable in the later afternoon. Soundings had to stop after 2:30 pm due to high winds and down drafts from thunderstorms.

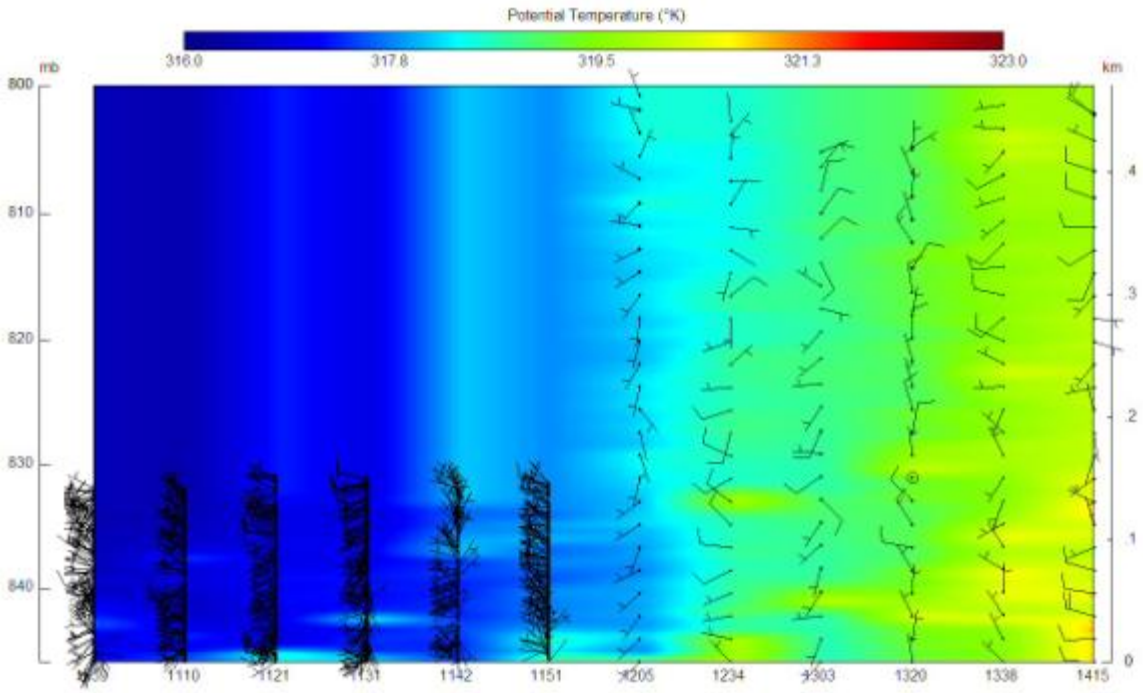

Figure 38. Tethered balloon wind and potential temperature profile summary for June 26, 2008

A shallow stable layer lasted until about 7:30 on June 27. After sunrise the 450 meter soundings revealed further extent of the stable layer not visible with the 150 meter soundings done in the early morning. This stable layer varied in height from 150 to 300 meters thick and eventually eroded by 9:30 am.

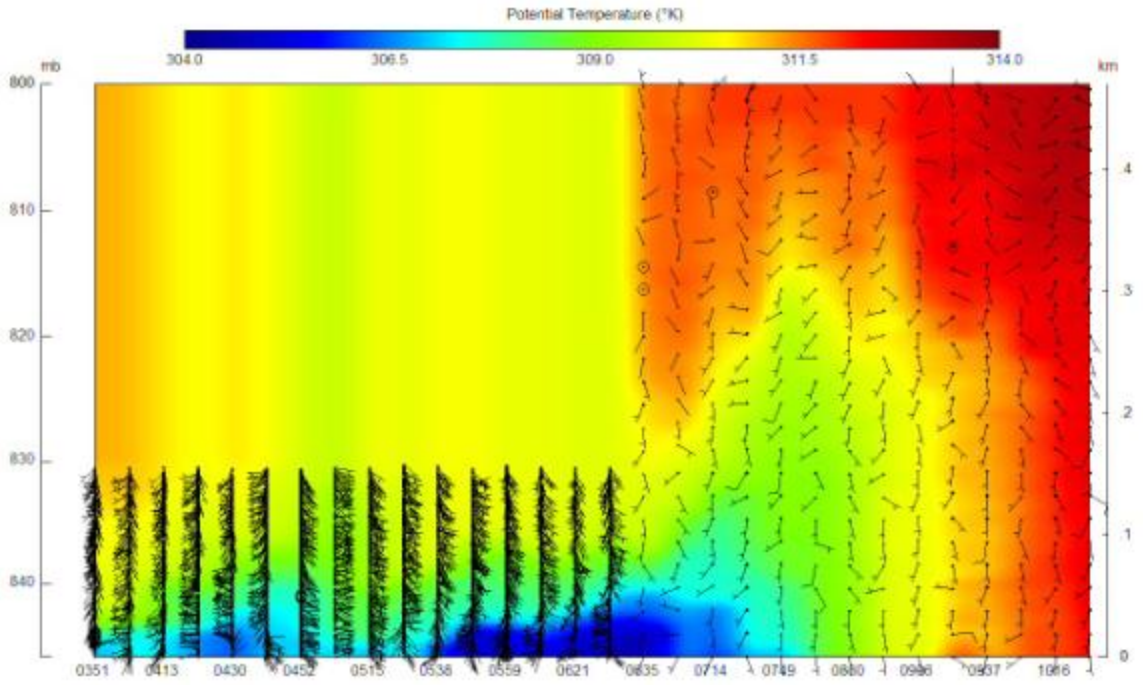

Figure 39. Tethered balloon wind and potential temperature profile summary for June 27, 2008

Highly variable southerly winds started off on June 28. The plot shows a deep stable layer that reaches up to 400 meters above the ground. Early in the day winds near the surface were variable from the southwest to southeast directions and remained that way after sunrise. After sunrise the lower levels of the mixed layer were flowing from the north but easterly above 300 meters. This shear continued until 9:30 am when we had to discontinue operations due to high winds.

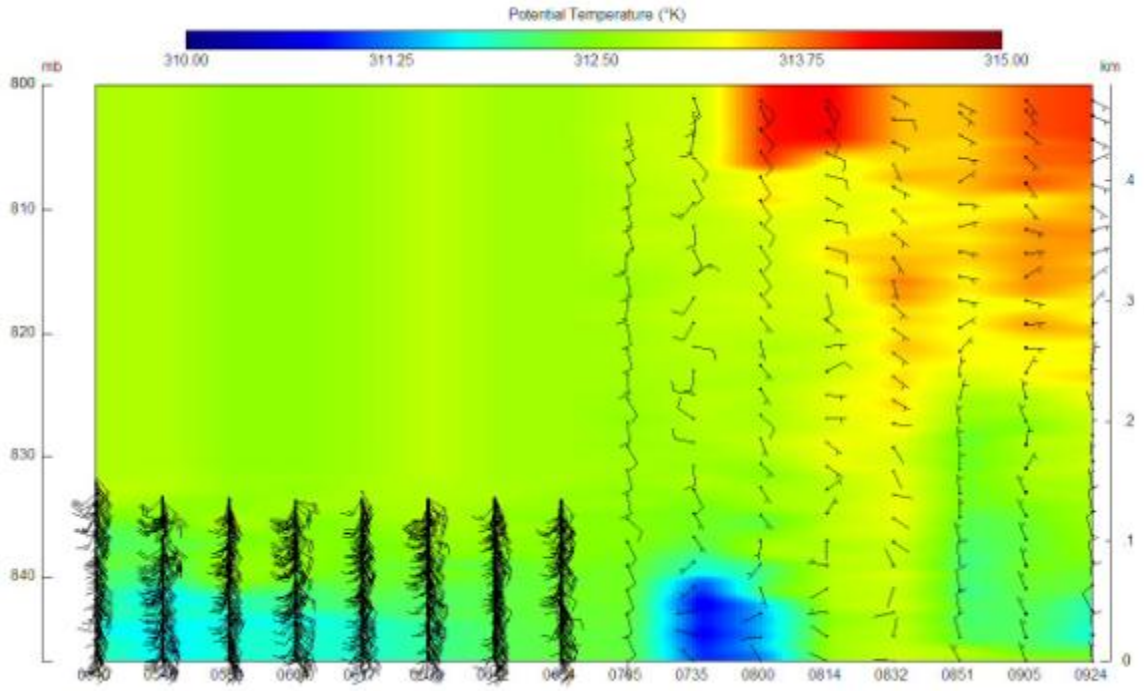

Figure 40. Tethered balloon wind and potential temperature profile summary for June 28, 2008

The plot for June 29 showed another shallow stable layer approximately 100 meters thick. Early in the morning the winds near the surface were from the northwest to westerly direction but shifted to southerly winds by 10 am.

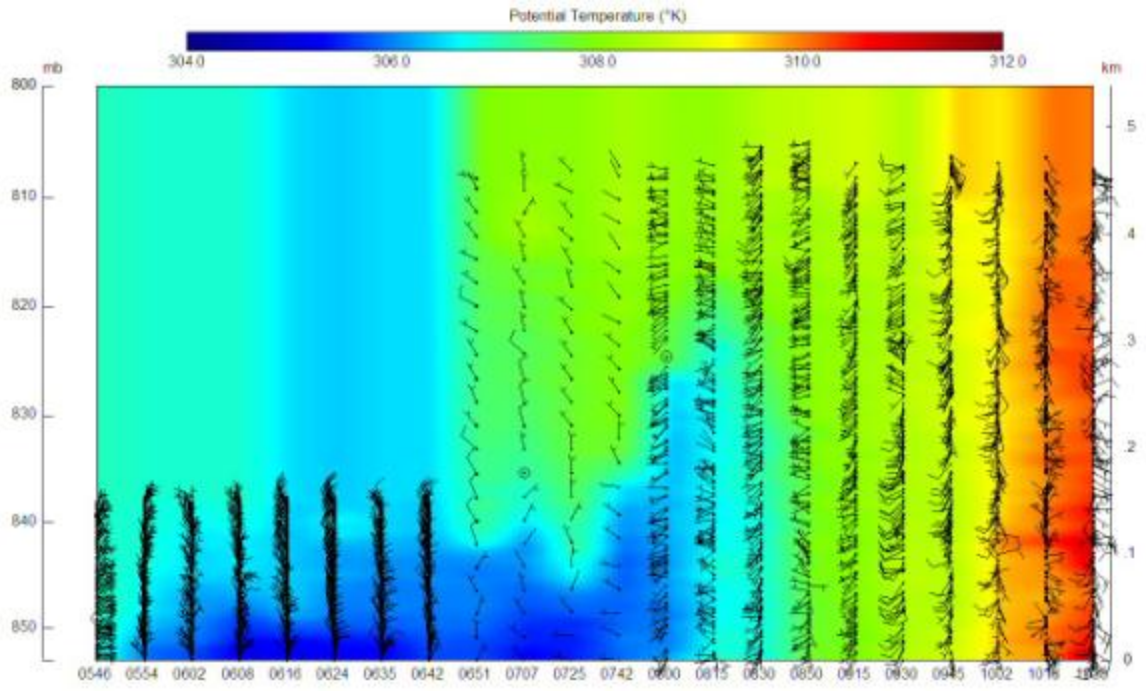

Figure 41. Tethered balloon wind and potential temperature profile summary for June 29, 2008

Sandia Tramway Profiles

Using the same instrumentation as the winter IMP, one gondola on the Sandia Tramway was instrumented to collect temperature and humidity during the summer IMP. Figures 33 through 39 show selected temperature profiles from the tram. On most days of the summer IMP the tram did not see a significant temperature inversion.

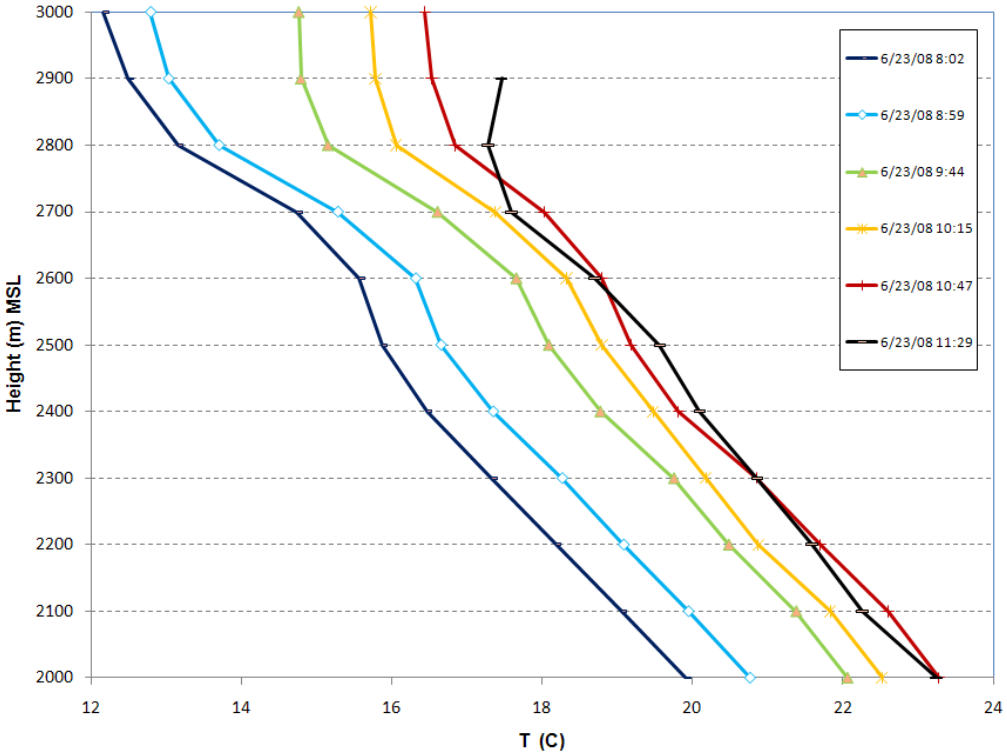

Figure 42. Morning tram temperature profiles on June 23, 2008

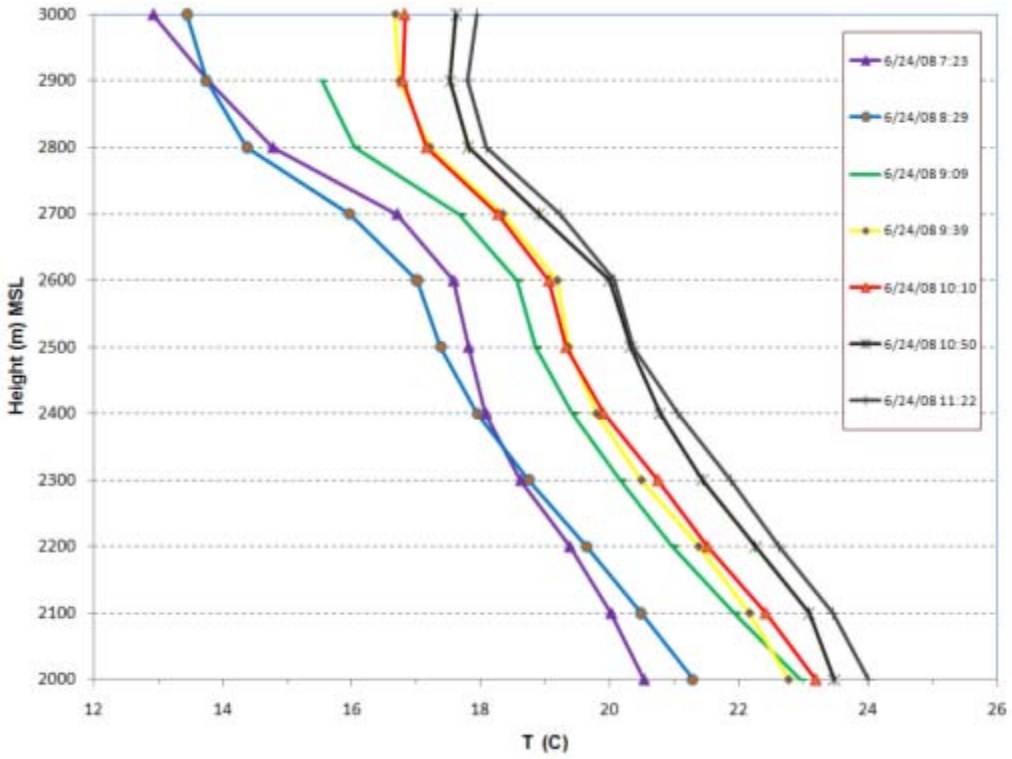

Figure 43. Morning tram temperature profiles on June 24, 2008

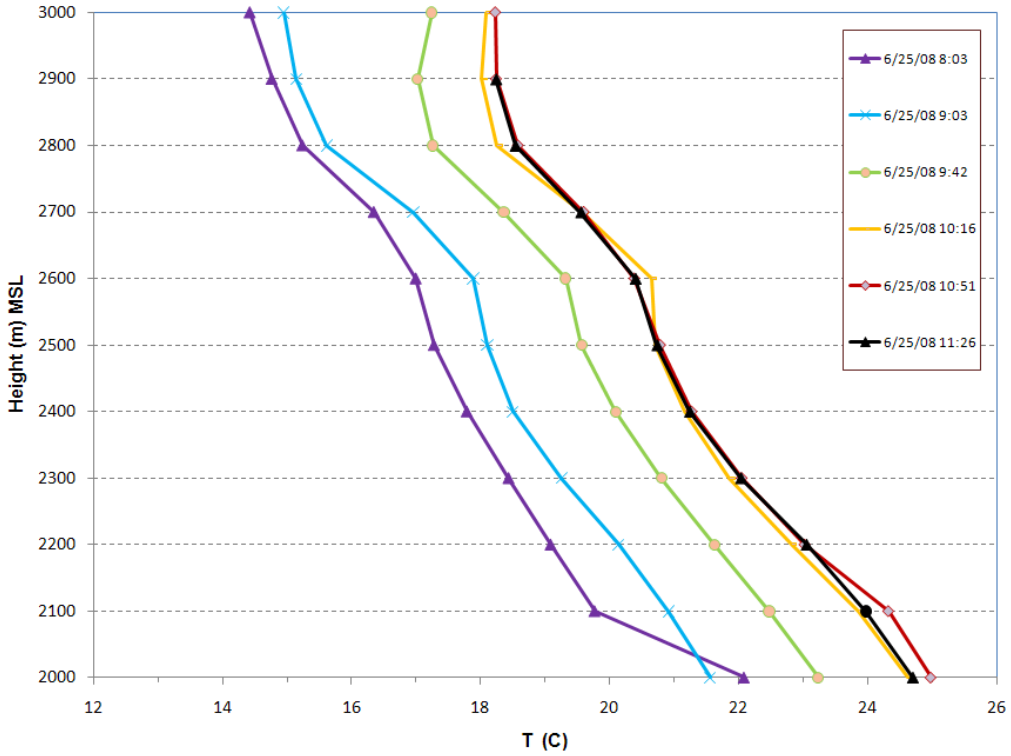

Figure 44. Morning tram temperature profiles on June 25, 2008

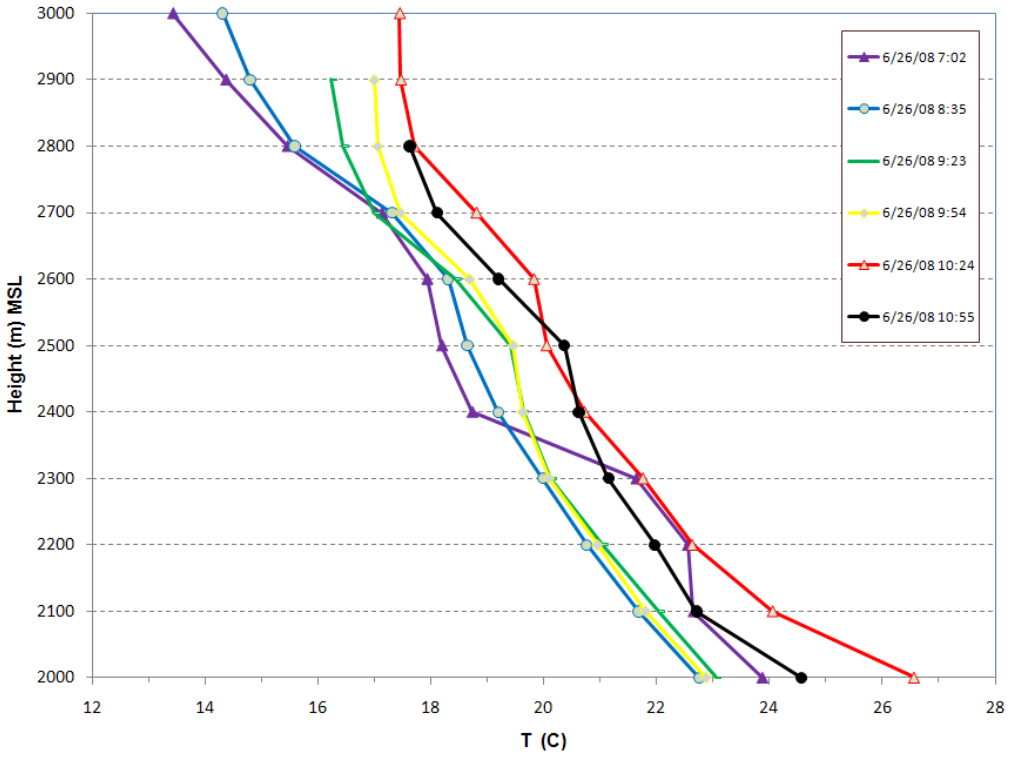

Figure 45. Morning tram temperature profiles on June 26, 2008

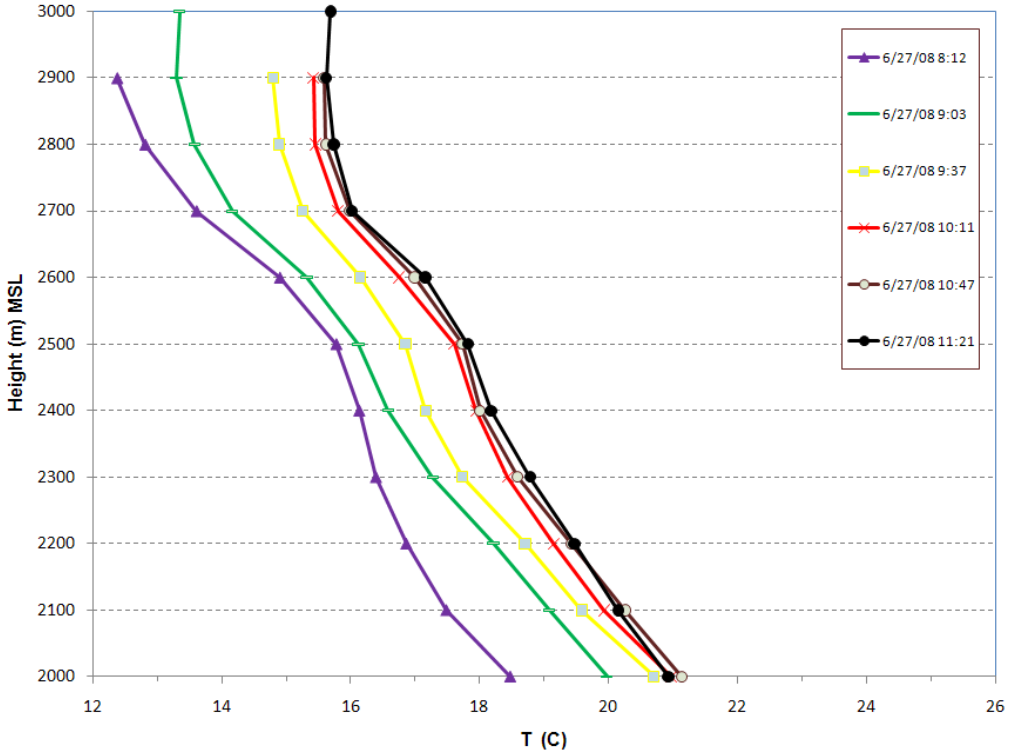

Figure 46. Morning tram temperature profiles on June 27, 2008

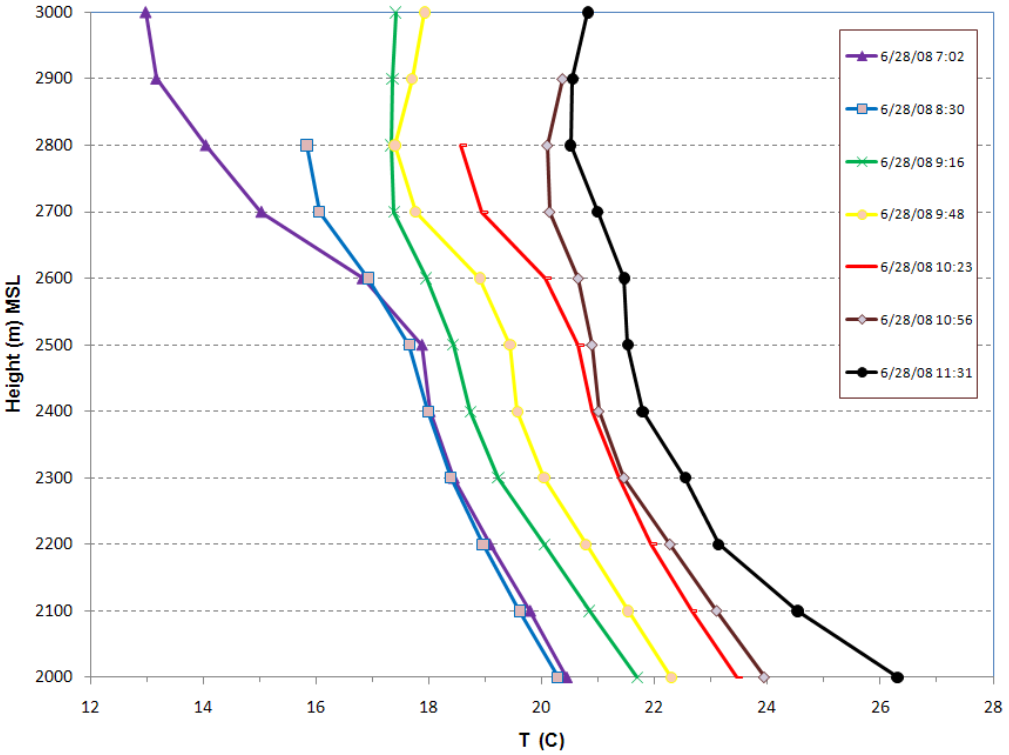

Figure 47. Morning tram temperature profiles on June 28, 2008

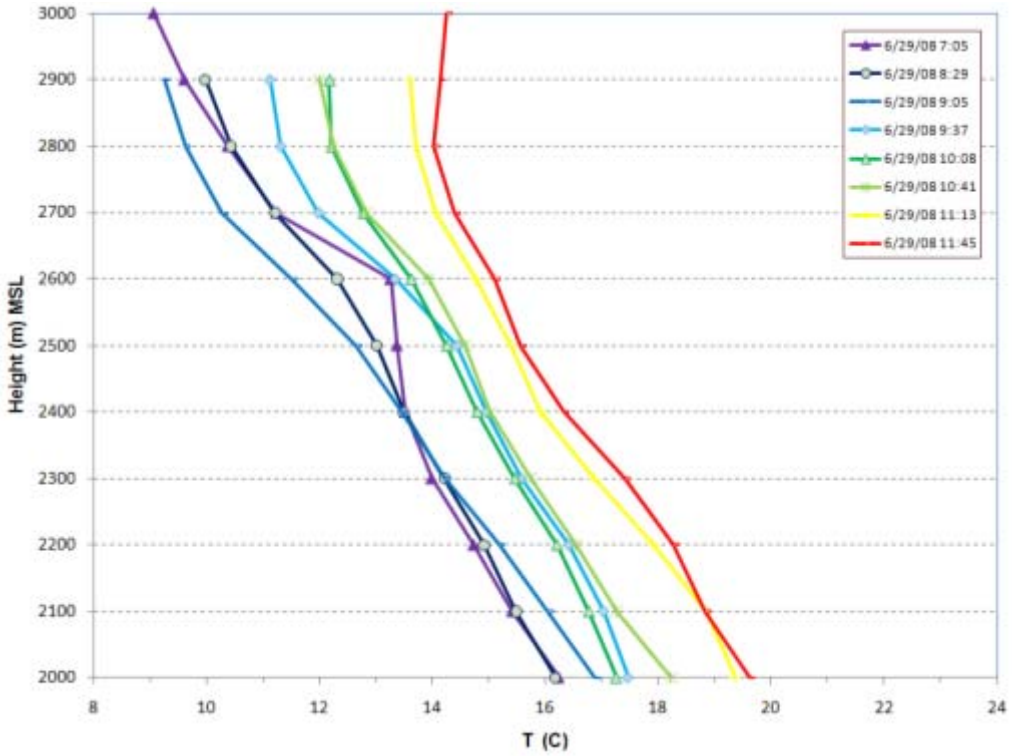

Figure 48. Morning tram temperature profiles on June 29, 2008

Ceilometer Data

The purpose of the ceilometer was to provide an additional method to estimate the boundary layer height as well as document aloft layers of pollutants and instances of clouds and precipitation during the summer study. The ceilometer was installed on Monday, June 16, 2008 and run through June 22 on the roof of the Del Norte site, 2ZM. The ceilometer was then operated at the balloon fiesta site while we were on site with the tethered balloon. The ceilometer was operated as a lidar with backscatter collected in units of steradan^{-1} km^{-1}. We used the Vaisala CL-VIEW software for data collection, and data storage. The software graphically shows cloud locations, cloud intensities and the backscatter profile graphs. In all three graphs also numerical cloud height information, ceilometer status, log status along with time and date are displayed. The ceilometer was connected to a laptop through a serial data port for data collection. The unit was operated to give a backscatter profile from the ground to 7.7 kilometers every 5 seconds. Each profile has a vertical resolution of 10 meters, providing a total of 770 discrete points in a vertical profile.

The mixed layer can often be seen as a strong gradient in backscattered intensity as a function of height. This usually works best when inversions are strong and there are sufficient aerosols within the mixed layer to act as scattering media. Various methods (Steyn et al., 1999; Endlich et al., 1979; Melfi et al., 1985; Menut et al., 1999) to differentiate the mixed layer depth can be investigated depending on the difference in aerosol concentrations above and within the mixed layer. The gradient method was used to find the hourly averaged mixing height (Endlich et al 1979; Munkel and Rasanen,

2004). The gradient method used the minimum of the first derivative of the backscatter profile, db/dz. This is one of the most straightforward methods and relatively simple to implement. I believe that is based on the Holzworth method. All of the hourly values are in the spreadsheet along with comparison plots. Note that there are significant differences in the two methods. I think the biggest contributor to the differences is the lack of stuff to backscatter when the mixing depths are high. The gradient method picks out the lower level aerosol and weighs them more since there's more signal to see.

Because of the size and proximity of the Big Spring wildfire, we took the opportunity to measure the smoke plume using the ceilometer. The ceilometer was operated along side of highway 337 just northeast of Tajique starting at 3:25 pm MDT. The location was at the intersection of 337 and county road A021 at 34.79772ºN,-106.2364ºW at an elevation of 5,094 feet MSL. The fire was calculated to be approximately 14 km from the ceilometer measurement site. The instrument showed the plume base elevation ranging from 2,400 (7,874') to 4,200 meters (13,780') AGL and moving toward the east-northeast. Figure 40 shows the backscatter profile for a short period of time. As the figure shows, the plume was elevated at approximately 3.6 to 4.5 km above the ground and did not reach the ground at first.

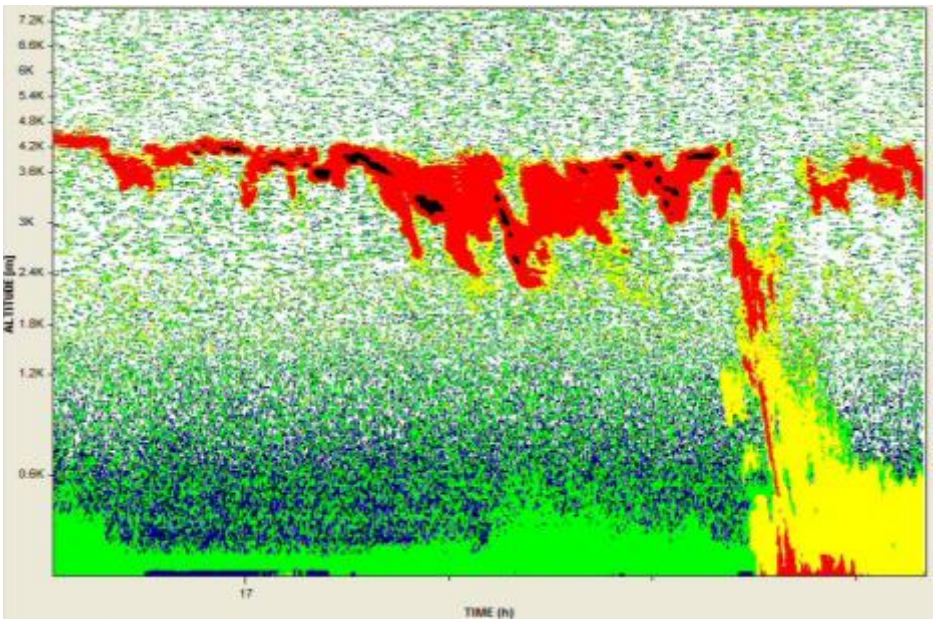

Figure 49. Backscatter of the Big Spring wildfire as the plume passed over the ceilometer from 4:45 to 5:15 pm on June 25, 2008

CALMET MODELING

CALMET Input Data

The primary types of inputs to the CALMET model include:

- Model domain, simulation time, time steps, computational grid size, map projection and number of vertical layers.

- Geophysical data (terrain elevation, land use categories, and optional parameters such as surface roughness length, albedo, Bowen ratio, soil heat flux, anthropogenic heat flux, and vegetative leaf area index).
- Surface meteorological data (hourly observations of wind speed and direction, temperature, surface pressure, relative humidity, and optionally cloud cover, ceiling height, hourly precipitation data).
- Upper-air data (vertical profiles of wind speed and direction, temperature, pressure, and elevation from the airport radiosonde every 12 hours).

CALMET Model Output

CALMET is a meteorological model that includes a diagnostic wind field module with objective analysis and parameterization of slope flows, kinematic terrain effects, terrain-blocking effects, and a micrometeorological module for overland and overwater boundary layers (Scire et al., 2000a). The diagnostic wind field module contains options that allow wind fields produced by complex atmospheric prognostic models (e.g., MM5) to be used as virtual meteorological stations or as initial conditions for the objective analysis procedure.

CALMET's diagnostic wind field module calculates winds in two steps. In the first step, an initial estimate is adjusted for kinematic effects of terrain, slope flows, and terrain-blocking effects. For the kinematic effects, the domain-scale winds are used to compute a terrain-forced vertical velocity subject to an exponential, stability-dependent decay function. The kinematic effects on the horizontal wind components are derived from a divergence minimization algorithm to the initial wind field estimate. Slope flows are parameterized by the balance of momentum, surface drag, and entrainment at the top of the flow layer. Specifics of the slope flows are determined from the slope angle, distance to the crest, and local sensible heat flux. The thickness of the flow layer is determined as a function of the elevation drop from the crest. The blocking effects of the terrain on the flow are parameterized in terms of the local Froude number and the wind direction of the flow is changed accordingly. In the second step, an objective analysis is used to produce a final wind speed.

The modeling domain was chosen to capture the local terrain features of the Albuquerque metropolitan area and to include locations of surface and upper air meteorological monitoring stations. The modeling domain covers an area of 55 x 55 kilometers with the southwest corner at UTM zone 13 coordinate of (325,000 meters Easting and 3,860,000 meters Northing). The modeling domain is larger than the area enclosing the city of Albuquerque so that terrain induced flows from the valley and mountain ranges can be simulated within CALMET.

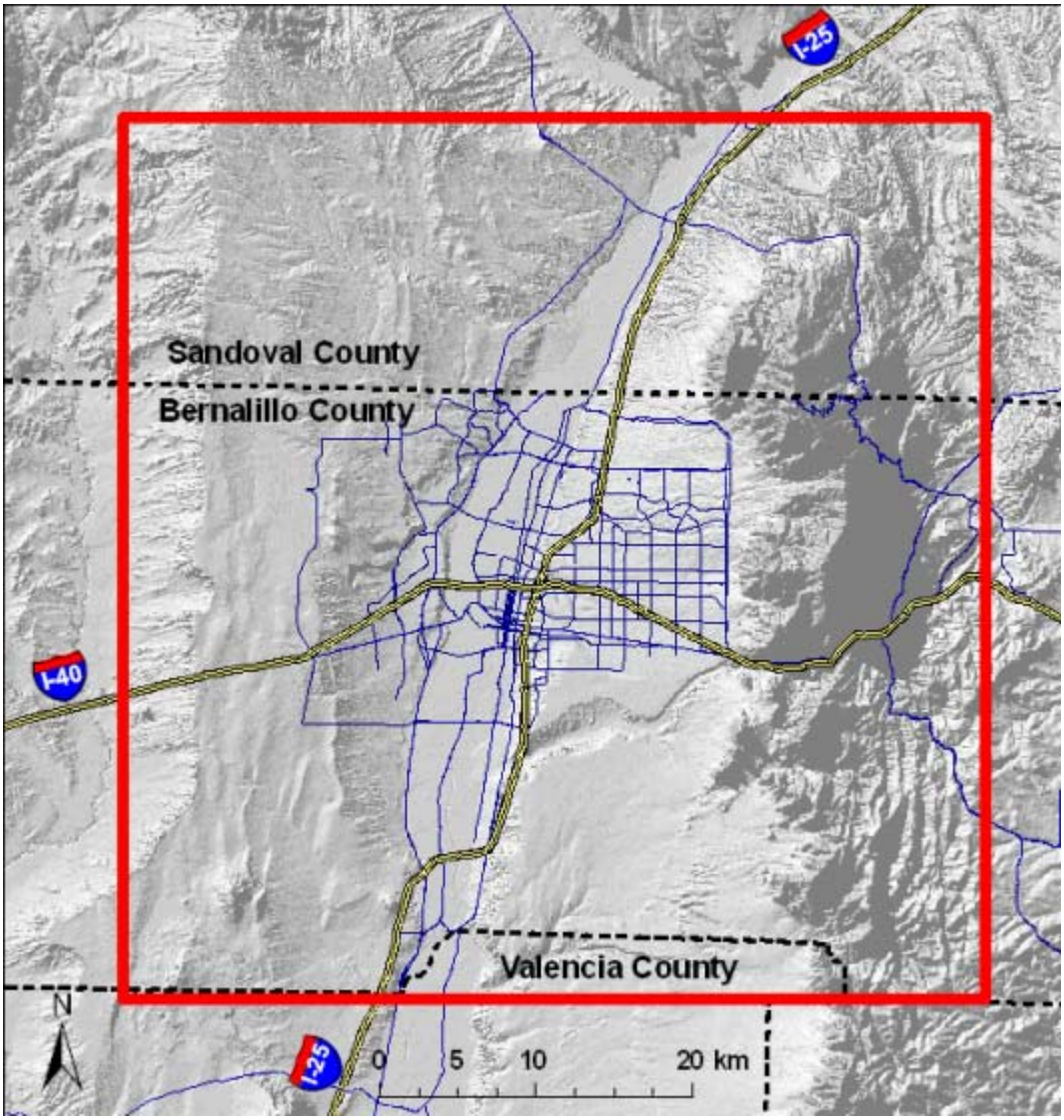

Figure 50. CALMET modeling domain (red box) for both summer and winter studies

Figure 51 shows the modeling domain and the terrain elevations used in the model. Elevation data were obtained from USGS digital elevation models with 10-meter resolution. These files were used as input for the CALMET preprocessing utilities such as TERREL.

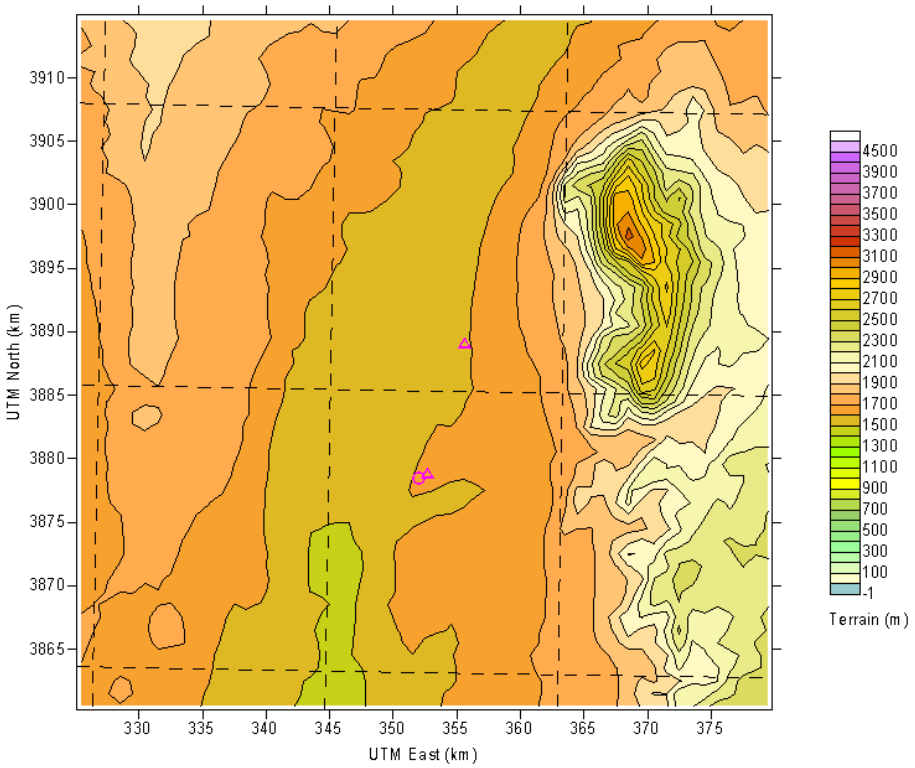

Figure 51. Topography within the modeling domain around Albuquerque with indicated meteorological stations used for meteorological modeling. Locations of the airport and the DelNorte site 2ZM are shown.

The CALMET model accepts a limited number of landuse databases in version 6. The CTGPROC is a pre-processor that formats the raw landuse files for the CALMET. CTGPROC accepts the following types:

- USGS Global landcover (GLCC v2) at 1 km resolution
- USGS LULC landcover landuse (CTG format) at 30 m resolution
- USGS National Landuse Land Cover NLCD92 at 30 m resolution

The first landuse database I used was the USGS LULC. As I stated in the draft report, the data originates from old satellite interpretations back in the mid-1980s. To compare this with a more recent database I downloaded the NLCD92 landuse database from the USGS. The NLCD92 was derived from mid-90s Landsat Thematic Mapper images at the USGS. All of these databases are linked from the CALMET/CALPUFF website. The NLCD92 file comes in the form of one 8-bit binary file for the whole state of New Mexico. USGS also provides a TIFF image with pixel values associated with the USGS landuse codes to view it in a visualization program. The following figures compares the landuse from the NLCD92 database (left) and LULC (right) as seen by CALMET using the CALVIEW utility.

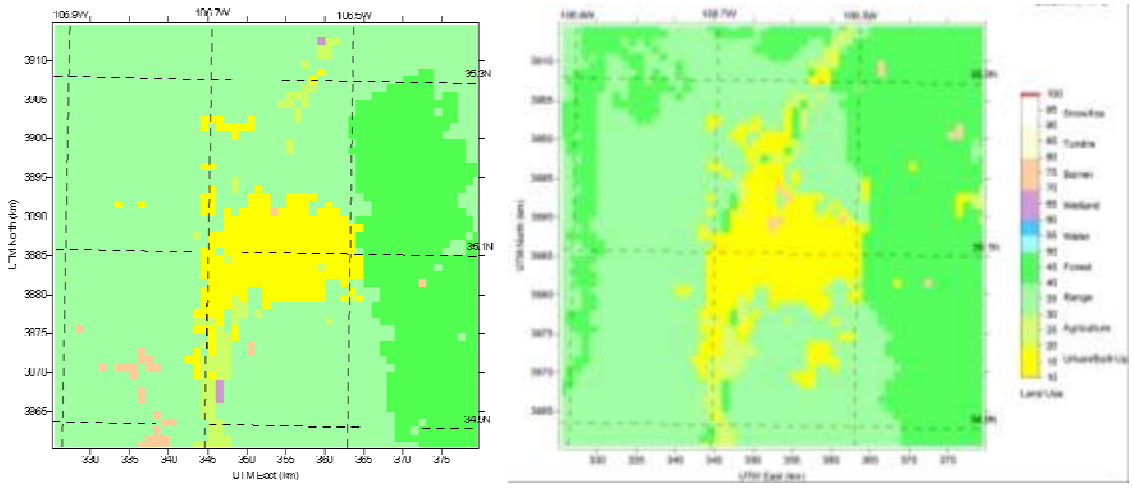

Figure 52. Landuse from NLCD92 (left) and LULC (right)

As you can see there are significant differences between the urban/built-up landuse categories. I also brought both of them into ArcGIS to look in detail at the land use categories and patterns between the two databases. An interesting find in the NLCD92 was that the landuse code 51 of shrubland was the dominant cover in the north valley and in Rio Rancho rather than urban. Shrubland appears as the tan color in the plot below.

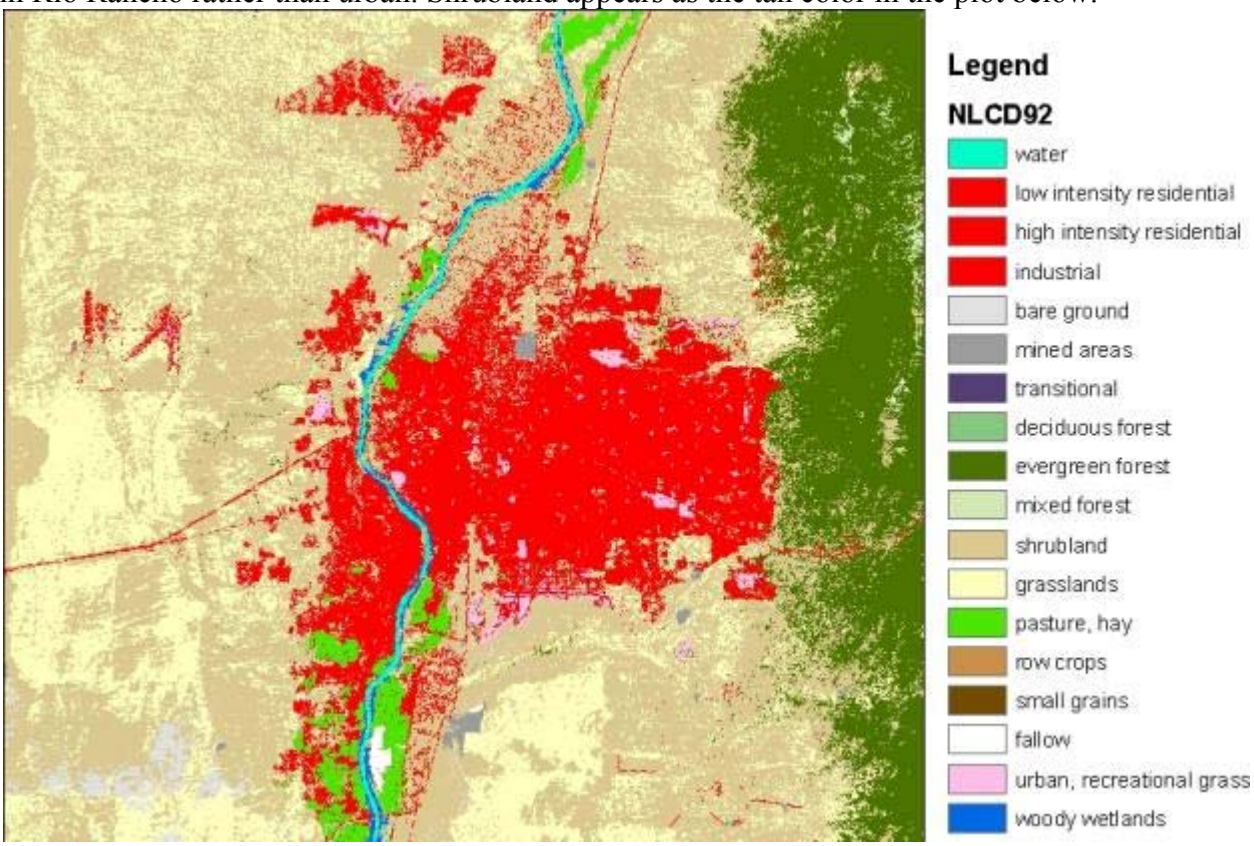

Figure 53. NLCD92 landuse in detail

I downloaded a recent aerial photo from 2009 and overlaid the NLCD92 landcover at several locations in the northern part of the modeling domain where the most noticeable

differences are. Figures 3 through 5 show some examples of NLCD92 and the aerial photos.

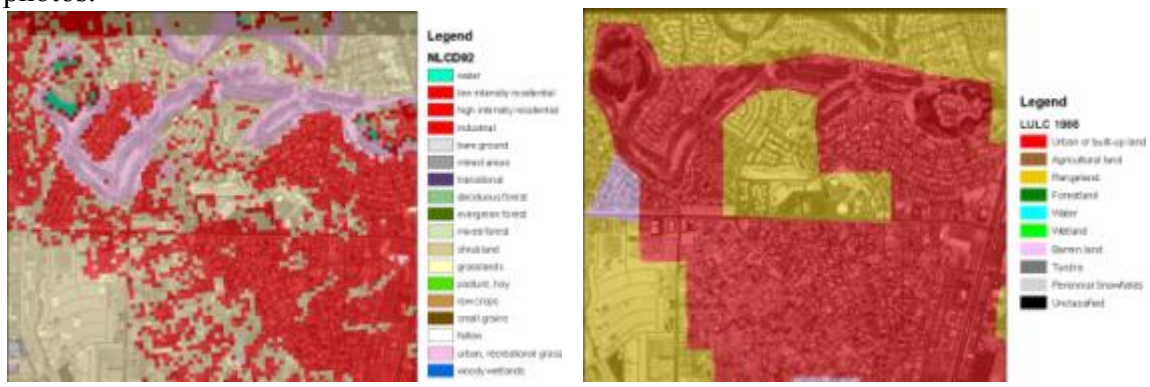

Figure 54. Chamisa Hills Golf Course in Rio Rancho with NLCD on left and LULC on right.

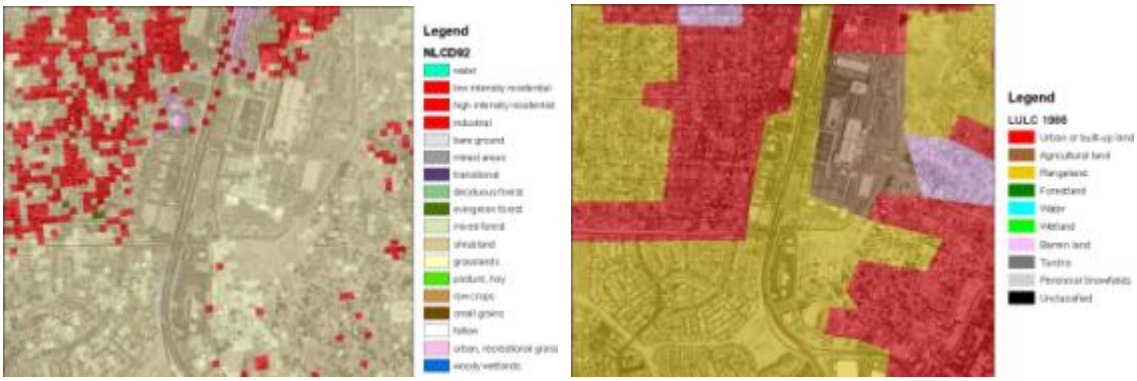

Figure 55. Intel in Rio Rancho with NLCD on left and LULC on right.

Figure 56. Rio Grande and Paso del Norte with NLCD on left and LULC on right.

Figures 4 and 5 are typical examples of the large expanse of shrubland in the north valley mixed with residential in the NLCD92 database. Figure 6 is a map of the older LULC database for the whole modeling domain. The older LULC database appears to better represent the urban landuse in the modeling domain.

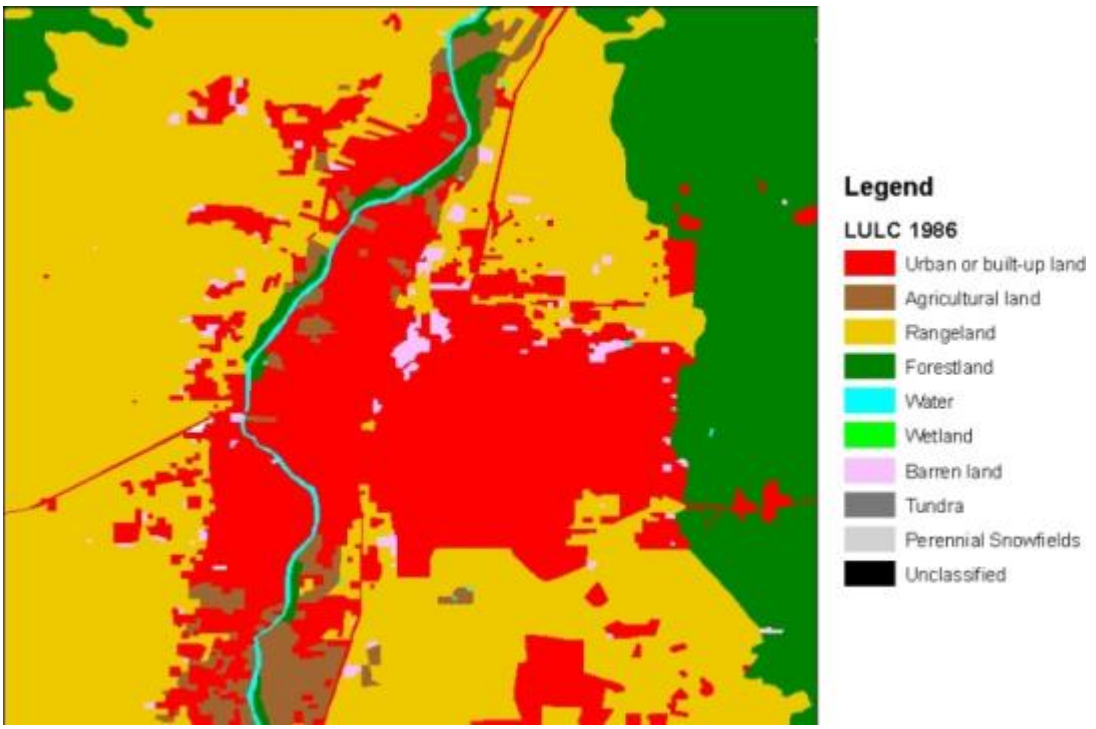

Figure 57. The USGS LULC database in detail

Landuse characteristics used in the model were obtained from the 1:250,000 scale USGS LULC database in the Composite Theme Grid (CTG) format. Landuse files in CTG format have a grid resolution of 30 meters. The LULC database has a total of 46 possible land use categories with Table 1 showing some of these relevant to the Albuquerque area.

Table 3. Land use categories from the USGS LULC database relevant to this study

Land Cover Code	Landuse Category	Land Cover Code	Landuse Category
1	Urban or Built-Up Land	4	Forest Land
11	Residential	41	Deciduous Forest Land
12	Commercial Services	42	Evergreen Forest Land
13	Industrial	43	Mixed Forest Land
14	Transportation, Communications	5	Water
15	Industrial and Commercial	51	Streams and Canals
16	Mixed Urban or Built-Up Land	52	Lakes
17	Other Urban or Built-Up Land	53	Reservoirs
2	Agricultural Land	7	Barren Land
21	Cropland and Pasture	71	Dry Salt Flats
22	Orchards, Groves, Vineyards, Nurseries	73	Sandy Areas Other than Beaches
23	Confined Feeding Operations	74	Bare Exposed Rock
24	Other Agricultural Land	75	Strip Mines, Quarries, and Gravel Pits
3	Rangeland	76	Transitional Areas
31	Herbaceous Rangeland	77	Mixed Barren Land
32	Shrub and Brush Rangeland	83	Bare Ground
33	Mixed Rangeland		

The CTGPROC processing utility was used to read these files and re-grid them in to the 1 kilometer grid resolution. Figure 42 shows the resulting gridded landuse as used in the

modeling. Although the landuse database was constructed from satellite imagery interpretations from the 1980s the overall urban category coverage matches the current area. The primary affect of landuse on the simulations would be in the predictions of mixing depth, wind speed and direction.

Table 5 presents the locations of the meteorological stations from which input data for CALMET were derived. Windroses for each site were generated and evaluated whether they made sense with regard to the flow in the area. If the windroses made sense then they were included in the CALMET simulation. One site that did not pass this test was the City of Albuquerque Double Eagle 2ZF site in the far northeast quadrant of the city. This site's windrose indicated only easterly winds and probably was not representative of the eastern foothills. Using this site's wind data in the CALMET simulation produced very tight gradients in wind flow that might not be reasonable. The wind field maps in this report did not use 2ZF in the calculations. Although not part of the city of Albuquerque network, the Los Lunas meteorological station data was used in the model to establish the southern Rio Grande valley boundary conditions since the airport station is influenced frequently by east canyon winds.

Table 4. Surface meteorological stations and their location as used in the CALMET model

ID	Name	UTM_E (km)	UTM_N (km)	Long (deg)	Lat (deg)	Elev (m)
KABQ	International Airport	352.658	3878.881	-106.615	35.042	1618
2ZM	DelNorte (CABQ)	355.582	3889.083	-106.585	35.134	1589
2ZE	Uptown (CABQ)	357.462	3886.059	-106.564	35.107	1620
2ZH	North Valley (CABQ)	353.079	3895.672	-106.614	35.193	1523
2ZL	Corrales (CABQ)	349.890	3896.712	-106.649	35.202	1531
2ZN	SE Heights (CABQ)	356.018	3881.181	-106.579	35.063	1616
2ZS	Singer (CABQ)	353.820	3890.228	-106.605	35.144	1555
2ZT	Taylor Ranch (CABQ)	345.428	3891.428	-106.697	35.154	1558
2ZU	San Pedro (CABQ)	356.235	3885.564	-106.577	35.103	1594
2ZV	South Valley (CABQ)	348.784	3876.194	-106.657	35.017	1509
2ZJ	Bernalillo (NMED)	359.340	3907.382	-106.547	35.300	1541
2ZR	Rio Rancho (NMED)	349.868	3900.700	-106.650	35.238	1606
2LL	Los Lunas (NMED)	340.893	3853.873	-106.740	34.815	1485

The primary source of upper air data was from the Albuquerque office of the National Weather Service near the International Airport. Atmospheric profiles were taken twice-daily at 12:00 and 00:00 UTC. In practice the radiosondes were launched approximately by 11 and 23 UTC.

Table 5. Upper air data used in CALMET

ID	Name	UTM_E (km)	UTM_N (km)	Long (deg)	Lat (deg)	Elev (m)
ABQ	International Airport	351.978	3878.466	-106.623	35.038	1614

Main outputs from CALMET are:

- Gridded fields of east-west (U), north-south (V), and vertical (W) wind components

- Surface friction velocity, convective velocity scale
- Monin-Obukhov length, mixing height, stability classes, air temperature, and precipitation rate.

CALMET was configured as follows for this study:

- Period of simulations: 12 February 2008 – 18 February 2008 for the winter IMP and 17 June 2008 – 30 June 2008 for the summer IMP
- Model horizontal grid: 55 km x 55 km
- Model horizontal resolution: 1 km x 1 km
- Model vertical grid: 11 layers
- Vertical layer heights: 0, 20, 50, 100, 500, 1000, 1500, 2000, 3000, 4000 and 5000 m
- Horizontal resolution of topography input to model: 10 m x 10 m.

Hourly wind fields for the study were generated for each IMP. Windroses were generated and compared to the measurements at each meteorological station location as a quality check of the model. One such comparison is shown in Figure 45 comparing wind roses at the airport during the summer IMP. From these plots we can see that the model predicts lighter winds compared with the measurements particularly in the northerly direction.

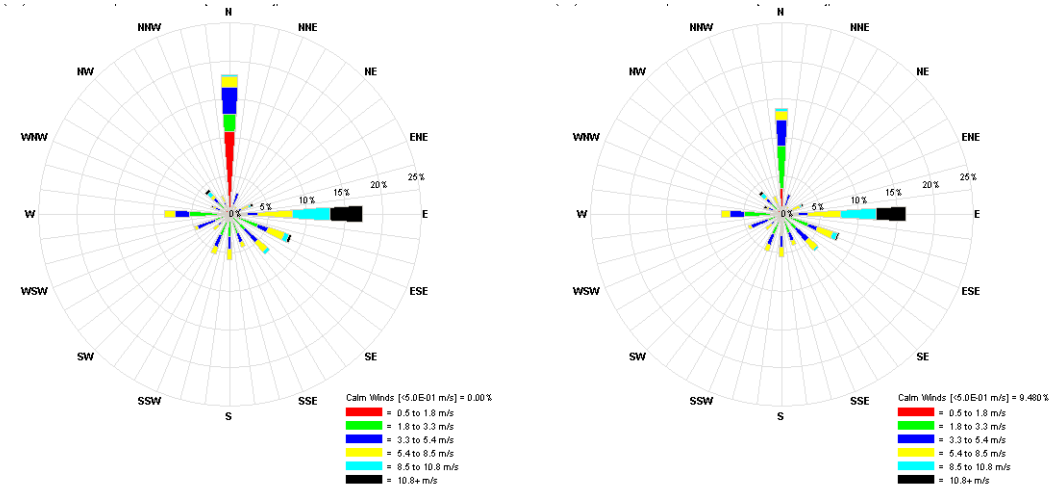

Figure 58. Frequency distribution of wind direction measured at the Albuquerque International Airport ASOS (left) and simulated with CALMET (right) during the summer IMP

The CALMET post-processor utility PRTMET was used to extract time series plots of mixing height and other meteorological outputs such as temperature, humidity and winds. Summary wind vector plots were generated for each IMP and in 1- and 6-hour time spans. Mean wind vectors were calculated by taking the means of the u and v wind components and computing a wind speed and direction from that mean value at each grid cell.

CALMET Winter Flows

CALMET was used to infer the temporal and spatial structure of the wind patterns across the Albuquerque metropolitan area. The hypothesis entering in the study was that the region has valley upslope and downslope winds in the absence of low pressure systems. With these valley slope flows come light and variable winds and a low level stable atmosphere. During winter storms high winds are typical and will appear more spatially uniform in the model.

To test the hypothesis, early morning wind patterns were used to examine the down-slope wind flows before sunrise. Morning wind patterns surrounding sunrise were analyzed to look at the transition between down-slope to upslope winds. Afternoon patterns were examined for up-slope flow toward higher terrain and up the Rio Grande River channel. Evening flow maps were calculated to show transition from upslope to down-slope flow.

Hourly wind vectors from 12 February 2008 to 18 February 2008 were generated by the model and displayed as maps. As expected, during the days when low pressure systems had a minimal effect, the valley showed down-slope winds across the region with winds blowing from the higher elevations toward the lower elevations. One hypothesis was that model would produce a narrow convergence zone along the Rio Grande River channel with NNW winds on the west side and NE winds on the east side of the river. However, this was not observed during the winter IMP. Overall the model predictions are consistent with the hypothesis for a nighttime flow regime having little influence from large scale synoptic forcing. For the north valley, this flow will tend to pull in air masses from areas to the north.

In the morning, between 6 am and 11 am, a northwest flow developed over most of the modeling domain. Based on the synoptic maps in Appendix A, these flow patterns were driven by the large scale synoptic flow during the winter IMP. On four of the days the area was under a building upper level ridge with northwest winds. On two of the days (February 14 and 15) an upper level trough produced southwest flow and southerly flow on February 17. The model produced the strongest northwest flow across the northern valley and lesser in the south valley. In the afternoon the flows are similar to the morning wind patterns but winds are higher. Again the wind patterns were driven primarily by the synoptic flow and to a lesser degree the terrain. By evening the wind patterns were split between a north and south valley pattern. In the north valley, a clear up-slope condition can be seen along the Rio Grande River channel. However in the south valley a strong east canyon wind influenced all points south of Tijeras Canyon and along I-40. This effect produced a 90 degree turning of the wind from areas along the I-40 corridor toward the river west of downtown. This circulation will bring in air masses from the east and south and transport them toward the north valley. During this time of the day the south valley has higher winds and will tend to be influenced by air masses to the east.

The calm period on February 18 is worth looking at since some of the gas phase pollutants peaked during that period. During that day winds were very light and several hours of calm winds were observed in the surface network. The following figures show snapshots of the winds during important hours and transition periods.

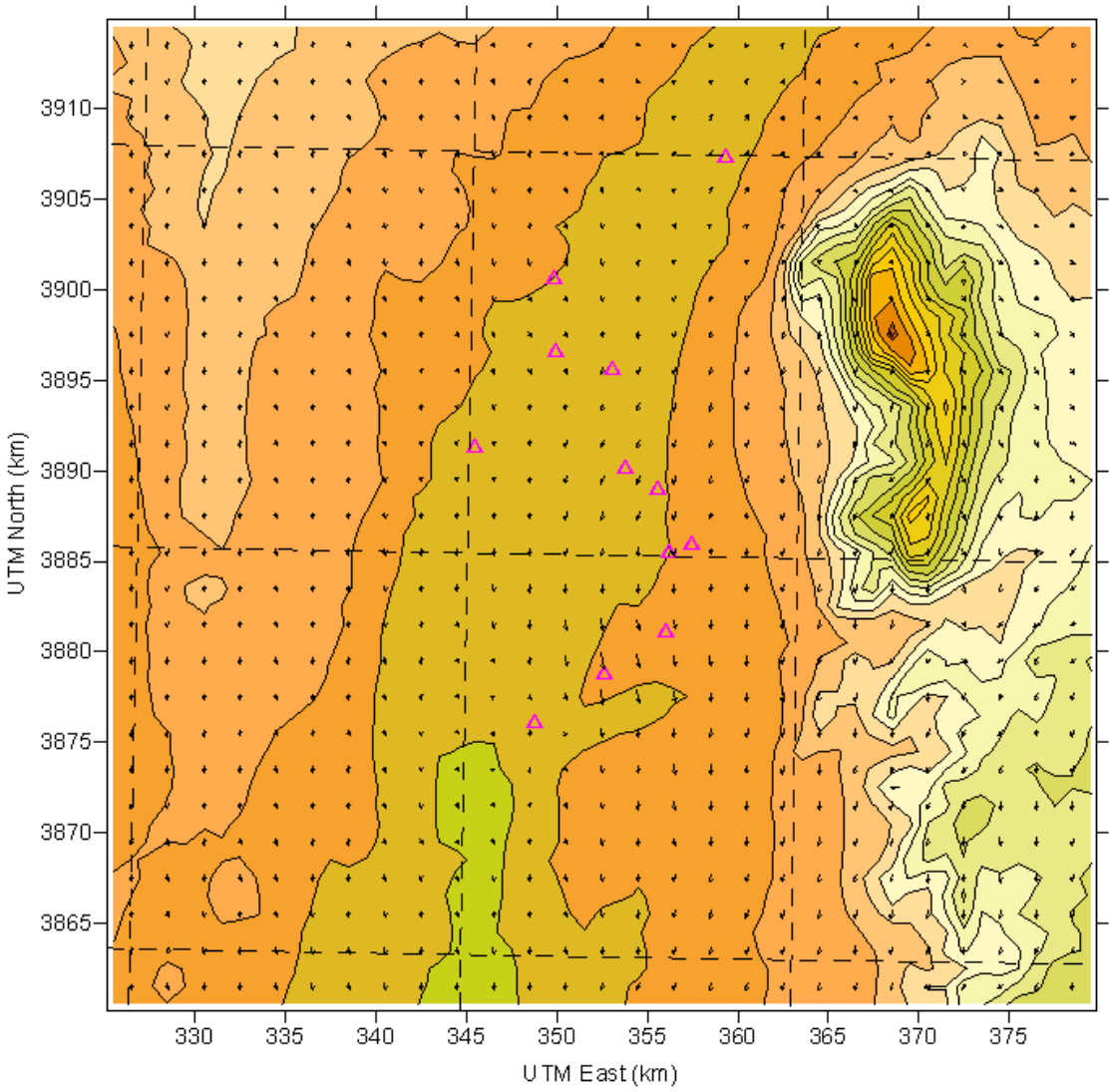

Figure 59. Wind field at 1 am on February 18, 2008

Very light winds with some hint of down slope winds but overall calm winds early in the morning at 1 am.

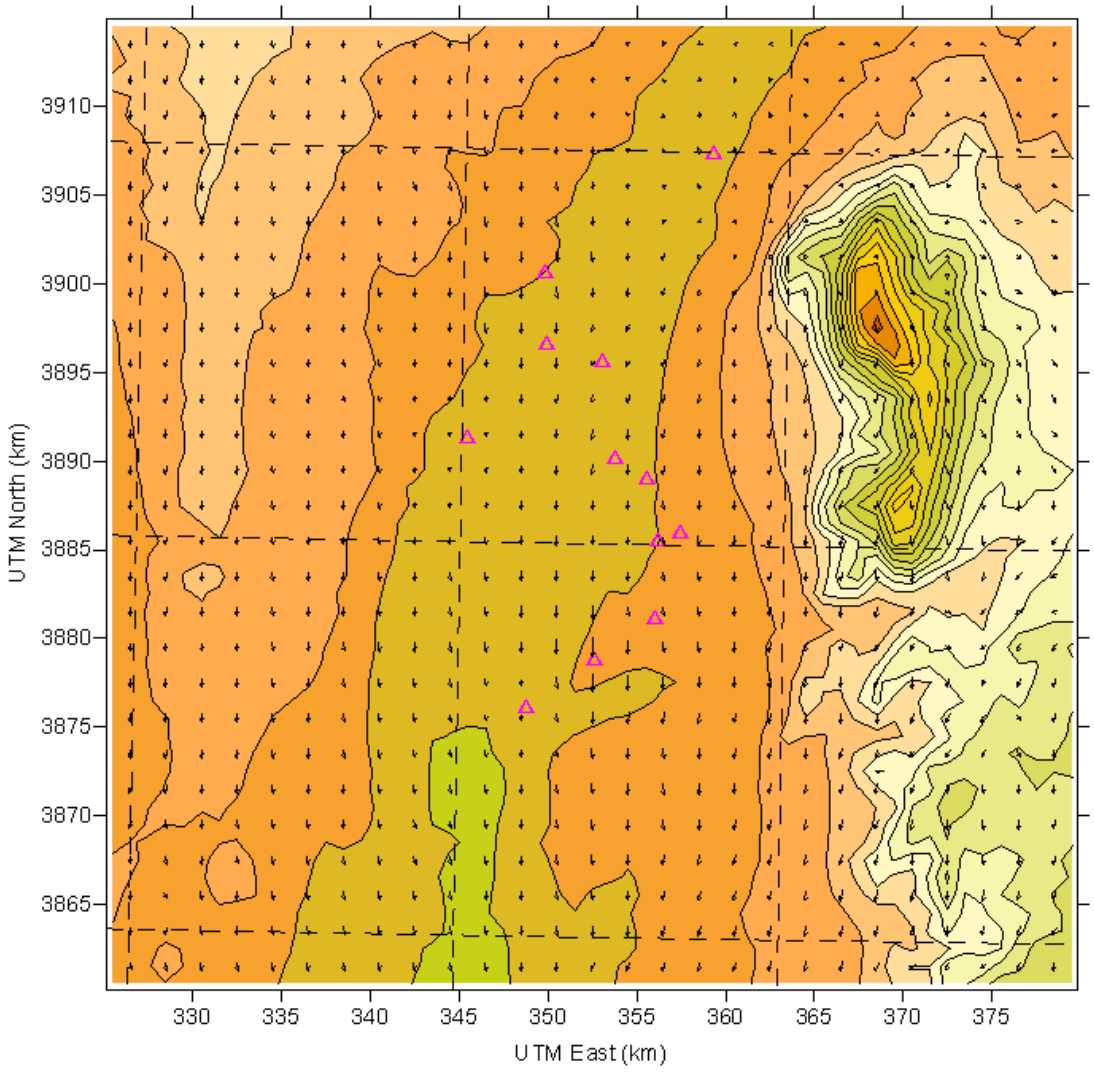

Figure 60. Wind field at 6 am on February 18, 2008

We continue to see some down-slope winds at 6 am but a transition starts to appear as the sun rises and heats the surface.

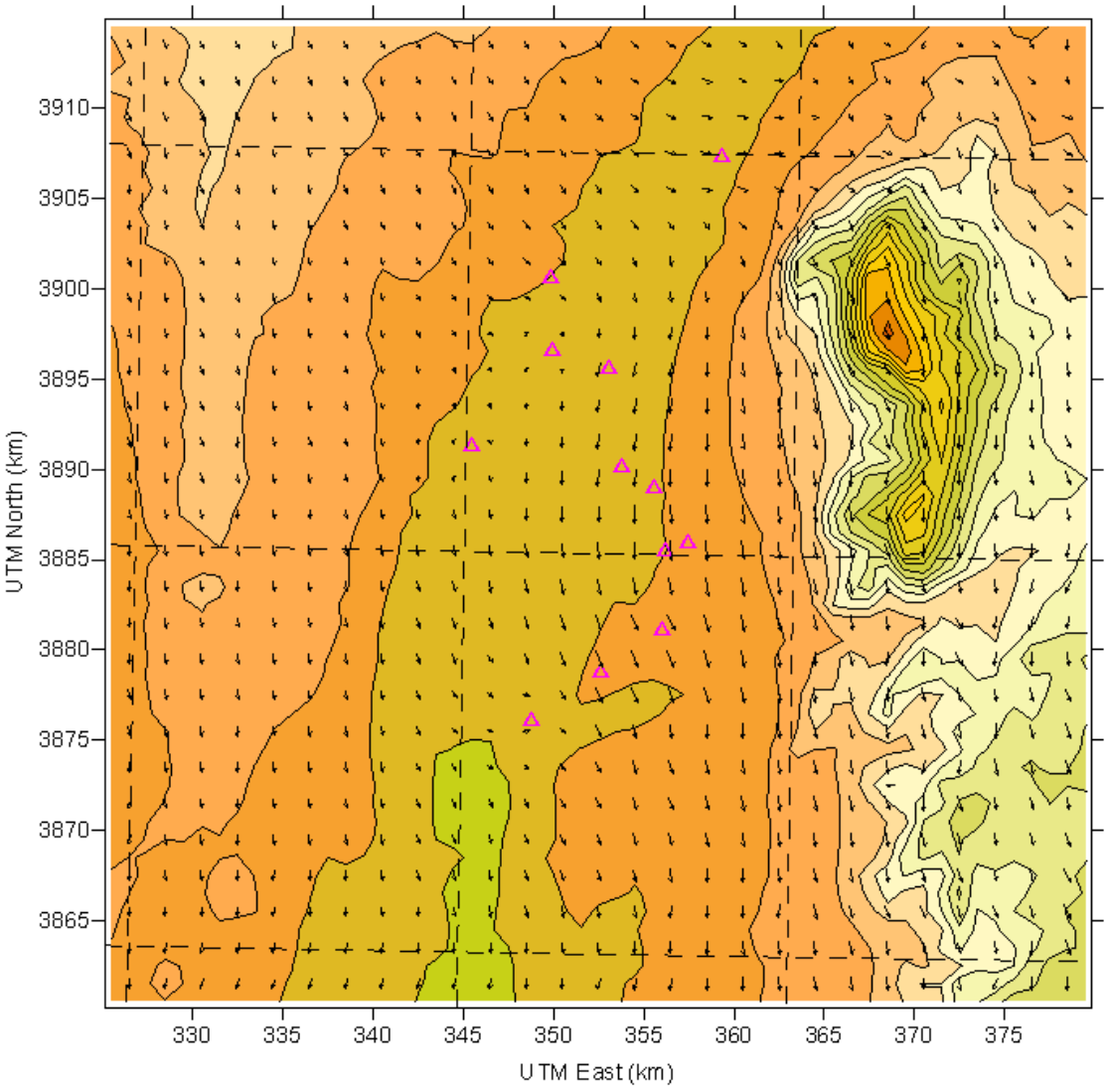

Figure 61. Wind field at 8 am on February 18, 2008

As the sun rises and we see stronger down-slope and down-valley winds continuing through 8 am.

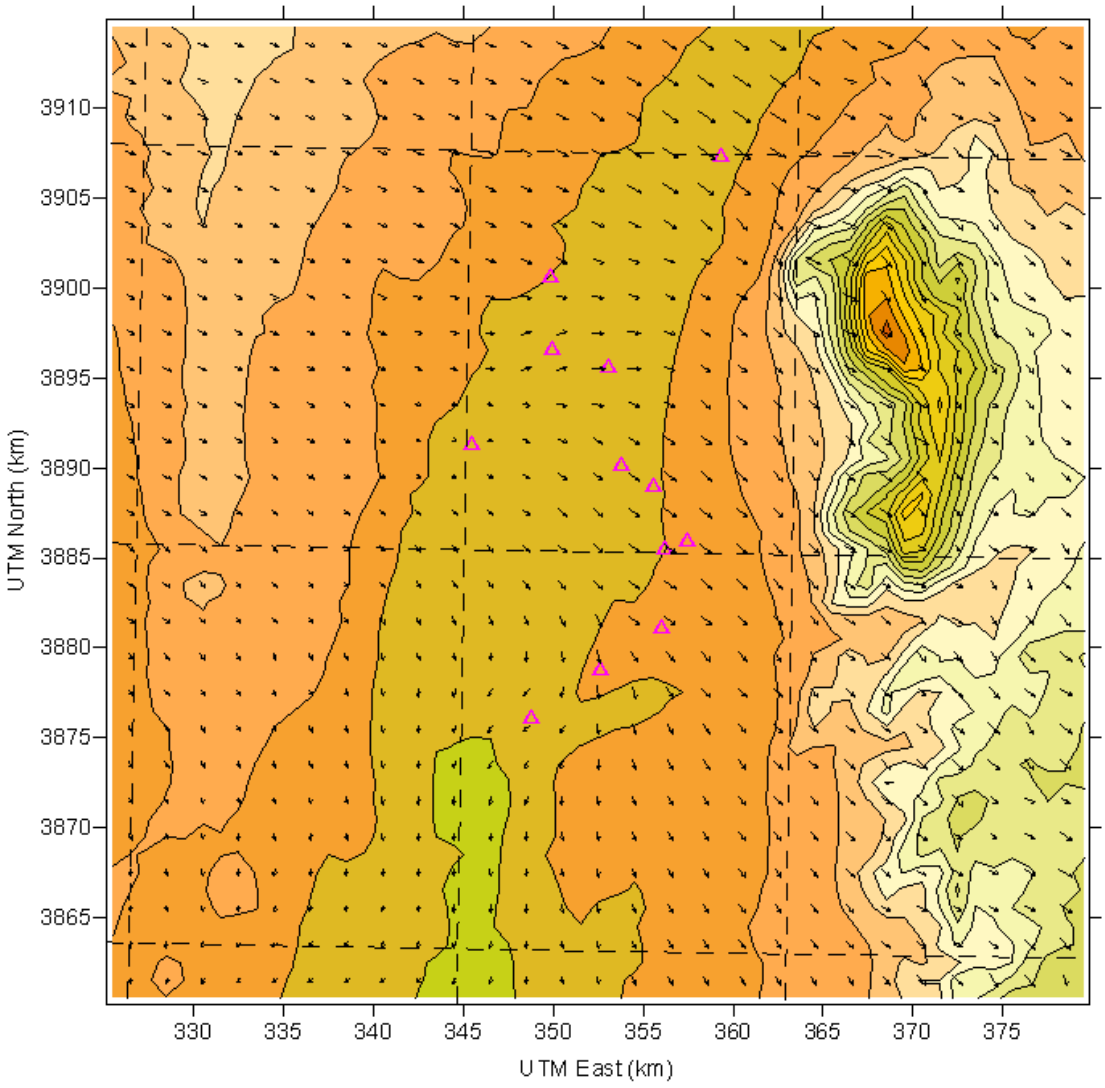

Figure 62. Wind field at 10 am on February 18, 2008

Late in the morning we transition to a more northwesterly pattern than down-slope.

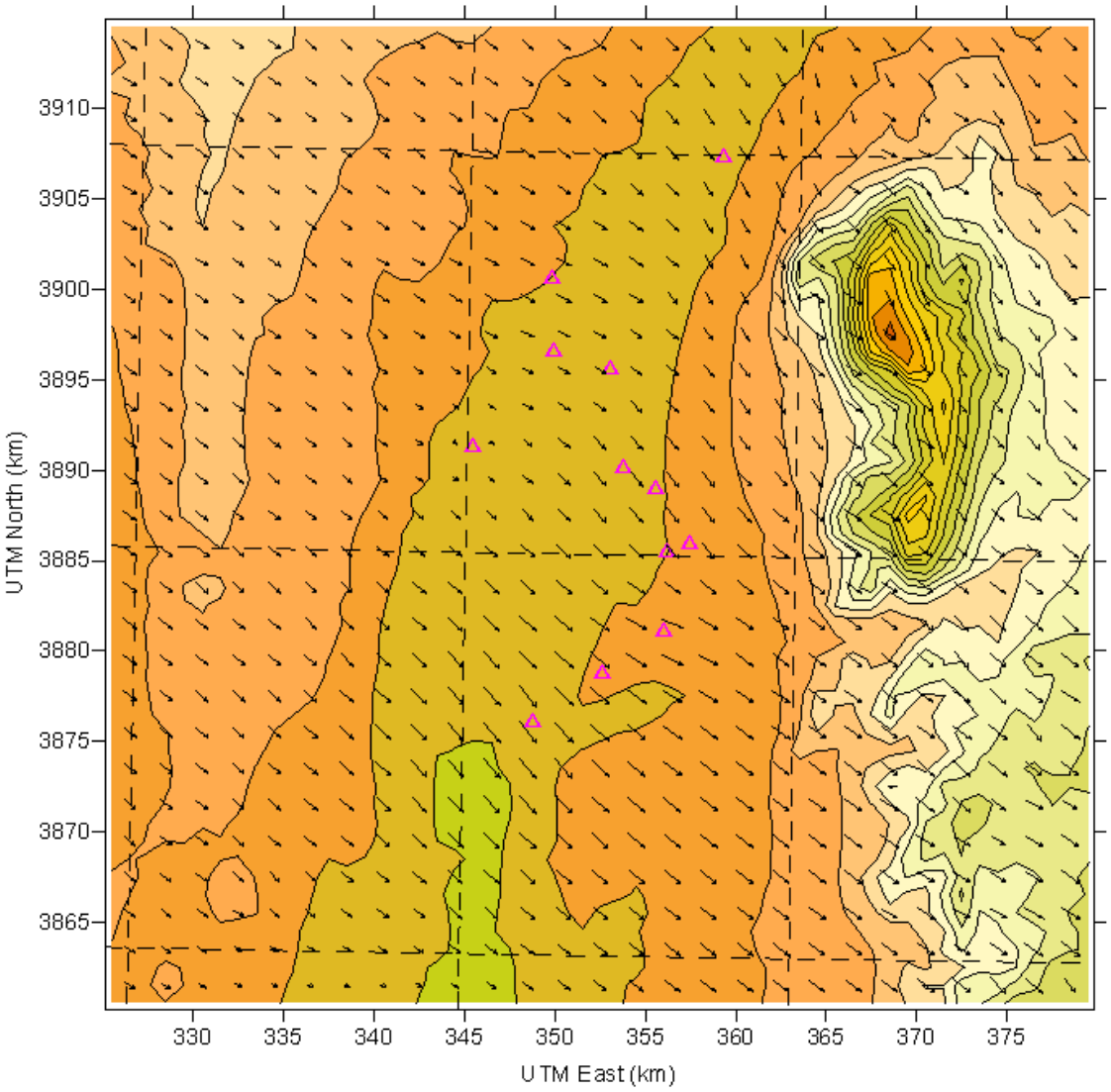

Figure 63. Wind field at 2 pm on February 18, 2008

In the early afternoon strong northwest winds dominate the wind flow patterns.

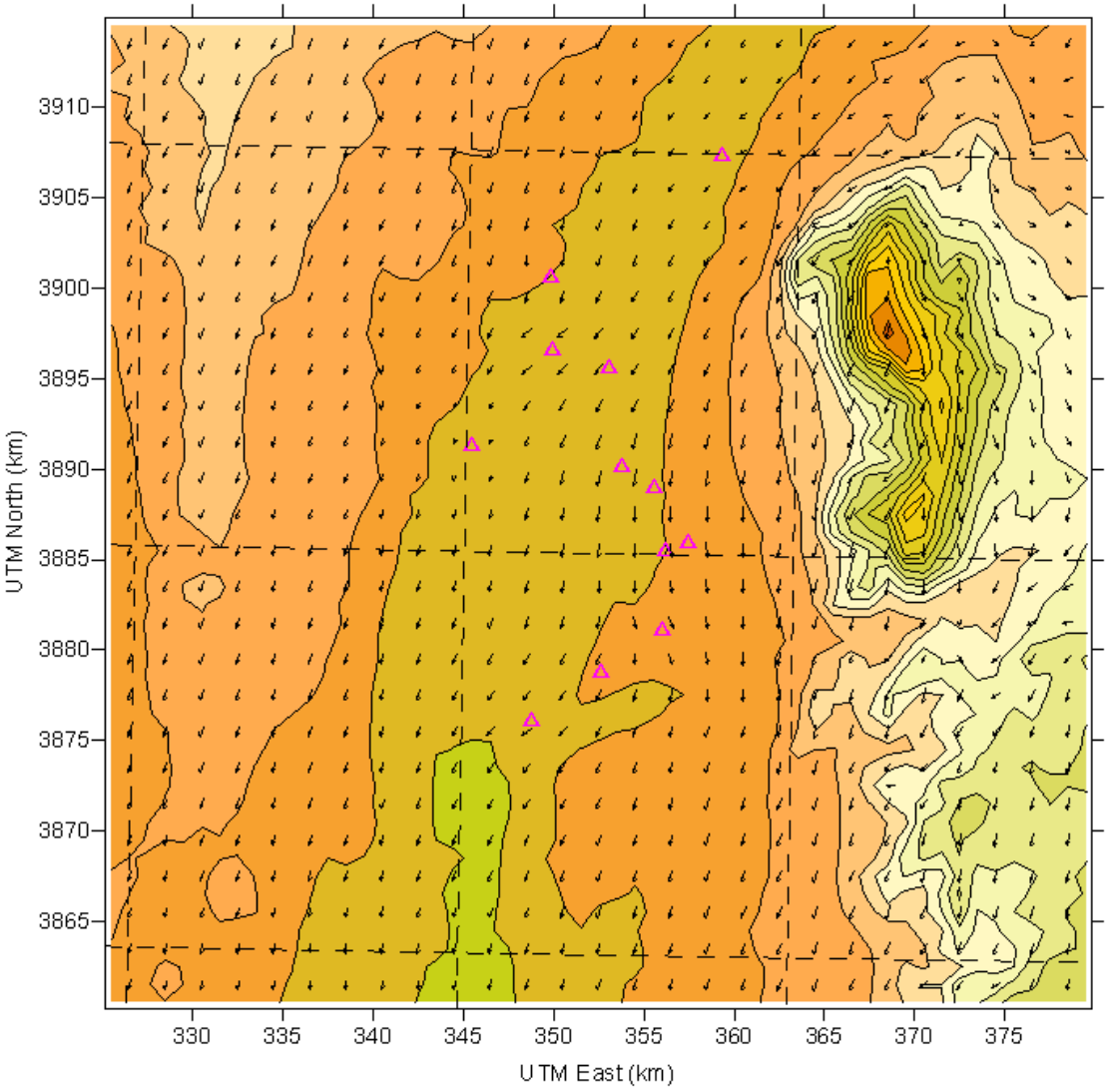

Figure 64. Wind field at 6 pm on February 18, 2008

Early in the evening as the sun sets, there is a transition to calmer winds from the northwest. At that time we see more of a down-slope pattern with winds from northeast.

CALMET Summer Flows

Hourly wind vector maps were generated for the time period between 17 June 2008 and 30 June 2008. Summer IMP wind patterns in the morning hours were similar to the winter except that that east canyon winds played a bigger role in the southern part of the modeling domain. Significant east canyon winds occurred on half of the 14 days in the IMP between the hours of midnight to 6 am. These days included June 17, 18, 20-21, 23, 25 and 29, 2008.

For example the east winds from June 18 brought in low level moisture from the Central Plains states and was driven by a large convective complex on the extreme eastern portion of NM and the Texas Panhandle. Surface weather maps showed a stationary front dividing this boundary with dewpoint temperatures in the upper 50s ºF on the east side and temperatures in the 30s ºF on the other side. North valley locales saw down-slope winds channeled by the valley terrain. The majority of the summer IMP was carried out during upper level ridge conditions with some weak but brief upper level disturbances as the 500 mb level maps in Appendix A show. These weak disturbances coupled with moist air masses brought in afternoon thunderstorms and wind gusts. Strong east canyon winds were observed on June 22 (late evening), June 18 (all evening) and on June 29 (early evening). Early in the morning wind patterns are dominated with a downslope flow that blows from the north toward the south.

The relatively calm period on June 24 is worth looking at since some of the gas phase pollutants were high during that period. During that day winds were very light in the morning and increased to the 5 m/s range in the afternoon. The following figure shows the frequency of winds based on CALMET at the South Valley and Del Norte sites on this day. Because of its location the South Valley site is more influenced by the valley drainage flow that runs along the Rio Grande River. This can be seen in the SW and SSW winds. This site also sees slightly higher winds being downwind of the east canyon wind flow as shown as in yellow.

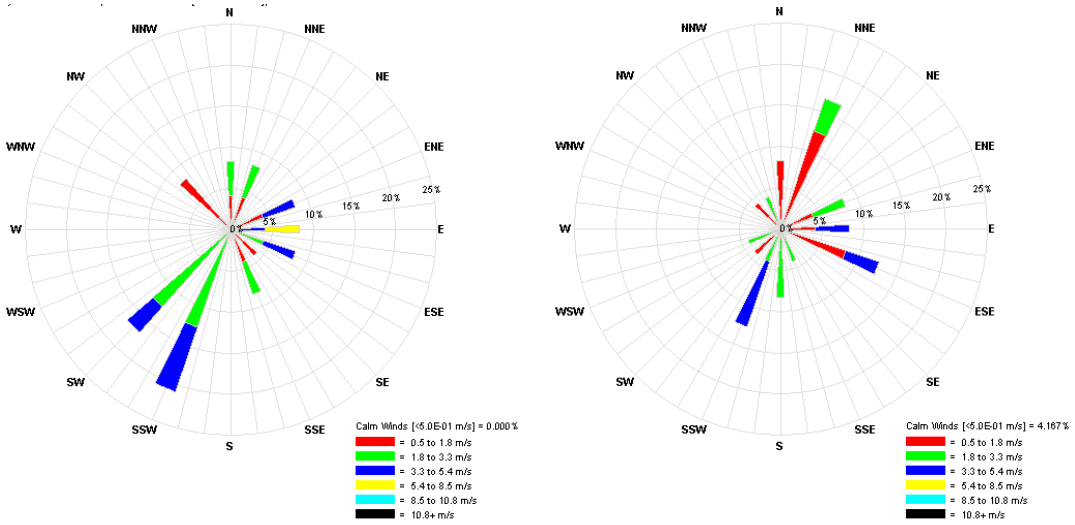

Figure 65. South Valley (left) and Del Norte (right) wind roses during June 24, 2008

The following figures show snapshots of the winds during important hours and transition periods.

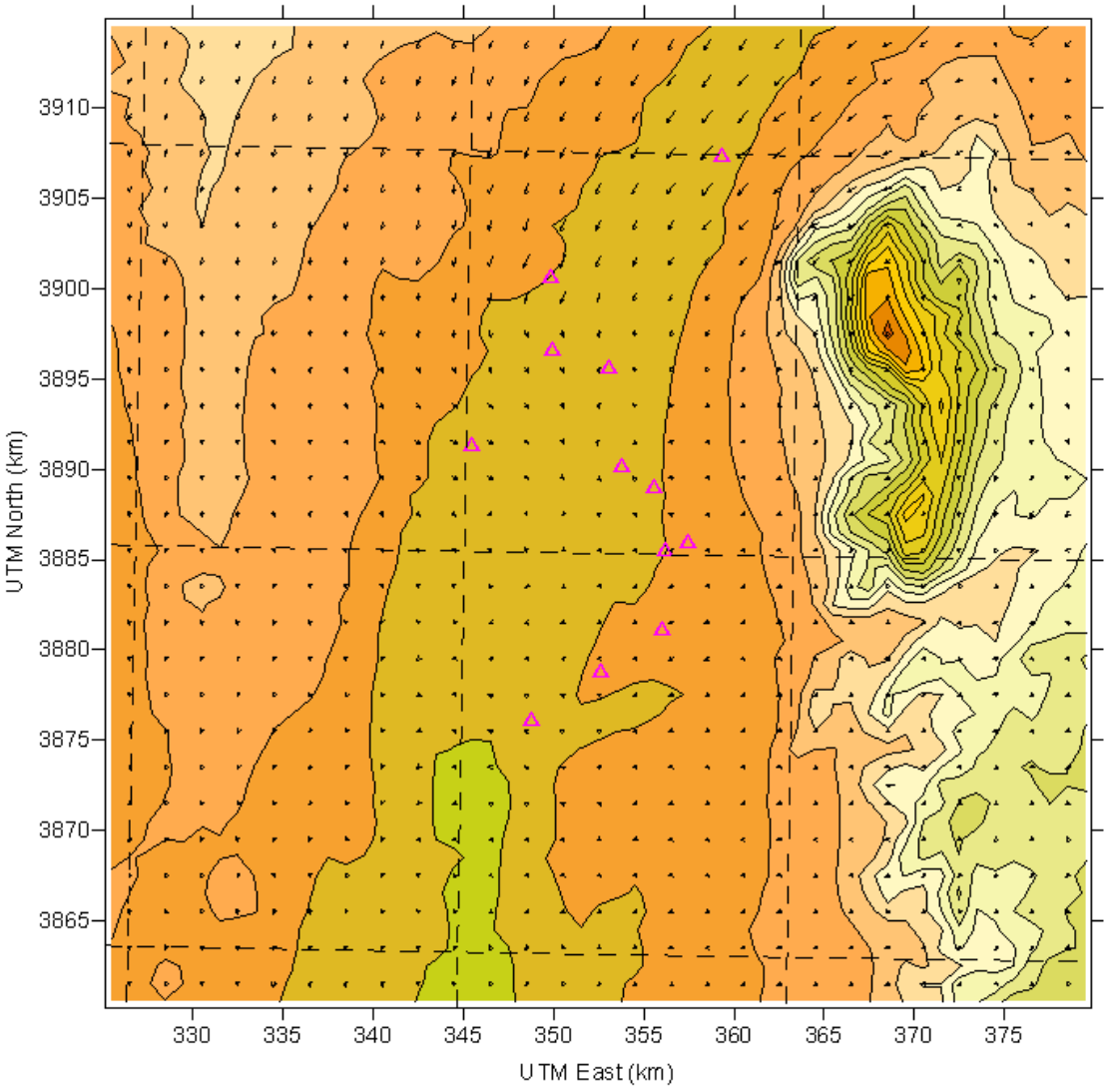

Figure 66. Wind flow at 4 am on June 24, 2008

The down-slope winds started off light but increased in magnitude over the course of the early morning. Initially the down-slope winds were seen mainly in the north valley and stronger toward Bernalillo. By 6 am the down-slope winds were well established.

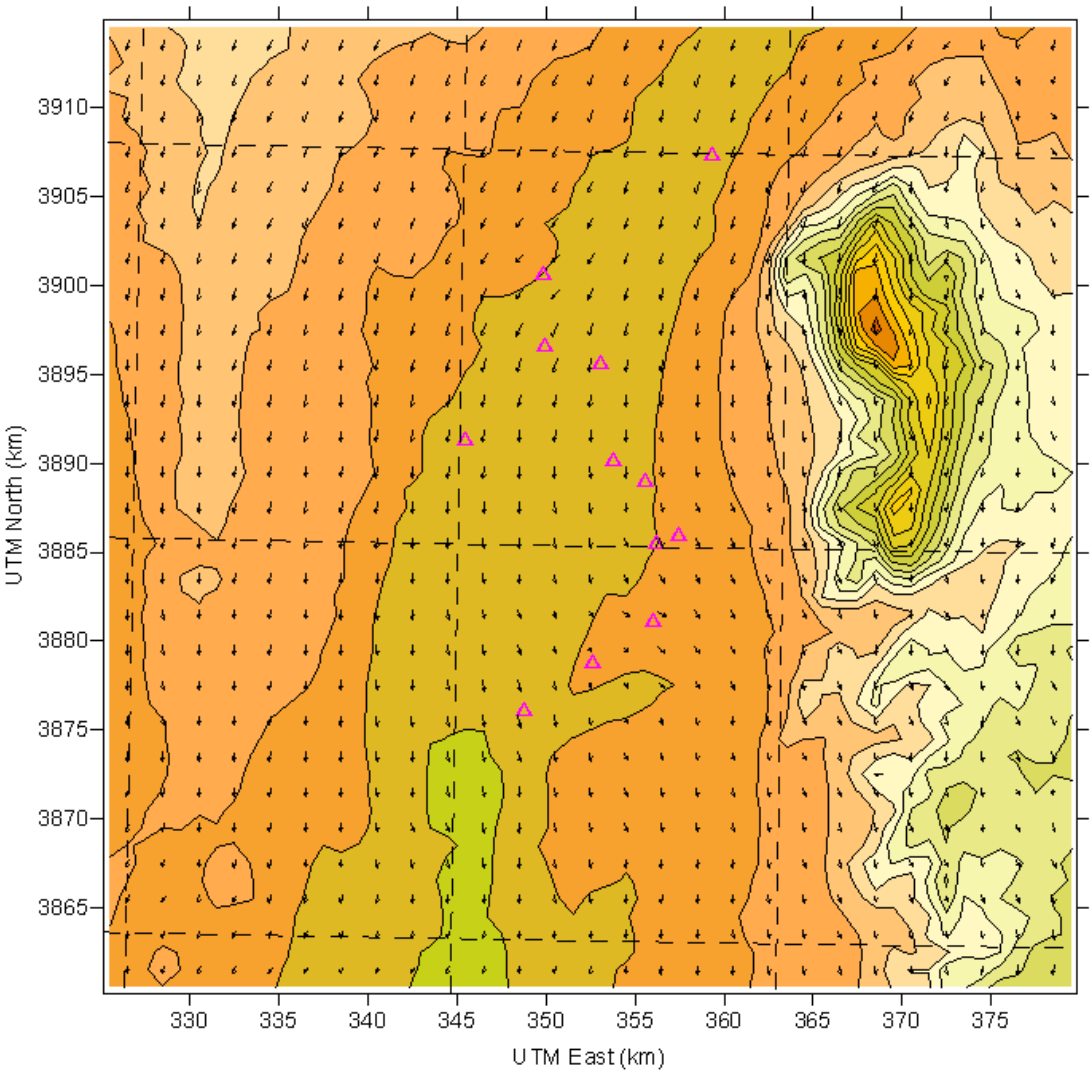

Figure 67. 6 am wind flow patterns on June 24, 2008

This figure shows the 6 am northerly down-slope winds are distributed throughout the valley. A transition starts approximately an hour after sunrise when slopes start to heat up.

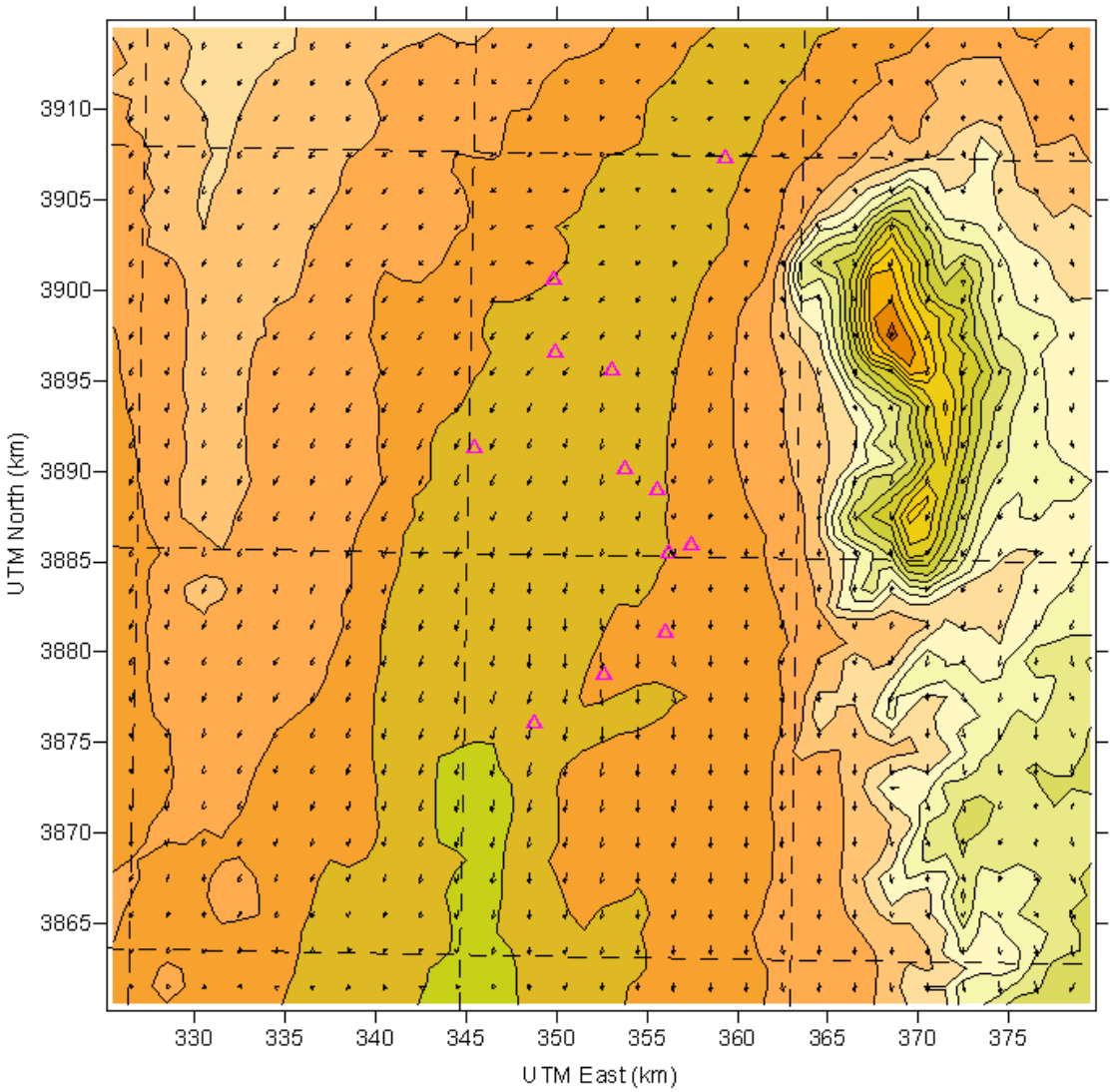

Figure 68. 7 am transition out of down-slope on June 24, 2008

This transition is shown in this figure with the 7 am wind flow.

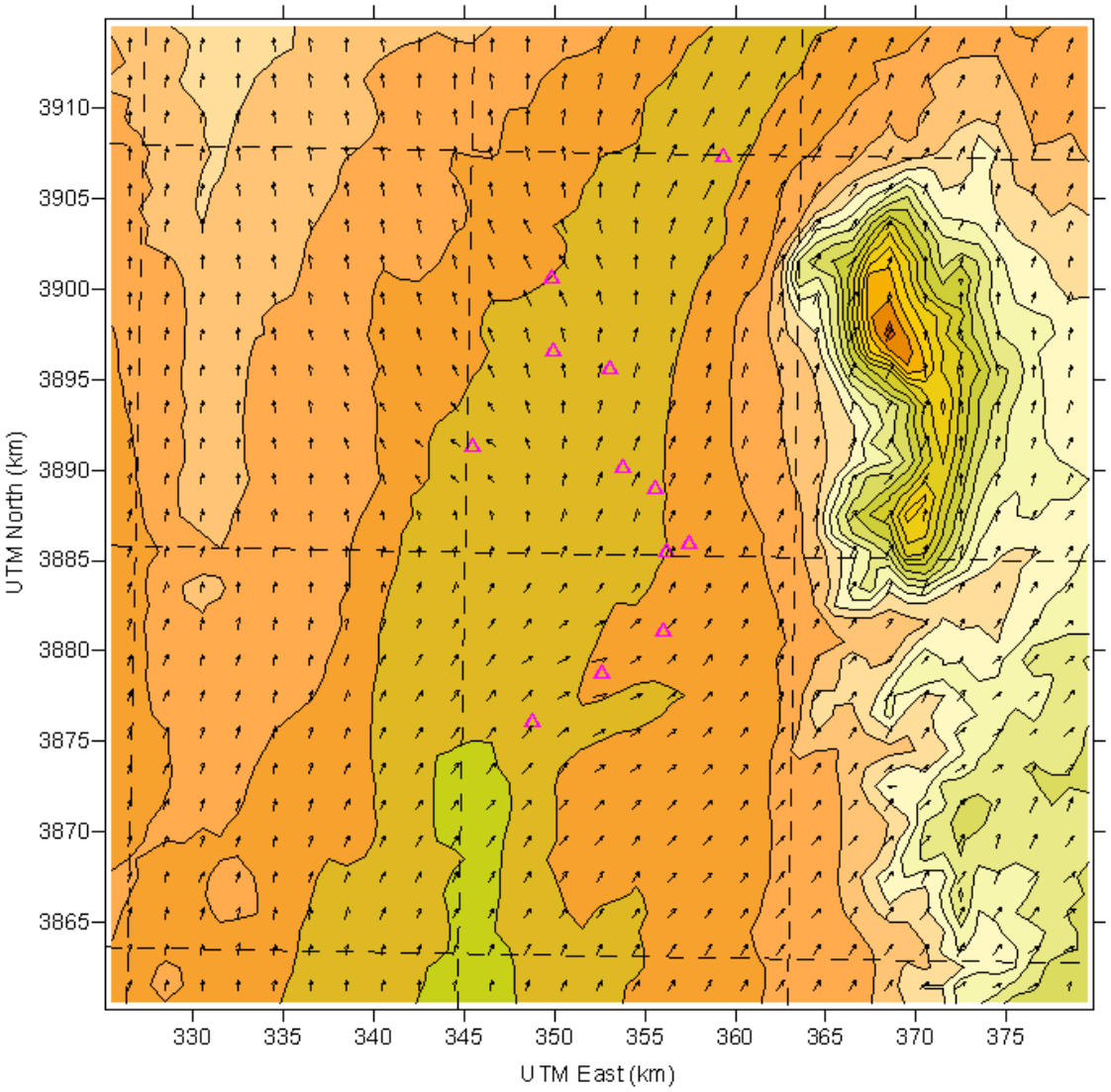

Figure 69. Beginning of upslope flow at 9 am, June 24, 2008

By 9 am the up-slope winds start to dominate the valley flow.

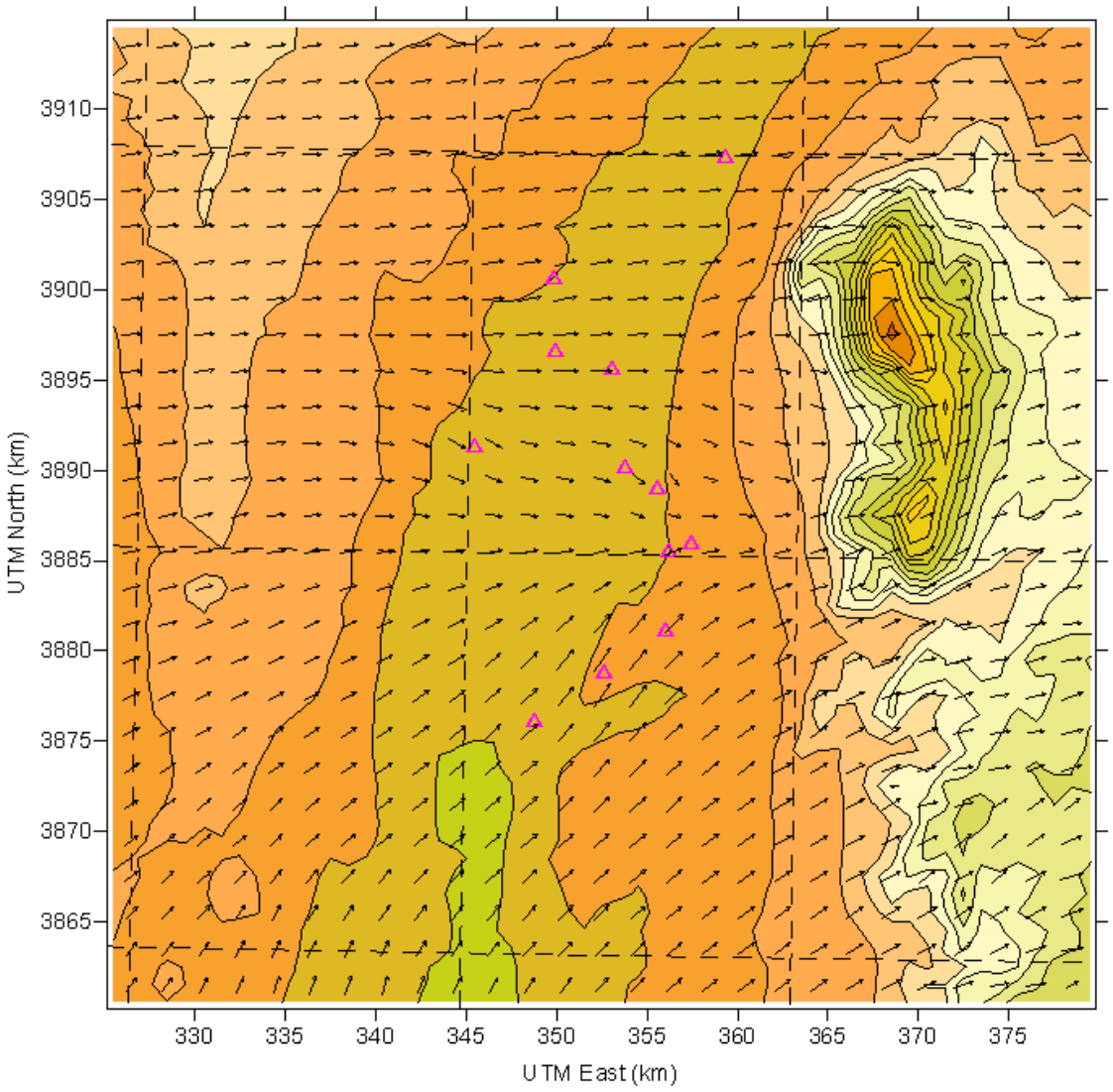

Figure 70. Westerly winds seen at north valley and southwesterly winds in south valley at 1 pm.

By 1 pm westerly winds take over the flow pattern throughout the valley. The southwesterly flow is part of the regional prevailing flow and could be enhanced by up-slope flow from the Sandia and Manzano Mountains.

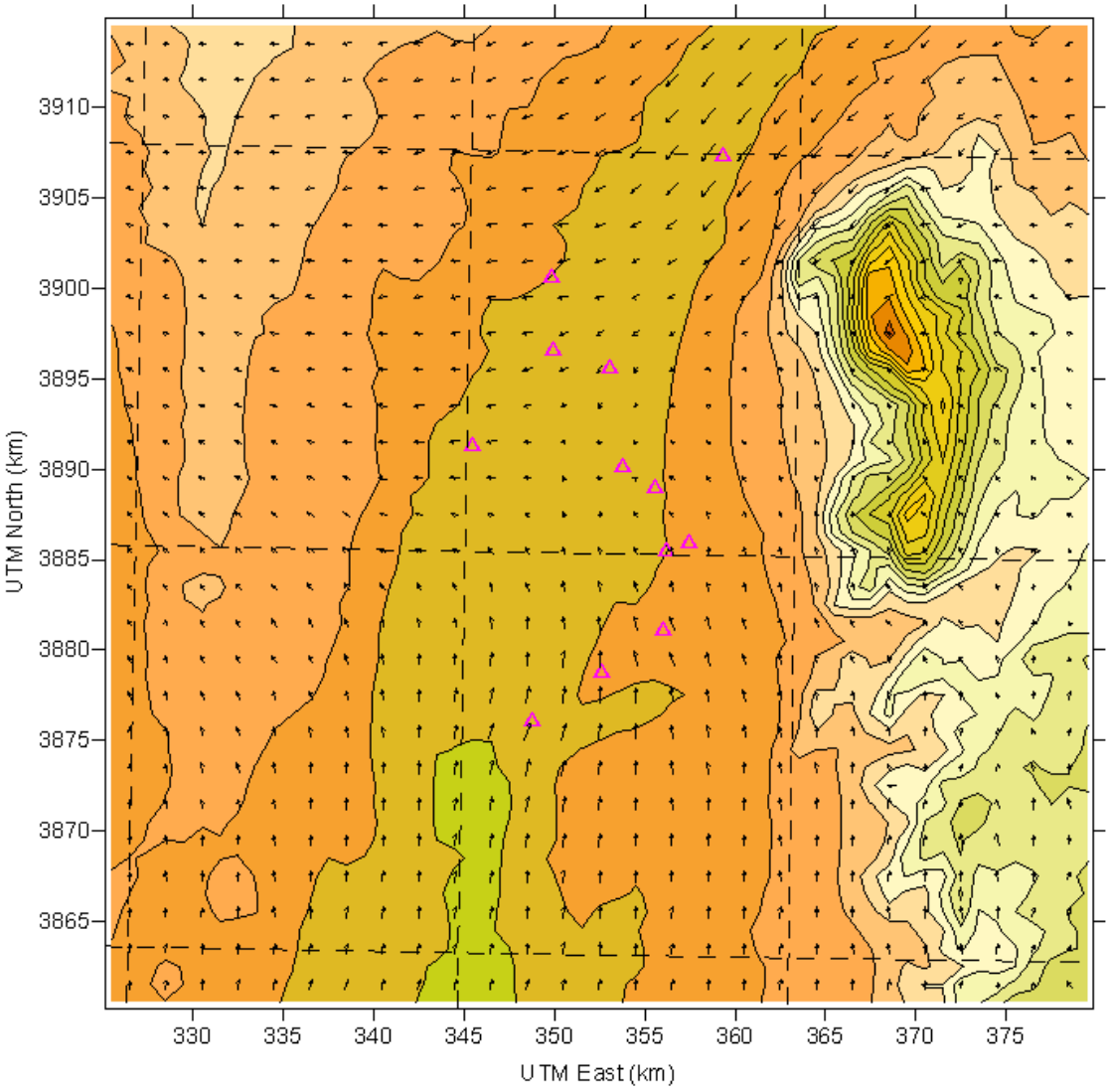

Figure 71. Downslope winds by 5 pm first seen at the northern part of the valley and strongest at Bernalillo. The southern part of the valley still sees a southerly flow.

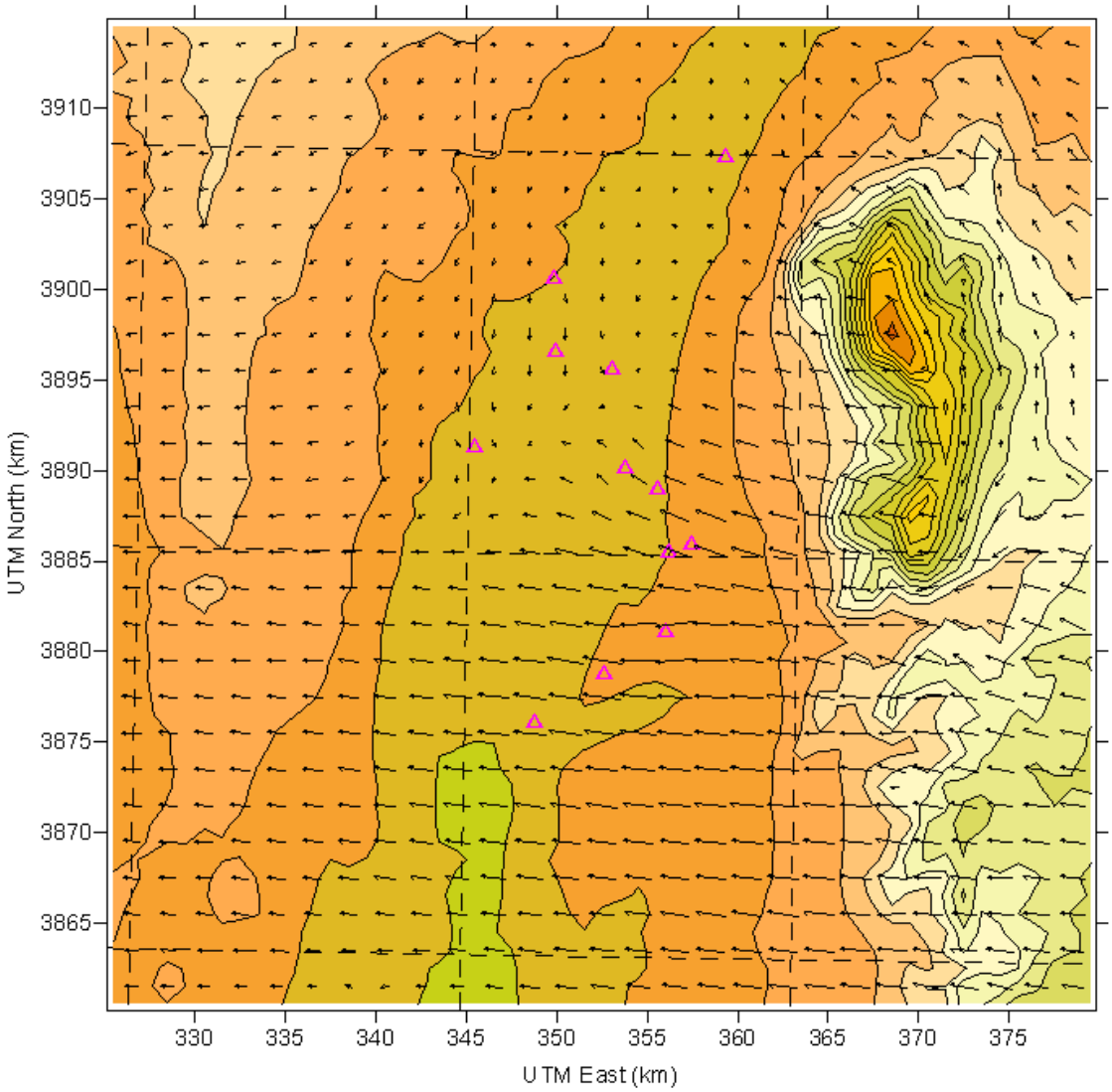

Figure 72. East canyon winds by 9 pm dividing the city into a north and south zone. The northern areas are less influenced by the east canyon winds while the areas directly facing the canyon and those to the south are affected by the easterly winds.

CALMET Surface Wind Roses

Wind roses are consistent with the conceptual model with nighttime down-slope, daytime up-slope and the east canyon winds depending on the location. The following figures show the distribution of winds at the air toxics study sites during the summer IMP.

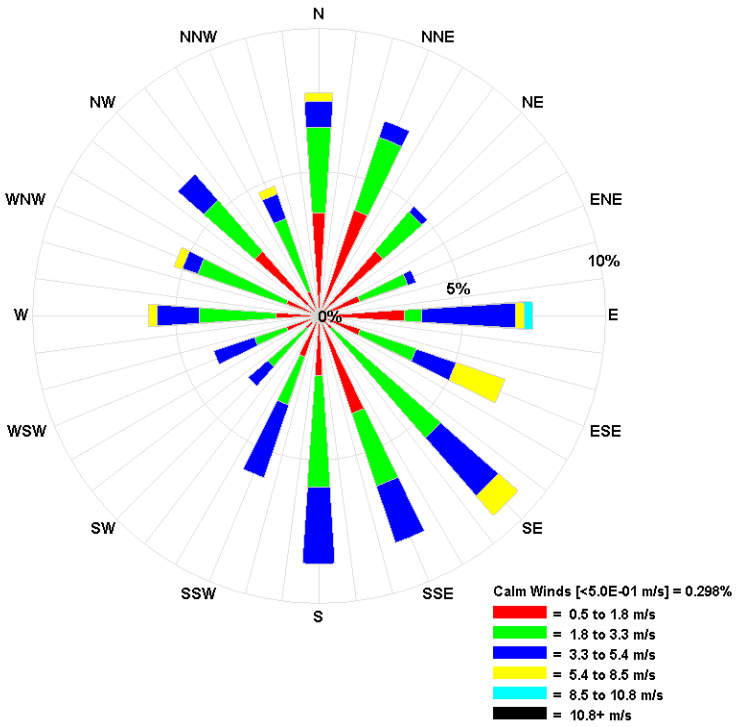

Figure 73. Frequency distribution of wind direction simulated by CALMET at the 2ZM site during the summer IMP

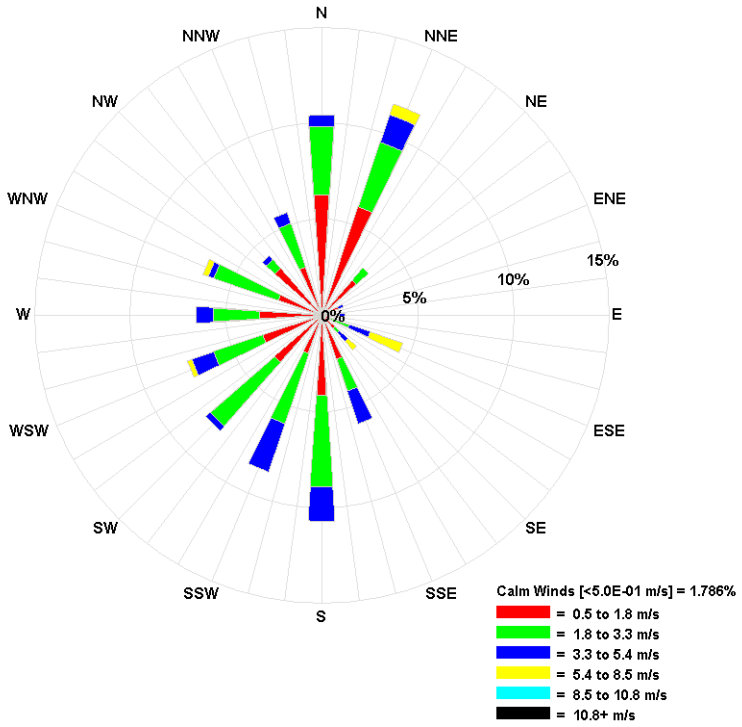

Figure 74. Frequency distribution of wind direction simulated by CALMET at the 2ZH North Valley site during the summer IMP

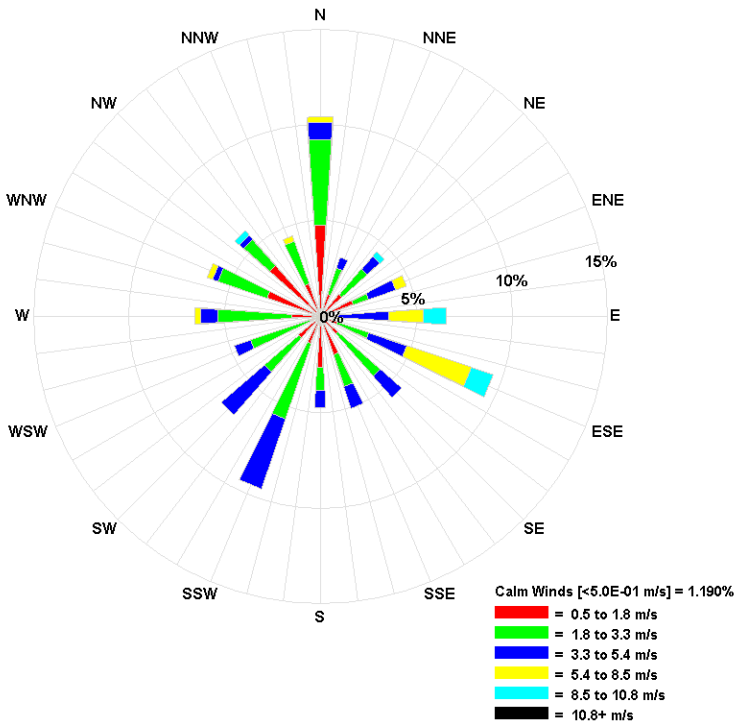

Figure 75. Frequency distribution of wind direction simulated by CALMET at the 2ZV South Valley site during the summer IMP

Estimates of Mixing Height

This section shows the calculated mixing height during the winter IMP at the Del Norte site based on the CALMET model. Also shown are estimates from the HYSPLIT model driven by the 12-km NAM meteorological model. While there are significant differences in the peak mixing heights, both methods produce low values in the morning hours.

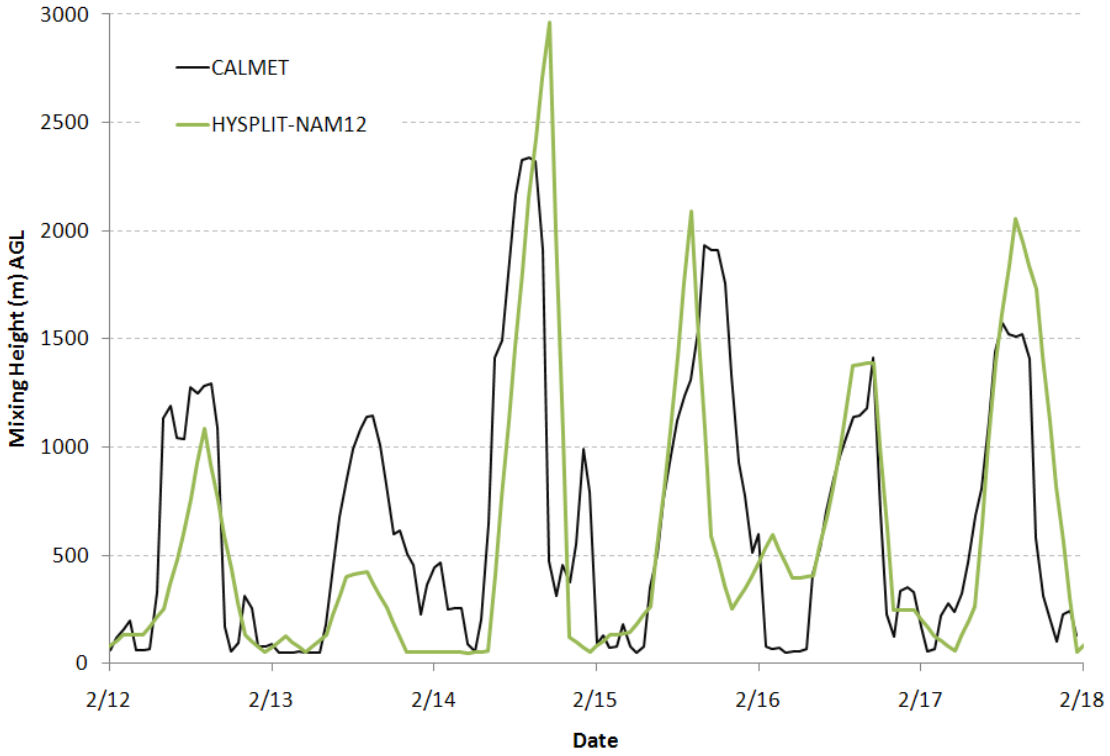

Figure 76. Winter IMP mixing heights at the 2ZM Del Norte site calculated from CALMET and HYSPLIT

The next figure shows the summer IMP mixing heights estimates from CALMET, HYSPLIT and the ceilometer using the gradient method.

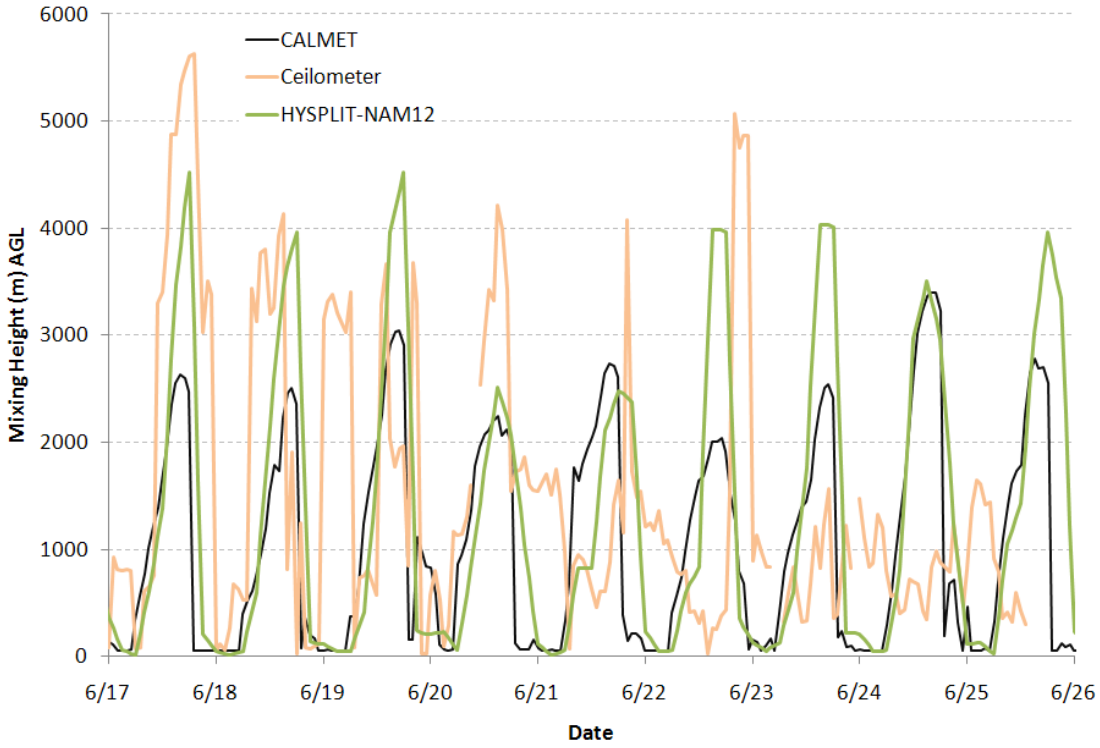

Figure 77. Summer IMP mixing height at the DelNorte site calculated from CALMET

The timing of the peak mixing heights agreed for both models but differed with the maxima. On several occasions the ceilometer picked mixing heights comparable to the models but agreement was poor overall. The ceilometers did not see the low morning mixing heights that the models estimated. This may be related to a sensitivity issue with the lack of aerosol scattering intensity near the surface in the shallow stable layer. More aerosols may be trapped in the higher residual layer several hundred or 1000 meters above the ground rather than the shallow layer less than 100 meters.

Conceptual Model of the Wind Flows

The City of Albuquerque is situated along the Rio Grande river valley that runs approximately south-north with the steep Sandia Mountain range to the east and a gradual upslope and plateau toward the west. Tijeras Canyon provides a drainage pathway between the Sandia and Manzano Mountains to allow airmasses to flow from the east. All of these terrain features induce local complex meteorology that includes channeled flow through the valleys and canyon, down-slope winds during the night, and up-slope flows during the day. Driving forces that change the wind flow patterns on a day to day basis include:

- synoptic forcing from high and low-pressure systems and fronts
- regional forcing such as outflow from thunderstorms, convective complexes
- frictional forces from the local terrain

- seasonal variation in the intensity of solar radiation
- diurnal variation in heating and cooling

Large-scale northwesterly flows occurred during the winter that were modified somewhat from the local terrain. Wind speeds and mixing depth in the winter were very low. A persistent down-slope drainage flow from the north in the morning was measured to be in the range of 50 to 200 meters thick. These stable layers eroded soon after the sun rose. Surface based pseudo-profiles verified these very shallow stable layers and they sometimes reached the height of the tramway base.

During summer, southerly and southwest flows are common in the day. Summer flows are also channeled along the Rio Grande River valley during days with light morning winds. Wind speeds and mixing depths in the summer are generally much higher than the winter. East canyon winds play a critical role in defining the wind circulation patterns in the city during the summer. Most of the strong east canyon winds occurred during the evening hours and lasted several hours. These winds tend to bring much more wind dynamics to the southern part of the valley with more wind gusts than in the north valley.

During summer IMP nights, local circulations develop with down-slope winds along the river channel. Evening wind speeds tend to be low in the absence of east canyon winds.

During the summer IMP days, southwesterly/southerly flows develop from the cooler valley floor air toward the warmer air over the gradual slope from the south. Wind speeds and the mixing depth are higher compared to the nighttime. Most of the afternoons brought in convective clouds and gusty winds and no precipitation.

CONCLUSIONS AND RECOMMENDATIONS

A meteorological measurement and wind field modeling study was undertaken to help understand the samples taken during the air toxics study. The purpose of the modeling study was to determine wind flows in the area. This was accomplished by applying the CALMET diagnostic meteorological model for the winter and summer IMPs.

During the night, local circulations develop with westerly, northwesterly, and northerly drainages from the western plateau toward the river valley. Wind speeds are low. During the day, mainly southwesterly/southerly flows develop from the cooler valley floor air toward the warmer air over the slope. Wind speeds and the mixing depth are higher during day compared to the nighttime. Model results are derived using sparse measurements and in some of the cases cannot fully represent atmospheric flows and thermal stability in this complex terrain. More detailed meteorological monitoring and prognostic meteorological modeling would provide better transport estimates.

REFERENCES

Endlich, R.M., F. Ludwig, E.E. Uthe (1979). An automated method for determining the mixing layer depth from lidar observations, Atmospheric Environment, 13:1051-1056

Fast, J.D.,J..C.Torcolini and R. Redman (2004). Pseudovertical temperature profiles and the urban heat island measured by a temperature datalogger network in Phoenix, Arizona, Journal of Applied Meteorology, 44:

Gertler, A., D. Koracin, J. Lewis, M. Luria, J. Sagebiel, and W. Stockwell, 2002: Development of a predictive model to assess the impact of coastal emissions on urban scale air quality. Proceedings, CRC Air Toxics Modeling Workshop, Houston, Texas, 26-27 February 2002.

Melfi, S.H., J.D. Spinhirne, S.-H. Chou, S.P. Palm (1985). Lidar observations of vertically orgainized convection in the planetary boundary layer ov erhte ocean, Journal of Climate and Applied Meteorology, 24:806-821

Menut, L., C. Flamant, J. Pelon, P.H. Flamant (1999). Urban boundary layer height determination from lidar measurements over the Paris area, Applid Optics, 38:945-954

Moschandreas, D.J.; Watson, J.G.; D'Abreton, P.; Scire, J.S.; Zhu, T.; Klein, W.; and Saksena, S. (2002). Chapter three: Methodology of exposure modeling. *Chemosphere*, **49**(9):923-946.

NASA 2008. CALIPSO expedited browse images, using release version 2.01. http://www-calipso.larc.nasa.gov/products/lidar/browse_images/expedited/

Steyn, D.G., M. Baldi, R.M. Hoff., (1999). The detection of mixed layer depth and entrainment zone thickness from lidar backscatter profiles. Journal of Atmospheric and Oceanic Techology, 16: 953-959

Scire, J.S., F.R. Robe, M.E. Fernau, R.J. Yamartino, 2000a: A User's Guide for the CALMET Meteorological Model. Available from Earth Tech Inc., 196 Baker Ave., Concord, MA 01742.

Scire, J.S., D.G. Strimaitis, R.J. Yamartino, 2000b: A User's Guide for the CALPUFF Dispersion Model. Available from Earth Tech Inc., 196 Baker Ave., Concord, MA 01742.

Strimaitis, D.G., J.S. Scire, and J.C. Chang, 1998: Evaluation of the CALPUFF dispersion model with two power plant data sets. Proceedings on 10th Joint Conference on the Applications of the Air Pollution Meteorology, 11-16 January 1998, Phoenix, AZ.

U.S. Government, 2000: Requirements for Preparation, Adoption, and Submittal of State Implementation Plan (Guideline on Air Quality Models), Part II. EPA, Federal Register, April 21, 2000.

Whiteman, C.D., J.M. Hubbe and W.J. Shaw (2000). Evaluation of an inexpensive temperature datalogger for meteorological applications, Journal of Atmospheric and Oceanic Technology 17:77-81

Whiteman, C.D., S. Eisenbach, B. Pospichal and R. Steinacker (2004). Comparison of vertical soundings and sidewall air temperature measurements in a small Alpine basin, Journal of Applied Meteorology 43:1635-1647

APPENDIX A-1: SYNOPTIC MAPS

– Synoptic scale maps during winter and summer IMPs.

Winter IMP 500 mb height maps

February 12, 2008

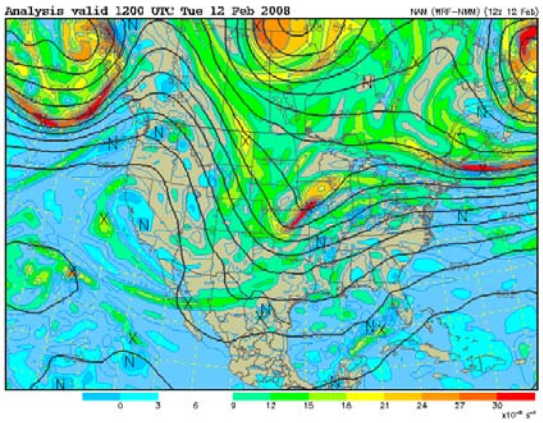

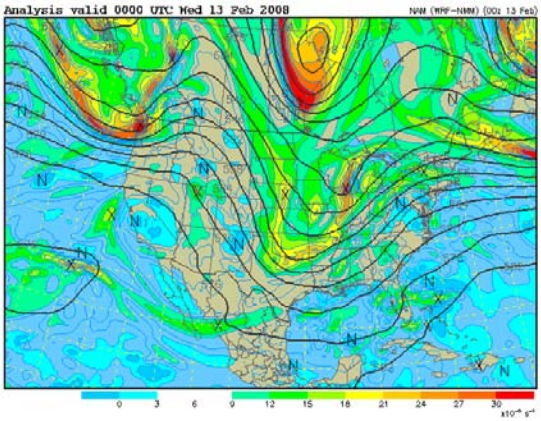

February 13, 2008

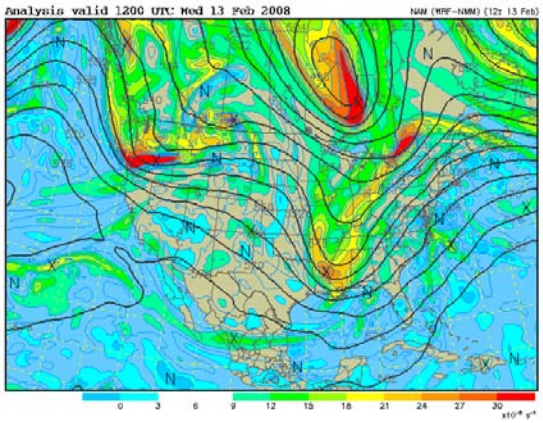

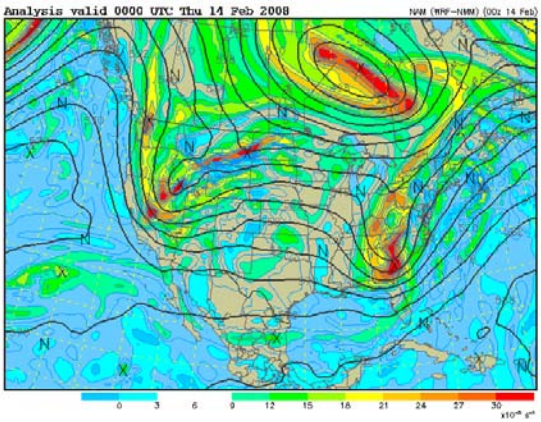

February 14, 2008

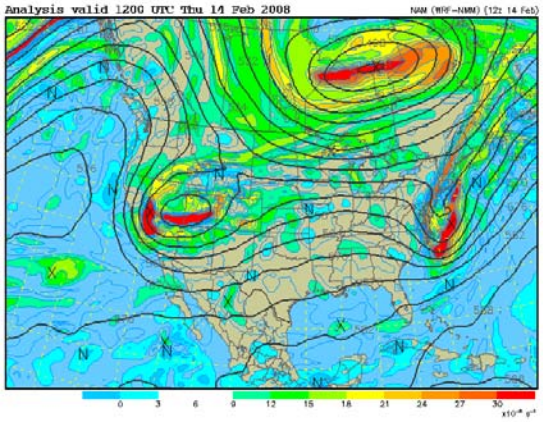

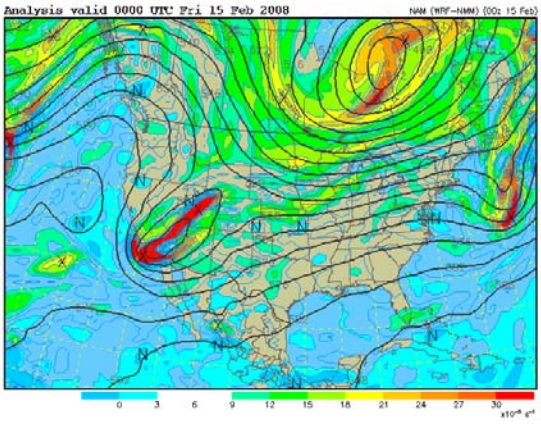

February 15, 2008

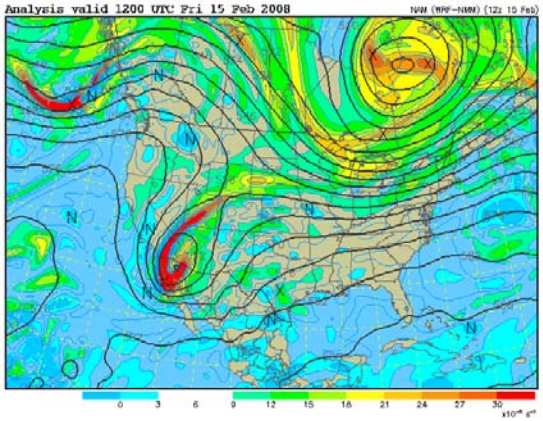

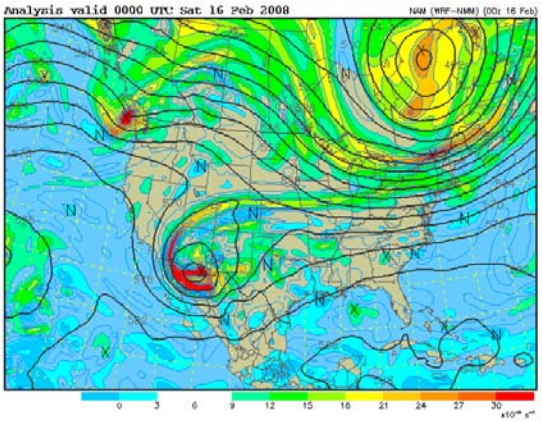

February 16, 2008

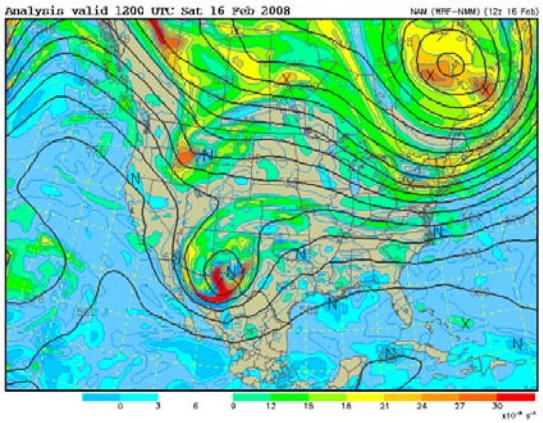

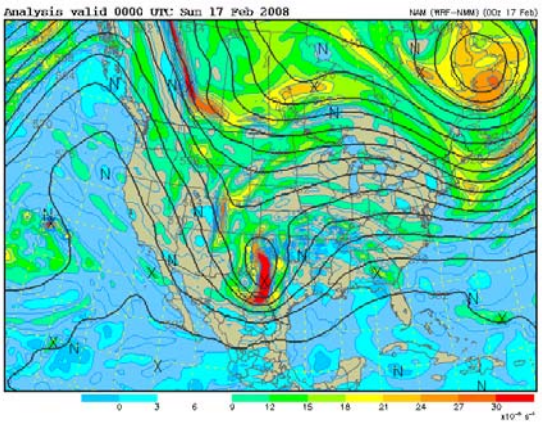

February 17, 2008

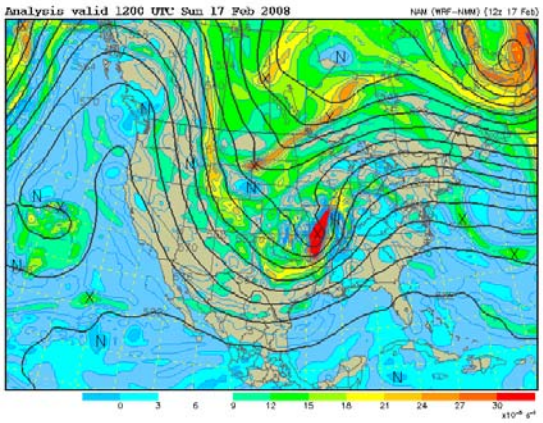

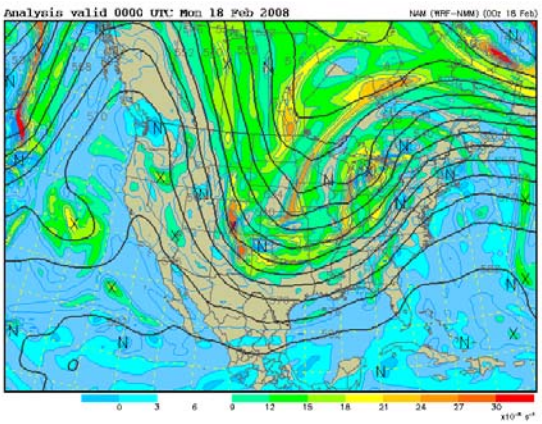

February 18, 2008

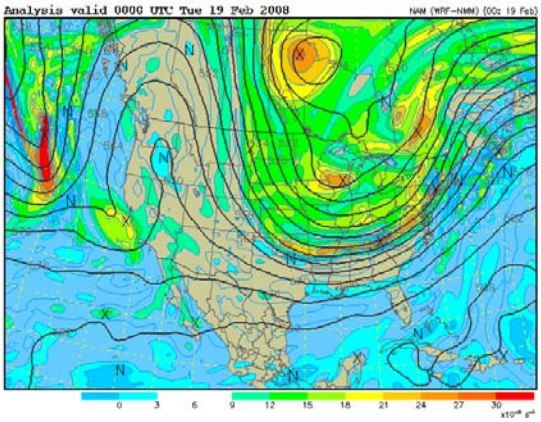

12 UTC map not available

Summer IMP 500 mb height maps

June 22

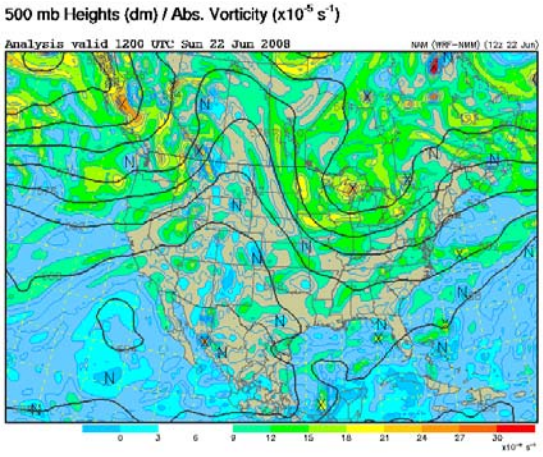

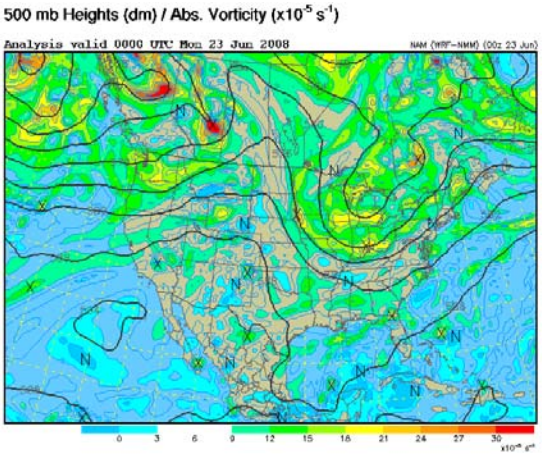

June 23

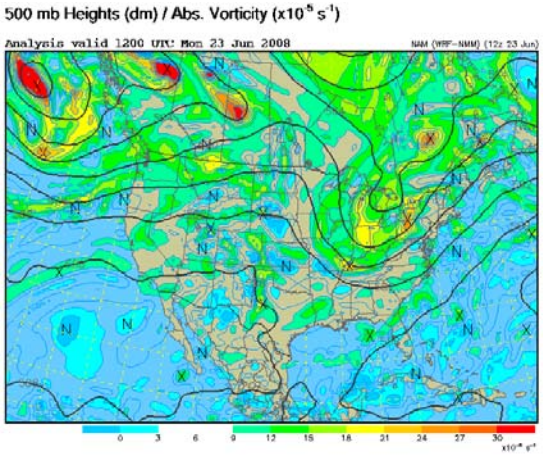

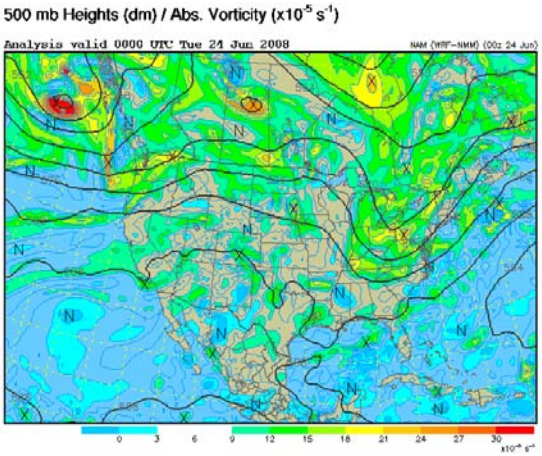

June 24

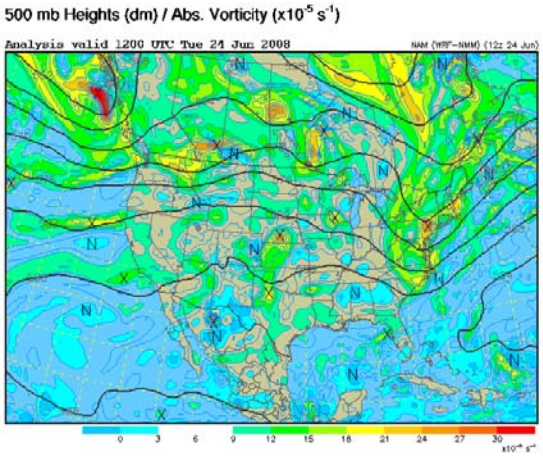

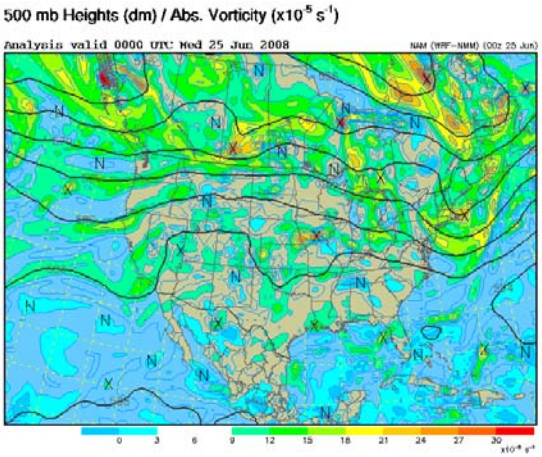

June 25

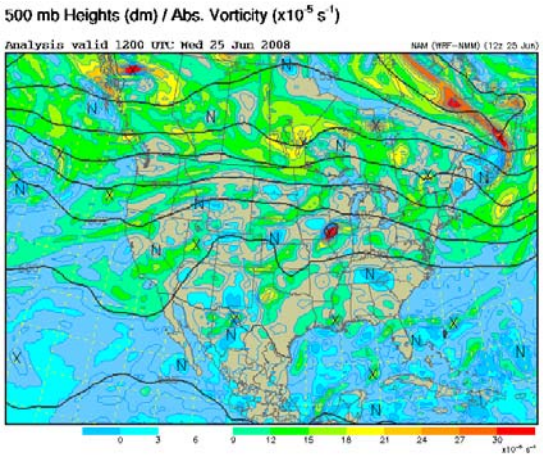

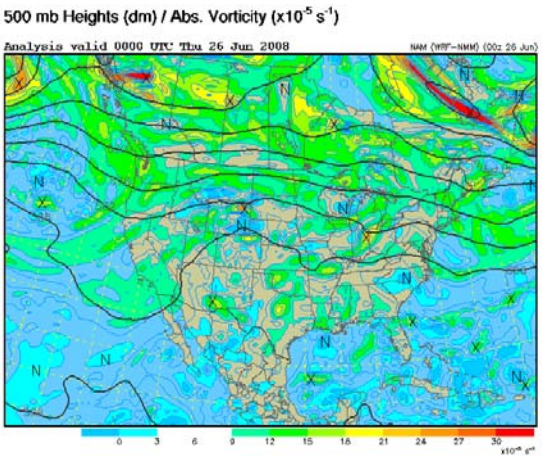

June 26

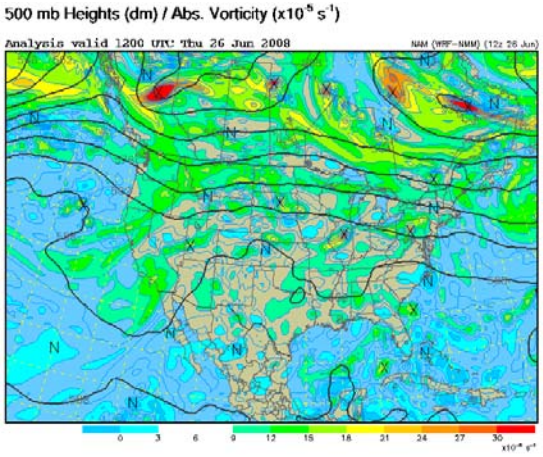

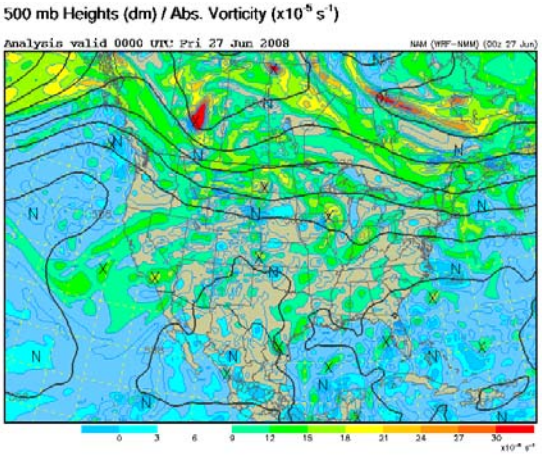

June 27

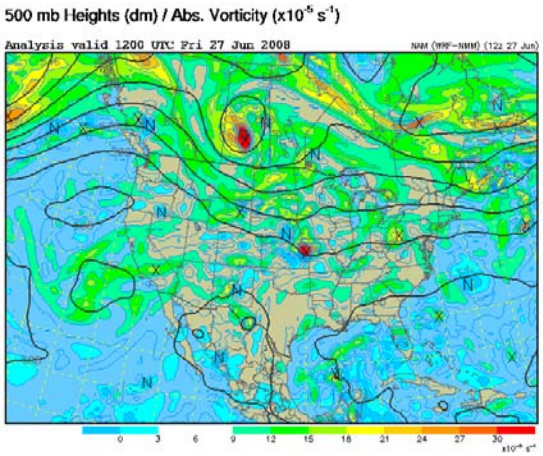

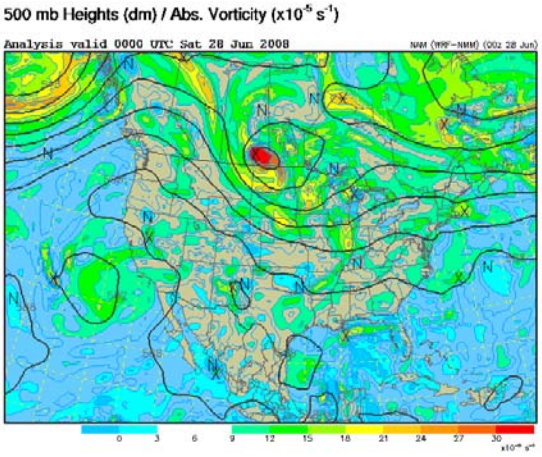

June 28

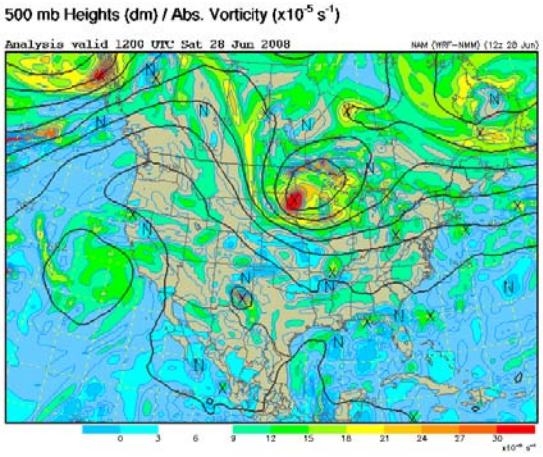

Afternoon map not available

June 29

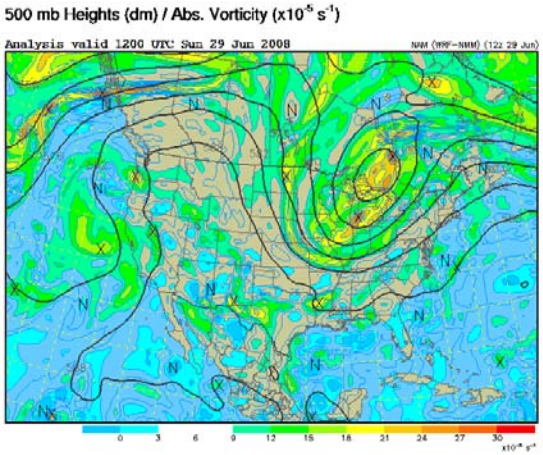

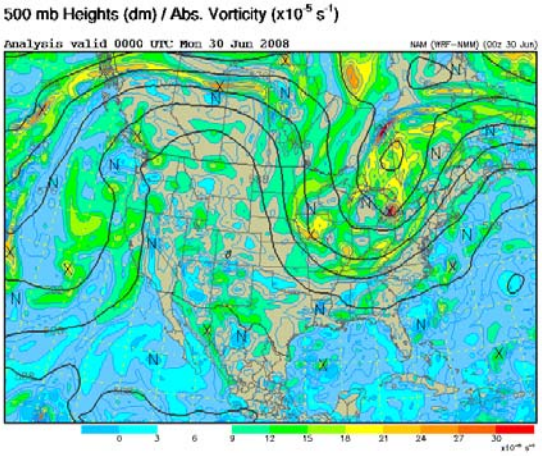

APPENDIX A-2: TETHERED BALLOON SOUNDING PLOTS

Winter IMP

February 13, 2008, from 09:33 to 12:17 local time

V-Component of wind (indication of up/down valley winds)

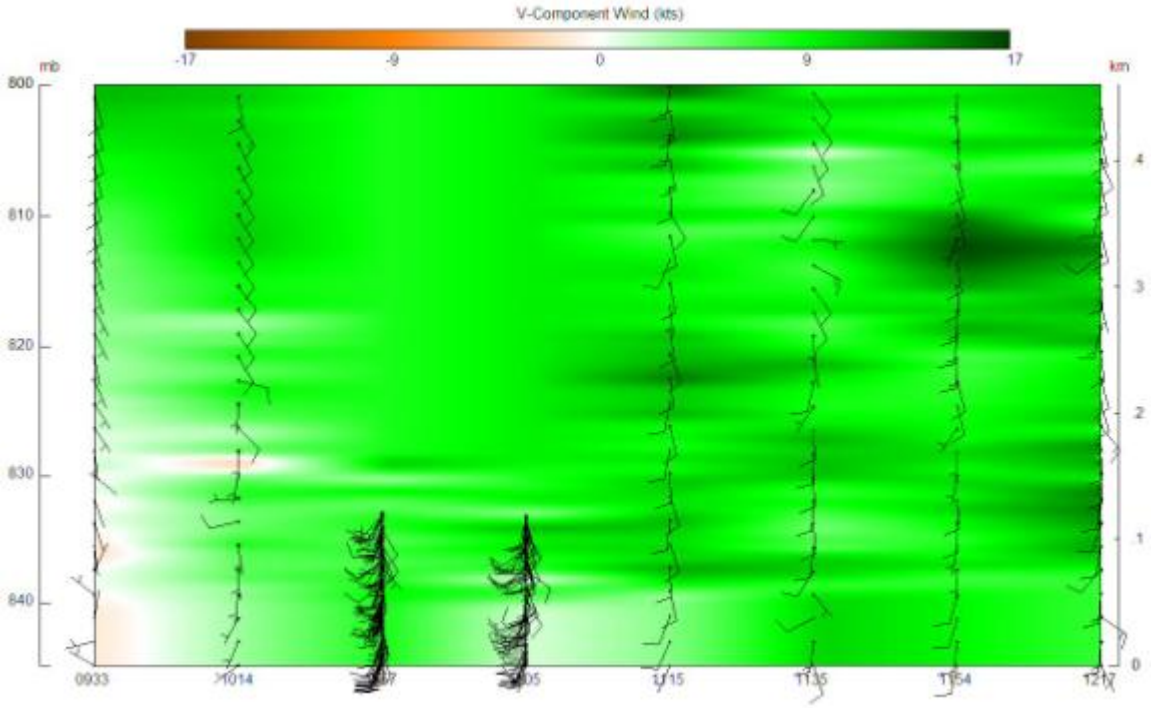

Mixing Ratio (g/kg)

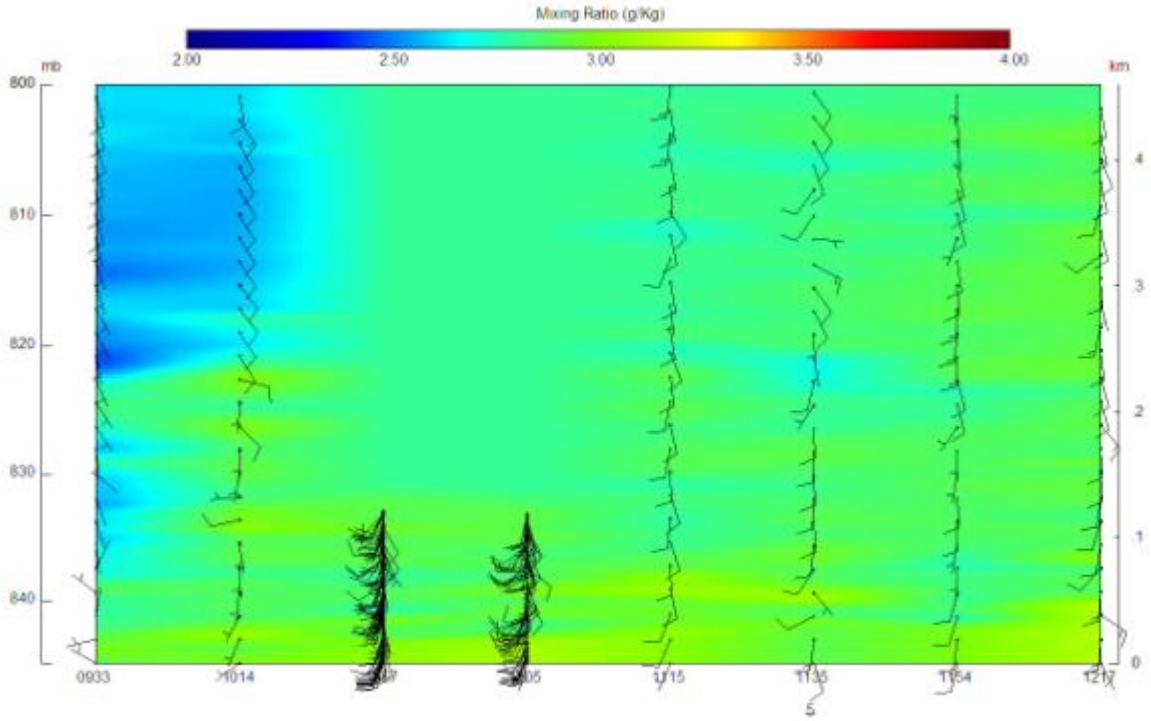

Relative Humidity (%)

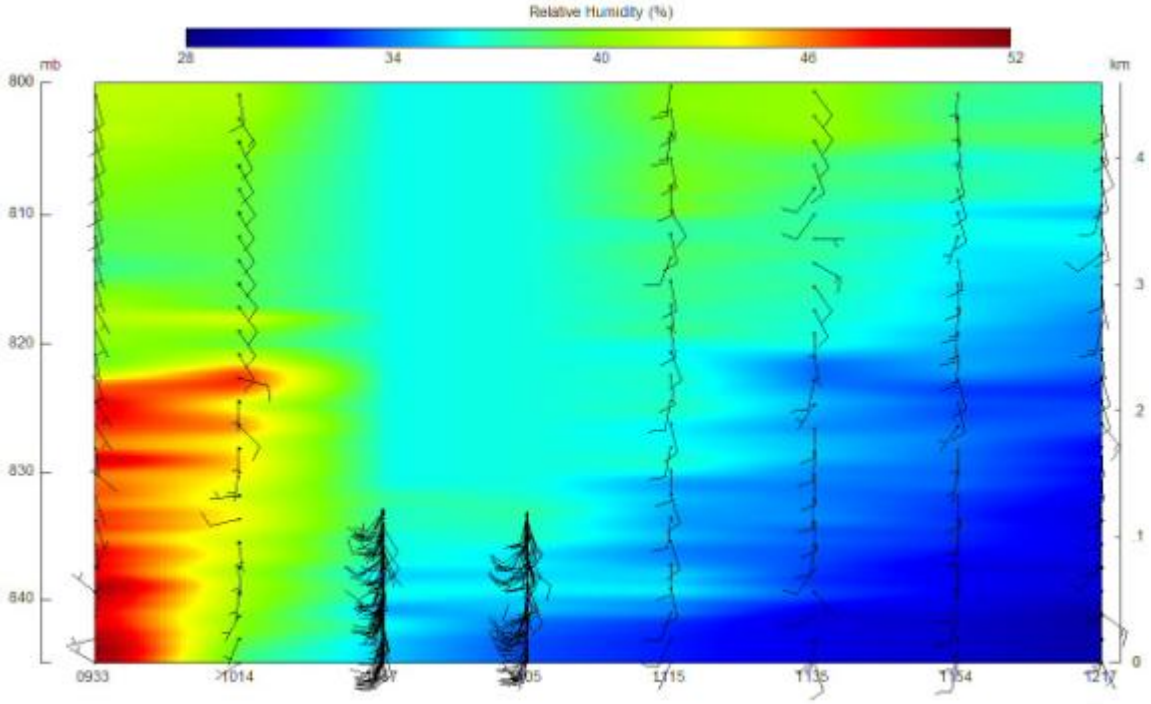

Temperature (°C)

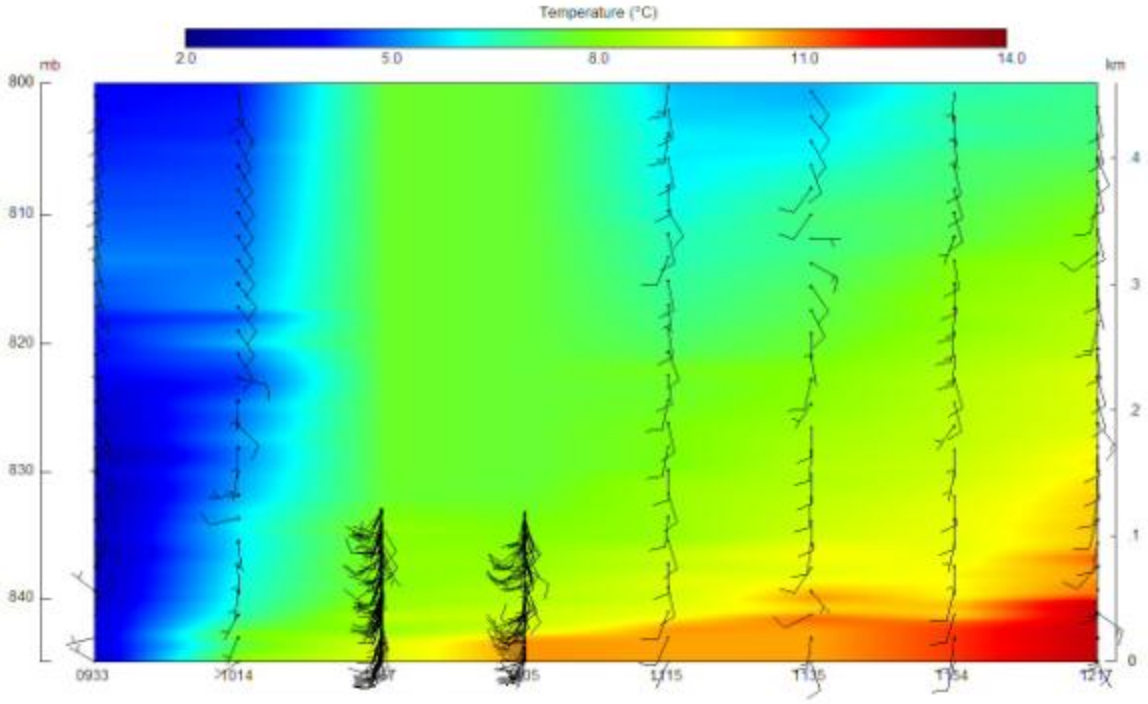

Potential Temperature (K)

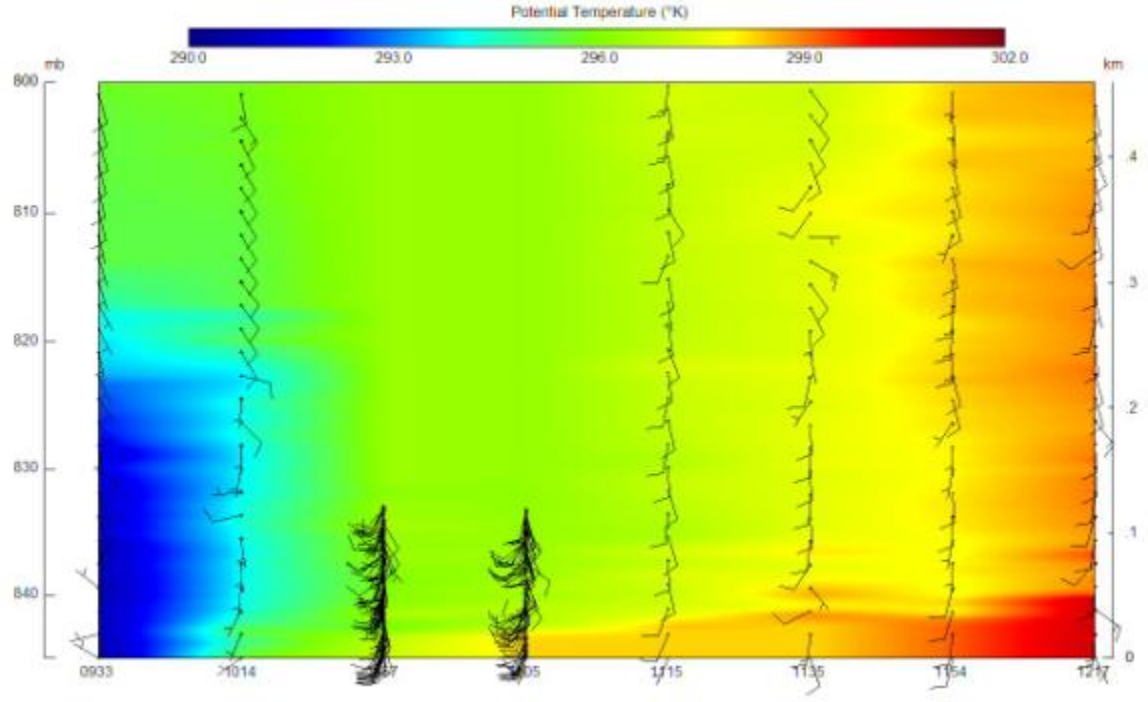

Equivalent Potential Temperature (K)

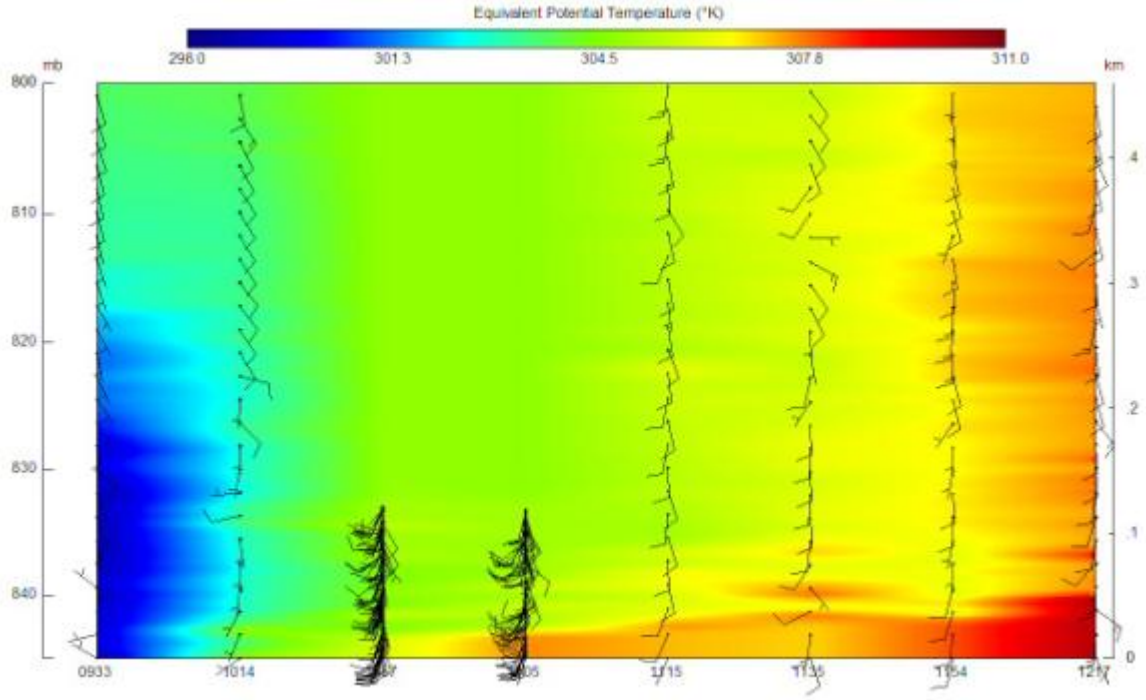

Wind Speed (knots)

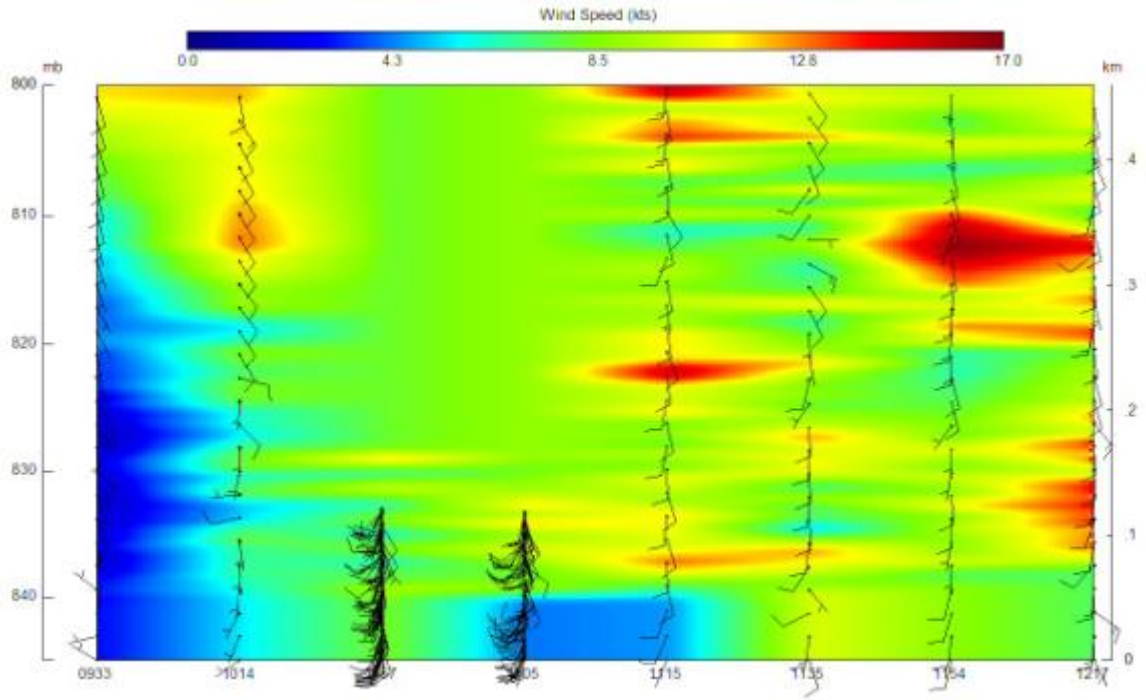

February 17, 2008

V-component of wind (indicator of up/down valley flow) in knots

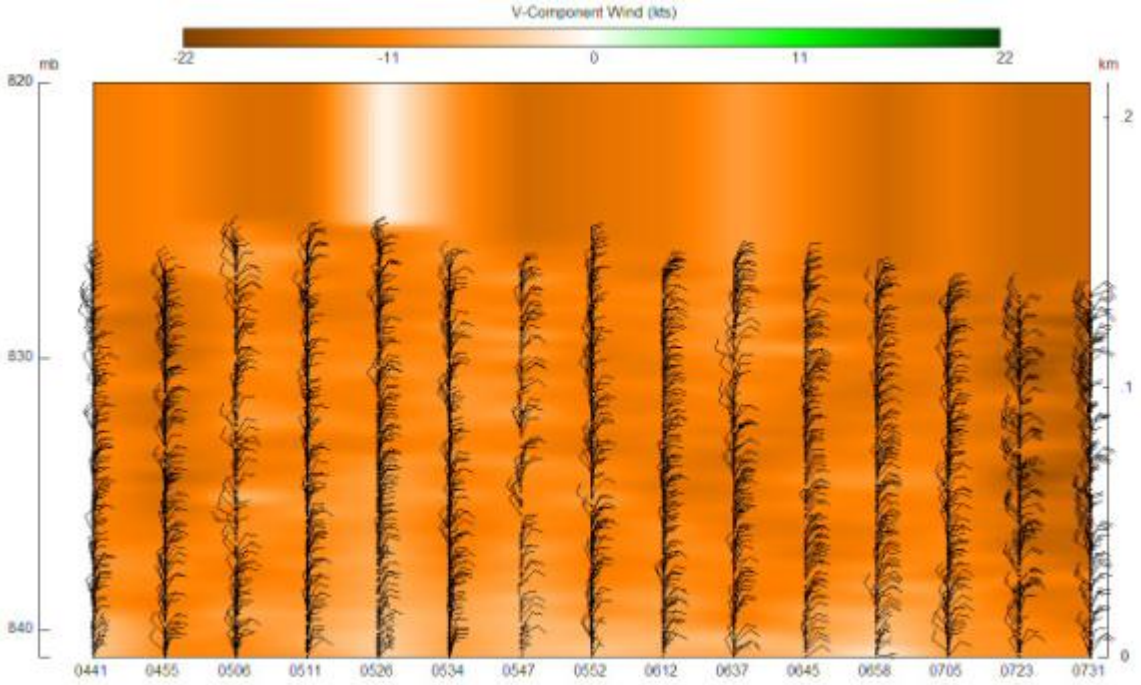

Mixing ratio (g/kg)

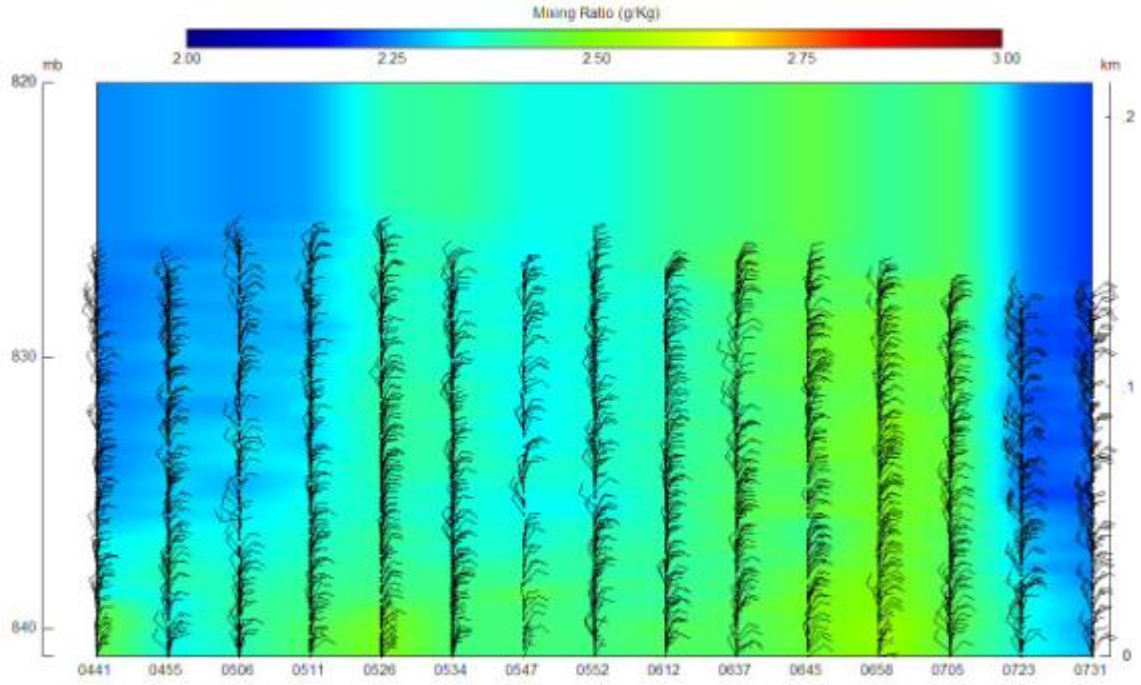

Relative Humidity (%)

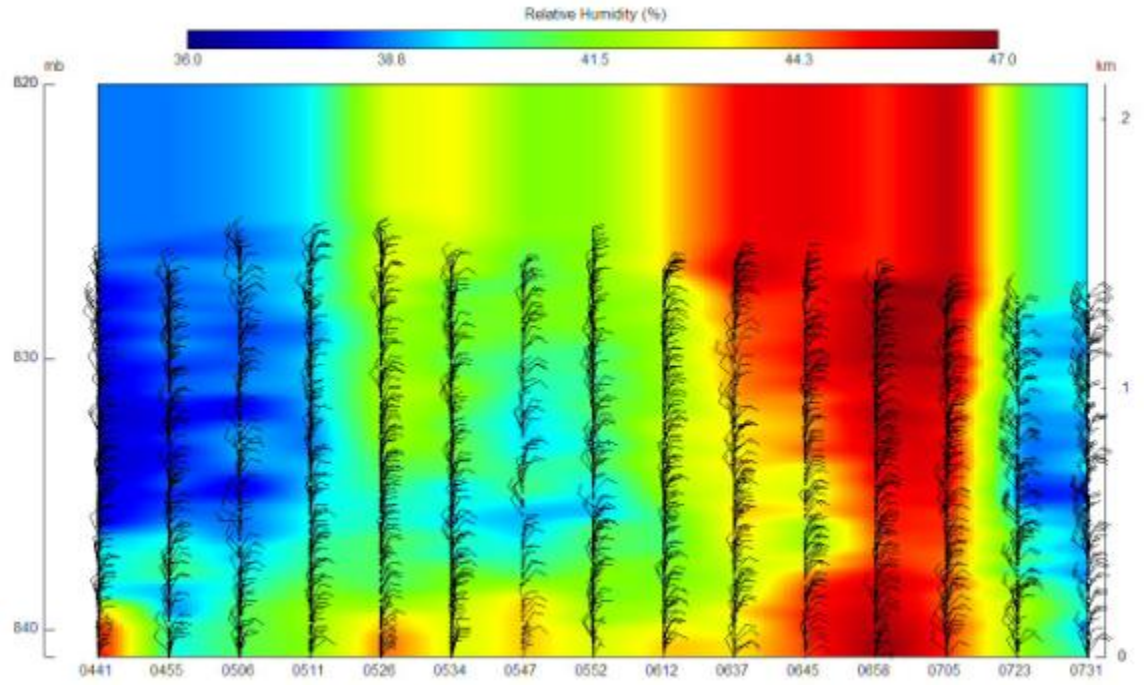

Temperature (°C)

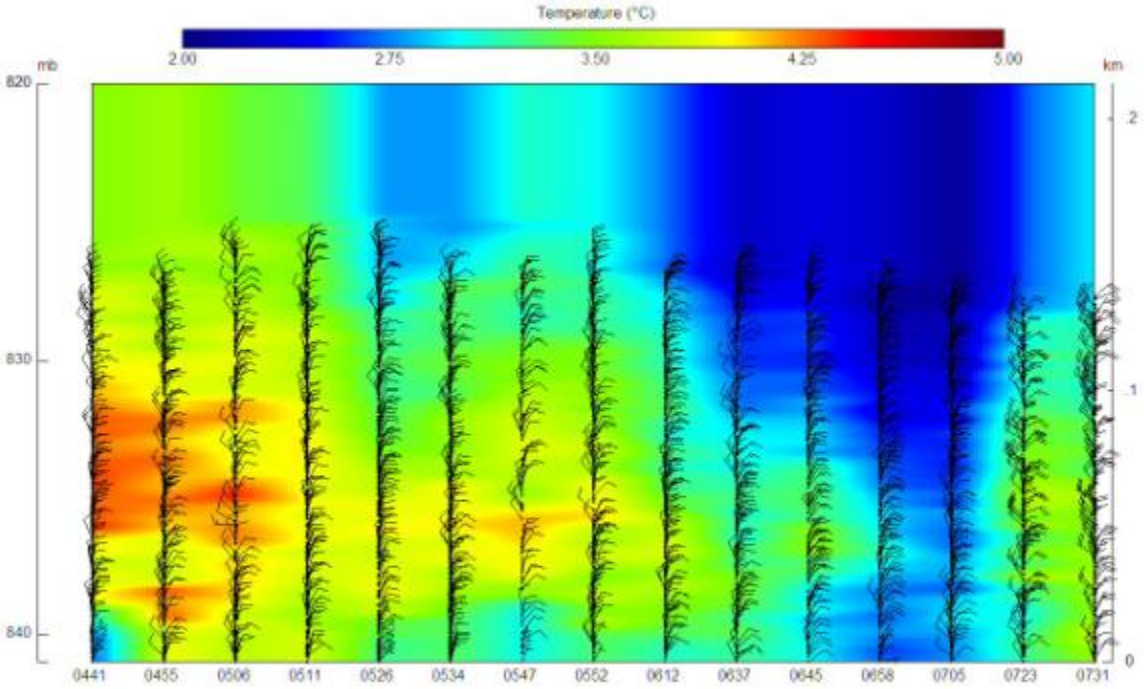

Potential Temperature (K)

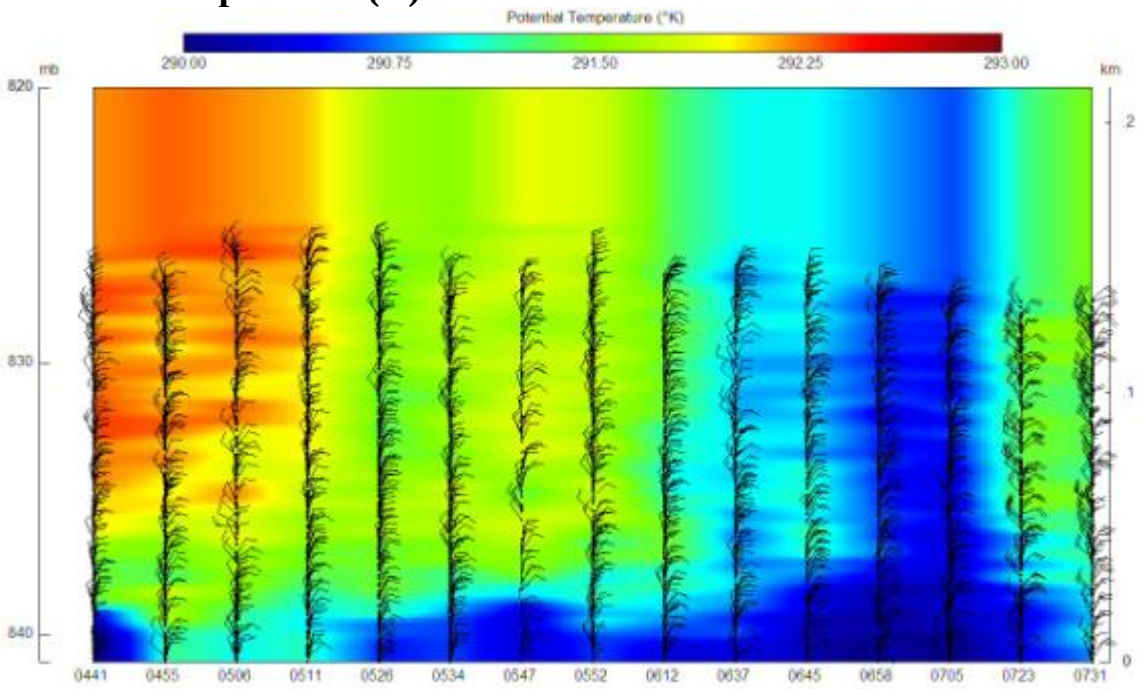

Equivalent Potential Temperature (K)

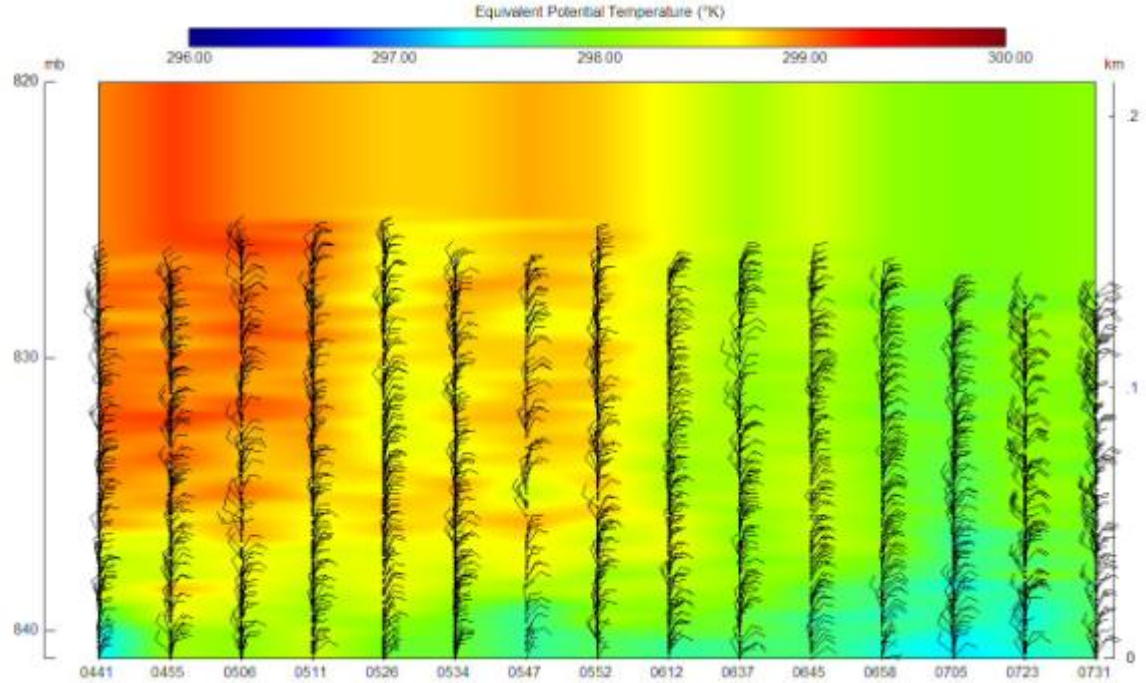

Wind Speed (knots)

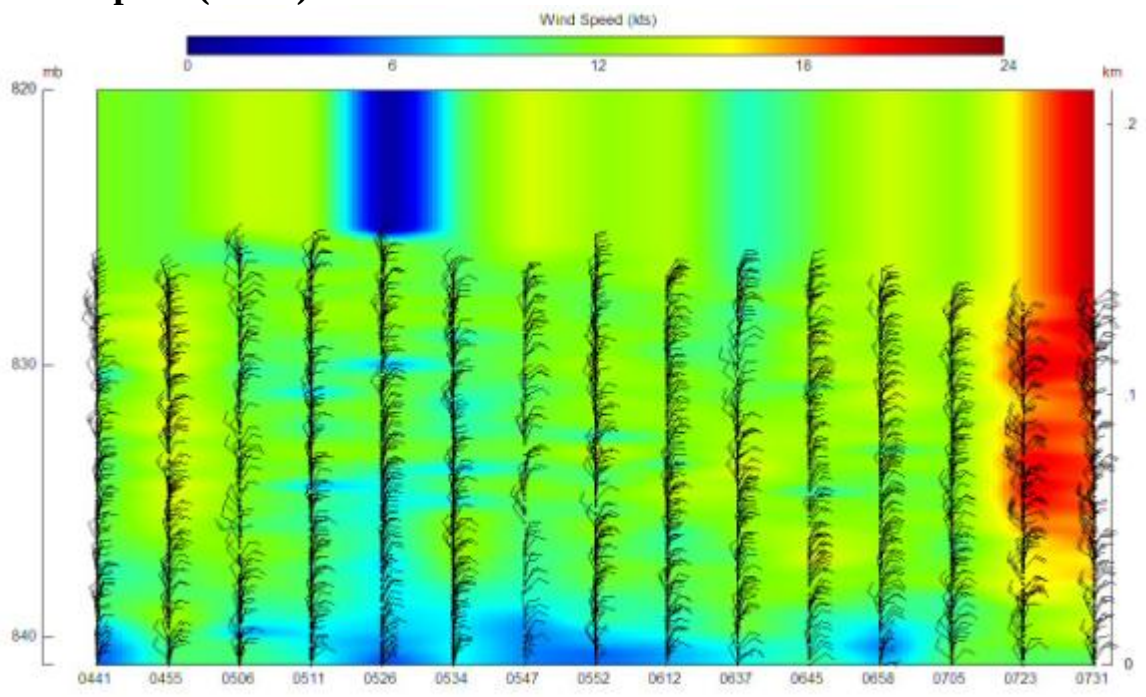

February 18, 2008

V-component of wind (knots)

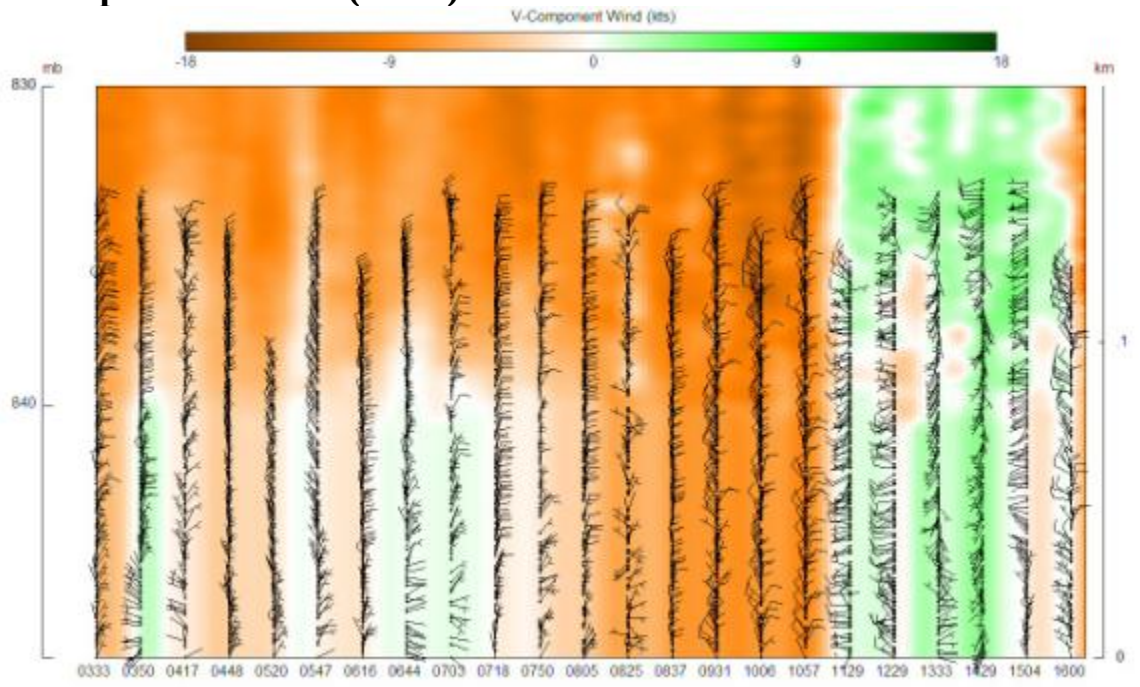

Mixing ratio (g/kg)

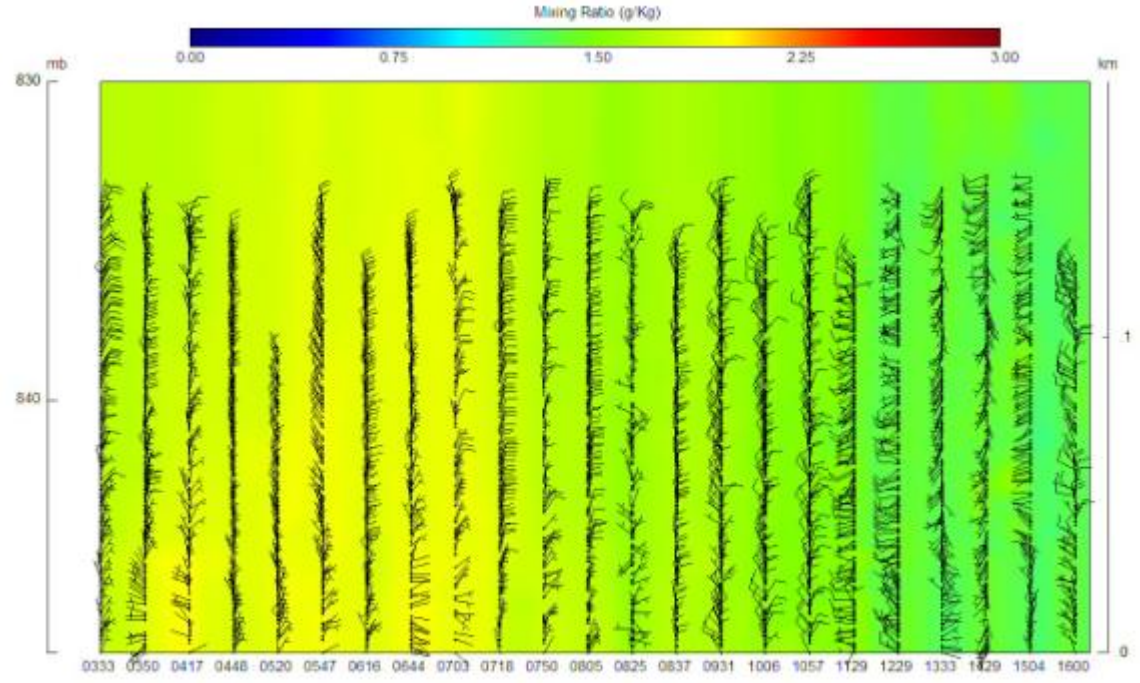

Relative Humidity (%)

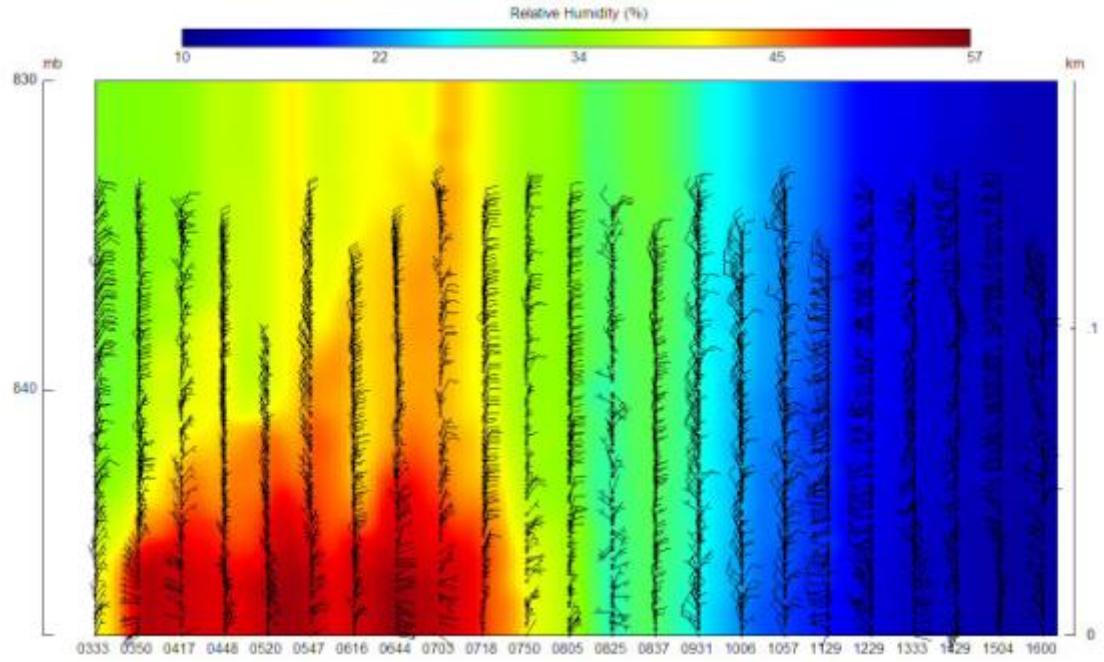

Temperature (°C)

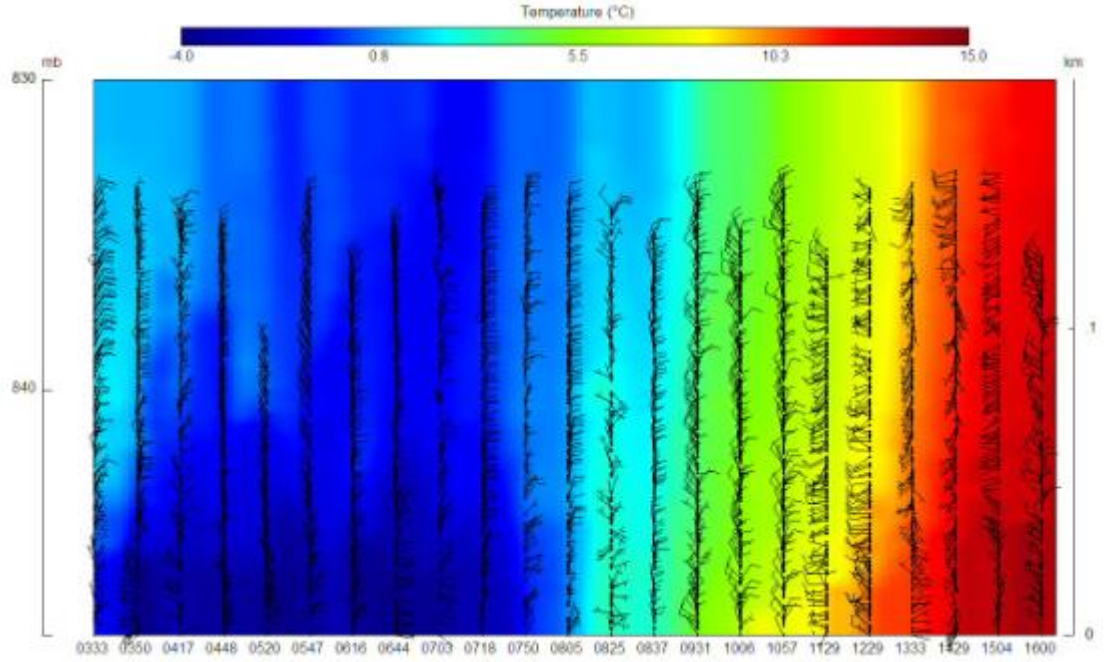

Potential Temperature (K)

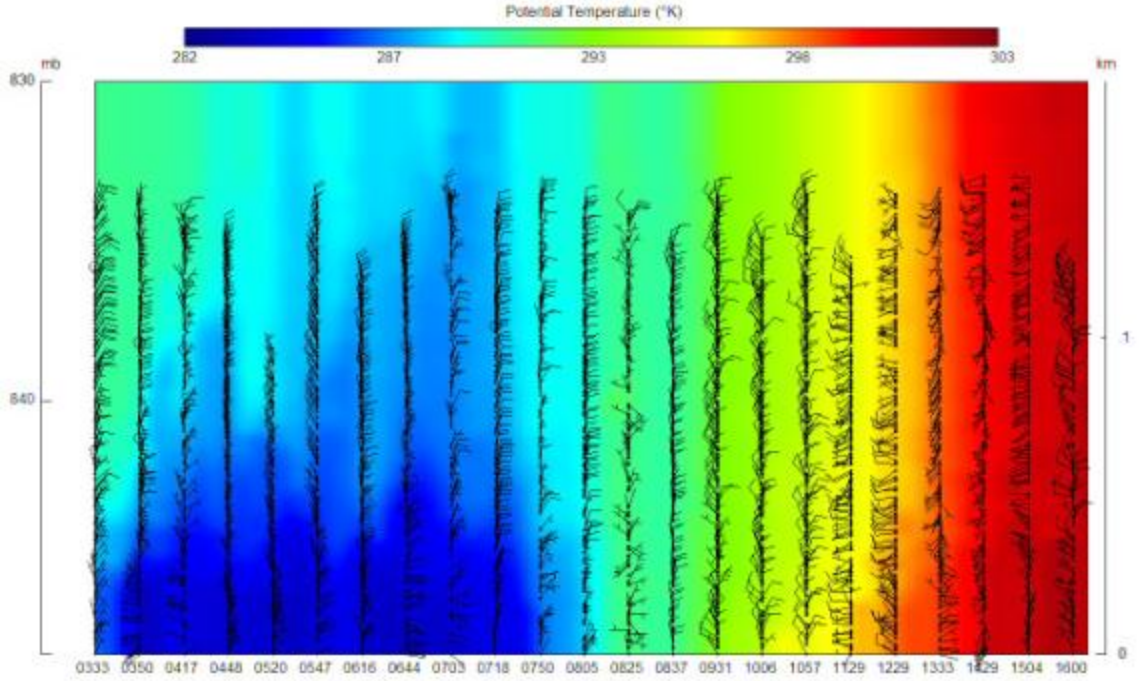

Equivalent Potential Temperature (K)

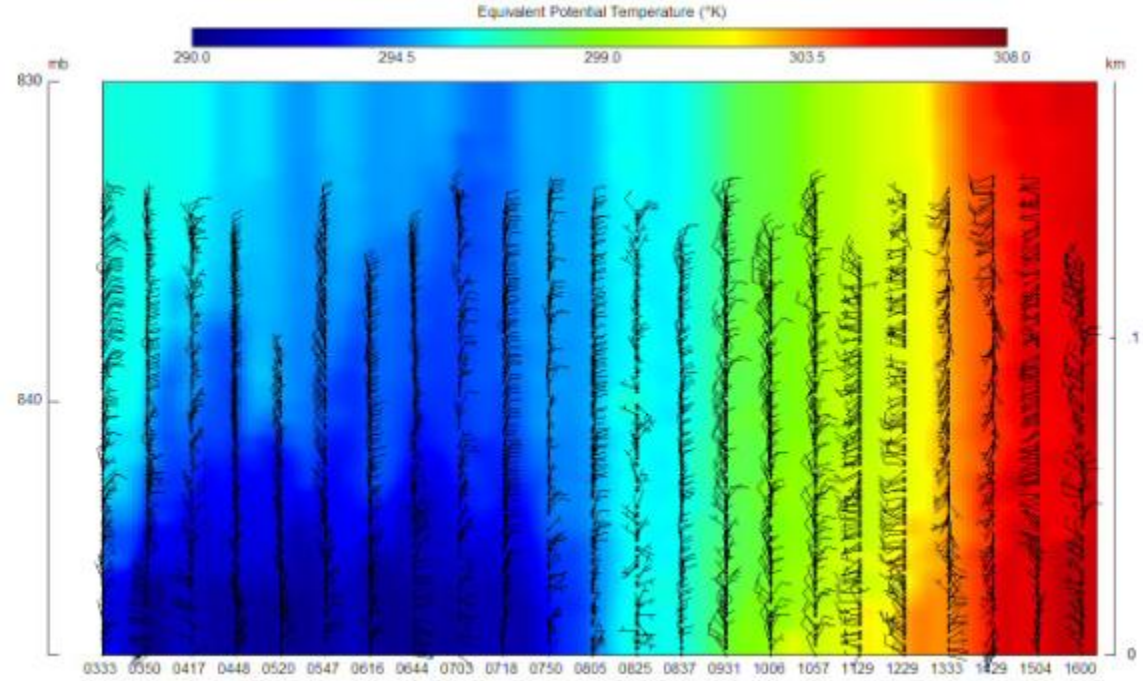

Wind Speed (knots)

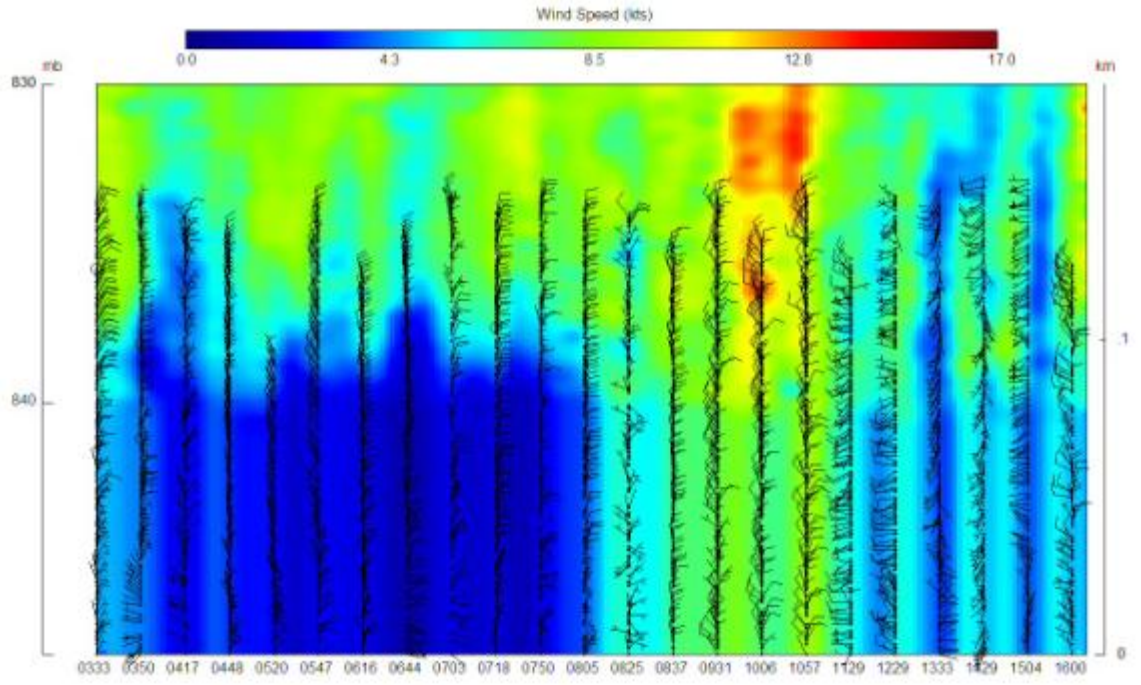

Summer IMP

June 23, 2008

Wind Speed (knots)

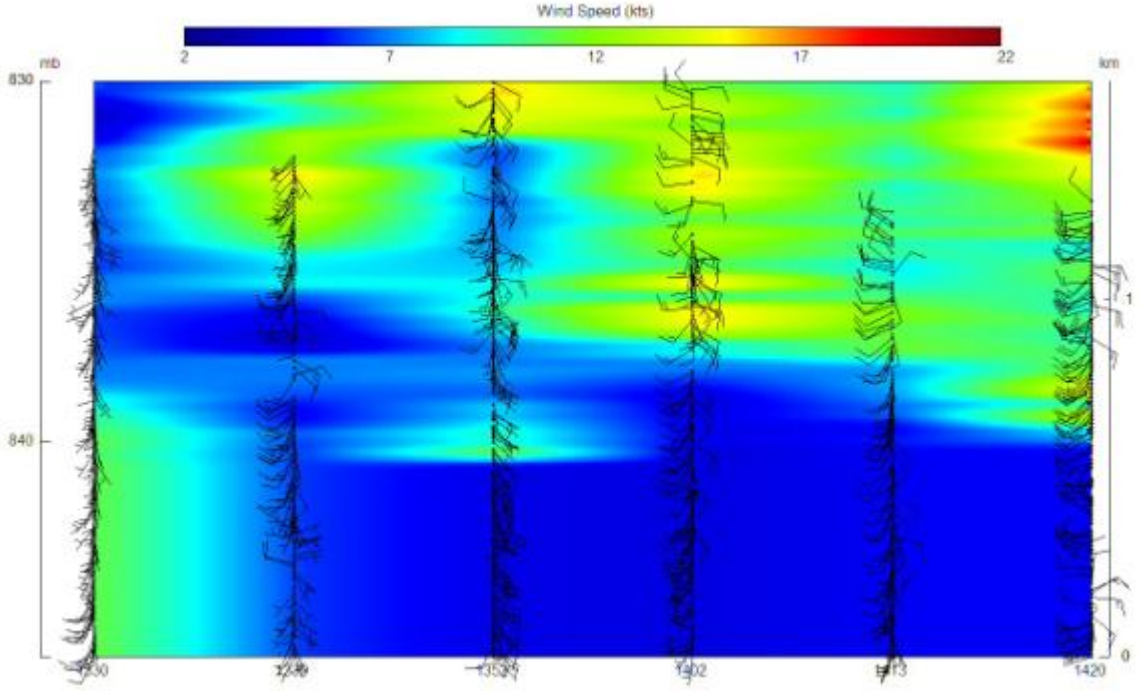

Mixing Ratio (g/kg)

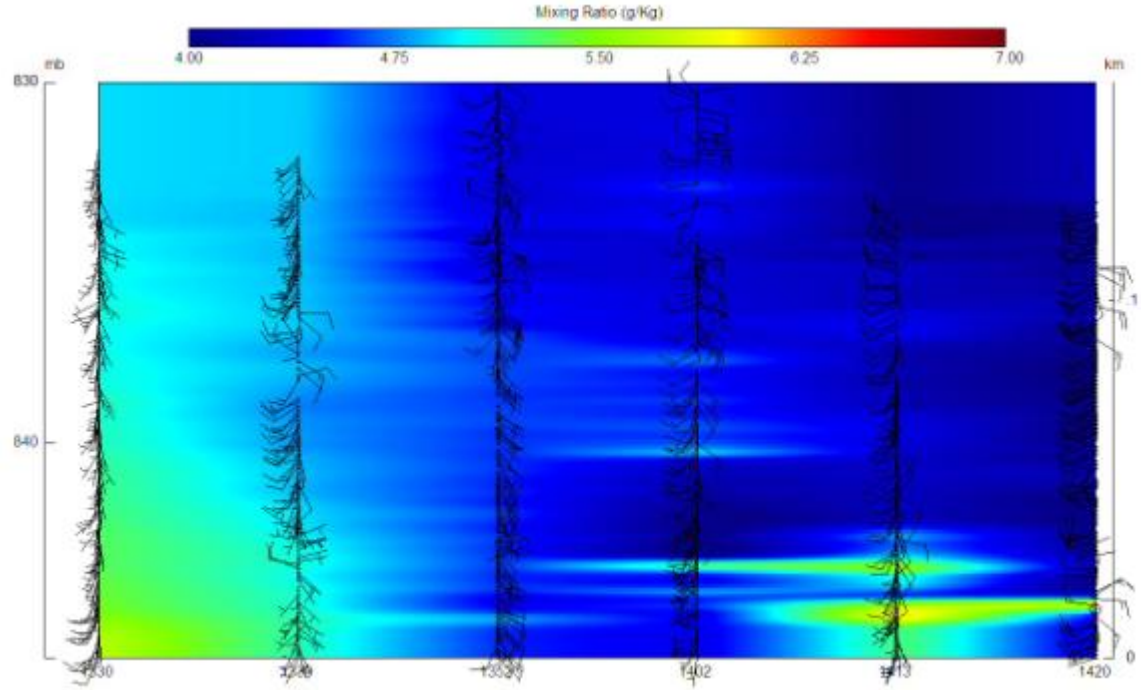

Relative Humidity (%)

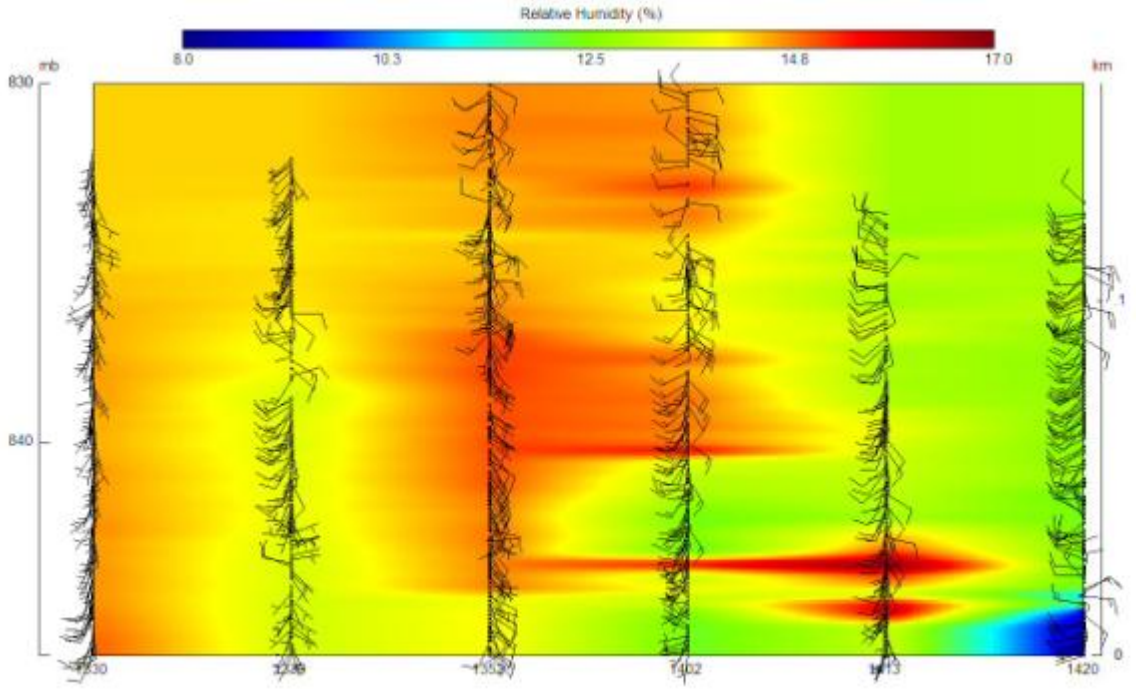

Temperature (°C)

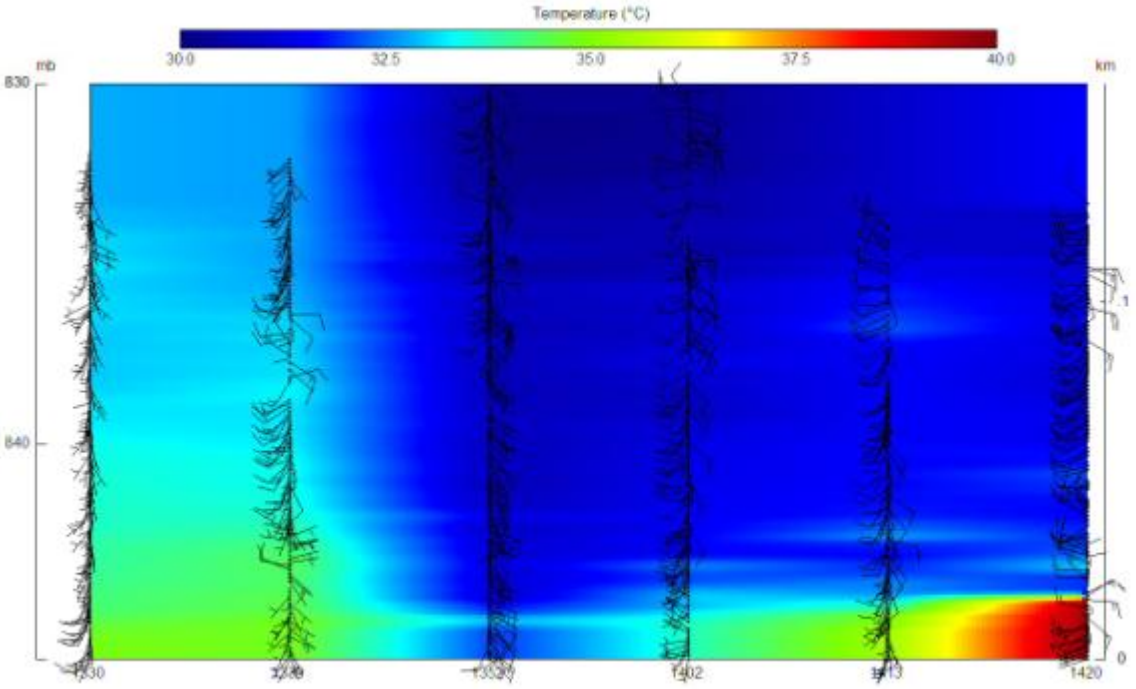

Potential Temperature (K)

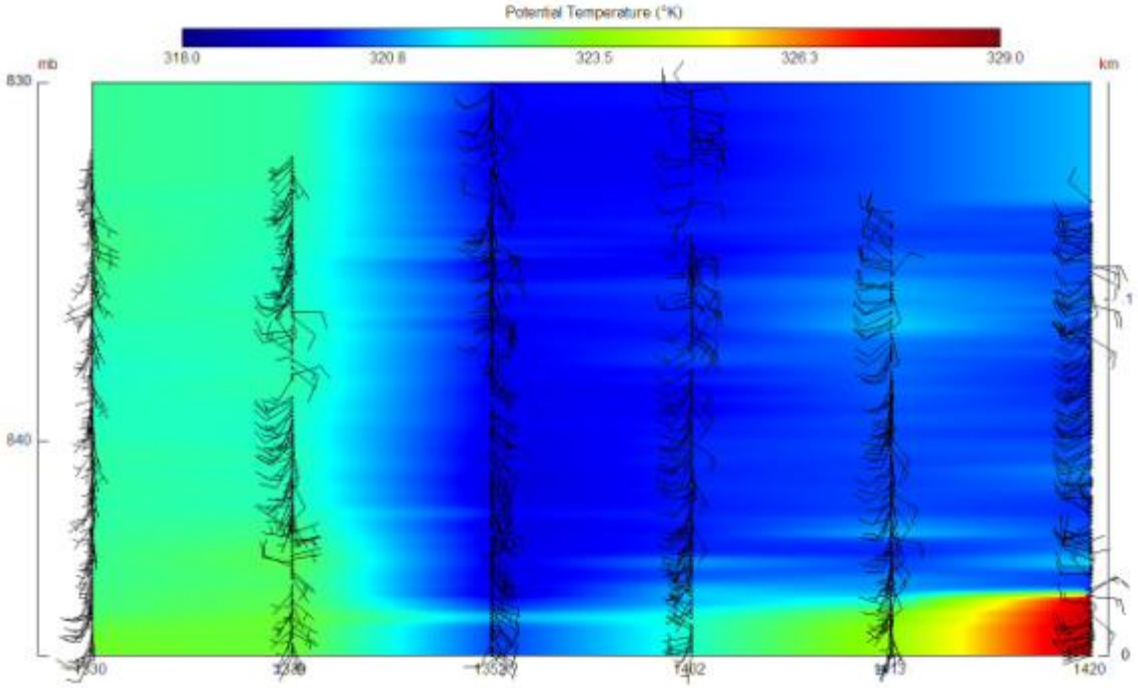

Equivalent Potential Temperature (K)

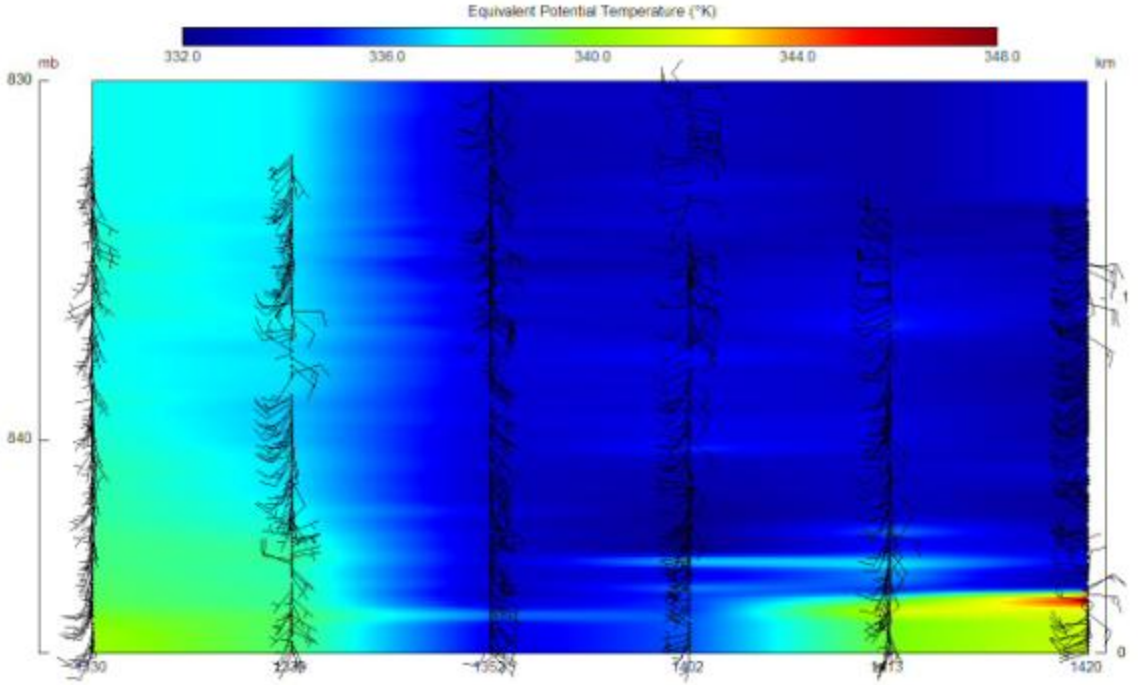

V-component of wind (knots)

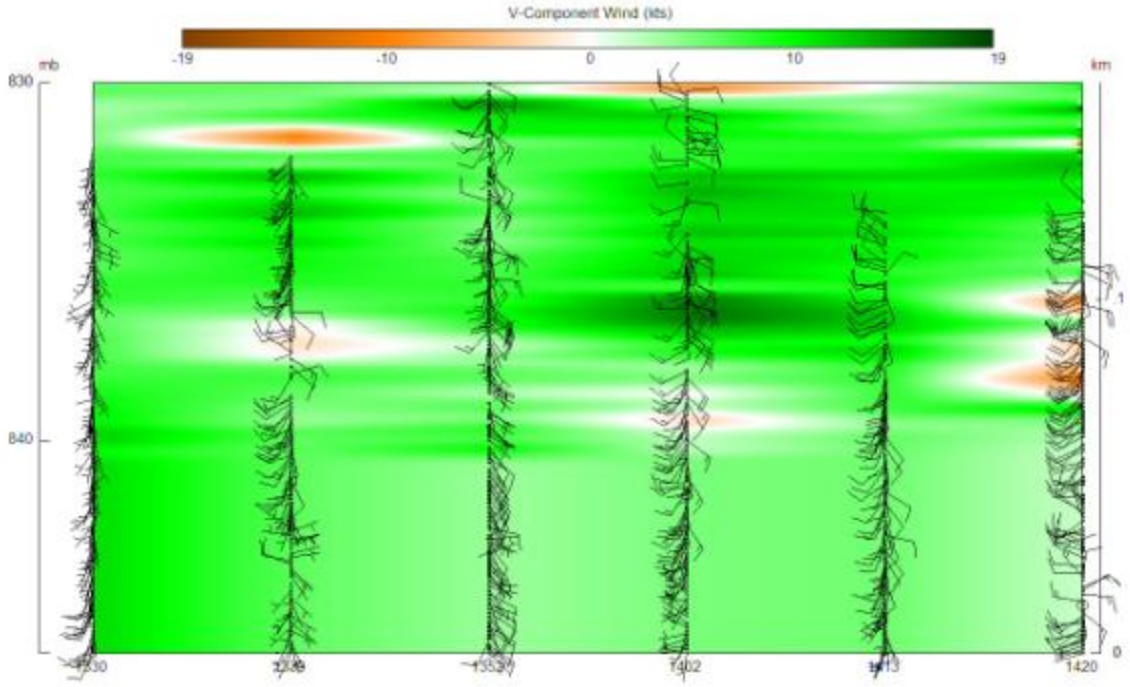

June 24, 2008

Wind Speed (knots)

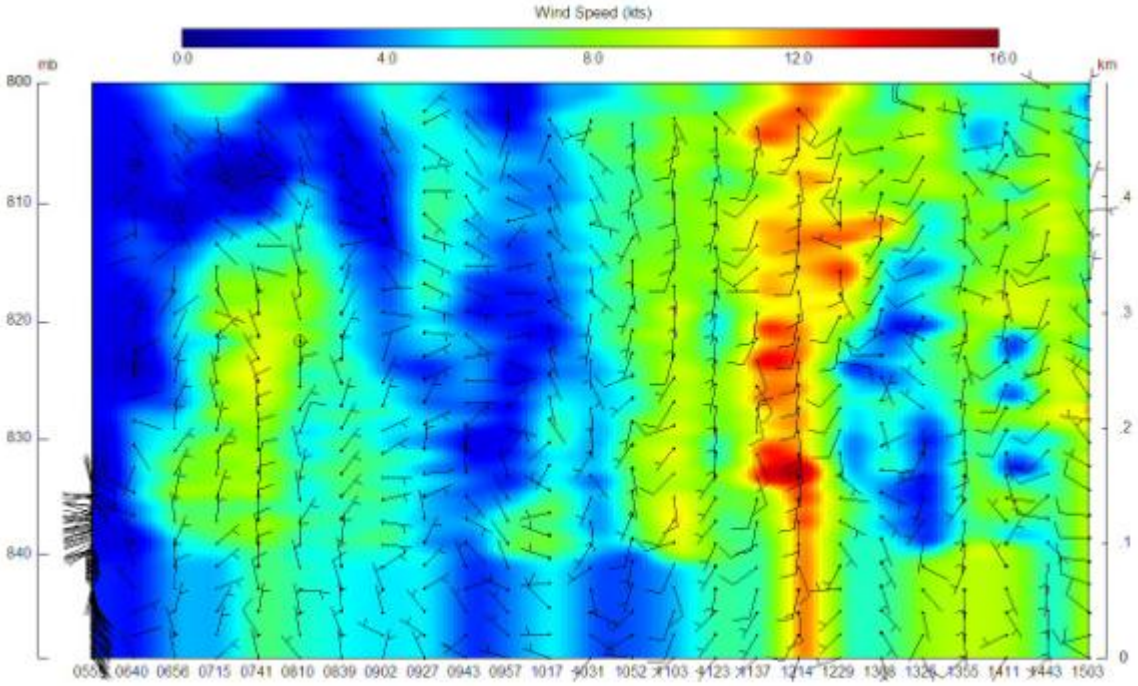

Mixing Ratio (g/kg)

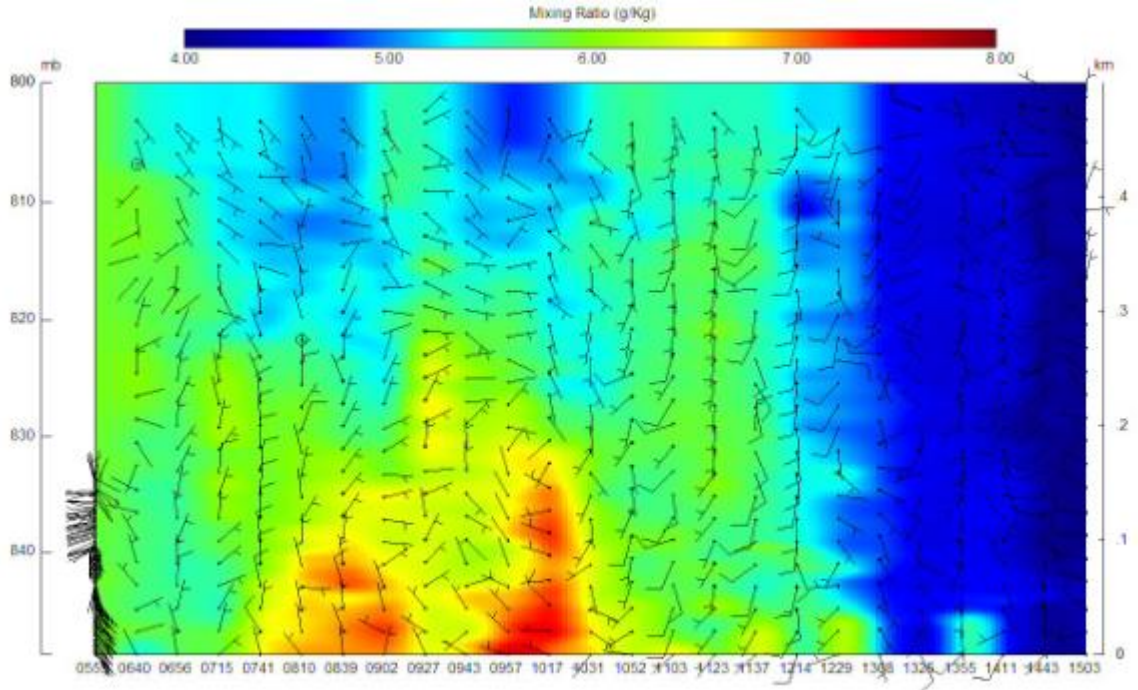

Relative Humidity (%)

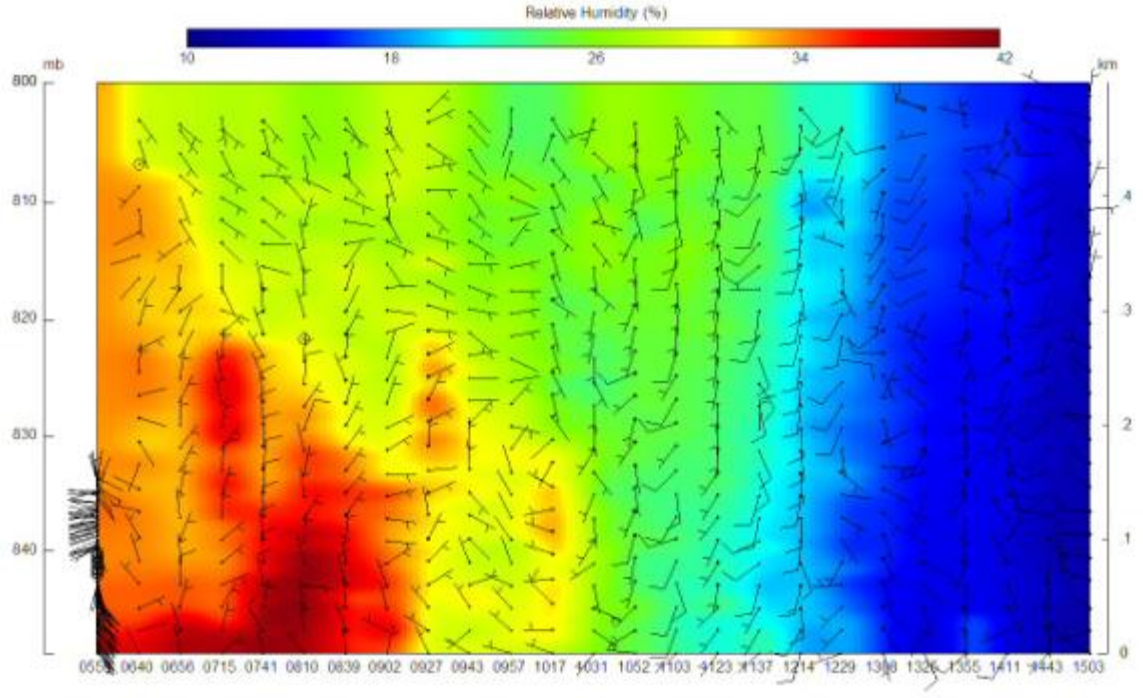

Temperature (°C)

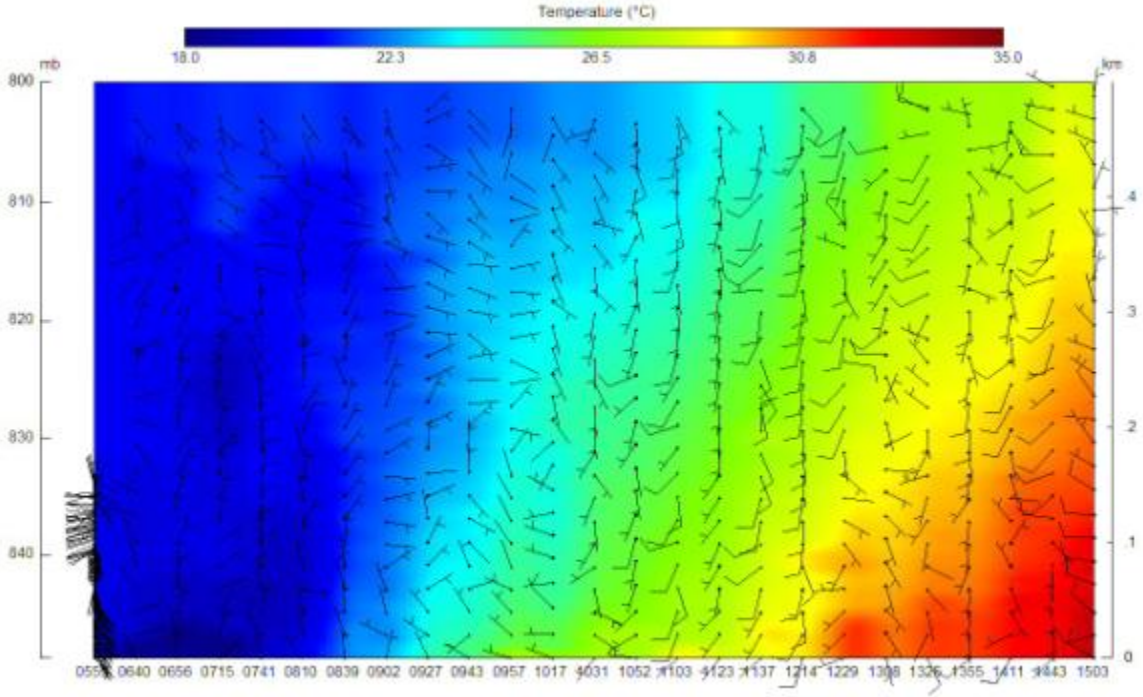

Potential Temperature (K)

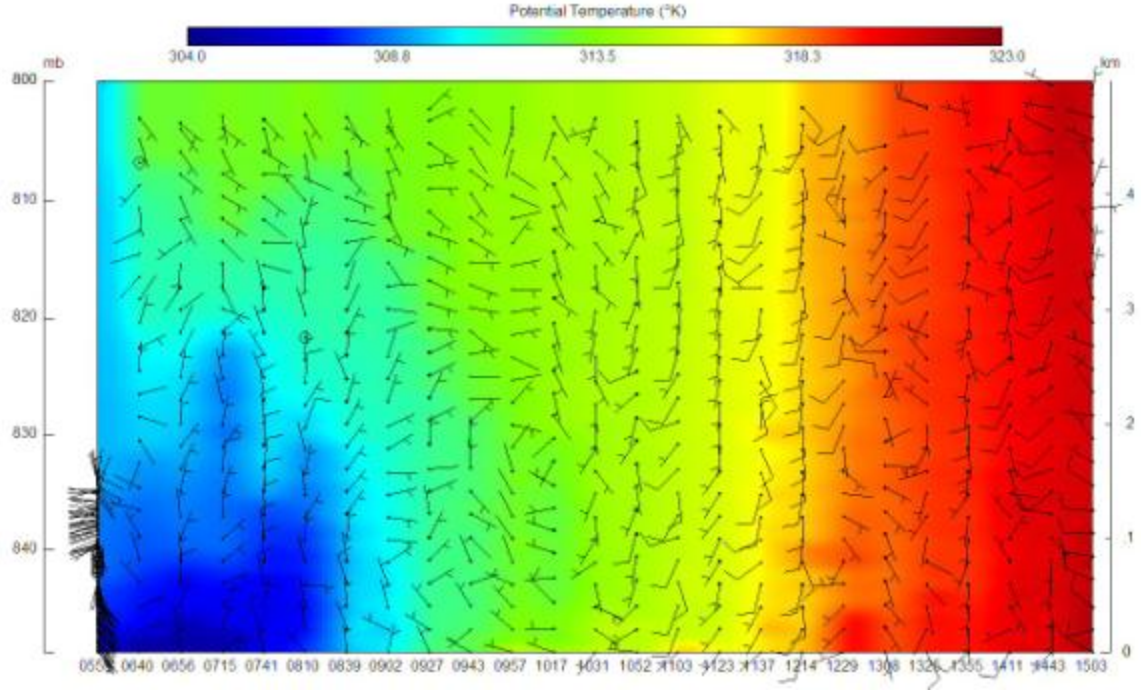

Equivalent Potential Temperature (K)

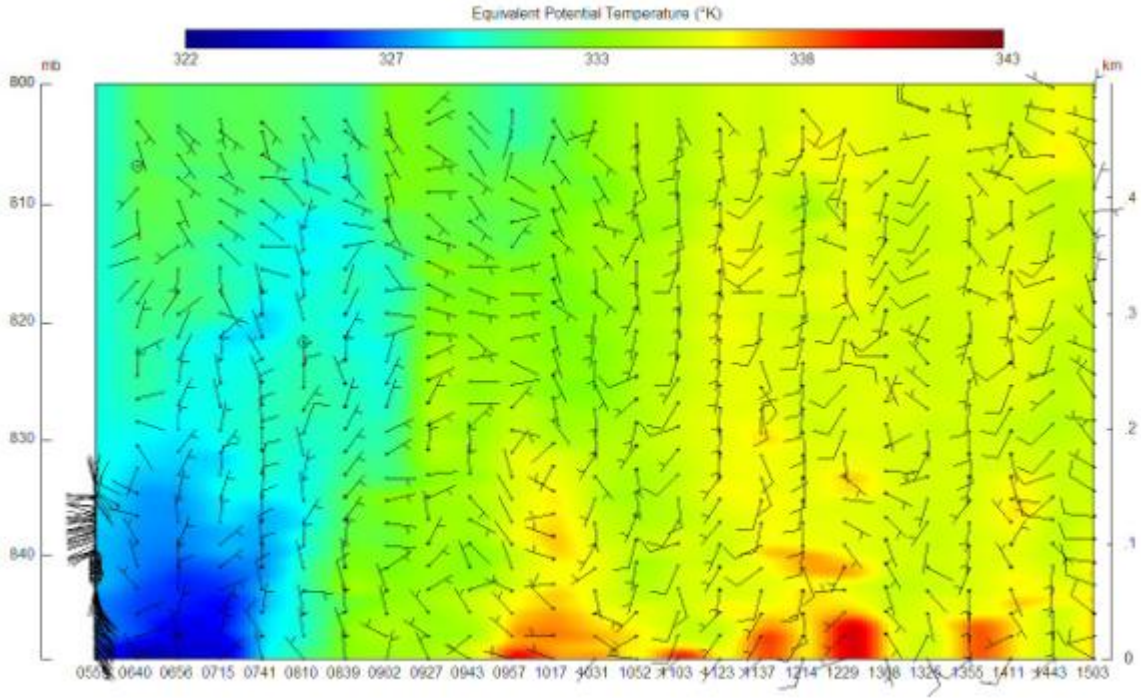

V-component of wind (knots)

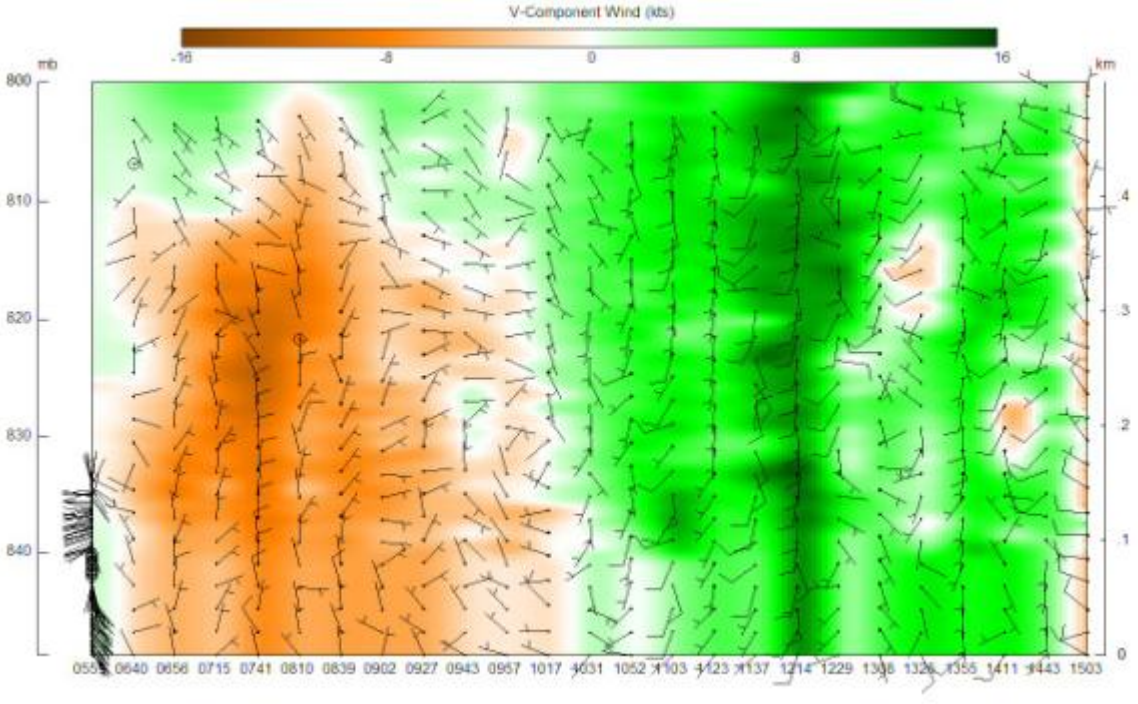

June 26, 2008

Wind Speed (knots)

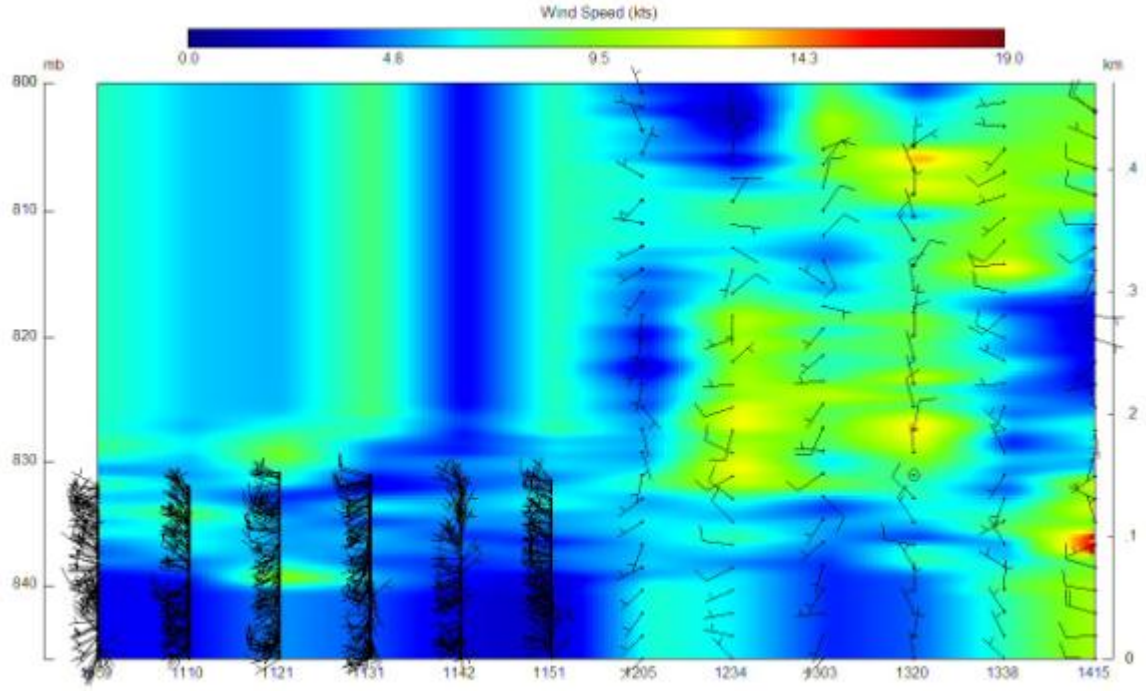

Mixing Ratio (g/kg)

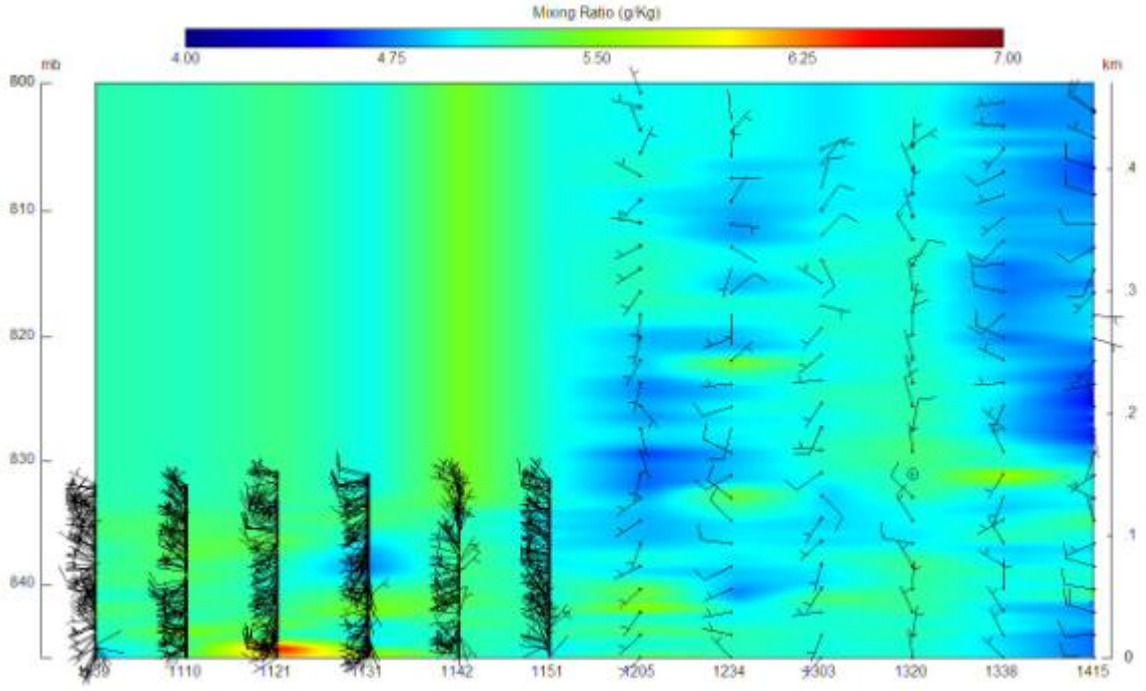

Relative Humidity (%)

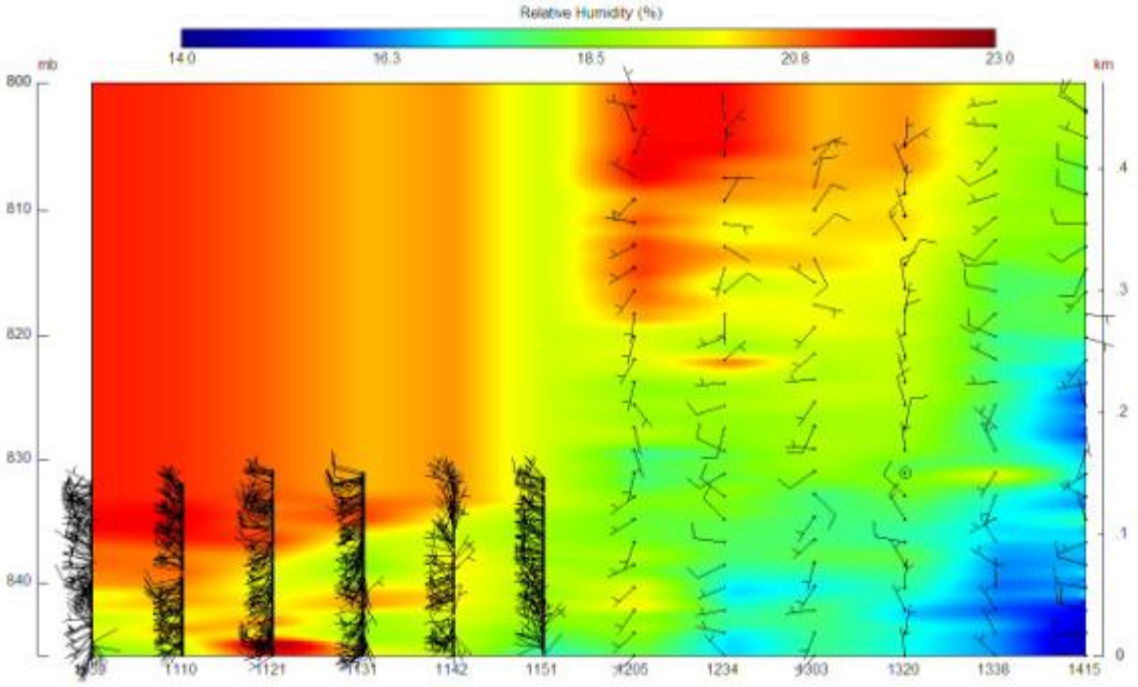

Temperature (°C)

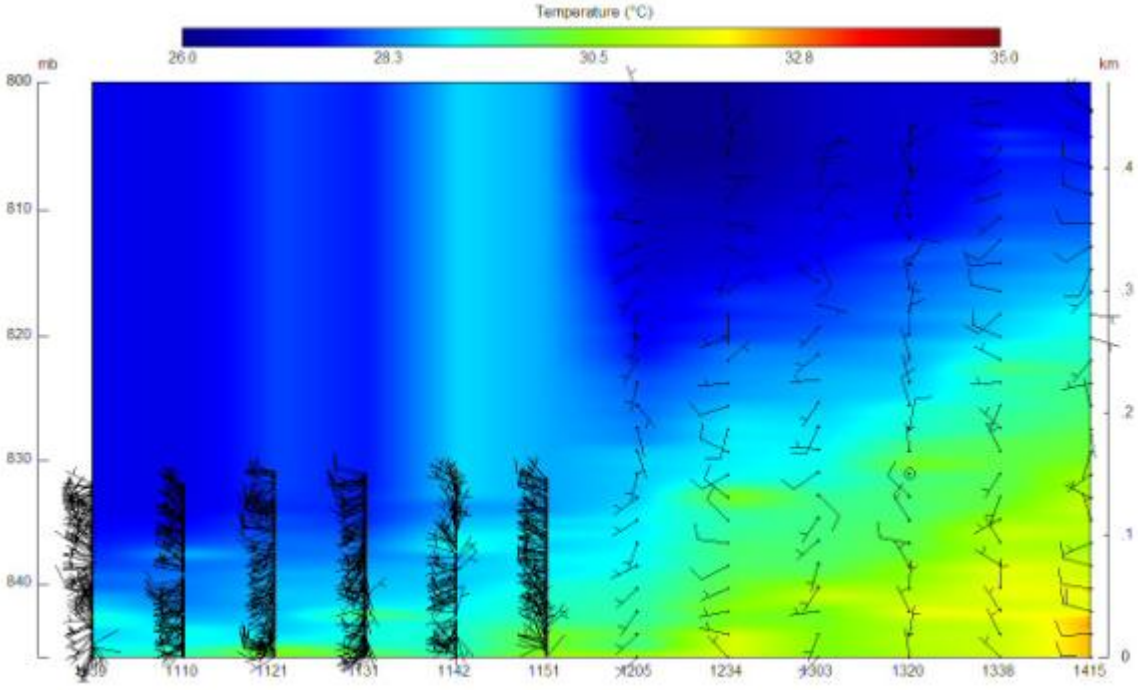

Potential Temperature (K)

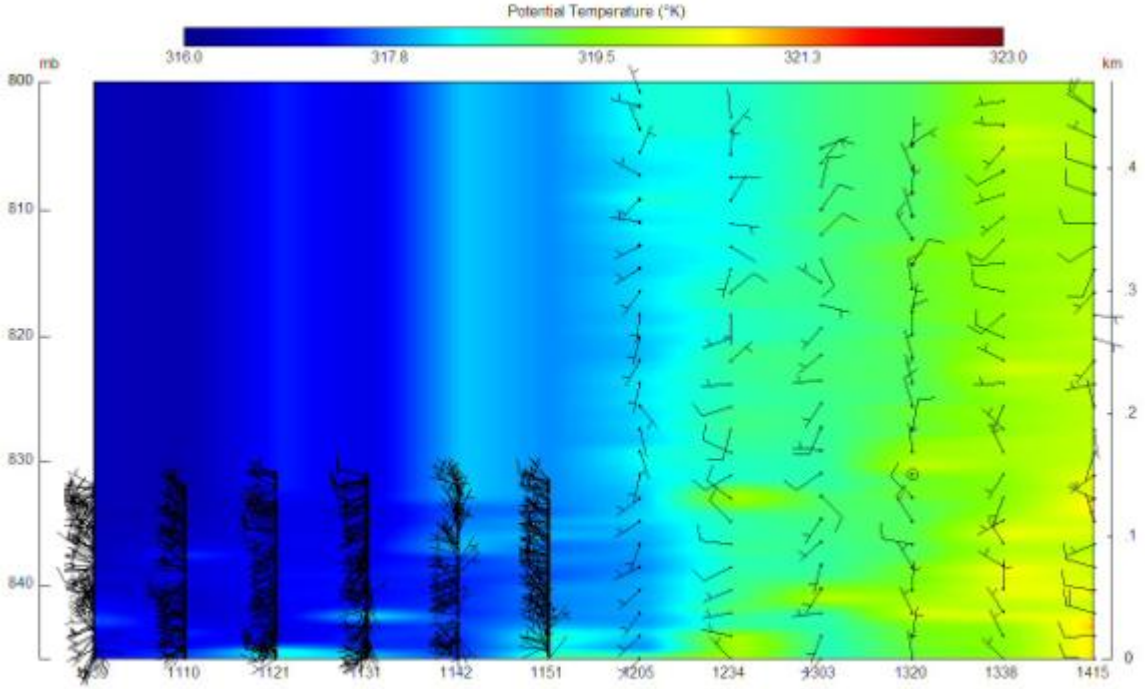

Equivalent Potential Temperature (K)

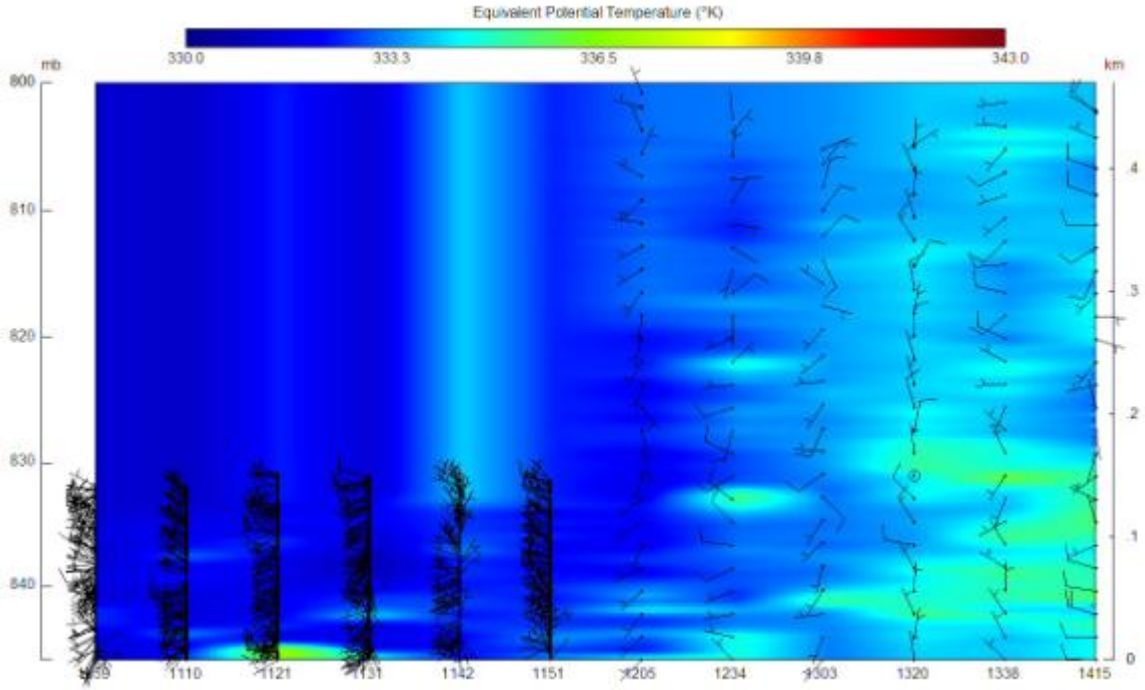

V-component of wind (knots)

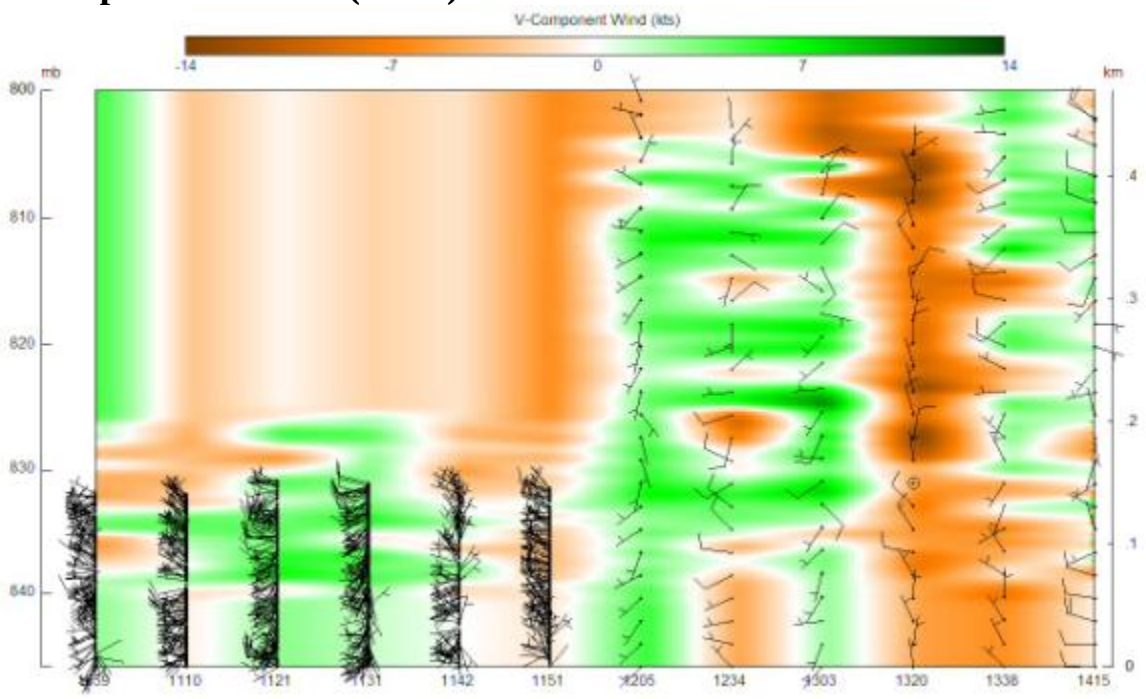

June 27, 2008

Wind Speed (knots)

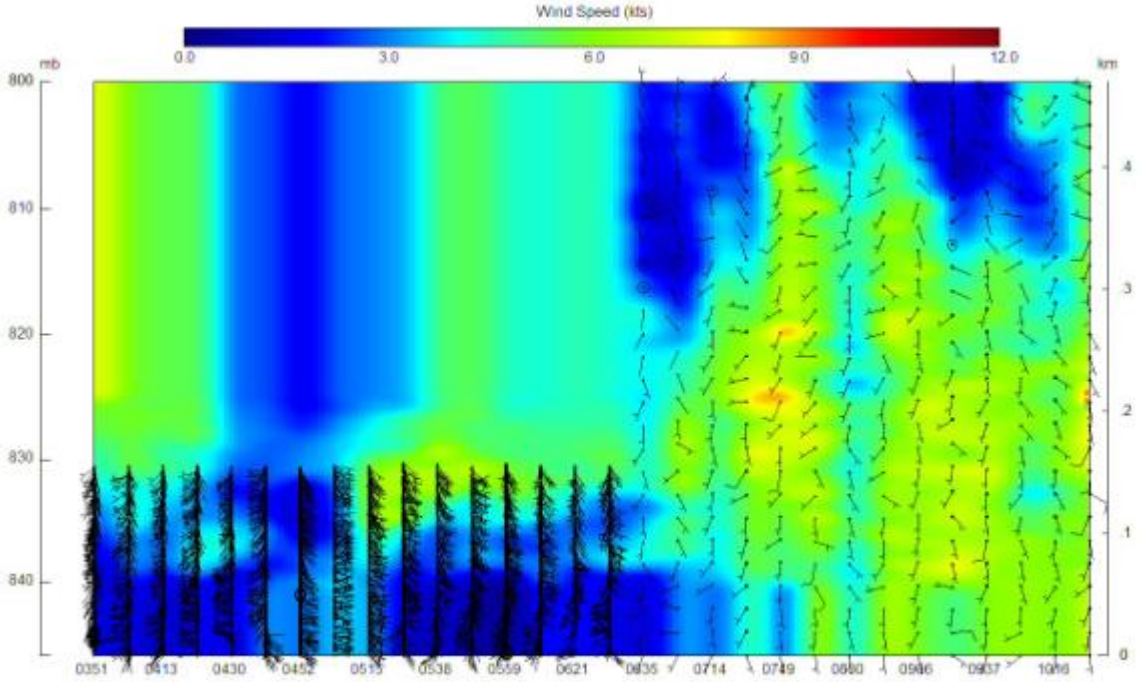

Mixing Ratio (g/kg)

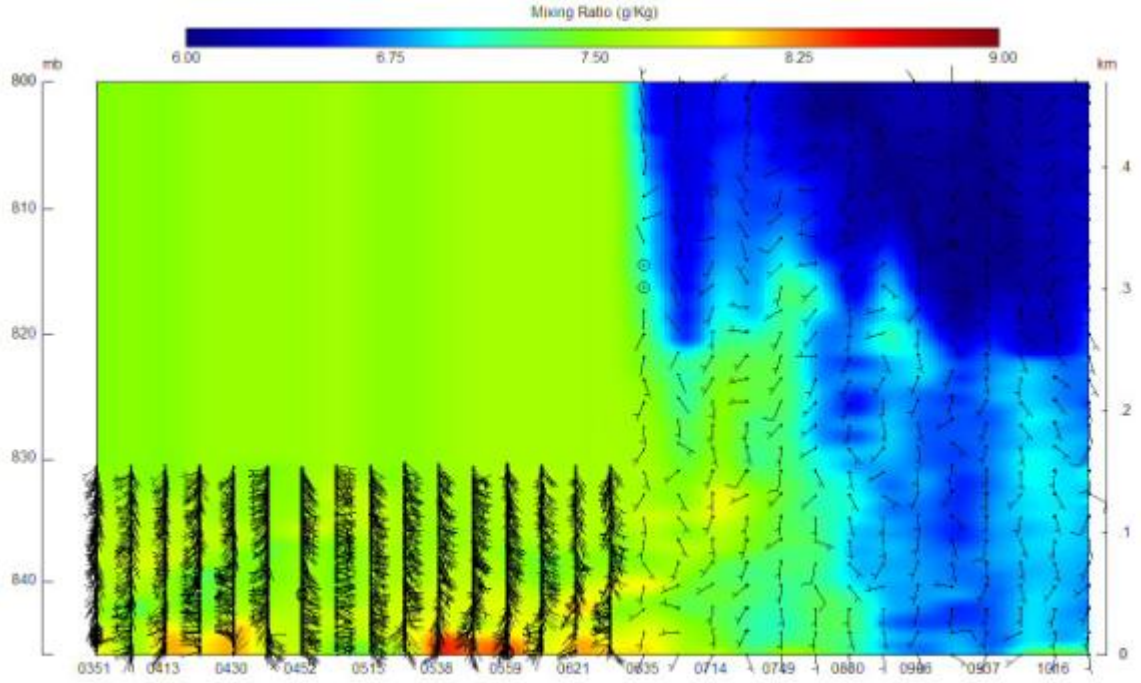

Relative Humidity (%)

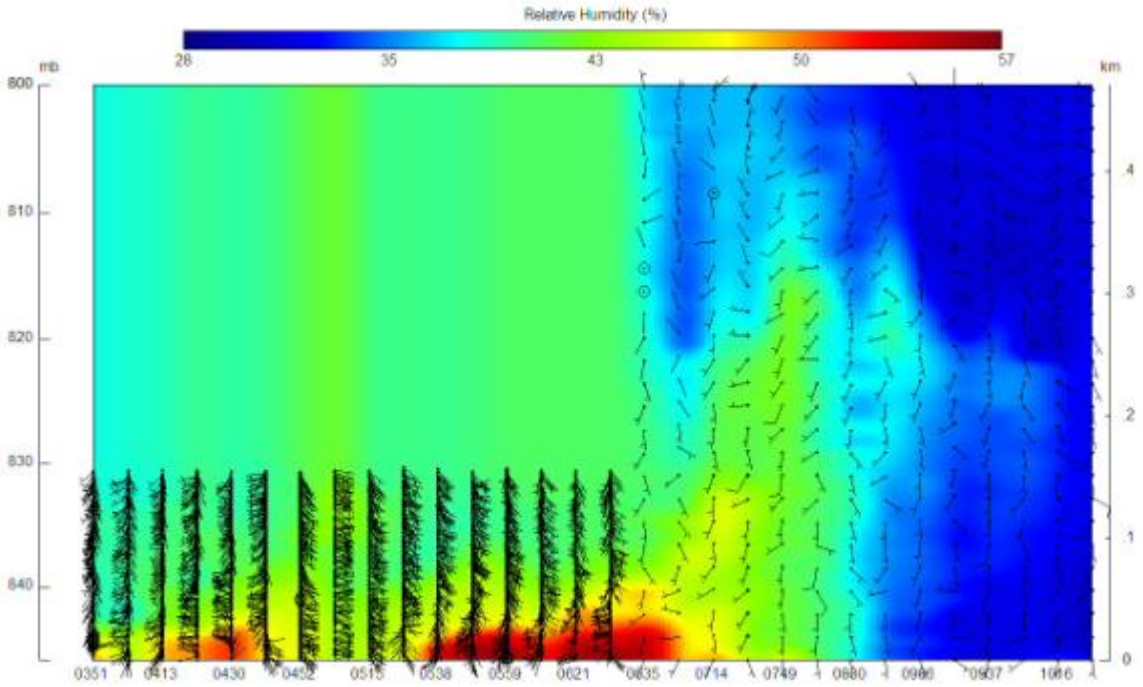

Temperature (°C)

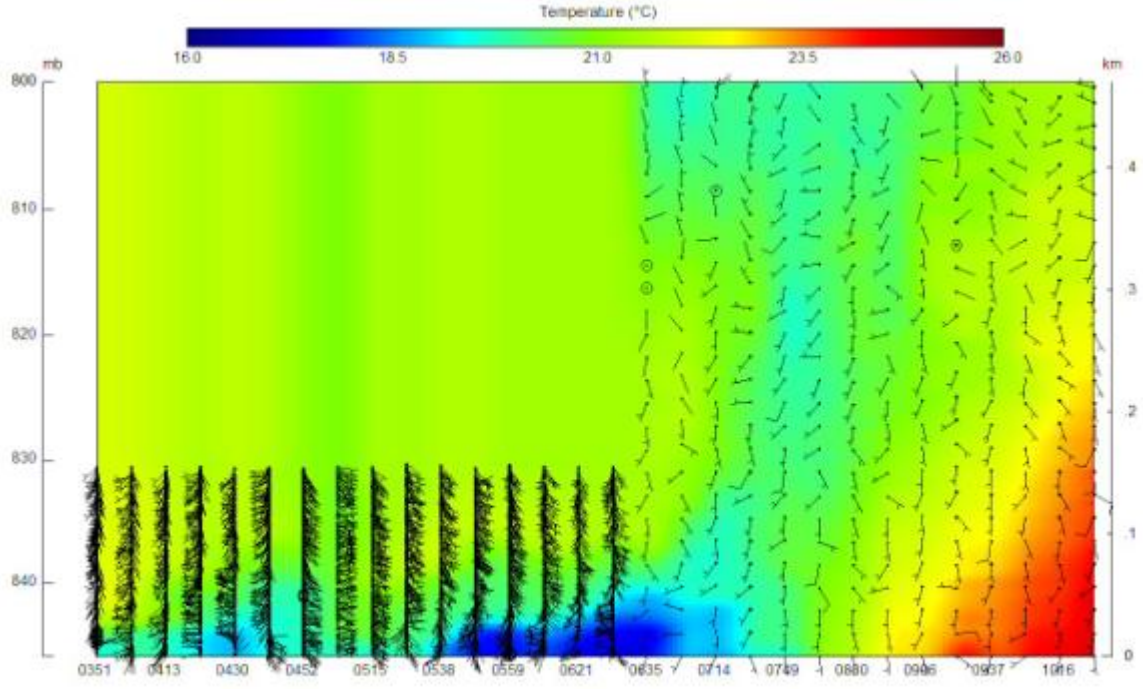

Potential Temperature (K)

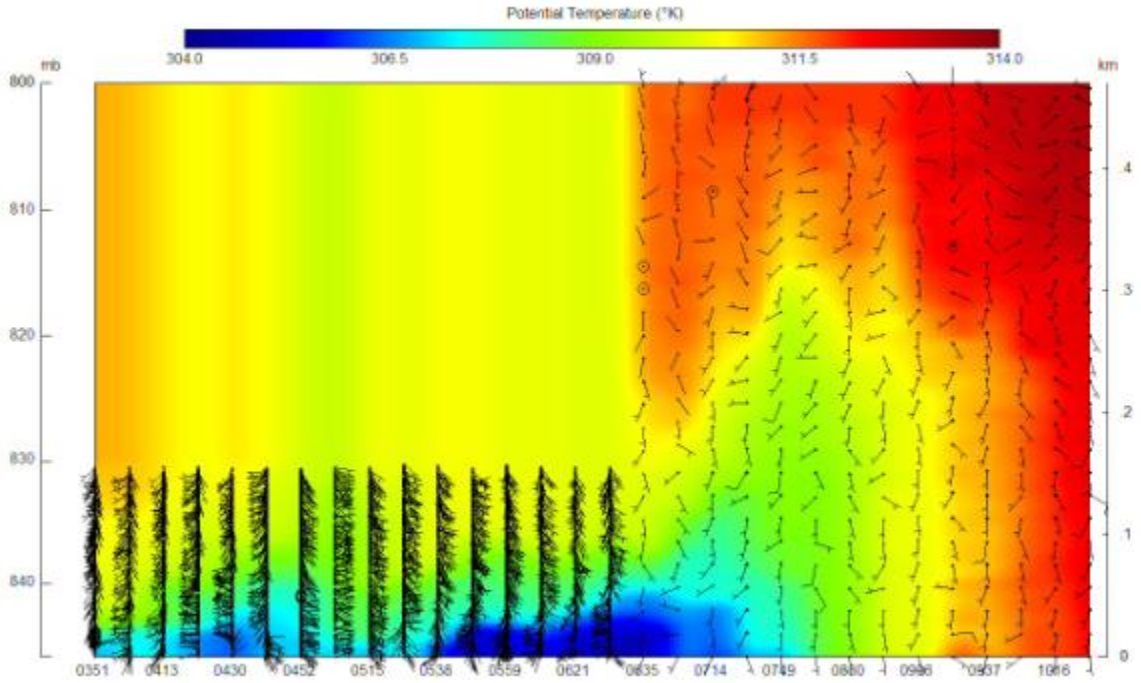

Equivalent Potential Temperature (K)

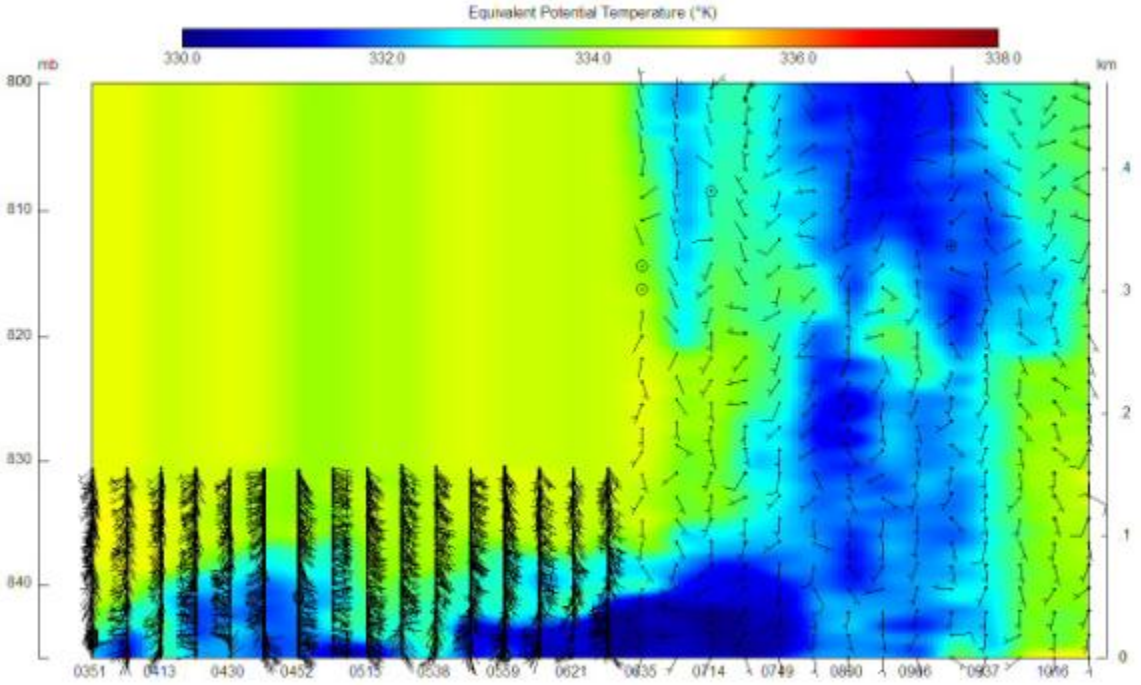

V-component of wind (knots)

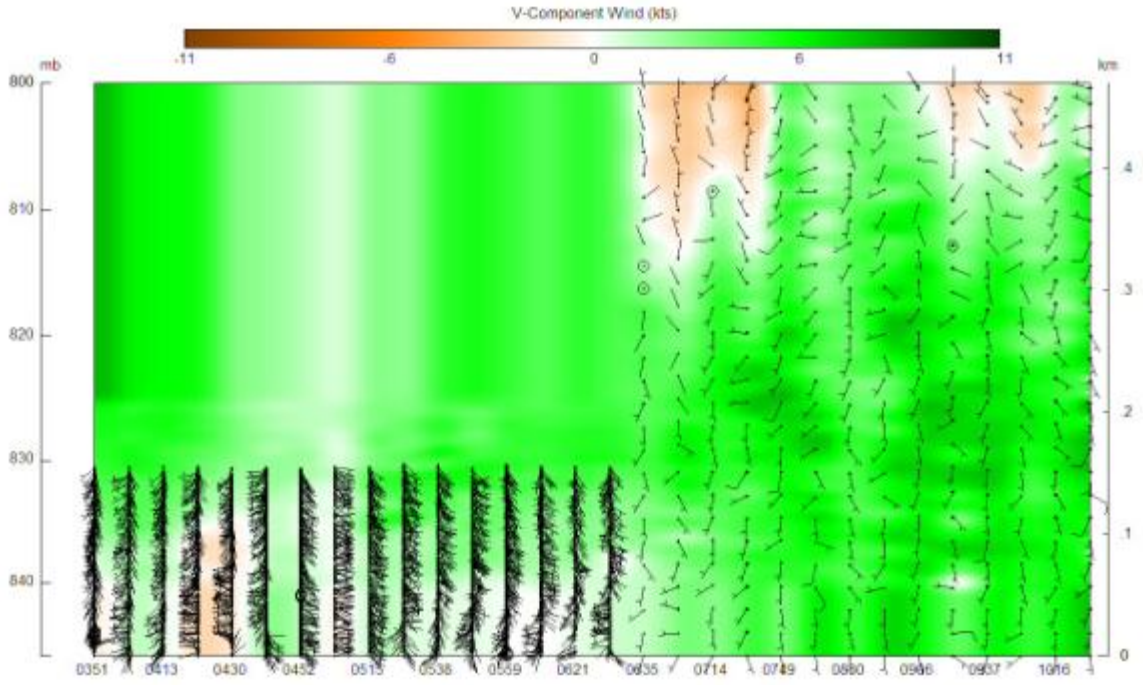

June 28, 2008

Wind Speed (knots)

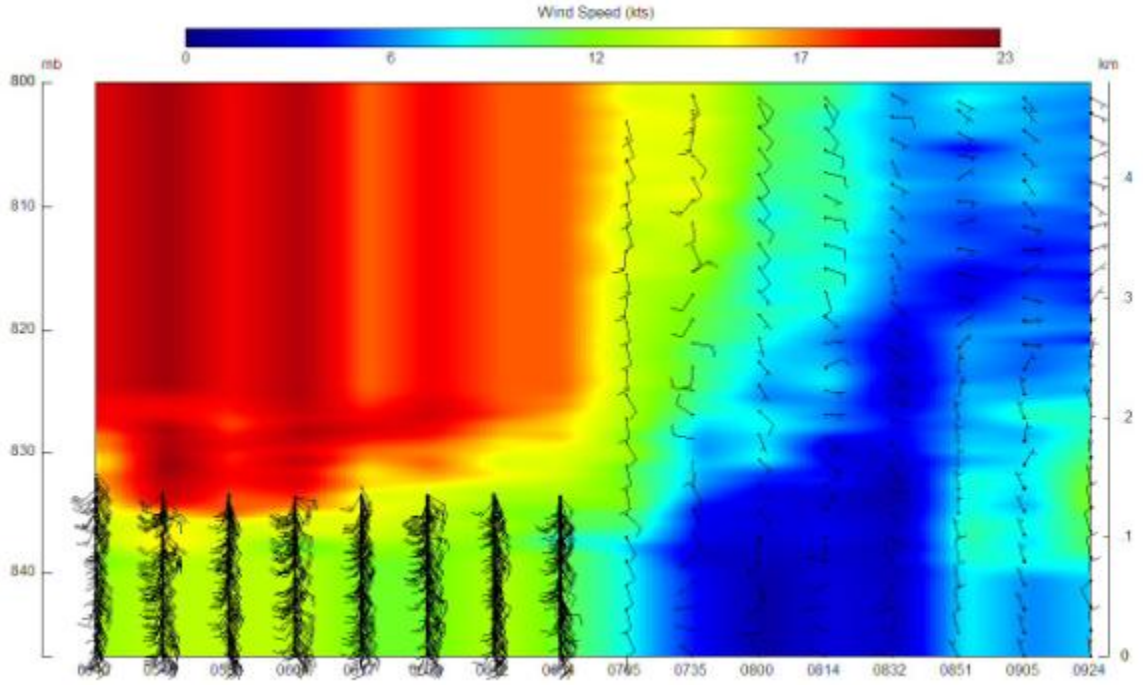

Mixing Ratio (g/kg)

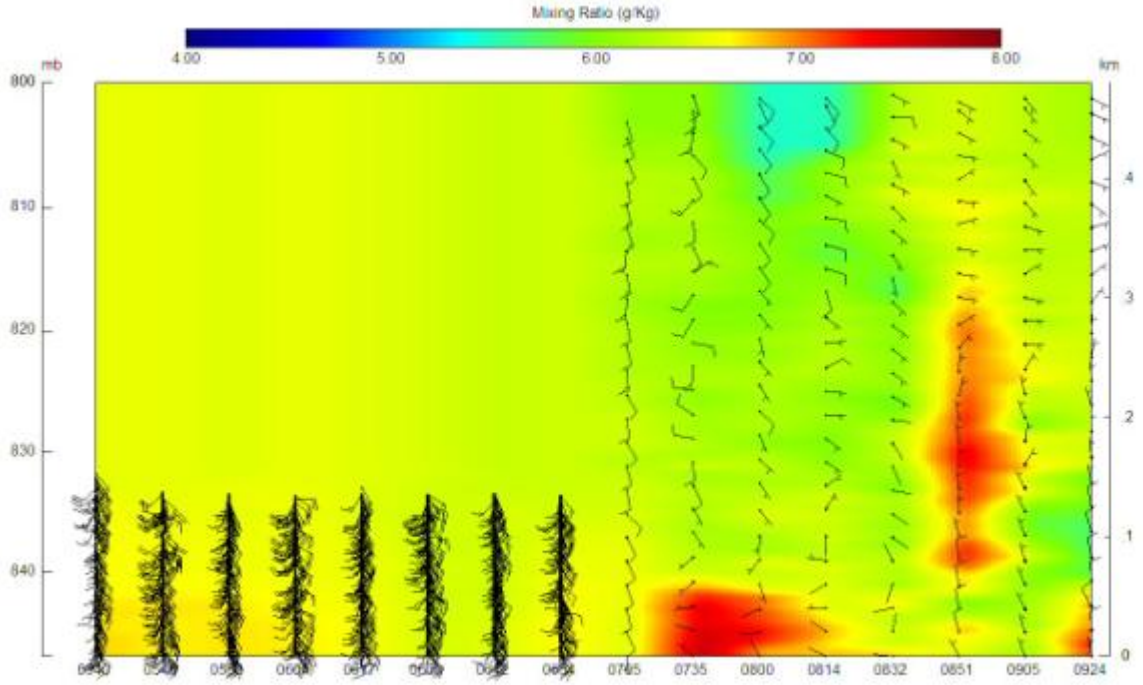

Relative Humidity (%)

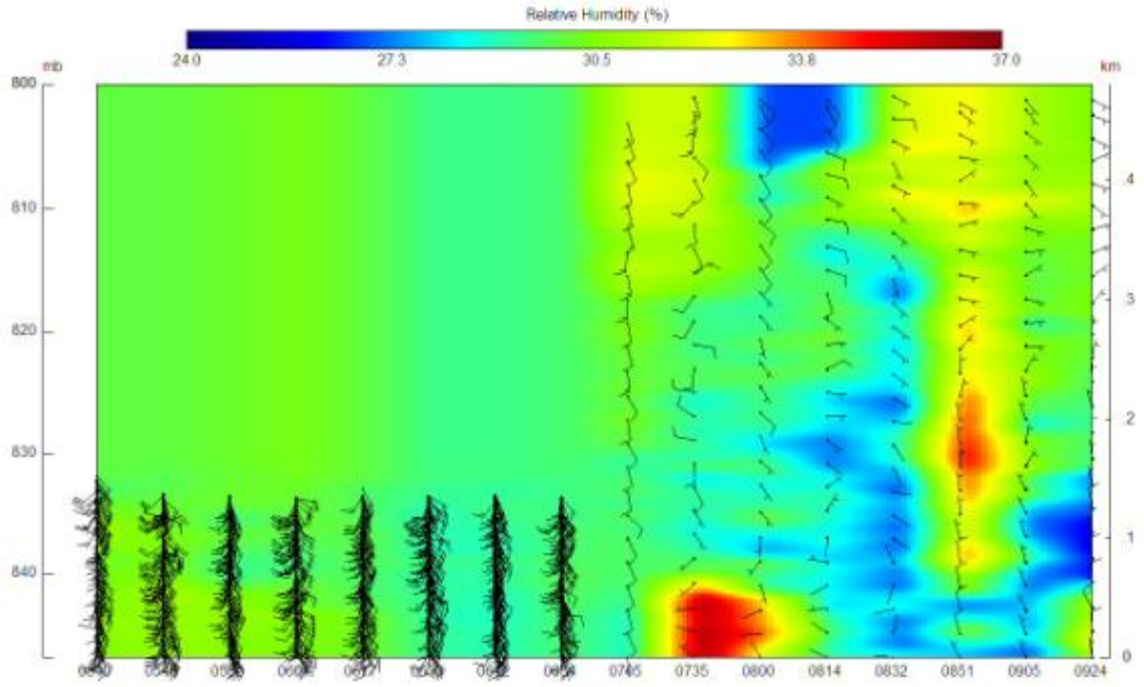

Temperature (°C)

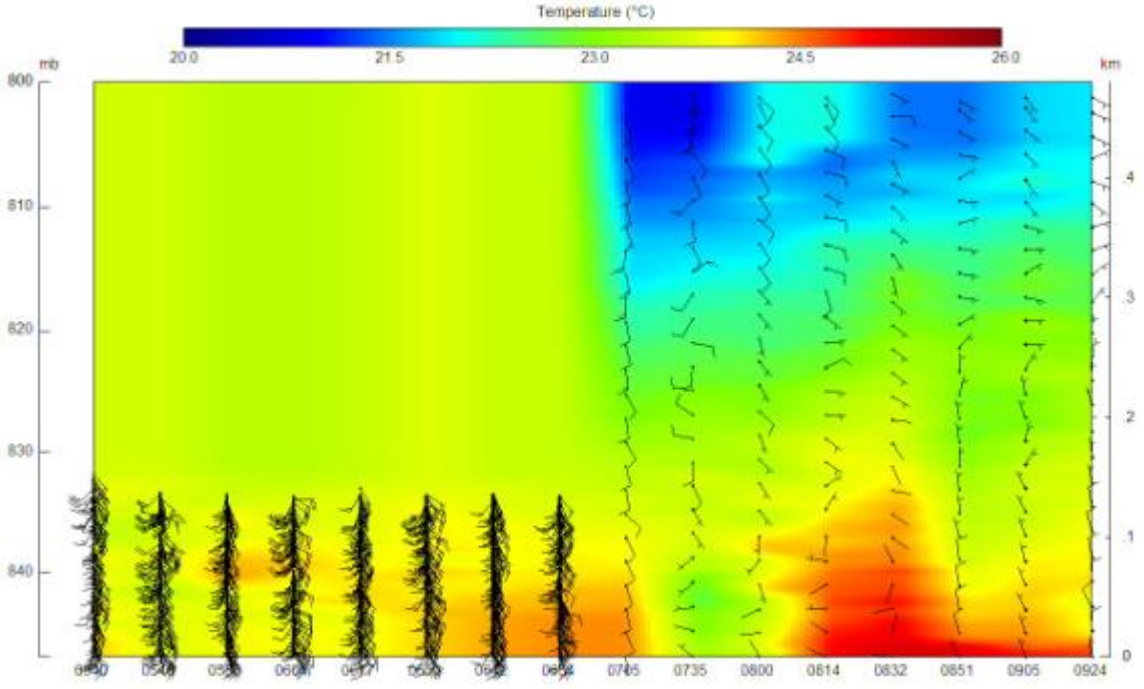

Potential Temperature (K)

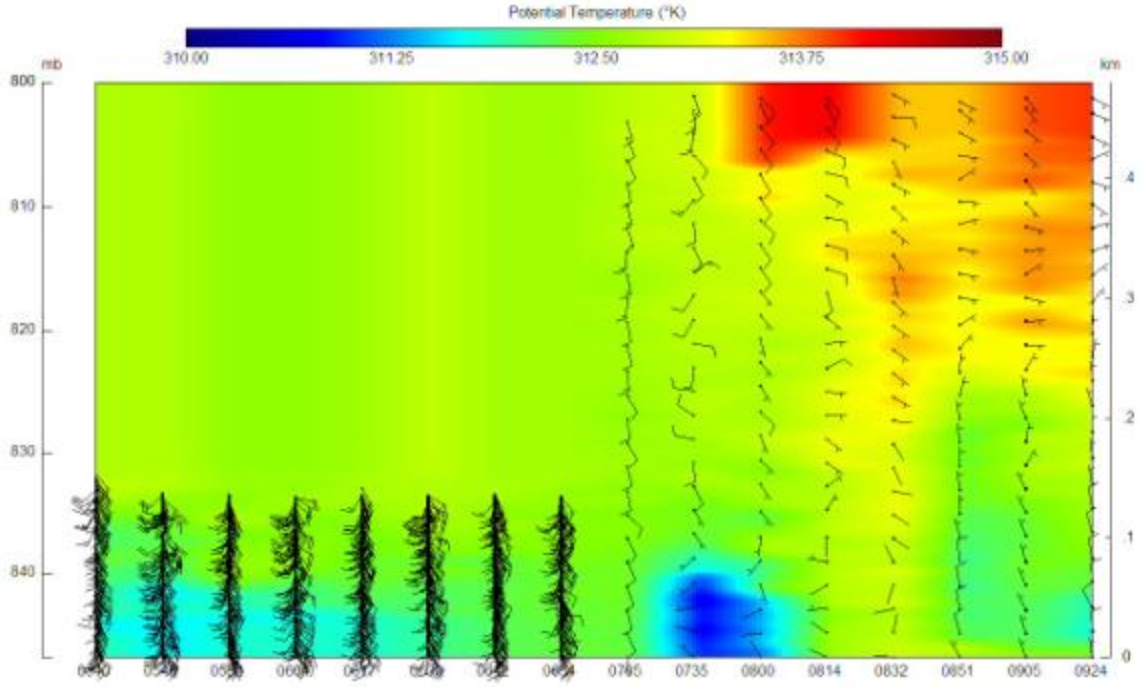

Equivalent Potential Temperature (K)

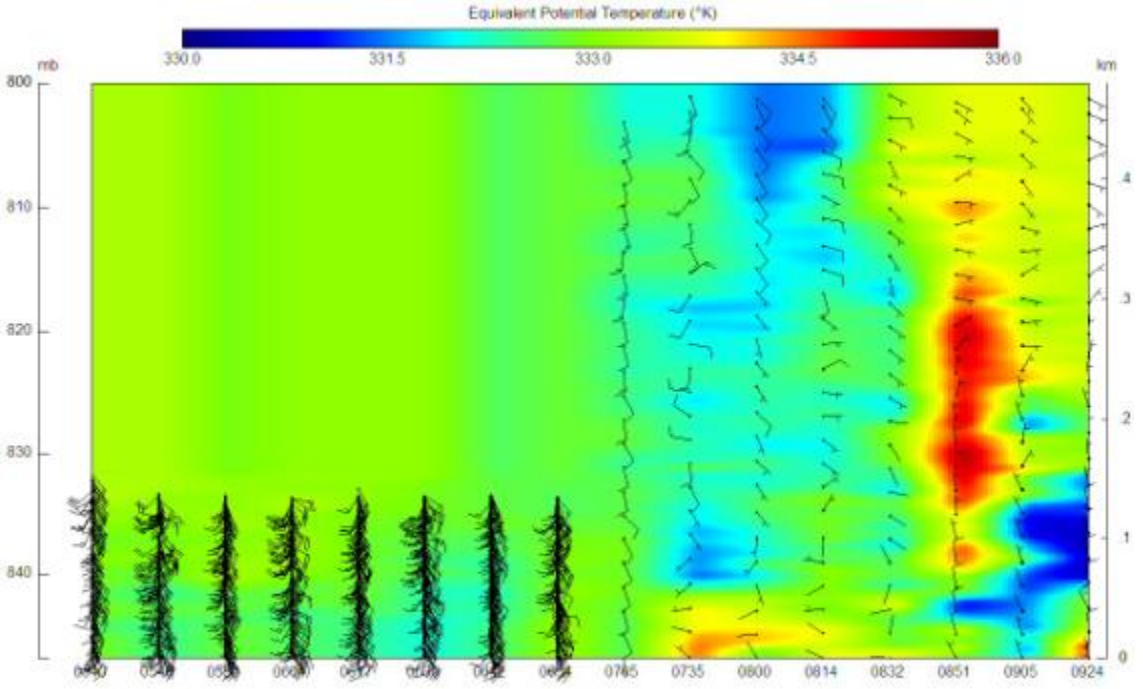

V-component of wind (knots)

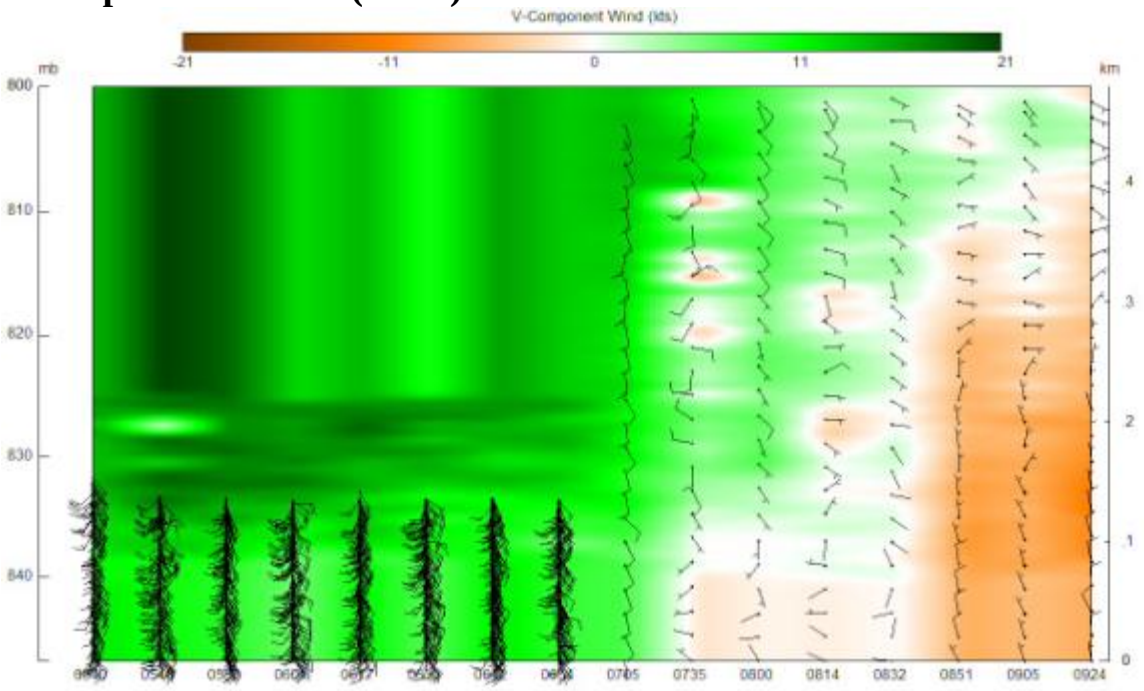

June 29, 2008

Wind Speed (knots)

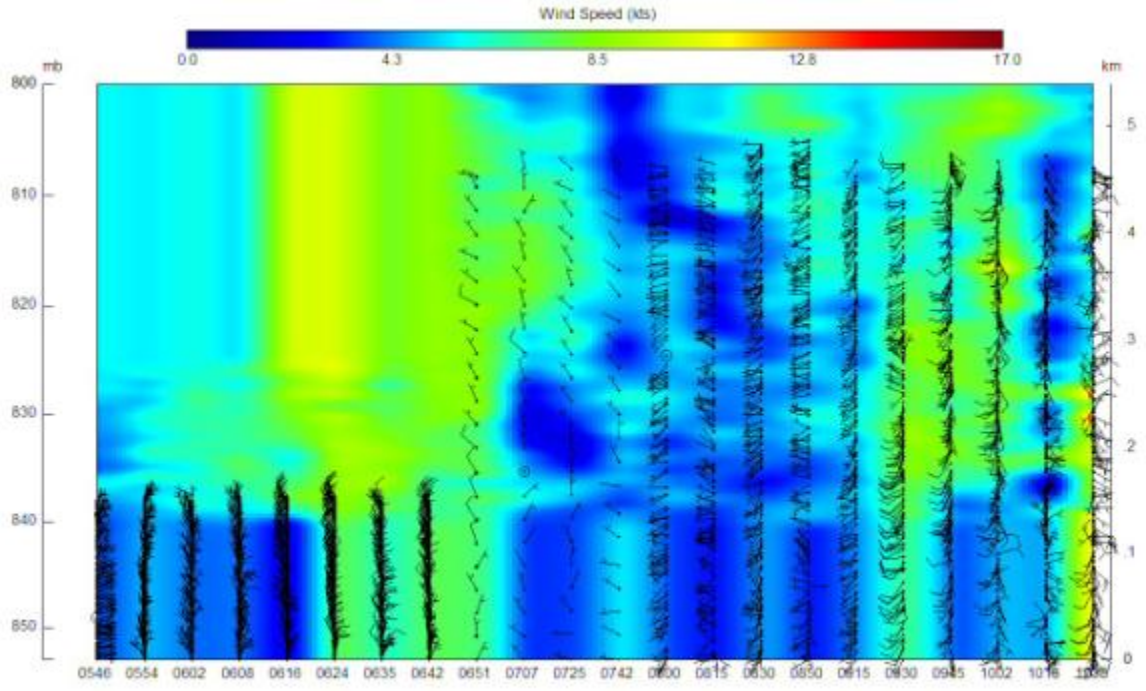

Mixing Ratio (g/kg)

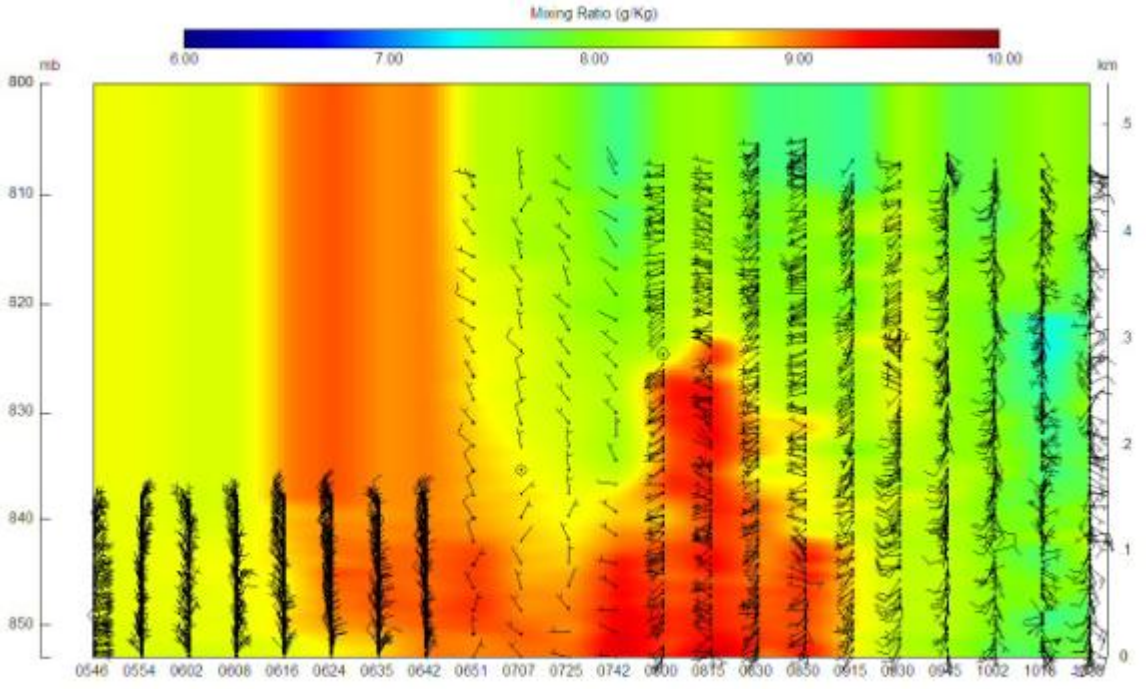

Relative Humidity (%)

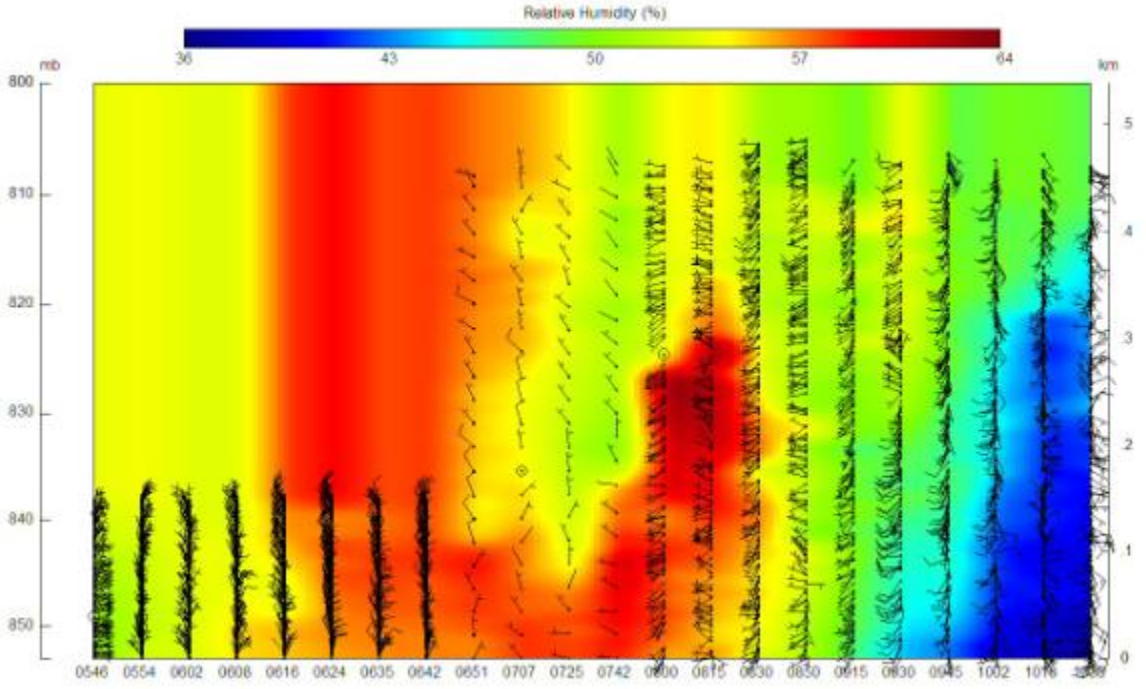

Temperature (°C)

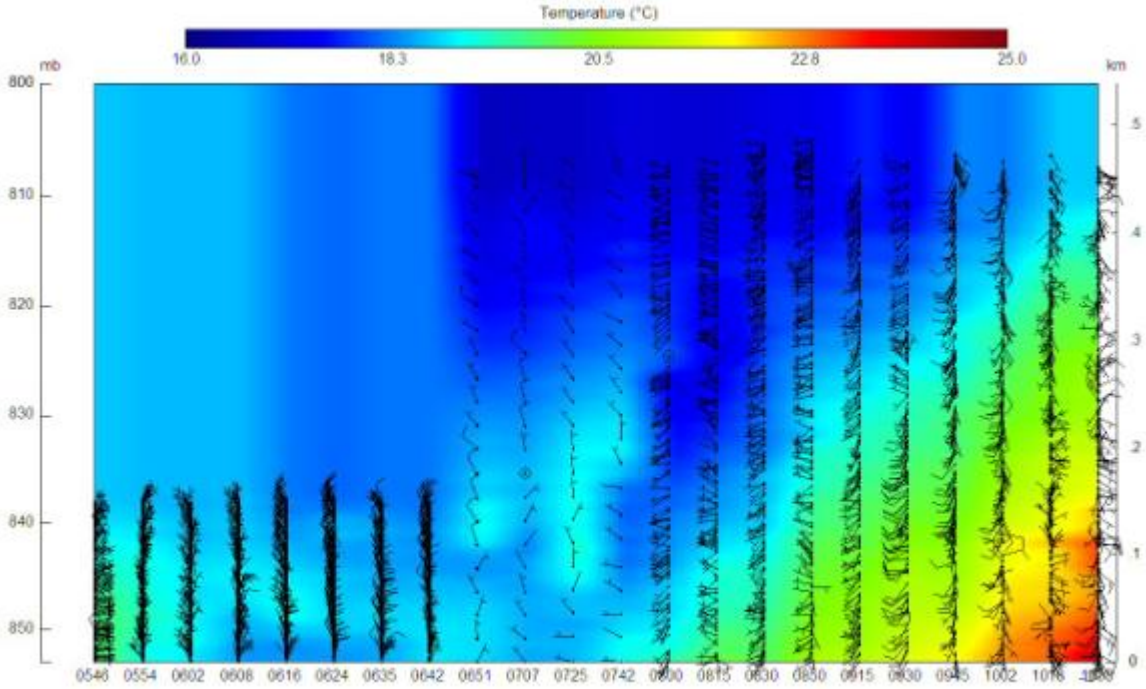

Potential Temperature (K)

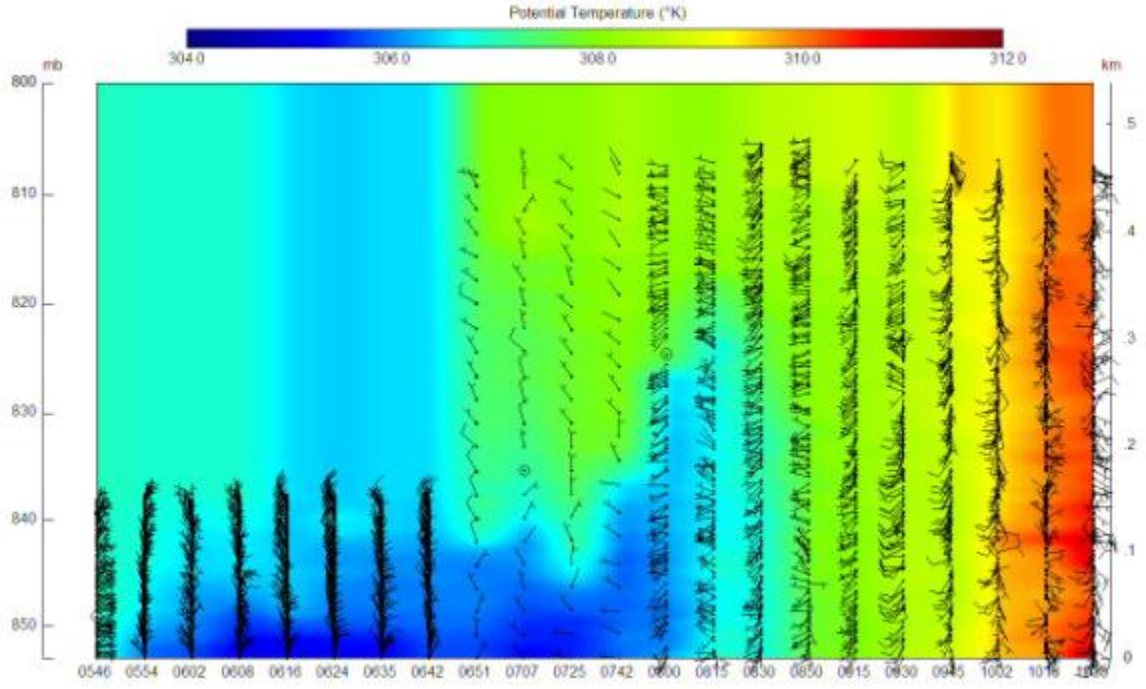

Equivalent Potential Temperature (K)

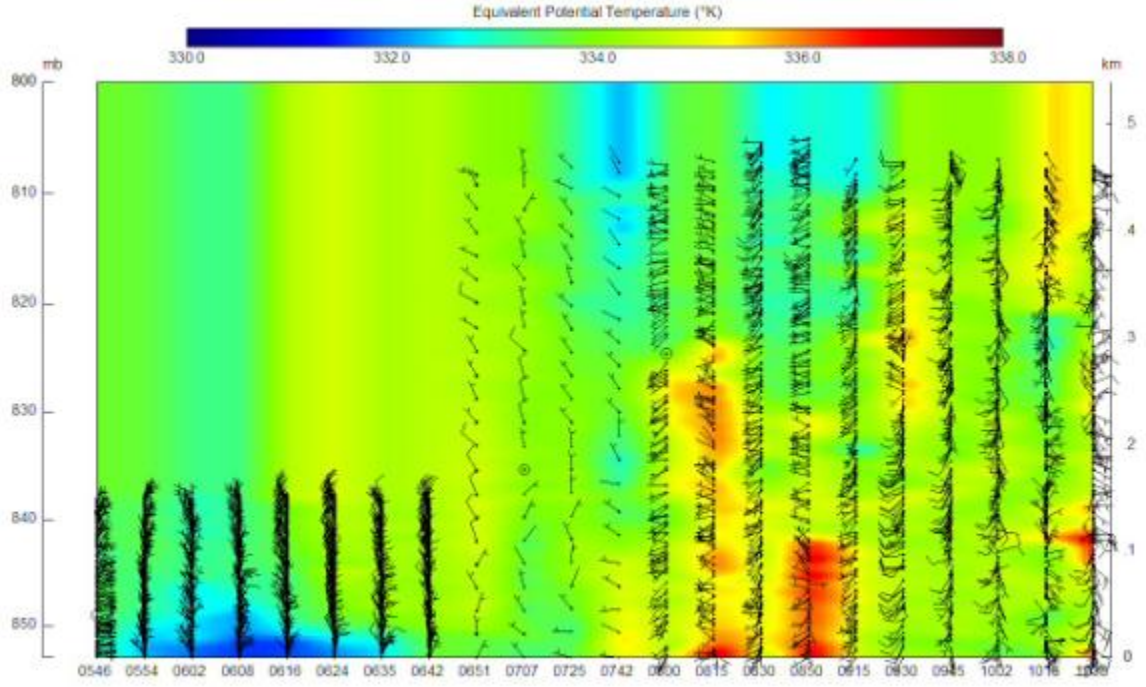

V-component of wind (knots)

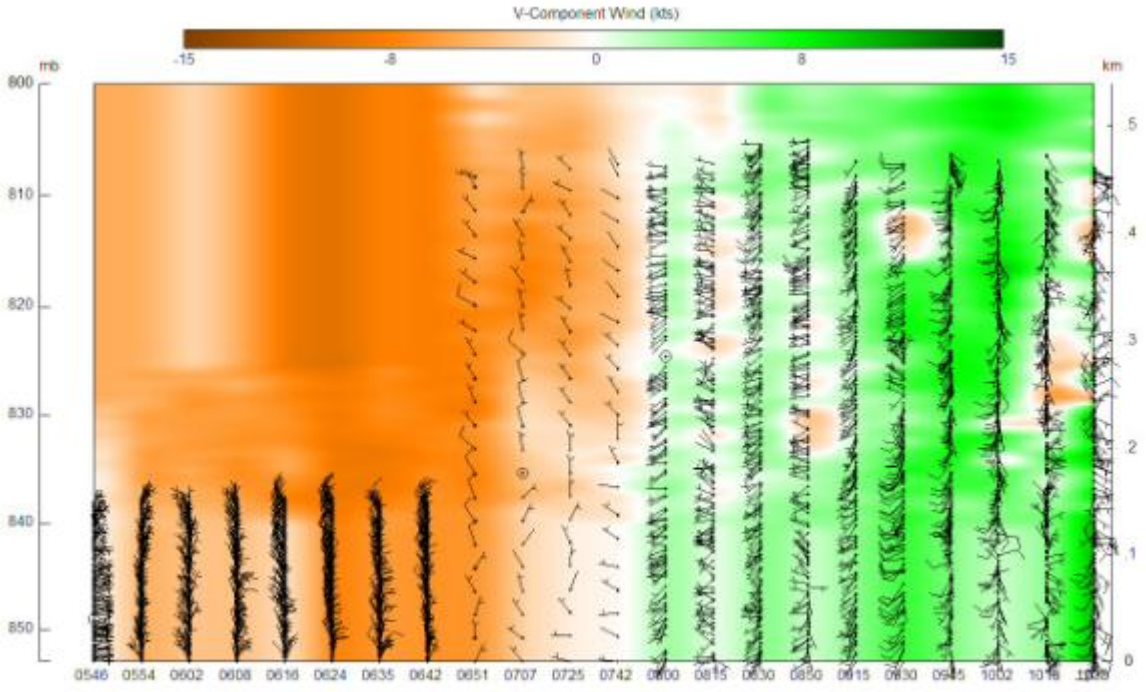

APPENDIX A-3: CEILOMETER BACKSCATTER PLOTS

– Plots of 15-minute average ceilometer backscatter during the summer IMP. Note that vertical heights need to be multiplied by 10 to get height in meters above ground.

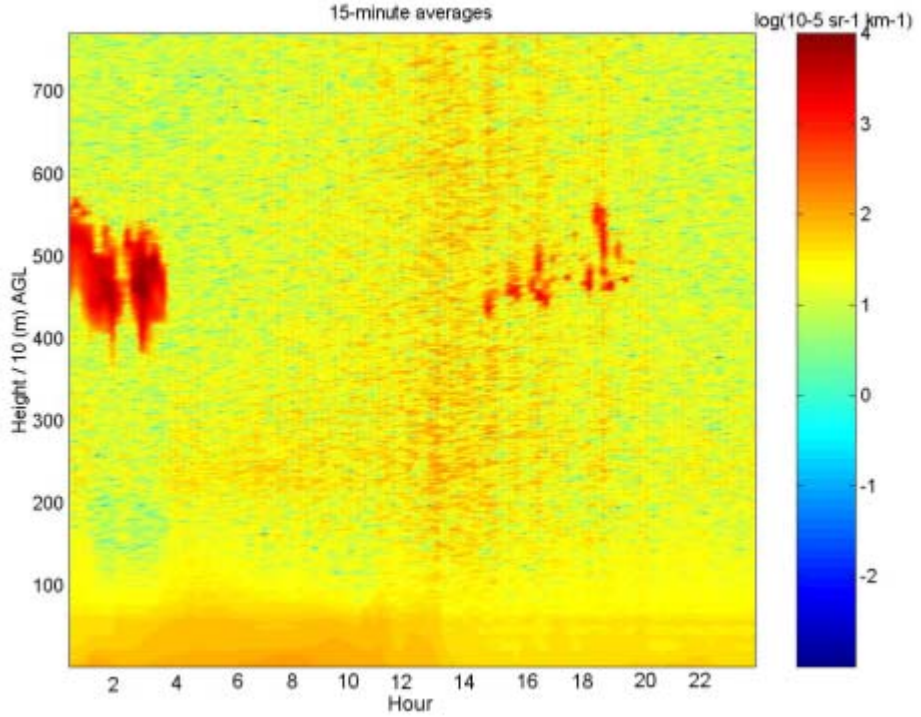

Figure 78. June 17, 2008

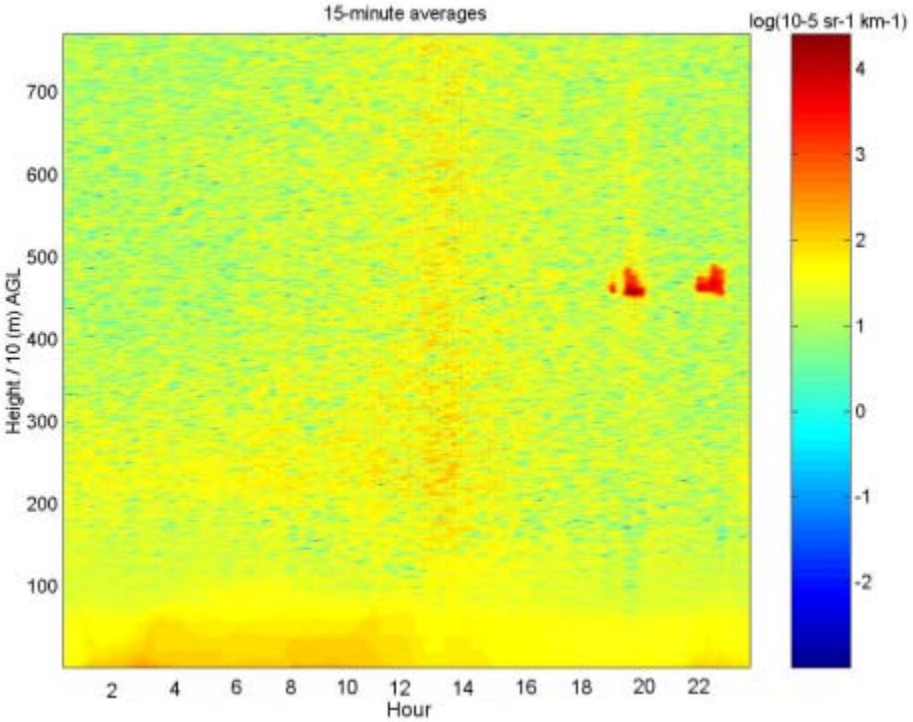

Figure 79. June 18, 2008

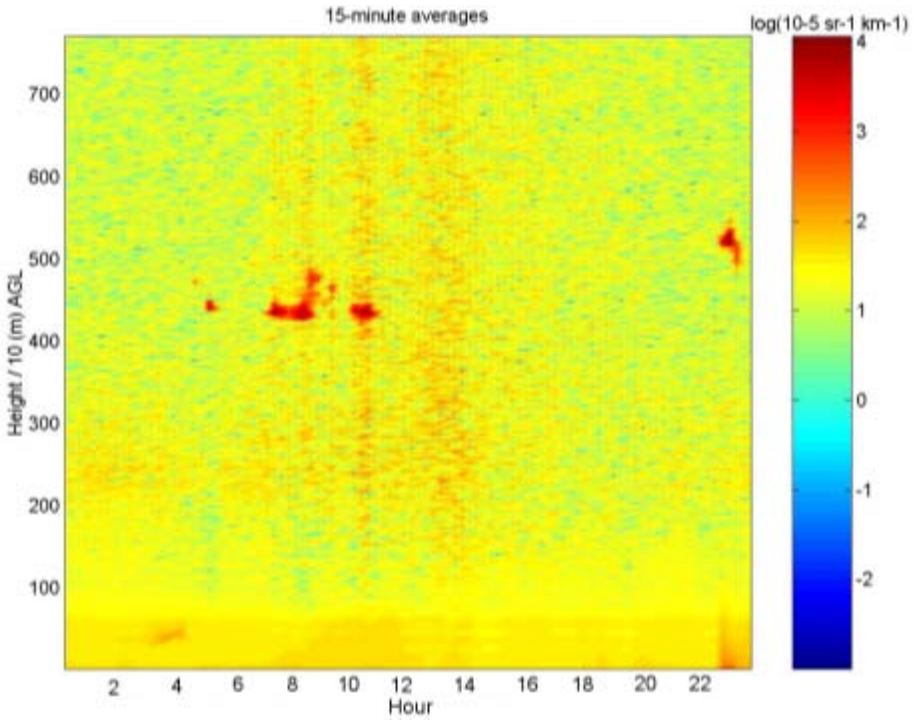

Figure 80. June 19, 2008

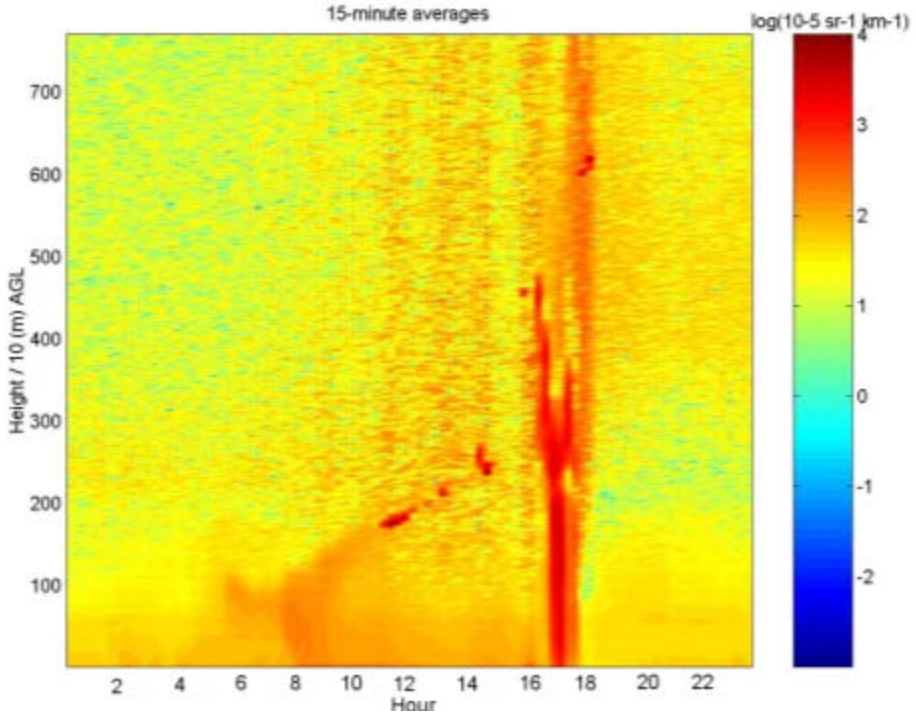

Figure 81. June 20, 2008

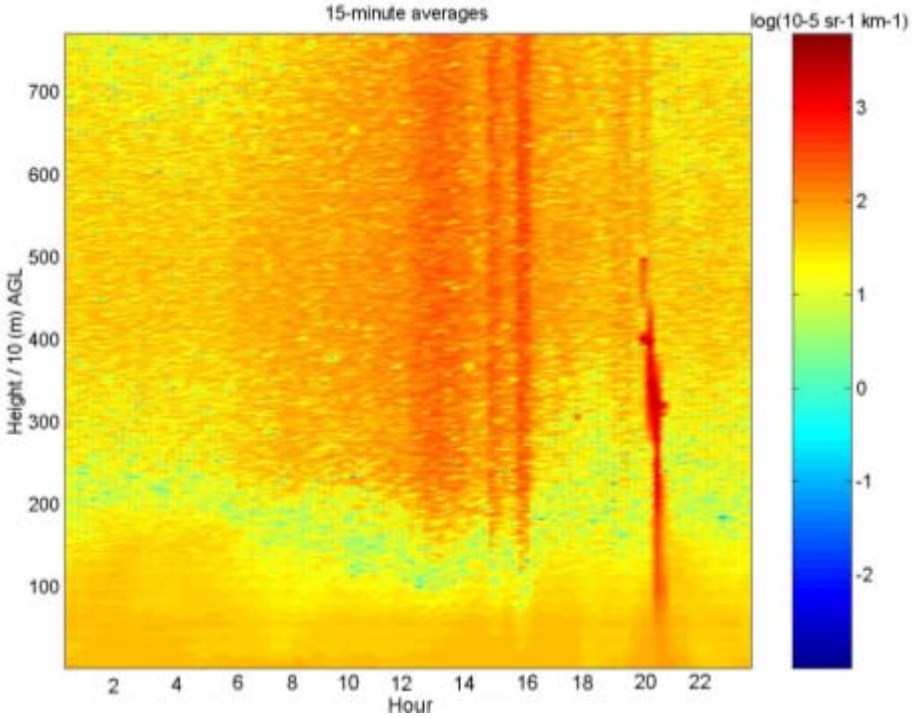

Figure 82. June 21, 2008

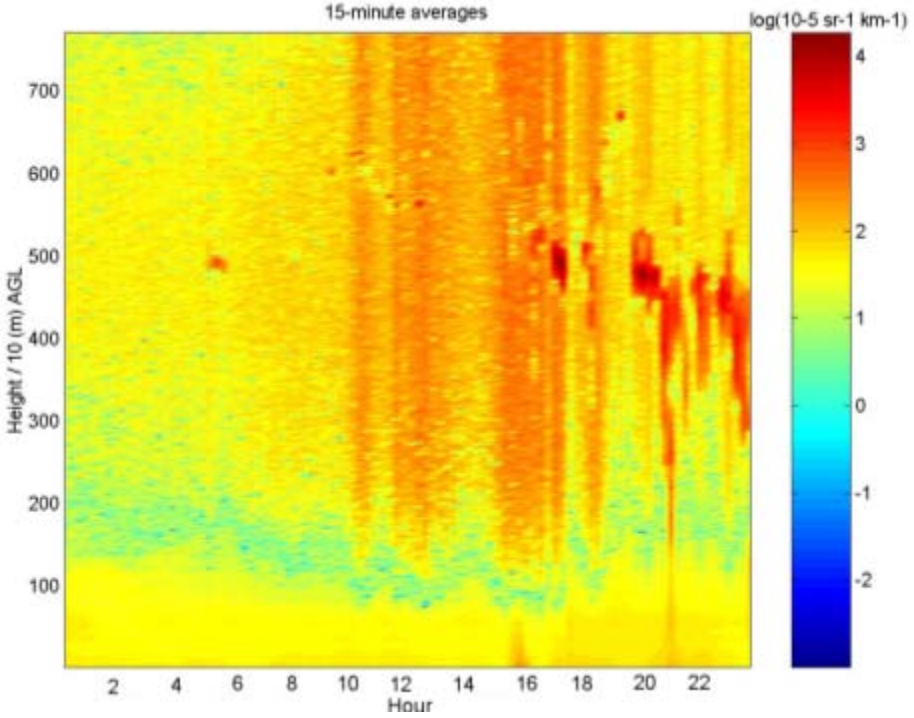

Figure 83. June 22, 2008

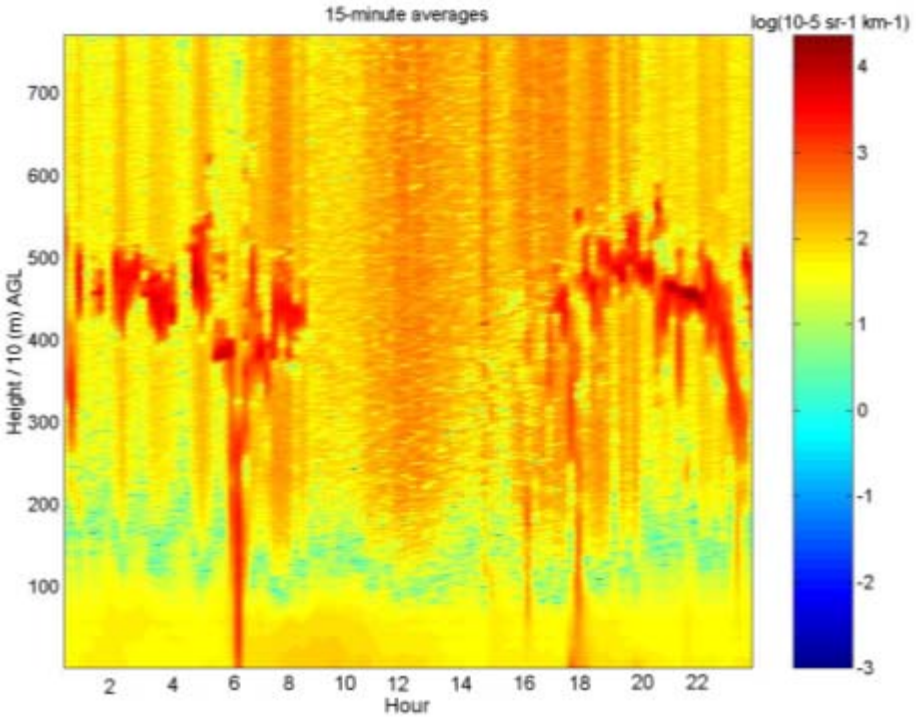

Figure 84. June 23, 2008

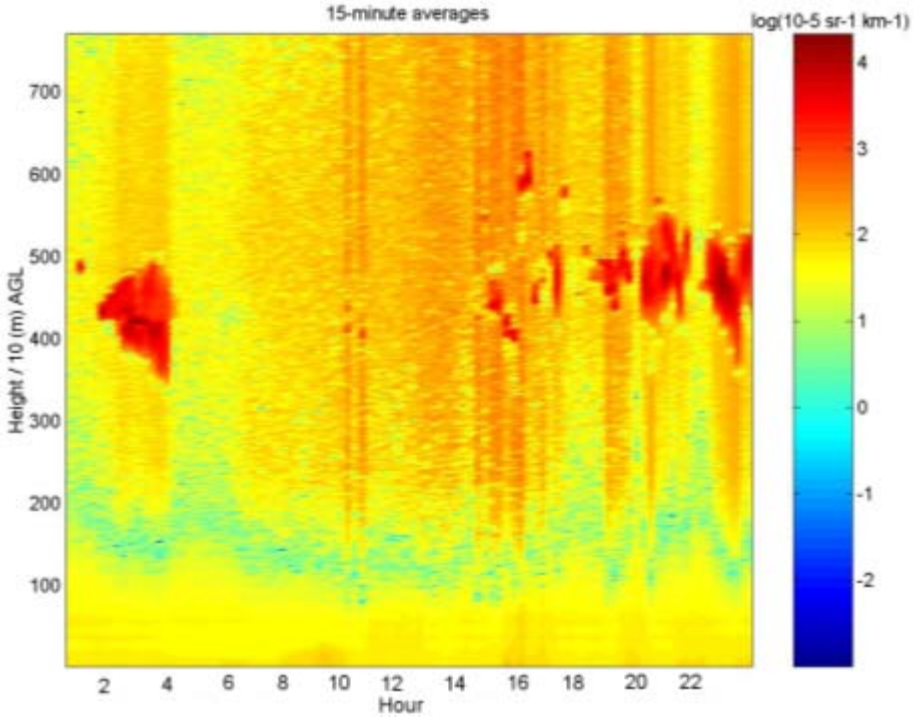

Figure 85. June 24, 2008

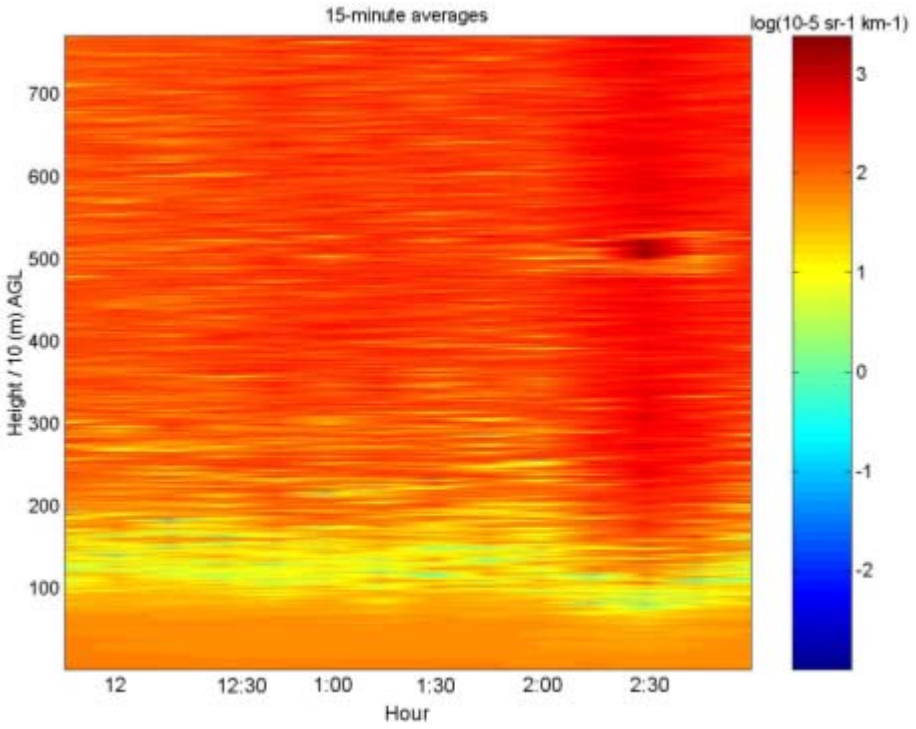

Figure 86. June 26, 2008

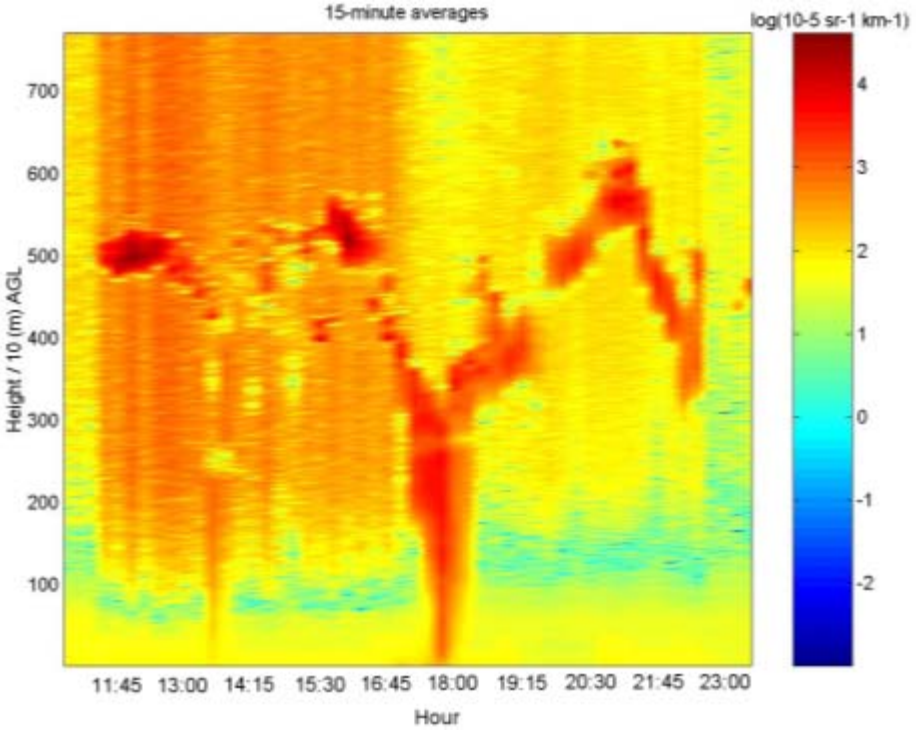

Figure 87. June 28, 2008 (2ZM)

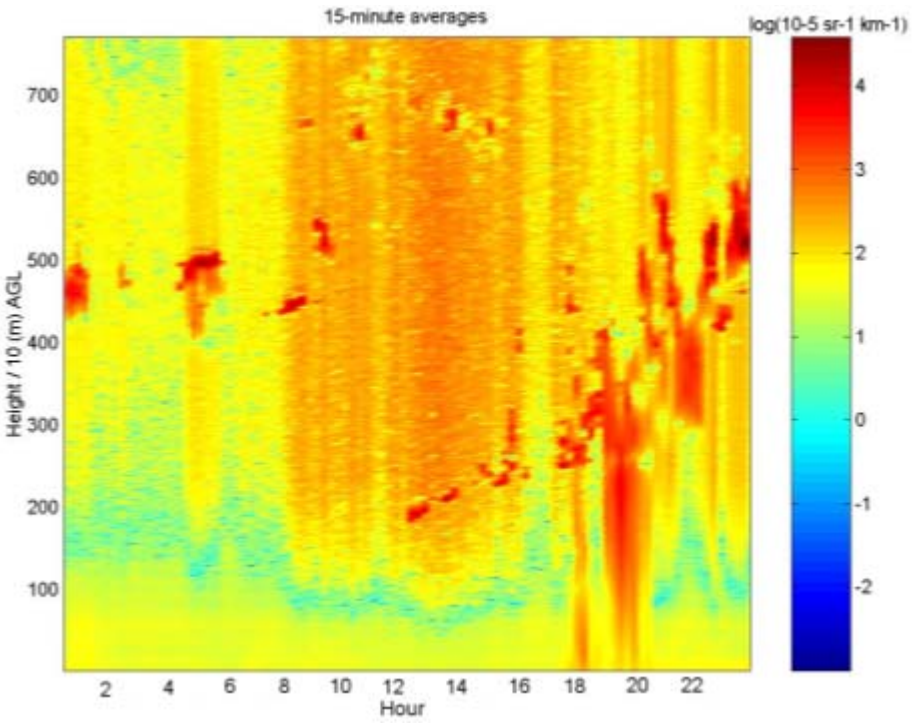

Figure 88. June 29, 2008

APPENDIX A-4: AIRPORT RADIOSONDE PROFILES

Winter IMP
12 and 00 UTC (5 am and 5 pm) soundings on Skew-T diagram

February 11, 2008

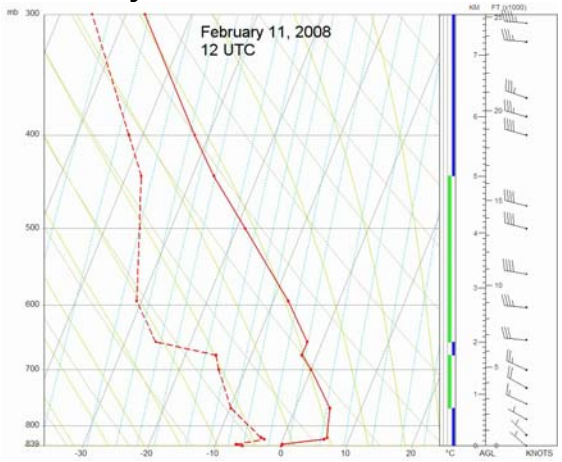

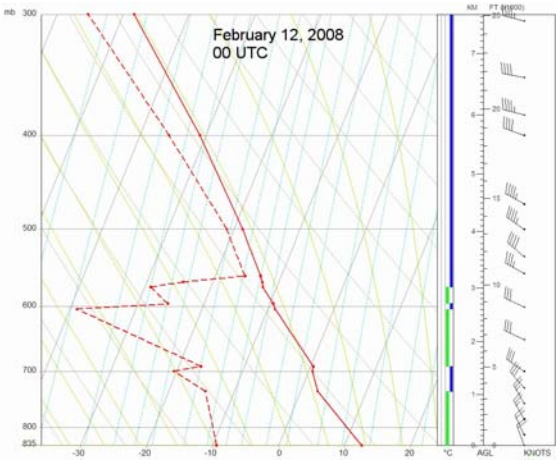

February 12, 2008

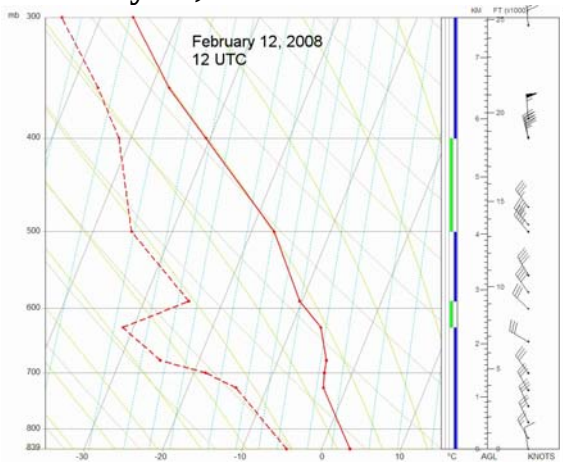

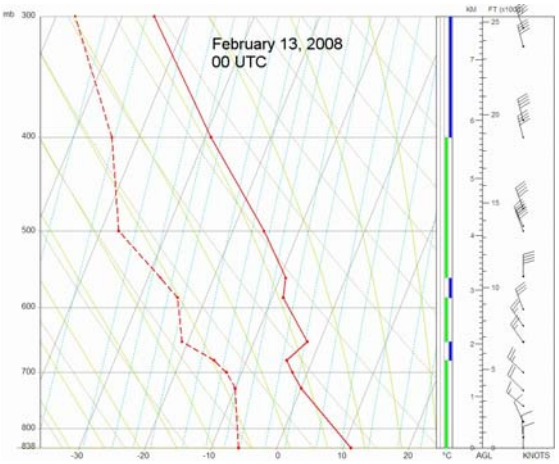

February 13, 2008

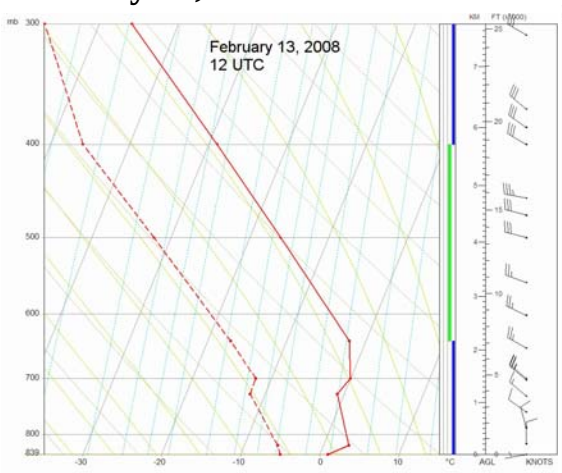

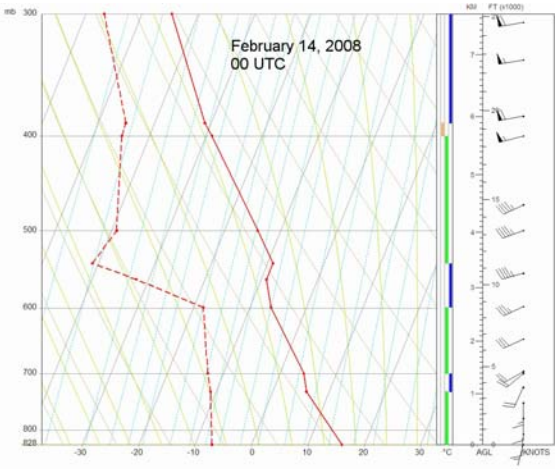

February 14, 2008

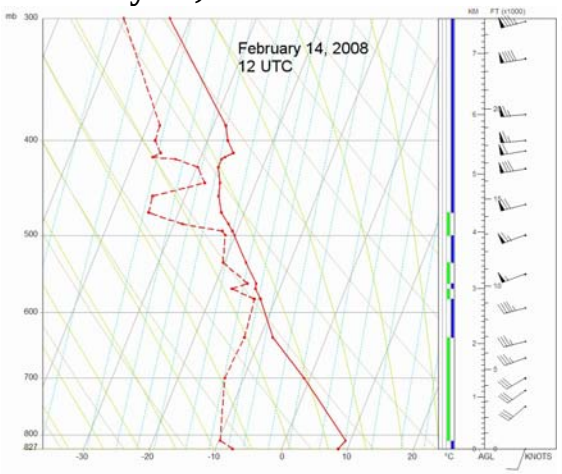

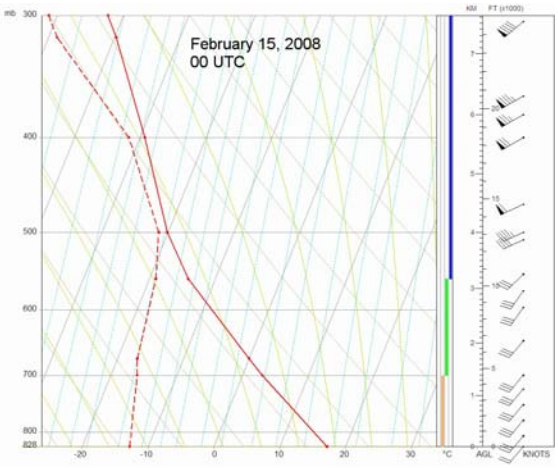

February 15, 2008

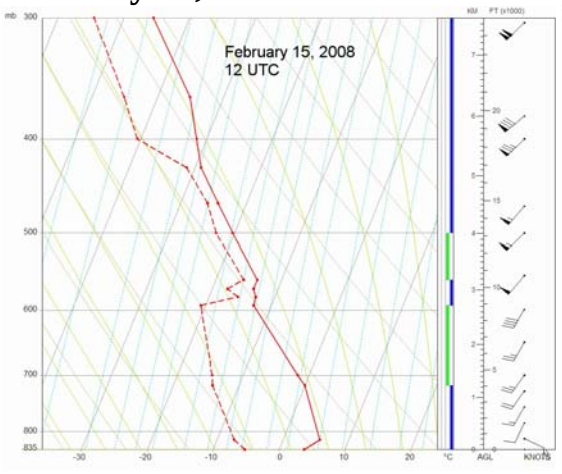

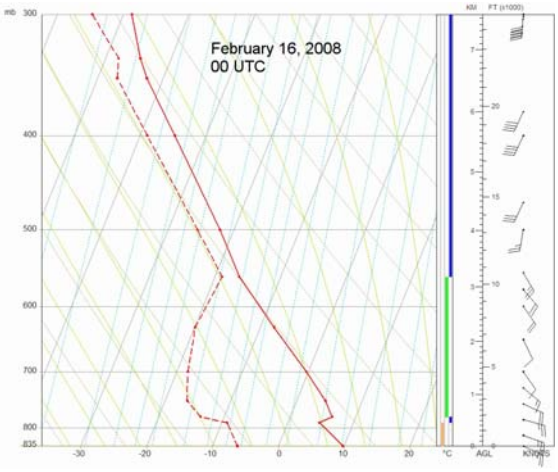

February 16, 2008

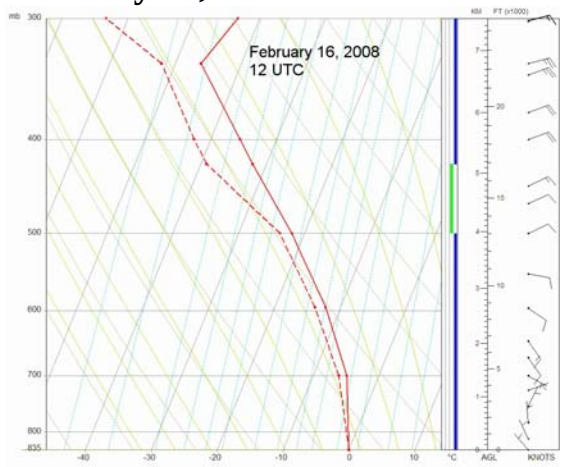

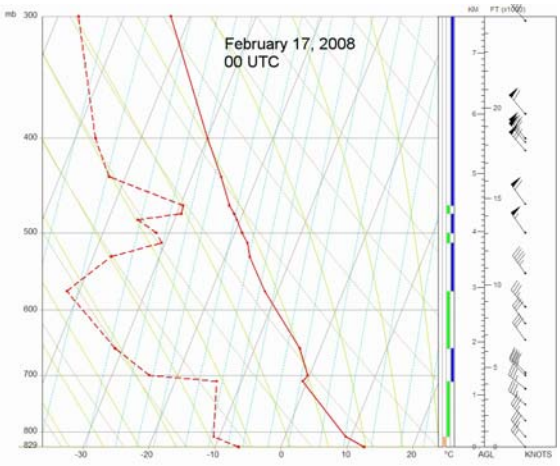

February 17, 2008

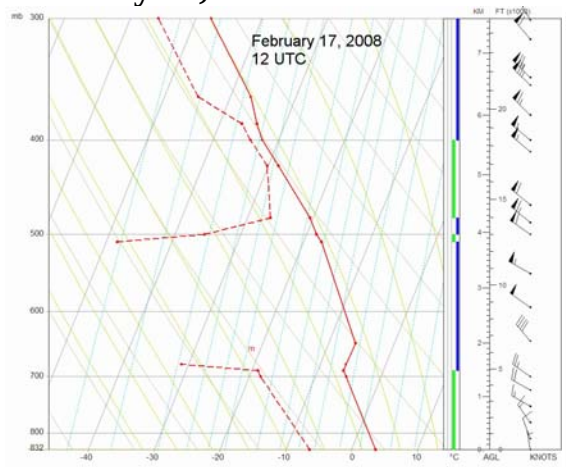

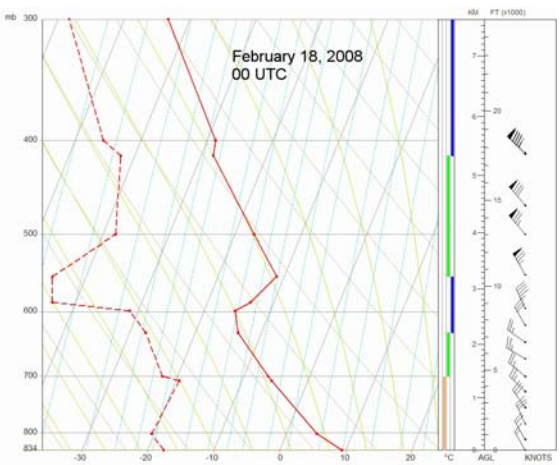

February 18, 2008

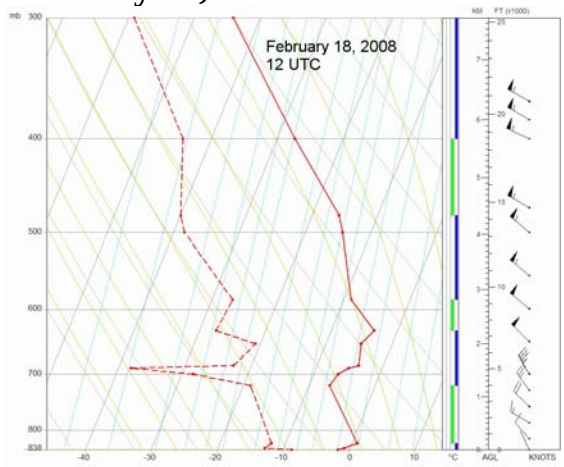

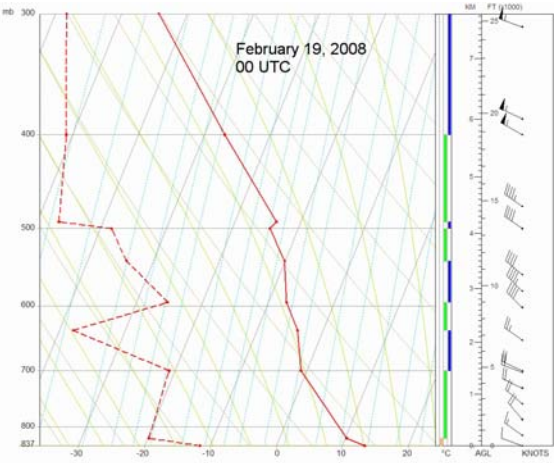

Summer IMP
12 and 00 UTC (6 am and 6 pm) soundings

June 17, 2008

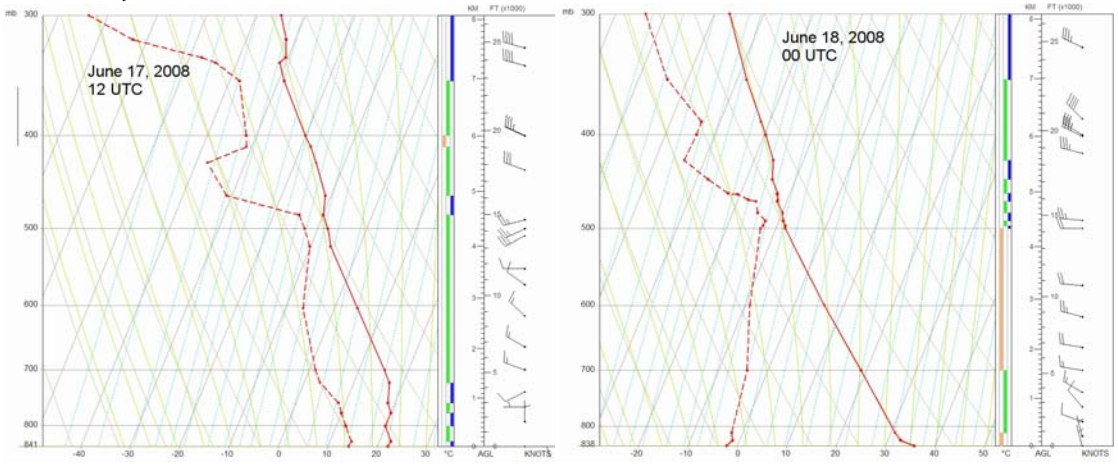

June 18, 2008

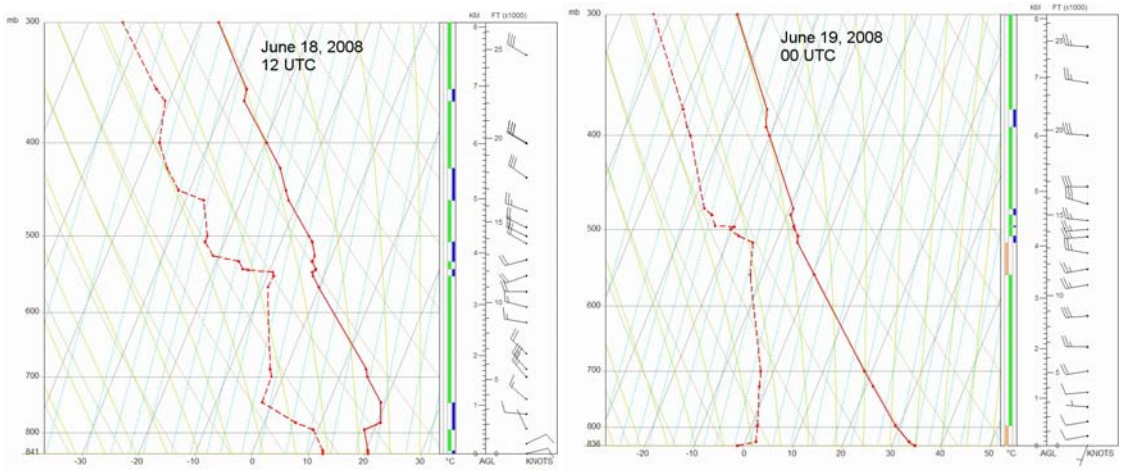

June 19, 2008

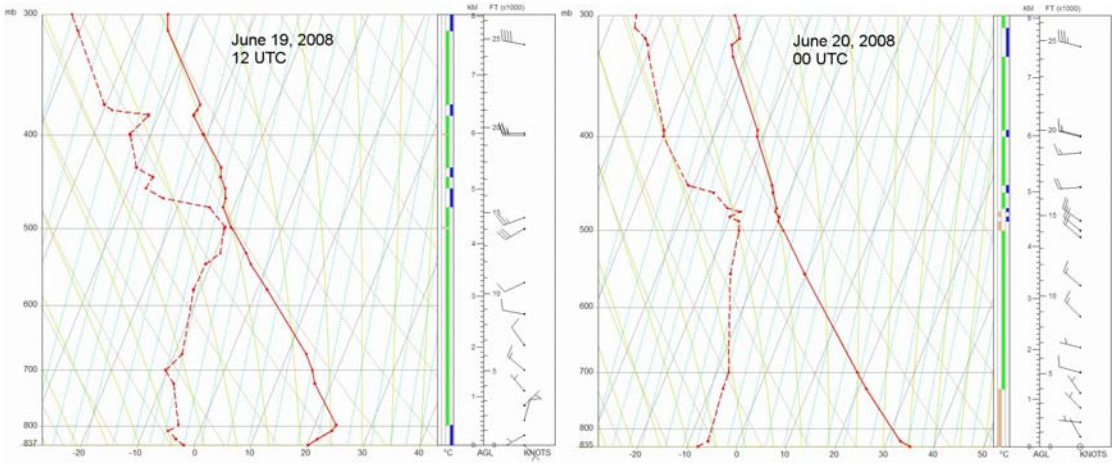

June 20, 2008

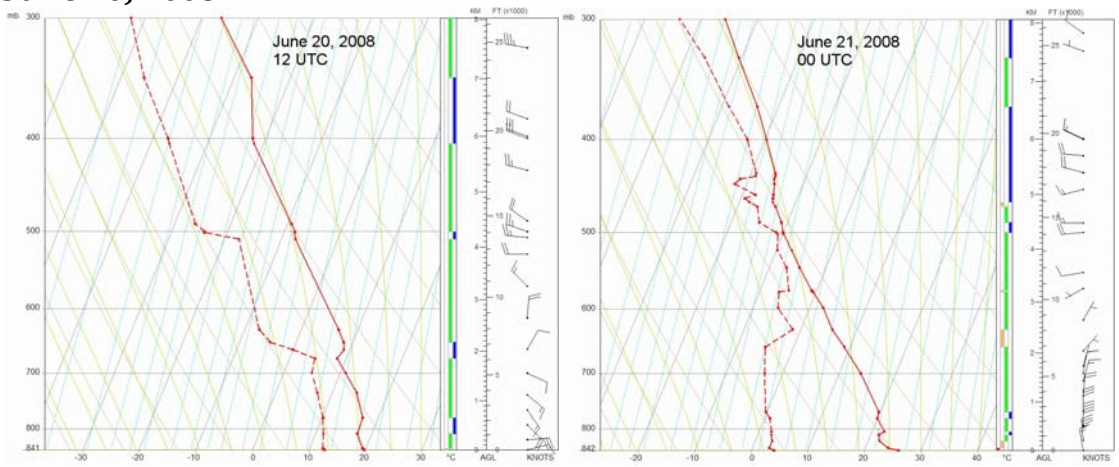

June 21, 2008

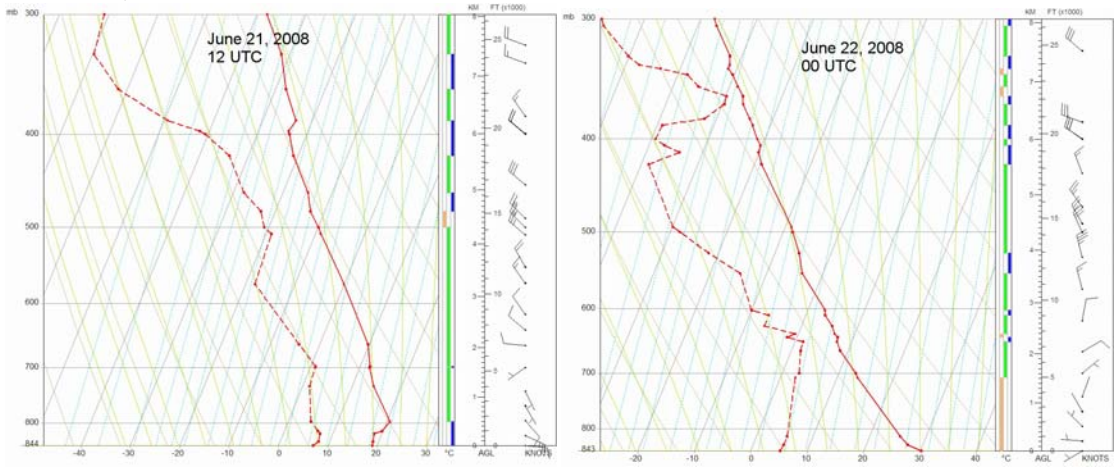

June 22, 2008

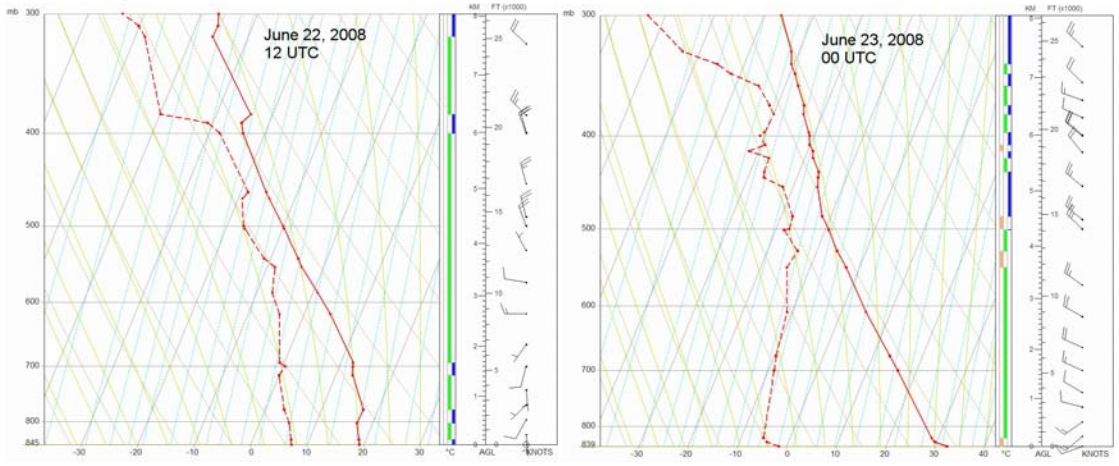

June 23, 2008

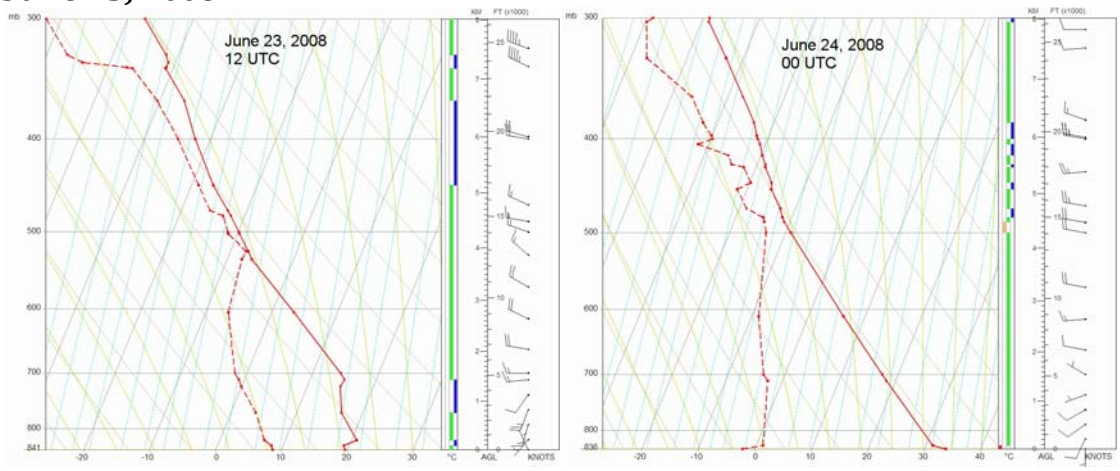

June 24, 2008

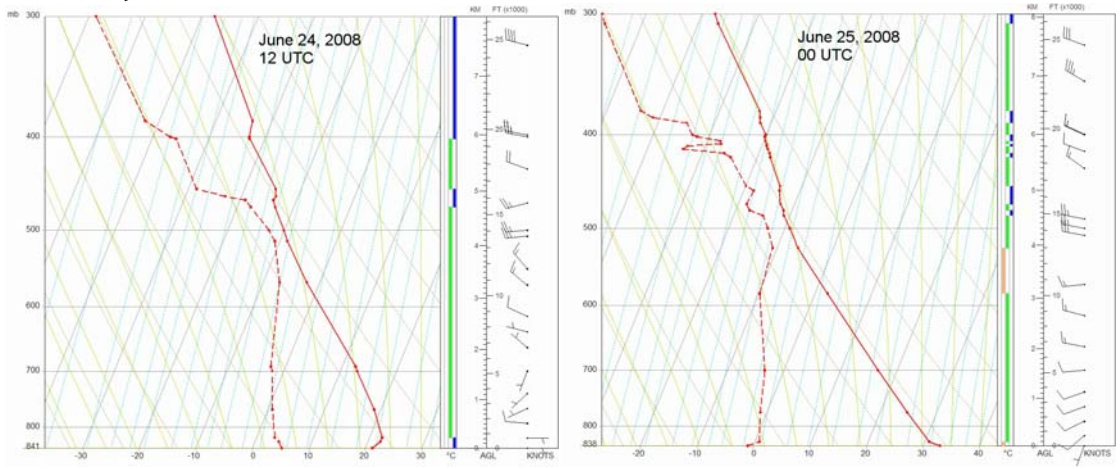

June 25, 2008

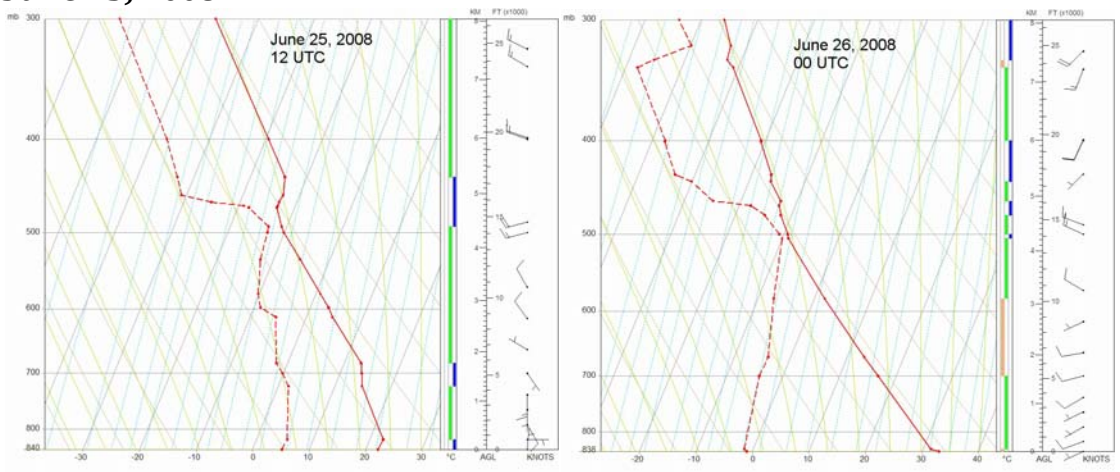

June 26, 2008

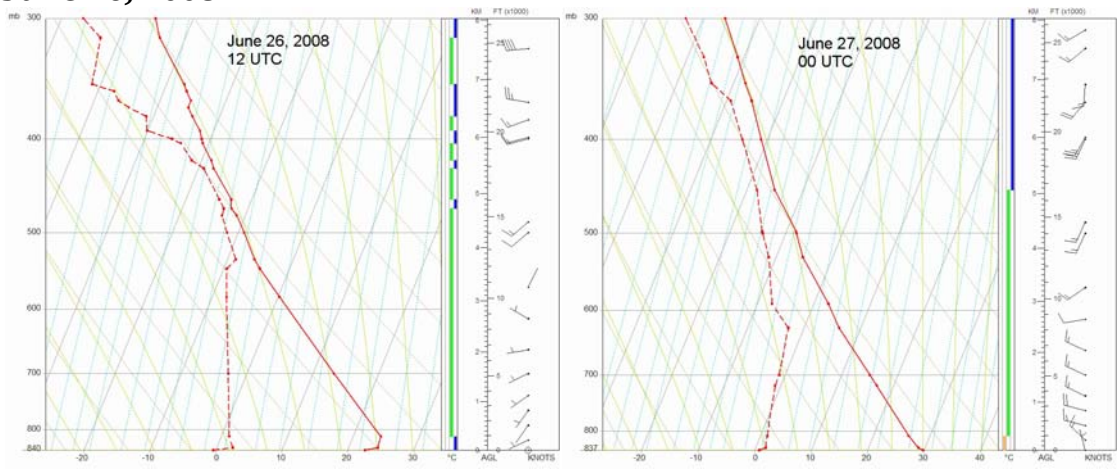

June 27, 2008

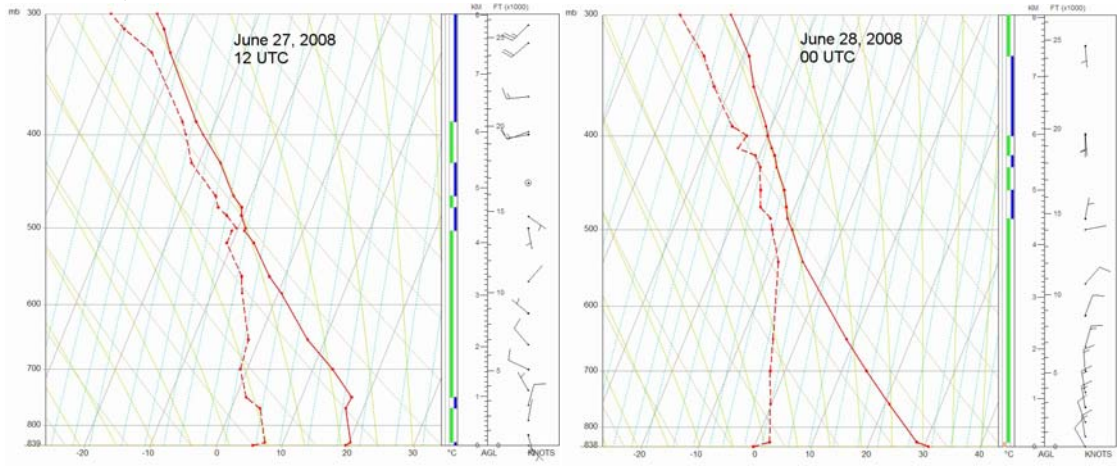

June 28, 2008

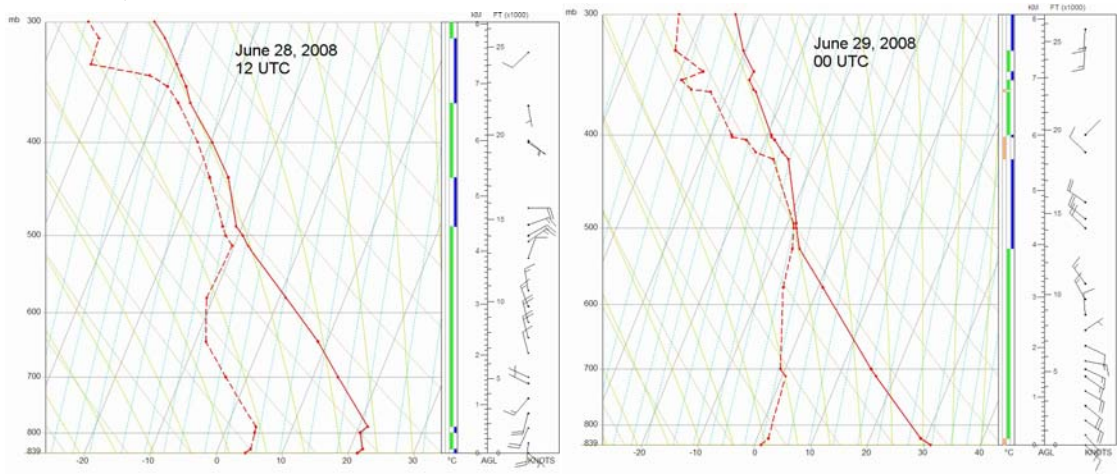

June 29, 2008

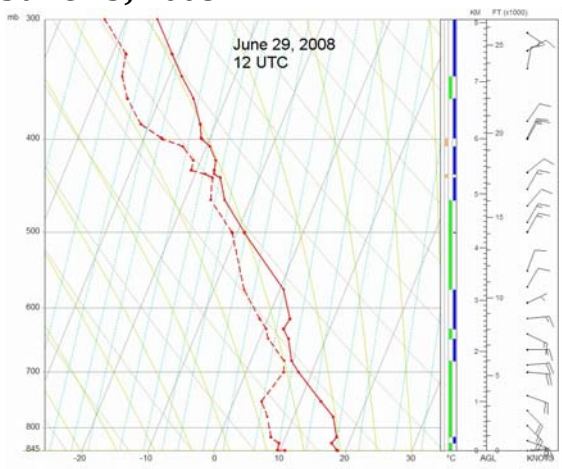

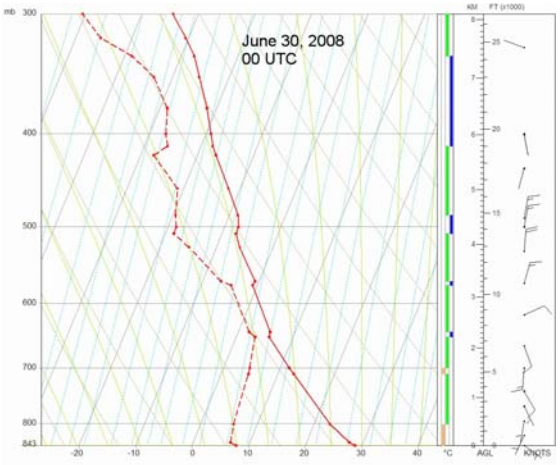

June 30, 2008

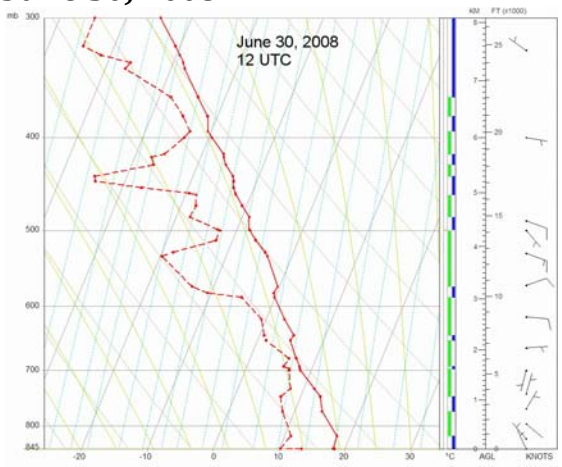

APPENDIX B

Albuquerque/Bernalillo County Community Scale Air Toxics Monitoring and Risk Assessment Project – Experimental Methods

Table of Contents

1. Intensive Monitoring Periods

The two IMPs were carried out on February 10-20, 2008 and on June 17-30, 2008. The details of each IMP and the parameters measured are presented below. Figure 1-1 shows the locations of all sites in which data were collected during one or more IMPs. Measurements during the two IMPs are categorized as follows:

- Primary, defined as those described in the award and the specifications are outlined in the QAPP (Kavouras et al., 2008). These measurements were: (*i*) continuous VOCs at the Del Norte site and; (*ii*) vertical profiles of meteorological and air quality parameters using a tethered balloon system at the Fiesta Balloon Park.

- Supplemental, defined as those obtained to understand the air transport and local conditions, but the details are not part of the QAPP. These measurements included: (*i*) temperature and relative humidity in different locations; (*ii*) meteorological and air quality parameters along the route of the tramway and; (*iii*) vertical profiles of aerosol scattering at the Del Norte and Fiesta Balloon Park.

Figure 1-1 Map showing the location of Primary Sites (Green balloons), Satellite Air Toxics sites (Yellow balloons) and Supplemental sites for both IMP (Blue balloons) or for the first IMP (Red (W) balloons)

No activities were carried out during the IMPs at the two Satellite sites in North and South Valley. At those sites, samples for HAPs were collected on a 1-in-6 day schedule.

IMP: 2/11/2008- 2/20/2008

Error! Reference source not found. describes the type and duration of measurements taken during the first IMP.

Primary measurements

Installation, calibration verification and tests of the online gas chromatography system at the Del Norte site were completed by noon on Monday, February 11, 2008. The GC system was running for the entire IMP with scheduled breaks for field blank and calibration verification tests. The operation ended on Wednesday, February 20, 2008. As a result, a total of 208 chromatograms were obtained.

Preparation, conditioning and pre-adjustment of ozonesondes sensors begun in Las Vegas 10 days prior to the arrival in Albuquerque. The electrochemical sensors of all three ozonesondes and the calibrator were prepared according to manufacturer's procedures. The final calibration and preparation for flights of the ozonesondes were completed by Wednesday, February 13, 2008. The balloon fiesta site was set up on Monday, February 11 and a Maloy container was delivered to the site as a shelter and for storage of the balloon and associated equipment. A waiver and Notice to Airmen (NOTAM) was obtained by the local FAA and the Air Traffic Control Tower (ATCT) of the Albuquerque Airport for balloon flights up to 1,500 feet AGL (450 m AGL) at this site. The waiver allowed us to operate the balloon to a maximum height of 6,600 feet MSL but since the ground elevation at the site was 5,100 feet MSL, that allowed us to 1,500 feet above the ground. We complied with the FAA regulations stated in 14 CFR section 101.13(A)(2) for operation of moored balloons. The FAA waiver had a stipulation that required us to only operate from sunrise to sunset each day. The observed sunrise actually occurred a few minutes after this due to the Sandia mountainous terrain to the east of Albuquerque. Preparations of the balloon started on Wednesday early morning under the supervision of an FAA representative. Balloon lift off was preceeded by a call to the ATCT notifying them that we are operating the balloon. A set of vertical profiles of meteorological parameters, particle number and VOCs were obtained for about four to five hours. During the preparation of the tethersonde to connect and transfer data from the ozonesonde, the tetherline that was holding the balloon broke, resulting in the immediate release and loss of the balloon. After this incident, the FAA informed us that and all tethered-balloon operations were suspended until a mitigation plan was in place to prevent this from happening again. The mitigation plan included purchasing a new and stronger 360 lb Spectra® tetherline and some operational procedures. We also found out that we could use a balloon with a diameter up to 6 feet and fly it up to 500 feet AGL at all hours of the day and night. That was very fortunate since it would have been difficult to obtain a replacement balloon from the manufacturer, Vaisala, in time for the remaining time of this IMP. Upon approval of the plan by FAA and the purchase of smaller balloons (5 and 6 ft diameter), balloon flights started again on Sunday, February 17, 2008 at 4:40 am. Because of the limited lifting capacity of the 6-ft balloons and the absence of safety valves, vertical profiles were obtained as high as 500 ft AGL (150 m AGL) but without time restrictions. We also acquired vertical profile measurements of meteorological conditions on Tuesday, February 18, 2008 from 2:00 am to 5:00 pm. Operations suspended due to high surface and aloft winds (higher than 10 m/s). As required by the FAA the ATCT was called to notify them that our measurements were completed for the February IMP.

Supplemental measurements

A set of HOBO temperature and relative humidity sensors were installed along the Paseo Del Norte Blvd. Two additional HOBO temperature/relative humidity sensors were also installed on the base and at the top of the Sandia Tramway on Monday, February 11, 2008.

A suite of temperature, relative humidity and barometric pressure sensors and, particle mass and a total VOC analyzer were installed on the roof of one of the trams on Monday, February 11, 2008 to obtain information from about the vertical profiles of the atmosphere at 1,500 to 6,500 ft above the balloon fiesta location. Measurements were obtained during the regular flights of the tramway.

Air Toxics measurements

During the first IMP, two sets of 24-h samples for VOCs and carbonyls were collected on Wednesday, February 12, 2008 and February 18, 2008 at Del Norte, North Valley and South Valley.

Table 1-1 Description of measurements during the first IMP (February 11 – February 19, 2008)

Description		11	12	13	14	15	16	17	18	19
VOCs (hourly) at Del Norte site		x	x	x	x	x	x	x	x	x
9 m^3 tethered balloon, altitude <500 m AGL; only daytime	Temp.			x						
	RH			x						
	Pressure			x						
	Wind direction			x						
	Wind speed			x						
	Particle number			*x*						
	VOCs			x						
6 ft tethered balloon, altitude <150 m AGL, night and day	Temp.						x	x	x	
	RH						x	x	x	
	Pressure						x	x	x	
	Wind direction						x	x	x	
	Wind speed						x	x	x	
Outdoor HOBO temperature/relative humidity sensors at Sandia Tramway route (three locations)		*x*	*x*	*x*	*x*	*x*	*x*	*x*	*x*	*x*
Outdoor HOBO temperature/relative humidity sensor along Paseo del Norte (four locations)						*x*	*x*	*x*	*x*	*x*
Hourly surface meteorological data at the balloon fiesta site from the 15 foot tower		*x*	*x*	*x*	*x*	*x*	*x*	*x*	*x*	*x*
Vertical profiles of temperature and relative humidity on tram			*x*	*x*	*x*	*x*	*x*	*x*		

IMP: 6/17/2008- 6/30/2008

Table 1-2 describes the type and duration of measurements taken during the second IMP.

Primary measurements

Installation, calibration, verification and tests of the online gas chromatography system at the Del Norte site were completed by noon on Monday, June 16, 2008. The GC system was running for the entire IMP with scheduled breaks for field blank and calibration tests. The operation ended on Monday, June 30, 2008. As a result, a total of 296 chromatograms were collected.

Preparation, conditioning and pre-adjustment of ozonesonde sensors begun in Las Vegas 10 days prior to the arrival in Albuquerque. The electrochemical sensors of all three ozonesondes and the calibrator were prepared according to manufacturer's procedures. The final calibration and preparation for flights of the ozonesondes was completed by Friday, June 20, 2008. A waiver and NOTAM was obtained by the local FAA and the Control Tower of the Albuquerque Airport for balloon flights up to 1,500 feet AGL (450 m AGL) at this site. The FAA waiver had a stipulation that required us to operate from sunrise to sunset each day for flying up to 450 m AGL. The observed sunrise actually occurred a few minutes after this due to the Sandia mountainous terrain to the east of Albuquerque. A set of vertical profiles of meteorological parameters were first obtained on June 23 starting in the morning. We began the study using the 6 foot diameter balloons in order to fly any time of the day. The 6 foot balloons were the only means of measuring profiles at night because of FAA regulations. We used the 6 foot balloons during the day as well to minimize the down time in switching balloons. Because of the limited lifting capacity of the balloons and the absence of safety valves, vertical profiles were obtained as high as 500 ft AGL (150 m AGL) during the night. With exception of June 25, balloon operations were done daily. Operations of the tethered balloons were completed on June 30, 2008.

Supplemental measurements

A suite of temperature, relative humidity and barometric pressure sensors and, particle mass and total VOC analyzer were installed on the roof of one of the trams on Tuesday, June 17, 2008 to obtain information from about 1,500 to 6,500 ft above the balloon fiesta base. Measurements were obtained during the regular flights of the tramway. Three HOBO Pro v2 temperature and relative humidity sensors were installed at the tram base, near the first tower and on the top of the Sandia Tramway on Monday, June 16, 2008. A 2B Technologies portable ozone monitor was installed on the top of the Sandia Peak on Wednesday, June 25, 2008.

Air Toxics measurements

Three samples of VOCs and carbonyl were collected on June 17, 2008, June 23, 2008 and June 30, 2008 and only one set of PAHs and heavy metals were collected on June 23, 2008 during the second IMP.

Table 1-2 Description of measurements during the second IMP (June 16 – June 30, 2008)

Description		16	17	18	19	20	21	22	23	24	25	26	27	28	29	30
VOCs (hourly) at Del Norte site		x	x	x	x	x	x	x	x	x	x	x	x	x	x	x
6 ft tethered	Temp.								x	x		x	x	x	x	

balloon, altitude <450 m AGL; daytime	RH								x	x		x	x	x	x	
	Pressure								x	x		x	x	x	x	
	Wind direction								x	x		x	x	x	x	
	Wind speed								x	x		x	x	x	x	
	O_3								x	x		x	x	x	x	
6 ft tethered balloon, altitude <150 m AGL, night	Temp.								x	x		x	x	x	x	
	RH								x	x		x	x	x	x	
	Pressure								x	x		x	x	x	x	
	Wind direction								x	x		x	x	x	x	
	Wind speed								x	x		x	x	x	x	
	O_3								x						x	
Outdoor HOBO temperature/relative humidity sensors at Sandia Tramway route (four locations)		*x*	*x*	*x*	*x*	*x*	*x*	*x*	*x*	*x*	*x*	*x*	*x*	*x*	*x*	*x*
2B portable ozone monitor at the Sandia Peak				*x*	*x*	*x*	*x*	*x*	*x*	*x*	*x*	*x*	*x*	*x*	*x*	*x*
Lidar (ceilometer) for aerosol vertical profiling		*x*	*x*	*x*	*x*	*x*	*x*	*x*	*x*	*x*	*x*	*x*	*x*	*x*	*x*	*x*

Description of the primary sites

The Del Norte air monitoring station and the site at Fiesta Balloon facility are shown in Table 1-3. A detailed description of the sites is presented in the QAPP for this study (Kavouras et al., 2008).

Table 1-3. Summary of Del Norte air monitoring site and the Fiesta Balloon location.

Site	Coordinates (NAD83 datum)	Location	Purpose
Del Norte	Lat: 35° 8’ 3.51” N Lon: 116° 35’ 6.67”W Elev: 814 m MSL	San Mateo Ln NE	Urban area, centrally-located site
Balloon Fiesta Park	Lat: 35° 12’ 1.91” N Lon: 106° 35’ 38.27”W Elev: 1,261 m MSL	Balloon Fiesta Pkwy	Open-dirt field for tethered-balloon flights

1.1.1 Del Norte Air Monitoring Site

The Del Norte air monitoring site (2ZM; EPA Site ID: 350010023) is adjacent to the Del Norte High School at the intersection of Montgomery Blvd NE and San Mateo Blvd NE (0.23 miles northeast of the intersection). This site has been used in a previous pilot-scale air toxics study (PCMP [2],[3]). The site is 0.06 miles east of San Mateo Blvd NE, 0.23 miles north of Montgomery Blvd NE, 0.30 miles south of McLeod Rd NE and 0.43 miles west of San Pedro Dr

NE (Figure 1-2). Both San Mateo and Montgomery Blvds are characterized by high traffic density. There are also a number of area sources that cover more than 2 million square feet such as filling stations, dry cleaners and automotive repair shops. The nearest business is Blaynes's Auto Superstore, a small used car dealer to the north of the site across the street. The site is also close to a small street (San Mateo Lane) that is frequented by school buses in the afternoon delivering children to the apartment complexes near the site.

O_3, CO, NO_x and meteorological parameters are currently monitored at this site by AQD. PM_{10} and $PM_{2.5}$ are also measured on a 1-in-6 day schedule. The site is also part of the Speciation Trends Network (STN) that determines the chemical composition of $PM_{2.5}$ on a 1-in-6 day schedule. A nephelometer is also operated at the site providing continuous light scattering, and an Aethelometer provides continuous Elemental/Organic Carbon (EC/OC) data.

Figure 1-2 Location of the monitoring site at Del Norte (Google Earth).

1.1.2 Balloon Fiesta Site

The Balloon Fiesta Park site was chosen to launch the tethered balloon flights during the two intensive periods. The site is located on the north end of the Balloon Fiesta facility at the end of Balloon Fiesta Parkway. The Balloon Fiesta Park is a 0.53 x 0.25 mile open area used to launch hot air balloons and for other outdoor activities and events. The site is 0.92 miles east of 2nd St NW, 1.09 miles north of Alameda Blvd NE, 0.46 miles south of Roy Ave NW and 0.90 miles west of Interstate-25 (Figure 1-3). A railroad is 0.20 miles west of the site. The park is about 1.3

miles east of the Rio Grande River, 4.45 miles north of the Del Norte monitoring site and 1.18 miles east of the North Valley site. The Tramway base is located 6.63 miles east of the Fiesta Balloon Park.

Figure 1-3 Location of the tethered balloon measurements at the Fiesta Balloon Park

Measurement Methods

Table 1-4 shows the instrumentation used for the monitoring of volatile organic compounds, O_3, and meteorological parameters as well as supplemental measurements taken during the IMPs. Description of the instruments, quality control requirements, calibration and maintenance procedures, and data management and validation are included in the Quality Assurance Project Plan for the City of Albuquerque Air Toxics Risk Assessment Study (Kavouras et al, 2008).

Table 1-4 Instrumentation for primary and supplemental measurements

Parameter	Instrument
Primary	
Volatile Organic Compounds	SRI TO-14 Gas Chromatography System
Total VOCs	RAE Systems ppbRAE
Vertical profiles	
Meteorological parameters	Vaisala Tethersonde
Ozone	Vaisala Ozonesonde

Total VOCs	RAE Systems ppbRAE
Supplemental	
Vertical profiles	
Meteorological parameters	HOBO Temperature/Relative humidity sensor Campbell barometric pressure sensor
Particle mass	TSI Dust Trak Model 8520
Particle number concentration	TSI CPC 3007 counter
Temperature/Relative humidity in four fixed locations	HOBO Temperature/Relative humidity sensor
Aerosol profiles	Vaisala CL31 laser ceilometer

1.1.3 Volatile Organic Compounds

A SRI TO-14 gas chromatography (GC) system composed of: (*i*) a complete sampling system (dryer, trap, mass flow meter, vacuum pump); (*ii*) a fully automated calibration system (clean air, calibration standard, regulators, dilution chamber); (*iii*) an analysis system (a temperature-controlled oven (capillary column) and; (*iv*) three in-series detectors (flame ionization (FID) (for hydrocarbons), photo-ionization (PID) (for aromatic hydrocarbons) and dry-electrolytic conductivity (DELCD) for halogen-hydrocarbons) was used to measure VOCs. The instrument was installed at the Del Norte site. A sampling copper line of approximately 3 meters (ID of 0.63 cm) was used to draw air from outside. A 47-mm Teflon filter was installed at the front of the sampling line to remove particles. The line was about 3 meters above ground and away from vertical structures or inlets of other samplers.

Figure 1-4 Photograph of the online GC system at the Del Norte site and the sampling inlet (left insert)

For the first IMP, a sample was collected for the first fifteen minutes of the run and was analyzed using a 35-minute temperature program A different method was used during the second IMP to collect a large volume of ambient air. For this method, a sample was collected for 45 min and analyzed. This was achieved by collecting an air sample for the last 45 minutes of a run. This sample was then analyzed during the second run using an 1-hour temperature program. During the last 45 minutes of the second run, a sample air was drawn that was subsequently analyzed during the third run. A multi-component certified calibration standard was obtained from Scott Specialty Gases (Item No. 0102AZ00004ZCL. The mixture was composed of 42 organic compounds. Table 1-5 presents the composition, molecular weight, concentration and accuracy of the calibration standard.

Table 1-5 Composition, concentration and accuracy of air toxics calibration mixture

Compound	Molecular weight (g/mol)	Conc. (ppm)	Accurary (%)
Acrylonitrile	53.062	1.07	± 10
Benzene	78.111	1.05	± 10
Bromomethane	94.938	1.04	± 10
1,3-Butadiene	54.090	1.04	± 10
Carbon tetrachloride	153.822	1.05	± 10
Chlorobenzene	112.556	1.06	± 10
Chloroform	119.377	1.05	± 10
3-Chloro-1-propene	76.524	1.07	± 10

cis-1,3-Dichloropropene	110.969	1.05	± 10
cis-1,2-Dichloroethylene	96.943	1.05	± 10
1,2-Dibromoethane	187.861	1.05	± 10
1,2-Dichlorobenzene	197.002	1.04	± 10
1,3-Dichlorobenzene	197.002	1.05	± 10
1,4-Dichlorobenzene	197.002	1.05	± 10
Dichlorodifluoromethane	120.913	1.04	± 10
1,1-Dichloroethane	98.959	1.05	± 10
1,2-Dichloroethane	98.959	1.03	± 10
1,2-Dichloropropane	118.985	1.05	± 10
1,1-Dichloroethylene	96.943	1.05	± 10
1,2-Dichlorotetrafluoroethane	170.921	1.04	± 10
1-Ethyl-4-methylbenzene	120.191	1.07	± 10
Ethyl-benzene	106.165	1.04	± 10
Ethyl-chloride	64.519	1.02	± 10
Hexachloro-1,3-butadiene	260.760	0.945	± 10
Methyl-chloride	50.487	1.04	± 10
Styrene	104.141	1.04	± 10
1,1,2,2-Tetrachloroethane	167.849	1.05	± 10
Tetrachloroethylene	165.833	1.05	± 10
Toluene	92.138	1.05	± 10
trans-1,3-dichloropropene	110.969	1.05	± 10
1,1,1-Trichlororethane	133.404	1.05	± 10
1,1,2-Trichloroethane	133.404	1.05	± 10
Trichloroethylene	131.388	1.05	± 10
1,2,4-Trichlorobenzene	181.447	0.915	± 10
Trichlorofluoromethane	137.368	1.04	± 10
1,1,2-Trichlorotrifluoromethane	187.675	1.05	± 10
1,2,4-Trimethylbenzene	120.192	1.05	± 10
1,3,5-Trimethylbenzene	120.192	1.04	± 10
Vinyl chloride	62.498	1.04	± 10
m-Xylene	106.165	1.05	± 10
o-Xylene	106.165	1.05	± 10
p-Xylene	106.165	1.05	± 10

Three dilution mixtures were used to obtain the calibration curves for each compound. The target concentrations were 20 ppbv, 40 ppbv and 80 ppbv. Table 1-6 shows the volumes of calibration standard and zero air to achieve the target concentrations. The dilution factor was computed as follows

$$C_{cal} = C_m \times D = C_m \times \frac{P_{calgas}}{P_{air} \times 100}$$

where C_{cal} is the concentration of the compound after the dilution (in ppmv). C_m is the concentration of the compound in the calibration mixture (in ppmv). D is the dilution factor

(dimensionless), P_{calgas} is the pressure of the calibration gas (in psi), P_{air} is the pressure of the dilution air (in psi)

Table 1-6 Dilutions of calibration standard

Mixture/Target	Dilution Air	Cal Gas	Dillution factor
1 / 20 ppbv	10	20	0.02
2 / 40 ppbv	10	40	0.04
3 / 80 ppbv	5	40	0.08

Field "blank" chromatograms were obtained using the calibration mode but without the activation of the calibration gas solenoid valve. Thus, only zero-grade air was introduced into the GC. The pressure of zero-grade air was set at 10 psi.

Because of the linear response of the FID and PID detectors, a simple linear model was used to compute the calibration curves for each compound. In some cases (mainly for the low molecular weight, high vapor pressure), a regression model produced moderate to poor correlations because of losses associated with the sampling and desorption. As a result, the concentration of each compound (C, in ppbv) in ambient air samples was calculated as follows:

$$C = a \cdot Area + b$$

where *Area* is the integrated area of the peak and *a* and *b* are the regression slope and intercept of the calibration curves.

Tethered-balloon measurements

Figure 1-5 shows the major components of the tethered balloon system that was composed of:
- a tethered balloon filled with helium ((1) in Figure 1-5),
- a TTS111 tethersondes((2) in Figure 1-5) for the monitoring of wind speed and direction, temperature, relative humidity, pressure and elevation,
- a winch ((3) in Figure 1-5) to control the release and retrieval of the balloon,
- an RM21 UHF telemetry antenna ((7) in Figure 1-5) to collect data from the tethesondes,
- a SPS220T sounding processor ((6) in Figure 1-5) that analyzes the signal received by the antenna and,
- a sounding workstation ((4) and (5) in Figure 1-5) that collects all the information.

For the needs of the study, a suite of other instruments was installed downstream of the tethersonde. These included:
- a TSI CPC 3007 particle counter;
- a ppbRAE total VOCs monitor;
- a TTO111 tethered ozonesonde and;
- a passive ozone monitor.

The tethered ozonesonde data were automatically transferred to the tethersonde while data from the other monitors were stored independently.

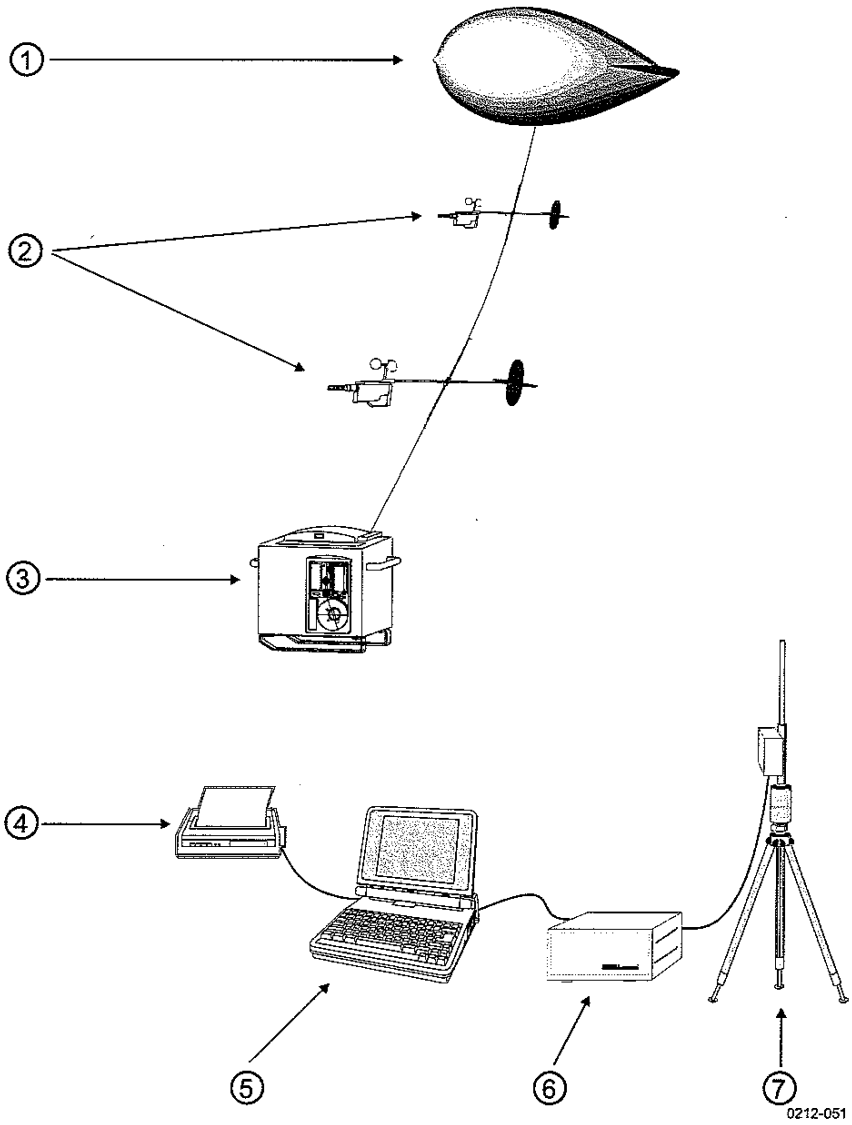

Figure 1-5 Schematic overview of the DigiCORA Tethersonde System TT12

Tethered balloon

During this study, two different types of balloon were used: a 9-m^3 balloon with a lifting capacity of 5 kg and a 6 ft diameter balloon with a lifting capacity of 2 kg (Figure 1-6). Because the 6 ft diameter balloon did not have any safety features, a new balloon ans stronger thetherlines were used for each launch day to compensate for regular ware and decomposition of the polypropylene material by wind and radiation.

Figure 1-6 Photos of the 9-m^3 balloon (left) and two 6-ft balloons (middle and right)

Tethersonde

The TTS111 Tethersonde consisted of an internal compass, an anemometer, a RSS911 PTU Sensor for pressure, temperature and humidity measurements, a transmitter that operated in the 400 MHz band, and a 9V lithium-ion battery. Table 1-7 presents the technical information for each sensor of the tethersonde. The tethersonde weighed about 300g and required a power source of 100mA at 9VDC. The compass was a dual-axis magnetometer which was calibrated every time the tethersonde battery was changed. After powering up, calibrating and balancing of the tethersonde, it was attached on the tether line approximately 6 ft below the balloon. Figure 1-7 shows the tethersonde attached on the tether line at about 3 meters above ground level for comparison against the meteorological tower. While all sensors have been calibrated in the factory before shipment and no field calibration is required, a mobile tower was used to compare readings between the tethersonde and meteorological instrumentation attached on the tower.

Table 1-7 Specification of tethersonde components

Measurement	Range	Resolution	Response time	Repeatability
Temperature	-50 – 60^{o}C	0.1^{o}C	0.2 sec	0.1 ^{o}C
Relative humidity	0 – 100%	0.1 %RH	< 0.5 sec	2 %RH
Pressure	500 – 1080 hPa	0.1 hPa		0.4 hPa
Wind speed	0 – 20 m/sec	0.1 m/sec		
Wind direction	0 – 360^o	1^o		
Analog-Digital	0 – 2000 VDC	0.001 VDC		

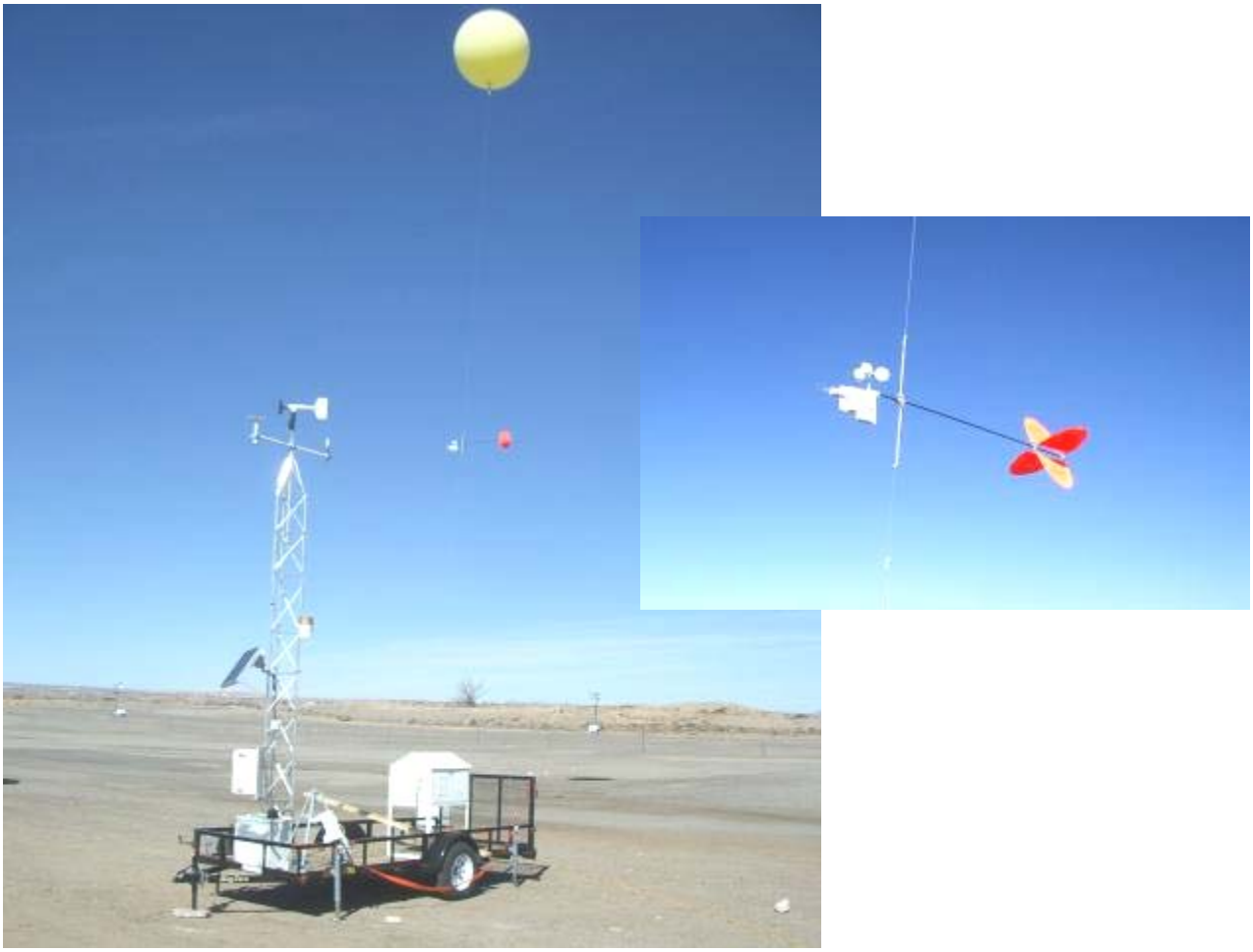

Figure 1-7 The tetheredsonde attached on the tetherline and the mobile meteorological tower (Insert: Tethersonde)

Tethered Ozonesonde

The TTO11 Ozonesonde utilized a SPC Model 6A ECC ozone monitor that included:

- a non-reactive PTFE gas sampling pump that was electronically controlled,
- a temperature sensor and,
- an ozone electrochemical sensor.

The ozonesonde weighed about 600g and required a power source of <115mA at 12VDC. Table 1-8 shows the specifications of the ozone and temperature sensor as well as the measurement of current from the electrodes. For accurate operation, a multi-step time consuming calibration of the ozonesondes was required. It involved the preparation of solutions for the anode and cathode electrodes, the preparation and activation of electrodes, the calibration of the response of the electrodes in comparison to a reference electrode that was attached on the calibrator and finally, the field verification before launch. Because of the nature of the sensors, the first steps were completed in Las Vegas, while the calibration and field verification were done in Albuquerque. The calibration procedures and methodologies suggested by the manufacturer were applied.

Table 1-8 Specifications of ozonesonde

Measurement	Range	Resolution	Sensitivity	Uncertainty	Noise
Ozone			2-3 ppb	± 10%	< 1%
Current	0 – 10,000 μA	0.003 μA			
Temperature	0 – 40 ^{o}C	0.1 ^{o}C			

The measurement of ozone relied on the measurement of current generated by the iodide-iodine redox reduction with ozone. The cathode was filled with an aqueous solution of KI, KBr, NaHPO4 and NaH_2PO_4, while the anode was loaded with a saturated KI solution. The redox reactions scheme is shown in Reaction 1.

$$\text{Cathode}: 3I^- \longrightarrow I_3^- + 2e^-$$

$$\text{Anode}: \quad I_2 + 2e^- \longrightarrow 2I$$

$$\text{Net}: \quad I^- + I_2 \longrightarrow I_3^- \qquad \text{(Reaction 1)}$$

or

$$2KI + O_3 + H_2O \longrightarrow 2KOH + I_2 + O_2$$

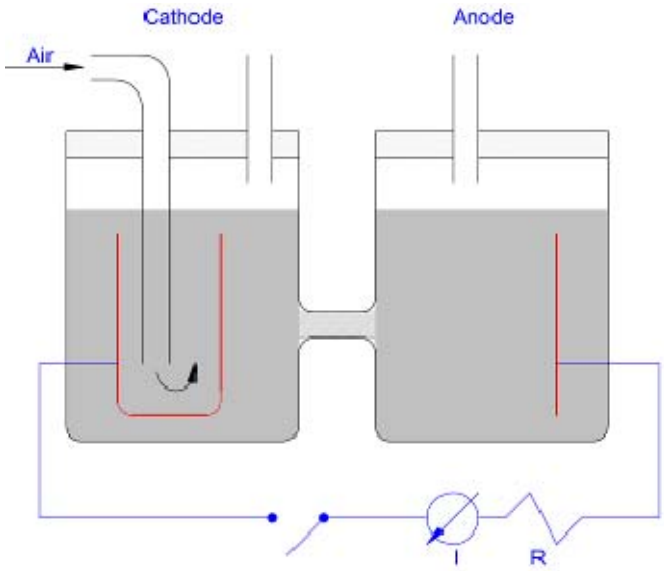

Figure 1-8 Drawing of the electrochemical sensor

The calibration of ozonesondes included exposure of the sensor to LOW and HIGH OZONE conditions and direct comparison of the sensor and the calibration unit. Table 1-9 and Table 1-10 show the calibration parameter for the three ozonesondes on February 13, 2008 and June 20, 2008.

Table 1-9 Calibration parameters of ozonesondes on February 13, 2008

	6A16465	6A16466	6A16467
Pump voltage (V)	12	12	12
Pump current (mA)	70	105	112

Head pressure (hPa)	760	700	500
Vacuum (hPa)	760	700	
Background response (μA)	0.10	0.20	
Flow rate (in sec/100 ml)	26.88	28.22	
Reading at 5 μA O3 (μA)	5.10	4.8	
Reading after 1 min (μA)	0.6	1.6	
Reading after 2 min (μA)	0.2	0.6	
Reading after 3 min (μA)	0.0	0.3	
	Passed	***Failed***	***Failed***

Table 1-10 Calibration parameters of ozonesondes on June 16, 2008

	6A16465	**6A16466**	**6A16467**
Pump voltage (V)	12	12	12
Pump current (mA)	55	105	70
Head pressure (hPa)	850	300	850
Vacuum (hPa)	850		700
Background response (μA)	0.15		0.0
Flow rate (in sec/100 ml)	25.61		27.23
Reading at 5 μA O3 (μA)	5.40		5.2
Reading after 1 min (μA)	0.9		0.3
Reading after 2 min (μA)	0.5		0.1
Reading after 3 min (μA)	0.3		0.0
	Passed	***Failed***	***Passed***

The ozone concentration (C, in ppbv) was computed as follows:

$$C = \frac{I \cdot t}{2 \cdot F \cdot 100} \cdot \frac{10^6}{0.0409}$$

where I is the measured current (in μA), t is the pumping time for 100 ml of air (in sec), F is the Faraday constant (9.6487 10^4 C/mol

ppbRAE VOC monitor

The ppbRAE Plus VOC instrument (Model PGM-7240) is a portable PID detector for continuous real-time detection and measurement of VOCs at ppb levels. It is composed of a photoionization detector (PID) with a 10.6 eV UV lamp and an integrated diaphragm-type pump that provide 450-550 ml/min flowrate. The range of measured VOC is 0-9999 ppb with resolution of 1 ppb. The accuracy of the measurements is 20 ppb (for isobutylene). One monitor was used to measure VOCs during the tethered balloon flights, while a second one was installed on the tramway to collect VOC measurements during the tram flights. However, a limited dataset of VOC measurements were obtained from the tethered-balloon system because of the limited lifting capacity of the 6 ft balloon. Figure 1-10 and Figure 1-11 show the VOC monitor and particle counter during one of the flights with the 9-m^3 balloon and inside a protective box placed on the roof of a tramway car. The ppbRAE was calibrated using a 10 ppm (±2%) isobutylene (P/N 600-0069-000; T C39M NRC 34/43 M1003) calibration standard. Individual calibration factors were obtained for benzene and toluene. In addition, a total (Air Toxics?) calibration factor was

obtained. Blank values were obtained using an activated carbon VOC Zeroing Tube (P/N 025-2000-010).

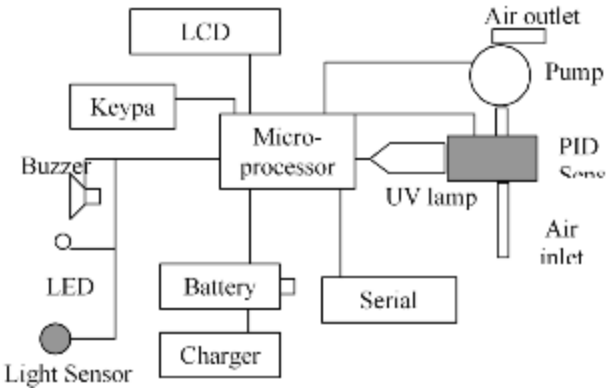

Figure 1-9 Schematic drawing of the ppbRAE VOC monitor

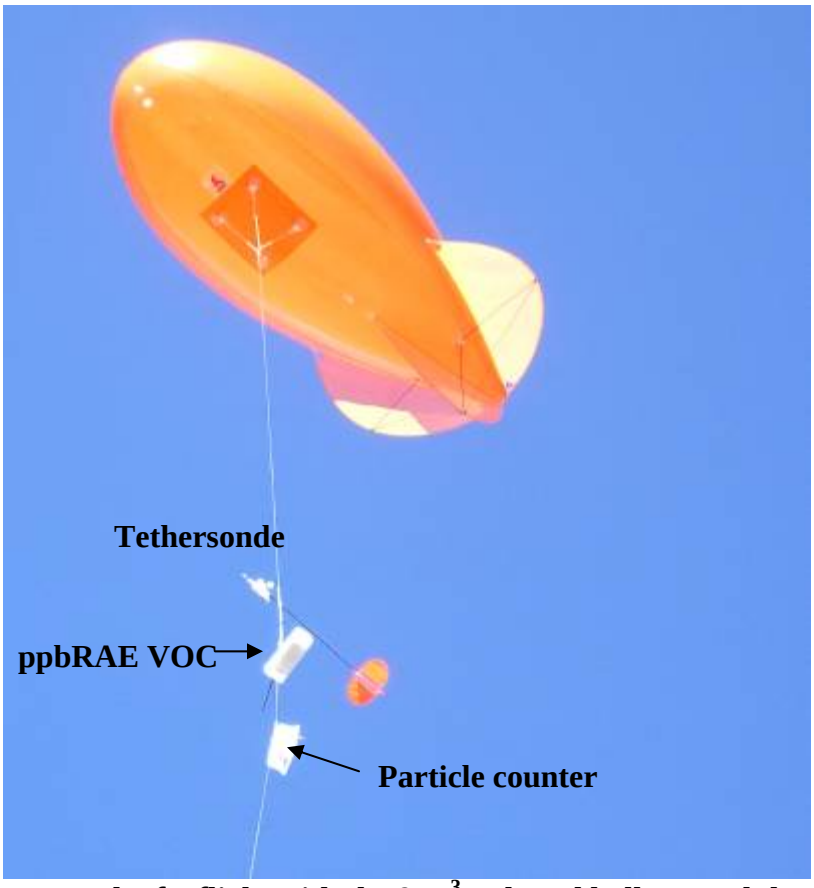

Figure 1-10 Photograph of a flight with the 9-m^3 tethered balloon and the ppbRAE VOC monitor and CPC3007 counter attached on the tether line after the tethersonde. Flight was on Wednesday, February 13, 2008.

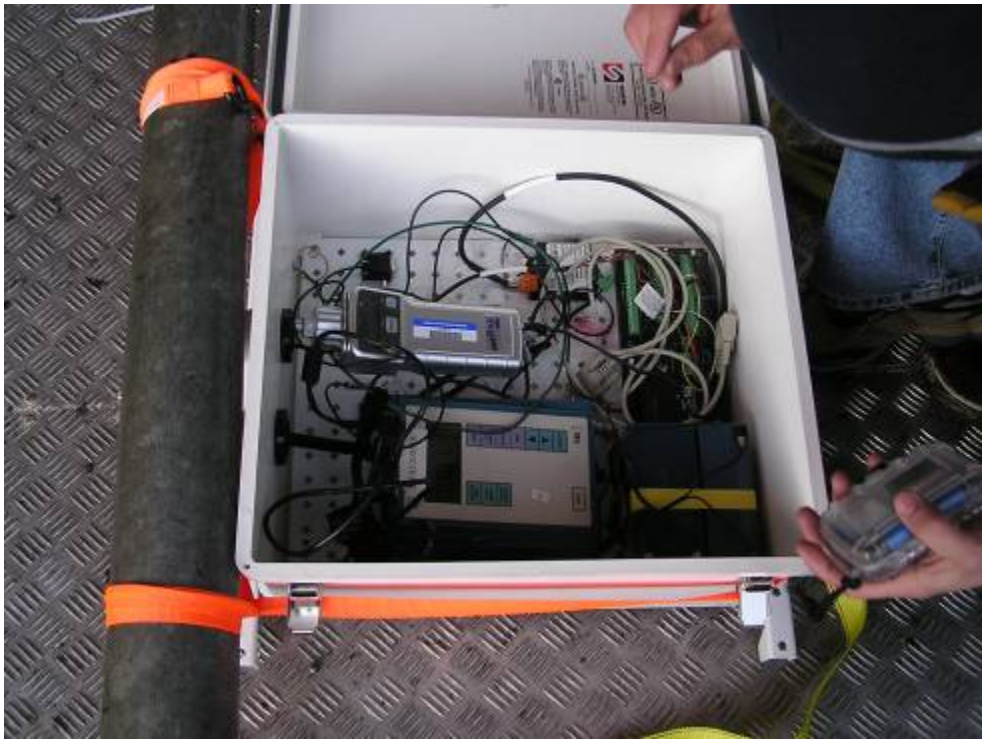

Figure 1-11 The ppbRAE VOC monitor, TSI Dust Trak particle mass monitor and other equipment inside a protective box on top of one of tramway cars

TSI CPC3007 particle counter

The TSI CPC3007 instrument is a portable particle counter for continuous real-time measurements of the particle number concentration. It is composed of a saturation chamber and a laser optical detector (Figure 1-12). Isopropanol is used to supersaturate the air inside the saturation chamber in order to increase the size of ultrafine and fine particles. Once particles exit the saturation chamber, they are directed to a laser detector in which the number of particles is counted. The measured concentration range from 0 to 10^5 particles/cm^3 for particles larger than 10 nm. A pump provides a total flow of 700 ml/min.

The monitor was used to measure VOCs during the tethered balloon flights; however, a limited dataset of VOC measurements were obtained from the tethered-balloon system because of the limited lifting capacity of the 6-ft^3 balloon. The instrument was calibrated by the manufacturer before shipment.

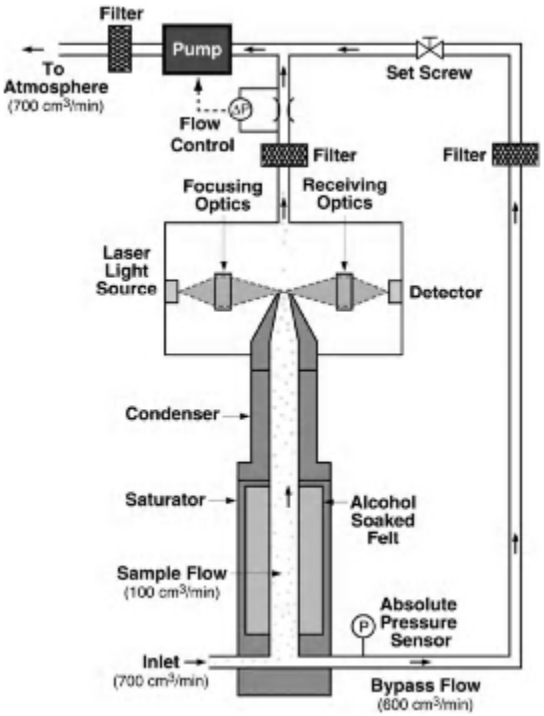

Figure 1-12 Schematic drawing of the particle number counter

Supplemental measurements

A set of supplemental measurements were obtained during the IMPs. These measurements were collected in order to obtain a better understanding of the spatial and temporal patterns of air transport and air quality. These data were collected with research-grade instrumentation and cannot be used to determine exposures and associated risks as well as compliance with existing federal regulations.

HOBO® T/RH Sensor

The HOBO Pro v2 external temperature/RH (U23-002) logger was used to collect temperature and relative humidity measurements in fixed locations along the tramway cable. A radiation shield was used to protect the external sensors from direct solar heating and precipitation. Except for the tram top, the sensors were attached to a fencepost approximately 1 meter above the ground. During the first IMP, sensors were installed at the tram base and peak of the Sandia Tramway. During the second IMP, a third sensor was installed at the first tower. A similar sensor was also attached on the roof of the tramway car. Table 1-11 presents the technical information for the sensor. Figure 1-13 shows the locations of the sensors. The sensors were calibrated by the manufacturer before shipment.

Table 1-11 Specification of HOBO Pro v2 components

Measurement	Range	Resolution	Response time	Repeatability
Temperature	-40 – 75°C	0.02°C	5 min	0.1 °C
Relative humidity	0 – 100%	0.03 %RH	10 min	1% RH

Figure 1-13 The locations of HOBO temperature/relative humidity sensors at the roof of the Sandia Tramway building at the peak (left), at the base of the Sandia tramway (middle) and on the roof of a tramway car (right)

TSI Dust Trak nephelometer

The DUSTTRAK™ Aerosol Monitor is a portable, battery operated laser photometer. The monitor provides measurements of particle mass based on 90^o light scattering. Atmospheric aerosol passes through a size selective inlet (either PM_{10} or $PM_{2.5}$) and is directed to an optics chamber at a flow rate of 1.7 l/min. The light source is a laser diode that emits light at a wavelength of 780 nm. The aerosol sample is drawn into the sensing chamber where it is illuminated with a narrow beam of laser light. Light scattered by aerosol particles is collected by a set of lenses and focused onto the photodetector. The detector signal is proportional to the amount of scattered light, which is proportional to the mass concentration of the aerosol. Voltage is read by the processor and multiplied by an internal calibration constant to yield mass concentration. The calibration constant is pre-set by the manufacturer for scattering characteristics of the respirable mass of ISO 12103-1, Al test dust. Local variations in aerosol particle size distribution and composition relative to this standard may result in differences in the actual response factor of the instrument. Figure 1-11 shows the TSI DustTrak on the roof of the tramway car. The instrument was calibrated by the manufacturer before shipment. The instrument was used for both IMPs at the tramway.

2B Model 202 Ozone monitor

The 2B Technologies Model 202 O_3 Monitor™ provides accurate and precise measurements of ozone ranging from 1 ppb to 100 ppm with a precision of 1 ppbv by absorption of ultraviolet radiation (at 254 nm). The amount of radiation absorbed is directly related to the concentration of the compound. The Ozone Monitor™ is simple to operate and has a fast response time. The O_3 monitor was placed in a temperature-controlled environmental enclosure (Figure 1-14 shows the environmental enclosure at the Sandia Peak). An 8-ft Teflon sampling line was used to draw air to the monitor. Particle contamination was eliminated by a Teflon filter.

The monitor was installed on Sunday, June 22, 2008 and run through the end of the second IMP (June 30, 2008). The instrument was calibrated by the manufacturer before shipment.

Figure 1-14 Environmental enclosure of the 202 O_3 Monitor

Vaisala CL31 Ceilometer

The Vaisala CL31 ceilometer is a compact and lightweight instrument for cloud base height and vertical visibility measurements. It is able to detect three cloud layers simultaneously. The ceilometer is ideal for aviation as well as meteorological applications where reliable detection of clouds is essential. The CL31 employs a pulsed diode laser LIDAR (light detection and ranging) technology, where short, laser pulses are sent out in a vertical or near vertical direction. The reflection of light (backscatter) caused by clouds, precipitation or other obscuration is analyzed and used to determine the cloud base height. Backscatter is given in units of steradan^{-1} km^{-1}. We used the CL-VIEW software for data collection, storage and presentation program designed for this ceilometer. The ceilometer was connected to a laptop through a serial data port for data collection. The unit was operated to give a profile from the ground to 7.7 kilometers every 5 seconds. Each profile is given with a vertical resolution of 10 meters, providing us with a total 770 points in a profile. The graphical presentations include cloud detection, cloud intensity and backscatter profile graphs. Numerical cloud height information, ceilometer status, log status along with time and date are displayed in all three graphs. An estimate of the mixed layer depth can be extracted from the backscatter signal as a function of time. The mixed layer can often be seen as a strong gradient in backscattered intensity as a function of height. This usually works best when inversions are strong and there are sufficient aerosols within the mixed layer to act as scattering media.

The ceilometer was installed on Monday, June 16, 2008 and run through June 22 on the roof of the Del Norte site. The ceilometer was then operated at the balloon fiesta site while we were on

site with the tethered balloon. Figure 2-21 shows the instrument installed at the two locations. The instrument was calibrated by the manufacturer before shipment.

Figure 1-15. Ceilometer located on the roof of the Del Norte site (left) and at the Balloon Fiesta site (right)

Laboratory Analyses for Elemental and Organic Carbon

Figure 1-16 shows the schematic diagram of the thermal-optical analyzer used for the measurement of elemental and organic carbon on filters collected at Del Norte, South Valley and North Valley sites. The operation of the DRI Model 2001 Thermal/Optical Carbon Analyzer is based on the preferential oxidation of organic carbon (OC) compounds and elemental carbon (EC) at different temperatures. Its function relies on the fact that organic compounds can be volatilized from the sample deposit in a non-oxidizing helium (He) atmosphere, while elemental carbon must be combusted by an oxidizer. The analyzer operates by:

1) liberating carbon compounds under different temperature and oxidation environments from a small sample punch taken from a quartz-fiber filter;
2) converting these compounds to carbon dioxide (CO_2) by passing the volatilized compounds through an oxidizer (heated manganese dioxide, MnO_2);
3) reducing CO_2 to methane (CH_4) by passing the flow through a methanator (hydrogen-enriched nickel catalyst); and
4) quantifying CH_4 equivalents with a *flame ionization detector* (FID).

The principal function of the optical (laser reflectance and transmittance) component of the analyzer is to correct for pyrolysis charring of OC compounds into EC. Without this correction, the OC fraction of the sample might be underestimated and the EC fraction might include some pyrolyzed OC. The correction for pyrolysis is made by continuously monitoring the filter reflectance and/or transmittance (via a helium-neon laser and a photodetector) throughout an analysis cycle. The reflectance and transmittance, largely dominated by the presence of light absorbing EC, decrease as pyrolysis takes place and increase as light-absorbing carbon is

liberated during the latter part of the analysis. By monitoring the reflectance and transmittance, the portion of the EC peak corresponding to pyrolyzed OC can be accurately assigned to the OC fraction. The correction for the charring conversion of OC to EC is essential for a less-biased measurement of carbon fractions. The Thermal Optical Reflectance (TOR) and Thermal Optical Transmittance (TOT) charring corrections are not necessarily the same, owing to charring of organic vapors adsorbed within the quartz fiber filter. OC and EC determined by both methods are reported. Carbonate carbon can be determined by measuring the CO_2 evolved upon acidification of the sample punch before the normal carbon analysis procedure. Seven temperature fractions, as well as the TOR and TOT charring correction, are individually quantified and reported when the IMPROVE temperature protocol is applied. Values routinely reported include total OC, total EC, total carbon (TC, sum of total OC and total EC), and pyrolyzed carbon, monitored by both reflectance (OPR) and transmittance (OPT).

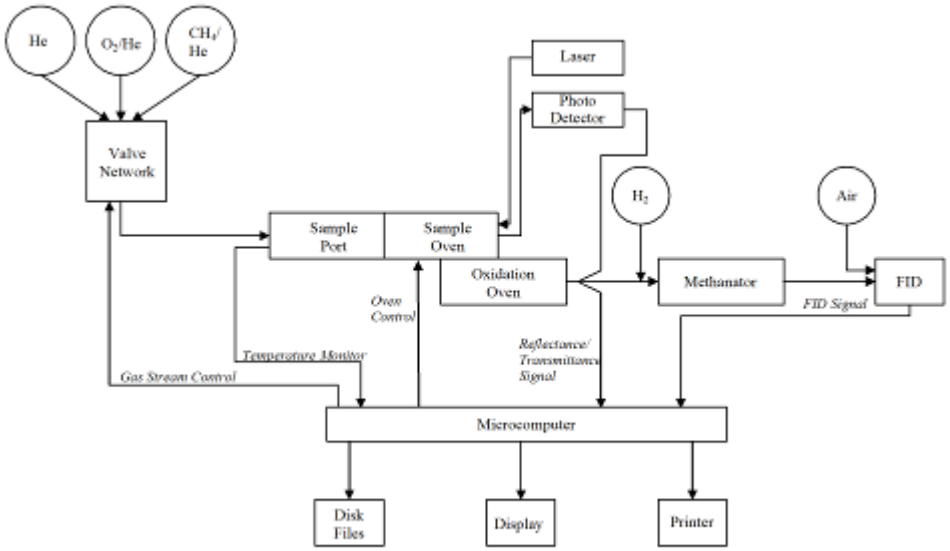

Figure 1-16 Schematic drawing of the DRI2001 Thermal/Optical Carbon analyzer

A small portion of the quartz filter (about 2.5 cm in diameter) was punched from the quartz filters used for the collection of particulate matter for PAHs analysis. The filters were placed in a petridish and stored at -10^{o}C until shipment to DRI's Environmental Analysis Facility in Reno. For the analysis, a punch of 1 cm^2 was obtained and analyzed, thus the results are reported in µgC/cm2. The concentration of organic and elemental carbon was calculated as follows:

$$EC(\text{or } OC) = \frac{C \cdot 113.0973355}{V}$$

where EC or OC are the concentrations of elemental and organic carbon in µg/m^3, C is the reading from the analyzer (in µg/cm^2) and V is the collected volume (in m^3). A factor of 113.0973355 cm^2 was used to estimate the total amount of carbon collected on a 12-cm diameter quartz filter.

2. References

Kavouras, I.G., Etyemezian, V., DuBois, D.W. (2008) QUALITY ASSURANCE PROJECT PLAN, CITY OF ALBUQUERQUE AIR TOXICS RISK ASSESSMENT STUDY, DESERT RESEARCH INSTITUTE July 2007 - September 2008 Revision 0

New Mexico Environment Department (NMED) (2004) Corrales Environmental health Evaluation Community Process Summary Report

U.S. Environmental Protection Agency (USEPA), (2002) Air Toxics Pilot Study Laboratory Intercomparison Office of Air Quality Planning and Standards, EPA-454/R-02-004

Appendices

Description of the online gas chromatography system

Figure 0-1 shows the gas chromatograph (GC) system and the individual components. It was composed of: (*i*) a complete sampling system (dryer, trap, mass flow meter, vacuum pump); (*ii*) a fully automated calibration system (clean air, calibration standard, regulators, dilution chamber); (*iii*) an analysis system (a temperature-controlled oven (capillary column) and; (*iv*) three in-series detectors (flame ionization (FID) (for hydrocarbons), photo-ionization (PID) (for aromatic hydrocarbons) and dry-electrolytic conductivity (DELCD) for halogen-hydrocarbons). Once sampling is completed, a 10-way solenoid valve switches to begin desorption and analysis of sample air. The functionality of the 10-port valve that was required to collect and inject the sample is presented in Figure 0-2.

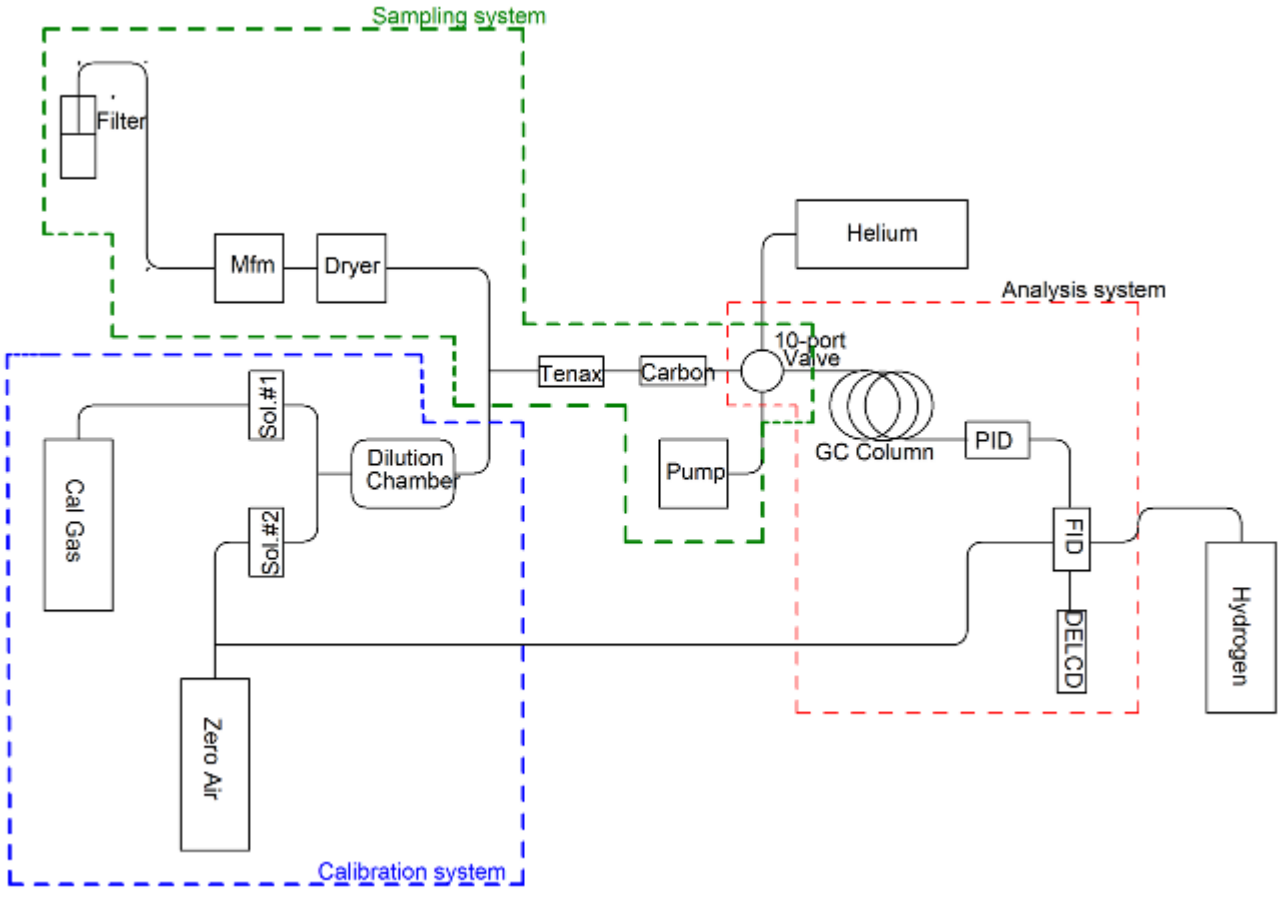

Figure 0-1 Drawing of the online gas chromatography system showing the components of each system

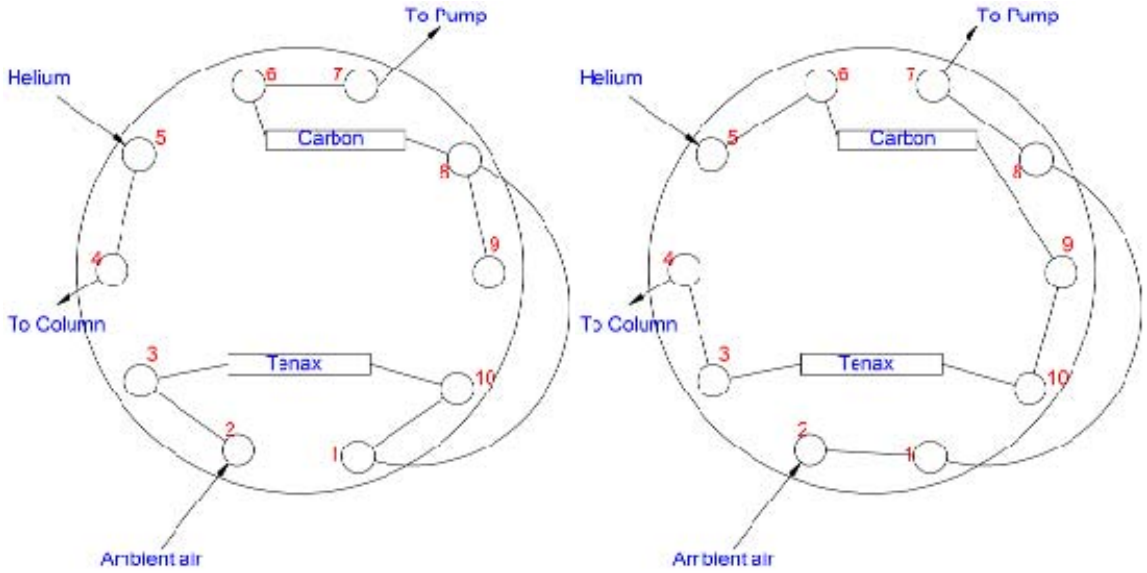

Figure 0-2 Schematic drawing of the 10-port valve in the LOAD (left) and INJECT (right) positions

The GC system runs in monitoring mode or calibration mode. During monitoring mode, VOC concentrations in ambient air were measured. On calibration mode, known VOCs mixtures were analyzed by the GC for identification and calibration of the compounds. All components of the GC were controlled through a series of switch on/off relays and a laptop. Table 0-1 shows the conditions of each relay. As a result, the system operated continuously, controlled by a pre-configured auto-sample method. The operating conditions of gases and detectors are presented in Table 0-2

On the measurement mode, the GC system ran as follows:

- Collection: The vacuum pump was automatically switched on. The 10-way valve was on LOAD position. The sample air was drawn through the filter (to remove particles), mass flowmeter (to measure the flowrate: Mfm) and Dryer prior to the collection of VOCs by the Tenax and Carbosieve traps (Figure 0-1). The temperature of the traps was at 35^{o}C. The carrier gas went direct to the capillary column.
- Analysis: The vacuum pump switched off and the two traps were heated to 190^{o}C. re. next sentence: I don't see a valve event on Figure 2-5 that corresponds to 3-min after reaching 190^{o}C. I do see an event 3-min after the temp reaches 150^{o}C After 3 minutes, the 10-way valve switched to the INJECT position and the carrier gas (helium) passed through the traps (Figure 0-2). As a result, concentrated VOCs were thermally desorpted and injected into the capillary column. The oven temperature increased as a function of time. VOCs were eluted from the capillary column at different times depending on the temperature in the oven and the interaction of the VOC with the solid phase of the capillary column. They were detected by the three detectors. Normal, unsaturated and aromatic hydrocarbons were identified by FID and PID. Halogenated hydrocarbons were determined by DELCD.
- Data collection: The signal of all detectors was automatically recorded by the software

On the calibration, the GC system ran as in the measurement mode but sample was drawn through the dilution chamber (Figure 0-2). The mixture in the dilution chamber was generated by releasing known amounts of the calibration gas and zero air for the duration of the sampling. The

concentration of the calibration mixture was controlled by adjusting the volumes of the calibration gas and zero air through the solenoid valves #1 and #2, respectively.

Table 0-1 Description of the function of relays

Relay	Function
A	Solenoid valve for calibration gas (OFF: no gas; ON: 10 ml/min for 10 psi)
B	Bake option for traps (ON: 50^{o}C above standby temperature for cleaning)
C	Heater for Trap2 (Carbosieve) (OFF: 35^{o}C; ON: 190^{o}C)
D	Vacuum pump (OFF: No flow; ON: 35-40 ml/min)
E	Solenoid valve for zero air for calibration (OFF: No air; ON: 1000ml/min)
F	Heater for Trap1 (Tenax) (OFF: 35^{o}C; ON: 190^{o}C)
G	10-port valve (OFF: LOAD position; ON: INJECT position)

Table 0-2 Sampling and analytical specifications of the online GC

Paramater	Value
Gases	
Helium (psi)	12 psi for 10 ml/min
Hydrogen (psi)	20 psi for 25 ml/min
Zero air (for FID) (psi)	5 psi for 250 ml/min
Cal Gas (psi)	10, 20 and 40 psi (10, 20 and 40 ml/min, respectively)
Zero air (for dilution)	10 psi for 1000 ml/min
Detectors	
FID Temperature	150^{o}C
DELCD Temperature	1000^{o}C
PID Current	150 mA

The parameters for the collection and analysis for the measurement and calibration methods during the first IMP are presented in **Error! Reference source not found.** a and b, respectively. Both programs are identical with the exception of the activation of CalGas and ZeroAir solenoid valves during the calibration in order to directly compare the retention time and the response of calibration and ambient chromatograms. A different method was used during the second IMP to collect a large volume of ambient air. For this method, a sample was collected for 45 min and analyzed. This was achieved by collecting an air sample for the last 45 minutes of a run. This sample was then analyzed during the second run using an 1-hour temperature program. During the last 45 minutes of the second run, a sample air was drawn that was subsequently analyzed during the third run. The sequence of three consecutive run is presented in Figure 0-4. The parameters for the collection and analysis for the measurement and calibration methods during the first IMP are presented in Figure 0-5 a and b.

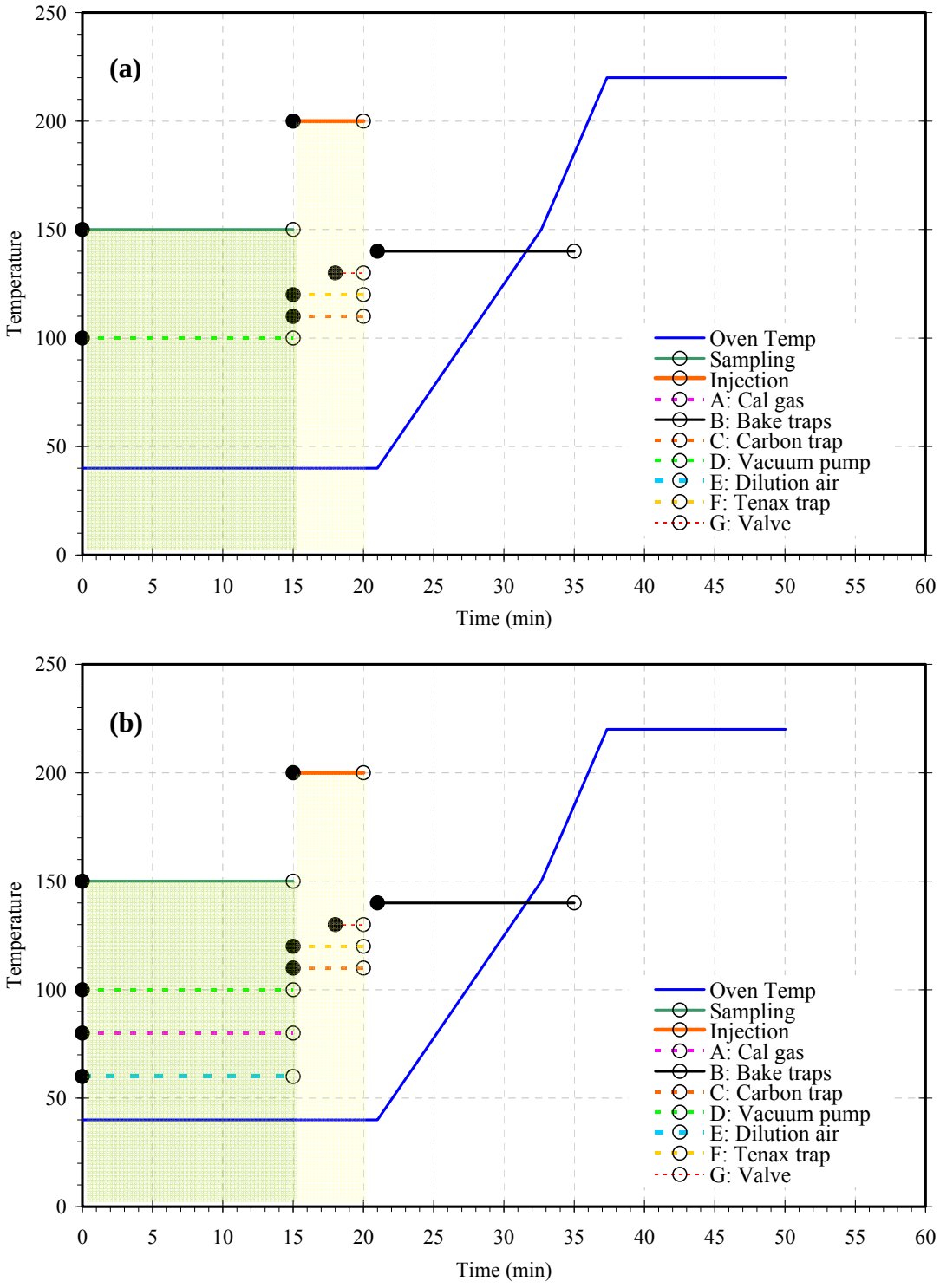

Figure 0-3 The temperature and relays program of the measurement (a) and calibration (b) method. Filled and open circles indicate the activation and de-activation of the relay, respectively. The green shaded area corresponds to the sampling phase and the yellow shaded area demonstrates the desorption/injection phase.

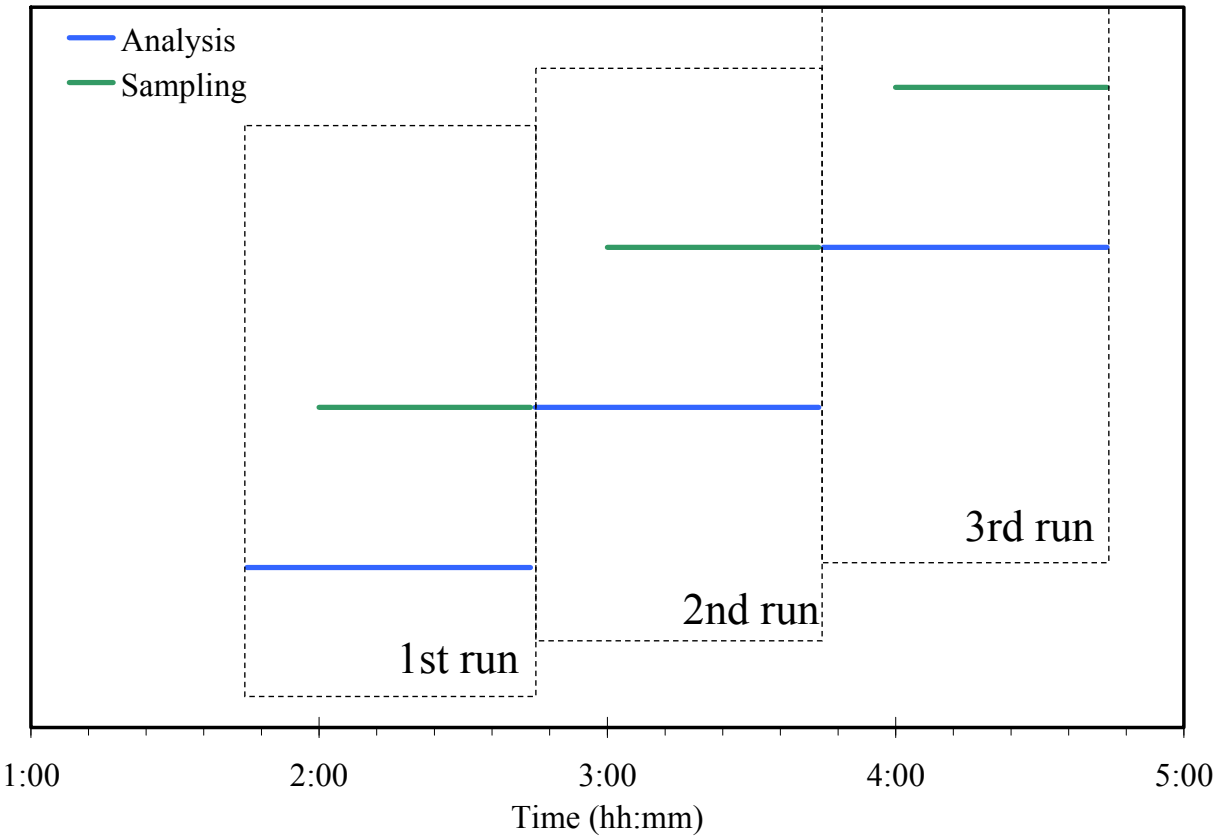

Figure 0-4 Sequence of sampling and analysis for the second IMP

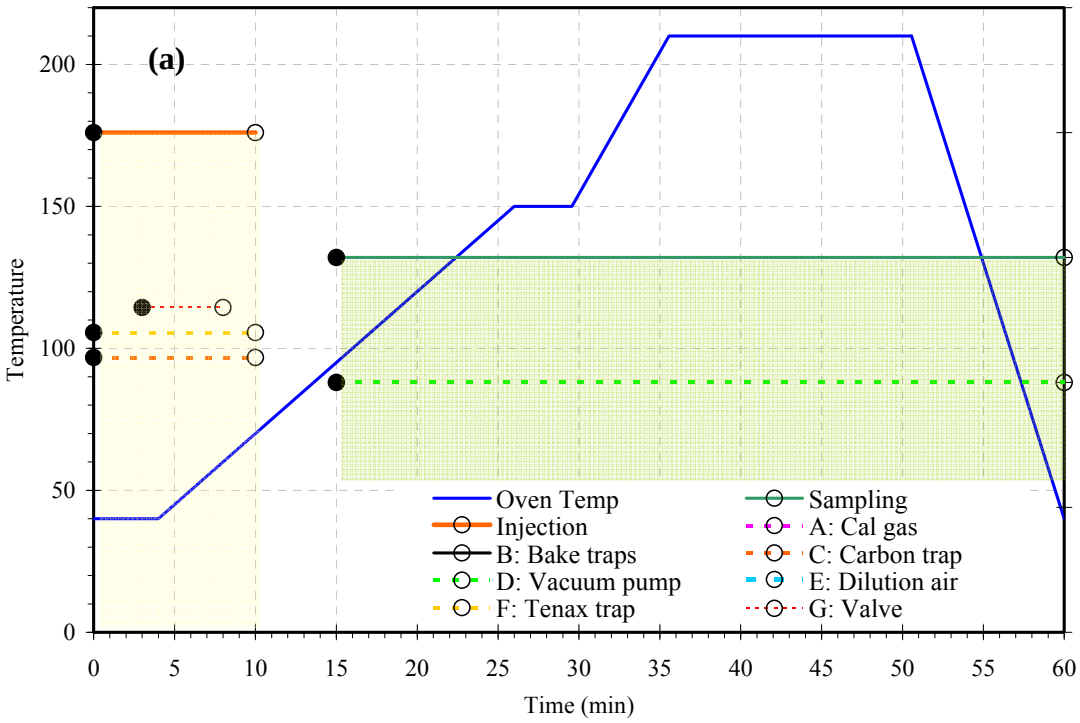

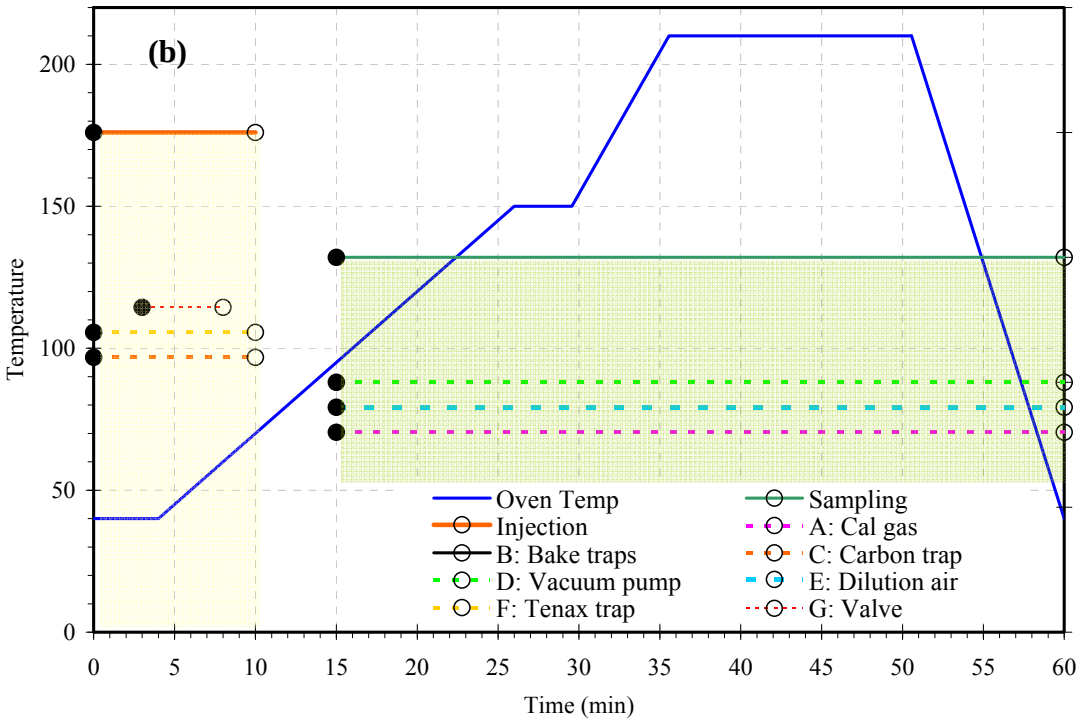

Figure 0-5 The temperature and relays program of the measurement (a) and calibration (b) method. Filled and open circles indicate the activation and de-activation of the relay, respectively. The green shaded area corresponds to the sampling phase and the yellow shaded area demonstrates the desorption/injection phase.

Chemical structure of target VOCs

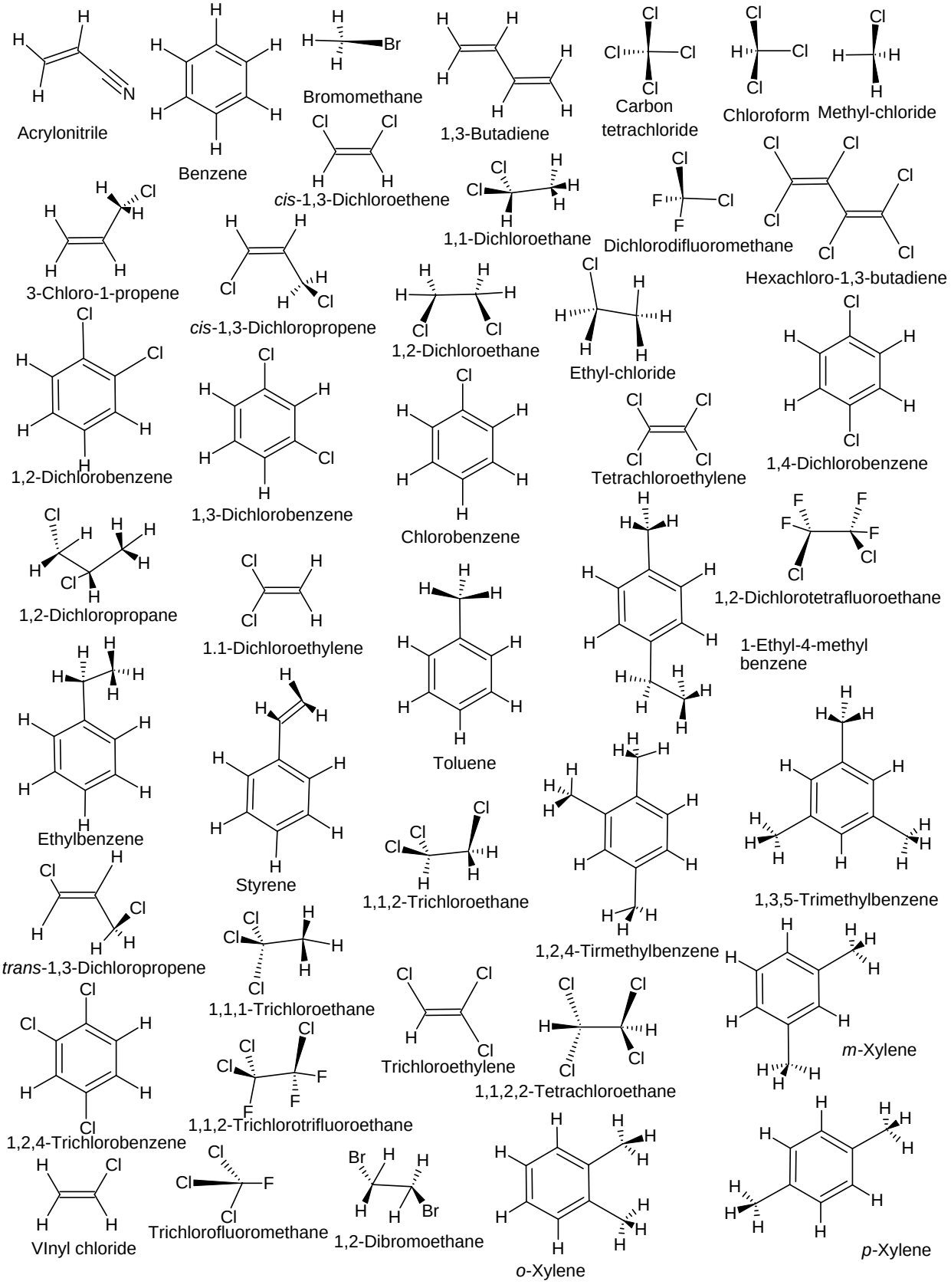

Calibration curves of target VOCs

Compund name	CalGas	Dil.Conc (1)	Dil.Conc (2)	Dil.Conc (3)	Area (1)	Area (2)	Area (3)	Slope	Intercept	R
vinylchloride	1.04	0.0416	0.0208	0.0832	549.1430	82.5490	835.4427	0.000079	0.009820	0.95
1,3-butadiene	1.04	0.0416	0.0208	0.0832	654.1857	105.7228	1058.4700	0.000064	0.009798	0.96
methylchloride	1.04	0.0416	0.0208	0.0832	735.0414	498.4144	1069.9540	0.000110	-0.036062	1.00
trichlorofluormethane	1.04	0.0416	0.0208	0.0832	603.8308	295.8180	1003.4270	0.000089	-0.007897	0.99
Bromomethane	1.04	0.0416	0.0208	0.0832	402.6818	77.8296	922.3092	0.000074	0.013713	1.00
1,1 dichloroethylene	1.05	0.0420	0.0210	0.0840	470.6818	237.0860	807.5402	0.000111	-0.007290	1.00
methylene chloride	1.04	0.0416	0.0208	0.0832	1101.9380	703.8290	3411.4750	0.000021	0.011468	0.98
1,1 dichloroethane	1.05	0.0420	0.0210	0.0840	862.4483	214.5442	1093.0960	0.000063	0.003302	0.90
cis-1,2-dichlroethylene	1.05	0.0420	0.0210	0.0840	483.2244	190.4977	622.7682	0.000134	-0.009074	0.92
3-chloro-1-propene	1.07	0.0428	0.0214	0.0856	760.3130	205.7168	1006.2950	0.000073	0.001852	0.92
chloroform	1.05	0.0420	0.0210	0.0840	667.9014	250.9780	959.3720	0.000086	-0.005020	0.96
1,2 dichloroethane	1.03	0.0412	0.0206	0.0824	542.0318	152.7856	741.1951	0.000098	0.001226	0.93
Benzene	1.05	0.0420	0.0210	0.0840	1595.4810	729.9072	3539.0760	0.000022	0.005430	1.00
1,1,1-trichloroethane	1.05	0.0420	0.0210	0.0840	159.5481	72.9907	353.9076	0.000223	0.005430	1.00
Carbon tetrachloride	1.05	0.0420	0.0210	0.0840	851.5853	377.1986	1406.6780	0.000062	-0.005117	0.99
trichloroethylene	1.05	0.0420	0.0210	0.0840	643.5316	271.2242	1111.9520	0.000076	-0.002045	0.99
cis-1,3-dichloropropene	1.05	0.0420	0.0210	0.0840	785.3326	347.6891	1256.1660	0.000070	-0.006427	0.99
trans1,3-dichlororpropene	1.05	0.0420	0.0210	0.0840	700.3326	285.3757	1043.9260	0.000082	-0.006438	0.97
1,1,2 trichlororethane	1.05	0.0420	0.0210	0.0840	638.6245	253.7657	962.2175	0.000088	-0.005311	0.97
toluene	1.05	0.0420	0.0210	0.0840	1453.7000	832.5288	2962.3480	0.000029	-0.002185	1.00
tetrachloroethylene	1.05	0.0420	0.0210	0.0840	568.3811	234.6431	918.9358	0.000092	-0.003978	0.98
chlorobenzene	1.06	0.0424	0.0212	0.0848	564.3012	247.4934	945.1718	0.000092	-0.004315	0.99
ethylbenzene	1.04	0.0416	0.0208	0.0832	1183.3460	681.2366	2336.7980	0.000037	-0.003856	1.00
m/p-xylene	2.1	0.0840	0.0420	0.1680	3334.3740	1820.4750	2913.7990	0.000045	-0.023858	0.55
styrene	1.05	0.0420	0.0210	0.0840	1530.6740	870.1050	6080.3530	0.000011	0.017780	0.98
1,1,2,2 tetrachloroethane	1.05	0.0420	0.0210	0.0840	961.6225	323.9850	1726.5640	0.000045	0.003570	0.99
o-xylene	1.05	0.0420	0.0210	0.0840	2531.2060	1268.9430	4331.5640	0.000021	-0.007268	1.00

1,3,5trimethylbenzene	1.04	0.0416	0.0208	0.0832	1577.2530	805.6850	2647.3160	0.000034	-0.008801	1.00
1-ethyl-4=methyl benzene	1.07	0.0428	0.0214	0.0856	2221.2040	1139.6660	3650.8430	0.000026	-0.010354	0.99
1,2,4 trimethylbenzene	1.05	0.0420	0.0210	0.0840	1762.8710	861.3430	2898.6890	0.000031	-0.008402	0.99
1,3 dichlorobenzene	1.04	0.0416	0.0208	0.0832	944.8136	483.9175	1562.6240	0.000058	-0.009669	0.99
1,4 dichlorobenzene	1.05	0.0420	0.0210	0.0840	1574.4640	828.7545	2635.8460	0.000035	-0.010094	1.00
1,2 dichlorobenzene	1.05	0.0420	0.0210	0.0840	1194.0220	660.4069	2097.5560	0.000044	-0.009116	1.00
1,2,4 trichlorobenzene	0.915	0.0366	0.0183	0.0732	784.8461	381.9250	986.4475	0.000084	-0.017832	0.93
hexachlororbutadiene	0.945	0.0378	0.0189	0.0756	968.4474	410.2620	1309.8360	0.000060	-0.009830	0.95